Evaluation of Prefabricated Construction Systems and Materials' Thermal Performance with Reference to Housing Construction in Saudi Arabia.

ABDULAZIZ AHMED ALKELANI

Bachelor of Building Engineering. IAU, Saudi Arabia

Master of Architectural Science (High Performance Buildings), University of Sydney, Australia.

Thesis Submitted to the University of Nottingham for the Degree of Doctor of Philosophy in Building Technology, United Kingdom.

January 2025

ABSTRACT

In light of recent revisions to international standards, such as those advocated by the American Society of Heating, Refrigerating and Air-Conditioning Engineers (ASHRAE), the prioritisation of improved air circulation to support more energy-efficient ventilation systems has become evident. These systems simultaneously enhance occupant satisfaction and thermal comfort. Within this framework, the current research systematically examines the thermal performance and comfort of prefabricated houses in Saudi Arabia, a subject of increasing importance given the rise in summertime temperatures, consistent with the global increase in temperatures.

The investigation distinctly outlines the implications of individual components of prefabricated buildings, particularly building envelope components, on the comprehensive thermal performance in the extreme climate conditions prevalent in Saudi Arabia. It ventures to shape innovative prospects in the Saudi prefabricated construction industry, emphasising the reduction of energy expenses while elevating the quality of the indoor environment through the introduction of high-performance prefabricated building components and systems.

In Saudi Arabia, characterised by a harsh and hot climate, the residential sector accounts for nearly 50% of national energy consumption. With energy demand expected to rise further, this research investigates the thermal performance and thermal comfort potential of prefabricated housing as a sustainable alternative. The study prioritises optimising building envelope components, developing high-performance precast systems, and providing design guidelines to reduce energy consumption and enhance indoor thermal comfort.

It is evident that the study centred its investigation on natural ventilation from the initial stage. Consequently, it revealed a significant reduction in total discomfort hours across various cities in Saudi Arabia. Optimal performance, characterised by minimal total discomfort hours, was observed in cities characterised by lower humidity levels. This suggests that cities with higher relative humidity, exemplified by Jeddah, exhibit extended discomfort hours and encounter challenges in achieving markedly low discomfort hours compared to drier cities like Riyadh, the capital city of Saudi Arabia.

The research employs field observations of existing prefabricated houses in Saudi Arabia and simulation tools to evaluate and optimise thermal performance. Findings reveal substantial reductions in total discomfort hours across various zones, with optimisations achieving up to 32% reductions in specific zones. Key innovations include the use of phase change materials (PCMs) with a melting point of 23°C, improved insulation strategies, and optimised window-to-wall ratios, achieving reductions of up to 48% in cooling loads, 99.95% in heating loads, and 51.6% in annual energy consumption for air conditioning. The study culminates in a tangible design product: a high-performance precast system tailored for extreme climates, offering transformative solutions for sustainable construction practices in Saudi Arabia.

ACKNOWLEDGMENT

My praise is to Allah, the Gracious and the Merciful, on whom we ultimately depend. His guidance and wisdom have been the illuminating forces that led me through the journey of this research.

First and foremost, my profound gratitude is extended to my supervisor, Associate Professor Dr. Mohamed Gadi. His unparalleled expertise, sagacious counsel, and perpetual encouragement have been instrumental in navigating the myriad challenges of this academic endeavour. His timely and incisive feedback was pivotal in moulding this work into its final form.

I am eternally indebted to my parents, whose relentless prayers and unwavering faith in me have fortified my resolve and spirit. Their ceaseless support and blessings have been the bedrock upon which my academic and personal pursuits have been built.

To my wife and children, whose love, patience, and sacrifice have been the silent, yet profound, cornerstones of this journey—I offer my heartfelt gratitude. Their perpetual optimism and unflagging support sustained me through moments of doubt and hardship.

I would also like to extend my sincere appreciation to the myriad individuals who lent their invaluable assistance during my visits and data collection. Their collaboration and insights were integral in imbuing this research with depth and authenticity.

May Allah reward all of you abundantly for the roles you played in this academic voyage. To all whom I have not mentioned but have in some way contributed to the fruition of this research, I remain grateful.

Table Of Contents

LIST OF FIGURES

LIST OF TABLES

LIST OF ABBREVIATIONS

AC/H	Air Changes Per Hour
ALPHA	External Surface Absorption Coefficient
AR	Alkali Resistant
ASHRAE	American Society of Heating, Refrigerating and Air-Conditioning Engineers
BEPS	Building Energy Performance Simulation
BESTEST	Building Energy Simulation Test
BFRP	Basalt Fibre Reinforced Polymers
CFRP	Carbon Fibre Reinforced Polymer
CIBSE	The Chartered Institution of Building Services Engineers
COP	Coefficient of Performance
DAS	Design Authoring Software
DBT	Dry Bulb Temperature
DDH	Discomfort Degree-Hours
DH	Discomfort Hours
DHW	Domestic Hot Water
DOE	Department of Energy
EMISS	External Surface Emissivity
EPS	Expanded Polystyrene
ETICS	External Thermal Insulation Composite Systems
EUI	Energy Use Index
FC	Foamed Concrete
FCU	Fan Coil Unit
FEM	Finite Element Method
FRP	Fibre-Reinforced Polymer
GDP	Gross Domestic Product
GCC	Gulf Cooperation Council
GRC	Glass Reinforced Concrete
HPC	High Performance Concrete
HSO	External Surface Heat Transfer Coefficient
HVAC	Heating, Ventilation, and Air Conditioning
IAQ	Indoor Air Quality
IES-VE	Integrated Environmental Solutions Virtual Environment
IEQ	Indoor Environment Quality
IWPP	Independent Water and Power Project

KACST	King Abdullah City of Science and Technology
KAPSARC	King Abdullah Petroleum Studies and Research Centre
LCA	Life Cycle Assessment
LHS	Latent Heat Storage
Low-E	Low-Emissivity
MDDH	Mean Discomfort Degree-Hours
MMC	Modern Method of Construction
NBSLD	National Bureau of Standards Load Determination
OSM	Offsite Manufacturing
PCMs	Phase Change Materials
PCI	Precast Concrete Institute
PDH	Percentage of Discomfort Hours
PEG600	Polyethylene Glycol
PEWPS	Prefabricated Enclosure Wall Panel Systems
PF	Phenolic Foam
PMV	Predicted Mean Vote
PPB	Prefabricated Public Buildings
PPD	Predicted Percentage Dissatisfied
PUR	Polyurethane
PCSPs	Precast Concrete Sandwich Panels
RAD	Incident Solar Radiation
RCJY	The Royal Commission for Jubail and Yanbu
RH	Relative Humidity
RLONG	The Longwave Loss
SABIC	Saudi Basic Industries Corporation
SBC	Saudi Building Code
SASO	Saudi Arabian Standards Organization
SET	Standard Effective Temperature
SHGC	Solar Heat Gain Coefficient
SIP	Structural Insulated Panels
SFRSCC	Steel Fibre Reinforced Self-Compacting Concrete
TDRY	External Dry Bulb Temperature
TRC	Textile Reinforced Concrete
UHPC	Ultra High-Performance Concrete
UNESCWA	United Nations Economic and Social Commission for Western Asia
VIPs	Vacuum Insulation Panels

WWR	Window-to-Wall Ratio
XPS	Extruded Polystyrene

LIST OF NOMENCLATURE

A	Area (m^2)
c	Specific Heat Capacity (Wh/kg.K)
G	Global Irradiance (W/m^2)
k_c	Concrete Thermal Conductivity (W/m.K)
k_i	Insulation Thermal Conductivity (W/m.K)
Ki	Internal Surface Conductance (W/m^2K)
Ko	External Surface Conductance (W/m^2K)
qa	Total Admittance (W/K)
Qs	Solar Heat Gain Rate (W)
R_{se}	External Surface Resistances (m^2K/W)
R_{si}	Internal Surface Resistances (m^2K/W)
sQ	Swing In Heat Flow Rate (W/m^2)
T	Transmission of Glass at Different Angles (ratio)
t_c	Thickness of the Concrete Layer (m)
t_i	Thickness of the Insulation Layer (m)
Y	Admittance (W/m^2K)

α	Absorptance, or Thermal Diffusivity (m^2/s)
α	Absorptivity of Glass (ratio)
κ	Conductivity Correction Factor (ratio)
λ	Thermal Conductivity (W/m.K)
μ	Decrement Factor (ratio)
ρ	Density (kg/m^3)
ρ	Reflectance (ratio)
τ	Transmittance (ratio)
θ	Solar Gain Factor (ratio)
ω	Angular Velocity (rad/s)

CHAPTER ONE – INTRODUCTION TO THE RESEARCH

1.1 INTRODUCTION

This chapter marks the start-up phase of the research, encompassing the research outlines, aims and objectives, research goals, and scientific questions that target thermal performance in prefabricated buildings. It also encapsulates research achievements and outlines of the thesis chapters.

Central to this thesis is an in-depth examination of the Saudi construction industry and real estate achievements, with a spotlight on the challenges and triumphs that characterise these sectors. A pivotal shift of focus to prefabricated housing allows for dissecting various facets such as construction innovation, thermal performance, and energy efficiency, particularly in regions with hot and humid climates.

This chapter offers an extensive country profile, presenting an overview of Saudi Arabia’s geographical, demographic, and economic landscape, along with a detailed exploration of construction materials used in residential buildings within the Kingdom. This serves as a foundational basis to delve into the multifaceted dimensions of prefabricated housing in Saudi Arabia, exploring its potential and implications within the distinctive context of the country’s construction and real estate sectors.

1.2 COUNTRY PROFILE: BACKGROUND OF SAUDI ARABIA

This section demonstrates statistical knowledge of Saudi Arabia.

1.2.1 GEOGRAPHICAL, CLIMATIC, DEMOGRAPHIC, AND CULTURAL BACKGROUND

The Kingdom of Saudi Arabia is a nation in development and holds the distinction of being the largest country on the Arabian Peninsula, covering a territory of approximately 2,250,000 square kilometres (868,730 square miles). Strategically situated in Southwest Asia, it is bordered by the Red Sea to the west, and to the east by the Arabian Gulf, the United Arab Emirates, and Qatar. The country shares its northern borders with Kuwait, Iraq, and Jordan, and to the south, it is neighboured by Yemen and Oman. Riyadh is the capital city, with other major cities including Jeddah, Makkah, and the Dhahran region, which encompasses Dammam and Khobar (General Authority for Statistics, 2024).

Saudi Arabia experiences a diverse climate owing to its varied topography and the influence of tropical high altitude. Generally, the Kingdom endures a continental climate, marked by hot summers and cold, rainy winters. The western and southwestern highlands experience temperate conditions, while the central regions are subjected to hot, dry summers and cold, dry winters. Additionally, coastal regions are characterised by high humidity mixed with elevated temperatures (National Center For Meteorology, 2020).

According to a study conducted by the Gulf Forum for Climate Outlook and Future Forecasting, surface temperatures are likely to be warmer than average over most of the Arabian Peninsula, except for the southern part. Temperatures in the northern and central parts of Saudi Arabia, Kuwait, Qatar, Bahrain, the United Arab Emirates, and Oman are expected to be above average, while temperatures in the southern parts of Saudi Arabia, western Oman, and most of Yemen are expected to be below normal (see Figure 1.1).

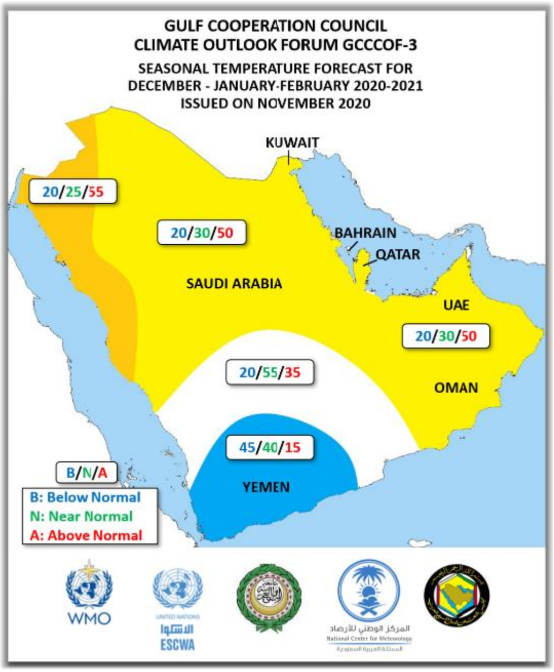

Figure 1.1: Seasonal Temperature Forecast over Arab Gulf Countries. Source: National Center For Meteorology (2020).

Moreover, as the largest Arab state in Western Asia, Saudi Arabia has witnessed rapid population growth, with an estimated total of 32,175,224 inhabitants and a real GDP growth rate of 2.8% (General Authority for Statistics, 2024).

Saudi Arabia's rich history is shaped by its Islamic heritage, its role as an ancient trading centre, and traditional Bedouin customs. Despite modernisation, the country has maintained its unique traditions and customs, adapting them to contemporary times. Its unique geographical location has established it as an international trade hub and a crossroads of cultures, acting as a bridge for cultural communication. Additionally, Saudi Arabia is the cradle of Arabism and Islam, home to the Two Holy Mosques, and Arabic is the official language, being the language of the Holy Quran. The country has achieved significant progress in literacy, with adult literacy reaching 95% in 2015, up from 71% in 1992(Nielsen, 2019, Saudi Arabian Cultural Mission, 2020). Moreover, in terms of labour dynamics, the second quarter of 2024 saw a decrease in the unemployment rate in Saudi Arabia to 7.1% (General Authority for Statistics, 2024).

Besides, in recent years, Saudi Arabia has undertaken numerous initiatives to preserve and promote its cultural heritage amidst modernisations. The Ministry of Culture's 2023 report, titled "Sustainability in the Cultural Sector," provides a comprehensive overview of the Kingdom's cultural landscape, highlighting efforts to integrate traditional arts and customs into contemporary society (NEWS, 2024).

1.2.2 ECONOMIC LANDSCAPE AND RESOURCE WEALTH OF SAUDI ARABIA

Saudi Arabia holds a significant position on the global stage as one of the leading oil producers, possessing approximately 17% of the world's proven petroleum reserves. This substantial reserve base underscores the Kingdom's pivotal role in the global energy market. Concurrently, there is a marked ascension in the Kingdom’s domestic market, which is characterised by its resilience and robustness, thus enhancing the consumer capacities and spending power of its inhabitants (Bulletin, 2024).

Furthermore, the strategic geographical location of Saudi Arabia has historically rendered the Kingdom a crucial axis in international trade. This advantageous position facilitates access to extensive export markets across Europe, Asia, and Africa, and acts as a central hub for fostering trade relations among major global economies, including India, China, and Europe. A deeper exploration of Saudi Arabia's economic fabric uncovers a legacy rooted in open philosophies, free-market principles, and private enterprise paradigms. The recent promulgation of the Foreign Investment Law exemplifies the Kingdom's economic adaptability and progressive stance, permitting full foreign ownership of businesses and real estate. The narrative of the Kingdom is one of enduring political and economic stability, complemented by its cutting-edge, world-class infrastructure (Unified National Platform, 2019).

Saudi Arabia is bestowed with a diverse array of natural resources and minerals, inclusive of industrial raw materials such as bauxite, limestone, gypsum, phosphate, and iron ore. The economic diversification of the Kingdom is manifested through its extensive spectrum of petrochemical and downstream industries, which span a variety of domains including, but not limited to, natural gas extraction and distribution, water desalination, electrical power generation, information technology, infrastructure development, industrial machinery, mining, and tourism. Additionally, the Kingdom's geomorphological features are underscored by the vastness of the Empty Quarter, the world's largest continuous sand desert, which houses a multitude of natural resources.

The monetary landscape of Saudi Arabia is marked by a stable currency and negligible foreign exchange fluctuations, thereby facilitating companies to repatriate their profits in full. The Kingdom is amongst a select few nations globally that allow businesses the fiscal leeway to carry forward losses indefinitely, thereby strategically reducing their tax obligations until profitability is achieved.

The landmark discovery of oil undeniably constituted a turning point in Saudi Arabia's economic history. The commencement of industrial oil extraction in March 1938, at a depth of 1,440 metres in the Dammam oilfield, marked a transformative epoch (OPEC, 2019). The Kingdom has outlined ambitious investment plans, allocating a substantial $200 billion across diverse sectors such as oil, gas, electricity, desalination, and petrochemicals. The oil and gas industries collectively contribute to nearly half of the country's GDP and account for 70% of export earnings. Forecasts by international oil conglomerates anticipate a considerable influx of investment, estimated at $100 billion, in natural gas production over the forthcoming two decades. The abundant wealth derived from oil has precipitated a phase of rapid urbanisation and industrialisation within the Kingdom. In 2019, the estimated value of petroleum exports rose to an impressive $202,370 million, with marketed production of natural gas accounting for 117,000 million cubic metres (ASB, 2020). Figure 1.2 presents a visual depiction of the total petroleum export values of OPEC members.

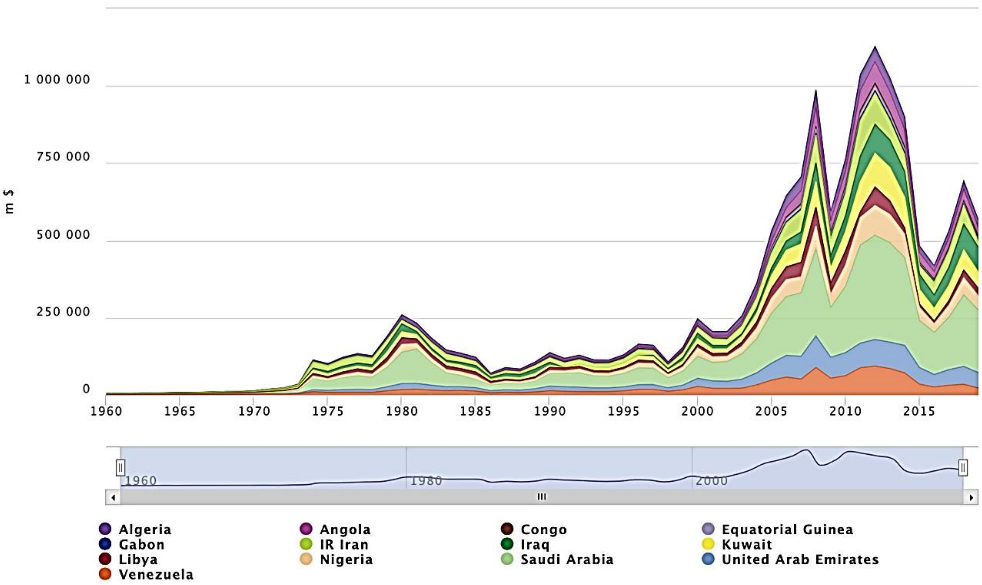

Figure 1.2: Values of petroleum exports by OPEC members (in millions of USD). Source: OPEC (2019).

1.2.3 CONSTRUCTION MATERIALS IN SAUDI ARABIA

Saudi Arabia is richly endowed with a plethora of natural resources, facilitating the production of a variety of high-quality materials. These include, but are not limited to, diverse types of glass, composite materials, ceramics, gypsum, reinforced steel, granite panels, bricks, marble, tiles, concrete, and cement (Lasker, 2016). The construction sector in the country makes extensive utilisation of such materials, a fact underscored by the existence of approximately 533 manufacturing facilities in 2004, as per the data garnered from the industrial census (Table 1.1).

Table 1.1. Enumeration of factories and labour force by section of construction materials (KACST, 2010; referenced in Lasker, 2016).

Description	Factory (No.)	Labor Force (People)	Investment Value (Million $)
Mosaic and pavement tiles	59	3350	521.13
Stones, marbles and granite	90	7202	1106.51
Cement	9	7666	14258.45
Gypsum products manufacturing	12	1058	431.74
Precast concrete panels, posts etc.	67	6860	1417.62
Fiberglass, Rockwall and glass	63	5322	1780.2
Clay, sand & cement bricks, and curbs	233	11103	3069.73
Total	**533**	**42561**	**22585.38**

The cement industry, within the broader construction materials sector in Saudi Arabia, holds a pivotal role. There are seven companies actively engaged in the production of Portland cement, with the annual yield reaching approximately 21.5 million tonnes. In addition to this, several companies specialise in the production of crushed clinker and white cement, with the cumulative annual production capacity for these materials approximating 370 thousand tonnes.

The major cement producers in Saudi Arabia include Saudi Cement Company, Southern Province Cement Company, Yamama Saudi Cement Company, Qassim Cement Company, Yanbu Cement Company, and Arabian Cement Company. These companies significantly contribute to the industry's output. Overall, Saudi Arabia's cement and construction materials industries are characterised by substantial production capacities and a diverse array of companies driving the sector's growth and development. In 2023, the Saudi Cement Company exported 1.5 million tonnes of cement and 1.86 million tonnes of clinker, marking increases of 36% and 81%, respectively, from the previous year (Figure 1.3) (Cement, 2023).

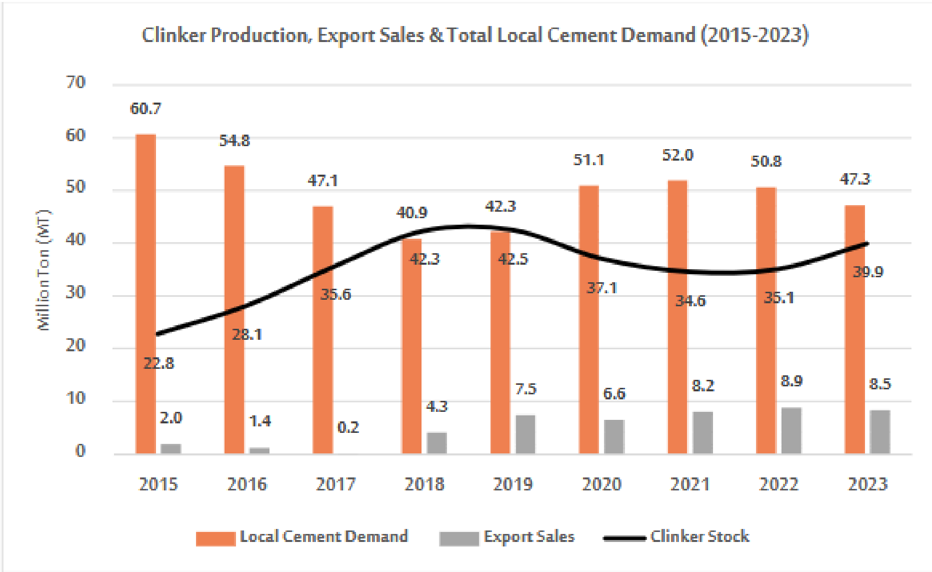

Figure 1.3: Clinker production, export sales, and total local cement demand (2015–2023). Source: Cement (2023).

Furthermore, the cement industry in Saudi Arabia plays a pivotal role within the broader construction materials sector. As of 2023, the Kingdom's cement production capacity is approximately 85 million tonnes per year, with 17 companies operating 22 active cement plants. In 2022, total cement production was 52.6 million tonnes, indicating a capacity utilisation rate of just over 60% (Jagdeep Verma, 2023)

1.2.4 MATERIALS FOR EXTERNAL WALLS IN SAUDI RESIDENTIAL BUILDINGS

Almujahid and Kaneesamkandi (2013) conducted experimental research on a custom-built room featuring a variety of external walls, mirroring those employed in Saudi Arabia. Within this investigation, a hybrid exterior wall structure was examined. The study revealed that cement-based materials are predominantly used in the construction of structures, particularly residences, with hollow building blocks being the most prevalent material for wall construction. These cement blocks are characterised by a thickness of 20 cm and a surface area of 60 x 20 cm².

In a detailed examination of the major cooling requirements for the building envelope in a typical Saudi Arabian detached villa dwelling, Alayed et al. (2021) segmented the envelope's construction into three critical components: insulated concrete blocks, the mortar connections between these blocks, and an uninsulated reinforced concrete frame. Consequently, exterior walls in such contexts typically comprise outside cement plaster, hollow brick, and inside cement plaster.

Further contributing to the body of knowledge on external wall materials, Al-Ghamdi and Al-Feridah (2011) incorporated brick, concrete blocks, and plaster for the exterior wall in a modelling experiment of a typical home in Dhahran, Saudi Arabia. Alaidroos and Krarti (2015b) employed a baseline energy model for a detached single-family house to develop energy-efficient design solutions for villas in Saudi Arabia. The model's specifications for wall construction materials were based on the findings of research conducted by King Abdullah City of Science and Technology (KACST), examining a newly constructed building at KACST. The model detailed the wall's construction materials as 20 mm plaster on the outside, 200 mm hollow concrete blocks, and 20 mm plaster on the inside.

From the foregoing, it is evident that the fundamental approach to external wall construction in Saudi Arabia has remained largely consistent over the past decade. The reviewed literature corroborates the notion that the external wall of a typical Saudi residence is structured with three primary layers: plaster on the outside, hollow brick in the middle, and plaster on the inside.

1.2.5 STANDARD INSULATION MATERIALS IN SAUDI ARABIA.

Following the guidelines set by the Saudi Electric Company, several insulation materials are typically employed in the Kingdom of Saudi Arabia:

1. **Foam Insulation:** Derived from oil-based polyurethane and polyisocyanurate, it is primarily used for wall insulation due to its water impermeability.
2. **Polystyrene:** Natural expanded and extruded forms are used for ceilings and walls, offering low water absorption and heat conductivity.
3. **Low-Conductivity Fibreglass:** Applied for insulating air conditioning ducts, its conductivity decreases with increased fibre density.
4. **Mineral Fibre:** Known for poor thermal conductivity, this synthetic material is produced by melting minerals.

Table 1.2: Thermal insulation materials in line with the requirements of the Saudi Building Code (601–602), released in 2021. Source: SBC (2021).

System	Material	Name	Density (kg/m^3)	Thermal conductivity (w/m·k)
Thermal insulation	Polystyrene	Polystyrene rigid foam	48-29	0.025-0.04
		Expanded polystyrene	12	0.046
			15	0.04
			18	0.038
			22	0.036
			29	0.034
			35	0.03
			42	0.028
		Extruded polystyrene	20	0.031
			30	0.029
			35	0.027
			42	0.026
			48	0.025
	Polyurethane	Polyurethane foam	14	0.054
			28	0.03
			30	0.028
			32	0.025
		Polyurethane foam board	28	0.032
			30	0.03
			32	0.028
			35	0.021
		Polyurethane, gas filled, rigid new	34-30	0.02-0.027
Multi-purpose	Cork	Cork board	160	0.04
		Cork board with asphalt or bitumen	240	0.055
			640	0.145
		Cork board with rubber	480	0.060

1.2.6 THERMAL INSULATION EFFICACY IN SAUDI RESIDENTIAL CONSTRUCTION

The application of insulation materials significantly contributes to the regulation of thermal properties within a building by minimising heat transmission loss. This results in the maintenance of stable internal temperatures, offering a shield against the severe heat of Saudi Arabian summers and the cooler winter nights, while also protecting against moisture. The insulation material's efficiency lies in its intrinsic properties that inhibit the transfer of thermal energy, thereby creating a barrier to external temperature fluctuations (Lasker, 2016).

The installation of insulation can be on either the exterior or interior sides of the façade. Ensuring a progression from the room side to the outside, materials used in constructing the wall should facilitate high diffusion permeability, enabling the free passage of moisture. It is essential to prevent thermal bridges at the junctures between floors and walls. Although the placement of thermal insulation primarily affects its effectiveness, external insulation tends to result in fewer thermal bridges and is more efficient in shielding against temperature variations. Internal thermal storage masses, when utilised, can significantly enhance indoor conditions during varying seasonal temperatures. For rooms with internal insulation and without thermal storage mass, there is the advantage of quick heating during the colder seasons (Hausladen et al., 2006).

Beyond an insulation thickness of 150 to 250 mm, the financial prudence of further investment in insulation becomes questionable. This is particularly evident given the juxtaposition of elevated insulation costs with relatively economical energy prices, resulting in a commonly adopted maximum insulation thickness of approximately 30 mm. This dichotomy presents a complex scenario for energy managers, complicating the projection of future energy expenditures despite having insights into energy percentages and the financial implications of insulation (El Bakkush et al., 2015)

Several studies have investigated the optimal thickness and placement of thermal insulation in Saudi residences. Alaidroos and Krarti (2015) conducted a study to assess the impact of different roof insulation and wall thicknesses (10cm, 5cm, and 7.5cm) on Riyadh's climate, in relation to heating and cooling loads. The National Bureau of Standards Load Determination (NBSLD) performed the energy simulations. The analysis indicated that satisfactory energy performance for heating and cooling loads was achieved with the application of 5 to 10 centimetres of thermal insulation to external walls. Moreover, insulation within the internal layer of the wall proved more effective in air-conditioned environments than insulation on the exterior layer (Alaidroos and Krarti, 2015).

Additionally, the research considered various construction materials, including prefabricated façades, sand-lime bricks, concrete blocks, and clay bricks. Clay bricks were found to be superior in terms of operational expenses, capital costs, and suitability for typical Saudi Arabian residential constructions. A standard Saudi residential building consumes around 185.4 kWh/m², with elevated consumption attributed to the absence of thermal insulation in roofs and external walls and the use of single-glazed openings.

1.2.7 THERMAL PERFORMANCE OF PRECAST CONCRETE WALLS IN SAUDI HOUSING

In countries with extremely hot climates, there is a notable scarcity of studies concerning the thermal insulation of exterior precast concrete system panels, as noted by Ang Soon Ern et al. (2017). However, Saudi Arabia has witnessed a significant proliferation of precast concrete wall systems in numerous housing projects. Precast concrete shares many characteristics with traditional concrete blocks, with the primary distinction being the higher concrete density found in precast concrete wall panels, which are typically employed as structural walls.

Ahmad et al. (2014) assessed the thermal performance of two exterior walls constructed using reinforced precast concrete panels, employing in situ measurements. The evaluation involved monitoring the thermal performance throughout the summer, during which three datasets were collected and analysed to determine the in situ thermal performance characteristics. Notably, due to the substantial size of the reinforced precast concrete wall panels, the researchers encountered limitations when attempting to ascertain the in situ thermal resistance values using the guarded hot plate method—a technique available in the laboratories of the King Fahd University of Petroleum & Minerals, specifically designed for surface-to-surface measurements. In contrast, conventional hollow concrete blocks have undergone laboratory testing and are extensively documented in relevant literature. Given the inherent variations in thickness between concrete blocks and reinforced precast concrete panels, a more meaningful comparison can be made by assessing their equivalent thermal conductivity rather than relying solely on their actual thermal conductivity values.

Figure 1.4 offers an illustrative example of a precast wall panel sourced from the Saudi local construction market. The figure highlights key attributes, including wall thickness, constituent materials, and thermal properties.

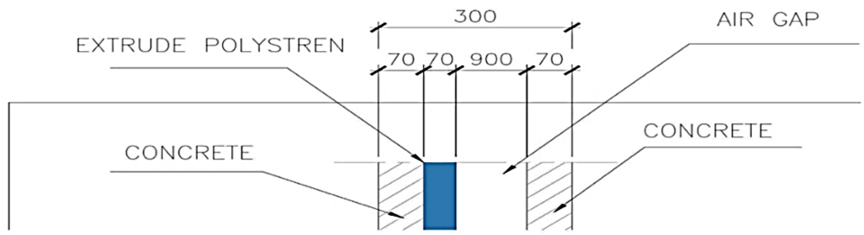

Thickness (m)	Material	K value (w/m.c)	R-value (m2.c/w)	R - value (ft2hf/btu)
0.07	Extrude Polystren	0.03	2.333333333	13.0298
0.09	Air gap	0.25634	0.3510962	1.960591402
0.14	Concrete	1.75	0.08	0.446736
Internal transtition resistance			0.123	0.6868566
External transtition resistance			0.055	0.307131
Total resisteance (R - VALUE)			**2.942429534**	**16.431115**
U - VALUE =1/ 2.942429534= .33986 W/M2.C				
U - VALUE =1/16.86680196= .06086 btu/ ft2hf				

Figure 1.4: Commonly used 30 cm precast external wall panel details in Saudi precast housing construction industries. Source: AL-SHAYEB (2021).

1.3 RESEARCH PROBLEM

Climate change is an indisputable fact, manifesting globally through escalating natural disasters and sustained increases in global temperatures. Notably, the persistent rise in the Earth's temperature is primarily driven by global warming. Despite numerous strategies deployed worldwide to mitigate this issue, the building and construction sectors accounted for 30% of total global energy consumption in 2015, with the residential sector consuming approximately 22% of this energy (Abergel et al., 2017). Consequently, achieving the target of limiting the global temperature increase to 2 °C by 2050 necessitates a 77% reduction in total carbon dioxide emissions in the building and construction sectors (Thompson, 2014).

In Saudi Arabia, the predominant harsh, hot, and dry climate conditions affect various aspects of daily life, including clothing, transportation, business operations, and housing. The nation experiences extreme heat during the summer, with temperatures exceeding 50 °C in some areas. Furthermore, Saudi Arabia's per capita energy consumption is nearly triple the global average, with the residential sector emerging as the leading contributor to national energy consumption, accounting for nearly 50% of the total annually (Ahmed et al., 2019). While countries such as the UK, Canada, Germany, Japan, Russia, and China have achieved significant reductions in CO_2

emissions, developing nations continue to experience increases, particularly in the residential and construction sectors (Nejat et al., 2015). Disturbingly, the Saudi residential construction market stands as one of the most unsustainable globally, evidenced by a nearly twofold increase in energy consumption from 2005 to 2016 (KAPSARC, 2020). This trend, driven by the demands of a growing population, forecasts further growth in the sector's energy consumption in the coming decade. Figure 1.5 illustrates the annual consumption by sector in Saudi Arabia.

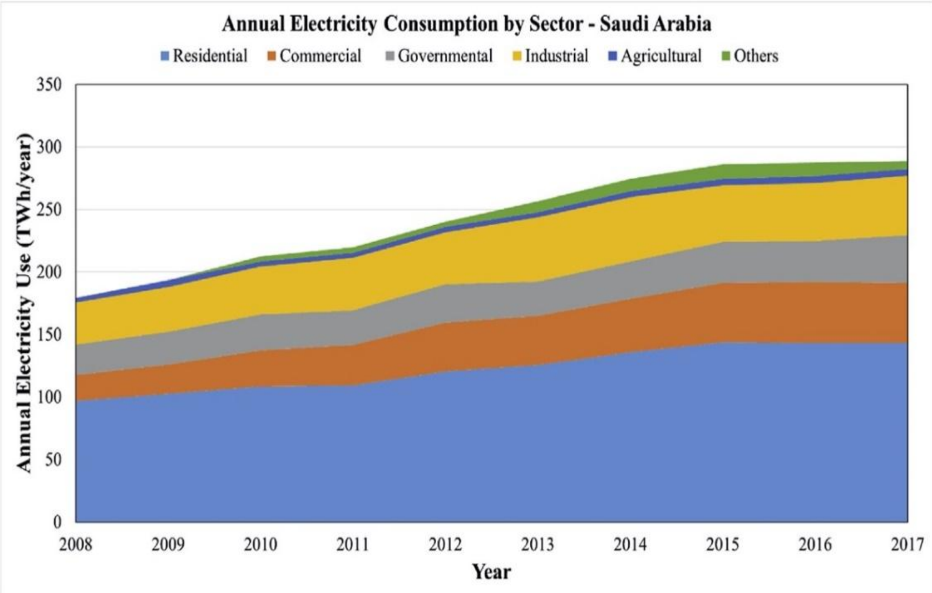

Figure 1.5: Annual electricity consumption by sector in Saudi Arabia. Source: SEC (2019).

According to Alrashed and Asif (2012), sustainability remains a low priority in Saudi Arabia's construction industry. Despite the harsh climate, approximately 70% of buildings are not thermally insulated, relying predominantly on conventional construction materials universally deemed standard by the industry (Mujeebu and Alshamrani, 2016).

Recently, there has been a growing interest in advancing prefabrication in Saudi Arabia's construction sector, focusing on state-of-the-art sandwich panels as prefabricated construction components. However, the lack of past regulations and the absence of standardised insulation layers within these components hinder sustainable construction practices. These gaps foster inconsistency and reliance on international building codes, such as the ACI standards for concrete material usage, predominantly in the private sector.

In late 2019, the government initiated a pivotal change by introducing the Saudi Building Code (SBC) (Saudi Building Code National Committee, 2019). Regrettably, the SBC does not specifically address the design and insulation of prefabricated components, a shortcoming that negatively influences the reliability and continued adoption of prefabricated construction. This oversight leads to hesitancy among potential building owners, despite the apparent advantages of prefabricated construction, such as improved thermal comfort and energy efficiency.

This research aims to tackle a tangible issue: the burgeoning demand for affordable, thermally regulated housing. By analysing the energy and thermal performance data of a fully prefabricated house, the study seeks to unlock the potential of prefabrication in optimally leveraging unused land while upholding modern housing attributes. Additionally, by utilising DesignBuilder software, the study will scrutinise the thermal efficiency of a representative prefabricated house situated in the Eastern Province region, specifically in Jubail Industrial City. The simulation will determine whether such houses can withstand Saudi Arabia's extreme heat, delineating the distinctions that justify this research. While in-situ construction remains prevalent, the research underscores the urgent need to explore the viability and benefits of prefabrication in the housing sector, aiming to devise strategies that foster energy conservation and indoor thermal comfort.

1.4 AIMS AND OBJECTIVES

The principal goal of this research is to evaluate the thermal performance of prefabricated houses in Saudi Arabia and provide optimal solutions for enhancing the thermal performance of their prefabricated envelope systems. The research objectives are as follows:

- To explore methods for reducing energy consumption and enhancing thermal performance in prefabricated houses.
- To investigate the thermal performance of prefabricated houses in Saudi Arabia.

- To assess the overheating potential of prefabricated houses during the summer months.
- To propose improvements to prefabricated houses, considering both thermal performance and energy conservation.

1.5 RESEARCH QUESTIONS

1. What are the indoor thermal conditions of prefabricated buildings in the extremely hot climate of Saudi Arabia?
2. To what extent do prefabricated houses maintain conditions conducive to thermal comfort throughout the year?
3. How effectively can the optimisation of prefabricated building components in Saudi Arabia deliver optimal thermal performance over the course of a year?

1.6 RESEARCH SIGNIFICANCE AND JUSTIFICATION

The trajectory of prefabricated buildings is firmly rooted in changes driven by economic, population, and socio-political factors. A pivotal moment for this construction method occurred during World War II, when there was an acute need to quickly provide housing in war-affected regions (El-Abidi and Ghazali, 2015). While the United States, Japan, and parts of Europe relied heavily on this building approach in the post-war period, newly independent nations formerly under European rule also embraced this technology to expedite urban and economic development (El-Abidi and Ghazali, 2015).

However, the 1960s saw a decline in the reputation of prefabricated buildings due to poor workmanship and design errors in earlier constructions. These setbacks reinforced a preference for traditional construction standards, a trend that continues today. The growing global population necessitates affordable and sustainable construction solutions, with prefabricated buildings serving as a mainstay for several decades. Their adaptability to diverse terrains makes them a valuable resource, particularly in regions with harsh weather conditions.

In the Kingdom of Saudi Arabia, active ventilation is the primary strategy employed to discharge undesired stored heat indoors (Alaidroos and Krarti, 2016). Consequently, a more innovative approach is required to provide occupants with maximum thermal comfort in such harsh climatic conditions while reducing the absolute reliance on HVAC systems. Moreover, a study conducted by Alrashed and Asif (2014) demonstrates that, in the Eastern Province, the energy use index (EUI) for a typical apartment is 196.5 kWh/m²/year, whereas traditional houses consume 156.5 kWh/m²/year. Furthermore, a survey conducted by Al Surf and Mostafa (2017) revealed that 92% of the general public reported increasing awareness of sustainability, which is a promising indicator for sustainable development. Figure 1.6 illustrates annual electricity consumption for residential buildings by region.

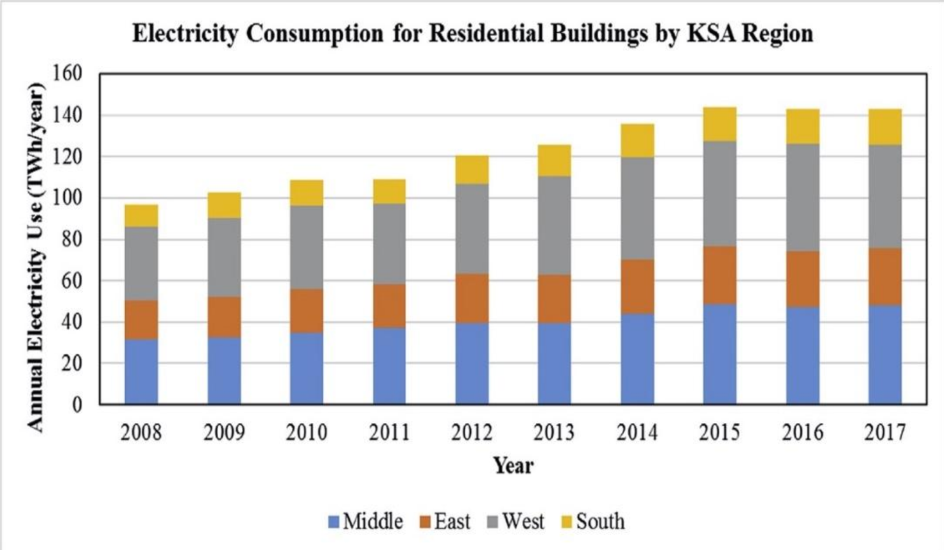

Figure 1.6: Annual electricity consumption for residential buildings by region in Saudi Arabia. Source :Krarti et al. (2020).

Asif et al. (2017) conducted a life cycle assessment, revealing that 91% of the materials used in Saudi houses account for approximately 43.4% of the total embodied energy, adversely affecting the environment. Despite this, numerous studies have advocated for sustainability in the Saudi construction market, urging engineers and architects to adopt sustainable practices during the preliminary phases of design.

In alignment with Saudi Vision 2030's emphasis on sustainable structure, there is an urgent need for collaboration between design experts and advanced prefabrication technologies within the construction industry. Conducting a rigorous analysis of the energy and thermal performance of existing prefabricated homes in Saudi Arabia is essential to this endeavour.

1.7 CONTRIBUTION TO KNOWLEDGE

This research makes substantial contributions to understanding the thermal performance of prefabricated buildings in extremely hot climates, particularly in Saudi Arabia. By addressing the thermal challenges associated with naturally ventilated structures, it identifies key factors influencing indoor thermal conditions and proposes enhancements. The findings emphasise the importance of optimising thermal insulation and ventilation strategies while considering the effects of surrounding structures. These insights provide valuable guidance for improving thermal comfort in prefabricated construction.

A significant contribution of this research lies in its detailed analysis of the thermal comfort range achievable by precast systems. The study underscores the critical role of heat balance within the building envelope in maintaining comfort across different seasons. It establishes that factors such as thickness, material density, and the sequencing of layers in precast concrete wall panels are crucial in reducing discomfort hours. By introducing an innovative design for precast sandwich wall panels—incorporating high thermal mass materials internally and lightweight materials externally—the research offers a transformative solution for enhancing thermal performance.

The research also advances industry-level understanding by evaluating the capacity of Saudi Arabia's prefabricated building sector to implement optimally insulated systems. A noteworthy finding is the comparable thermal performance of air cavities and polyurethane foam in precast concrete sandwich panels (PCSPs). Additionally, the study emphasises the importance of strategically selecting and arranging thermal insulation materials. It further demonstrates how increasing the window-to-wall ratio (WWR) and employing shading devices can significantly improve indoor thermal conditions and mitigate overheating risks.

One of the most innovative contributions of this research is the integration of phase change materials (PCMs) within PCSP designs. The study demonstrates that PCMs with a melting point of 23°C, strategically positioned internally, can significantly enhance thermal regulation. When combined with high thermal mass concrete, these materials achieve notable reductions in cooling loads (up to 48%), heating loads (up to

99.95%), and energy consumption by air conditioning systems (up to 51.6%). These findings represent a significant step forward in promoting sustainable building practices.

Importantly, the research culminates in the development of an optimised precast system specifically designed for the extreme hot climates of Saudi Arabia. By focusing on reducing discomfort hours and improving thermal performance through innovative material selection and system design, the study delivers a tangible design product. This integrated approach bridges theoretical advancements with practical applications, contributing to both academic discourse and industry practices in sustainable construction.

1.8 STRUCTURE OF THE THESIS

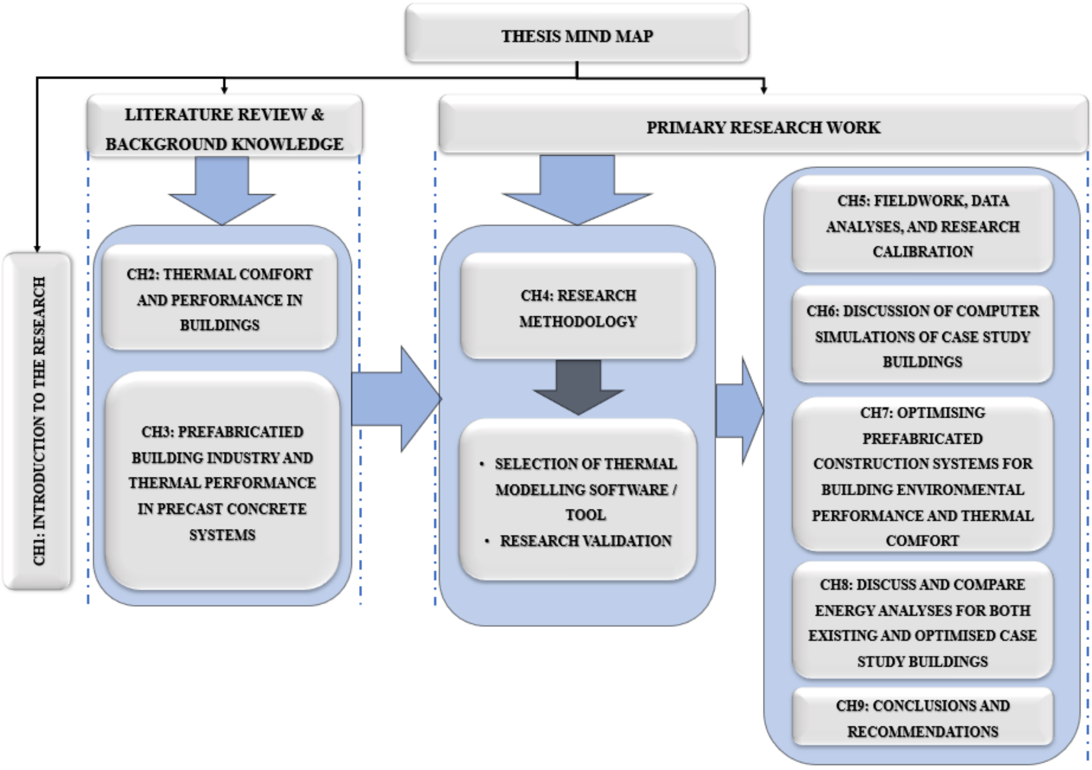

Figure 1.7: Illustration of thesis outline.

The thesis is structured into nine chapters, as shown in Figure 1.7, and described under the following headings:

Chapter 1:

Introduction to the thesis, including background information on Saudi Arabia and foundational knowledge.

Chapter 2:

A review of methods for estimating thermal comfort in buildings. Additionally, design considerations affecting thermal performance in hot climates are reviewed.

Chapter 3:

This chapter examines prefabrication in buildings, focusing on their history and the use of precast concrete panels, as well as their architectural considerations within the construction market. It also explores the relationship between current developments and prospects of prefabricated precast housing in Saudi Arabia.

Furthermore, the chapter reviews precast wall panels, specifically sandwich panels, with an emphasis on the thermal properties of the materials used and their thermal mass heat exchange principles. It evaluates the properties of transparent elements and their interaction with precast systems, contributing to a comprehensive understanding of how these components influence building performance.

Chapter 4:

This chapter illustrates the research methodology, discussing the methods used for developing the study. It also examines computer simulation tools and validates the selected simulation tool.

Chapter 5:

Fieldwork data collection and analysis are explained in this chapter. It presents the selected case study houses and their architectural and parametric data. Additionally, calibration for both indoor and outdoor air temperatures is discussed.

Chapter 6:

This chapter focuses on thermal modelling and computer simulations of the case study buildings. It critically analyses the simulation results based on designated thermal measurement levels.

Chapter 7:

Building on the findings from thermal modelling and simulation, this chapter focuses on improving thermal performance and comfort in the studied prefabricated precast houses. The chapter also discusses contributions to advancing prefabricated construction systems and materials to enhance environmental performance and user thermal comfort.

Chapter 8:

This chapter discusses and compares energy analyses for both existing and optimised case study buildings. It comprehensively examines overall energy consumption, including lighting, HVAC, and hot water, as complementary components of energy usage.

Chapter 9:

This chapter concludes the findings from the simulations and data conducted in the research. It revisits each research question posed at the beginning of the thesis and provides recommendations, as well as potential future work and opportunities.

1.9 SUMMARY

This chapter underscored the urgent need to address energy consumption in the building and construction sectors, which are responsible for a substantial portion of global energy usage. Within this context, Saudi Arabia was highlighted, with its residential sector identified as a significant contributor to the nation’s elevated per capita energy consumption. This scenario has drawn the attention and support of the government, resulting in initiatives to improve energy consumption, notably through the Saudi Vision 2030 reform programme. The discussion emphasised the untapped growth potential of the prefabricated building construction industry in Saudi Arabia, where the adoption rate of such innovative solutions remains modest.

Moreover, the chapter explored the distinct benefits of prefabricated housing, particularly in hot and humid climates such as that of Saudi Arabia. These advantages include reduced workplace safety risks, diminished noise pollution, and less disruption to surrounding structures. Despite these substantial benefits, the chapter noted that the adoption of prefabricated houses in such challenging climates remains limited.

A significant portion of the chapter was dedicated to exploring the role of the external envelope system in determining building thermal performance. It highlighted that external façades play a critical role in maintaining indoor comfort and modulating energy demands. The narrative reviewed various studies examining the materials used in building façades, revealing a growing trend towards the use of energy-conserving, recyclable materials in prefabricated houses, which also offer considerable environmental benefits. Within this framework, Saudi Arabia's abundance of natural resources, including oil and high-quality materials, was acknowledged, emphasising the influential role of the cement industry in the construction materials sector.

In conclusion, the chapter emphasised that advancing research and development in the domain of prefabricated building components and systems is pivotal for achieving energy conservation, fostering sustainable construction, and enhancing thermal performance in regions characterised by hot and humid climates, such as Saudi Arabia. By embracing and refining prefabricated solutions, the Saudi Arabian construction industry can significantly contribute to global efforts to reduce carbon emissions and address climate change, with a particular focus on the housing sector.

CHAPTER TWO – THERMAL COMFORT AND PERFORMANCE IN BUILDINGS

2.1 INTRODUCTION

Thermal comfort is defined as "that condition of mind that expresses satisfaction with the thermal environment" (ASHRAE Standard 55-2010). Thermal comfort can be achieved only when the amount of heat produced by metabolism balances the amount of heat lost by the body. It is also essential to consider thermal comfort when evaluating a building's efficiency and potential for energy savings. Consequently, studying the thermal behaviour of buildings is imperative for predicting occupant comfort and identifying a building's energy consumption.

This chapter discusses the variables affecting thermal comfort to aid in determining strategies for predicting thermal comfort, which will be addressed later. The major variables influencing comfort, specifically the measurable factors that impact the body's heat balance, are explained. Additionally, the thermal comfort preferences of individuals living in hot-humid regions are explored. The adaptive comfort model is thoroughly investigated, along with an in-depth analysis of the cooling effects of elevated air movement.

This chapter also outlines design strategies for improving the thermal performance of buildings in hot, humid climates. It identifies key issues inherent to passive design and other proven strategies that enhance indoor thermal comfort, particularly in hot climates, while minimising reliance on mechanical and active ventilation systems.

2.2 MAJOR VARIABLES INFLUENCING THERMAL COMFORT

Numerous debates surround the precise definition of thermal comfort. One definition, proposed by ASHRAE, describes it as a psychological state reflecting an individual's satisfaction with their surrounding thermal conditions (ASHRAE, 2023). Thermal comfort is often inferred through an individual's thermal perceptions, suggesting that a "state of mind" encompasses elements of perception, cognitive processing, and overall mood or disposition. Consequently, comfort is recognised as a subjective psychological condition that can vary due to different circumstances (De Dear, 2011b). Various methods are available for assessing the comfort of an indoor environment, with ISO 7730 (Predicted Mean Vote, PMV) and ASHRAE/55 being the most widely used standards (Wilde, 2023). To conduct such evaluations, several metrics must be identified and incorporated into the calculation model.

Commonly, an assessment model incorporates six crucial parameters: four related to the environment (air temperature, relative humidity, mean radiant temperature, and air velocity) and two pertaining to individual occupants (metabolic rate and clothing insulation values). These factors, which are essential to thermal comfort, can be broadly organised into two primary categories, as outlined below.

2.3 ENVIRONMENTAL FACTORS

ASHRAE Standard 55 is based on the heat balance model of the human body, proposing that thermal sensation is determined solely by four environmental factors (temperature, thermal radiation, humidity, and air velocity) and two personal determinants (activity level and clothing) (De Dear and Brager, 2002). The environmental factors are discussed below.

2.3.1 AIR TEMPERATURE

Air temperature is often regarded as the most significant environmental factor influencing an individual's sense of comfort. It directly impacts the rate of heat transfer between the skin and the surrounding atmosphere. Specifically, when the air temperature equals or exceeds skin temperature, heat loss through both convection and evaporation is reduced and, in some cases, ceases entirely.

2.3.2 RELATIVE HUMIDITY

Relative humidity is a critical environmental factor that significantly influences thermal comfort within a building. Jing et al. (2013) investigated the impact of relative humidity on thermal comfort using an environmental chamber. Their findings indicated that increased humidity can adversely affect an individual's thermal comfort. Furthermore, their study recommended that constraints on relative humidity should be considered to prevent discomfort. Consequently, building codes should specify a humidity limit within the permissible air temperature range to ensure effective indoor environment control. Notably, elevated relative humidity can cause individuals to perceive their surroundings as hotter than the actual temperature. This phenomenon is illustrated in the "de Dear model of thermal sensation votes," which integrates a thermal sensation vote with indoor operative temperature to represent the regression curve across various relative humidity levels (Figure 2.1).

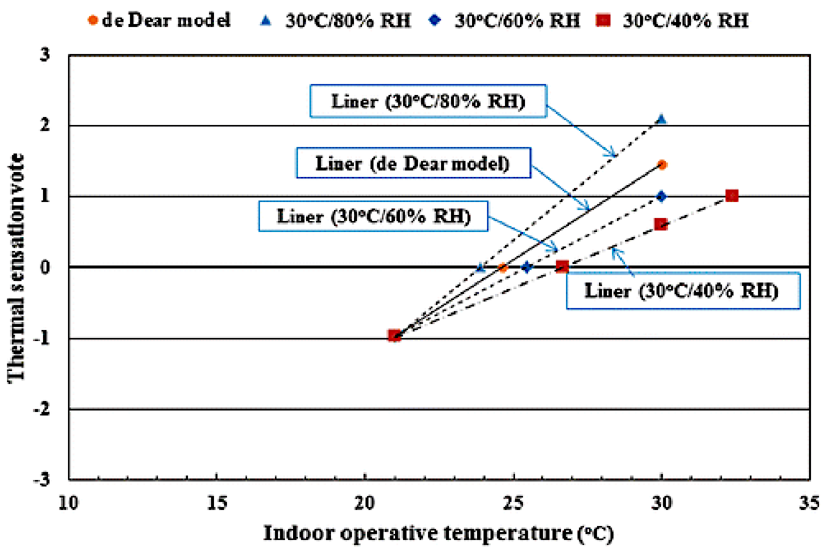

Figure 2.1: Regression curve based on de Dear’s model using different relative humidity levels. Source: Jing et al. (2013).

2.3.3 AIR VELOCITY

The effects of air movement on comfort have been extensively studied across a variety of settings. Air movement significantly influences occupants' thermal sensation and comfort in both ventilated and air-conditioned environments, affecting comfort locally and across the entire body. For the past 60–70 years, thermal comfort experts have investigated the impact of air movement on human comfort (Toftum, 2004). Notably, air movement plays a critical role in heat loss from the body through convection and evaporation, with increased air velocity enhancing heat loss via both mechanisms.

2.3.4 MEAN RADIANT TEMPERATURE

Mean radiant temperature is a critical environmental factor influencing both building performance and the thermal comfort of occupants (Zhao et al., 2024). Although they do not come into direct contact with the human body, objects within a space significantly affect thermal comfort. These objects absorb or emit heat based on their thermal properties and the temperature difference between themselves and the surrounding air. Radiative heat loss from the body occurs when the mean radiant temperature is lower than the body surface temperature. Conversely, when the temperature of nearby surfaces—thus influencing the prevailing radiant temperature—is higher than the body surface temperature, the body gains heat through radiation.

2.4 PERSONAL FACTORS

Personal factors, including activity levels and clothing, are perceived by occupants as key determinants of comfort. Moreover, these factors are controlled by the occupants themselves, rather than by architects or designers. Consequently, standards such as ASHRAE 55 have adopted constant values for these variables to evaluate thermal comfort among occupants.

2.4.1 ACTIVITY

The metabolic rate is arguably the most essential of the six fundamental metrics in the standard heat balance model of human thermal comfort, despite being the most imprecisely estimated in practice (Luo et al., 2018). The rate at which the body produces heat is determined by its activities. The metabolic rate, or the amount of heat or energy produced by the human body, is often expressed in units called "Met." A relaxed, seated individual has a metabolic rate of one (1). Accordingly, activity is measured in metabolic rate units, with one Met unit defined as 58 W/m^2 (356 Btu/hr). Typically, a higher degree of activity requires cooler temperatures to alleviate thermal stress. Metabolic rates corresponding to various activities are detailed in Table 2.1.

Table 2.1: Metabolic rates. Source: Engineering Toolbox (2004), ISO 7730 (1984).

Activity	**Met - Metabolic Rate**	
	W/m^2	**Met Units**
Reclining, Sleeping	46	0.8
Seated relaxed	58	1.0
Standing at rest	70	1.2
Sedentary activity (office, dwelling, school, laboratory)	70	1.2
Car driving	80	1.4
Graphic profession - Book Binder	85	1.5
Standing, light activity (shopping, laboratory, light industry)	93	1.6
Teacher	95	1.6
Walking on the level, 2 km/h	110	1.9
Standing, medium activity (shop assistant, domestic work)	116	2.0
Building industry - Brick laying (Block of 15.3 kg)	125	2.2
Washing dishes standing	145	2.5

2.4.2 CLOTHING

Clothing acts as a regulator for heat exchange between the human body and its surroundings. The unit 'Clo' is used to measure the thermal insulation provided by clothing. On this scale, 1 Clo represents the insulation of typical winter attire, whereas 0.5 Clo corresponds to the lighter insulation of summer clothing. The insulation properties of clothing are measured in 'Clo', with 1 Clo equalling 0.155 $K \cdot m^2/W$. In this context, 0 Clo represents a nude person, while 1 Clo describes the insulation required for an individual wearing a business suit to remain comfortable in a 21°C room with an air movement of 0.1 m/s and humidity below 50%. Table 2.2 lists typical Clo values.

Table 2.2: Clothing insulation values for typical ensembles. Source: ASHRAE (2010). The table has been revised for clarity and enhancement.

Clothing Description	**Garments Included**	***I*cl (Clo)**
Trousers	Trousers, short-sleeve shirt	0.57
	Trousers, long-sleeve shirt	0.61
	#2plus suit jacket	1.04
	#2 plus suit jacket, vest, T-shirt	1.14
	#2 plus long-sleeve sweater, T-shirt	1.20
	#5 plus suit jacket, long underwear bottoms	1.30
Skirts/Dresses	Knee-length skirt, short-sleeve shirt (sandals)	0.54
	Knee-length skirt, long-sleeve shirt, full slip	0.67
	Knee-length skirt, long-sleeve shirt, half-slip, long-sleeve sweater	1.00
	Knee-length skirt, long-sleeve shirt, half-slip, suit jacket	1.20
	Ankle-length skirt, long-sleeve shirt, suit jacket	1.30
Shorts	Walking shorts, short-sleeve shirt	0.36
Overalls/Coveralls	Long-sleeve coveralls, T-shirt	0.72
	Overalls, long-sleeve shirt, T-shirt	0.89
	Insulated overalls, long-sleeve thermal underwear tops and bottoms	1.37
Athletic	Sweatpants and a long-sleeve sweatshirt.	0.74
Sleepwear	Long-sleeve pyjama top, long pyjama trousers, and a short 3/4-length robe (slippers, no socks).	0.96

2.5 ADAPTATION HYPOTHESIS

The adaptive theory suggests that environmental factors and past thermal experiences shape the thermal preferences and expectations of individuals within buildings (De Dear and Brager, 1998). Furthermore, De Dear and Brager (1998) propose that the adaptive theory predicts a preference for higher indoor temperatures among residents of warmer regions compared to those in colder areas. The term "adaptation" can be defined as the gradual diminishing of an organism's reaction in response to repeated environmental stimuli. Accordingly, and as summarised by De Dear and Brager (1998), three distinct types of thermal adaptation can be identified as follows:

2.5.1 BEHAVIORAL ADJUSTMENT

This refers to all modifications an individual might undertake, whether intentionally or automatically, that influence the exchange of heat and mass to maintain the body's thermal balance. These modifications can be further categorised into personal actions, technological measures, and cultural habits (De Dear and Brager, 1998).

2.5.2 PHYSIOLOGICAL

De Dear and Brager (1998) provide a comprehensive explanation of physiological adaptation, defining it as the changes in physiological responses to thermal environmental stimuli that result in a sustained reduction in the strain caused by these conditions. According to the authors, physiological adaptation manifests in two primary forms: genetic adaptation, which evolves over generations, and acclimatisation, which develops within an individual's lifetime.

2.5.3 PSYCHOLOGICAL

Thermal adaptation includes a psychological aspect characterised by an altered perception of and reaction to sensory stimuli. As a result, residents of naturally ventilated structures display a significantly broader acceptance of varied temperatures. This phenomenon can be attributed to a combination of behavioural and psychological adjustments (De Dear and Brager, 1998).

2.6 THERMAL COMFORT ESTIMATION METHODS

Global standards such as ISO 7730 and ASHRAE Standard 55 define comfort zones using Fanger's PMV–PPD method, which is derived from laboratory settings. This method, based on the heat-balance model, is favoured for its inclusion of a comprehensive range of indoor environmental factors, as well as human activity and clothing levels. However, it excludes elements such as climatic conditions, socio-economic factors, expectations, and adaptive psychological and behavioural responses (Yao et al., 2009).

ASHRAE Standard 55 defines the metrics of the thermal environment in relation to an acceptable proportion of satisfied occupants. This facilitates the establishment of a comfort zone, considering distinct levels of humidity, air movement, metabolic rates, and clothing insulation values. Essentially, this zone is defined as a range of operative temperatures that provide conditions deemed thermally comfortable (see Table 2.3) (ASHRAE, 2013).

Note: The patterns from ASHRAE define the thermal comfort zone for PPD < 10% and -0.5 < PMV < 0.5.

Table 2.3: Thermal comfort zone as outlined by ASHRAE. Source: ASHRAE Standard-55 (2013).

Season	Thermal Comfort Zone (°C)	Operative Temperature (°C)	Clothing Insulation (Clo)
Summer	23–26	24.5	0.5 Clo (Light Clothing)
Winter	20–23	22	1.0 Clo (Heavy Clothing)

2.6.1 ANALYTICAL METHOD

The standard further outlines an analytical method whereby users document metrics such as operative temperature, air velocity, humidity levels, metabolic rate, and clothing insulation values. The method then predicts probable thermal sensation, categorising it on a scale ranging from -3 (indicative of feeling cold) to +3 (suggestive of feeling hot). Notably, ASHRAE/ANSI Standard 55 recommends that comfort assessments be conducted using Fanger's PMV/PPD index. Additionally, this method applies to spaces with occupants who maintain average metabolic rates between 1.0 and 2.0 met and who wear clothing with a thermal insulation of 1.5 Clo or less, as identified by ASHRAE (2013). For clarification, the ASHRAE thermal sensation scale is defined as follows:

+3 Hot

+2 Warm

+1 Slightly warm

0 Neutral

–1 Slightly cool

–2 Cool

–3 Cold

Table 2.4: Acceptable thermal environment for general comfort. Source: ASHRAE (2013).

PPD	PMV Range
<10	–0.5 < PMV < +0.5

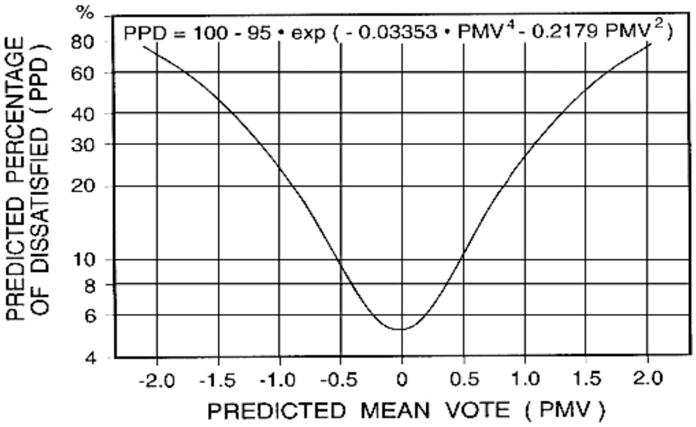

Figure 2.2: Predicted percentage dissatisfied (PPD) as a function of predicted mean vote (PMV). Source: ASHRAE (2013).

For further explanation, the predicted mean vote (PMV) model employs heat balance principles to relate the six main factors affecting thermal comfort to the average vote of individuals on the thermal sensation scale. As illustrated in Figure 2.2, the predicted percentage dissatisfied (PPD) index is linked to the PMV. It is based on the premise that individuals voting +3, +2, –2, or –3 on the thermal sensation scale are dissatisfied, with the assumption that PPD is symmetric around a neutral PMV (ASHRAE, 2013). Additionally, Table 2.4 specifies the recommended ranges for PPD (Predicted Percentage of Dissatisfied) and PMV (Predicted Mean Vote) in common applications. It is important to note that this methodology underpins the graphical comfort zone approach in ASHRAE standards. However, this method is considered robust and requires calculations using the ASHRAE thermal comfort tool.

2.6.2 GRAPHICAL METHOD

This standard adopts a streamlined graphical comfort zone methodology, enabling the determination of suitable comfort zones across various standard applications (Turner, 2011). For a broader range of applications, comfort zones are established using computer software based on a heat balance model. The graphical method is represented on a psychrometric chart, as shown in Figure 2.3. It illustrates the requisite operative temperatures and humidity levels for maintaining thermal comfort during winter (1.0 Clo) and summer (0.5 Clo) seasons. At its core, this technique is grounded in the Predicted Mean Vote (PMV) model.

In this system, participants input specifics such as operative temperature (encompassing both air temperature and mean radiant temperature), air velocity, humidity levels, metabolic rate, and the insulation value of clothing. The system, in turn, estimates their thermal sensation, rated on a scale ranging from -3 (signifying cold) to +3 (suggesting heat). However, despite their simplicity, these methods are acknowledged to have certain limitations in their applicability.

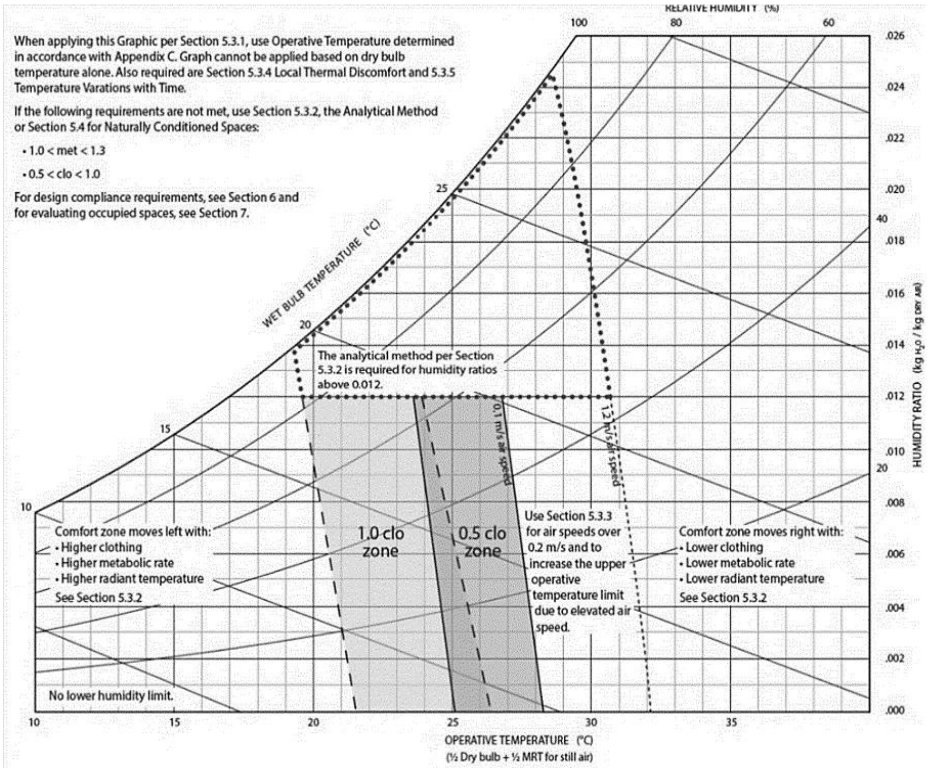

Figure 2.3: The graphical comfort zone method showing the acceptable range of operative temperature and humidity. Source: Figure 5.3.1 in Standard 55-2013.

2.6.3 ELEVATED AIR SPEED METHOD

This methodology is employed to increase the maximum permissible operative temperature and the highest allowable average airspeed, as determined by both the graphical comfort zone method and the analytical comfort zone method, subject to two specific conditions. The first condition stipulates that when occupants can adjust local airspeed, it must not exceed 1.2 m/s, in accordance with the Standard Effective

Temperature (SET) model within the ASHRAE Thermal Comfort Tool. Airspeed control should be either continuous or adjustable in maximum increments of 0.25 m/s at the occupant's position.

Under the second condition, if there is no provision for occupants to control local airspeed, the application of the SET model is subject to the following constraints:

A. For operative temperatures exceeding 25.5°C, the mean airspeed must remain below 0.8 m/s.
B. For operative temperatures below 22.5°C, the maximum average airspeed permitted is 0.15 m/s.
C. For operative temperatures ranging from 22.5°C to 25.5°C, the peak average airspeed should conform to the curve depicted in Figure 3.4, located between the areas of darker and lighter shading.

Notably, the ASHRAE Thermal Comfort Tool employs the SET model to evaluate comfort scenarios with elevated airspeeds exceeding 0.2 m/s, as illustrated in Figure 2.4. Additionally, it is important to highlight that the elevated airspeed method typically adjusts the graphical or analytical method to account for the increased air velocity (ASHRAE, 2013).

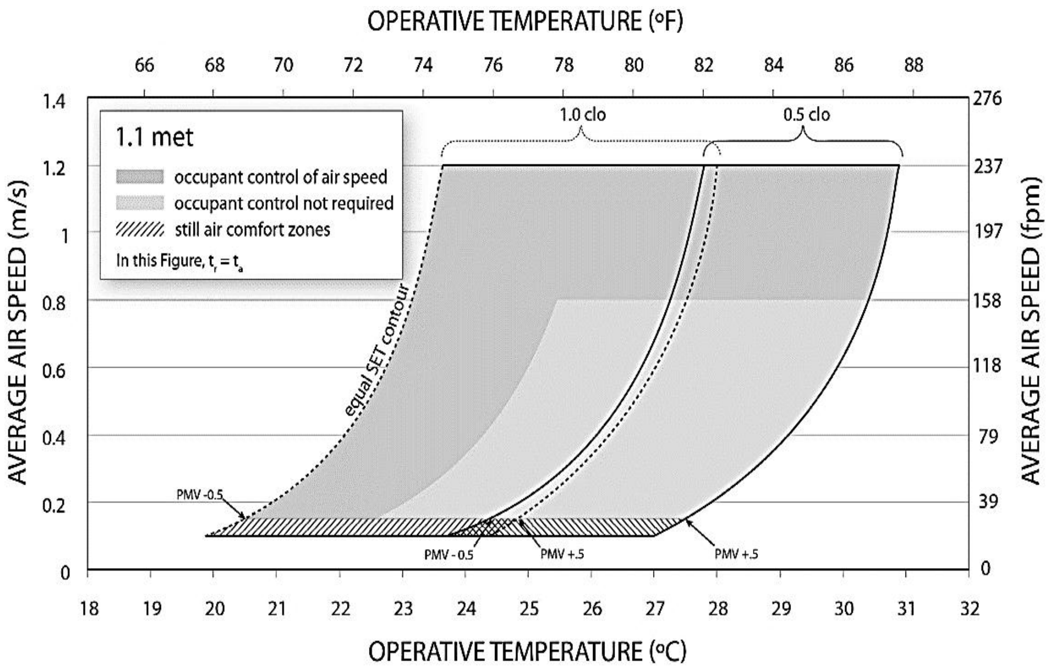

Figure 2.4: Elevated airspeed method in ASHRAE/ANSI Standard 55-2013.

2.6.4 ADAPTIVE METHOD

This methodology is specifically designed for naturally ventilated spaces without mechanical heating or cooling systems, where occupants retain control. The origins of the adaptive comfort theory are attributed to Charles Webb of the Building Research Establishment in the UK. During the 1960s, Webb conducted longitudinal field studies in diverse climates, including Singapore, Baghdad, northern India, and north London (Efeoma and Uduku, 2014). His findings indicated that occupants found the average temperatures they experienced to be the most agreeable, suggesting an adaptation to their unique environmental conditions. Nicol and Humphreys (1973) later expanded on this work, proposing a holistic, self-regulating system encompassing both the occupants and their indoor environment, a concept further supported by McCartney and Humphreys (2002). This culminates in the concise articulation of the adaptive principle: "If a change occurs that produces discomfort, people will tend to act to restore their comfort."

However, it is critical to acknowledge that the early works on adaptive comfort by scholars such as Webb, Humphreys, Nicol, and Auliciems did not gain significant traction in contemporary academic and practical realms. De Dear highlighted this oversight, pointing to the preference for Fanger's heat-balance model (PMV/PPD) within the comfort research community. In-depth field studies by De Dear exploring these competing theories (adaptive versus heat balance) revealed notable differences, particularly in warmer regions, that were unaccounted for by Fanger's foundational comfort factors (De dear, 1985b, De dear, 1985a, Auliciems and Dear, 1998), as referenced by Efeoma and Uduku (2014).

With these insights, ASHRAE 55 has evolved to accommodate a range of design strategies that prioritise comfort while aligning with the sustainability imperative of modern building practices. Interestingly, since the introduction of the adaptive standard in 2004, practitioners have frequently inquired about incorporating elevated air velocity into the adaptive model, as discussed by De Dear (2011a). Consequently, ASHRAE 55 requires that optimal indoor operative temperatures be determined using the 80% acceptability limits, as detailed in Figure 2.5.

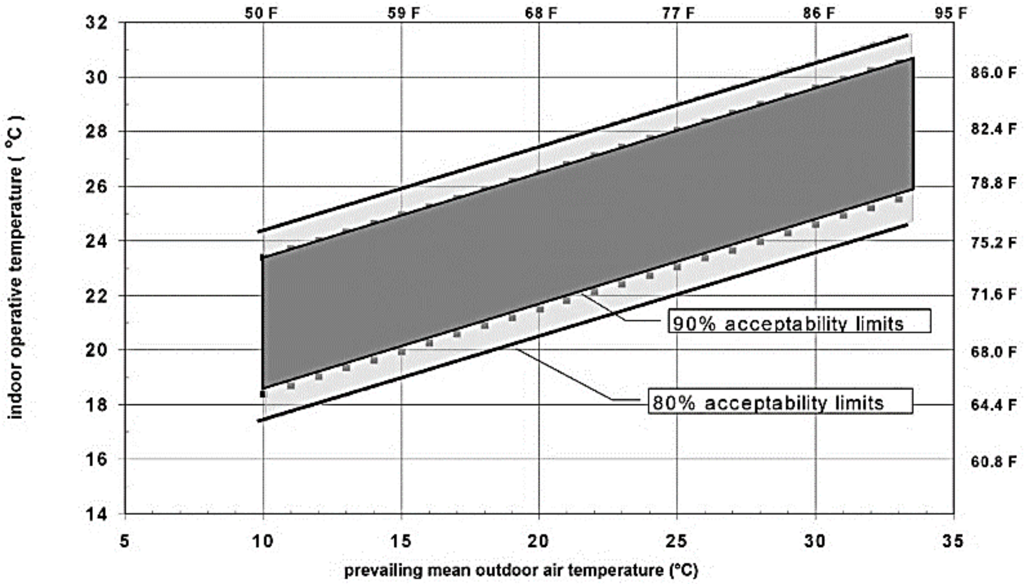

Figure 2.5: Acceptable operative temperature ranges for naturally conditioned spaces according to the ASHRAE comfort standard, using the 80% acceptability limits.

2.7 NATURALLY VENTILATED SPACES

Over the past several decades, there has been a significant increase in interest in naturally ventilated spaces. This shift is primarily driven by the substantial energy loads required to maintain the 'thermally neutral' conditions recommended by static thermal comfort models. According to Fanger (1970), integrated HVAC systems are largely responsible for this rise in energy consumption within buildings.

Additionally, the Fanger framework is widely used globally, and its recommendations are well-recognised due to their association with the ASHRAE standard. Guided by this mathematical framework, achieving occupant satisfaction within buildings became feasible, primarily because the risk of draughts led to a significant reduction in both air velocity and set points. Consequently, new models are being developed in which a slightly warm environment is also considered acceptable by individuals, as noted by De Dear and Brager (1998). Furthermore, both PMV and PPD have demonstrated a preference for these alternative techniques due to their efficacy in managing increases in air velocity within indoor settings. This successful approach allows for the dispersion of latent heat and the adjustment of the occupant's comfort set point, as the thermoreceptors in human skin respond favourably to these conditions.

The academic body of ASHRAE has also recognised and endorsed these advantages, offering a broader range of airflow options and personal controls within spaces, thereby enabling optimal performance in dynamic settings. Accordingly, as noted by Candido and Dear (2012), contemporary research on naturally ventilated buildings highlights three critical factors that have driven conventional adjustments: thermal delight, enhanced airflow, and customisable controls.

2.8 AIR MOVEMENT AS A PRIMARY THERMO-REGULATOR

Air movement has long been recognised as an effective technique for thermoregulation in buildings. The Roman architect Vitruvius experimented with this method and evaluated its benefits for the indoor environment. Numerous advantages of this strategy have been explored, with the most significant being the reduction of air temperature in interior spaces through the adjustment of air volume, which enhances indoor air quality (De Dear, 2011b). However, the rapid introduction of mechanical ventilation systems, such as HVAC systems, in the twentieth century led to significant changes. De Dear and Schiller Brager (2001) observed that modern technology has created thermally isolated indoor spaces, negatively impacting overall occupant comfort in the built environment and resulting in unexpectedly high energy consumption.

In hot and humid environments, the primary cause of discomfort is not unwelcome air. Natural ventilation is considered an effective strategy for improving indoor air quality. Additionally, it aids in temperature regulation, reducing the risk of occupants overheating and lowering energy consumption (Candido and Dear, 2012). Historically, several environmental specialists have conducted research to determine the optimal indoor air velocity. Rohles (1974) explored the influence of air velocity on mean temperature, revealing that excessive air speed could significantly increase indoor temperature set points. Specifically, the findings indicate that elevating airspeed to 1 m/s would result in an effective temperature of 29°C. Subsequent experimental studies reported a high acceptability rate, with the temperature threshold nearing 28°C (Candido and De Dear, 2012). Moreover, peak rates of 1.6 m/s were identified as ideal for providing a comfortable temperature experience for occupants, with temperatures reaching approximately 31°C.

Thus, these research studies assert a critical finding, demonstrating a strong correlation between thermal comfort sensation and air movement, emphasising the importance of air movement in occupants' thermoregulatory systems.

2.9 NATURAL VENTILATION HOURS POTENTIALS IN HOT CLIMATES

Globally, several regions demonstrate substantial potential for utilising natural ventilation (Fig. 2.6), as studied by Chen et al. (2017). The Mediterranean climate, for instance, is well-suited to the use of natural ventilation. Moreover, the authors observed that desert areas exhibit unexpectedly high natural ventilation potential, with estimates ranging from 3,000 to 4,000 NV hours. Even during the sweltering conditions of summer days, temperatures experience a significant decline at night due to radiative cooling under clear skies. This phenomenon makes night-purge ventilation a widely applicable strategy in various regions, including the Middle East, Central Australia, and Egypt (Chen et al., 2017).

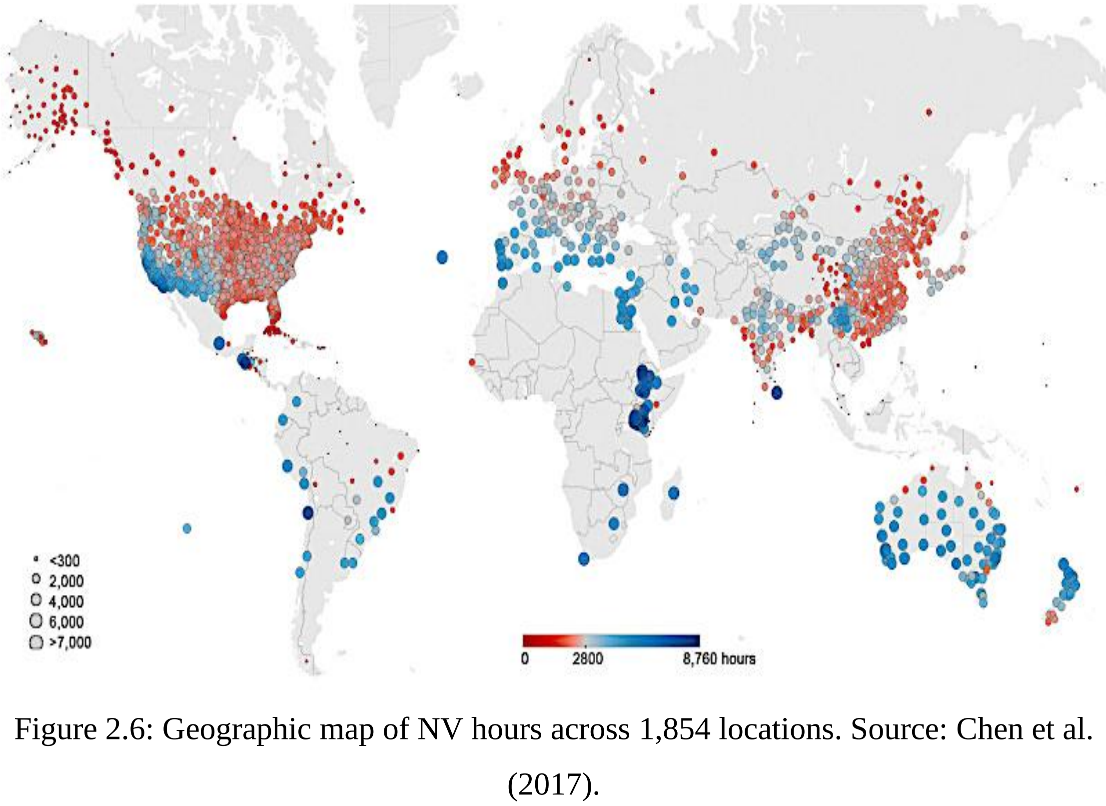

Figure 2.6: Geographic map of NV hours across 1,854 locations. Source: Chen et al. (2017).

The number of NV hours can increase substantially if the higher temperature threshold is raised by a few degrees. However, as indicated by the authors, this increase varies by region. Figure 2.7 illustrates the additional NV hours achieved by adopting the adaptive thermal comfort model. Notably, cities in the polar climatic zone exhibit only a minor increase in NV hours, typically exceeding 1,000. In contrast, cities located in desert and semi-arid climates, such as Central Australia, Central East Africa, and the Middle East, show a significant rise (Chen et al., 2017).

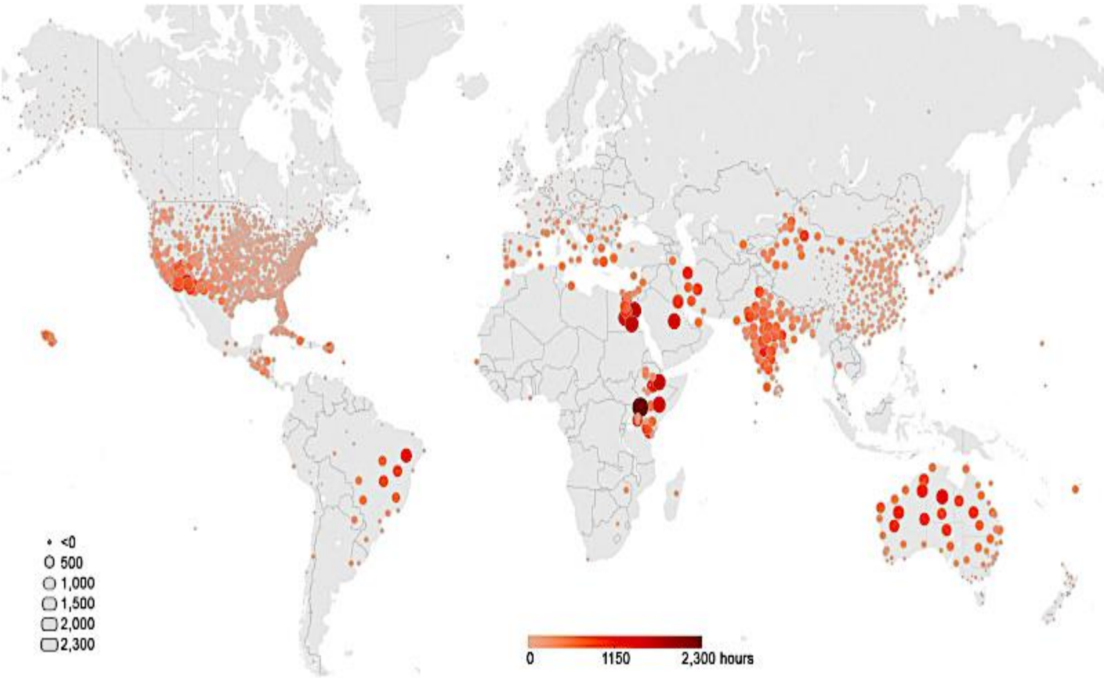

Figure 2.7: Ge Geographic map of additional NV hours achieved using the adaptive thermal comfort model. Source: Chen et al. (2017).

Table 2.5: Recorded natural and non-natural ventilation hours in the world's largest cities. Source: Chen et al. (2017).

City	NV hour	Non-NV hour (hot and humid)	NV%	ES%	City	NV hour	Non-NV hour (hot and humid)	NV%	ES%
Tokyo	2633	2131	55.3%	27.5%	Nagoya	3031	2241	57.5%	24.9%
Delhi	3331	4572	42.1%	13.3%	Hyderabad	2471	6283	28.2%	6.0%
Manila	7	8753	0.1%	0.0%	Chicago	2808	1368	67.2%	20.7%
Seoul	2423	1967	55.2%	26.5%	Johannesburg	6105	219	96.5%	30.3%
Karachi	2701	5799	31.8%	7.6%	Shenyang	2182	1682	56.5%	20.1%
Shanghai	2302	3325	40.9%	20.8%	Wuhan	2122	3433	38.2%	16.1%
Mumbai	1373	7387	15.7%	1.9%	Kuala Lumpur	0	8760	0.0%	0.0%
New York	2966	1573	65.3%	23.0%	Hong Kong	2840	5671	33.4%	16.8%
Sao Paulo	5164	3215	61.6%	27.2%	Boston	2745	1136	70.7%	27.3%
Beijing	2651	1907	58.2%	21.7%	Zhengzhou	2553	2404	51.5%	17.5%
Mexico City	7161	104	98.6%	32.3%	Hangzhou	2193	3428	39.0%	17.8%
Guangzhou	2434	5358	31.2%	15.1%	Dusseldorf	3294	136	96.0%	46.5%
Dhaka	2240	6428	25.8%	4.6%	Toronto	2489	702	78.0%	26.3%
Osaka	2969	2381	55.5%	24.2%	Dallas	2938	3174	48.1%	16.9%
Moscow	2378	193	92.5%	31.7%	San Francisco	5337	57	98.9%	49.2%
Cairo	4886	3187	60.5%	26.1%	Nanjing	2246	3015	42.7%	19.8%
Bangkok	606	8154	6.9%	0.8%	Madrid	4074	703	85.3%	36.1%
Los Angeles	7197	526	93.2%	49.8%	Santiago	4297	565	88.4%	39.2%
Buenos Aires	4514	1690	72.8%	39.2%	Houston	2927	4595	38.9%	16.9%
Kolkata	1785	6928	20.5%	4.5%	Miami	1906	6675	22.2%	6.4%
Tehran	4253	1240	77.4%	24.0%	Riyadh	4916	3110	61.3%	24.7%
Istanbul	3577	1436	71.4%	28.5%	Singapore	0	8760	0.0%	0.0%
Tianjin	2643	2076	56.0%	19.3%	Xi'an	2735	2145	56.0%	21.7%
Rio de Janeiro	1518	7241	17.3%	3.6%	Philadelphia	2883	1775	61.9%	25.4%
Lima	5974	2784	68.2%	38.9%	Nairobi	8435	179	97.9%	43.5%
Chengdu	2660	3153	45.8%	24.2%	Milan	3221	934	77.5%	28.9%
Paris	3451	161	95.5%	45.4%	Atlanta	2674	2798	48.9%	21.3%
Bangalore	3100	5660	35.4%	7.3%	St. Petersburg	2164	82	96.3%	37.2%
London	2885	57	98.1%	45.9%	Washington	2601	2169	54.5%	22.5%
Chennai	120	8640	1.4%	0.0%	Barcelona	3803	1776	68.2%	38.1%

Moreover, the Energy Plus programme was used to evaluate the energy-saving potential of the world's 60 largest cities (as shown in Table 2.5), according to the author. Notably, out of 8,760 hours in a year, the study found that Riyadh (desert climate) has 4,916 NV hours, with 3,110 NV hours deemed unusable due to excessive heat. This is reflected in the table, which presents a list of the world's largest cities, including NV hours (out of 8,760 hours), non-NV hours due to high temperatures and humidity, energy-saving hour percentages (NV%), and corresponding energy-saving percentages achieved through natural ventilation (ES%), as investigated by Chen et al. (2017).

2.10 RECOMMENDED COMFORT ASSESSMENT METHOD

The comfort zone encompasses the combination of the six previously mentioned thermal comfort factors, where the PMV lies within the permissible range. The PMV model calculates thermal comfort based on air temperature, mean radiant temperature, metabolic rate, clothing insulation, air velocity, and moisture levels. Conditions are considered within the comfort zone if the model yields a PMV value within the desired range. It is worth noting that, as stated by the ASHRAE standard: "Since the two personal characteristics of occupants (metabolic rate and clothing level) vary, operating setpoints for buildings are not mandated by this standard" (ASHRAE 55, 2013). Over time, numerous models for predicting comfort have been developed. Based on the comfort zone method and the previous understanding, Table 2.6 lists the four recommended methods, considering the reviewed environmental and personal factors.

Table 2.6: Recommended comfort assessment methods based on the type of space and occupants. Source: ASHRAE Standard 55 (2013).

Air speed	**Humidity Ratio**	**Met**	**Clo**	**Other**	**Comfort Zone Method in ASHRAE**
<0.2 m/s (40 fpm)	<0.012 kg H_2O/kg dry air	1.0 to1.3 met	0.5 to 1.0 Clo		S 5.3.1 (graphical method)
0.2 m/s (40 fpm)	Any	1.0 to2.0 met	0 to 1.5 Clo		S 5.3.2 (analytical method)
>0.2 m/s (40 fpm)	Any	1.0 to2.0 met	o to 1.5 Clo		S 5.3.3 (elevated air speed method)
Any	Any	1.0 to1.3 met	Free to adjust within a range of 0.5 to 1.0 CIO	No cooling installed, heat not operating, occupants control openings, prevailing mean OAT 10 ^{0}c to 33.5 ^{0}C	S 5.4 (adaptive method)

2.11 ENHANCING THERMAL PERFORMANCE THROUGH PASSIVE DESIGN STRATEGIES IN HOT CLIMATES

In regions with hot and humid conditions, substantial opportunities exist for energy savings by reducing cooling demands. This can typically be achieved by minimising solar and heat conduction gains while promoting natural ventilation for both cooling and dehumidification. Alassaf (2024) highlights various essential strategies for reducing cooling needs, including appropriate building alignment and spatial arrangement, effective shading techniques, and the selection of suitable materials, colours, and textures. Additionally, recent studies have emphasised the significance of passive design applications in hot climates (Aldabesh et al., 2021).

To clarify, passive design is one of the most widely recognised terms used to describe a method that uses existing meteorological conditions and inherent energy resources to create desirable comfort conditions. This approach reduces energy consumption and lessens reliance on HVAC and active systems. It is well established by several institutes specialising in building and energy studies (such as the Passive House Institute) that a range of passive design principles has been standardised as design benchmarks for architects and engineers. These principles help mitigate excessive energy consumption in buildings while producing thermal comfort.

Moreover, Roaf et al. (2014) outline several passive design opportunities, organised in order of importance, as design opportunities form the foundation for delivering comfort, while other factors are supplementary and support the degree of satisfaction. Key design opportunities include orientation, shape, apertures, solar access, floor and building height, ventilation strategies, solar shading, insulation, and building materials. Opportunities for adaptation encompass opening windows, infiltration, furnishings, cooling systems, landscaping, shades, curtains, and blinds, as well as the occupants' lifestyle. Finally, the third level of opportunities involves sensation and perception, colour and lighting, vistas and connections to nature, architectural style, and the presence of ambient noise.

2.11.1 ADAPTIVE PASSIVE STRATEGIES FOR ENERGY SAVINGS IN HOT CLIMATES

Since its inception in 1988, the passive house concept has been attributed to the work of Dr Wolfgang Feist and Bo Adamson. According to the Passive House Institute (2015), the concept was first validated in 1990 with the completion of their initial project, the Kranichstein Passive House in Darmstadt, Germany, as noted by Trubiano (2013). In 1996, Dr Feist established the Passivhaus Institute as a research organisation comprising a multidisciplinary team of architects, engineers, and construction experts to advance energy-efficient building design concepts (Trubiano, 2013, Alshenaif, 2015). Figure 2.8 depicts the early prototype of a passive house developed by Dr Feist in 1996.

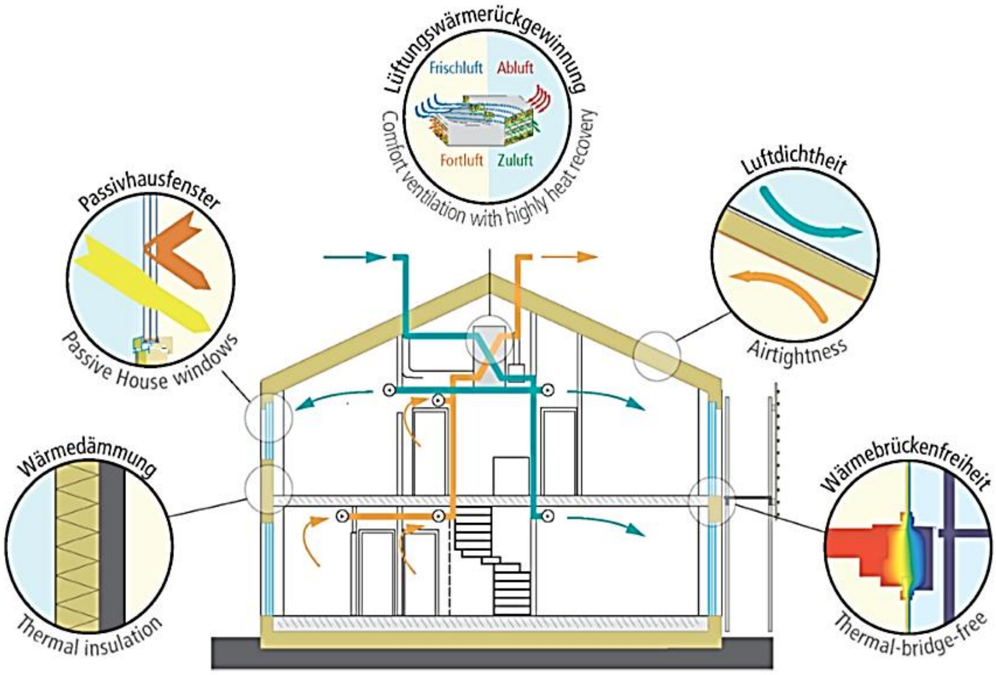

Figure 2.8: Overview of a typical passive house from 1996. Source: Passive house Institute (2015), cited in Alshenaif (2015).

Accordingly, as a basic rule of thumb in hot climates, the design of a passive house must adhere to the following five principles:

1. The structure should be well insulated, with continuous insulation throughout the entire exterior envelope system.
2. Thermal bridging should be minimised in the building's design.
3. The exterior envelope of the structure must be exceptionally airtight.
4. The façade should incorporate high-performance windows.
5. The building should use a heat recovery ventilation system and minimise the use of air conditioning.

Within the Kingdom of Saudi Arabia, numerous studies have evaluated the effectiveness of passive cooling strategies in reducing thermal loads and energy consumption for air conditioning in residential buildings (Albogami and Boukhanouf, 2019). A key study frequently cited in the context of passive methodologies for Saudi Arabia's hot and dry conditions is the work of Alaidroos and Krarti (2015a). Their research examined three passive cooling strategies: natural ventilation, downdraft evaporative cooling, and earth tube cooling. These strategies were applied to a standard Saudi residential villa model with an optimised building envelope. The analysis employed an advanced simulation tool to evaluate performance across various Saudi regions, each representing distinct climatic characteristics.

The findings from Alaidroos and Krarti's research demonstrated significant energy savings in a representative Riyadh villa through the use of natural ventilation and evaporative cooling. Specifically, implementing natural ventilation resulted in a 22% reduction in cooling energy requirements and a 10% decrease in the villa's total energy consumption. In contrast, the evaporative cooling approach achieved a 64% reduction in cooling energy needs and a 32% decrease in overall energy usage for the villa. Furthermore, Alaidroos and Krarti (2015a) suggested that while natural ventilation shows considerable potential across all Saudi climates, evaporative cooling is particularly well-suited to hot and dry regions such as Riyadh and Tabuk.

The documented savings in cooling energy achieved through natural ventilation across five distinct Saudi climatic regions are illustrated in Figure 2.9. In contrast, Figure 2.10 depicts the energy savings resulting from the implementation of passive evaporative cooling systems for villas in these regions.

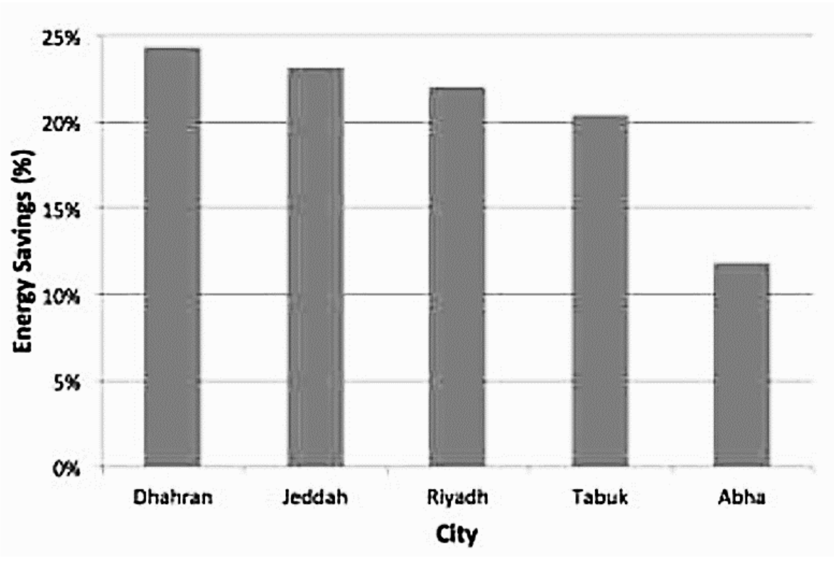

Figure 2.9: Annual energy savings achieved through natural ventilation across five climate zones in Saudi Arabia. Source: Alaidroos and Krarti (2015a).

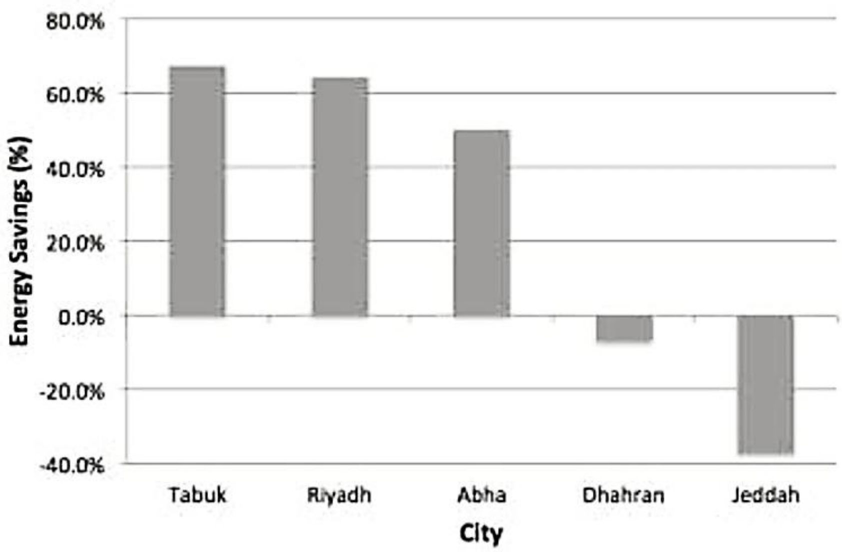

Figure 2.10: Annual reductions in cooling energy achieved through the use of a passive evaporative cooling system in a villa across five climate zones in Saudi Arabia. Source: Alaidroos and Krarti (2015a).

From the above analysis, with reference to Dhahran and Jeddah, it is evident that the natural ventilation strategy significantly reduces cooling energy consumption by approximately 24% and 23%, respectively, as illustrated in Figure 2.9. This finding supports the recommendation of adopting natural ventilation as a primary enhancement strategy in this thesis. However, as shown in Figure 2.10, passive evaporative cooling systems demonstrate nearly 0% and -40% effectiveness for improving building performance in Dhahran and Jeddah, respectively. Consequently, the passive evaporative cooling strategy is deemed an invaluable approach to addressing cooling load challenges in these regions, as argued by the author.

In other words, the figure indicates that evaporative cooling provides little to no energy savings in Dhahran and Jeddah due to the high humidity levels in these regions, which diminish the effectiveness of such systems. In these areas, alternative or complementary cooling strategies, such as enhanced insulation, shading devices, or advanced ventilation techniques, may be more suitable for addressing cooling loads under humid climatic conditions. This observation underscores the adaptability and importance of tailoring evaporative cooling to specific regional climates.

2.11.2 NATURAL VENTILATION PRINCIPLES AND STRATEGIES FOR ENHANCED AIRFLOW

Khayyaminejad and Fartaj (2024) identify natural ventilation as a fundamental passive cooling strategy that reduces energy consumption in buildings while improving indoor air quality and comfort. This approach leverages the principles of wind pressure and the buoyancy effect to channel fresh air through the building (Khan et al., 2008). The effectiveness of this method lies in the pressure difference created by wind on the building's exterior—specifically, the contrast between the windward side and the leeward side. This pressure differential, combined with the variation caused by indoor and outdoor temperature contrasts, facilitates air movement within the building.

Alaidroos and Krarti (2015a) investigated the potential for reducing cooling demands in a villa across various climatic regions in Saudi Arabia through natural ventilation, using the Airflow Network Model in Energy Plus. They emphasised that effective management and control strategies are essential for accurately simulating natural ventilation. The study highlighted that airflow through windows, particularly in single-storey buildings like villas, is significantly influenced by wind, making this form of ventilation highly suitable for residential settings.

The practice of ventilating through windows is common in residential buildings due to its simplicity and ease of management (Adeyemi et al., 2024). Alaidroos and Krarti (2015a) further identified specific times of the year when external temperatures are suitable for cooling a villa through natural ventilation, highlighting its seasonal applicability in warmer regions. They emphasised the annual temperature variations in Riyadh and the viable periods for employing natural ventilation to cool the villa, as illustrated in Figure 2.11.

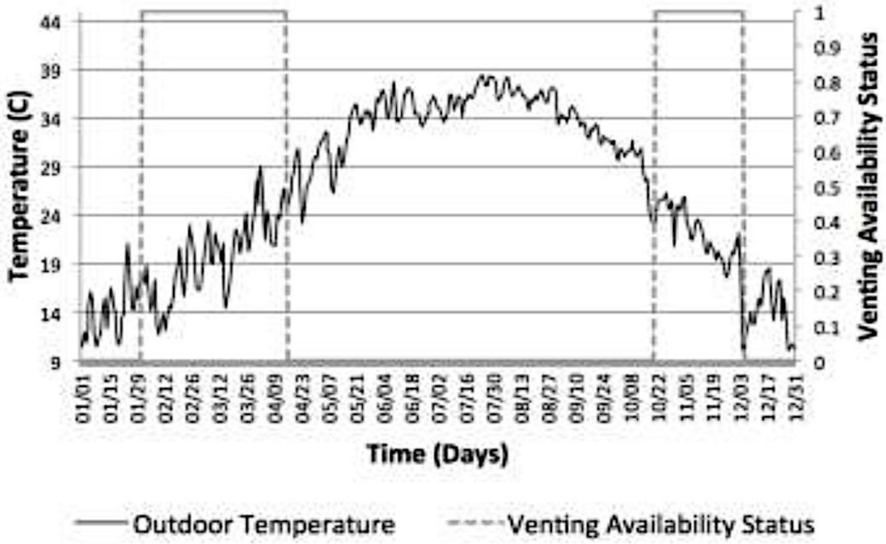

Figure 2.11: Annual fluctuations in outdoor temperature indicating opportunities for employing natural ventilation in a villa in Riyadh. Source: Alaidroos and Krarti (2015a).

Their research emphasises that windows should be strategically positioned and opened only when outdoor conditions are conducive to natural ventilation, as depicted in Figure 2.11. The figure identifies two primary periods suitable for natural ventilation in Riyadh: from 1 February to 15 April and from 10 October to 5 December, when external temperatures range between 15 °C and 25 °C. For the remainder of the year, natural ventilation is less effective due to excessively high temperatures during summer or the cold during the brief winter period (6 December to 31 January). The research employs temperature-based controls, operating continuously, to facilitate the opening of windows during these optimal periods.

This review highlights the importance of establishing comprehensive design and control guidelines to maximise the effectiveness of passive design strategies, particularly in hot and humid climates for naturally ventilated residences. These guidelines will serve to inform the thermal performance enhancement strategies applied to the case studies examined in this research.

Regarding the efficacy of natural ventilation in hot and humid conditions, Al-Tamimi (2015) investigated enhancing indoor thermal comfort through passive cooling techniques in residential buildings without relying on additional cooling devices

(Figure 2.12). The study revealed that, despite high-velocity air during the day, ventilation alone could not lower indoor temperatures below outdoor levels, irrespective of window orientation. While night-time ventilation had a limited impact on daytime indoor temperatures, the research demonstrated that natural ventilation could reduce temperature differences by 80% during the day and 50% at night. Notably, continuous ventilation throughout the day and night provided superior thermal conditions in hot, humid climates compared to ventilation applied only during the day or night.

Al-Tamimi (2015) also found that a room with an opening equivalent to 14.5% of the glass area does not provide sufficient natural ventilation to achieve a comfortable environment. However, a design incorporating two windows on opposite sides enhances airflow, even when the door is closed. This cross-ventilation has the potential to offset significant heat gains from large glass areas, depending on external temperatures, thereby creating a more comfortable indoor environment.

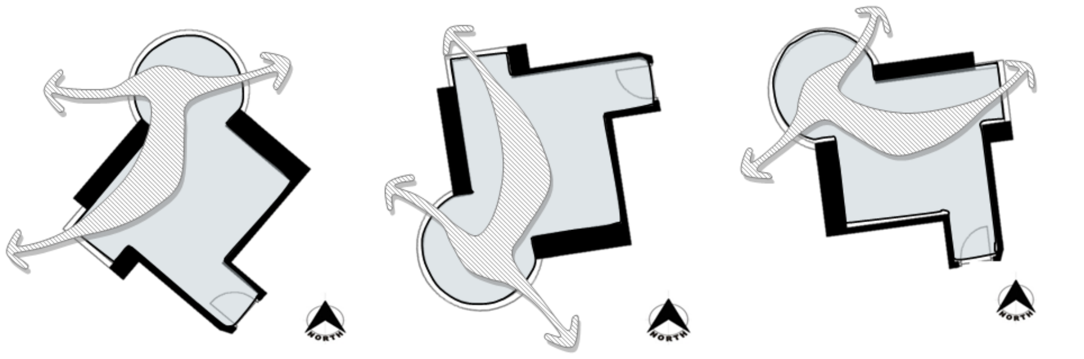

R3 at unit A9	R3 at unit B3	R3 at unit A10

Figure 2.12: Estimated indoor air behaviour influenced by operable windows. Source: Al-Tamimi (2015).

Furthermore, Figures 2.13 illustrate a significant rise in internal air temperature compared to the outside throughout the day. These rooms, as highlighted in the study, are exposed to intense solar radiation without any protective shading. However, when adequate ventilation is provided (as shown in Figures 2.14), the indoor air and surface temperatures closely align with external conditions. This results in a substantial 79.72% reduction in indoor temperature across the three rooms compared to their non-ventilated states, as reported by Al-Tamimi (2015). Nevertheless, despite the considerable cooling effect of natural ventilation, the interior air temperature remains above levels typically considered comfortable. This underscores the pivotal role of natural ventilation in dwellings within hot and humid climates.

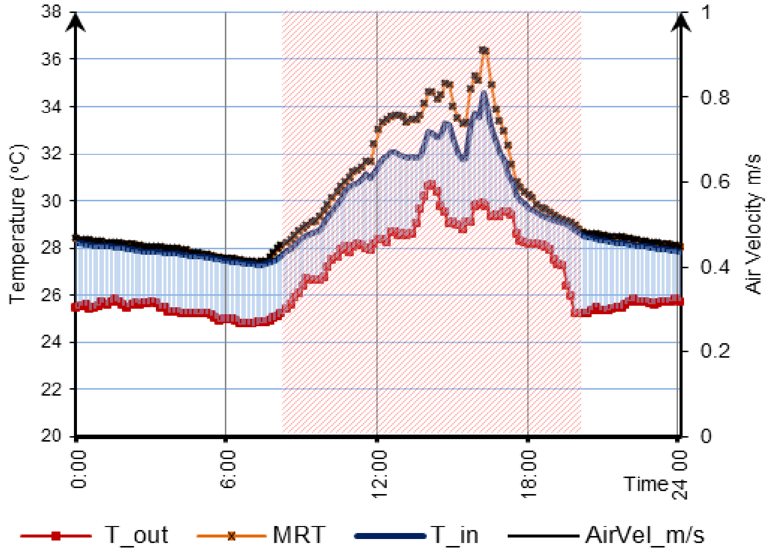

Figure 2.13: Room (A9) unventilated on 13 April 09. Source: Al-Tamimi (2015).

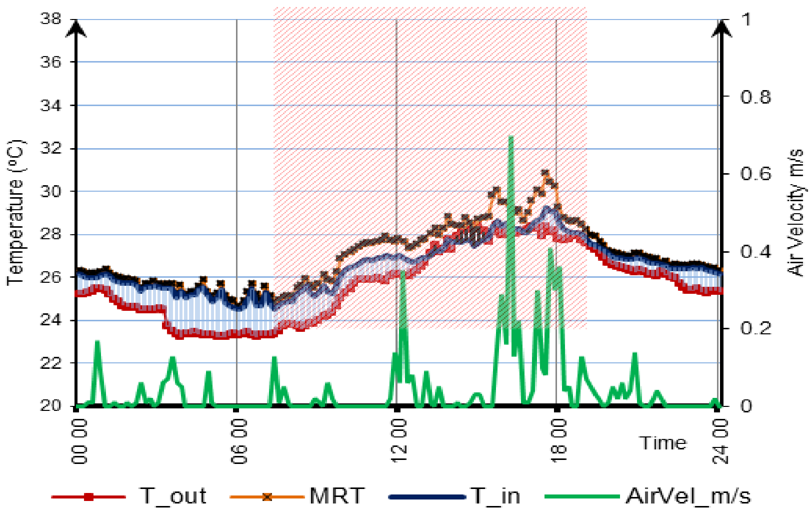

Figure 2.14: Room (A9) ventilated on 21 April 09. Source: Al-Tamimi (2015).

2.11.3 ORIENTATION AND ARCHITECTURAL LAYOUT

The climatic influence on a building is shaped by its exposure to solar radiation and the surrounding average temperature. These factors determine the energy required for heating, cooling, and lighting. Unwanted solar energy entering a structure is termed 'solar excess'. As architectural trends increasingly incorporate glass and glazing systems designed to absorb solar heat, orientation becomes a critical consideration. A study by Haase and Amato (2009) evaluated 12 distinct sites, primarily in Asia's warm-humid region, with the remainder located in China. The study found that while buildings displayed various orientations, a predominant preference for a north-south alignment was evident, minimising the exposure of the east and west facades. However, this trend was not universal across all warm-humid locations.

Designing a building to optimise winter sun exposure does not inherently address summer conditions. A crucial consideration is to minimise solar exposure during peak heat, particularly given the 90° seasonal shift in solar angles. When the ideal orientations for summer and winter do not align perpendicularly, a careful balance is required, guided by the comparative thermal discomforts, as outlined by Haase and Amato (2009). Research conducted in the UAE by Alshuhail and Taleb (2020) revealed that the southern aspect experienced temperatures approximately 9.4% higher than its northern counterpart.

Contemporary studies affirm that building orientation significantly influences operational efficiency, particularly in warmer climates. Southern and western orientations are generally less favourable due to their heightened solar exposure, even at elevated positions. When a building's eastern and western facades are compact, the northern orientation proves to be the most advantageous. Consequently, in hotter regions, buildings with facades facing either north or south tend to provide a more comfortable internal environment compared to those oriented east or west.

Lastly, Liping and Hien (2007) emphasised that for naturally ventilated buildings, it is advisable to avoid sealed daylighting windows on the east and west facades to ensure optimal internal thermal conditions.

2.11.4 OPTIMISING SHADING DEVICES FOR THERMAL COMFORT IN HOT CLIMATES

In hot regions, the use of external shading mechanisms is a common strategy for controlling the infiltration of solar radiation into residential buildings, as noted by Bena et al. (2019). However, this approach often limits the penetration of natural light and airflow, which are essential for passive thermal regulation within these structures. The effectiveness and implications of various shading solutions have been a focal point of research conducted across different climatic conditions.

In one study, Hien and Istiadji (2003) evaluated six distinct external shading alternatives applied to a residential building in Singapore. Their objective was to enhance natural illumination and ventilation, using CFD and LIGHTSCAPE models for detailed analysis. The findings highlighted a general reduction in indoor temperatures due to shading applications. However, the study revealed differences in effectiveness between vertical shading (refer to Figure 2.15) and horizontal shading (see Figure 2.16), with the latter proving more effective in promoting daylight and fresh air circulation. The temperature reduction was measured at approximately 0.5 to 1 °C, corresponding to a variation of 1.3 to 2.8%.

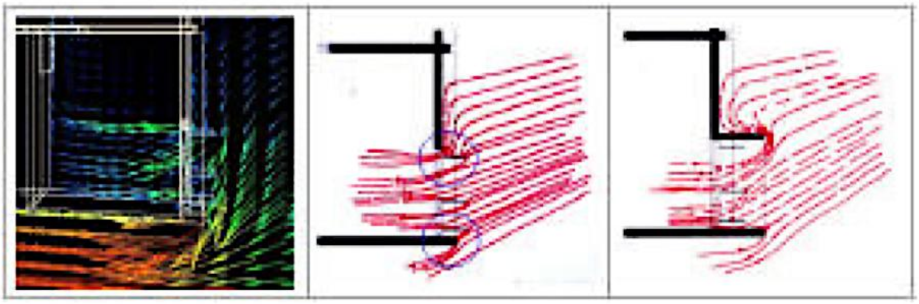

Figure 2.15: Depiction of vertical shade's influence on airflow. Source: Hien and Istiadji (2003).

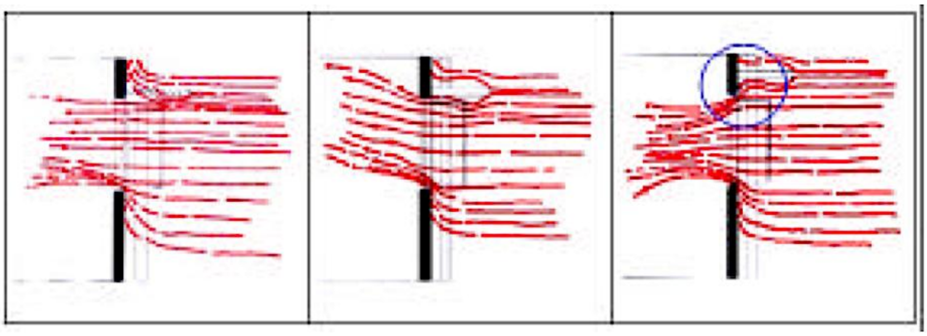

Figure 2.16: Representation of airflow alteration by horizontal shades. Source: Hien and Istiadji (2003).

In a convergent finding, Liping and Hien (2007) advocated for an increase in the window-to-wall ratio, up to 0.24, as a means to significantly improve indoor thermal dynamics. They emphasised the importance of integrating horizontal shading across all cardinal orientations to further optimise indoor thermal conditions.

Expanding on this perspective, the strategic adoption of external shading methods acts as a regulator for solar penetration, reducing reliance on mechanical cooling systems while enhancing both thermal comfort and daylight quality (Corrado et al., 2004, Bouchlaghem, 2000, Muniz, 1985, Liping and Hien, 2007). However, as noted by Haase and Amato (2009), variations in average monthly temperatures across different climatic zones necessitate a nuanced understanding of solar radiation characteristics specific to each locale. Such insights are essential for the tailored implementation of shading techniques. Building on this, Alwetaishi et al. (2020) stressed the importance of carefully incorporating shading solutions to manage excessive solar radiation, particularly for larger window surfaces facing south and west.

The current body of scholarly work highlights a notable gap in research on thermal comfort in naturally ventilated structures, particularly in harsh climates, where studies are largely limited to advanced façade solutions. This scarcity underscores the need for detailed investigations into adaptive ventilation and façade strategies tailored to Saudi Arabia's unique climate and cultural context. Ineffective shading implementations can obstruct the transition of air from external to internal spaces, highlighting the importance of designing shading elements that align with local wind patterns and the building's thermal characteristics.

2.11.5 WINDOW-TO-WALL RATIO'S ROLE IN THERMAL COMFORT

The Window-to-Wall Ratio (WWR), representing the proportion of window area to wall surface in a building, plays a crucial role in influencing indoor thermal comfort and lighting energy requirements. Extensive research has been conducted on the effects of WWR on buildings' thermal performance and comfort levels. Pathirana et al. (2019) conducted a comprehensive study examining various architectural factors, including building form, orientation, and WWR, and their impact on lighting energy use and thermal satisfaction in naturally ventilated tropical residences. Using DesignBuilder software, the study simulated thermal discomfort averages (based on ASHRAE 55, 80% acceptability limits) across 300 distinct two-storey residential models, while also comparing four WWRs across three architectural configurations.

The findings revealed that optimal thermal comfort was achieved with a central-staircase, rectangular layout at a 20% WWR, whereas L-shaped configurations performed best when the stairwell was located at the shorter end or centrally, depending on the WWR. Interestingly, thermal comfort improvements of 20%–55% were observed with increased WWR, alongside a modest 1.5%–9.5% reduction in lighting energy demand.

Consequently, adjustments to the WWR aimed at improving occupant thermal comfort have minimal impact on internal lighting energy requirements, underscoring the prioritisation of thermal comfort in WWR design decisions. Figures 2.17 and 2.18 graphically illustrate these variations in thermal comfort and lighting energy demand resulting from WWR modifications.

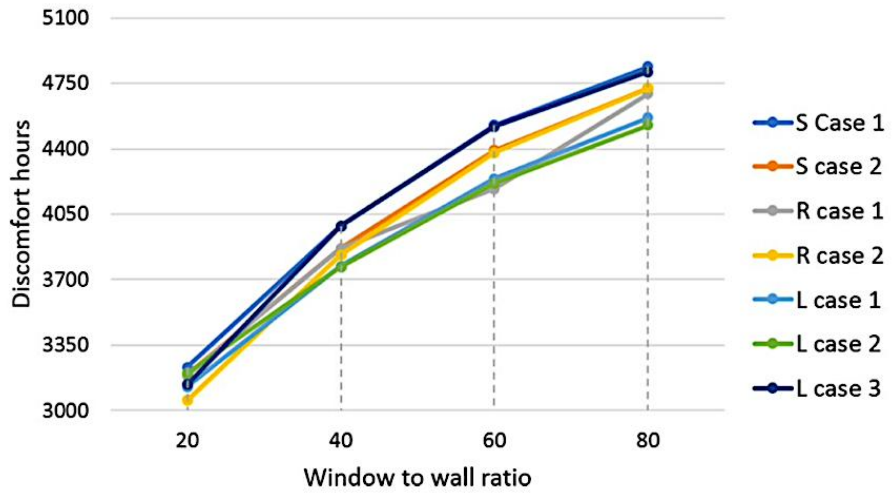

Figure 2.17: Thermal comfort across various cases with different WWRs. Source: Pathirana et al. (2019).

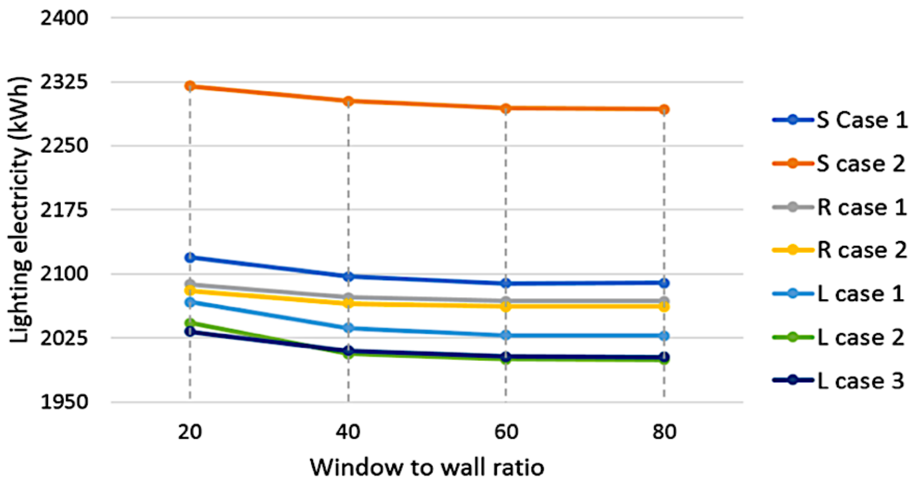

Figure 2.18: Influence of WWR on lighting energy consumption. Source: Pathirana et al. (2019).

The study highlights the pivotal role of WWR in optimising daylight usage, as evidenced by discomfort rates and lighting energy data for seven primary models at WWRs of 20%, 40%, 60%, and 80%. As shown in Figures 2.17 and 2.18, WWR directly correlates with discomfort rates, with a 20% WWR providing the most favourable thermal conditions. However, increasing the WWR to 40% significantly raises the discomfort rate by over 20%.

In an assessment comparing various strategies, Asfour (2020) explored the benefits of de-lighting and the incorporation of courtyards within Saudi Arabia's extreme climate. The study advocated for a conservative approach to the Window-to-Wall Ratio (WWR) and endorsed extensive use of external shading mechanisms. It highlighted the drawbacks of increasing the WWR beyond 50%, a threshold where cooling demands and the risk of glare-induced discomfort significantly rise. This perspective prioritises WWR adjustments over maximising daylight, reaffirming the critical role of passive design elements. These measures, including a carefully calibrated WWR, are essential for reducing reliance on energy-intensive cooling systems, thereby enhancing thermal comfort and improving conditions for building occupants.

Alwetaishi et al. (2020) emphasised the predominant impact of glazing on indoor environments, surpassing the influence of thermal mass. This finding underscores the need for meticulous selection of window systems in warmer regions, particularly at higher elevations. Moreover, Al-Saggaf et al. (2020) identified that glazing choices have a greater impact on energy consumption in hot climates than factors such as building orientation, shape, or the number of floors. This highlights the importance of focusing on the thermal properties of glass. In this context, Su and Zhang (2010) observed that while single-glazed windows significantly increase energy requirements, the use of low-emissivity (low-E) glass can dramatically enhance a building's overall energy efficiency over its lifespan (Troup et al., 2019).

Focusing on the aspect of openings, the proportion of inlet aperture area in relation to windows is a crucial consideration. To ensure comfort levels in naturally ventilated buildings, it is recommended that the inlet area constitutes approximately 20% of the total floor area (Liping and Hien, 2007, Tantasavasdi et al., 2001). Liping and Hien (2007) also stressed the importance of keeping windows open when daylighting is intended in naturally ventilated buildings, particularly on facades exposed to intense solar radiation. Similarly, Al-Mofeez (1991) noted that fenestration could account for nearly 22% of energy consumption in residential buildings. This issue arises when window heat gain is poorly managed, leading to excessive heat and undermining thermal efficiency.

Uncontrolled window heat gain often results in overheating, compromising a building's thermal performance. In naturally ventilated buildings, it is essential to control fenestration effectively while adhering to the recommended inlet aperture area. This balance involves designing fenestration systems that manage solar heat gain and ensuring reasonable control over opening percentages, enabling occupants to regulate ventilation and maintain thermal comfort.

2.11.6 THERMAL MASS UTILISATION FOR ENHANCED COMFORT IN HOT CLIMATES

According to Li and Yam (2004), thermal mass (TM) can be categorised into two broad types: interior TM, which includes furniture, and exterior TM, which comprises walls, roofs, and floors. In hot and temperate climates, incorporating thermal mass into building walls is a common practice for regulating indoor temperatures via night-time natural ventilation.

The ability of a building's thermal mass to store heat, either as sensible or latent energy, is crucial in managing interior temperatures, reducing energy demands, and enhancing occupant comfort. Reilly and Kinnane (2017) underscore the significance of thermal mass during dynamic heating and cooling phases—conditions prevalent in most global structures—compared to those maintaining near-constant steady-state environments. Thermal mass, therefore, emerges as an effective strategy in arid climates characterised by pronounced diurnal temperature variations. Likewise, Lind et al. (2023) advocate for the potential of thermal mass and its energy storage capacity as robust solutions for improving energy efficiency and thermal comfort, particularly within the context of indoor air quality.

Reilly and Kinnane (2017) introduced innovative metrics to measure the impact of thermal mass on energy consumption related to building heating and cooling. Their findings indicate that structures with substantial thermal mass provide significant advantages in warmer climates. However, in colder climates, the drawbacks of increased thermal mass frequently outweigh its benefits, often resulting in higher energy consumption.

Similarly, Alwetaishi et al. (2020) investigated the thermal comfort of historic buildings in Saudi Arabia's elevated desert regions. Using TAS EDSL software, thermal cameras, and data loggers, their study found that while thermal mass had a limited effect on indoor temperatures and energy consumption, it notably enhanced thermal comfort.

Conversely, ventilation enhances thermal comfort. Alwetaishi et al. (2020) suggested that buildings with substantial thermal mass in high-altitude warm climates could achieve year-round comfort, although air conditioning may be required during summer months when temperatures exceed 35°C. Similarly, Mousa et al. (2017) compared historical stone structures with modern brick buildings in Egypt's hot climate, demonstrating that the stone structures were capable of reducing indoor temperatures by approximately 1.4°C.

Numerous scholars agree on the advantages of thermal mass, particularly in extreme heat conditions (Reilly and Kinnane, 2017, Kumar et al., 2017, Wolisz et al., 2020). However, Rodrigues et al. (2019) emphasised the necessity of accounting for local climate when evaluating the application of thermal mass in Mediterranean environments.

Furthermore, a study investigating the correlation between thermal mass and energy consumption examined the effects of varying the exterior concrete wall thickness of a villa from 5 cm to 40 cm. Preliminary findings indicated that increased thermal mass had a significant impact in temperate climates, whereas its advantages were marginal in the intense heat of Jeddah. Alaidroos and Krarti (2015) posited that thermal mass performs optimally in regions with pronounced day-night temperature fluctuations, enabling efficient heat absorption and dispersion. Consequently, due to the limited energy savings observed, the study excluded shading apparatuses from its evaluation.

Synthesising these findings, thermal mass is fundamentally linked to thermal comfort. Kumar et al. (2018) estimated that incorporating thermal mass could reduce thermal discomfort by 40–98%. Similarly, Deng et al. (2019) underscored the dual advantages of thermal mass in reducing energy consumption and enhancing occupant comfort.

2.12 SELECTION AND EVALUATION OF THERMAL MODELLING TOOLS

The foremost and most critical criterion for selecting a thermal modelling tool is its ability to address the intended application while providing the necessary accuracy and reliability. The chosen software must predict internal conditions, such as temperature and humidity, estimate heating and cooling loads, assess thermal comfort, and evaluate the performance of alternative constructions. These capabilities are essential to achieving improved indoor thermal environments and reducing energy consumption within the scope of this study. The following subsections systematically compare and evaluate potential tools to identify the most suitable option for meeting the study's specific requirements.

Based on the explanation provided in this chapter, collecting reliable data is a critical starting point before commencing the simulation phase. The building's geometrical layout is initially designed in the first section and subsequently exported to the simulation software, which evaluates the thermal performance of the structure by analysing its designated parameters. The software is required to assess thermal performance by considering multiple factors, including conduction through building fabrics (using an approach adapted from the ASHRAE response technique), convection at the building's surfaces, long- and short-wave radiation, and solar radiation (both direct and diffuse) absorbed, reflected, and transmitted, utilising the solar data provided in the meteorological file.

Additionally, the software must account for internal gains, such as lighting, miscellaneous equipment, computers, and other devices; sensible heat gain from occupants; solar gains from exterior windows; zone sensible cooling; and zone sensible heating. The following capabilities are essential within the simulation software:

- Air temperature
- Operative temperature
- Relative humidity

• Fanger PMV/PPD

• Comfort and discomfort hours as per ASHRAE standards

• Energy consumption

2.12.1 BUILDING ENERGY PERFORMANCE SIMULATION

The term "early design stage" often appears in research as a reference to the phase of conceptual design development. According to Attia et al. (2012), as cited by Mahmoud et al. (2020), this stage holds significant potential for enhancing energy efficiency but is frequently overlooked in the implementation of regulations and standards. Over the past three decades, Building Energy Performance Simulation (BEPS) tools have become essential for predicting and optimising energy demands during the design process, which accounts for over 73% of the total energy consumed in a building's lifecycle. Attia et al. (2012) emphasise that integrating BEPS tools earlier in the design process can result in more energy-efficient and cost-effective solutions. Despite their advantages and widespread availability, the application of energy modelling tools during the early design stage remains limited, with most tools primarily used for post-design validation.

Originally developed for engineers to evaluate building performance and HVAC systems during the later stages of design, the integration of Building Energy Performance Simulation (BEPS) tools into mainstream architectural practices has faced significant challenges. These difficulties primarily arise from the differing operational frameworks and expectations between architects and engineers, as noted by Alsaadani and De Souza (2012), cited in Mahmoud et al. (2020). Engineers typically rely on well-defined models to perform simulations, a process that is often incompatible with the fluid and iterative approach characteristic of early-stage architectural design.

In response to these challenges, several advancements in BEPS technologies have been introduced, including plug-ins, cloud-based simulations, and parametric analysis tools, designed to support the dynamic nature of architectural workflows. However, researchers argue that the development of specialised tools, while promising, is insufficient if these tools are not aligned with the practical demands of real-world architectural practice. Without this alignment, such innovations are unlikely to fully address the evolving objectives of greenhouse gas (GHG) reduction.

2.13 SUMMARY

In this chapter, factors influencing indoor thermal comfort have been examined based on the most recent studies conducted in the area of focus. These factors vary in their effects depending on the climatic conditions of the selected region. Accordingly, the prediction of thermal comfort in buildings has been identified, alongside an investigation of the thermal comfort zone methods outlined in ASHRAE standards. Four distinct comfort zone methods—graphical, analytical, elevated airspeed, and adaptive—have been explored in detail. It is important to note that each method requires specific conditions to align with the standards.

The use of simulation tools for assessing thermal comfort has been introduced in ASHRAE standards and supported by numerous highly regarded studies. However, the ASHRAE thermal comfort models do not fully account for all climatic conditions. This research focuses on identifying the conditions under which these standards can be applied. For instance, while excessive heat or cold days simulated in the models may fall outside the ASHRAE standards' scope, compliance is achievable on most moderate days throughout the year, provided outdoor temperatures align with the recommended ranges specified by the standards. Consequently, the development phase (model enhancement or retrofitting) considers naturally ventilated buildings during most months of the year, ensuring compliance with the standards' requirements and recommendations.

The literature extensively explores passive elements, including shading solutions and natural ventilation, highlighting their significant influence on thermal comfort within buildings. Although these passive design strategies have a considerable impact, findings from both historical and contemporary studies indicate that they alone cannot fully secure thermal comfort in buildings. However, they play a vital role in energy conservation. Furthermore, the literature demonstrates that natural ventilation (NV) hours are particularly advantageous in Mediterranean climates as well as in various climatic regions within Saudi Arabia.

CHAPTER THREE – PREFABRICATIED BUILDING INDUSTRY AND THERMAL PERFORMANCE IN PRECAST CONCRETE SYSTEMS

3.1 INTRODUCTION

This chapter provides a comprehensive examination of advancements and challenges inherent in prefabricated building technologies, with a particular focus on the components of precast concrete sandwich panels (PCSPs). Key elements such as solid (concrete) wythes, insulation layers, and connection systems are analysed for their critical roles in ensuring system coherence and optimising thermal performance. Innovations in materials and connection technologies are explored within the context of minimising panel thickness and enhancing thermal efficiency. A detailed review of the history of prefabricated building systems is included, illustrating the evolution of these technologies across diverse contexts. Furthermore, the chapter evaluates factors such as fixability, economy, security, and mobility to provide a holistic perspective on the performance and usability of prefabrication.

The chapter also investigates the role of the building envelope as a mediator between indoor and outdoor environments, focusing on the classification of building fabrics and the analysis of thermal properties in precast concrete systems (PCS). Emphasis is placed on understanding multi-layer fabric elements and the mathematical methods employed to model thermal exchanges across building envelopes. The specific thermal properties of materials and components within PCS are defined to elucidate their behaviours during heat exchange. This foundational understanding is essential before conducting thermal analysis using simulation tools. By addressing a wide range of material properties and calculation methods, the chapter establishes a robust framework for advancing the thermal efficiency of precast building systems.

3.2 HISTORICAL EVOLUTION OF PREFABRICATED BUILDING SYSTEMS

The development of prefabricated building solutions was primarily driven by the need to enhance efficiency and provide a more cost-effective alternative to conventional construction practices (Knaack et al., 2012). These innovative systems were influenced by various factors, including the prevailing culture of the people, the availability of natural resources, geographic features, technological advancements, and the vision of architects and engineers. Identifying the exact origin of prefabrication in building construction is challenging due to the diverse perspectives and methodologies adopted by different nations.

The Mongolian Yurt, with a history spanning over 2,000 years, is a notable example of early prefabrication (Figure 3.1). It originated in the steppe regions of Mongolia, where nomadic tribes used it as a portable dwelling while travelling with their families in search of pastures and trade opportunities. The Yurt’s design is celebrated for its lightweight structure, portability, and ease of assembly. Constructed from wood, wool blankets, yak and horsehair ropes, and linen sheets, it can be assembled in as little as 60 minutes and transported using camels. Its unique design effectively shields occupants from wind, while the wool blankets act as thermal insulators, protecting against extreme external temperatures that can drop as low as -40°C (Knaack et al., 2012).

Figure 3.1: The early mongolian Yurt. Source: National Geographic (2017).

Continuing the exploration of historical prefabricated building elements, the Tatami mat from Japan presents another compelling example. Renowned for its floating design, the Tatami mat has been utilised across Asia for over a thousand years and serves as a modified standard module of architectural measurement (Figure 3.2). With its precise dimensions of 190 cm by 95 cm, the Tatami mat embodies principles of design and functionality that remain highly valued today. This meticulous approach has fostered an exceptional level of craftsmanship and facilitated the standardisation of technical and functional aspects, reflecting the enduring influence of traditional Japanese design.

 

Figure 3.2: Crafting Tatami mats (Flooring) during the late 19th century. Source: Motoyama Tatami shop (2016).

In architectural terminology, the term "module" refers to a standard unit of measurement used to establish the proportions of building components. Over time, various modules have been developed, with significant contributions from architects such as Leonardo da Vinci and Le Corbusier. This traditional concept of a module contrasts markedly with its modern interpretation in prefabricated construction, where it typically denotes fully prefabricated, often interlocking units manufactured as complete living products (Knaack et al., 2012).

3.3 MASS PRODCTION AND THE PREFABRICATION DEBATE IN ARCHITECTURE

The Industrial Revolution, spanning from the late 18th century to the 1840s, initiated shifts in technical, socioeconomic, and cultural conditions, the impacts of which continue to permeate our lives and the built environment (Knaack et al., 2012). This era marked the substitution of manpower with machines. Subsequently, the second phase of the revolution commenced in the 1850s, heralding the emergence of new industrial powerhouses like Germany and the United States. These nations, drawing inspiration from the United Kingdom and possessing substantial financial resources, ascended to prominence.

Reyner Banham, a pivotal figure in the articulation of modern architectural terminology and an advocate of machine aesthetics, delineated the evolving roles and trends of architecture and design within the Industrial Age framework (Banham, 1980). In 1960, he authored Theory and Design in the First Machine Age, a seminal work on architecture and design, elucidating the transformative effects of the Industrial Revolution (Knaack et al., 2012).

Mass production, characterised by the manufacturing of standardised goods on a large scale, typically through assembly lines or automation technology, facilitated the swift production of identical items. Le Corbusier, a leading architect of the modern movement, envisioned the mass production of housing. Captivated by automobiles and factory assembly lines, he proposed that housing components should be products of automobile factories. Despite the advancements, the public harboured mixed feelings towards the concept, associating it with both the merits and pitfalls of contemporary functionalist architecture and mass manufacturing. The notion of prefabricated homes encountered initial resistance, as alterations in the perception of 'home' unsettled residents. Consequently, conservatives, upholding values of identity, heritage, craftsmanship, and architectural professionalism, persisted in their opposition to the mass production and prefabrication of architecture into the 1960s (Knaack et al., 2012).

3.4 THE EMARGENCE OF PREFABRICATED HOUSING SYSTEMS

Following World War I, the United Kingdom emerged as one of the pioneering nations to subsidise social housing programmes. Housing authorities recognised building systems as a rapid and efficient method for home construction. Although various innovative systems, such as precast concrete frames and concrete blocks, were developed and implemented, their anticipated success was not fully realised.

With the end of the Second World War in 1945, inadequate housing conditions and a severe housing shortage caused by wartime destruction highlighted the need for renewed attention to system housing, particularly for temporary accommodation. The Ministry of Works in the UK initiated a series of projects, most notably the Portal Building, a prefabricated bungalow constructed on a lightweight steel frame in 1944 (Figure 3.3). However, the extensive use of steel made the Portal prohibitively expensive, preventing it from achieving mass production. Despite this, the Portal set a precedent for numerous subsequent experiments in alternative construction techniques (Knaack, 2012).

Figure 3.3: AIROH aluminium bungalows. Source: Knaack (2012).

In the 1960s, modular coordination emerged as a significant milestone in governmental development. This coordination was instrumental in linking modular systems to facilitate the prefabrication of interchangeable components, an endeavour too complex for standalone commercial enterprises. Within the UK, the modular system was particularly suited to large-panel concrete structures. Precast concrete components, complete with integrated internal and external finishes, lighting, and plumbing, were predominantly used in extensive housing projects, typically ranging from eight to twenty storeys (Knaack, 2012). The centralised modular approach demonstrated its effectiveness across a wide variety of building types.

3.5 EVOLUTION AND BENEFITS OF PRECAST CONCRETE SANDWICH PANEL TECHNOLOGY

Precast concrete sandwich panels (PCSPs) have undergone significant advancements over time. Initially, sandwich panels were non-composite, comprising a thick structural wythe, an insulation layer, and a non-structural wythe. The introduction of composite sandwich panels represented a key innovation in this technology (Losch et al., 2011). As composite external wall systems, PCSPs integrate two to three wythes with thermal insulation layers, functioning as both thermal barriers and inner walls (Ang Soon Ern et al., 2017). Traditionally utilised in low-rise structures, these panels are now being incorporated into a wider range of building types, including high-rise developments (O'Hegarty and Kinnane, 2020). Nevertheless, challenges such as seismic concerns have hindered their broader adoption. Interestingly, countries like Japan and New Zealand, which regularly contend with seismic activity, remain major users of this system (Lee, 2016, Cao et al., 2015).

The robust nature of concrete renders PCSPs superior to many conventional building systems. They are scalable for mass production, allowing for extensive facade coverage with fewer connections (Frankl et al., 2011). This prefabrication method not only enhances a building's thermal performance but also ensures consistent quality and minimises on-site construction errors (Kim and Allard, 2014, O'Hegarty et al., 2020). Typically reinforced with steel, PCSPs are characterised by their considerable wall thickness and weight (Losch et al., 2011). Recent research has focused on developing slimmer sections without compromising the panels' structural integrity and thermal properties (O'Hegarty and Kinnane, 2020).

PCSPs are highly efficient, offering both structural and thermal benefits, including a reduction in energy costs of approximately 20% (Geeta et al., 2013). Beyond thermal advantages, they provide strength, sound insulation, safety, and cost-effectiveness compared to traditional construction methods (Ang Soon Ern et al., 2017). Their numerous benefits include durability, cost-efficiency, fire resistance, and versatility in terms of relocation and expansion (O'Hegarty et al., 2021).

In many countries, the evolution of prefabricated building technologies has been deeply rooted in precast technologies. This approach involves manufacturing building components off-site and assembling them on-site, thereby improving efficiency and minimising waste. Although the term "prefab" encompasses other materials such as steel and wood, the precast method most accurately represents the concept in the context of concrete structures (Figure 3.4).

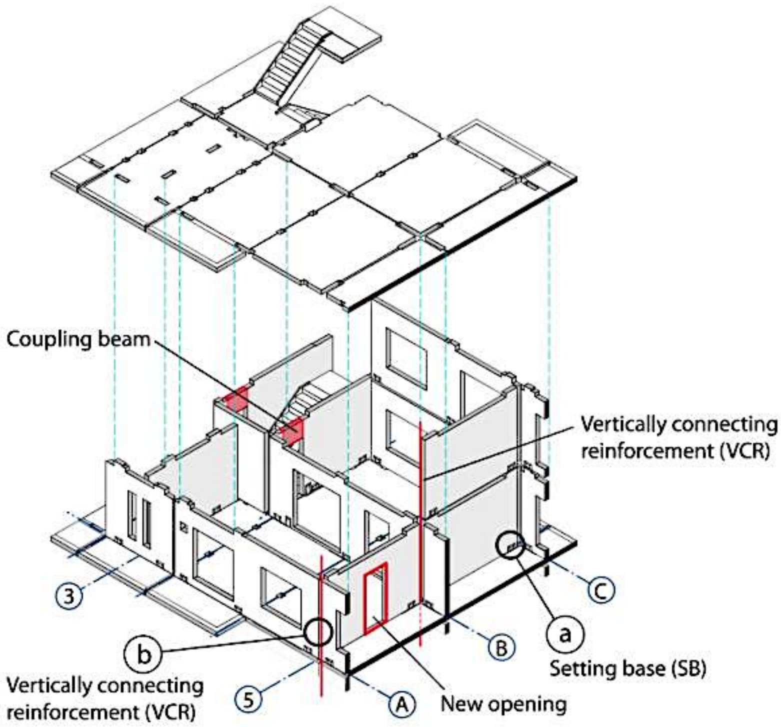

Figure 3.4: Precast element of a precast concrete building. Source: Takagi et al. (2012).

3.6 PRECAST CONCRETE SANDWICH PANELS IN MODERN CONSTRUCTION

Since the 1950s, precast concrete sandwich panels (PCSPs) have been adopted within the building sector ((Losch et al., 2011). The original design of PCSPs consisted of two wythes connected by concrete ribs. Over time, these continuous ribs were replaced with solid square concrete zones to reduce the volume of concrete permeating the insulating layer, while still facilitating the transfer of lateral shear stresses between the wythes (Gleich, 2007). Subsequently, steel trusses were introduced to further minimise material intrusion into the insulating layer. However, these trusses exhibited significant thermal bridging due to the high thermal conductivity of the steel connections as claimed by O'Hegarty and Kinnane (2020).

The 1980s marked a shift towards the use of thinner steel ties, which improved thermal performance by reducing the amount of steel but still allowed notable heat loss and compromised the panel’s structural integrity (Lee and Pessiki, 2008b). The introduction of fibre-reinforced polymer (FRP) connectors as replacements for metal connectors represented a pivotal innovation for the industry. FRP connectors, with their significantly lower thermal conductivity compared to steel, transmit less heat across the insulating layer and are now widely used (Keenehan et al., 2012).

Recent research has focused on reducing the total thickness of panels, employing high-performance insulation materials or textile-reinforced concrete to maintain both structural and thermal efficiency (Richard et al., 2019, Shams et al., 2014, O'Hegarty et al., 2021).

Precast concrete sandwich panels are integral to a wide range of structural applications, including residential buildings, offices, educational establishments, storage facilities, industrial complexes, and healthcare institutions. Renowned for their durability, cost-effectiveness, and environmentally friendly attributes, these panels, while predominantly employed as external walls, have also been adapted for internal applications such as partition walls, particularly in temperature-controlled environments. Additionally, these panels exhibit significant versatility in architectural applications. Treatments typically associated with standard architectural panels can be applied to the outer 'wythe' of the precast system, enhancing the aesthetic appeal of precast constructions (Losch et al., 2011). This adaptability underscores the multifaceted utility of precast concrete sandwich panels, demonstrating their substantial value in meeting a diverse array of architectural and construction requirements (Sah et al., 2024).

3.7 FABRICATION TECHNIQUES OF PRECAST CONCRETE SANDWICH PANELS

As described by O'Hegarty and Kinnane (2020), the standard fabrication process for precast concrete sandwich panels begins with the assembly of formwork, irrespective of the specific panel type or the nature of the precast facility. Following site preparation, reinforcing steel is placed, and the first concrete layer is poured. For prestressed concrete panels, strands are arranged and prestressed either before or after the concrete pour. Connectors and insulation are then installed according to technical specifications, followed by the addition of a second layer of steel reinforcement above the insulation. The final concrete layer is subsequently poured. The exposed concrete surface can be finished in various ways, ranging from smooth finishes achieved with trowels to textured finishes created with brushes, while the base surface retains a smooth formwork finish. Once cured, the panels are removed, placed upright, and extracted from the formwork for storage until they are transported to the site.

Over recent decades, significant industry advancements have sought to enhance production speed. Precast facilities frequently use rapid-mixture cement to accelerate strength development within 12 to 24 hours. Heat curing is commonly employed to further expedite early strength gain. For PCSPs, it is essential to cap the maximum curing temperature to prevent differential volume changes between the insulation and concrete layers (Losch et al., 2011). O'Hegarty and Kinnane (2020) also discussed an innovative casting technique involving an initial cast with connectors, followed by tilting and immersion into a second fresh concrete layer. While this method provides dual formwork surface finishes, it necessitates specialised machinery, extends curing times, and limits flexibility in finishing and shaping. The following sections explore various production techniques and finishes employed in PCSP fabrication.

3.7.1 METHODS OF CASTING SANDWICH PANELS

Wet-cast sandwich panels are manufactured using extensive steel formwork with intervening bulkheads. The process begins with the placement of the bottom-wythe strand, reinforcement steel, and other essential components. The initial concrete layer is then compacted using vibratory methods, including spud vibrators and vibrating drop screeds. Insulation is subsequently introduced, with wythe ties employed to connect the two concrete layers. To ensure the accurate placement and finishing of the final concrete layer, measures such as the use of rebar slugs are implemented to minimise insulation displacement during vibration. Furthermore, during these initial stages, some manufacturers may choose to stress both the upper and lower strands.

In contrast, dry-cast refers to a production method involving the use of non-slumping concrete. This technique relies heavily on machinery, particularly extruders for dry mixes. Initially developed for the production of hollow-core slabs, this method has been adapted to facilitate the manufacture of sandwich panels using the same concrete type.

Lastly, machine casting encompasses a suite of technologies designed to enhance panel quality and cost-effectiveness. These techniques provide manufacturers with the flexibility to select either wet-cast or dry-cast methods, depending on specific project requirements.

3.7.2 MATERIALS AND FINISHING TECHNIQUES FOR PRECAST CONCRETE PANELS

Precast panels are primarily composed of elements commonly utilised in the precast concrete production industry, including structural concrete, reinforcing bars, weld-wire reinforcement, steel embedment, and prestressing strands. A distinctive feature of sandwich panels is the incorporation of insulating materials in various forms, alongside a range of wythe connections. Sandwich panels can be produced with a diverse array of finishes, determined by design specifications, casting methods, and budgetary constraints.

The base layer of the sandwich panel, typically moulded in steel or wooden formwork, generally provides a smooth finish that is suitable for both internal and external applications. This finish can be further enhanced with coatings such as paint or varnish. Additionally, form liners may be used to achieve textured finishes. By contrast, the top layer can be treated to achieve a variety of finishes, applied either manually or through advanced technological processes. These finishes include rake, rolled, imprinted, broomed, or hard steel trowelled surfaces.

Due to the broad spectrum of consumer preferences and the significant investments made by manufacturers in developing specialised finishes, not all manufacturers provide the same finish options. Consequently, it is essential for designers to liaise with local manufacturers to ascertain the costs associated with each finish, particularly as the selection of non-standard finishes can substantially increase panel costs (Losch et al., 2011).

The appeal of precast concrete sandwich panels continues to grow among architects due to the precision and consistency they offer. Similar to single-layer concrete, sandwich panels can undergo a variety of surface treatments, applied either to freshly poured or hardened concrete. These treatments include water washing, brushing, sand casting, and others, as illustrated in Figure 3.5. O'Hegarty and Kinnane (2020) highlight that refining processes such as polishing produce a glossy finish by removing coarse particles, while the use of finer abrasives results in an even smoother texture.

Techniques such as acid etching, which imparts a textured effect by treating concrete with diluted acid, and sandblasting, which provides a deeper surface finish, are now performed with improved precision.

Moreover, setting materials like stone, ceramics, or brick into the mould prior to overlaying it with concrete enables the creation of prefabricated panels with veneers. This innovative approach exemplifies the evolving nature of finishing techniques for concrete panels, reflecting the advancements that continue to enhance their functionality and aesthetic appeal in architectural applications.

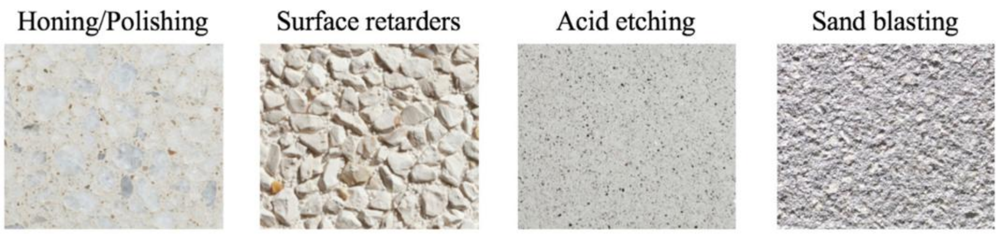

Figure 3.5: Illustrating different precast panels' surface finishes. Source: O'Hegarty and Kinnane (2020)

3.8 SANDWICH PANELS DIMENSIONAL CONSTRAINTS AND HANDLING PROTOCOLS

The dimensions of sandwich panels are determined by project specifications, form size, handling equipment capabilities, transportation constraints, worksite limitations, and design considerations. With ongoing advancements in manufacturing and finishing techniques for precast concrete sandwich panels (PCSPs), recent academic research has increasingly focused on reducing their size and weight. The shift towards lighter and thinner PCSPs brings advantages in shipping and installation processes. For example, certain regions in the United States permit the transport of panels up to 3.7 metres wide without requiring an escort, while others impose a maximum width limit of 3 metres. Remarkably, panels measuring up to 4.6 metres in width and 23 metres in length have been successfully manufactured and transported (Losch et al., 2011, Woltman et al., 2017).

The handling of sandwich panels necessitates strict adherence to design specifications. According to O'Hegarty and Kinnane (2020), standard lifting tools such as vacuum lifts are indispensable for back-stripping, with edge-picking designated for panels on tilt tables. Side-clamp mechanisms are suitable for narrower panels, which are transported on their edges. Proper care during handling is essential to prevent damage, as depicted in Figure 3.6, since neglect may necessitate extensive repairs or complete panel replacement. Furthermore, O'Hegarty and Kinnane (2020) highlight the importance of a bolt size of at least 19 mm for handling precast panels, underscoring the need to adhere to specific thickness standards alongside other design requirements.

Figure 3.6: PCSP damage during transport. Source: O'Hegarty and Kinnane (2020).

3.9 SANDWICH PANELS CLASSIFICATIONS

Precast concrete sandwich panels are known by various names, such as insulated precast concrete panels, sandwich walls, sandwich elements, prefabricated precast insulated walls, and others. A myriad of options is available, with choices in materials, dimensions, and scales often dictated by project or client specifications. Much academic attention on sandwich panels revolves around the structural assessment of emerging panel designs to ensure compliance with design standards. Central to these evaluations are investigations into the panels' flexural strength, shear capacity, and the extent to which concrete layers share loads (termed composite or non-composite behaviour).

Certain panels are explicitly crafted to bear the static loads of structures above them. Given the elevated load-bearing demands of these panels, there is an increasing emphasis on innovative designs capable of accommodating varying load intensities.

This makes the exploration of new design approaches and testing methods a continual area of research. In addition to structural considerations, research also examines the thermal efficiency of PCSPs, particularly with regard to heat loss.

3.9.1 COMPOSITE AND NON-COMPOSITE PANELS

Composite precast concrete sandwich panels (PCSPs) are designed for integrated structural behaviour, capitalising on the collective strength of both concrete wythes against bending forces and behaving as a unified unit. In composite panels, the two concrete wythes work in tandem under applied loads, with shear transmission fully shared between the wythes.

In contrast, non-composite PCSPs feature independent load-bearing by each wythe. These panels are constructed with the understanding that the two wythes function separately. Typically, non-composite panels consist of two types of wythes: structural and non-structural, with the latter usually being thicker. During the design phase of non-composite panels, each wythe is treated distinctly, focusing on its unique attributes. Calculating the bending moment capacity—the maximum bending moment a section can withstand before failing—requires consideration of the specific bending stiffness of each wythe individually. Conversely, in fully composite panels, the wythes collaborate to resist bending forces. This behaviour depends on the connectors' ability to transfer horizontal forces effectively between the wythes. Consequently, many practical PCSPs exhibit behaviours that fall between entirely composite and non-composite systems(Sah et al., 2024).

3.9.2 PARTIALLY COMPOSITE

Sandwich panels that are only partially composite include shear ties connecting the wythes; however, these connections do not produce complete composite action within the panel. Such sandwich panels exhibit bending stiffnesses and strengths that lie between those of fully composite sandwich panels and non-composite sandwich panels, respectively (Losch et al., 2011).

3.9.3 LOAD BEARING AND NON-LOAD BEARING PANELS

Loadbearing precast concrete sandwich panels (PCSPs) are designed to support the weight of walls and/or floors situated above them. As illustrated in Figures 3.7-a and 3.7-b, this weight is vertically transferred towards the foundation. In contrast, non-loadbearing PCSPs, depicted in Figure 3.7-c, do not bear the weight of other structural components within the building. Their slimmer profile arises from their non-loadbearing nature, making them lighter compared to their loadbearing counterparts. Typically, these panels are supported at each floor level via a supporting structure positioned at either the top or bottom of the panel. This structure directs the panel's self-weight to the main structure. Additionally, a restraint at the panel's opposing end ensures stability, functioning similarly to a beam supported from floor to floor (O'Hegarty and Kinnane, 2020).

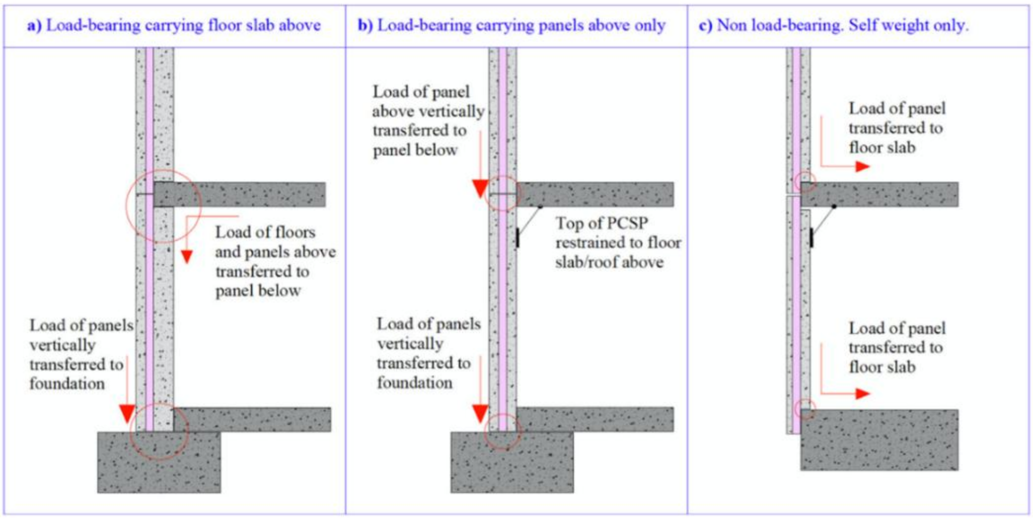

Figure 3.7: Section illustrating examples of loadbearing and non-loadbearing precast concrete sandwich panel. Source: O'Hegarty and Kinnane (2020).

3.10 CONTEMPORARY SYSTEMS AND MATERIALS IN PRECAST CONCRETE WYTHES OF SANDWICH PANELS

Concrete wythes, constituting the internal and external façades of a wall, play a critical role as structural elements of the wall system. According to Lee and Pessiki (2004, 2006), some designs for PCSPs incorporate three wythes. However, the more common design incorporates two concrete wythes, as illustrated in Figure 3.8. For uniformity, both wythes typically use the same type of concrete. Various forms of concrete are used in the production of PCSPs, including normal concrete, foamed concrete, self-compacting concrete, high-performance concrete (HPC), glass-reinforced concrete (GRC), and ultra-high-performance concrete (UHPC). It is imperative to apply a concrete overlay to both reinforced and prestressed concrete, protecting embedded steel components from corrosion. The majority of bearing-wall PCSPs are constructed from prestressed concrete (Frankl et al., 2008, 2011; Hassan and Rizkalla, 2010; Lee and Pessiki, 2008a).

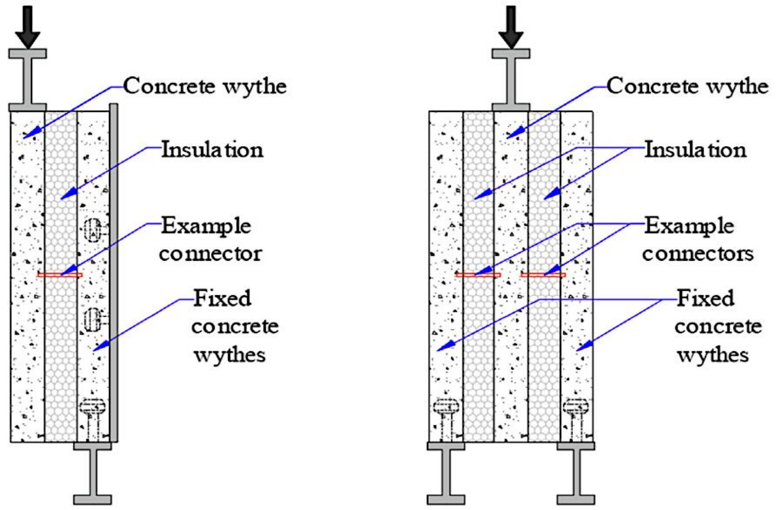

Figure 3.8: Section illustrating examples of typical two and three wythes PCSP systems. Source: O'Hegarty and Kinnane (2020).

In addressing issues of corrosion, various studies have proposed the use of non-corrosive textile-reinforced concrete (TRC) for the wythes in sandwich panel designs. A variety of textile types have been evaluated in PCSP research, each highlighting beneficial properties. For instance, although carbon fibre is more expensive, its strength surpasses that of alkali-resistant (AR) glass fibre. Williams Portal et al. (2017) integrated HPC with an epoxy-coated carbon textile grid in a PCSP. Horstmann and Hegger (2011) utilised TRC wythes reinforced with a carbon fibre-reinforced polymer (CFRP) mesh, while Shams et al. (2015) employed CFRP pre-tensioned tendons in their high-performance PCSP. Among other concrete types used are GRC (Hegger et al., 2008; Choi et al., 2015; Enfedaque et al., 2011), geopolymer concrete (Hyde and Kinnane, 2016; Hyde et al., 2017), and phase change material (PCM) concrete (Niall et al., 2016; Niall et al., 2017). Notably, Shams et al. (2015) highlighted the use of UHPC in a curved PCSP design with impressive strength, and Lee et al. (2018) demonstrated similar strength using UHPC in a PCSP.

3.10.1 CELLULAR CONCRETE

Cellular concrete encompasses both aerated and foamed concrete variants, each designed for specific construction applications due to their intrinsic characteristics, as illustrated in Figure 3.9. Foamed concrete (FC) is a comparatively recent addition to the construction domain compared to conventional concrete. It is distinctively composed, integrating not only standard concrete components but also a foaming agent, compressed air, ultra-fine materials, and specialised chemical additives (Ang Soon Ern et al., 2017). Due to its adaptability, FC is increasingly employed as an insulation layer in diverse construction undertakings (Portal et al., 2017). Its properties, such as mechanical and thermal attributes, can be tailored to fit particular requirements, with a noteworthy correlation between its compressive strength and density, predominantly governed by the air content (Flansbjer et al., 2018).

On the other hand, aerated concrete achieves its porous nature through a chemical reaction between cement and aluminium powder, which acts as a gas-forming agent. This process results in a sustained porous structure, even after solidification. Such porosity endows the concrete with lightweight properties and durability, enhancing its thermal retention capabilities and making it more robust compared to other forms of concrete.

In terms of production costs, aerated concrete tends to be more expensive than FC, despite FC's higher material expenditure. For perspective, a wall constructed of aerated concrete with a density of 600 kg/m^3 can exhibit comparable strength and thermal qualities at a reduced thickness. Furthermore, Adilkhodjaev et al. (2021) conducted a study to evaluate techniques for optimising the pore structure of aerated concrete, specifically for external walls. Their investigation into the physical, mechanical, and thermal characteristics of walls made from cellular concrete determined the optimal porosity values. The research highlighted the potential of aerated concrete to reduce energy consumption throughout a building's lifespan.

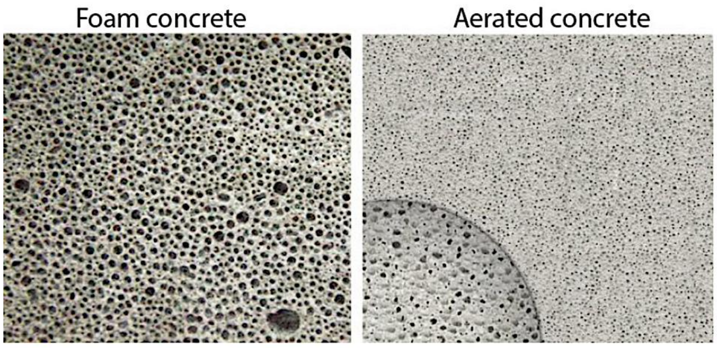

Figure 3.9: Microsections of foamed concrete (left) and aerated concrete. Source: Techcon (2020).

3.10.2 AEROGEL-ENHANCED FOAM CONCRETE

Recent research highlights aerogel as a remarkable insulating material (Chen et al., 2022). Consequently, the integration of aerogel into traditional foamed concrete has given rise to a new class of high-performance construction materials, with their thermal properties, resilience, and strength being subjects of comprehensive investigation. Notably, the effect of humidity on the thermal conductivity of these aerogel-incorporated materials is found to surpass that of temperature (Liu et al., 2022).

In an innovative endeavour, Yoon et al. (2020) aimed to enhance both thermal conductivity and moisture resistance by combining aerogel technology with standard foamed concrete. This amalgamation involved the inclusion of a supremely insulating, hydrophobic aerogel with nanoscale voids distributed evenly within the porous structure of the foamed concrete. A noteworthy outcome of this experiment was the thermal conductivity of the aerogel-enhanced foamed concrete, recorded at just 0.08 W/m·K, signifying substantial improvement in its water resistance.

Building upon this foundational research, Liu et al. (2022) explored the implications of the thermal and moisture transfer properties of aerogel-integrated foamed concrete precast wall panels on a building's energy consumption. They selected Shanghai and Beijing as representative cities for hot-summer-cold-winter and cold climates, respectively. Their research involved the development and validation of a mathematical model, focusing solely on temperature and relative humidity as the driving factors. Notably absent from the study was an investigation into air infiltration and the effect of temperature on the wall's equilibrium moisture content.

The comparative analysis revealed significant differences in energy consumption due to solar radiation. Specifically, the variation in cooling load in Shanghai exceeded 55%, while in Beijing it escalated to 62.4%. Conversely, the disparity in heating load between the two locations was minimal, at approximately 9%. The overarching conclusion from these findings underscores the remarkable insulating capability of aerogel in construction applications.

3.11 THERMAL INSULATION MATERIALS IN PRECAST CONCRETE SANDWICH PANELS

Concrete is primarily responsible for the structural and durable properties of the prefabricated wall panel. However, its thermal resistance capabilities emerge from the integration of insulation materials. Within the scope of PCSPs, this study provides an overview of the diverse insulation types cited in existing literature. Various studies, such as those by Asdrubali et al. (2015) and Schiavoni et al. (2016), have conducted comprehensive analyses of insulating materials used in buildings, illustrating that the thermal properties of these materials can differ substantially.

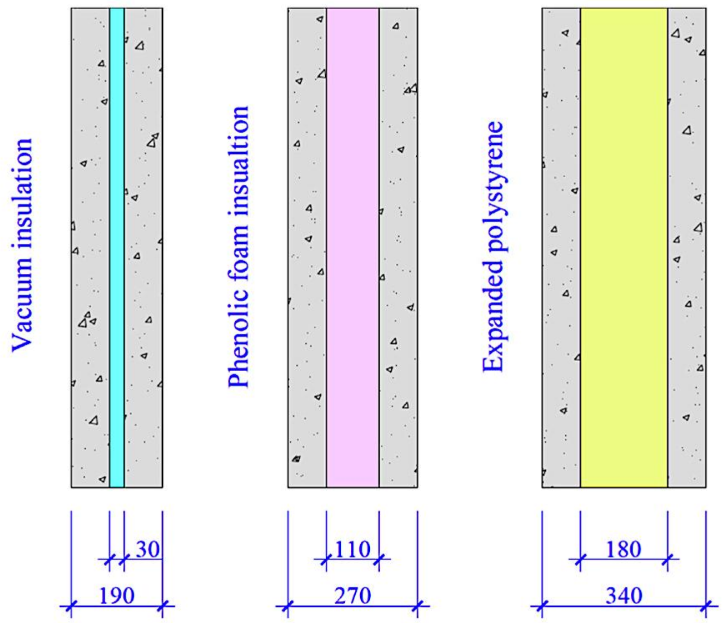

Figure 3.10: Section illustrating examples of insulation thickness for a PCSP using different materials. Source: O'Hegarty and Kinnane (2020).

There are numerous insulation materials available in the current market. Nevertheless, cellular (rigid) insulation is favoured for sandwich panels due to its compatibility with the intrinsic properties of concrete (Woltman et al., 2017). Such compatibility is characterised by factors such as moisture absorption, dimensional stability, coefficient of expansion, and compressive and flexural strengths. The selection of insulation material to enhance energy efficiency is as crucial as reinforcing it to augment structural performance. Factors such as geographic location, climate, and operational conditions can influence the choice of insulation, potentially affecting the anticipated efficiency and longevity of the panel (Sah et al., 2024).

Several common thermal rigid insulation materials are in use, namely expanded polystyrene (EPS), extruded polystyrene (XPS), polyurethane (PUR), and polyisocyanurate foam (PIR) – the latter being regarded as a slight advancement over PUR. Phenolic foam is another widely used option. Continuous research in this area has led to the exploration and innovation of insulation materials. Notable examples include the growing popularity of vacuum insulation panels (VIPs) and foamed concrete (FC), both presenting compelling alternatives as insulation materials. Figure 3.10 illustrates the thickness variations among these insulation materials, demonstrating that high-efficiency insulation enables thinner designs without sacrificing thermal performance. Additionally, Table 3.1 provides an overview of various insulation types used in precast panels, highlighting their distinct properties as outlined by O'Hegarty and Kinnane (2020).

Table 3.1: Overview of various insulation materials used in precast panels and their respective properties. Source: O'Hegarty and Kinnane (2020).

Reference	Date	U ($W.m^{-2} \bullet K^{-1}$)	Total panel thickness (mm)	Insulation Type	Thickness (mm)
Hodicky et al.	2013	0.08	330	PF	290
O'Hegarty et al.	2019	0.09	150	PF + VIP	90
Hegger et al.	2009	0.16	180	PUR	150
Shams et al.	2015	0.2	280	EPS	160
Shams et al.	2014	0.2	260	EPS	160
Teixeira et al.	2016	0.22	270	EPS	150
Tomlinson & Fam	2015	0.22	270	EPS	150
Frankl et al.	2008	0.31	255	EPS	102
Chen et al.	2015	0.31	254	EPS	102
Portal et al.	2017	0.31	230	FC	150
Choi et al	2015	0.31	260	EPS	100
Flansbjer	2018	0.31	200	FC	150
Choi et al	2015	0.31	220	EPS	100
Kim and You	2015	0.31	220	EPS	100
Hopkins et al.	2017	0.31	254	EPS	102
Frankl et al.	2011	0.32	200	EPS	100
Joseph et al.	2018	0.32	150	EPS	100
Colombo et al.	2015	0.32	120	EPS	100
Enfedaque et al.	2011	0.35	110	EPS	90
Al-Rubaye et al.	2017	0.41	280	XPS	76
Bush and Stine	1994	0.57	203	EPS	51
Pessiki and Mlynakrzyk	2003	0.57	203	EPS	51
Benayoune et al.	2006	0.7	121	EPS	41
Amran et al.	2016	0.89	150	EPS	30
Amran et al.	2016	1.04	125	EPS	25
Lee et al.	2018	3.55	65	EPS-concrete	55

3.11.1 MINERAL WOOL

Mineral wool, depending on its specific variety, has a thermal conductivity ranging from 0.03 to 0.04 W/m·K. This positions its thermal performance close to that of conventional foam-based insulations (Bagarić et al., 2020). A distinct challenge with mineral wool, however, is its lack of rigidity. Load transfer between the concrete wythes relies solely on the connecting elements. This limitation means that traditional fabrication methods, which involve pouring an additional layer directly onto the insulation, may not be suitable. Consequently, more substantial and robust connectors are required to bridge the two concrete wythes, which can result in pronounced thermal bridges (Bagarić et al., 2020).

Correia et al. (2006) incorporated both mineral wool and EPS into their panel configuration but used 10 mm thick concrete ribs to link the two wythes. Despite these challenges, mineral wool offers an economic advantage and demonstrates superior fire resistance compared to some alternatives (Schiavoni et al., 2016). Given certain authorities' restrictions on the use of flammable materials, wool-based products are expected to shape the future of the precast panel industry, particularly in warmer climates.

3.11.2 PHENOLIC FOAM

Phenolic foams have a density range of 35 kg/m³ to 200 kg/m³ and exhibit thermal conductivities varying from 0.018 W/m·K to 0.023 W/m·K. With an exceptionally low thermal conductivity of 0.018 W/m·K, phenolic insulation is regarded as offering the highest thermal performance among insulation boards currently available on the market. Compared to rigid polyurethane or extruded alternatives, phenolic foam's remarkably low thermal conductivity makes it approximately 50% more efficient than many conventional insulation materials (O'Hegarty et al., 2021).

3.11.3 VACUUM INSULATION PANELS

Vacuum insulated panels (VIPs) exhibit thermal conductivities 5 to 8 times lower than those of traditional thermal insulation materials (Ciobanu and Iacob, 2013). This characteristic makes them a particularly compelling choice in situations where overall wall thickness is constrained. As described by Johansson (2012), VIPs typically consist of a rigid core, often made of fumed silica, which is evacuated and hermetically sealed within a wrapper, frequently crafted from aluminium foil.

In recent years, the adoption of VIPs in PCSP design and construction has increased, reflecting the growing trend of minimising both wall thickness and U-value (Ribeiro, 2024). While VIPs boast significantly lower thermal conductivities compared to conventional insulating materials, their brittle nature makes them susceptible to damage. Such damage can reduce their insulative performance by around a third (Hülsmeier, 2014).

To mitigate this vulnerability, Voellinger et al. (2014) advocate for incorporating a composite insulation layer that encapsulates the VIPs within solid foam insulation, thereby shielding them from potential harm. Aligning with this recommendation, several industry leaders in the precast concrete sector, including the UK's Kingspan, have introduced products featuring PIR foam-protected VIPs, primarily targeting roofing and flooring applications, as documented by O'Hegarty and Kinnane (2020).

3.12 WYTHES CONNECTORS

Wythe connectors in PCSPs play a pivotal role in addressing multiple structural challenges. These connections, when horizontally stripped from their form, must support the tensile stresses arising from the bottom wythe's weight and any applied pressure. Additionally, they counteract out-of-plane forces such as wind suction and, where applicable, seismic pressures. The primary function of wythe connectors in a PCSP is to link the insulating layer with the concrete one, enabling lateral shear stress transfer between them and fostering composite action. The effectiveness of this action varies depending on the connector type (Fahmy et al., 2024).

Earlier PCSP designs used cast-concrete connectors, but modern panels tend to favour metal and plastic ties. Every connector forms a thermal bridge across the insulating layer, with its impact depending on the connector's characteristics. Balancing structural shear transfer and thermal bridge reduction remains a challenge, prompting extensive academic scrutiny (O'Hegarty and Kinnane, 2020). Manufacturers typically supply data on tensile and shear capacities for specific embedment depths, with some also providing stiffness ratings to guide design specialists. Figures 3.11 and 3.12 illustrate various shear connectors.

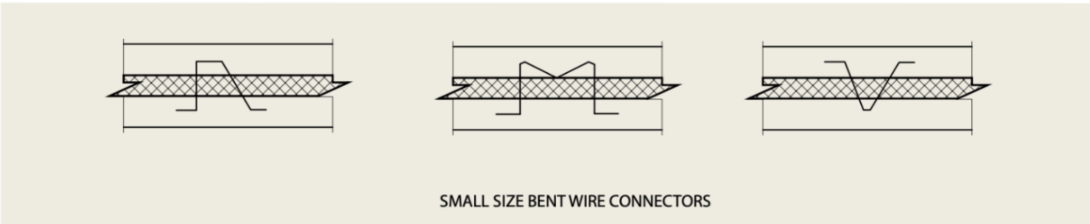

Figure 3.11: One-way shear connectors. Source: Losch et al. (2011).

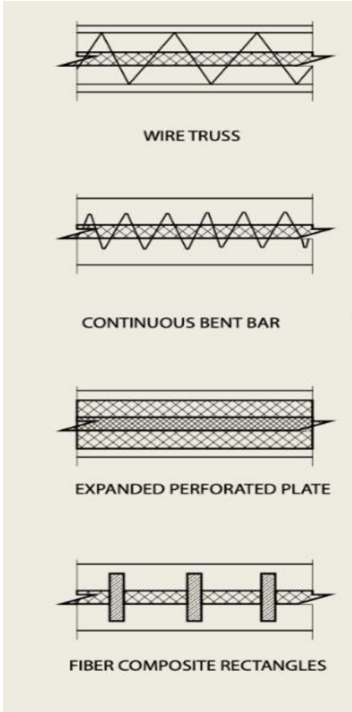

Figure 3.12: One-way shear connectors. Source: Losch et al. (2011).

3.12.1 CONCRETE CONNECTORS

Precast concrete typically consists of two layers, interconnected by concrete ribs or specific areas where concrete transversely penetrates the insulating layer. Joseph et al. (2018) conducted an experiment incorporating continuous concrete sections at both the top and bottom edges of the panels and around the panel's perimeter. However, such concrete connections introduce significant thermal bridges, diminishing the thermal resistance of the PCSP. Lee and Pessiki (2008a, 2006) also examined PCSPs with three wythes, incorporating varying insulation levels and concrete areas. Yet, these three-wythe designs complicate fabrication and do not significantly enhance the system's overall thermal performance (O'Hegarty and Kinnane, 2020). Refer to Figure 3.13.

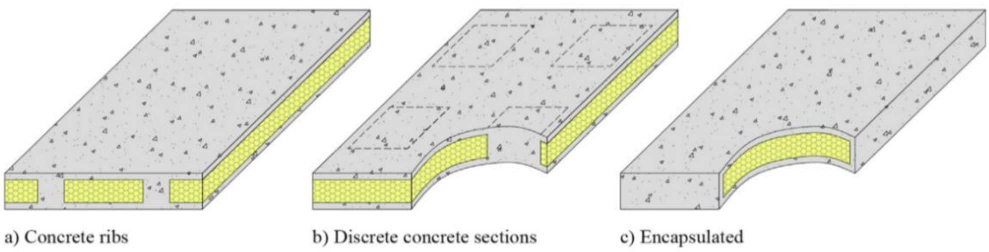

Figure 3.13: Example of concrete connections. Source: O'Hegarty and Kinnane (2020).

3.12.2 METALLIC CONNECTORS

To enhance the thermal performance of concrete connections, metallic connectors are often employed, reducing the amount of insulation "bridged" by the connection. Depending on whether composite action is required, these connectors can be designed as a truss, tube, or plate (Bush and Stine, 1994; Tomlinson and Fam, 2015; Mugahed Amran et al., 2016; Daniel Ronald Joseph et al., 2018; Salmon et al., 1997; Losch et al., 2011), or as discrete pin-type connections when composite action is not required (Pessiki and Mlynarczyk, 2003; Palermo and Trombetti, 2016).

Various industries manufacture metallic connectors, as illustrated in Figure 3.14. Hou et al. (2019) designed a fully composite PCSP with evenly spaced diagonal steel connections. Conversely, Hegger et al. (2009) proposed limiting metallic connections to the panel edges only. However, due to their high thermal conductivities, metallic connections create significant thermal bridges over the insulation layer (Kim and Allard, 2014; Lee and Pessiki, 2006). This has prompted recent research to focus on PCSPs with non-metallic connectors that offer reduced thermal conductivities.

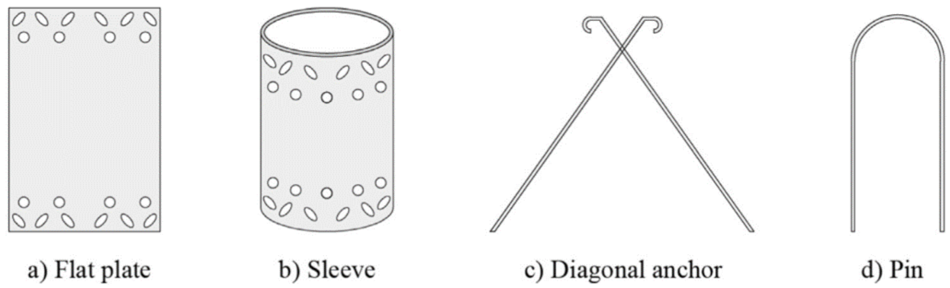

Figure 3.14: Example of typical metallic connectors. Source: O'Hegarty and Kinnane (2020).

3.12.3 FIBRE REINFORCEMENT CONNECTORS

Fibre-reinforced polymer (FRP) represents a category of composite materials composed of a polymer matrix reinforced with fibres. These materials offer varied and versatile properties, significantly enhancing the thermal performance of concrete connections by minimising the formation of thermal bridges (O'Hegarty and Kinnane, 2020; O'Hegarty et al., 2021; Huang et al., 2022).

Among these, carbon fibre-reinforced polymers (CFRP) are manufactured with carbon fibres to achieve a high carbon content of over 90% (Portal, 2013). Glass fibre-reinforced polymers (GFRP) incorporate fibres derived from silica sand, augmented with zircon to improve alkali resistance and enhance durability (Jawdhari et al., 2022). Basalt fibre-reinforced polymers (BFRP) use fibres derived from basalt minerals. A notable advantage of BFRP is the absence of additives in their production, simplifying manufacturing and resulting in cost savings (Tomlinson, 2015).

Huang et al. (2022) emphasised the thermal efficiency of FRP tube connectors, employing two types of GFRP connections in PCSP specimens. Their research demonstrated that such FRP connectors effectively mitigate thermal bridging, enhancing the panels' fire resistance. Furthermore, Lameiras et al. (2021) introduced an innovative sandwich panel design that utilised FRP connections to eliminate thermal bridging. The design incorporated steel fibre-reinforced self-compacting concrete (SFRSCC) layers, connected by novel GFRP connectors.

3.13 THERMAL CONSIDERATIONS IN PRECAST CONCRETE SANDWICH PANELS

Over the past three decades, advancements in insulating technologies have aimed to reduce or eliminate solid concrete zones and steel connections. The choice of insulation materials for sandwich panels should take into account the local climate, structural performance requirements, and the implications of building regulations. While PCSPs must bear any applied load, this can often be achieved with a single reinforced concrete wythe. What distinguishes PCSPs from traditional reinforced concrete walls is the inclusion of an insulation layer, providing essential thermal resistance. Much of the existing research has focused on the structural attributes of PCSPs; however, experimental thermal testing has been less explored (Kim and Allard, 2014, Lee and Pessiki, 2008b, Voellinger et al., 2014, Woltman et al., 2017, Lee and Pessiki, 2004, Zhai et al., 2018). In this context, it is noteworthy to mention O'Hegarty and Kinnane (2020), who argue that, when accounting for thermal bridging connections, effective U-values can represent up to 70% of heat loss in a highly insulated precast concrete sandwich panel.

3.13.1 THERMAL PERFORMANCE AND BRIDGING IN PCSPS

The thermal transmission within a sandwich panel's insulation is often considered its most critical attribute. The insulation system's capacity to hinder thermal energy transfer directly influences the panel's resistance to energy flow across its thickness. This resistance is pivotal in defining its effectiveness as a thermal barrier. There is a considerable push to bolster energy efficiency and curtail heat loss within buildings. PCSPs stand out from many alternative panelling systems due to their ability to achieve superior thermal resistance.

In Europe, thermal effectiveness is typically assessed using thermal transmittance or U-value, while the United States employs thermal resistance, termed R-value. This distinction is determined by Equation (3.1), where 't_c' and 't_i' correspond to the thicknesses of the concrete and insulation layers, respectively, in line with ISO (2007):

$$\frac{\mathbf{1}}{\mathbf{U}} = \boldsymbol{R_{se}} + \frac{\boldsymbol{t_c}}{\boldsymbol{k_c}} + \frac{\boldsymbol{t_i}}{\boldsymbol{k_i}} + \boldsymbol{R_{si}} \quad \text{......Eq. 3.1}$$

The U-value, a measure of heat transfer across a building component, directly correlates with the extent of heat loss under a specific temperature gradient. Thus, a heightened U-value equates to an increased rate of heat loss when a temperature difference exists.

Geographical locale and its associated climatic conditions significantly dictate building regulations related to U-values. In colder regions, regulations often prescribe lower U-values for construction materials, aimed at diminishing heat loss and elevating energy efficiency and thermal comfort. In contrast, warmer areas tend to have less rigorous specifications, mirroring varied thermal demands due to environmental divergences (Kayello et al., 2017).

Moreover, considering thermal bridging is vital. A thermal bridge refers to a section within a building's insulation layer that facilitates heat transfer, leading to increased heat flux across that zone and potentially compromising the insulation's effectiveness. In PCSPs, these bridges typically occur at intersections between panels. Such points often manifest as weak spots in the insulation, resulting in increased heat flow and reduced thermal efficiency.

The impact of these thermal bridges on the thermal performance of PCSPs depends on several factors, notably the dimensions and composition of the connectors joining the panels. The size and material of these connectors can either amplify or mitigate the thermal bridging effect, significantly influencing the energy efficiency and thermal behaviour of PCSPs. Consequently, larger, thermally conductive connectors, such as steel trusses, result in greater heat loss compared to smaller, less conductive alternatives (O'Hegarty and Kinnane, 2020).

3.13.2 EFFECT OF INSULATION LAYER THICKNESS ON PCSPS

Zhai et al. (2018) investigated the effect of insulation layer thickness on the thermal transmittance of PCSP walls, with insulation thicknesses ranging from 20 to 120 mm in 10 mm increments. The study found that PCSP walls with a greater thermal bridge effect, as shown in Figure 3.15 (e.g., PU-t-Y and PU-t-Y), exhibit a smaller reduction in thermal transmittance as the insulation thickness increases. Regardless of the insulation materials illustrated in the figure, it is evident that significantly increasing the insulation layer thickness becomes ineffective beyond a certain point. This may result in higher material costs without proportional performance benefits.

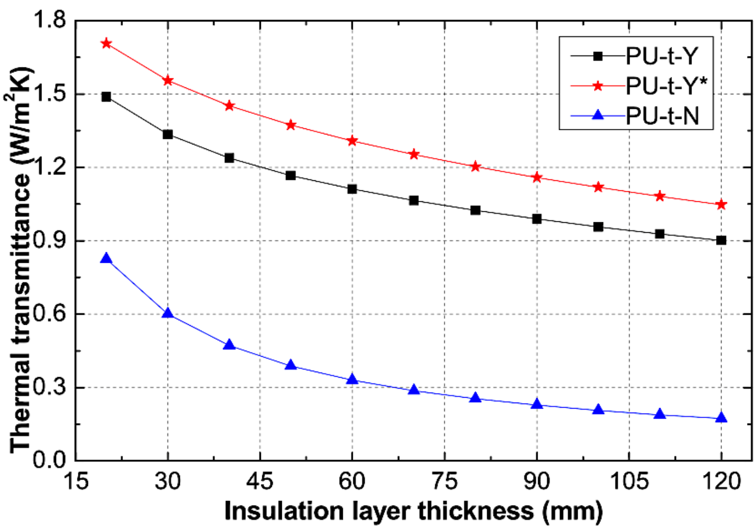

Figure 3.15. Thermal transmittance vs insulation layer thickness. Source: Zhai et al. (2018).

3.13.3 THERMAL PERFORMANCE OF THREE WYTHE SANDWICH PANELS

Lee and Pessiki (2004) explored the thermal performance of precast three-wythe concrete wall panels. They suggested that the three-wythe panel system offers superior thermal performance compared to its two-wythe counterpart. This enhanced performance is attributed to the elongated thermal path across the concrete panels inherent in the three-wythe system. Such a configuration forces heat to traverse a longer distance, thereby improving insulation and thermal performance. This indicates that the length of the thermal path is a critical factor in the system. For two-wythe panels, a similar elongation can be achieved by increasing the panel's thickness (Ahmad et al., 2014).

Moreover, Lee and Pessiki further critiqued the accuracy of the ASHRAE Handbook R-value calculation methods for three-wythe panels, suggesting that alternative calculation approaches, such as FEM-based experimental methods, would yield more accurate R-value estimations (Lee and Pessiki, 2006; Zhai et al., 2018). Contrary to what one might expect, they highlighted that the concrete wythe thickness does not markedly influence the R-value in either two- or three-wythe systems. Instead, the insulation thickness is the key determinant of the total R-value. Additionally, their research indicated that the surface temperature of the three-wythe system closely mirrors the ambient temperature, unlike the two-wythe system. This similarity could be instrumental in reducing surface layer condensation.

Lee and Pessiki (2004) emphasised the profound impact of thermal bridging on the overall thermal performance of a building envelope, particularly in the context of precast concrete sandwich panels. Thermal bridging, often a result of solid concrete zones devoid of insulation, creates direct conduits for heat transfer. This leads to heightened thermal conductivity, compromising the panel's thermal efficiency. These solid regions, crucial for aspects like panel connection, lifting, handling, and attachment to floors and roofs, must be accounted for in thermal performance predictions of prefabricated building components. Such zones can notably influence the thermal efficiency of even three-wythe panels. The disruption of insulation continuity by the presence of solid concrete establishes a thermal bridge, facilitating heat transfer and impacting the system's thermal performance. This underscores the importance of thorough thermal analyses, encompassing potential thermal bridging, to guarantee accurate forecasts and optimal efficiency for precast concrete sandwich panels (Lee and Pessiki, 2004).

3.13.4 PHASE CHANGE MATERIALS IN PREFABRICATED SANDWICH PANELS

Research on materials for their overall behaviour is varied, but studies focusing on the potential to alter thermal performance by integrating high- or low-thermal-mass materials within the building envelope are scant. By combining different materials with existing construction components, significant changes can occur in their thermal behaviour, particularly in terms of temperature absorption and discharge over short periods (Olivieri et al., 2018). Phase change materials (PCMs) have notably transformed the thermal behaviour of concrete materials, enhancing thermal properties in construction components. Their application within building envelopes improves indoor thermal comfort.

Many studies have explored the use of PCMs in the construction sector, particularly in high-temperature regions. These focus on improving indoor thermal comfort, conserving energy, and mitigating temperature fluctuations on building surfaces. However, much of the current research concentrates on integrating PCMs into cement plaster mixtures for facades or in mats, as noted by Sarı et al. (2018) and Tsoka et al. (2020).

Tsoka et al. (2020) presented a multifunctional prefabricated component integrating the building envelope with PCM to increase its thermal mass storage. They found that incorporating latent heat storage components, such as PCMs, into walls can regulate peak cooling loads and benefit indoor temperature control. They used PCMs with melting temperatures of 24°C and 28°C, chosen based on environmental conditions.

Olivieri et al. (2018) also investigated the integration of PCMs in a microencapsulated form into concrete mixtures to enhance thermal efficiency. Commonly, PCMs are added to the inner concrete panel to manage interior surface temperature, thereby improving indoor comfort and energy efficiency.

Marani and Madhkhan (2021) studied multi-layered concrete wall specimens with a PCM layer. Their findings on Polyethylene glycol (PEG600) showed it had a favourable melting temperature for interior comfort in buildings (17–22 °C). However, practical applications of macro-encapsulated PCM in concrete require further design and structural considerations.

Both Soares et al. (2013) and Ascione et al. (2014) researched optimal phase change temperatures for PCMs in the Mediterranean region. They found that a PCM concentration of 20% led to significant energy savings without compromising the mechanical strength of concrete panels.

In conclusion, while PCMs can enhance energy efficiency, their concentration must be carefully balanced against the mechanical strength of building elements. It is also crucial to select the appropriate melting point of PCMs based on climatic conditions. Future research should include a comprehensive cost-effectiveness analysis, assessing durability and performance over extended periods.

3.14 THERMAL DYNAMICS IN PRECAST CONCRETE SYSTEMS

The envelope system is integral to the thermal performance of buildings, influencing both heating and cooling loads. A pragmatic, cross-disciplinary approach to facade design encompasses considerations of the environment, climate, building design, material properties, and functionality, thereby promoting energy efficiency. Particularly, the characteristics of envelope materials are vital for managing heat transfer through external wall systems. In Saudi Arabia's extreme heat, the emphasis is on well-oriented, large windows, where their size, orientation, and glazing properties hold more significance for energy savings and thermal comfort than facade properties.

Utilising design rules and tools early in the design process is essential for evaluating building envelope efficacy, acknowledging that design decisions at various stages influence energy consumption and thermal performance. Climate-driven variations cause heat transfer and thermal exchange shifts at the fabric's external surface, predominantly due to solar radiation's impact on air temperature and subsequent heat exchange forms (Hashim, 1991). The quantity of heat received by fabric elements hinges on their orientation and the extent of external absorption, as substantiated by the sol-air temperature theory (Mostafaeipour et al., 2019).

Subsequent sections will categorise building fabrics, analyse thermal performance in PCS, and delineate a spectrum of values for such systems, demonstrating the multi-layer fabric elements theory. This approach not only clarifies the role of PCS in thermal dynamics but also guides efficient envelope system design amidst Saudi Arabia's climatic challenges.

3.15 THE USE OF MULTI-LAYER BUILDING ELEMENTS

Fabric's primary function can be viewed as a protective barrier against the external environment. However, from a thermal perspective, this becomes more complex. The building envelope can resist external conditions temporarily. If the external temperature is stable, heat will continue to transfer until equilibrium with the surroundings is achieved. Since external conditions shift daily, the fabric can also function to balance heat between day and night, utilising the temperature variations to achieve internal comfort.

Each fabric element can be designed with a time-lag, allowing peak external temperatures to permeate internally when the outside temperatures are at their lowest (Szokolay, 2014). This aids in stabilising temperatures. The desired time of occupation also influences this; spaces for daytime use need a considerable time-lag to temper diurnal temperature shifts. Conversely, spaces for nighttime use require minimal time-lag for cooling post-sunset. Hence, two distinct strategies emerge for responding to external climatic changes. The first involves minimal time delays between building components and the external environment, taking advantage of cooler temperatures post-sunset. The second uses elements with prolonged time-lags, such as thick walls, roof slabs, or insulating layers, to moderate temperature variations.

Gregory et al. (2008) explored how thermal mass affects the performance of various construction materials, considering both the thickness of insulation and its location. They found that using a higher amount of thermal mass, or materials with significant heat capacity, led to reduced temperature differences. This sentiment was supported by Al-Sanea and Zedan (2011), who observed that thermal mass lessens daily temperature fluctuations, causing the interior surfaces to align more closely with the average daily external temperature. Building fabric's thermal strategies often depend on the specific climatic conditions. Numerous studies presented in *Design with Climate* offer guidelines for regions with extreme temperatures. In places experiencing sharp seasonal and daily temperature swings, it is essential to balance both the heat capacity and insulation levels. In conditions marked by extreme seasonal temperatures, insulation's role becomes crucial, ensuring comfort. While precast concrete systems can often function with a single layer of fabric, situations demanding more insulation and thermal mass may require multiple layers, especially in hotter climates where daily temperatures can exceed comfort levels.

3.16 INTERACTION OF THE FABRIC WITH THE HEAT

Different approaches can be utilised for the evaluation of the fabric. Each conducts its own investigation into the structure's fabric, examining (1) the thermal properties of the materials and (2) the thermal properties of the elements (Evans, 1980). The following sections describe these approaches, with a focus on the precast concrete system.

3.17 THERMAL PROPERTIES OF PRECAST CONCRETE SYSTEM’S MATERIALS

In Saudi Arabian precast concrete systems, the primary material of choice is reinforced concrete, although supplementary materials like glass-reinforced concrete (GRC) may be incorporated for added strength. Insulation layers are often integrated as needed. In housing projects, precast concrete systems are frequently employed as load-bearing walls and slabs, a practice commonly observed in the region. This preference is attributed to the controlled quality achieved through prefabrication in specialised factories. The frame system represents the primary alternative in traditional Saudi Arabian housing construction. While historical research has focused on concrete's mechanical properties, recent years have witnessed a growing interest in studying both the thermal conductivity and mechanical characteristics of concrete. This shift is driven by the imperative to conserve energy in the construction sector. In general, materials characterised by low thermal conductivity values (k-values) are recognised as energy-efficient solutions within the building and construction industries (Asadi, 2018).

3.17.1 HEAT BUILD-UP AT EXTERNAL SURFACES

Sol-air temperature is a concise metric that combines the impact of air temperature, solar radiation, orientation, and external absorption on a building. Although typically employed to gain insights into how these factors collectively influence a building's thermal design, in this context, it will be treated as an approximation for external surface conditions. This approach will subsequently guide the selection of pivotal thermal considerations for further examination in the upcoming simulation.

Various equations can be applied to compute the sol-air temperature, with more complex equations offering greater precise results. The Chartered Institution of Building Services Engineers (CIBSE) has formulated a series of equations for determining the sol-air temperature (Butcher, 2006). The sol-air temperature for external surfaces can be expressed by Equation 3.2:

$\mathrm{TSOL} = \mathrm{TDRY} + (\mathrm{ALPHA} * \mathrm{RAD} - \mathrm{EMISS} * \mathrm{RLONG})/\mathrm{HSO}$………………...Eq. 3.2

Where:

TDRY: External dry bulb temperature

ALPHA: External surface absorption coefficient

RAD: Incident solar radiation = sum of direct, ground reflected and sky diffuse solar radiation, as appropriate.

EMISS: External surface emissivity

RLONG: The longwave loss

HSO: External surface heat transfer coefficient

The thermal absorptance, also known as emissivity, of a material is directly proportional to the amount of incident long-wavelength radiation it absorbs. This parameter plays a crucial role in determining long-wavelength radiative exchange across distinct surfaces and, consequently, impacts surface heat balances, both indoors and outdoors. Its values typically range between 0.0 and 1.0, with 1.0 representing "blackbody" conditions.

Conversely, in the material input syntax, the solar absorptance field denotes the fraction of incident solar energy absorbed by the material. Solar radiation encompasses visible, infrared, and ultraviolet wavelengths. This parameter is instrumental in quantifying the amount of incident solar radiation absorbed by various surfaces, influencing surface heat balances. Its values must also fall within the range of 0.0 to 1.0.

Table 3.2: Absorptivity and emissivity of various surfaces. Source: Boltzmann (2021).

Surface material	Absorptivity	Emissivity
Aluminium Foil	0.05	0.05 - 0.04
Aluminium Heavily Oxidized	0.15	0.2 - 0.31
Steel Galvanized New	0.25	0.23 - 0.25
Aluminium paint	0.50	0.67
white/Lime wash	0.12	0.9 - 0.91
Oil paints, all colours	0.20	0.90 - 0.96
Black Body Matt	0.85 - 0.95	1.00
Ordinary black colour	0.85	0.90
Gray colour, light	0.70	0.90
Gray colour, dark	0.40	0.90

Furthermore, sol-air temperatures for the design day, signifying the hot season, were determined using the CIBSE technique. Given the precision of the simulation software in performing these calculations, some locally suitable finishes were considered. Table 3.2 presents an array of potential building finishes, encompassing both absorptivity and emissivity values for different materials and colours. However, as a general guideline, the emissivity values provided are based on a temperature of 85 °C as reported by Boltzmann (2021).

3.17.2 PROPERTIES OF CONCRETE MATERIALS

The thermal conductivity of concrete varies with its density, with a strong correlation between concrete's unit weight and its thermal conductivity, as noted by Sengul et al. (2011) and referenced in Asadi (2018). Normal concrete typically ranges in density from 200 to 2400 kg/m³, but moisture content can affect this ratio. On the other hand, high-density concrete, characterised by densities between 6000 and 6400 kg/m³, is primarily employed in applications such as radiation shielding and counterweights.

The relationship between density and thermal conductivity serves as a foundational principle in designs emphasising the thermal performance of concrete materials. This correlation is illustrated in Figure 3.16, which is based on 185 experimental datasets from various literature sources cited by Asadi (2018). It demonstrates strong correlations for different types of cement mortar and concrete. Asadi (2018) affirms the validity of this connection, which can be used to predict the thermal conductivity of concrete within a density range of 150 to 2350 kg/m³. Furthermore, the thermal conductivity of lightweight concrete falls within the range of 0.2 to 1.9 W/m·K, while that of standard (Normal weight) concrete ranges from 0.6 to 3.3 W/m·K (Asadi, 2018).

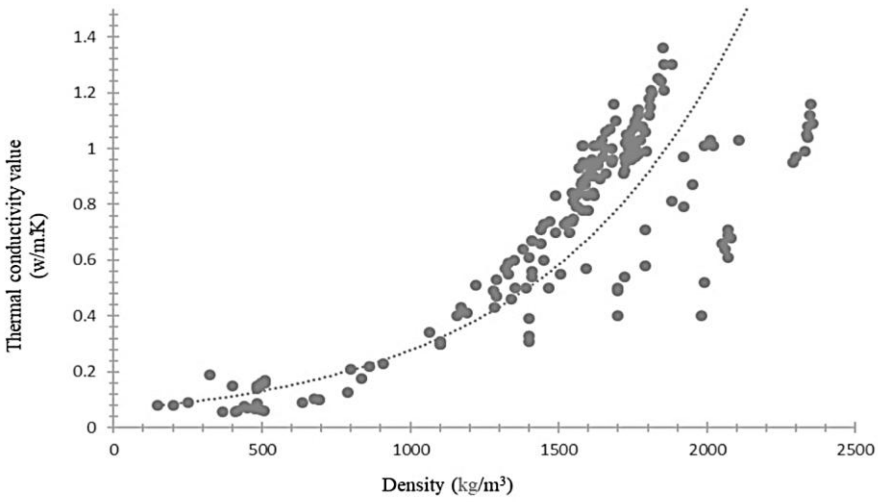

Figure 3.16: General correlation between thermal conductivity and density. Source: Asadi (2018).

The thermal conductivity of concrete can be influenced by various factors, including humidity, temperature, aggregate type, the use of PCMs, concrete mixture composition, and concrete density.

In high-humidity conditions, research has shown that the k-value of cement-based materials is 1.4 to 3 times higher in saturated conditions than in dry conditions, due to water's higher thermal conductivity compared to air. This variation can be attributed to differences in porosity types, sizes, and the water absorption capacities of materials. Additionally, the k-value decreases as the temperature increases, with most studies indicating a 50% reduction in the k-value at 500°C compared to ambient temperature for cement-based materials.

The use of lightweight aggregate and/or foam in concrete results in a decrease in the concrete's thermal conductivity due to increased porosity. A 1% increase in concrete porosity approximately corresponds to a 0.6% reduction in its thermal conductivity. Additionally, concrete's heat capacity falls within the range of 840 to 1000 J/kg·°C

(Szokolay, 2014). The choice of aggregates in concrete also plays a significant role, particularly for heavier concrete types. Furthermore, the properties of other materials, such as glass and wood, are considered, as they are commonly utilised in the openings of precast concrete systems (Szokolay, 2014).

Regarding insulation materials, the selection is based on their average conductivity values. Most insulation materials exhibit conductivity values below 0.05 W/m·K, with those commonly used in applications typically ranging from 0.02 to 0.04 W/m·K. Tables 3.3 and 3.4 provide an overview of the thermal properties of relevant materials and elements.

Table 3.3: Thermal properties of key materials used in precast concrete systems. Source: Szokolay (2014); Clarke et al. (1991).

	Conductivity (W/m K)	**Density (kg/m3)**	**Specific heat (J/kg K)**
Concrete			
Cast, Lightweight	0.380	1200	1000
Dense	1.400	2100	840
Concrete block, heavy	1.630	2300	1000
Concrete block, medium	0.510	1400	1000
Concrete block, light	0.190	600	1000
Concrete slab, dense	1.130	2000	1000
Concrete slab, aerated	0.160	500	840
Glass	1.100	2500	840
Aggregates			
Sand (dry)	0.300	1500	800
sandstone	1.300	2000	800
granite	2.300	2600	820
Steel	47	7800	480
Insulations			
Glass fibre (batt)	0.035	25	1000
Polyurethane board	0.025	30	1400
polystyrene	0.035	25	1400
Timber			
Softwood	0.130	610	1420
Hardwood	0.150	680	1200
External rendering	0.500	1300	1000

Table 3.4: Thermal properties of key windows, roofs, and floors. Source: Szokolay (2014).

	U-value (W/m^2K)	Admittance (W/m^2K)	Time-lag (hours)	Decrement factor
Windows				
Metal frame, single 6 mm glass	6.0	6.0	0	0
same, but discontinuous frame	5.7	5.7	0	1
Metal frame, double glazing	3.6	3.6	0	1
same, but discontinuous frame	3.3	3.3	0	1
Flat roofs				
150 concr. slab, plastered, 75 screed + asphalt	1.80	4.50	8	0.33
same, but lightweight concrete	0.84	2.30	5	0.77
Floors				
Concrete slab on ground, 2 edges exposed				
3×3m	1.07	6.0	-	0.01
6×6m	0.57	6.0	-	0
7.5×7.5m	0.45	6.0	-	0
15×7.5m	0.36	6.0	-	0
15×15m	0.26	6.0	-	0
30×15m	0.21	6.0	-	0
Concrete slab on ground, 4 edges exposed				
3×3m	1.47	6.0	-	0.02
6×6m	0.96	6.0	-	0.01
7.5×7.5m	0.74	6.0	-	0.01
15×7.5m	0.62	6.0	-	0
15×15m	0.45	6.0	-	0
30×15m	0.36	6.0	-	0

3.18 THERMAL PROPERTIES OF PCS AS A MULTILAYER ELEMENT

In building elements, particularly in multilayer elements, a number of properties are considered that directly influence the thermal indoor conditions. These properties include U-value, admittance, solar heat gain factor, time-lag, and decrement factor. Therefore, in precast concrete sandwich wall panels, homogeneous elements with their thermal properties can be easily identified.

The admittance (Y) of an element indicates its capacity to absorb and release heat in response to indoor temperature fluctuations. It plays a crucial role in determining indoor temperatures resulting from heat flows (Szokolay, 2014). The admittance for a uniform, solid, homogeneous element, expressed in SI units, is dimensionally $W/m^2 \cdot K$: $Y = \sqrt{\lambda \bullet \rho \bullet c \bullet \omega}$ ………………………………………………………………………. Eq. 3.3

Where:

λ = thermal conductivity (W/m.K).

ρ = density (kg/m^3).

c = specific heat capacity (Wh/kg.K).

ω = angular velocity of the diurnal temperature wave.

Also, the total admittance of a building (or of a room) is qa (in W/K) and can be calculated using Equation 3.4:

$qa = \sum(A \times Y)$ ………………………………………………………………………. Eq. 3.4

The solar heat gain factor quantifies the proportion of solar energy passing through openings such as windows, doors, or skylights, directly transmitting or subsequently emitting as heat inside a dwelling. This factor is gauged on a scale from 0 to 1, commonly ranging between 0.25 and 0.80. A lower factor signifies minimal solar heat conduction, indicating greater shading capacity for the interior (Straube and Eng, 2008).

The phenomenon where the real heat flow curve experiences a slight delay, expressed in hours, behind the zero-mass curve is identified as the time-lag (represented as φ), measured in hours (Szokolay, 2014). Consequently, the time-lag for a large wall heated by solar energy is determined by the interval between the peak of solar input and the point at which the heat is required.

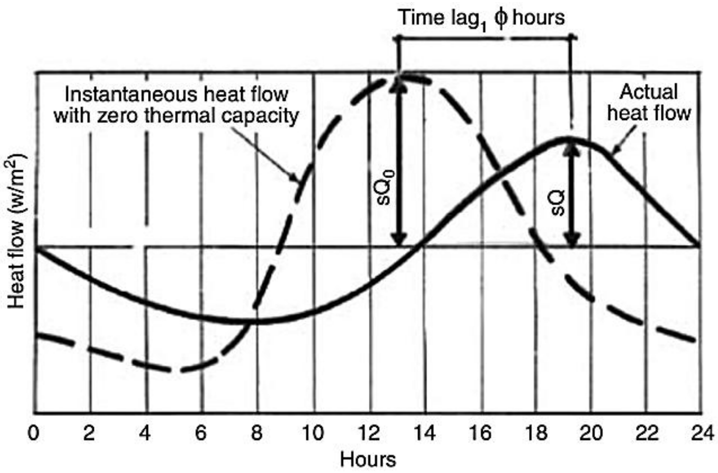

Figure 3.17: Illustration of the phase shift between the time-lag curve and the actual heat flow curve. Source: Szokolay (2014).

Besides, the time lag (φ) is always related to another parameter called the decrement factor (μ). Both are related to the admittance theory of thermal transmission, as well as aim to account for thermal behaviour's time dependency. Therefore, the time-lag is defined as the time difference between the external maximum temperature and the internal maximum temperature during periodic cycles, whereas the decrement factor is the ratio of external to inside temperature. Figure 3.17 illustrates the phase shift between the time-lag curve and the actual heat flow curve.

The peak amplitude, or swing, relative to the daily average heat flow is less pronounced for the solid line (sQ) than it is for the dashed line, which depicts the zero-mass wall (sQ0). This leads to the concept of the decrement factor or amplitude decrement, represented by μ, as established in Equation 3.5. It is the ratio of the two amplitudes, indicating the extent of damping in the heat flow's oscillation.

$\mu = \frac{sQ}{sQ0}$ ....Eq. 3.5

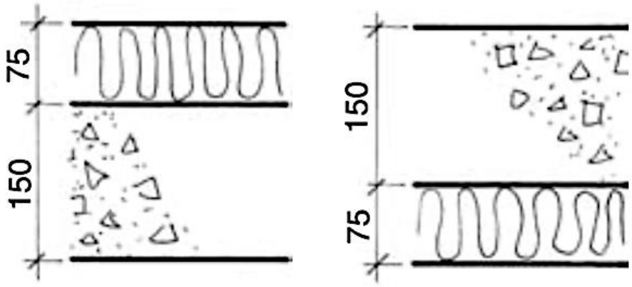

Figure 3.18: Sequence of layers in an insulated concrete roof slab. Source: Szokolay (2014).

The dynamic characteristics of multilayer elements, including time-lag, decrement factor, and admittance, as observed in systems like precast concrete walls, depend on the composition and thickness of the individual layers and their sequential arrangement relative to the heat flow direction. This relationship is effectively visualised in Figure 3.18. Additionally, Figure 3.19 provides a representation of both time-lag and decrement specifically for solid homogeneous walls, as explained by Szokolay (2014).

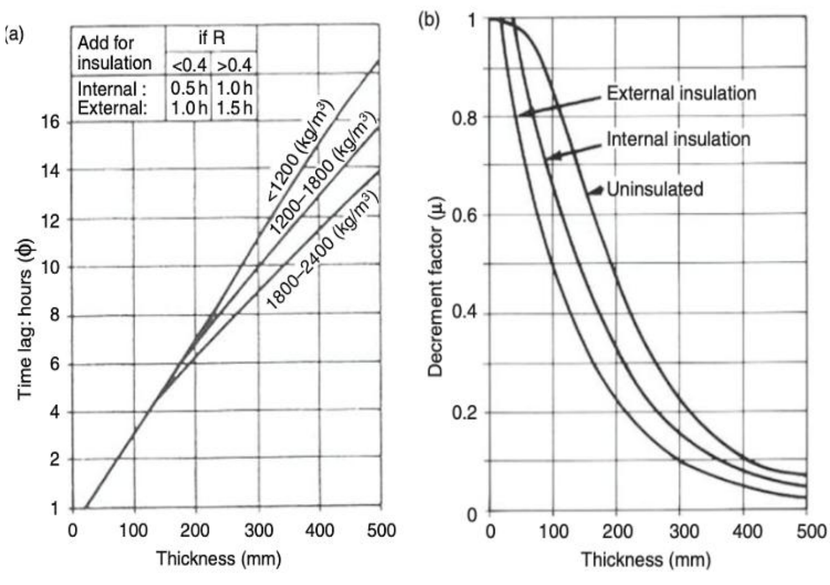

Figure 3.19: Depiction of time-lag and decrement factors in solid homogeneous walls. Source: Szokolay (2014).

Based on the above understanding, Table 3.5 lists the most relevant elements used in precast concrete wall systems including their previously mentioned thermal properties.

Table 3.5: Thermal properties of key elements used in precast concrete wall systems. Source: Szokolay (2014).

	U-value (W/m^2K)	Admittance (W/m^2K)	Time-lag (hours)	Decrement factor
Concrete, precast panel, 75 mm	4.28	4.9	1.9	0.91
Concrete, precast panel, 75 mm + 25 cavity + 25 EPS + plasterboard	0.84	1.0	3.0	0.82
Concrete, precast, 75 + 25 EPS + 150 Lw concrete	0.58	2.3	8.7	0.41
Concrete, precast, 75 + 50 EPS + 150 Lw concrete	0.41	2.4	9.2	0.35
Concrete, dense, cast, 150 mm	3.48	5.3	4.0	0.70
Concrete, dense, cast, 150 mm+ 50 mm woodwool slab, plastered	1.23	1.7	6.0	0.50
Concrete, dense, cast, 200 mm	3.10	5.5	5.4	0.56
Same above + 50 mm woodwool slab, plastered	1.18	2.2	7.7	0.36

3.19 THERMAL PROPERTIES IN PRECAST PANELS' ELEMENTS

In precast panels, windows that interrupt wall systems should be thermally analysed at their interface with the opaque element. Thus, the properties of these elements can be classified into two categories: one relating to opaque elements and the other relating to transparent elements.

3.19.1 PROPERTIES OF OPAQUE FABRIC ELEMENTS

In opaque elements, the solar heat input is conceptualised through the sol–air temperature model. It represents the radiant heat received by a surface unit and is closely tied to its absorptance. Furthermore, the solar heat gain on opaque surfaces is influenced by the building's shape and orientation, along with surface factors such as reflectance. To reduce solar heat gain, the shape should be determined by solar geometry: larger surfaces should receive the least solar exposure (Szokolay, 2014).

In general, opaque fabric elements include concrete walls and roofs, as well as the insulating materials used in conjunction with these elements. Homogeneous single-layer concrete elements with a thickness of 10 to 30 cm can have a U-value of 4.0 to 2.5 $W/m^2 \cdot K$ for 2100 kg/m^3 high-density concrete and 1.4 to 0.6 $W/m^2 \cdot K$ for 800 kg/m^3 low-density concrete. This equates to a thermal resistance of 0.25 to 0.10 $m^2 \cdot K/W$ for such high-density concrete elements and 0.71 to 1.67 $m^2 \cdot K/W$ for the previously specified low-density concrete elements. The time-lag for such elements is between 2.5 and 9 hours for 10 to 30 cm high-density concrete elements and between 3 and 12 hours for 10 to 30 cm low-density concrete elements (Evans, 1980).

When insulation is applied in combination to form multi-layered components, the previously stated values might significantly vary. This is because the thermal behaviour of insulating materials is indeed different from that of concrete. Thermal insulation works on the concept of using a non-conductive substance or trapping air or other gases within the insulation layer. If the cavity is enclosed with reflective sheets on one, or even both sides, this significantly increases the cavity's ability to insulate the structure. When only one side of a cavity is enclosed with reflective material, the conductance reduces from 5.56 to 2.86 $W/m^2 \cdot °C$; when both sides are lined with reflective material, the conductance decreases from 1.61 to 0.35 $W/m^2 \cdot °C$.

Cavities, on the other hand, require the employment of two distinct parts in the building. This is impossible in a precast concrete system. As a result, alternative materials, such as polystyrene, are more commonly used with the system.

Because the effectiveness of an insulating material is dependent on its porous nature, water penetration and humidity have a significant impact on its efficiency. As a result, measures should be taken to ensure that the insulating material is kept dry at all times. The location of insulation also plays a crucial role in its efficiency. Placing the insulation on the outside increases the element time lag and reduces the decrement factor, while placing it on the interior surface appears to offer a benefit in cold regions (Burberry, 1978; Szokolay and Koenigsberger, 1973), as mentioned by (Hashim, 1991).

Hashim (1991) stated that some precast concrete systems, such as hollow-core slabs, have cavities that are not continuous. These tend to reduce the cavity's insulating effectiveness by creating cold bridges. Other insulating materials are used in PCS because it is impractical to create a hollow of this size in the material. Materials with a conductivity of 0.03–0.035 W/m·K and a thickness of 5 cm can readily create a resistance of 1.43–1.67 m^2·K/W when used in an element with the same conductivity range.

3.19.2 PROPERTIES OF TRANSPARENT ELEMENTS.

While transparent components are frequently associated with glass, they can also refer to open windows that are not covered or are covered with louvres, blinds, or curtains. Most of this section, however, will focus on glass elements, as open windows have little influence on material or element behaviour. Glass components serve as barriers against a variety of external influences, such as hot air, dust, and insects. Additionally, they provide natural light and views to the interior.

The transmission of light to interior spaces depends on the wavelength distribution of the radiation, the elemental composition and thickness of the pane, as well as the angle of incidence. In addition to being transparent to short-wave radiation, glass has the property of being opaque to long-wave radiation from low-temperature emitters such as warm building envelopes. This phenomenon, known as the greenhouse effect, results from this occurrence.

When it comes to the transmission, reflection, or absorption of radiation on any glazing surface, glass exhibits high transparency and a high U-value (5.38 W/m^2·K for 6 mm glass), allowing significantly more incoming heat compared to opaque materials. As a result, a number of alternatives to single clear glazing have been developed, including double glazing, heat-absorbing glazing, and heat-reflecting glazing.

One of the most significant characteristics in window technology is the thermal transmittance value, often known as the U-value. In general, a window's thermal and optical performance may be summarised using the following important indicators: U-value, Solar Heat Gain Coefficient (SHGC), and visible transmittance (Aguilar-Santana et al., 2019). Table 3.6 shows the U-values of uncoated glass with different configurations.

Table 3.6: List of U-values for different glass configurations. Source: Lolli and Andresen (2016).

Glass configuration	U-value (W/m^{2}K)
Uncoated single glass 6 mm	5.70
Uncoated double glass 12 mm cavity	2.80
Uncoated double glass 15 mm air cavity	1.40
Uncoated double glass 15 mm argon cavity	1.20
Uncoated triple glass 16 mm with argon	0.79
Uncoated double glass 22 mm monolithic aerogel	0.65
Uncoated double glass 33 mm granular aerogel	0.44

3.19.3 SOLAR HEAT GAIN

Solar heat gain is addressed distinctively for transparent and opaque surfaces (Szokolay, 2014). For both types, it is essential to ascertain the global irradiance (G) striking the surface, expressed in W/m^2. For transparent elements like windows, solar gain is computed by multiplying the irradiance (G) by the window's area and the solar gain factor (θ), a decimal indicating the fraction of incident radiation permeating the interior. Incident radiation comprises transmitted (τ), reflected (ρ), and absorbed (α) components within the glass, as detailed in Equation 3.6 (Szokolay, 2014).

$\tau + \rho + \alpha = 1$..Eq. 3.6

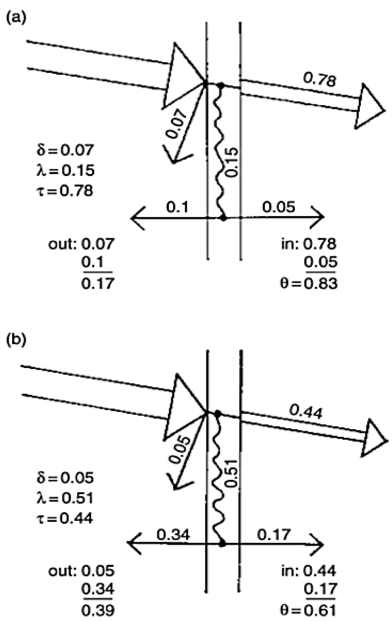

Figure 3.20: Transmission through glass: (a) clear 6-mm glass, (b) heat-absorbing (tinted) glass. Source: Szokolay (2014).

The energy absorbed by the glass leads to its heating, causing the glass to radiate a portion of this heat externally and convey some internally through re-radiation and convection, as depicted in Figure 3.20. The combination of this inwardly re-radiated heat and the direct transmission is denoted as θ. Consequently, the solar gain via a window is articulated in Equation 3.7.

$$\mathrm{Qs} = \mathrm{A} \times \mathrm{G} \times \theta \quad \text{Eq. 3.7}$$

Additionally, the use of various types of glass in conjunction with other shading devices, such as blinds, has resulted in a more detailed application of the solar gain factor. This can be calculated using Equation 3.8, as introduced by Evans (1980) and cited by Hashim (1991):

$$\theta = \mathrm{T} + \alpha \left(\frac{\mathrm{Ki}}{\mathrm{Ko}} + \mathrm{Ki}\right) \quad \text{Eq. 3.8}$$

The following Table 3.7 illustrates the solar gain factor for the most relevant glazing systems.

Table 3.7: Solar gain factors for most relevant glazing system. Source: Szokolay (2014).

	Instantaneous (SGF or θ)	**Alternating solar gain factor (lightweight)**	**Alternating solar gain factor (heavyweight)**
Single glazing			
Clear, 6 mm glass	0.76	0.64	0.47
Surface tinted 6 mm glass (STG)	0.60	0.53	0.41
Body tinted 6 mm glass (BTG)	0.52	0.47	0.38
Body tinted 10 mm glass (BTG)	0.42	0.39	0.34
Clear glass, with reflective film	0.32	0.29	0.23
Same but strongly reflective film	0.21	0.19	0.16
Clear, with tinted reflective film	0.28	0.26	0.23
Reflecting glass	0.36	0.33	0.27
Strongly reflecting glass	0.18	0.17	0.15
Double glazing (outer pane first)			
Clear 6 mm + clear 6 mm	0.64	0.56	0.42
STG + clear 6 mm	0.48	0.43	0.34
BTG 6mm + clear 6mm	0.40	0.37	0.30

BTG 10mm + clear 6mm	0.30	0.28	0.24
Reflecting + clear 6 mm	0.28	0.25	0.21
Strongly reflecting + clear 6 mm	0.13	0.12	0.10
Lightly reflecting sealed double unit	0.32	0.29	0.21
Strongly reflecting sealed double unit	0.15	0.14	0.11
Single glazing + External shade			
Clear 6 mm + light horizontal slats+	0.16	0.11	0.09
+ light vertical slats+	0.18	0.13	0.10
+ dark horizontal slats+	0.13	0.09	0.08
+ holland blind	0.13	0.10	0.08
+ miniature louvres*	0.16	0.10	0.09
Double glazing + External shade Clear 6 + clear 6			
+ light horizontal slats+	0.13	0.09	0.07
+ light vertical slats+	0.15	0.10	0.08
+ light roller blind	0.10	0.09	0.07
+ miniature louvres*	0.12	0.07	0.06
Triple glazing			
Clear 6 + clear 6 + clear 6	0.55	0.50	0.39
+ mid-pane light slats	0.28	0.26	0.24

3.19.4 VISIBLE TRANSMITTANCE

These optical characteristics measure the amount of visible light that passes through a particular glazing material. It typically varies between 90% and 10% for transparent glazing. This parameter is influenced by the glass type, the number of panes, and the presence of coatings that reduce visibility. A high visual transmittance value indicates an increased amount of daylight in a room and, in most cases, a reduction in the demand for artificial lighting. A typical double-glazed window has a visual transmittance of 78%, which may be further reduced with the addition of low-E coatings and tinted films(Hammarberg and Roos, 2003).

3.19.5 GLASS THICKNESS AND MULTI-PANE GLAZING

As previously shown in Table 4.6, the effect of glass thickness on thermal performance is significantly correlated. For glass panes with a thickness greater than 12 mm, a considerable drop in the U-value was observed. However, the reduction in heat transmission comes at the expense of visible transmittance and increased weight. Double-glazed windows contribute to reduced building energy consumption by enhancing insulation, attributed to the pane spacing that serves as a thermal barrier. Figures 3.21, 3.22, and 3.23 respectively illustrate heat transfer in double-glazed windows, the solar heat gain coefficient for various tints of single glass, and visible transmittance across different coatings used in double-glazed windows.

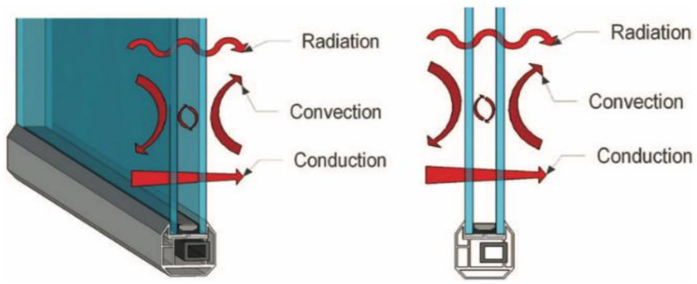

Figure 3.21: Heat transfer through double-glazing windows. Source: Aguilar-Santana et al. (2019).

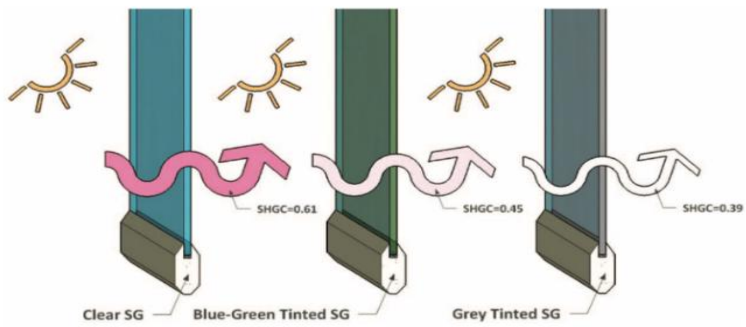

Figure 3.22: Illustrates the solar heat gain coefficient of single glass for different tinting types. Source: Aguilar-Santana et al. (2019).

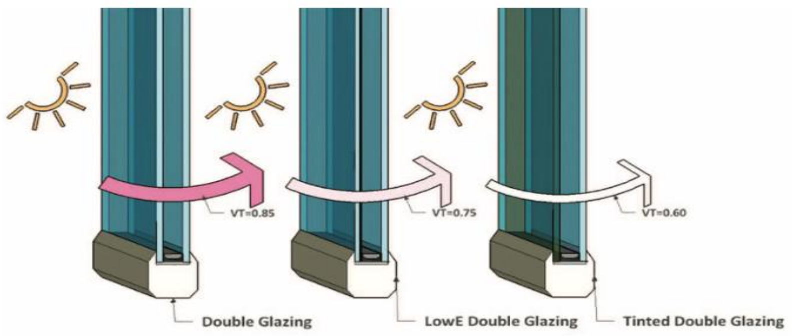

Figure 3.23: Illustrates the visible transmittance for different coatings in double-glazing windows. Source: Aguilar-Santana et al. (2019).

3.20 STATE OF THE ART SAUDI BUILDING PERFORMANCE RESEARCH

Precast concrete sandwich panels (PCSPs) are increasingly utilised in Saudi Arabia's construction industry due to their superior thermal performance, structural efficiency, and cost-effectiveness. These panels consist of two concrete layers (wythes) separated by an insulating core, typically made of materials such as EPS or PIR foam. This configuration enhances thermal insulation, making PCSPs particularly suitable for the region's hot climate.

The choice of insulation significantly impacts the panel's thermal resistance. Materials such as EPS and PIR are favoured for their low thermal conductivity, contributing to effective thermal insulation. For instance, sandwich panels with PIR insulation can achieve thermal conductivity as low as 0.023 W/m·K, enhancing energy efficiency in buildings (TSSC, 2024).

A study by Jithin and Joseph (2023) analysed PCSPs with different insulation materials—Expanded Polystyrene (EPS), Extruded Polystyrene (XPS), Phenolic Foam (Pungercar et al.), and Polyisocyanurate Foam (PIR)—and varying insulation thicknesses. The findings indicated that PF insulation achieved the lowest thermal transmittance (U-value) of 0.053 W/m²·K, outperforming other materials. Increasing insulation thickness from 80 mm to 160 mm further enhanced thermal resistance, underscoring the importance of both material selection and adequate insulation thickness in hot climates.

The thermal mass of PCSPs plays a pivotal role in regulating indoor temperatures by absorbing and releasing heat. Shareef et al. (2024) conducted a holistic analysis of the thermal mass performance of precast concrete panels in hot climates in UAE. Their study revealed that employing heavyweight PCSPs with increased insulation thickness (50 mm) can reduce cooling loads by up to 15.8%. This reduction is attributed to the panels' ability to moderate indoor temperature fluctuations, thereby decreasing reliance on mechanical cooling systems.

3.20.1 THE USE OF PHASE CHANGE MATERIALS

Phase Change Materials (PCMs) have been explored to enhance the thermal performance of precast concrete sandwich panels by increasing their thermal storage capacity. PCMs absorb and release thermal energy during phase transitions, helping to regulate indoor temperatures.

A study conducted by Niall and West (2024) involved designing and manufacturing precast cladding sandwich panels with a PCM–concrete inner layer, used in full-scale huts monitored over 18 months. The PCM–concrete composite effectively reduced internal air temperatures by up to 16% with overnight ventilation and 12% without it in a temperate climate. However, PCM located deeper than 60 mm from the internal surface was less effective. The study highlighted that the thermal conditions required to activate the PCM only occurred during 30% of the year. Figure 3.24 illustrates the increased thermal mass provided by PCM and its impact on internal temperatures.

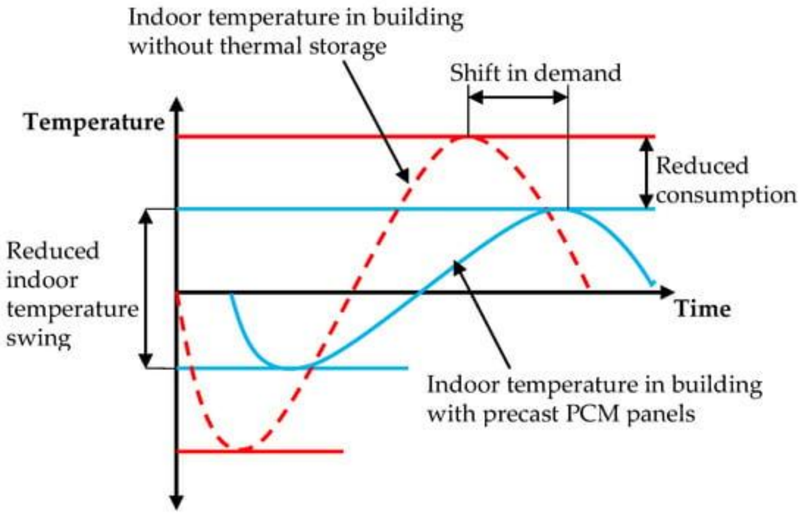

Figure 3.24: Schematic showing impact of increased thermal mass provided by PCM–concrete panels on internal temperature. Source: Niall and West (2024).

The effectiveness of PCMs depends on factors such as the phase change temperature of the PCM, the depth of its incorporation within the panel, and the building's ventilation strategy. While PCMs can enhance thermal performance, their integration requires careful design to ensure they function as intended.

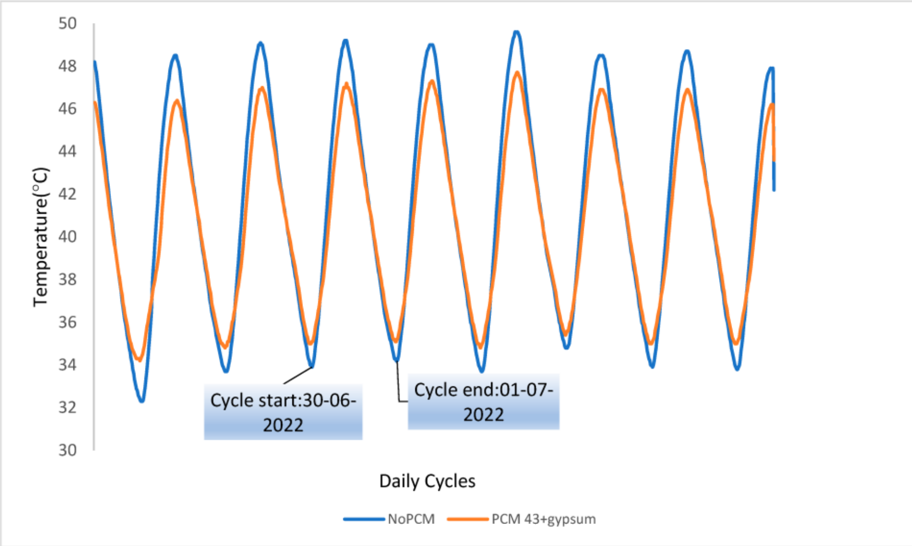

Figure 3.25: Daily temperature fluctuations in PCM43+gypsum and control chambers. Source: Alrashdan et al. (2024).

In their 2024 study, AlRashdan et al. explore the thermal efficiency of building envelopes integrated with PCMs in Saudi Arabia. They particularly focused on microencapsulated paraffin-based PCMs with melting points of 37°C and 43°C, assessing their performance in cement and gypsum composites within service areas often excluded from thermal analyses, such as underground garages. The findings indicated that the 43°C PCM significantly outperformed the 37°C PCM in reducing heat loads as shown in Figure 3.25. A subsequent comparison revealed that cement-based composites with 20% PCM content were more effective, reducing the highest daily temperature by 5.2°C and overall heat load by approximately 63%, thereby enhancing thermal comfort in building interiors (Alrashdan et al., 2024).

Fagehi and Hadidi (2022) examined the thermal behaviour of three buildings in NEOM, focusing on the application of Phase Change Materials (PCMs) in building envelopes to enhance energy efficiency. Their study compared a reference building with 29 cm-thick walls and no PCM to two PCM-filled buildings with 34 cm-thick walls. The results highlighted the significant impact of PCM integration across all wall orientations (north, south, east, and west), achieving a 63.5% reduction in heat exchange compared to the non-PCM building. The study further evaluated the effect of PCM thickness, demonstrating that increasing the thickness from 5 cm to 10 cm and 20 cm resulted in energy exchange reductions of 4500, 7546, and 11,681 kWh/year, respectively, for the second building. Although the third building exhibited diminishing returns with increased PCM thickness, it achieved higher overall energy savings of 17,120, 19,835, and 21,215 kWh/year for 5 cm, 10 cm, and 20 cm, respectively.

These findings underscore the transformative potential of PCMs in reducing energy demand and improving thermal performance in hot climates, aligning with NEOM's vision for sustainable urban development and energy-efficient smart cities.

While the integration of PCMs into PCSPs offers potential benefits for thermal regulation, their application in Saudi Arabia and similar hot climates remains limited. Further research and development are needed to address the challenges associated with PCM integration and to evaluate its feasibility and effectiveness in these regions.

3.20.2 RECENT RETROFITTING STRATEGIES

Improving existing building envelopes can significantly enhance energy efficiency. Al-Tamimi (2022) explored various retrofitting strategies for office buildings, in hot-arid climate, emphasising the importance of tailored solutions for different building types. The assessments were conducted to determine the reduction in energy usage achieved by upgrading the building envelope. The DesignBuilder simulation tool was employed to examine the impact of various retrofitting approaches, including changing the window glass type, adding layers of thermal insulation, and installing shading devices. The findings indicated that implementing a combination of these strategies led to a 26.81% decrease in total energy consumption relative to the existing baseline. In conclusion, the study underscores the effectiveness of comprehensive retrofitting in significantly enhancing energy efficiency in buildings.

Rababa and Asfour (2024) conducted a comprehensive analysis of façade retrofit strategies aimed at enhancing energy efficiency in Saudi Arabian buildings. Their research evaluated the effectiveness of upgrading external walls, replacing windows, and installing shading devices. The optimal combination involved an External Thermal Insulation Composite System (ETICS) for walls, louvres for windows, and low-emissivity, argon gas-filled glazing, which collectively reduced cooling energy consumption by approximately 16% with a payback period of 14.8 years. This study highlights the significant potential for energy savings through targeted facade improvements in regions with hot climates.

The study by Balabel et al. (2024) evaluates the impact of green roofs on building sustainability within the context of Saudi Arabia, particularly focusing on how these systems contribute to achieving Saudi Vision 2030 and the Sustainable Development Goals. Green roofs are shown to significantly enhance the sustainability ratings of buildings, offering up to 32% of the total credits in the MOSTADAM rating system. This improvement not only underscores the environmental benefits of green roofs, such as reduced energy consumption and better thermal regulation, but also promotes broader societal and economic benefits by fostering sustainable urban development.

In their 2024 study, Mezaein and Baltazar examine the regenerative impact of integrating cultural vernacular elements, specifically *rowshans*, into modern architecture in Jeddah, Saudi Arabia. Utilising building performance simulation and computational fluid dynamics (CFD), their research demonstrates that *rowshans* can significantly enhance air movement and reduce cooling loads, resulting in a 15% to 22% decrease in indoor air temperatures during midday from November to April. This strategic implementation not only promotes energy efficiency but also aligns with sustainable architectural practices, thereby supporting environmental and economic sustainability in the region (Mezaien and Baltazar, 2024).

A study conducted by Magzoub et al. (2024) critically evaluates the Energy Active Window (EAW) systems designed to enhance thermal performance in hot climates. Their innovative approach integrates low-grade air from HVAC systems into window systems to maintain the internal surface temperature close to that of the indoor air, reducing heat transfer. Using Computational Fluid Dynamics (CFD), they demonstrated a reduction in surface temperature by 4 to 7°C when outdoor temperatures reached 45°C, with an 8% margin of error. The study's findings emphasise the potential of EAW systems to significantly lower energy consumption in buildings by optimising various factors such as air velocity, air gap width, and glazing layers, enhancing the sustainability of architectural designs in regions with hot climates.

Besides, a study conducted by Alyami (2024) in Riyadh, Saudi Arabia, utilised the DesignBuilder tool to optimise thermal insulation in a residential building. By adjusting the type, thickness, and placement of insulation, especially in walls and roofs, the study achieved a 42.5% reduction in energy consumption and carbon emissions. This approach not only improved thermal performance but also yielded 33% cost savings over 30 years, along with a payback period of 7.98 years, underscoring the economic and environmental benefits of optimal insulation strategies in hot-arid regions like the Gulf states.

3.21 SUMMARY

The literature review highlights significant advancements in the design of precast concrete sandwich panels (PCSPs), transitioning from their early role as cladding to highly efficient building systems. Modern concrete technologies, including ultra-high-performance fibre-reinforced and textile-reinforced concretes, have enabled the production of thinner panels, complemented by corrosion-resistant reinforcements and high-performance insulation materials, such as vacuum insulation. These developments have improved thermal efficiency, achieving low U-values without increasing the structural footprint.

While many thin PCSP designs have undergone structural testing, comprehensive thermal performance assessments remain limited. Initial findings indicate that some designs meet stringent benchmarks, such as the passive house standard of 0.15 $W/m^2 \cdot K$, though thermal bridging remains a challenge. The durability, reduced weight, and logistical benefits of slimmer panels enhance their appeal as energy-efficient, sustainable solutions, positioning PCSPs as a versatile option for future building applications.

This chapter also focuses on the thermal characteristics of typical PCS materials and elements, categorised into material thermal properties and element thermal properties. The study distinguishes two primary types of materials: solid structural concrete and lightweight insulating materials. Structural concrete encompasses heavy mix "high-density" and light mix "low-density" categories. Precise values for density, conductivity, and specific heat capacity are elusive due to variations in the manufacturing process. Attention is required to the proportionality of materials to achieve desired thermal properties. In this research, typical values considered for simulation inputs include densities of 800 kg/m^3 for lower-density concrete and 2100 kg/m^3 for higher-density concrete.

Heavy-mix concrete, comprising elements like gravel, sand, and various stones, inherits its properties from these constituents, with a standard option having 2100 kg/m³ density, 1.39 W/m·K conductivity, and 830 J/kg·K specific heat. Standard polystyrene, in contrast, has properties of 30 kg/m³ density, 0.025 W/m·K conductivity, and 1400 J/kg·K specific heat (refer to Table 3.8).

Table 3.8: Highlighting the thermal properties of typical precast dwellings in Saudi Arabia.

Construction material	Conductivity (W/m.K)	Density (kg/m^3)	Specific heat (J/kg. K)
Concrete	1.39	2100	830
Insulation materials	0.025	30	1400
Glass	1.1	2500	840

Despite the diversity in glass types and coatings, a standard set of properties (2500 kg/m³ density, 1.1 W/m·K conductivity, and 840 J/kg·K specific heat) is acknowledged for window components.

The literature review identified several thermal strategies for envelope systems, including the use of low thermal mass materials, optimisation of glazing area, strategic insulation placement, multi-layered glazing, and the implementation of shading systems to protect against solar radiation. These methods contribute to the thermal efficiency of building components.

CHAPTER FOUR - RESEARCH METHODOLOGY

4.1 INTRODUCTION

This chapter presents the research methodology and tools used to analyse the thermal performance of prefabricated houses in Saudi Arabia. The methodology is structured following Saunders' Research Onion framework to ensure a coherent and systematic approach. The chapter begins by establishing the research philosophy and approach, followed by the justification for the methodological choice and research strategy. The chapter also explains the rationale for employing case studies, describes the data collection and analysis techniques, and outlines the process of software validation to ensure reliable results.

4.2 RESEARCH PHILOSOPHY

The research adopts a pragmatic philosophy, which focuses on addressing real-world problems through practical and flexible methodologies. Pragmatism allows the integration of both qualitative and quantitative methods to comprehensively analyse the thermal performance of prefabricated houses. This philosophy aligns with the objectives of this study, as it seeks to balance theoretical insights with practical solutions, particularly in the context of improving energy efficiency and thermal comfort in extreme climates.

4.3 RESEARCH APPROACH

This study employs an abductive approach, which facilitates iterative reasoning between data collection and theoretical frameworks. The research begins by observing the real-world challenges of thermal inefficiency in prefabricated houses and uses these observations to inform simulations and analyses. Insights derived from simulation results are then used to refine hypotheses and propose optimisations for building envelope systems. This cyclical process ensures a comprehensive understanding of the research problem.

4.4 METHODOLOGICAL CHOICE

A mixed-methods approach is adopted in this research to combine the strengths of both qualitative and quantitative methods. Qualitative methods, such as field observations, provide detailed insights into construction materials, architectural features, and environmental factors. Quantitative methods, including simulations using

DesignBuilder software, offer precise numerical data on energy consumption, thermal comfort, and performance improvements. This combination ensures a robust and balanced investigation.

4.5 RESEARCH STRATEGY

The research employs a case study strategy, which is well-suited for examining the thermal performance of prefabricated houses in their real-world context. Case studies allow for an in-depth analysis of individual buildings, capturing the complex interactions between materials, design, and environmental conditions. This strategy is particularly relevant for investigating the effects of building envelope components on energy efficiency and indoor thermal comfort.

Three case study houses were selected from Jubail Industrial City based on specific criteria, including the use of precast concrete systems, accessibility, and the unoccupied status of the buildings. These houses serve as representative examples, enabling detailed analysis and simulation of thermal performance.

4.6 TIME HORIZON

This research adopts a cross-sectional time horizon, focusing on specific time periods to analyse the thermal performance of the case study houses. Although the study examines performance during particular seasons, the simulations incorporate annual variations to provide a comprehensive understanding of energy demands throughout the year.

4.7 DATA COLLECTION AND ANALYSIS

4.7.1 FIELD OBSERVATIONS

Field observations were conducted to gather qualitative data on the architectural and structural characteristics of the selected houses. Key tasks included:

- Documenting construction materials and building layouts.
- Measuring indoor and outdoor air temperatures.
- Collecting technical drawings and other relevant documentation.

These observations provided the foundational data required for simulation and validation.

4.7.2 SIMULATION TOOLS

The thermal performance of the selected houses was simulated using DesignBuilder, a validated Building Energy Performance Simulation (BEPS) tool. The software was assessed against ANSI/ASHRAE Standard 140-2017 to ensure accuracy and reliability. Key parameters analysed include:

- Thermal properties of building envelope components.
- Internal heat gains from occupants, lighting, and equipment.
- Energy consumption for cooling and heating.

Simulation results were used to evaluate and optimise building envelope designs, focusing on factors such as wall thickness, material density, and the integration of phase change materials (PCMs).

4.8 JUSTIFICATION OF METHODS

The selection of a case study strategy and mixed-methods approach is justified by the need to comprehensively investigate the thermal performance of prefabricated houses in a specific context. Case studies provide detailed insights into the interactions between building materials, design features, and environmental conditions, while the mixed-methods approach ensures a balance between qualitative observations and quantitative analysis.

The use of BEPS tools is justified by their ability to accurately predict energy performance and identify optimisation opportunities. By integrating simulations at an early stage, the study contributes to the development of energy-efficient design solutions tailored to Saudi Arabia's climate.

4.9 LIMITATIONS

While the case study methodology offers detailed insights, it has inherent limitations. Results are context-specific and may not be fully generalisable to other regions or building types. Resource constraints and the COVID-19 pandemic also limited the number of case studies conducted. However, these limitations were mitigated through rigorous data collection, validation, and the use of reliable simulation tools.

4.10 RELEVANCE AND APPLICABILITY TO THE RESEARCH APPROACH

Johansson (2007) analysed the work of previous authors and concluded that case studies are recommended over other methodologies because case studies use a combination of other research strategies, thus making it a meta-method. The researcher emphasised the special importance of case studies in practice-oriented research and fact-finding such as planning and architecture (Johansson, 2007). This attribute directly highlights the relevance and applicability of the case study methodology to investigate the thermal performance of precast concrete wall systems. Johansson (2007) further characterised the characteristic of case studies to limit the scope to a particular case while simultaneously taking stock of the context as explicative rather than reductive and experimental.

Other fields, centred on research education, have expanded the importance of case studies to learning methods, despite the approach being adamant about the analytical purpose of that type of study and ignoring concerns about data collection and analysis because its application is limited to producing exercises for students. Alternatively, case studies are provided as a systematic description in architecture and engineering, focused on construction, design, and management. A good example of this notion is explored in Arup's work in 1995 which laid out a case study guide for designers (Savvides, 2013). In this example, the constraint on the method's application, which concentrated on its descriptive purpose, affected the method's other qualities, such as its exploratory and explanatory roles.

4.11 THE QUALITATIVE AND QUANTITATIVE APPLICATION OF CASE STUDY METHODOLOGY

Unlike other extensively used approaches, case study research is not founded in any one social scientific tradition. As a result of this broad and diverse base, case studies can be both qualitative and quantitative. According to Harrison et al. (2017), differences in case study methodologies in the dimensions of intrinsic, instrumental, and collaborative approaches facilitate both qualitative and quantitative analysis. Many longitudinal studies of solitary subjects use qualitative data from academic journals that report detailed recordings of development over time. One of the most used approaches in qualitative research is the case study methodology. Rich qualitative descriptions obtained from case studies, on the one hand, help to explain the complexities of real-world settings that may not be fully explored and explained by experiments or other forms of research, in addition to aiding data descriptions in a real-world environment.

Researchers may perform in-depth analyses of complicated relationships within a given context using the qualitative case study techniques. A qualitative case study is an evidence-backed methodology that allows for the investigation of a phenomenon in a specific setting utilising a variety of data sources and several levels of analysis to reveal many aspects of the phenomenon. Effective case studies are contingent on real-time occurrences being examined in their natural setting, based on the underlying premise that the context has a significant effect on the outcome. On the other hand, many researchers gather and use quantitative data to supplement qualitative data. The use of quantitative data to support qualitative data improves our knowledge of the linkages between occurrences. In numerous case study settings, certain data analyses, such as theme and pattern analysis, may bring a range of viewpoints and insights to the research.

4.12 LIMITATIONS OF CASE STUDY METHODOLOGY IN BUILT ENVIRONMENT RESEARCH

Despite the many applications of case study methodology, there are some drawbacks to using this form of research method. According to Houghton et al. (2013), case studies are time-consuming, expensive, and involve large volumes of data, the depth of analysis of which can be affected by available resources and time restrictions. A prominent argument levelled against the case study methodology is that it relies on a single case investigation, making it hard to derive generalisable and applicable conclusions. As a result, some academics regard case methodology as microscopic due to the small sample size. Case study approaches, according to Yin (2013), are criticised for lacking a scientific foundation, thus providing insufficient justification for extrapolating the findings to a larger audience. Furthermore, since case studies lack direct methods to conduct formal research with comparable and generalisable settings, they are more difficult to replicate. This issue is more prominent in built environment research, where a single case study could face challenges in producing generalisable results and recommendations. The thermal performance of a built structure is highly susceptible to regional attributes, local landmarks, climate change, and other factors that differ from one location to another.

4.13 ASHRAE STANDARD TEST FOR BUILDING THERMAL ENVELOPE AND FABRIC LOAD

ANSI/ASHRAE Standard 140-2017 provides test protocols aimed at determining the effectiveness and capabilities of software meant for assessing the thermal performance of buildings and their related environmental control systems. These tests allow for the comparison of one program's outcomes with analytical and quasi-analytical solutions, as well as with the outcomes of other software. While these tests are not exhaustive in scope, they are designed to pinpoint major issues or constraints.

For DesignBuilder, the tests have dual objectives. Firstly, they offer a comparative measure of DesignBuilder's performance against a set of leading building energy computation programs, detailed in Table 4.1. Secondly, they enable the juxtaposition of future iterations of DesignBuilder with its earlier versions, as part of DesignBuilder's Quality Assurance process.

Table 4.1: Computer programs and associated authors employed for comparative analysis. Source: EnergyPlus (2021b).

Computer Program (Abbrev.)	Authoring Organization
BLAST-3.0 level 193 v.1 (BLAST-US/IT)	CERL,[a] United States (U.S.)
DOE-2.1D 14 (DOE21D)	LANL/LBNL,[c] U.S.
ESP-RV8 (ESP-DMU)	Strathclyde University, United Kingdom (U.K.)
SERIRES/SUNCODE 5.7 (SRES/SUN)	NREL/Ecotope, U.S.
SERIRES 1.2 (SRES-BRE)	NREL/BRE,[d] U.S./U.K.
S3PAS	University of Sevilla, Spain
TASE	Tampere University, Finland
TRNSYS 13.1 (TSYS-BEL/BRE)	University of Wisconsin, U.S.

- [a]CERL-U.S. Army Construction Engineering Research Laboratories.
- [b]NREL-National Renewable Energy Laboratory.
- [c]LANL/LBNL-Los Alamos National Laboratory/Lawrence Berkeley National Laboratory.
- [d]BRE-Building Research Establishment.

4.14 COMPARATIVE ANALYSIS OF BEPS TOOLS

This section outlines the key parameters and scenarios used in the ASHRAE Standard Test to evaluate building energy performance. The fundamental modelling information includes weather data DRYCOLD.TMY (converted to EPW format), infiltration: 0.5 ach, sensible internal gains = 200W (60% radiative, 40% convective, continuously), and latent internal gains = 0W. The heating system activates if the temperature drops below 20°C, while the cooling system activates if the temperature exceeds 27°C.

The simulations encompass various scenarios. The base case, coded as 600FF, represents a rectangular, single-zone, low-mass structure (interior dimensions: 8 x 6 x 2.7 m) with two windows (3 x 2 m) on the south-facing façade. An "ideal" mechanical system, which is 100% efficient with no duct losses or capacity limitations, provides heating and cooling.

Case 650FF, akin to the base case 600, is considered a night ventilation scenario but with a distinct thermostat and ventilation fan control strategy. The inputs for this case are: vent fan capacity = 1703.16 m^3/h (13.14 ach), 08:00 – 07:00 vent fan = ON (else OFF), heat = OFF, 07:00 – 18:00 cool = ON if > 27°C (else OFF). Both cases 600 and 650 use lightweight material specifications as depicted in Table 4.2.

Table 4.2: Material specifications for Lightweight cases 600 and 650. Source: EnergyPlus (2021b).

Element	k, W/(m·K)	Thickness, m	U, $W/(m^2·K)$	R, $(m^2·K)/W$	Density, kg/m^3	c_p, J/(kg·K)
Lightweight Case: Exterior Wall (inside to outdoors)						
Interior surface coefficient			8.290	0.121		
Plasterboard	0.160	0.012	13.333	0.075	950.000	840.000
Fiberglass quilt	0.040	0.066	0.606	1.650	12.000	840.000
Wood siding	0.140	0.009	15.556	0.064	530.000	900.000
Exterior surface coefficient			29.300	0.034		
Total air-air			**0.514**	**1.944**		
Total surf-surf			**0.559**	**1.789**		
Lightweight Case: Floor (inside to outdoors)						
Interior surface coefficient[a]			8.290	0.121		
Timber flooring	0.140	0.025	5.600	0.179	650.000	1200.000
Insulation	0.040	1.003	0.040	25.075	0[b]	0[b]
Total air-surf			**0.039**	**25.374**		
Total surf-surf			**0.040**	**25.254**		
Lightweight Case: Roof (inside to outdoors)						
Interior surface coefficient[a]			8.290	0.121		
Plasterboard	0.160	0.010	16.000	0.063	950.000	840.000
Fiberglass quilt	0.040	0.1118	0.358	2.794	12.000	840.000
Roofdeck	0.140	0.019	7.368	0.136	530.000	900.000
Exterior surface coefficient			29.300	0.034		
Total air-air			**0.318**	**3.147**		
Total surf-surf			**0.334**	**2.992**		

Summary: Lightweight Case				
Component	**Area, m^2**	**UA, W/K**		
Wall	63.600	32.715		
Floor	48.000	1.892		
Roof	48.000	15.253		
S. window	12.000	36.000		
Infiltration		18.440[c]		
Total UA (with south glass)		**104.300**		
Total UA (without south glass)		**68.300**		
		ach	**Volume, m^3**	**Altitude, m**
		0.500	129.600	1609.000

On the other hand, the simulations also explored scenarios involving heavyweight construction materials, specifically case 900FF and case 950FF, which are defined as high-mass base building and high-mass night ventilation, respectively. These cases are identical to the base case 600FF, except for the use of heavyweight material for the walls and floor. As a result, the high-mass scenarios mirror their low-mass counterparts in the 600-series, the only difference being that the material properties are derived from Table 4.3.

Table 4.3: Material specifications for heavyweight cases 900ff and 950ff. Source: EnergyPlus (2021b).

Element	k, W/(m·K)	Thickness, m	U, W/(m^2·K)	R, m^2·K/W	Density, kg/m^3	c_p, J/(kg·K)
Heavyweight Case: Exterior Wall (inside to outside)						
Interior surface coefficient			8.290	0.121		
Concrete block	0.510	0.100	5.100	0.196	1400	1000
Foam insulation	0.040	0.0615	0.651	1.537	10	1400
Wood siding	0.140	0.009	15.556	0.064	530	900
Exterior surface coefficient			29.300	0.034		
Total air-air			**0.512**	**1.952**		
Total surf-surf			**0.556**	**1.797**		
Heavyweight Case: Floor (inside to outside)						
Interior surface coefficient[a]			8.290	0.121		
Concrete slab	1.130	0.080	14.125	0.071	1400	1000
Insulation	0.040	1.007	0.040	25.175	0[b]	0[b]
Total air-surf			**0.039**	**25.366**		
Total surf-surf			**0.040**	**25.246**		
Heavyweight Case: Roof (inside to outside)[c]						
Interior surface coefficient[a]			8.290	0.121		
Plasterboard	0.160	0.010	16.000	0.063	950	840
Fiberglass quilt	0.040	0.1118	0.358	2.794	12	840
Roofdeck	0.140	0.019	7.368	0.136	530	900
Exterior surface coefficient			29.300	0.034		
Total air-air			**0.318**	**3.147**		
Total surf-surf			**0.334**	**2.992**		

Summary: Heavyweight case			
Component	**Area, m^2**	**UA, W/K**	
Wall	63.600	32.580	
Floor	48.000	1.892	
Roof	48.000	15.253	
S. Window	12.000	36.000	
Infiltration		18.440[d]	
Total UA (with south glass)		**104.165**	
Total UA (without south glass)		**68.165**	
	ach	**Volume, m^3**	**Altitude, m**
	0.500	129.6	1609.0

Moreover, Figures 4.1 and 4.2 compare the results of the earlier identified cases' ANSI/ASHRAE Standard 140-2017 Building Thermal Envelope and Fabric Load Tests. Based on this comprehensive analysis, the results show that DesignBuilder performs exceptionally well when compared to the comparative results.

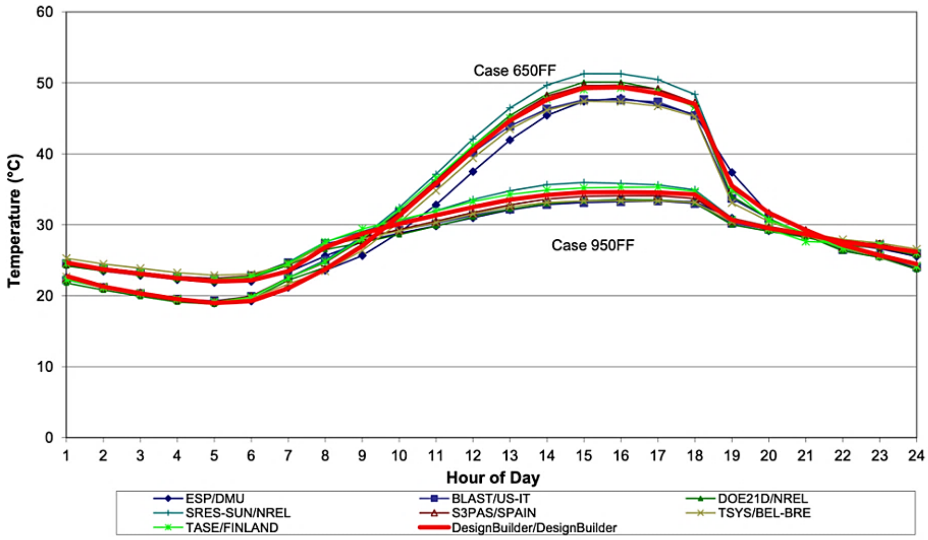

Figure 4.1: Hourly free float temperatures on a clear hot day simulation comparison for cases 650FF and 950FF, using lightweight and heavyweight material specifications, respectively, with night ventilation case. Source: EnergyPlus (2021b).

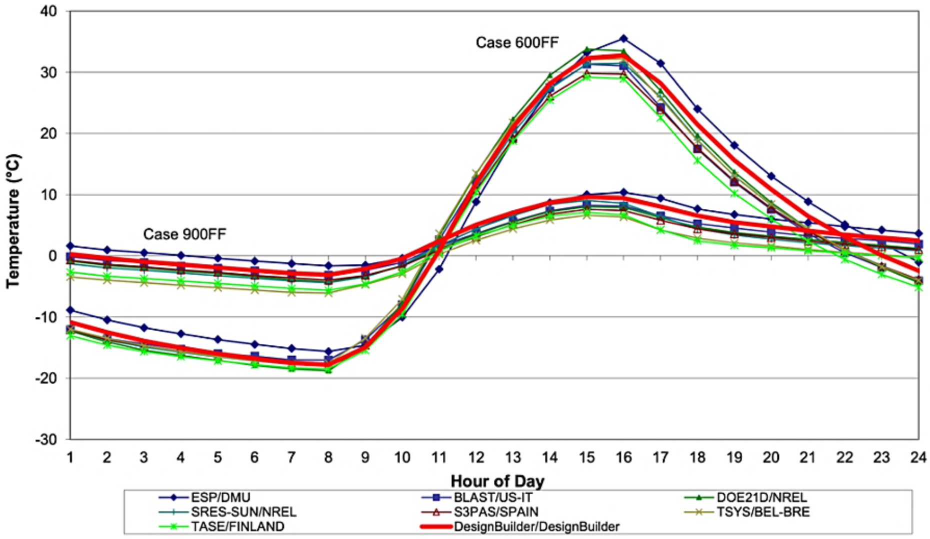

Figure 4.2: Hourly free float temperatures on a clear cold day for cases 600FF and 900FF, using lightweight and heavyweight material specifications, respectively, without night ventilation. Source: EnergyPlus (2021b).

Each figure presents 8 lines of data. These data represent the results of individual Building Energy Performance Simulation tools. Originally, the base-case model was a rectangular, low-mass, single-zone structure (interior dimensions: 8 x 6 x 2.7 m) with two south-facing windows (3 x 2 m). Heating and cooling are provided by an "optimal" mechanical system (100% efficient, with no duct losses and no capacity limits). The figures summarise the results of the ANSI/ASHRAE Standard 140-2017 Building

Thermal Envelope and Fabric Load Tests. The results indicate that EnergyPlus compares very well to the comparative results across all scenarios.

The development of dynamic thermal models capable of predicting hourly internal temperatures in buildings in the late 1980s necessitated the creation of criteria for determining whether a building was likely to overheat. This was especially critical for free-running buildings, as defined by the CIBSE Guide A as those that do not consume energy for heating or cooling at the time in question. The term 'naturally conditioned' is also used elsewhere, for example, in the ASHRAE Standard 55 (Lomas and Giridharan, 2012).

The EnergyPlus (2021) simulation compared heavyweight and lightweight construction materials across various scenarios, analysing hourly free-float temperatures during clear hot and cold days to account for climatic variations. Negative temperature values in Figure 4.2 indicate room temperatures below zero on a typical cold day. Among state-of-the-art simulation tools, DesignBuilder demonstrated superior performance, achieving an optimal balance in simulating the thermal performance of building envelopes, as validated by the ASHRAE standard test for building fabric and load.

Evidently, DesignBuilder software produces accurate results that lie in the middle range of all the other simulation tools. Hence, the results examining the tools consider a maximum temperature of around 52°C and a minimum of around -20°C, while the DesignBuilder result remains consistent. In other words, the result lies somewhere between all the other simulation tools' outputs, providing an outstanding average result.

4.15 RESEARCH VALIDATION OF ENERGY SIMULATION TOOLS FOR SAUDI RESIDENCES

DesignBuilder is a BEPS tool developed in the UK. It employs the EnergyPlus simulation engine, making it a user-friendly building simulation software interface. The accuracy of DesignBuilder has been validated using the Building Energy Simulation Test (BESTEST) approach, which the US Department of Energy and an international community of building modellers utilise to test computer simulation tools' capabilities (Alayed et al., 2021). Based on previous scientific investigations, DesignBuilder is the recommended BEPS tool for this study. To gauge the uncertainty of the EnergyPlus tool, findings were juxtaposed against measured and simulated models for dwellings in

Saudi Arabia. Given the extreme weather conditions, Saudi Arabia stands as one of the most challenging global locations concerning household power consumption. The nation faces a hot-humid environment in its coastal regions, making the uncertainty around yearly energy loads particularly pronounced.

This research further seeks to compare the EnergyPlus model with studies examining energy use and thermal performance in Saudi Arabian residences. The BEPS tool's accuracy and reliability were ascertained to justify its selection. This study has taken steps to validate the tool's reliability and accuracy. This investigation chose the DesignBuilder (EnergyPlus, Version 8.9.0 Simulation) tool to assess energy consumption. The overarching aim was to pinpoint the EnergyPlus model's position amongst other developed models, especially those relating to typical Saudi Arabian dwellings. Consequently, the EnergyPlus model's validity was determined using data from prior research, as well as from observed projected models. The subsequent section delves deeper into the comparison of the EnergyPlus model with other studies focusing on Saudi Arabian residences.

Note: previous research into the use of BEPS tool is attached in Appendix E.

4.15.1 RESEARCH VALIDATION USING A CASE STUDY COMPARISON

Alayed et al. (2021) scrutinised the thermal envelope performance of typical detached villa housing in Saudi Arabia, utilising DesignBuilder analysis software. Their research entailed an exhaustive energy assessment of the entire structure, conducted using DesignBuilder v6.1.2.009. The materials and wall type investigated in their study epitomise a conventional Saudi Arabian residential villa (Table 4.4) and provide a foundation for evaluating the thermal performance of the envelope and, subsequently, the energy load of certain building typologies.

The case study was selected for validation as it closely resembled one of the pre-existing developed case study models in terms of construction materials and average usage. Accordingly, the model presented by Alayed et al. encompasses a traditional construction system situated in the Riyadh region. The replicated (developed) model employed identical construction materials and weather location. Consequently, the annual electricity consumption for the Alayed model and the replicated model was recorded as 140 and 150 kWh/m², respectively, indicating that the replicated model consumes 10 kWh/m² more electricity annually.

Table 4.4: Modelled villa construction properties. Source: Alayed et al. (2021)

Latitude position	Riyadh (latitude 24.710 N, longitude 46.725 E, Elevation 635)
Face direction	Front elevation facing East
No. of floors	3
height of floors	3.5 m
Total floors area	288 m^2
Total roof area	120 m^2
Total walls area	406 m^2
WWR	6.5%
Window type	Double layered glazing (6 mm, 12 mm, 6 mm)
External walls	Model-1 bridged walls U-value = 1.27 W/(m^2·K) Model-2 un-bridged walls U-value = 0.47 W/(m^2·K)
Roof construction	20 mm cement plaster, 200 mm reinforced concrete slab, 50 mm EPS expanded polystyrene, 4 mm waterproof membrane, 50 mm lightweight cast concrete and 20 mm Terrazzo tiles
Air conditioning system	Split unit
Heating system	Electrical heater
Thermostat setpoint	25 °C for cooling and 20 °C for heating

In their research, the primary objectives were to ascertain whether the prevailing envelope construction practices in Saudi Arabia can comply with the new SBC 2018 requirements, and whether the recommended modelling tools in these codes can appropriately represent the complex geometries of the vertical envelope and, consequently, thermal bridging (Figures 4.3 and 4.4). This study was selected for inclusion in this research to validate the reliability of employing the recommended simulation tool, DesignBuilder, as a means of validation within this research alone.

The study was conducted in Riyadh, and as such, the chosen weather data pertains to the Riyadh weather data file. Similarly, the reproduced model accounted for the Riyadh weather data file to ensure accurate and comparable results. Additionally, in their investigation, the U-value used in the comprehensive building analysis was determined using the Finite Element Method (FEM) via ANSYS software. This calculated U-value was then used as an input for the building envelope material properties within the reproduced model. Consequently, this research solely compares the DesignBuilder model with a similarly developed model using the U-value as calculated by Alayed et al.'s FEM simulation.

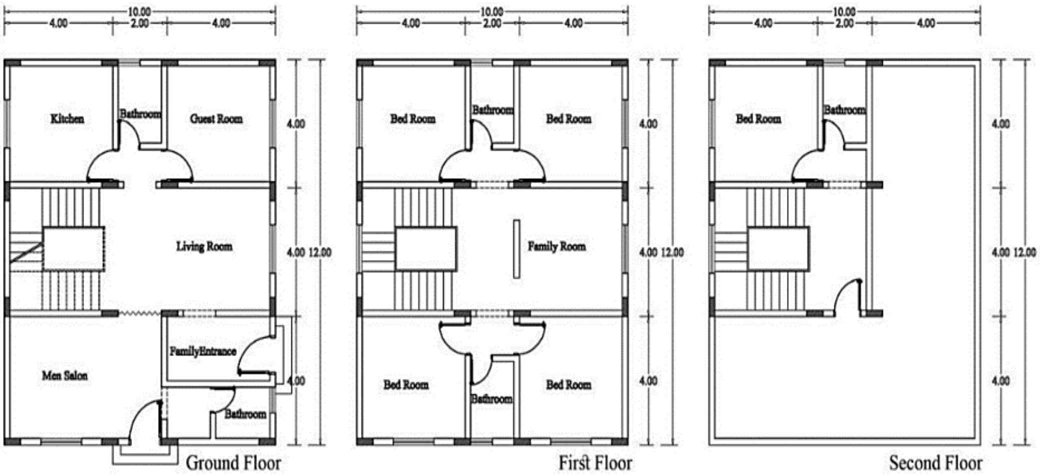

Figure 4.3: Floor plans of the analysed case study house by Alayed et al. (2021).

Despite the modest discrepancy between the two cases, the variance could potentially stem from distinctions in the HVAC system's intricate details, which were not elaborated upon in Alayed et al.'s study. Specifics such as the HVAC's Coefficient of Performance (COP), capacity, and the like were omitted, with only a reference to a split HVAC system that may have resulted in minor variations in the outcomes. Additionally, the unspecified window heights in the study could have contributed to this marginal difference. Nevertheless, the difference in energy consumption between the two cases is a mere 10 kWh/m^2, thereby encouraging the reliability of the analysis programme as shown it table 4.5.

Table 4.5: Modelled villa and developed model analysis comparison.

Reference	Alayed et al. (2021) model	Developed model
Building location	Riyadh (Latitude 24.710° Longitude 46.725°, elevation 635	Riyadh (Latitude 24.70° Longitude 46.80°, elevation 612
Face direction	Front elevation facing East	Front elevation facing East
No of floors	3	3
Roof Area [m^2]	120	120
Walls area [m^2]	406	406
WWR%	6.5	6.5
Climate zone	1	1
Total floors area (m^2)	288	288
One year energy consumption (MWh)	32	32
Total energy consumption per floor area (kwh/m^2/yr.)	140	150

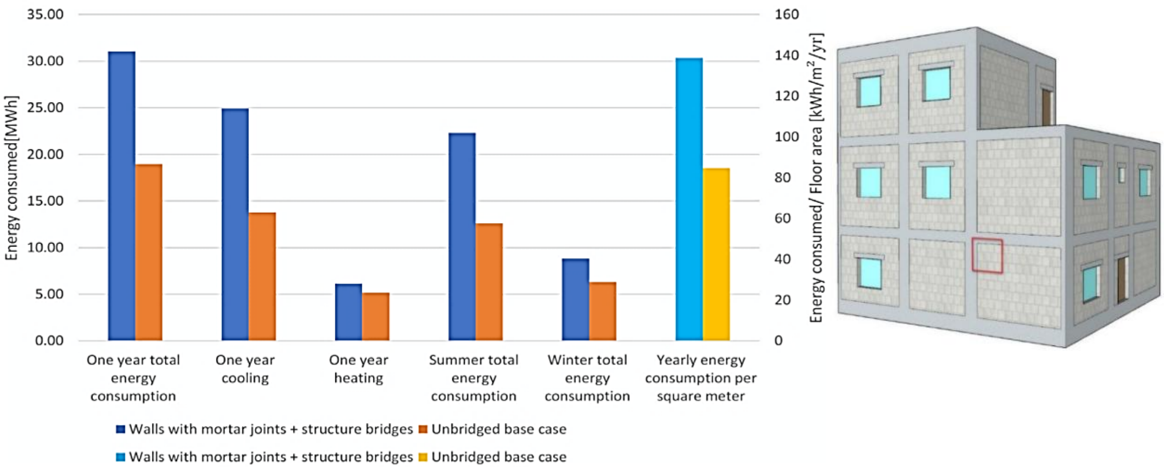

Figure 4.4: Alayed et al.'s (2021) model's energy consumption with bridged and hypothetical unbridged envelopes (simulated for one year using DesignBuilder).

According to Alayed et al.'s model, Figure 4.4 provides a comprehensive representation of energy consumption metrics over a year, covering total, cooling, heating, summer, winter, and energy consumption per square metre. The results elucidate the distinction between "bridged" scenarios, which account for the entirety of thermal bridging effects, and "unbridged" scenarios, which exclude the thermal bridging effects originating from mortar and concrete structures.

As a result, Figure 4.4 explores the impact of thermal bridging caused by mortar joints and structural components. It reveals a significant increase in the annual total energy consumption, which escalates from 19 MWh to 32 MWh due to the introduction of thermal bridges. When compared with Alayed et al.'s base case scenario – featuring a continuous insulating layer absent of thermal bridges – the cooling load undergoes a substantial increase of 78%, surging from 14 MWh to 25 MWh. Concurrently, the heating demand experiences a reasonable rise, from 5 MWh to 6 MWh. This increase is predominantly observed during the winter nights when temperatures descend below 10°C, a condition persisting for approximately three months across diverse regions of Saudi Arabia.

Alayed et al. (2021) highlight that the summer energy load discrepancy between the bridged and unbridged configurations is notably accentuated, witnessing a 70% increase, equating to an additional 10 MWh, driven by an augmented demand for air conditioning.

According to Alayed et al.'s model, Figure 4-4 provides a comprehensive representation of energy consumption metrics over a year, covering total, cooling, heating, summer, winter, and energy consumption per square meter. The results elucidate the distinction between "bridged" scenarios, which account for the entirety of thermal bridging effects, and "unbridged" scenarios, which exclude the thermal bridging effects originating from mortar and concrete structures.

In summary, thermal bridging results in an elevation in annual energy consumption per square metre of floor space from around 85 to 140 kWh/m²/year, with the impact being especially pronounced during the summer months, where cooling is of utmost importance.

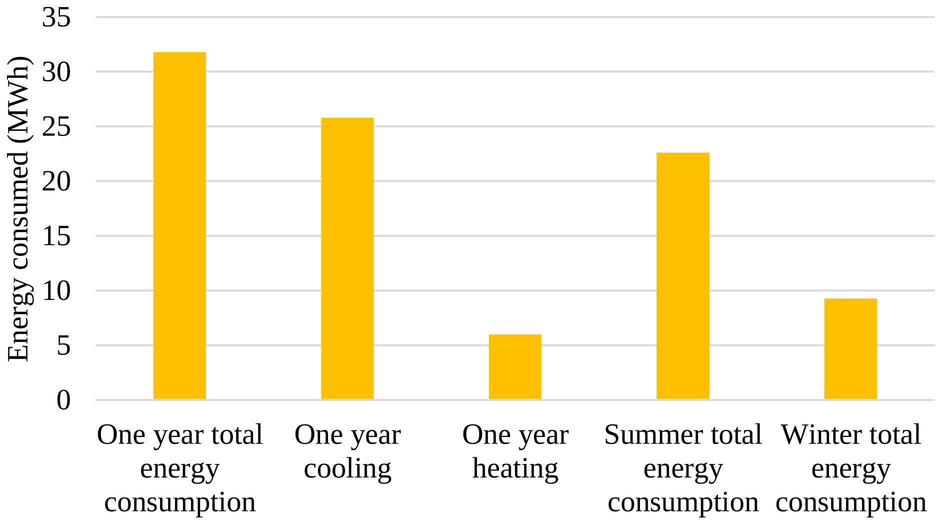

Figure 4.5: The reproduced model's simulation results for one year of energy consumption in the building with the bridged envelopes scenario. Data gathered from the generated model and reproduced using Excel.

As depicted in Figure 4.5, the reproduced model simulation considers only the bridged scenario, aligning with the results presented in Alayed et al.'s Figure 4.4. The results from the reproduced model indicate a one-year total energy consumption of 32 MWh, closely aligning with the 32 MWh reported by Alayed et al. Additionally, the one-year cooling and heating energy consumption of the reproduced model are 25.8 MWh and 6 MWh, respectively, akin to the 25 MWh and 6 MWh observed in Alayed et al.'s model. The summer and winter total energy consumption for both models also bear a resemblance, approximately 22.6 MWh and 9.2 MWh, respectively, as depicted in Figures 4.4 and 4.5.

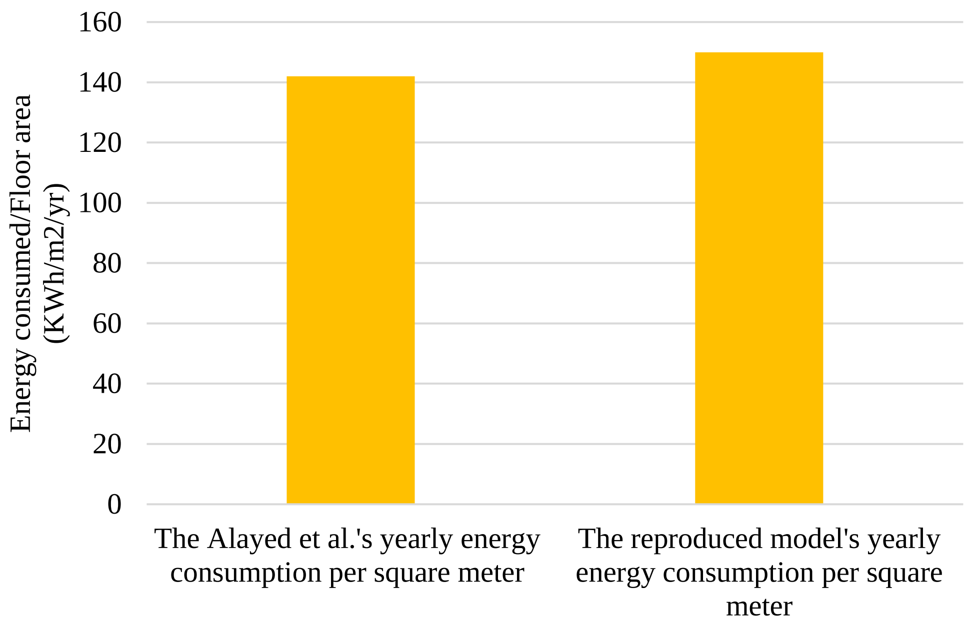

Figure 4.6: Alayed et al.’s and the reproduced developed model's yearly energy consumption per square metre. Data gathered from the generated model and reproduced using Excel.

As shown in Figure 4.6, the analysis reveals that the overall energy consumption for the thermally bridged case study scenario of a villa-type structure in Saudi Arabia is 140 kWh/m²/year. Meanwhile, the reproduced model, utilising the same construction parameters and considering the thermally bridged scenario, reports an overall energy consumption of 150 kWh/m²/year. The discrepancy in the yearly energy consumption per floor area between Alayed et al.’s model and the reproduced model is justifiable, given that the reproduced model did not account for accurate lighting and other energy loads (from both equipment and appliances). These factors were assumed as they were not detailed in Alayed et al.’s study; thus, the reproduced model simulation focused on cooling and heating demands overall.

4.15.2 ETHICAL CONSIDERATION

This study adhered to ethical research practices by ensuring the proper acknowledgement of existing studies and their authors when comparing analysis results. The use of the same house as the original study was conducted with respect to intellectual property and academic integrity. All referenced materials, data, and findings from the original study were credited appropriately, ensuring transparency and avoiding misrepresentation. Additionally, the comparative analysis was solely intended to validate the research methodology and contribute to the academic discourse, without compromising the originality or significance of the referenced work.

4.16 SELECTION OF HOURLY WEATHER DATA FOR THERMAL SIMULATION

The Department of Energy (DOE) supplies the hourly meteorological data used by DesignBuilder, which simulates external environmental conditions using the EnergyPlus format for hourly weather data. This data is location-specific, providing detailed records of external temperature, solar radiation, and air conditions for each hour of the year. Typically, this 'typical' weather data is sourced from the hourly observations made by the National Weather Service or similar meteorological bodies, collected at specific sites. In instances where hourly weather data is not available for a certain location, it may be necessary to use data from a nearby area to estimate the conditions at the intended site (Designbuilder, 2022).

With this consideration, the hourly weather data from King Fahad Airport was chosen for its geographical proximity; it is the closest available dataset. King Fahad Airport, located in Dammam City, approximately 80 kilometres from Jubail City, provides a weather dataset that is used to infer the environmental conditions of Jubail Industrial City.

The initial phase of the field study entails a comprehensive examination and documentation of the selected case study houses, detailing their locations, areas, and architectural layouts. For the purposes of simulation, the hourly weather data from King Fahad Airport is utilised, allowing for a more precise simulation of the thermal performance of the residences under study, reflective of the environmental conditions pertinent to Jubail Industrial City.

4.17 SUMMARY

The methodology, structured according to Saunders' Research Onion framework, provides a systematic approach to investigating the thermal performance of prefabricated houses. By integrating field observations, validated simulation tools, and a case study strategy, the research ensures a comprehensive analysis of energy efficiency and thermal comfort in the context of Saudi Arabia's unique climatic conditions.

Additionally, it conducts an extensive comparative analysis of various Building Energy Performance Simulation (BEPS) tools, evaluating their capabilities in assessing zone loads, building envelopes, daylighting, solar gains, infiltration, ventilation, zone airflow, HVAC systems and components, renewable energy systems, and economic factors. Moreover, the chapter addresses the pertinence of ASHRAE Standard 140-2017, which is fundamental in evaluating the software employed for determining the thermal performance of buildings.

For this study, the BEPS tool of choice is DesignBuilder, a UK-developed tool utilising the EnergyPlus simulation engine. Its reliability has been validated through the BESTEST approach, a stringent testing method sanctioned by the US Department of Energy and the international building modelling community. The robustness of DesignBuilder is further examined by comparing measured and simulated data for houses in Saudi Arabia, where the climate poses significant challenges to domestic energy management.

CHAPTER FIVE - DISSCUTION OF FIELD MEASURMENTS OF CASE STUDY BUILDINGS

5.1 INTRODUCTION

This chapter delves into the practical implementation of the research through a comprehensive field study, aimed at validating and calibrating the outcomes of the research methodology. Centred on evaluating thermal performance, the study highlights residential precast concrete structures in Jubail Industrial City, Saudi Arabia. It emphasises data collected from these dwellings, analysing key factors that affect their thermal characteristics.

The chapter begins by outlining the tasks involved in the field study, detailing the systematic approach adopted to gather significant data essential for achieving the research objectives. The criteria for selecting the projects or houses are meticulously discussed, emphasising the importance of choosing representative samples aligned with the research goals. The selection process for prefabricated precast case study houses is examined for their suitability for in-depth analysis and comparison within the research framework.

Furthermore, this chapter provides a contextual understanding of the selected projects' developments, offering insights into their historical background and geographical context. The physical aspects of the case study houses are examined in detail, providing insights into their structural and architectural characteristics. The arrangement of spaces within the selected houses is thoroughly analysed, considering their impact on energy performance and indoor comfort.

A critical focus of this chapter is the validation of indoor and outdoor air temperatures from software simulations against in-field measurements. The instrumentation and methodology employed for indoor and outdoor air temperature measurement are rigorously discussed, ensuring standardised and precise data collection procedures. Through meticulous attention and adherence to precise methodologies, this chapter aims to produce highly validated outcomes essential for advancing knowledge in the field of building energy performance simulation.

5.2 FIELDWORK INSIGHTS FOR ASSESSING INDOOR CONDITIONS

The primary method employed to investigate indoor environmental conditions in the case study houses was a comprehensive fieldwork investigation. This fieldwork aimed to gather detailed information on various aspects, including the houses' locations, surroundings, and materials used in their prefabricated construction. Additionally, indoor observations were conducted to obtain insights into cooling and heating methods, finishing materials, and the properties of internal and external prefabricated walls, among other factors. This rich dataset is crucial for use in the computer model, ensuring accurate simulation outcomes.

Specifically defining tasks, sequencing operations, and identifying survey materials were essential for completing the fieldwork efficiently and within the scheduled period. Special attention was given to locating prefabricated houses, as assessments were conducted exclusively in unoccupied dwellings. The fieldwork unfolded in three distinct phases, each contributing essential insights into the indoor conditions of the prefabricated houses. Further details regarding these phases are provided in Figure 5.1.

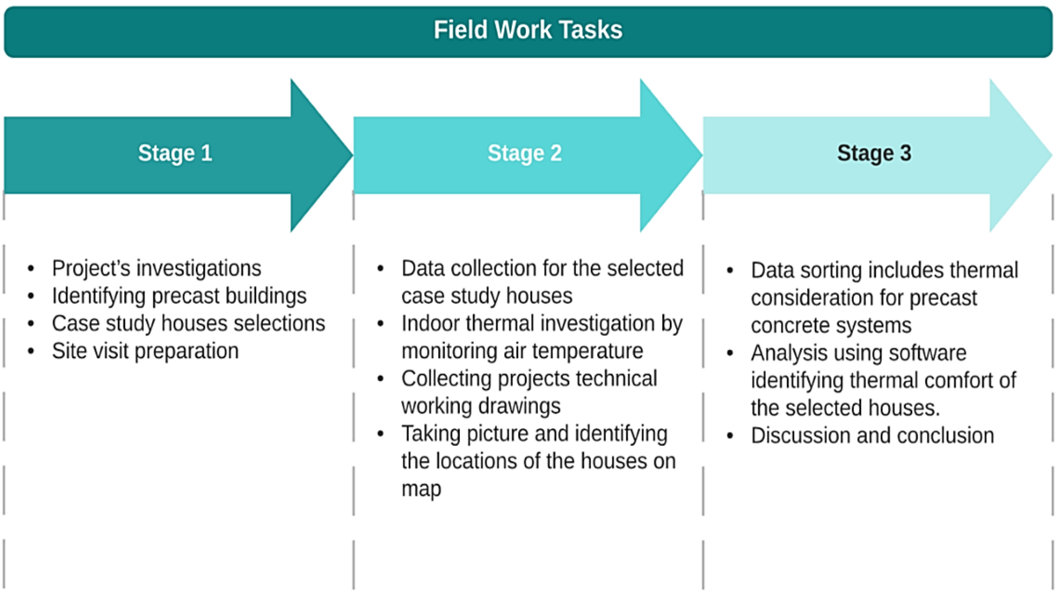

Figure 5.1: Illustration of the fieldwork tasks.

5.2.1 CRITERIA FOR SELECTING THE PROJECT/HOUSES

The following criteria are employed to select the projects or houses:

1. Precast Concrete System: The project must exclusively implement a precast concrete system.
2. Occupancy Status: The house must be unoccupied. This ensures easy access and consistent conditions for validation, aligning with simulation settings for a closed, unoccupied house.
3. Construction Completion: The house must be fully constructed.
4. Accessibility: The house must be accessible.
5. Regional Development: The project must be part of a regional development housing initiative, reflecting significant housing development in the area.
6. Amenities: The house must be equipped with sanitary facilities, including a kitchen and toilet.

The data collection phase began with the identification of several local projects within the Kingdom of Saudi Arabia, designated as potential candidates for selecting houses for the case study. Notably, a significant proportion of these projects consist of housing developments initiated by private sectors in collaboration with the Ministry of Housing. The Ministry's strategic collaboration involves contracting local developers to create high-quality projects tailored to meet the needs of end users.

The distinguishing feature of these projects is the use of precast concrete systems, enabling rapid construction completion and cost reduction compared to other large-scale housing projects within the country. Appendix A outlines the theoretically examined prefabricated projects in the Kingdom of Saudi Arabia, with a particular focus on those exclusively incorporating precast concrete systems.

However, it is worth noting that there may be other projects that remain undiscovered due to accessibility issues, study limitations, and data collection constraints. To mitigate this, information about potential projects is carefully gathered and compiled using official government websites, ensuring a comprehensive overview of the available options for inclusion in the case study.

5.2.2 FIELDWORK TASKS

The research methodology indicates that the field study, encompassing case study investigations, is considered a primary phase of the research. Consequently, several tasks are identified and executed during the investigation of the prefabricated houses, as follows:

1. Location Mapping: The identified precast houses are located by plotting their positions on the district's map.
2. Occupancy Check: Ensuring that the houses are completely empty and unoccupied.
3. Technical Drawings Collection: Gathering all architectural technical working drawings (AutoCAD drawings) for the development of a thermal/energy simulation model using EnergyPlus.
4. Material Investigation: Investigating the construction materials used in the prefabricated houses.
5. Thermal Monitoring: Conducting an indoor thermal investigation by monitoring the indoor air temperature using a thermometer device for a minimum period of 7 days.
6. Energy Consumption Data: Collecting monthly energy consumption readings, if possible.
7. HVAC System Identification: Identifying the originally designed HVAC system of each house.
8. Site Layout Update: Updating any changes to the site layout of each house, including any new nearby buildings or surrounding objects.
9. Height Verification: Confirming the uniformity of the surrounding buildings' heights.
10. Data Collection: Taking notes, capturing pictures, and gathering any useful data relevant to the simulation phase.
11. Software Calibration: Collecting relevant data for calibrating the software intended for the parametric analysis.

The survey device used is illustrated in the validation section of this chapter. Data collected during the fieldwork stage, such as indoor air temperature and technical drawings, are organised into Excel sheets and documented to serve as input data for the thermal simulation.

5.2.3 SELECTION OF PREFABRICATED PRECAST CASE STUDY HOUSES

As previously indicated, several projects featuring prefabricated construction technology were identified in the initial phase of the study. From these projects, a selection of prefabricated houses was identified and investigated during the second phase. Various parameters were defined to find the most suitable building for the study's needs. These parameters include location, climate zone, total floor area, floor height, number of floors, building origin, construction systems and materials used, the implementation of solar shading devices or other integrated shading systems, building age, and the intensity of surrounding buildings or objects that may impact the thermal performance of the building. A crucial criterion considered in both phases was the ability to visit and investigate the project, and the requirement for the building to be empty and unoccupied to align with the research objectives.

From this perspective, the projects in Jubail Industrial City emerged as the preferred choice among all the projects considered. The Royal Commission for Jubail Industrial City developed these projects in accordance with international standards for housing criteria, formulated by a team of architects and engineers. Additionally, a number of special criteria for selecting the projects or houses were considered, as discussed in the following section.

5.2.4 DESCRIPTION OF THE SELECTED PROJECTS' DEVELOPMENTS

The Royal Commission for Jubail Industrial City undertook the construction of 2,197 villas between 1978 and 1982, employing various materials such as precast concrete (1,140 units), aerated concrete (931 residential units), Polyfab (51 residential units), and Cast-in-Situ (51 residential units). The project saw an expansion in 2006 with an additional 123 units made of precast concrete. Between 2009 and 2017, the Royal Commission approved a housing development contract with private sectors, introducing approximately 3,915 residential units made of precast concrete. From 2013 to 2020, the Royal Commission developed around 13,000 residential units to accommodate the rising population, according to a report conducted in 2011 by the Royal Commission. Typically, a residential villa comprises 3 to 4 bedrooms, spanning a total built area of 337m². It is anticipated that by 2030, three additional districts will be established within the residential area, contributing over 27,000 residential units as part of the expansion programme (Royal commission for jubail and yanbu industrial city, 2011).

The aim of the selected projects was to establish a housing scheme consisting of a substantial number of villas, categorised into distinct types based on their built-up areas. This approach was intended to offer customers a variety of choices to align with their income levels. The project includes primary and intermediate schools, a clinic, and apartments, strategically positioned near main streets for easy accessibility. Since all the villas and apartments are constructed within Jubail Industrial City on Royal Commission lands, the project ensures ready access to all amenities necessary for a modern urban lifestyle, while being situated in a green environment near the sea. Additionally, the villas are designed with a focus on individual privacy, adhering to bylaws mandating setbacks on all sides. A standard feature across all villas is a carport capable of accommodating at least two cars.

5.2.5 CITY AND SELECTED PROJECT'S GEOGRAPHICAL LOCATION

Jubail Industrial City, situated on the Arabian Gulf approximately 100 kilometres north of Dammam, benefits from access to international sea lanes and proximity to energy and raw material sources for refining and petrochemical products (Figure 5.2).

Figure 5.2: Map of cities developed by the Royal Commission within the Kingdom of Saudi Arabia. Source: (Royal commission for jubail and yanbu industrial city, 2011).

Jubail, situated in the Eastern Province of Saudi Arabia, had a population of 684,531 people as of 2021. This vibrant urban centre is divided into two distinct zones: the historic Old Town and the extensive expanse of the Industrial City, which is the largest industrial hub in the world. Established in 1975, Jubail Industrial City has grown into a thriving metropolis, serving as the nucleus for a multitude of industrial endeavours. Notably, it accommodates the headquarters of the Middle East's largest petrochemical conglomerate, Saudi Basic Industries Corporation (SABIC), and hosts the world's largest Independent Water and Power Project (IWPP). This monumental endeavour yields an impressive daily output of 2,743.6 megawatts of electricity and supplies 800,000 cubic metres of potable water.

In the pursuit of economic diversification, the Kingdom of Saudi Arabia established the Royal Commission for Jubail and Yanbu in 1975. This strategic move aimed to bolster the nation’s economy by leveraging the potential of industrial development. The commission was tasked with overseeing and coordinating the establishment and growth of key industrial cities, including Jubail, Yanbu, Ras Al-Khair, and Jazan. These cities were envisioned as vital hubs for various industries, ranging from petrochemicals to manufacturing, with the aim of reducing the Kingdom’s dependence on oil revenue.

The Royal Commission for Jubail and Yanbu (RCJY) operates under a mandate to effectively manage and develop these cities, ensuring their sustainable growth and economic viability. This mandate encompasses a multifaceted approach, which includes urban planning, infrastructure development, regulatory oversight, and the facilitation of investment opportunities. The commission works closely with government agencies, private sector entities, and international partners to achieve its objectives.

At the core of the RCJY’s mission is a commitment to a customer-centric approach. This entails prioritising the needs and interests of residents, businesses, and other stakeholders in the development and management of the cities. The commission seeks to create an enabling environment that fosters innovation, entrepreneurship, and economic prosperity. Moreover, the RCJY recognises the importance of collaboration and partnerships in achieving its goals. The commission actively engages with a diverse range of stakeholders, including local communities, industry associations, educational institutions, and research organisations. By leveraging collective expertise and resources, the RCJY aims to optimise the impact of its initiatives and drive sustainable development.

The Royal Commission for Jubail and Yanbu plays a pivotal role in Saudi Arabia's economic diversification strategy. Through strategic planning, effective governance, and collaboration with stakeholders, the commission endeavours to create vibrant, sustainable cities that contribute to the Kingdom's long-term prosperity and resilience.

Figure 5.3: Map showing the Jubail 1 and Jubail 2 areas within the region. Source: (Royal commission for jubail and yanbu industrial city, 2011).

Figure 5.3 illustrates the geographical locations of Jubail 1 and Jubail 2. Since its inception, Jubail Industrial City has evolved into a leading global centre for petrochemical production and related industries. The persistent demand for investment in this sector prompted the establishment of Jubail 2, underscoring the unwavering commitment of the Royal Commission to fostering economic growth and industrial development. Furthermore, Jubail Industrial City serves as a catalyst for the advancement of downstream industries by facilitating access to raw materials essential for the manufacturing of value-added products destined for both domestic consumption and international markets.

In line with this vision, various strategic initiatives, such as the PlasChem initiative, have been implemented to incentivise the establishment of downstream industries. These initiatives are designed to streamline production processes and reduce operational costs, thereby enhancing the attractiveness of Jubail Industrial City as a preferred destination for investment in downstream manufacturing.

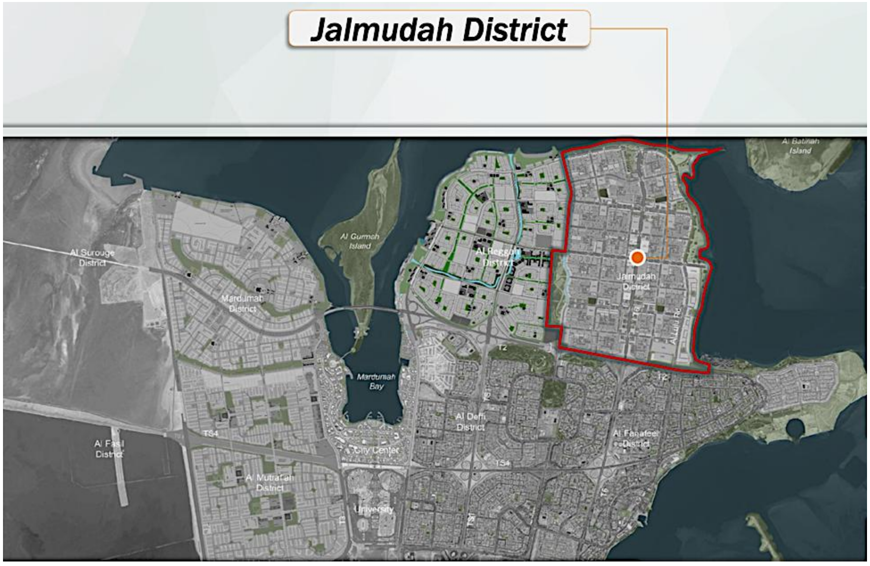

Figure 5.4: Illustration of Jalmudah District. Source: (Royal commission for jubail and yanbu industrial city, 2011).

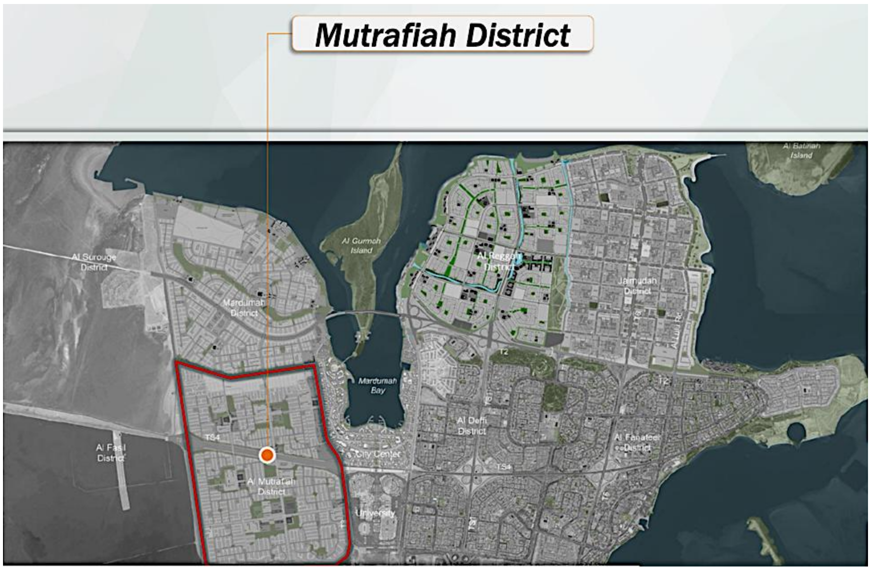

Figure 5.5: Illustration of AL-Mutrafiah District. Source: (Royal commission for jubail and yanbu industrial city, 2011).

Figures 5.4 and 5.5 provide insights into Jalmudah and Al-Mutrafiah, respectively, highlighting their pivotal roles within Jubail Industrial City's residential landscape. These districts, situated in Jubail 1, are among the meticulously planned residential zones within the city. Notably, the road networks within these districts not only facilitate vehicular movement but also enhance the overall urban aesthetics and functionality. Positioned near the city centre, both Jalmudah and Al-Mutrafiah play crucial roles in shaping the residential experience within Jubail Industrial City, offering residents a blend of convenience and accessibility.

Furthermore, Figure 5.6 provides additional context by visually illustrating the spatial relationship between the city centre and these residential districts. This depiction underscores the strategic placement of Jalmudah and Al-Mutrafiah within the broader urban framework of Jubail Industrial City, emphasising their importance in enhancing the city’s residential fabric.

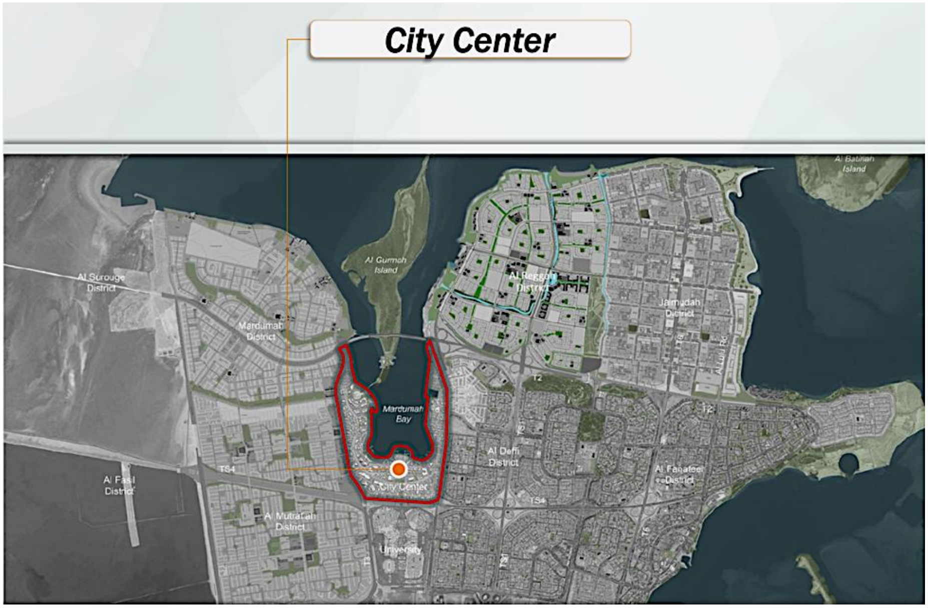

Figure 5.6: Map illustrating the city centre and the nearby Al-Mutrafiah district. Source: (Royal commission for jubail and yanbu industrial city, 2011).

5.2.6 PHYSICAL ASPECTS OF CASE STUDY BUILDINGS

In the development projects of Jalmudah and Al-Mutrafiah, the predominant architectural feature is detached single-family houses, complemented by a selection of apartments integrated within detached structures. These houses exhibit diversity in terms of schemes or types, each characterised by distinct sizes and layouts. Tables 5.1 and 5.2 meticulously outline the array of schemes and types of houses prevalent in the Al-Mutrafiah and Jalmudah districts of Jubail Industrial City, respectively.

As depicted in Figures 5.7 and 5.8, houses constitute the predominant construction within both development projects, reflecting the emphasis on single-family dwellings.

Apartments, on the other hand, are primarily situated at the edges of the sites, contributing to a balanced and harmonious urban landscape within the districts.

Table 5.1: Different types of houses investigated in Jalmudah District (developed by the Royal Commission) in Jubail Industrial City. Data gathered from a site visit.

House type	Total building Area (M^2)	Number of rooms	Ground floor area (M^2)	First floor area (M^2)	Roof room area (M^2)
A-1	378	4	177	157	44
B-2	408	4	194	170	44
B-3	423	4	195	177	51

Table 5.2: Different schemes of houses investigated in Al-Mutrafiah District (developed by SABIC) in Jubail Industrial City. Data gathered from a site visit.

House type	Total building Area (M^2)	Number of rooms	Ground floor area (M^2)	First floor area (M^2)	Roof room area (M^2)
Scheme 1	378	4	188	162	28
Scheme 2	376	4	188	163	25
Scheme 3	371	4	188	163	20
Scheme 4	367	4	183	166	18
Scheme 5	352	4	179	157	16
Scheme 6	359	4	176	167	16

Table 5.1 illustrates the diversity of house types within the Jalmudah District of Jubail Industrial City, supervised by the Royal Commission, while Table 5.2 lists a range of housing schemes in the Al-Mutrafiah District, managed by SABIC. These tables detail the total building area, number of rooms, and floor area distribution for each type and scheme, providing valuable insights into the architectural characteristics of these residential areas.

Upon detailed inspection of the projects and design criteria, three houses were identified for closer examination: one A-1 house type (1-J) from Jalmudah and two Scheme 5 houses (1-M and 2-M) from Al-Mutrafiah. These selections were based on their representative characteristics, suitability for in-depth analysis, and availability.

Moreover, the chosen houses share some common construction materials, including precast concrete insulated panels for exterior walls and precast solid wall panels for interior walls. Additionally, roofs and floors are constructed using precast hollow-core slabs, underscoring the standardised building techniques employed in both districts.

5.2.7 HOUSES LOCATIONS AND DESCRIPTIVE IMAGES

House 1-J is situated at a corner block comprising 22 single-detached houses and faces northeast (Figure 5.7). Its energy and thermal performance are assessed with consideration of the surrounding houses of similar height, ensuring an accurate simulation of environmental influences such as shading. Architectural technical drawings and images of House 1-J are shown in Figures 5.9 to 5.13.

Conversely, Houses 1-M and 2-M, both of the Scheme 5 type, are situated in a block containing 14 single-detached houses in the Al-Mutrafiah District (Figure 5.8). All the houses in the block share identical architectural and structural attributes. The distinction between Houses 1-M and 2-M lies in their respective locations: 1-M is nestled between detached houses and includes an attached green area, while 2-M is positioned at the corner of the block. This slight difference might influence their thermal behaviour due to varying shading from adjacent buildings and the effects of the green surfaces. Both houses face southwest and are surrounded by houses of the same height. Figures 5.14 to 5.17 provide a visual representation of the architectural technical drawings and images of Houses 1-M and 2-M.

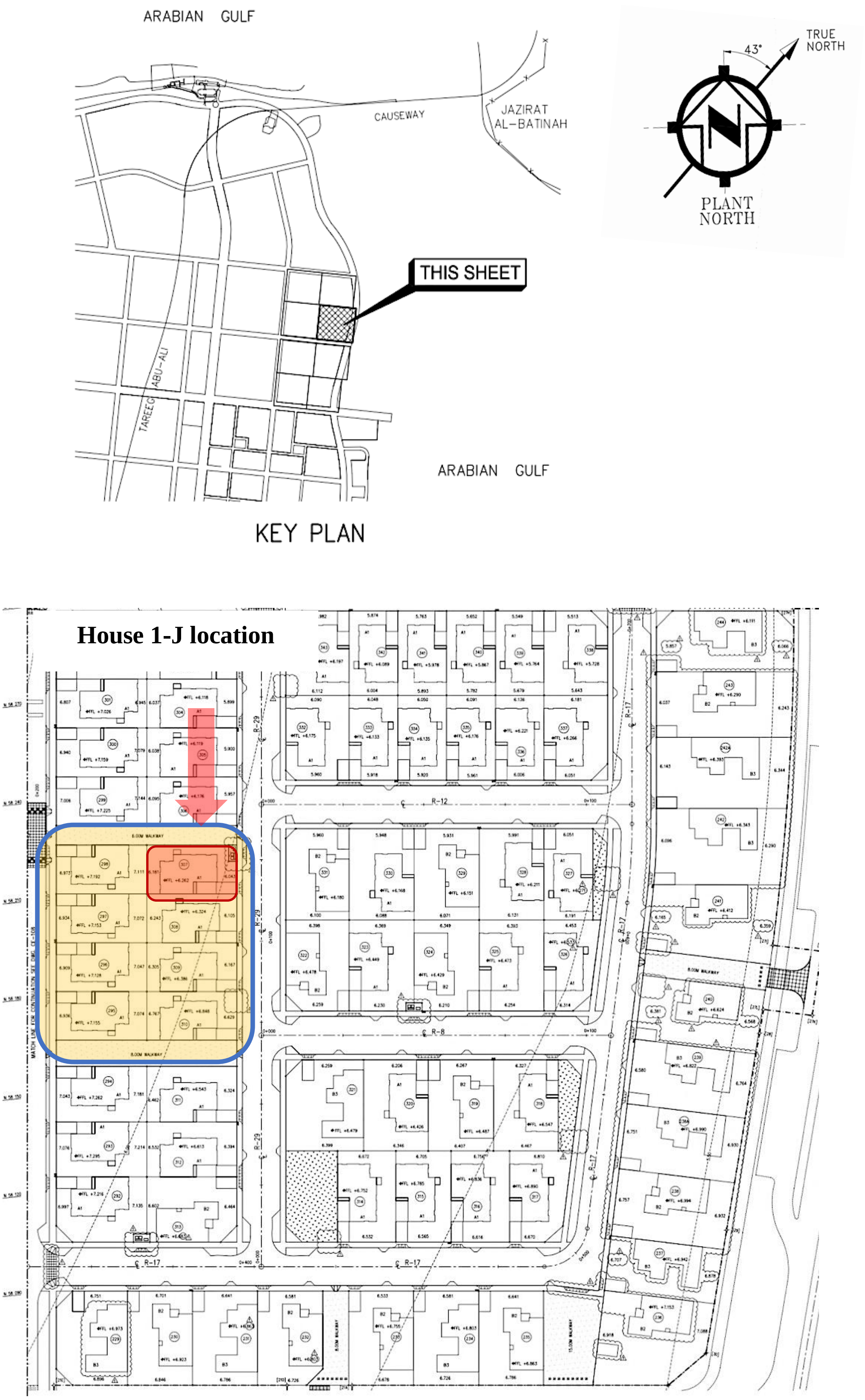

Figure 5.7: District plan showing the location of the selected house (1-J), facing northeast. Source: Royal Commission for Jubail Industrial City. Data gathered from a site visit and document collection.

House 2-M location

House 1-M location

Figure 5.8: District plan showing the locations of the selected houses (1-M and 2-M), facing southwest. Source: Royal Commission for Jubail Industrial City. Data gathered from a site visit and document collection.

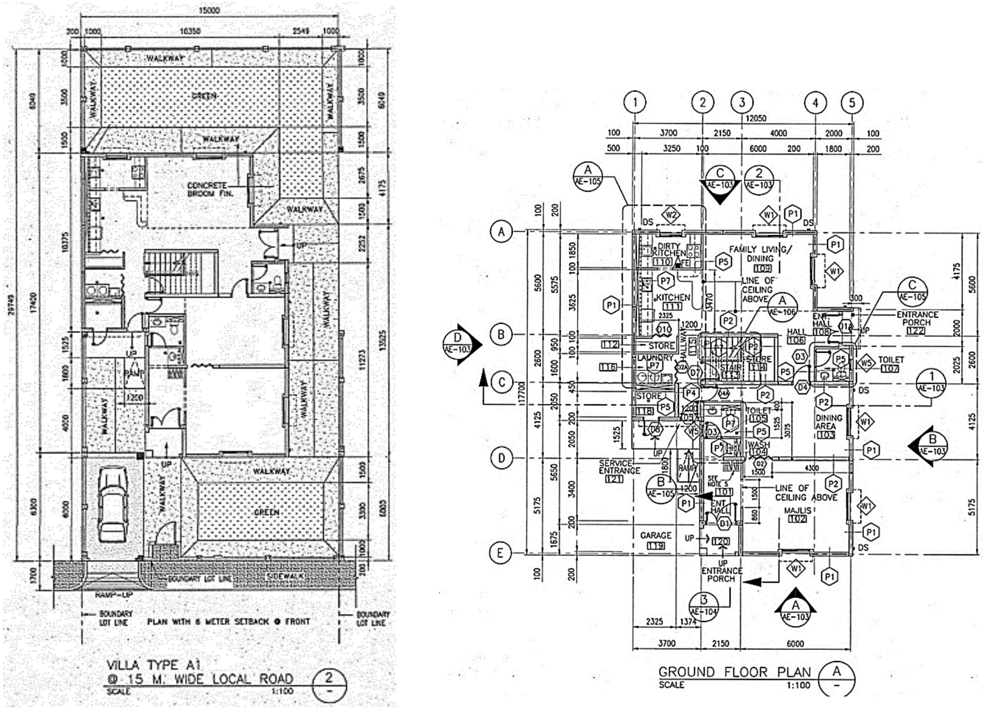

Figure 5.9: Site and ground floor plans for House 1-J. Source: Royal Commission for Jubail Industrial City. Data gathered from a site visit and document collection.

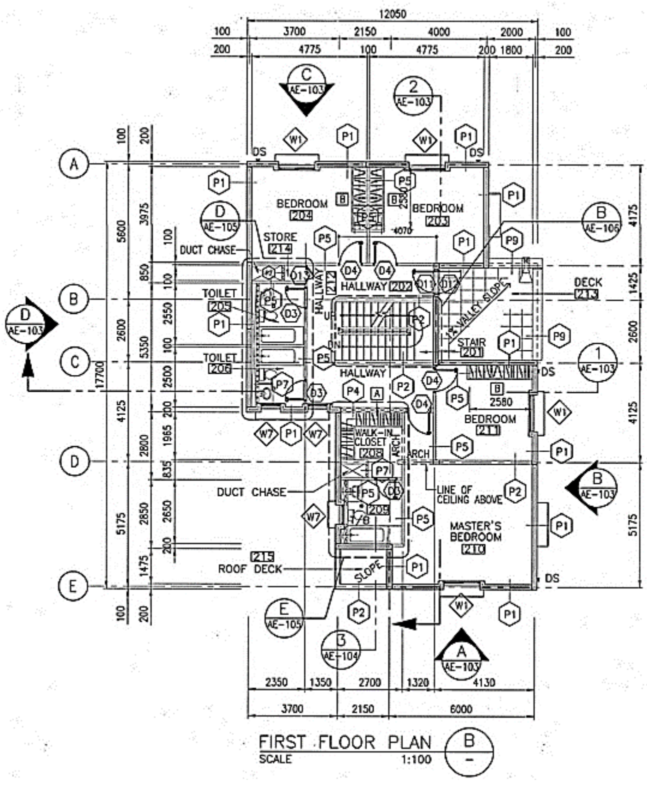

Figure 5.10: First floor plan for House 1-J. Source: Royal Commission for Jubail Industrial City. Data gathered from a site visit and document collection.

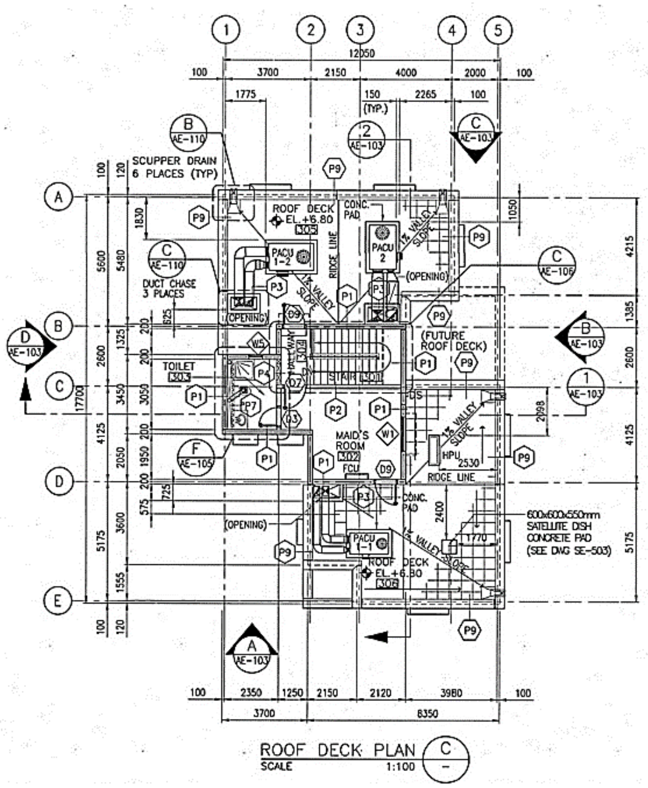

Figure 5.11: Roof floor plan for House 1-J. Source: The Royal Commission for Jubail Industrial City. Data gathered from site visit and document collection.

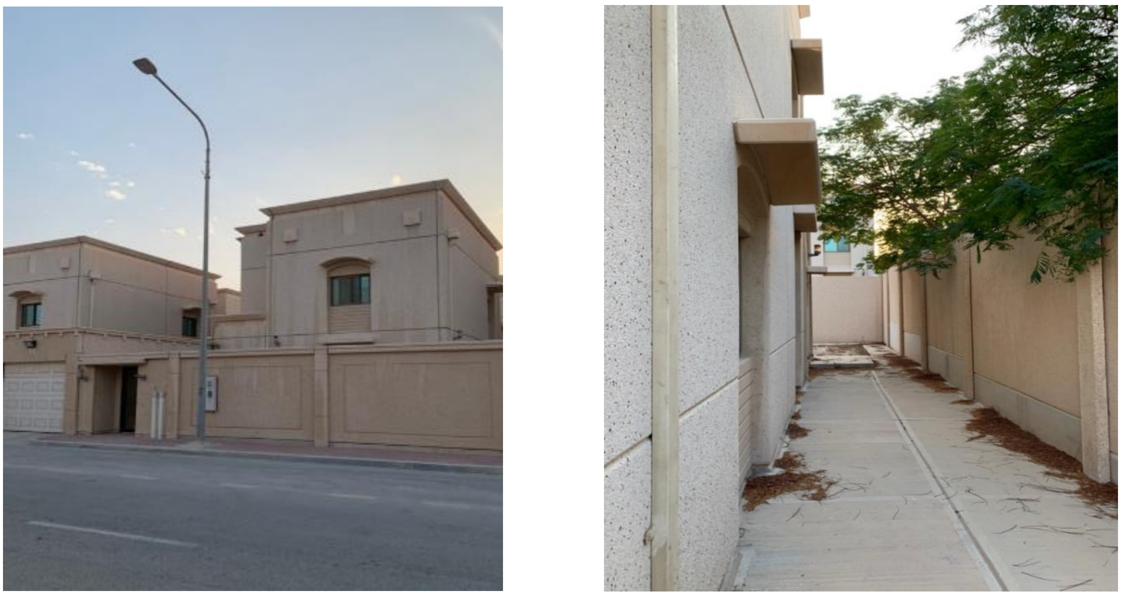

Figure 5.12: Image showing the elevation and side corridor of House 1-J. Source: Self-taken photograph.

Figure 5.13: Images showing the front façade and living room interior of House 1-J. Source: Self-taken photographs.

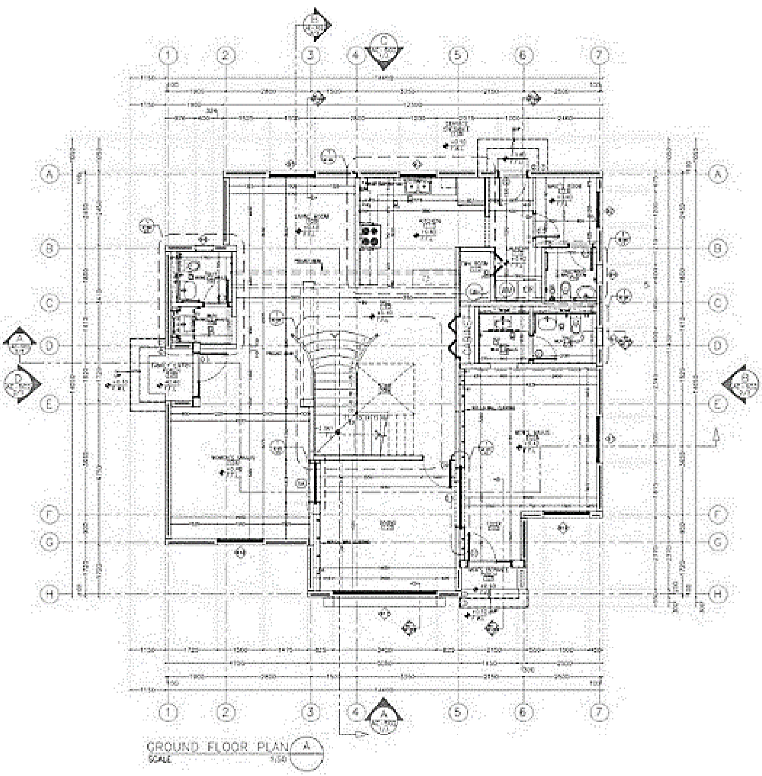

Figure 5.14: Ground floor plan for Houses 1-M and 2-M. Source: Royal Commission for Jubail Industrial City. Data gathered from a site visit and document collection.

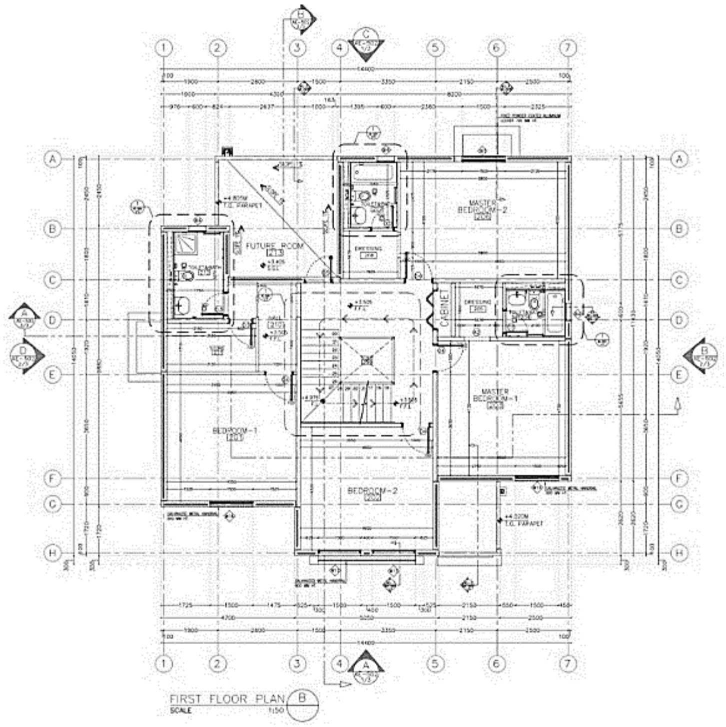

Figure 5.15: First floor plan for Houses 1-M and 2-M. Source: Royal Commission for Jubail Industrial City. Data gathered from a site visit and document collection.

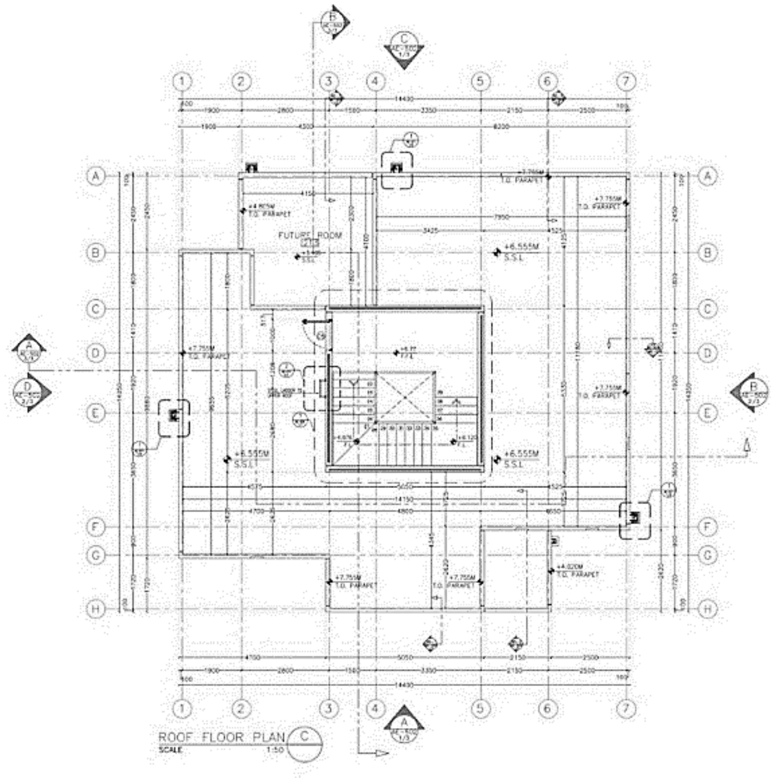

Figure 5.16: District plan for Houses 1-M and 2-M. Source: Royal Commission for Jubail Industrial City. Data gathered from a site visit and document collection.

Figure 5.17: Images showing houses of Scheme 5 (Houses 1-M and 2-M). Source: Self-taken photographs.

5.3 ARRANGEMENT OF SPACES IN THE SELECTED HOUSES

The architectural layout of the selected houses is meticulously designed to meet the varied needs of residents, ensuring functionality and comfort throughout. Comprising four bedrooms, a generously sized living room, a guest room, well-appointed kitchens, and a designated dining area, these houses offer ample space for various activities and social gatherings. Additionally, the inclusion of six bathrooms enhances convenience and privacy for occupants, facilitating their daily routines with ease.

One of the distinctive features of these houses is the strategic placement of three entrances, facilitating seamless access to different areas within the home. Whether entering through a small hall or a corridor, residents are provided with efficient pathways leading to key living spaces such as the dining room, living room, or kitchen.

This thoughtful arrangement optimises movement and enhances the overall functionality of the house.

Central to the architectural composition of these houses is the centrally positioned staircase, serving as a hub adjacent to the living room. This design feature not only acts as a focal point but also ensures accessibility between the ground floor and the first floor, promoting ease of movement throughout the house.

Furthermore, the distribution of bedrooms exclusively on the first floor maximises privacy and creates a calm environment for rest and relaxation. Meanwhile, the strategic placement of bathrooms and toilets, including within the master bedrooms and on both floors, ensures accessibility from all areas of the house, addressing the various needs of residents.

Thus, the arrangement of spaces within the selected houses reflects careful consideration of functionality, convenience, and aesthetics, providing residents with a comfortable and harmonious living environment.

5.4 STRUCTURE AND ENVELOPE

All the identified houses employ concrete skeleton constructions, utilising reinforced precast concrete systems in both architectural and structural elements such as external and internal walls, floors, and roofs (hollow-core slabs). The external walls are constructed from double-wythe precast concrete panels with an intermediate insulation layer, often referred to as a precast sandwich panel. Additionally, the exterior wall is coated with either a dark or light colour and may have a hard or light sandblast finish. This variation in finishes aims to introduce contrast in the architectural patterns, highlight the architectural mass, and distinguish between neighbouring buildings of the same type or scheme.

Floors are typically finished with either ceramic tiles for toilets and kitchens or unglazed porcelain tiles for the remaining rooms. These are installed with a concrete screed topping placed on the precast hollow-core concrete slab. Roofs, on the other hand, are precast hollow-core concrete slabs comprising several layers of thermal and moisture insulation and top finishes. The roof layers include:

1. Precast hollow-core concrete slab: 150 mm for houses 1-M and 2-M, and 200 mm for house 1-J.
2. 20 MPa concrete screed with fibre, thickness varying from 50 mm to 100 mm.
3. Polyurethane foam, 35-45 mm thick.
4. Polytex liquid UV protection coat.
5. Polyfab filter membrane, 120 gsm.
6. Protective sloped screed, thickness varies from 50 mm to 100 mm.
7. SBR bonding agent and Polytex combo-top coat, 800 microns thick.

The total roof thickness amounts to 495 mm. Furthermore, the internal partitions consist of 18 cm and 15 cm precast concrete wall panels for Houses 1-J, 1-M, and 2-M, respectively. All interior wall surfaces are finished with white paint as per approved specifications. The windows are sliding glass panels with double-glazed reflective glass, 6/4 mm, and a 12 mm air gap. The frame is made of powder-coated aluminium, inclusive of the aluminium screen. External shading, in the form of a precast concrete canopy, is only present in House 1-J.

The literature review outlined challenges and trends influencing the system features of precast housing in Saudi Arabia. These findings were leveraged to establish the physical properties of the selected case studies and to generate assumptions regarding variables affecting the thermal performance of the precast concrete system. This informed the subsequent steps of the methodology. A set of parameters was considered based on data collected during the in-field investigation, review of published data, local energy efficiency building standards and regulations in Saudi Arabia, and visits to housing projects in the Eastern Province of Saudi Arabia.

Certain parameters were assumed based on the ASHRAE standard, which played a significant role and was implemented in the selected projects. Chapter 4 delineates a number of thermal properties of precast concrete systems, including elements and material properties usually considered within the precast concrete system. Important building configurations and parameters have been defined in Tables 5.3 to 5.7, establishing a base case scenario based on available technical working drawings and data collected from both literature and in-field investigations

Table 5.3: General information for the selected case study houses collected from the site visit and technical working drawings.

Project	Bldg. Ref.	Geographical Location	Climate Zone	Surrounding Buildings Density	Year	House Type	Building Form
Jalmudah Housing Project	House 1-J	Jubail Ind. City, Saudi Arabia	1A	High	2015	Detached Single House	Rectangular
Mutrafiah Housing Project	House 1-M	Jubail Ind. City, Saudi Arabia	1A	High	2013	Detached Single House	Square
Mutrafiah Housing Project	House 2-M	Jubail Ind. City, Saudi Arabia	1A	High	2013	Detached Single House	Square

Table 5.4: Architectural data for the case study houses collected from the site visit and technical working drawings.

Bldg. Ref.	Built Area (m2)	Floor Height (mm)	Bldg. Height	No. of Floors	No. of Bedroom	Orientation	Const. System	Shading System	Depth-To-Length (%)
1-J	378	GF-3400-FF-3400-SF-3100	10550	3	4	North-East	Precast Concrete System	Precast Conc. Canopy	68.07
1-M	352	GF-3105-FF-3050	9900	2	4	South-West	Precast Concrete System	None	97.56
2-M	352	GF-3105-FF-3050	9900	2	4	South-West	Precast Concrete System	None	97.56

Table 5.5: Envelope systems and floor data for the case study houses, collected from the site visit and technical working drawings.

Bldg. Ref.	Ext. Wall Thick. (mm)	Ext. Wall System	Insu. R-Value (M2·K/W)	Int. Wall Thick. (mm)	Int. Wall System	Roof Slab Thick. (mm)	Roof System	Floor Slab Thick. (mm)	Floor System
1-J	200	Precast Concrete Sandwich Panel (75 mm - 50 mm – 75 mm)	13	180	Precast Aerated Concrete Wall Panel	200	Hollow core Roof Slab + Conc. screed	200	Hollow-core floor Slab
1-M & 2-M	200	Precast Concrete Sandwich Panel (50 mm - 50 mm – 100 mm)	13	150	Precast bearing concrete wall panel	150	Hollow core Roof Slab + Conc. screed	150	Hollow-core floor Slab

Table 5.6: Opening data for the case study houses collected from the site visit.

Bldg. Ref.	Window/Glazing Type	Frame Type	Number Of Panes	Window-To-Wall Ratio (%)
House 1-J	Tinted tempered insulated glass sliding windows with heat mirror film	Powder coated aluminium frame	2	4
Houses 1-M & 2-M	Sliding Glass Panel/ reflective glass of 6/4mm,12mm airgap glazing	Powder coated aluminium frame	2	8.5

Table 5.7: Air conditioning data for the case study houses collected from the site visit.

Bldg. Ref.	Cooling Set Point (°C)	Heating Set Point (°C)	HVAC System	HVAC Operational Hours
House 1 J	24	20	Central packaged system	Referenced as per ASHRAE standard for each single zone
House 1 M	24	20	Split units' system	Referenced as per ASHRAE standard for each single zone
House 2 M	24	20	Split units' system	Referenced as per ASHRAE standard for each single zone

5.5 INSTRUMENTATION AND METHODOLOGY FOR INDOOR AIR TEMPERATURE MEASUREMENT

The process of measuring indoor air temperature in the selected house is facilitated using a precision measurement device, the technical details of which are outlined in Table 5.8. This device, carefully selected for its suitability and accuracy, is employed to gauge the temperature in a room situated on the northeast side of the house, specifically designated as the Visitor Room. Figures 5.18 and 5.19 provide detailed images of the measurement tool, displaying its design and functionality in capturing accurate temperature readings.

This careful approach ensures that the gathered data is reliable and representative of the indoor thermal conditions, contributing to the comprehensive analysis of the house's thermal performance.

Figure 5.18: Image showing the manufactured shape of the product. Source: Elitech.

Figure 5.19: Image of the product used in the study, showing the three devices. Actual device images were taken in person.

Table 5.8: Description of the measurement device and product specifications used for the validation part of this research. The tool was used during the site visit, and information was gathered from the data provided with the product.

Brand	Elitech
Model no	Rc-4hc
Measuring parameters	Temperature – relative humidity
Sensor	Internal, optional external sensor
Temperature	-30°C to +60°C
Accuracy	±0.5(-20°c/+40°c): ±1.0
Resolution	0.1 °c
Humidity	0 to 99%RH
Accuracy	±3%RH (25°C,20%RVI to 90%RVI), others; 5% RH
Resolution	0.1 %rh
Operating temperature	-30°C to +60°C
Record capacity	16000 points (MAX} Interval:10s-24hour adjustable
Communication	USB interface
Power supply	Inner CR2450 battery or power supply via USB interface
Battery life	In normal temperature, if the record interval sets as 15 minutes, it could be used above one year
Engineering units	°C or °F optional, set through RC-4H data management Software.
Calibration	Provided along with and valid for 2 years (Certificates on Appendix D)
Protection grade	IP67
Dimensions	84 X 44 X 20 mm
Weight	35grams

Figure 5.20: Image showing the camera tripod positioned in the living room. Image taken for methodology illustration purposes.

Figure 5.21: Image showing the camera tripod with the thermometer device positioned on top. Image taken for methodology illustration purposes.

Figure 5.22: Image showing the thermometer positioned on top of the camera tripod. Image taken for methodology illustration purposes.

For in-field temperature measurement in the real building, a thermometer, as described above, was utilised. The thermometer was strategically positioned at a height of 1.70 m, in accordance with the recommended occupant height as per the ASHRAE Standard (ASHRAE, 2013), atop a camera tripod stand, as depicted in Figures 5.20 to 5.22. Care was taken to place the stand at two locations within the room to negate any influence from heat radiation emanating from external walls or windows.

Additionally, the room, which has two windows and a side entrance to the villa, is situated on the northeast front elevation of the villa at an angle of 64 degrees. The devices were operational for 10 consecutive days in March, recording the temperature at one-hour intervals throughout the duration. Accordingly, the analysis conducted not only validates the accuracy of the simulation results but also provides insights into the dynamic interplay between the simulated model and the actual indoor thermal behaviour.

This underscores the importance of accurate monitoring and analysis in ensuring the reliability and effectiveness of building thermal performance simulations.

5.5.1 INDOOR AIR TEMPERATURE VALIDATION BETWEEN SOFTWARE AND IN-FIELD MEASUREMENT

In this section, the objective is to conduct a detailed comparison between in-field air temperature readings and those generated through simulations using DesignBuilder software. To facilitate this comparison, a case study house constructed from precast concrete, situated within Jubail Industrial City, Saudi Arabia, is selected. This chosen structure serves as the basis for our analysis within the software, aimed at understanding the variation in air temperatures over an entire year, recorded at one-hour intervals.

At the same time, a thermometer device placed indoors is utilised to record air temperature readings at similar one-hour intervals over a period of 10 days. To ensure methodological consistency and strengthen the reliability of the analysis, both sets of readings are adjusted to match the one-hour intervals, facilitating a more direct and accurate comparison while minimising potential differences.

Subsequently, a comprehensive validation test is conducted, where the in-field air temperature readings are compared with those simulated by the DesignBuilder software. This thorough evaluation process aims to confirm the reliability and accuracy of the software-generated temperature data in replicating real-world conditions. Specifically, the analysis focuses on comparing the temperature data of a selected zone within the case study house, providing valuable insights into the performance and effectiveness of the simulation model in reflecting indoor air temperature variations.

Table 5.9: General information about the selected case study house used for validation analysis.

Building type	Detached single house
Location	Jalmudah, Jubail, Eastern province, Saudi Arabia
Total floors Area	378 m^2
Project Year	2015
Project Owner	The Royal Commission for Jubail Industrial City
Climate zone	Hot-Dry Maritime subzone (1A)

Table 5.10: Technical and thermal performance information about the selected case study house used for validation analysis.

Component	**Materials/Description**	**U-Value (W/m^2-k)**
Ground Floor	heavy weight concrete	2.2
External walls	heavy weight precast insulated	0.43
Internal partitions	Precast concrete panels	3.0
Flat Roof	heavy weight concrete insulated	1.9
Openings	Clear glass double Blue 6mm/6mm Air (as original design)	2.89

The simulation of indoor air temperature for the selected vacant house in Jubail Industrial City is integral to this research, serving as a cornerstone in understanding thermal dynamics and energy performance. This two-storey villa, constructed from precast concrete materials, is modelled using the technical specifications outlined in Tables 5.9 and 5.10, ensuring accuracy and precision in the simulation process.

Emphasising the absence of HVAC or any ventilation systems, the simulation focuses on the free-floating temperature as the central element in assessing the house's thermal behaviour. This approach allows for a comprehensive evaluation of natural temperature fluctuations and heat transfer mechanisms within the building envelope.

Moreover, the analysis relies fundamentally on the EnergyPlus weather data, as mentioned earlier, to accurately replicate the climatic conditions prevalent in Jubail Industrial City throughout the simulation period. By incorporating real-world weather data, the simulation captures the dynamic interplay between external environmental factors and internal thermal conditions, providing valuable insights into the house's thermal performance under varying weather conditions.

Thus, DesignBuilder is the primary Building Energy Performance Simulation (BEPS) tool employed in this simulation, chosen for its comprehensive capabilities and suitability for detailed analysis. The findings derived from DesignBuilder are subsequently compared with in-field air temperature measurements, as detailed in the subsequent sections.

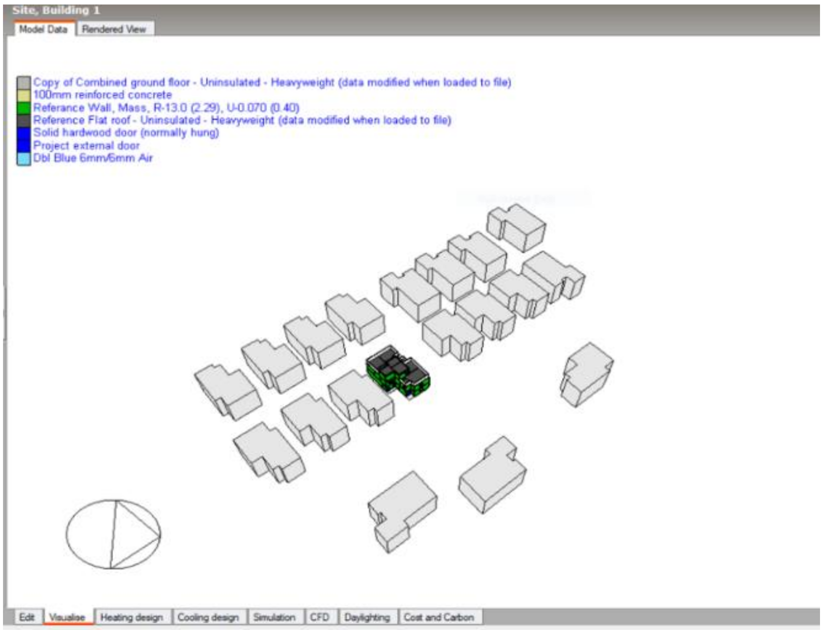

Figure 5.23: Illustration of the developed house, including the surrounding structures, using DesignBuilder software.

The house, oriented towards the northeast as illustrated in Figure 5.23, is situated among several other residences. These neighbouring houses play a crucial role in both the modelling and analysis phases, as their presence is considered to enhance accuracy and provide a comprehensive understanding of the impact of the surrounding environment on the thermal performance of the selected house.

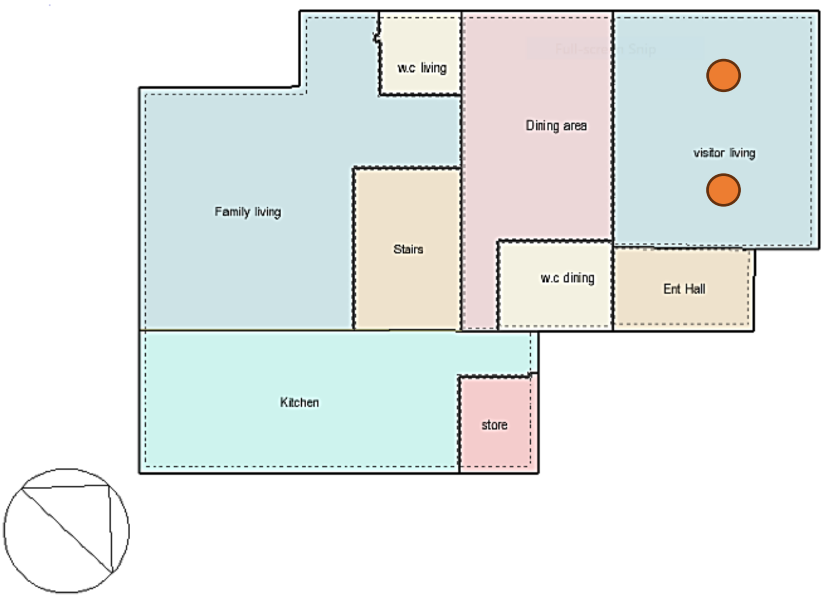

Figure 5.24: Illustration of the ground floor plan for the studied house, showing monitoring locations. Floor layout developed using DesignBuilder software.

Two data logger devices, strategically positioned within the indoor environment as depicted in Figure 5.24, were systematically employed for indoor air temperature monitoring. These devices continuously recorded indoor air temperature readings over a period spanning 22 March to 31 March (10 days).

The subsequent section offers an in-depth comparison, incorporating both the carefully gathered field study data and the outputs generated from the analysis tool for the selected zone. This detailed analysis aims to provide a comprehensive understanding of indoor air temperature dynamics and validate the accuracy of the simulation results.

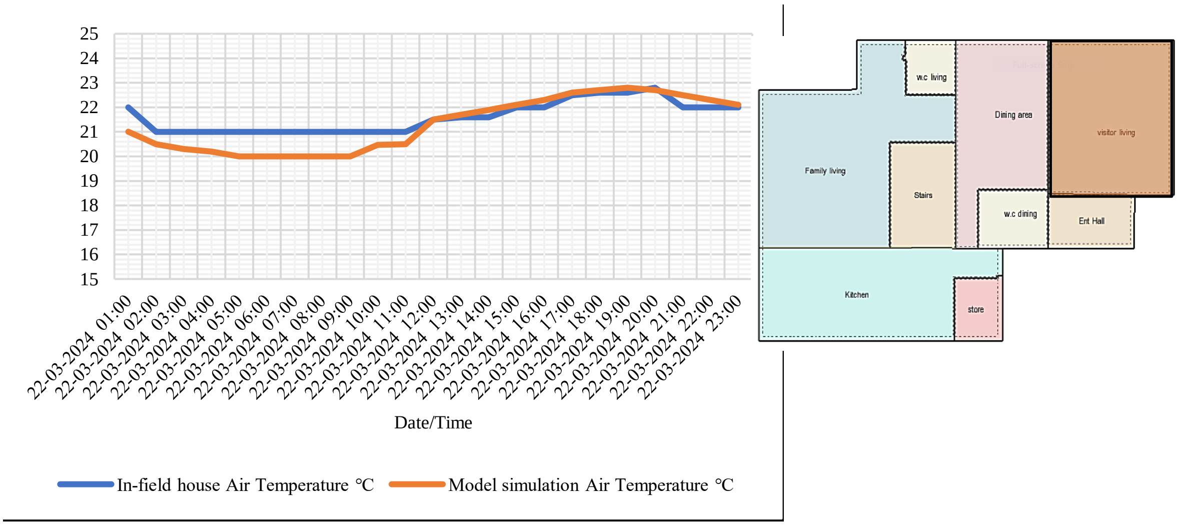

Figure 5.25: Illustration of one-day air temperature distribution on an hourly basis, comparing in-field measurements (shaded zone in the layout plan) with DesignBuilder simulation software on 22 March 2024.

The air temperature readings were carefully compiled to illustrate the alignment between the simulated model's analysis and the in-field measurements. It should be noted that a ten-day measurement period is generally considered sufficient to determine the indoor temperature profile of the house.

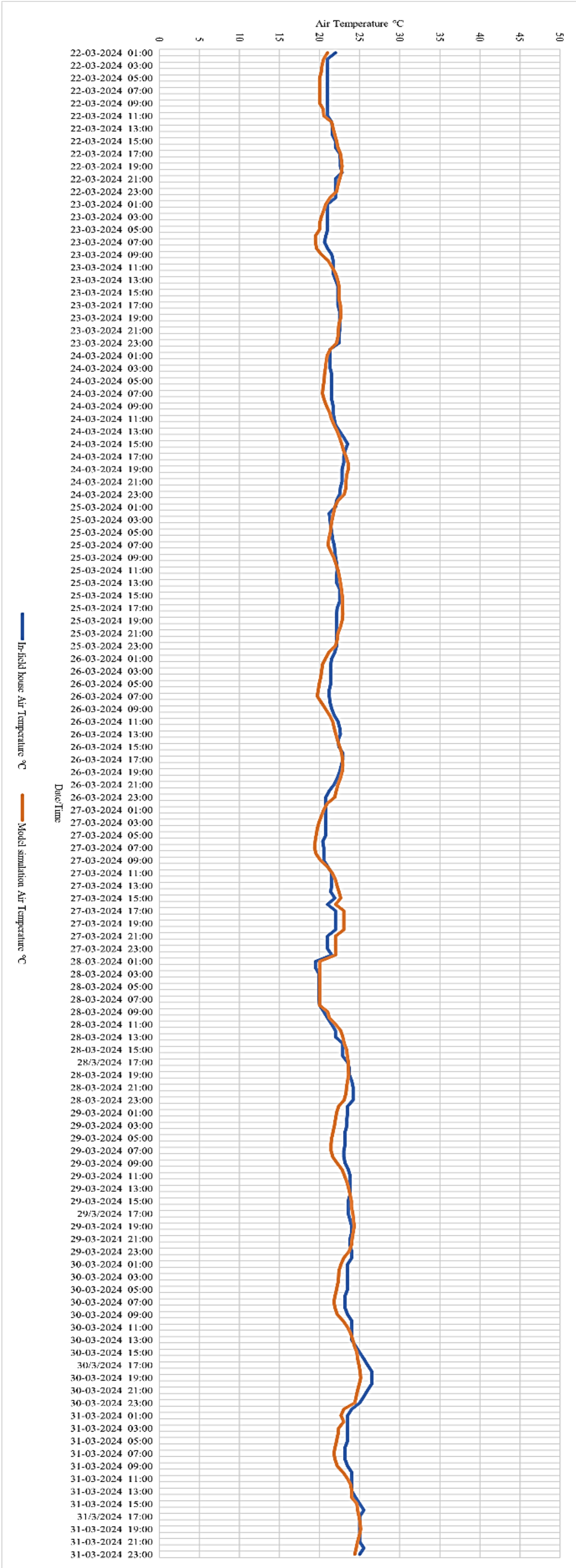

Figure 5.26: Illustration of 10-day air temperature distribution on an hourly basis, comparing in-field measurements with DesignBuilder simulation from 22 March 2024 to 31 March 2024.

The comparison analysis was conducted in two segments: firstly, a comprehensive examination for a full day on an hourly basis (Figure 5.25), and secondly, an extended evaluation spanning a period of 10 full days, also on an hourly basis (Figure 5.26). These figures highlight a significant correlation between the simulated model and the in-field measurements. Despite occasional minor temperature deviations, they remain insignificant. Such deviations could be attributed to presumed differences in infiltration rates during the monitoring period compared to the simulated model.

In this study, the Root Mean Squared Calibration (RMSC) method was used to validate the accuracy of the model's predicted indoor air temperatures by comparing them with observed real-world data. This approach calculates the square of the differences between the model's predicted values and the actual observed temperatures, then averages these squared differences and takes the square root of the result. The resulting RMSC value provides a measure of how closely the model's predictions match the observed data, with lower values indicating a better fit.
After applying the RMSC method using Equation (5.1), the results showed an exceptionally low RMSC value (Table 5.11), indicating a near-perfect alignment between the model's predicted indoor air temperatures and the observed data. This suggests that the model is highly accurate in replicating indoor climate conditions, with minimal discrepancies between the predicted and actual temperatures.

The excellent RMSC result underscores the model's capability to effectively simulate indoor temperature variations, making it a reliable tool for further analysis in energy management, building design optimisation, and climate control systems.

$$RMSC = \sqrt{\frac{1}{n}\sum_{i=1}^{n}(y_{\text{pred},i} - y_{\text{obs},i})^2} \quad \text{...Eq. 5.1}$$

where $ypred$ is the predicted value, $yobs$ is the observed value, and n is the total number of data points.

Table 5.11: RMSC analysis assessing validation accuracy over a 10-day period between observed and simulated air temperatures. Data gathered from both in-field measurements and DesignBuilder software, reproduced using Excel.

	Date/Time	Observed Air Temperature ℃	Simulated Air Temperature ℃	Residuals	Squared Residuals
Day 1	22-03-2024 01:00	22.00	21.0	-1.00	1.00
	22-03-2024 02:00	21.00	20.5	-0.50	0.25
	22-03-2024 03:00	21.00	20.3	-0.70	0.49
	22-03-2024 04:00	21.00	20.2	-0.80	0.64
	22-03-2024 05:00	21.00	20.0	-1.00	1.00
	22-03-2024 06:00	21.00	20.0	-1.00	1.00
	22-03-2024 07:00	21.00	20.0	-1.00	1.00
	22-03-2024 08:00	21.00	20.0	-1.00	1.00
	22-03-2024 09:00	21.00	20.0	-1.00	1.00
	22-03-2024 10:00	21.00	20.5	-0.53	0.28
	22-03-2024 11:00	21.00	20.5	-0.50	0.25
	22-03-2024 12:00	21.50	21.5	0.00	0.00
	22-03-2024 13:00	21.60	21.7	0.10	0.01
	22-03-2024 14:00	21.60	21.9	0.30	0.09
	22-03-2024 15:00	22.00	22.1	0.10	0.01
	22-03-2024 16:00	22.00	22.3	0.30	0.09
	22-03-2024 17:00	22.50	22.6	0.10	0.01
	22-03-2024 18:00	22.60	22.7	0.10	0.01

	22-03-2024 19:00	22.60	22.8	0.20	0.04
	22-03-2024 20:00	22.80	22.7	-0.10	0.01
	22-03-2024 21:00	22.00	22.5	0.50	0.25
	22-03-2024 22:00	22.00	22.3	0.30	0.09
	22-03-2024 23:00	22.00	22.1	0.10	0.01
Day 2	23-03-2024	22.00	21.3	-0.70	0.49
	23-03-2024 01:00	21.00	20.8	-0.20	0.04
	23-03-2024 02:00	21.00	20.5	-0.50	0.25
	23-03-2024 03:00	21.00	20.2	-0.80	0.64
	23-03-2024 04:00	21.00	20.0	-1.00	1.00
	23-03-2024 05:00	21.00	20	-1.00	1.00
	23-03-2024 06:00	20.80	19.5	-1.30	1.69
	23-03-2024 07:00	20.60	19.5	-1.10	1.21
	23-03-2024 08:00	21.00	20	-1.40	1.96
	23-03-2024 09:00	21.50	20.2	-1.28	1.64
	23-03-2024 10:00	21.70	21.1	-0.62	0.38
	23-03-2024 11:00	21.70	22	-0.13	0.02
	23-03-2024 12:00	21.70	22.0	0.30	0.09
	23-03-2024 13:00	22.00	22.2	0.24	0.06
	23-03-2024 14:00	22.30	22.4	0.10	0.01
	23-03-2024 15:00	22.30	22.4	0.12	0.01
	23-03-2024 16:00	22.30	22.4	0.13	0.02

	23-03-2024 17:00	22.30	22.6	0.30	0.09
	23-03-2024 18:00	22.50	22.6	0.13	0.02
	23-03-2024 19:00	22.50	22.6	0.13	0.02
	23-03-2024 20:00	22.50	22.4	-0.10	0.01
	23-03-2024 21:00	22.50	22.3	-0.18	0.03
	23-03-2024 22:00	22.40	22.3	-0.12	0.01
	23-03-2024 23:00	22.40	22.1	-0.28	0.08
Day 3	24-03-2024	21.30	21.3	0.03	0.00
	24-03-2024 01:00	21.30	21	-0.35	0.13
	24-03-2024 02:00	21.30	21	-0.47	0.22
	24-03-2024 03:00	21.30	21	-0.54	0.29
	24-03-2024 04:00	21.50	21	-0.89	0.79
	24-03-2024 05:00	21.50	21	-0.95	0.91
	24-03-2024 06:00	21.50	20.4	-1.07	1.14
	24-03-2024 07:00	21.50	20.3	-1.15	1.32
	24-03-2024 08:00	21.50	21	-0.92	0.85
	24-03-2024 09:00	21.70	21	-0.82	0.66
	24-03-2024 10:00	21.70	21.3	-0.44	0.19
	24-03-2024 11:00	21.80	21.5	-0.33	0.11
	24-03-2024 12:00	22.00	22	-0.20	0.04
	24-03-2024 13:00	22.50	22.2	-0.30	0.09
	24-03-2024 14:00	23.00	22.5	-0.51	0.26

	24-03-2024 15:00	23.50	23	-0.73	0.53
	24-03-2024 16:00	23.20	23.0	-0.24	0.06
	24-03-2024 17:00	23.00	23.3	0.29	0.08
	24-03-2024 18:00	23.00	23.5	0.54	0.29
	24-03-2024 19:00	22.80	23.6	0.79	0.62
	24-03-2024 20:00	22.80	23.3	0.55	0.30
	24-03-2024 21:00	22.80	23.3	0.46	0.22
	24-03-2024 22:00	22.60	23.3	0.67	0.44
	24-03-2024 23:00	22.50	23.1	0.56	0.32
Day 4	25-03-2024	22.10	22.3	0.20	0.04
	25-03-2024 01:00	22.00	22	-0.10	0.01
	25-03-2024 02:00	21.20	21.7	0.52	0.27
	25-03-2024 03:00	21.30	21.5	0.25	0.06
	25-03-2024 04:00	21.40	21.4	0.01	0.00
	25-03-2024 05:00	21.50	21.3	-0.17	0.03
	25-03-2024 06:00	21.60	21.2	-0.45	0.20
	25-03-2024 07:00	21.80	21.0	-0.78	0.60
	25-03-2024 08:00	21.90	21.4	-0.51	0.26
	25-03-2024 09:00	22.00	22	-0.24	0.06
	25-03-2024 10:00	22.10	22.1	-0.05	0.00
	25-03-2024 11:00	22.20	22.3	0.10	0.01
	25-03-2024 12:00	22.10	22.5	0.37	0.14

	25-03-2024 13:00	22.10	22.6	0.48	0.23
	25-03-2024 14:00	22.50	22.7	0.20	0.04
	25-03-2024 15:00	22.50	22.8	0.30	0.09
	25-03-2024 16:00	22.50	22.9	0.35	0.12
	25-03-2024 17:00	22.20	22.9	0.66	0.43
	25-03-2024 18:00	22.10	22.9	0.80	0.64
	25-03-2024 19:00	22.10	22.8	0.72	0.52
	25-03-2024 20:00	22.10	22.6	0.49	0.24
	25-03-2024 21:00	22.10	22.3	0.21	0.04
	25-03-2024 22:00	22.10	22.2	0.08	0.01
	25-03-2024 23:00	22.10	22.0	-0.11	0.01
Day 5	26-03-2024	21.90	21.2	-0.75	0.56
	26-03-2024 01:00	21.50	21	-0.77	0.59
	26-03-2024 02:00	21.40	20.4	-1.03	1.07
	26-03-2024 03:00	21.40	20.3	-1.13	1.28
	26-03-2024 04:00	21.40	20.1	-1.25	1.57
	26-03-2024 05:00	21.40	20	-1.46	2.13
	26-03-2024 06:00	21.20	20	-1.38	1.90
	26-03-2024 07:00	21.20	20	-1.51	2.29
	26-03-2024 08:00	21.30	20.2	-1.09	1.18
	26-03-2024 09:00	21.50	21	-0.77	0.59
	26-03-2024 10:00	21.80	21.3	-0.53	0.28

	26-03-2024 11:00	22.30	22	-0.68	0.46
	26-03-2024 12:00	22.50	22	-0.68	0.47
	26-03-2024 13:00	22.60	22.0	-0.56	0.31
	26-03-2024 14:00	22.30	22.3	-0.04	0.00
	26-03-2024 15:00	22.40	22.5	0.09	0.01
	26-03-2024 16:00	22.90	23	-0.14	0.02
	26-03-2024 17:00	22.90	22.8	-0.07	0.00
	26-03-2024 18:00	22.70	22.9	0.18	0.03
	26-03-2024 19:00	22.50	22.8	0.30	0.09
	26-03-2024 20:00	22.20	22.6	0.39	0.15
	26-03-2024 21:00	21.80	22.3	0.50	0.25
	26-03-2024 22:00	21.20	22.1	0.86	0.75
	26-03-2024 23:00	20.80	22	1.11	1.24
Day 6	27-03-2024	20.80	21.0	0.16	0.03
	27-03-2024 01:00	20.80	20.5	-0.27	0.07
	27-03-2024 02:00	20.80	20.2	-0.58	0.34
	27-03-2024 03:00	20.80	20	-0.87	0.75
	27-03-2024 04:00	20.80	20	-1.11	1.23
	27-03-2024 05:00	20.80	20	-1.21	1.46
	27-03-2024 06:00	20.40	19.4	-0.97	0.94
	27-03-2024 07:00	20.50	19.4	-1.14	1.30
	27-03-2024 08:00	20.50	20	-0.92	0.85

	27-03-2024 09:00	20.50	20.1	-0.37	0.14
	27-03-2024 10:00	21.00	21.0	-0.05	0.00
	27-03-2024 11:00	21.50	21.5	0.04	0.00
	27-03-2024 12:00	21.50	22	0.44	0.19
	27-03-2024 13:00	21.50	22.2	0.65	0.43
	27-03-2024 14:00	21.40	22.4	1.01	1.02
	27-03-2024 15:00	21.90	22.6	0.75	0.56
	27-03-2024 16:00	21.00	22.0	1.00	1.00
	27-03-2024 17:00	22.00	23.0	1.00	1.00
	27-03-2024 18:00	22.00	23.0	1.00	1.00
	27-03-2024 19:00	22.00	23.0	1.00	1.00
	27-03-2024 20:00	22.00	23.0	1.00	1.00
	27-03-2024 21:00	21.00	22.0	1.00	1.00
	27-03-2024 22:00	21.00	22.0	1.00	1.00
	27-03-2024 23:00	21.00	22.0	1.00	1.00
Day 7	28-03-2024	21.50	22.0	0.50	0.25
	28-03-2024 01:00	19.50	20.0	0.50	0.25
	28-03-2024 02:00	19.50	20.0	0.50	0.25
	28-03-2024 03:00	19.90	20.0	0.10	0.01
	28-03-2024 04:00	19.90	20.0	0.10	0.01
	28-03-2024 05:00	19.90	20.0	0.10	0.01
	28-03-2024 06:00	19.90	20.0	0.10	0.01

	28-03-2024 07:00	19.90	20.0	0.10	0.01
	28-03-2024 08:00	20.00	20.0	0.00	0.00
	28-03-2024 09:00	20.50	21.0	0.50	0.25
	28-03-2024 10:00	21.00	21.2	0.19	0.04
	28-03-2024 11:00	21.50	22.0	0.47	0.22
	28-03-2024 12:00	22.00	23	0.65	0.42
	28-03-2024 13:00	22.00	23	0.89	0.79
	28-03-2024 14:00	22.90	23.1	0.18	0.03
	28-03-2024 15:00	22.90	23.4	0.47	0.22
	28-03-2024 16:00	22.90	23.5	0.55	0.31
	28/3/2024 17:00	23.50	24	0.06	0.00
	28-03-2024 18:00	23.70	24	-0.12	0.01
	28-03-2024 19:00	23.70	24	-0.07	0.00
	28-03-2024 20:00	24.00	23.5	-0.52	0.27
	28-03-2024 21:00	24.20	23.3	-0.86	0.73
	28-03-2024 22:00	24.20	23.3	-0.91	0.83
	28-03-2024 23:00	24.20	23.1	-1.13	1.27
Day 8	29-03-2024	23.50	22.4	-1.11	1.23
	29-03-2024 01:00	23.50	22.1	-1.40	1.96
	29-03-2024 02:00	23.40	22.0	-1.40	1.95
	29-03-2024 03:00	23.40	21.9	-1.54	2.38
	29-03-2024 04:00	23.20	21.7	-1.53	2.35

	29-03-2024 05:00	23.20	21.5	-1.68	2.83
	29-03-2024 06:00	23.20	21.4	-1.79	3.19
	29-03-2024 07:00	23.00	21.4	-1.59	2.52
	29-03-2024 08:00	23.00	21.6	-1.35	1.83
	29-03-2024 09:00	23.20	22.2	-1.00	0.99
	29-03-2024 10:00	23.60	23	-0.81	0.66
	29-03-2024 11:00	23.80	23.1	-0.69	0.47
	29-03-2024 12:00	23.80	23.4	-0.40	0.16
	29-03-2024 13:00	23.80	23.6	-0.17	0.03
	29-03-2024 14:00	23.80	23.8	-0.01	0.00
	29-03-2024 15:00	23.60	23.9	0.35	0.12
	29-03-2024 16:00	23.60	24.0	0.37	0.14
	29/3/2024 17:00	23.60	24.1	0.52	0.27
	29-03-2024 18:00	23.80	24.2	0.42	0.17
	29-03-2024 19:00	24.00	24.3	0.31	0.10
	29-03-2024 20:00	24.00	24.2	0.20	0.04
	29-03-2024 21:00	23.80	24.1	0.27	0.07
	29-03-2024 22:00	23.80	24.0	0.19	0.03
	29-03-2024 23:00	24.00	24	-0.33	0.11
Day 9	30-03-2024	24.00	23.0	-0.98	0.96
	30-03-2024 01:00	23.50	23	-0.82	0.67
	30-03-2024 02:00	23.50	22.4	-1.10	1.20

30-03-2024 03:00	23.50	22.4	-1.12	1.26
30-03-2024 04:00	23.50	22.3	-1.22	1.49
30-03-2024 05:00	23.50	22.1	-1.39	1.92
30-03-2024 06:00	23.20	22	-1.25	1.57
30-03-2024 07:00	23.20	22	-1.44	2.07
30-03-2024 08:00	23.20	22	-1.27	1.61
30-03-2024 09:00	23.50	22.2	-1.31	1.71
30-03-2024 10:00	24.00	23	-1.08	1.16
30-03-2024 11:00	24.00	23.5	-0.52	0.27
30-03-2024 12:00	24.00	24	-0.13	0.02
30-03-2024 13:00	24.00	24.1	0.13	0.02
30-03-2024 14:00	24.50	24.4	-0.13	0.02
30-03-2024 15:00	25.00	25	-0.33	0.11
30-03-2024 16:00	25.50	25	-0.76	0.57
30/3/2024 17:00	26.00	25	-1.10	1.20
30-03-2024 18:00	26.50	25.0	-1.47	2.15
30-03-2024 19:00	26.50	25.1	-1.39	1.93
30-03-2024 20:00	26.50	25.0	-1.53	2.35
30-03-2024 21:00	26.00	25	-1.25	1.56
30-03-2024 22:00	25.50	25	-0.91	0.83
30-03-2024 23:00	25.00	24.4	-0.61	0.37

Day 10	31-03-2024	24.00	23.0	-0.98	0.96
	31-03-2024 01:00	23.50	23	-0.82	0.67
	31-03-2024 02:00	23.50	23.0	-0.50	0.25
	31-03-2024 03:00	23.50	22.4	-1.12	1.26
	31-03-2024 04:00	23.50	22.3	-1.22	1.49
	31-03-2024 05:00	23.50	22.1	-1.39	1.92
	31-03-2024 06:00	23.20	22	-1.25	1.57
	31-03-2024 07:00	23.20	22	-1.44	2.07
	31-03-2024 08:00	23.20	22	-1.27	1.61
	31-03-2024 09:00	23.50	22.2	-1.31	1.71
	31-03-2024 10:00	24.00	23	-1.08	1.16
	31-03-2024 11:00	24.00	23.5	-0.52	0.27
	31-03-2024 12:00	24.00	24	-0.13	0.02
	31-03-2024 13:00	24.00	24.0	0.00	0.00
	31-03-2024 14:00	24.50	24.0	-0.50	0.25
	31-03-2024 15:00	25.00	25	-0.33	0.11
	31-03-2024 16:00	25.50	25	-0.76	0.57
	31/3/2024 17:00	25.00	25	-0.10	0.01
	31-03-2024 18:00	25.00	25.0	0.03	0.00
	31-03-2024 19:00	25.00	25.1	0.11	0.01
	31-03-2024 20:00	25.00	25.0	-0.03	0.00

31-03-2024 21:00	25.00	25	-0.25	0.06
31-03-2024 22:00	25.50	25	-0.91	0.83
31-03-2024 23:00	25.00	24.4	-0.61	0.37
Mean				**0.59**
RMSC				**0.770**

After verifying and validating the indoor air temperature readings of the house (in-field measurements) against the air temperatures generated by the simulation program, Table 5.11 presents the RMSC analysis to assess validation accuracy over a 10-day period within the simulated duration.

With an error value of 0.770, it can be confirmed that the DesignBuilder software is validated and thus deemed reliable.

5.6 INSTRUMENTATION AND METHODOLOGY FOR OUTDOOR AIR TEMPERATURE MEASUREMENT

In the pursuit of accurate outdoor air temperature measurement, precise instrumentation and methodology are essential. The Elitech temperature monitor, housed within an outdoor plastic enclosure (Table 5.12), was employed to validate outdoor temperature readings relevant to the studied location, in conjunction with the simulation tool, DesignBuilder.

Table 5.12: Description of Product Specifications.

Manufacturer	TFA Dostmann
Material type	Plastic
Product dimensions	10.2 × 9.5 × 71.5 cm; 291 grams
Item display heights	17.5 centimetres
Item display length.	10.2 centimetres
Item display Width	9.5 centimetres
Material type	Plastic

This approach ensures the integrity and accuracy of outdoor temperature data captured, thereby enhancing the reliability of weather simulations conducted via the DesignBuilder software. By employing the Elitech temperature monitor, housed within the specified outdoor plastic enclosure, this research not only validates simulated weather conditions with real-world observations but also refines the precision and applicability of the analyses conducted.

Figures 5.27 to 5.33 illustrate product details and installation methods, providing a comprehensive visual reference for the setup and utilisation of the Elitech temperature monitor in outdoor environments.

Figure 5.27: Image showing the TFA Dostmann plastic case product shape. Original product illustration.

Figure 5.28: Image showing the components of the TFA Dostmann plastic case. Self-taken image illustrating the product contents.

Figure 5.29: Image showing the side ventilation area of the TFA Dostmann plastic case. Self-taken image illustrating the product’s side ventilation openings.

Figure 5.30: Image showing the box base ventilation area of the TFA Dostmann plastic case. Self-taken image illustrating the product’s base ventilation openings.

Figure 5.31: Image showing the Elitech device attachment area inside the TFA Dostmann plastic case. Self-taken image illustrating the installation method.

Figure 5.32: Image showing both Elitech device attachment areas inside the TFA Dostmann plastic case. Self-taken image illustrating the installation method.

Figure 5.33: Image showing the Elitech device inside the TFA Dostmann plastic case, on top of the tripod, located outdoors monitoring outdoor air temperature. Self-taken image explaining the method used.

5.6.1 OUTDOOR AIR TEMPERATURE VALIDATION BETWEEN SOFTWARE AND IN-FIELD MEASUREMENT

This section conducts a comprehensive comparison between outdoor air temperature readings and those simulated using DesignBuilder software. The studied location, situated in Jubail Industrial City, Saudi Arabia, necessitates the selection of the most applicable weather file by distance, which is Dammam King Fahd International Airport.

To ensure a thorough validation of air temperatures throughout the year, the comparison encompasses one-hour intervals over a continuous five-day period, commencing from

31 March to 4 April, as illustrated in Figure 5.28. This thorough approach allows for a detailed assessment of the agreement between in-field and software-generated data. The validation test aims to ascertain the reliability and accuracy of the simulated outdoor air temperature readings for the studied location.

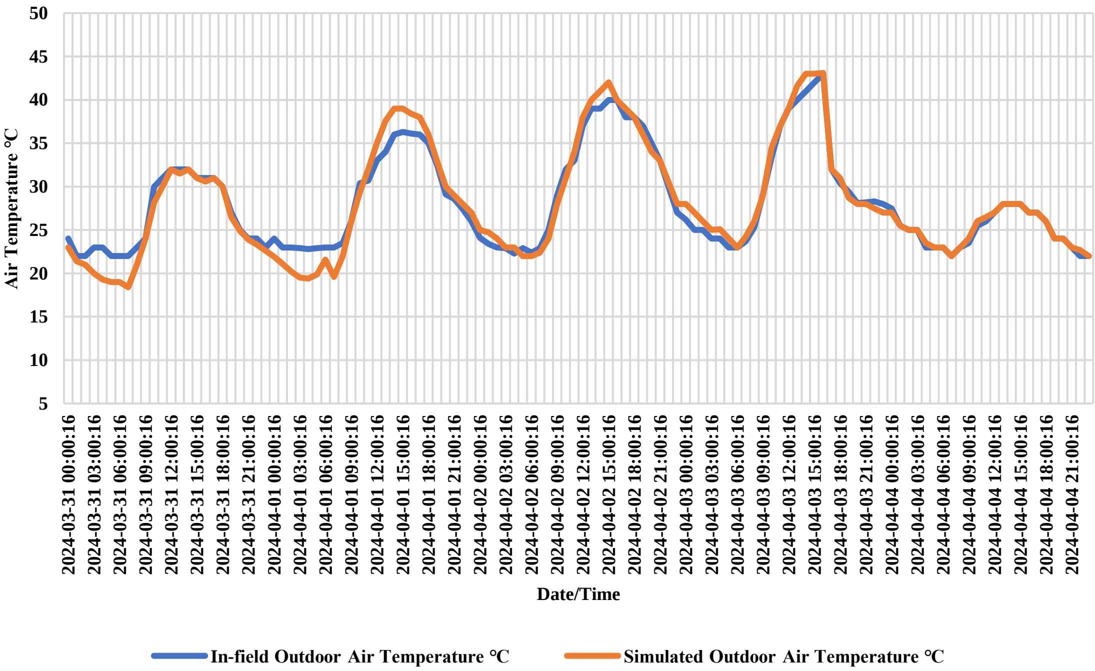

Figure 5.34: Illustrating the correlation between in-field outdoor air temperature readings and simulated outdoor air temperature over a period of 5 days. Data gathered from both the data logger device and DesignBuilder software, reproduced using Excel.

Figure 5.34 provides a detailed comparison between in-field outdoor air temperature readings and simulated outdoor air temperature readings. The analysis aims to evaluate the consistency between these two datasets over a 5-day period. Hourly temperature readings were collected meticulously to capture the nuances of outdoor temperature variations.

Upon examination of the data, it is evident that there are slight variations between the in-field and simulated temperatures at different points throughout the observation period, particularly noticeable during the first 2 days. These variations are presumed to be attributed to several factors, including local microclimatic effects, such as wind corridors or nearby building components, which can influence the actual outdoor temperature.

Furthermore, the comparison allows for a comprehensive understanding of the performance of the simulation tool in replicating real-world outdoor temperature conditions. By scrutinising these differences, valuable insights can be gained into the accuracy and reliability of the simulation model, aiding in further refinement and improvement. Consequently, while minor discrepancies between the in-field and simulated temperatures are observed, the general alignment between the two readings indicates that the simulation tool effectively captures the outdoor temperature dynamics.

The comprehensive analysis undertaken demonstrates a notably high correlation in the overall readings between the in-field and simulated outdoor air temperature readings. Across the observed period spanning five days, both sets of readings exhibit markedly similar fluctuations and trends, attesting to the simulation model's proficiency in capturing the nuanced dynamics of outdoor air temperature variations within the study area.

This robust alignment underscores the reliability and efficacy of the simulation model in accurately representing the existing environmental conditions prevalent in Jubail Industrial City, Saudi Arabia. This validation of the simulation model's accuracy enhances its utility for various applications, including energy performance assessments and building design optimisations, within the specific context of Jubail Industrial City's climatic conditions.

Table 5.13: RMSC analysis assessing validation accuracy over a 5-day period between observed and simulated air temperatures. Data gathered from both in-field measurements and DesignBuilder software, reproduced using Excel.

Column1	Date/Time	Observed Air Temperature ℃	Simulated Air Temperature ℃	Residuals	Squared Residuals
Day 1	2024-03-31 00:00:16	24	23	-1.00	1.00
	2024-03-31 01:00:16	22	21.4	-0.60	0.36
	2024-03-31 02:00:16	22	21	-1.00	1.00
	2024-03-31 03:00:16	23	20	-3.00	9.00
	2024-03-31 04:00:16	23	19.3	-3.70	13.69
	2024-03-31 05:00:16	22	19	-3.00	9.00
	2024-03-31 06:00:16	22	19	-3.00	9.00
	2024-03-31 07:00:16	22	18.4	-3.60	12.96
	2024-03-31 08:00:16	23	21	-2.00	4.00
	2024-03-31 09:00:16	24	24	0.00	0.00
	2024-03-31 10:00:16	30	28.2	-1.80	3.24
	2024-03-31 11:00:16	31	30	-1.00	1.00
	2024-03-31 12:00:16	32	32	0.00	0.00
	2024-03-31 13:00:16	32	31.5	-0.50	0.25
	2024-03-31 14:00:16	32	32	0.00	0.00
	2024-03-31 15:00:16	31	31	0.00	0.00
	2024-03-31 16:00:16	31	30.6	-0.40	0.16
	2024-03-31 17:00:16	31	31	0.00	0.00

	2024-03-31 18:00:16	30	30	0.00	0.00
	2024-03-31 19:00:16	27	26.5	-0.50	0.25
	2024-03-31 20:00:16	25	24.9	-0.10	0.01
	2024-03-31 21:00:16	24	23.9	-0.10	0.01
	2024-03-31 22:00:16	24	23.3	-0.70	0.49
	2024-03-31 23:00:16	23	22.6	-0.40	0.16
Day 2	2024-04-01 00:00:16	24	21.9	-2.10	4.41
	2024-04-01 01:00:16	23	21.1	-1.90	3.61
	2024-04-01 02:00:16	23	20.2	-2.80	7.84
	2024-04-01 03:00:16	22.9	19.5	-3.40	11.56
	2024-04-01 04:00:16	22.8	19.4	-3.40	11.56
	2024-04-01 05:00:16	22.9	19.9	-3.00	9.00
	2024-04-01 06:00:16	23	21.6	-1.40	1.96
	2024-04-01 07:00:16	23	19.6	-3.40	11.56
	2024-04-01 08:00:16	23.5	22	-1.50	2.25
	2024-04-01 09:00:16	26	26	0.00	0.00
	2024-04-01 10:00:16	30.4	29.4	-1.00	1.00
	2024-04-01 11:00:16	30.7	32	1.30	1.69
	2024-04-01 12:00:16	33	35	2.00	4.00
	2024-04-01 13:00:16	34	37.6	3.60	12.96
	2024-04-01 14:00:16	36	39	3.00	9.00

	2024-04-01 15:00:16	36.3	39	2.70	7.29
	2024-04-01 16:00:16	36.1	38.4	2.30	5.29
	2024-04-01 17:00:16	36	38	2.00	4.00
	2024-04-01 18:00:16	35	36	1.00	1.00
	2024-04-01 19:00:16	32.5	32.9	0.40	0.16
	2024-04-01 20:00:16	29.1	30	0.90	0.81
	2024-04-01 21:00:16	28.6	29	0.40	0.16
	2024-04-01 22:00:16	27.4	28	0.60	0.36
	2024-04-01 23:00:16	26	27	1.00	1.00
Day 3	2024-04-02 00:00:16	24.1	25	0.90	0.81
	2024-04-02 01:00:16	23.4	24.7	1.30	1.69
	2024-04-02 02:00:16	23	24	1.00	1.00
	2024-04-02 03:00:16	22.9	23	0.10	0.01
	2024-04-02 04:00:16	22.3	23	0.70	0.49
	2024-04-02 05:00:16	22.9	22	-0.90	0.81
	2024-04-02 06:00:16	22.4	22	-0.40	0.16
	2024-04-02 07:00:16	22.9	22.4	-0.50	0.25
	2024-04-02 08:00:16	25	24	-1.00	1.00
	2024-04-02 09:00:16	29	28	-1.00	1.00
	2024-04-02 10:00:16	32	31	-1.00	1.00
	2024-04-02 11:00:16	33	34	1.00	1.00

	2024-04-02 12:00:16	37	38	1.00	1.00
	2024-04-02 13:00:16	39	40	1.00	1.00
	2024-04-02 14:00:16	39	41	2.00	4.00
	2024-04-02 15:00:16	40	42	2.00	4.00
	2024-04-02 16:00:16	40	40	0.00	0.00
	2024-04-02 17:00:16	38	39	1.00	1.00
	2024-04-02 18:00:16	38	38	0.00	0.00
	2024-04-02 19:00:16	37	36	-1.00	1.00
	2024-04-02 20:00:16	35	34	-1.00	1.00
	2024-04-02 21:00:16	33	33	0.00	0.00
	2024-04-02 22:00:16	30	30.5	0.50	0.25
	2024-04-02 23:00:16	27	28	1.00	1.00
Day 4	2024-04-03 00:00:16	26.2	28	1.80	3.24
	2024-04-03 01:00:16	25	27	2.00	4.00
	2024-04-03 02:00:16	25	26	1.00	1.00
	2024-04-03 03:00:16	24	25	1.00	1.00
	2024-04-03 04:00:16	24	25.1	1.10	1.21
	2024-04-03 05:00:16	23	24	1.00	1.00
	2024-04-03 06:00:16	23	23	0.00	0.00
	2024-04-03 07:00:16	23.7	24.2	0.50	0.25
	2024-04-03 08:00:16	25.3	26	0.70	0.49

	2024-04-03 09:00:16	29.1	29	-0.10	0.01
	2024-04-03 10:00:16	33.4	34.5	1.10	1.21
	2024-04-03 11:00:16	37	37	0.00	0.00
	2024-04-03 12:00:16	39	39	0.00	0.00
	2024-04-03 13:00:16	40	41.6	1.60	2.56
	2024-04-03 14:00:16	41	43	2.00	4.00
	2024-04-03 15:00:16	42	43	1.00	1.00
	2024-04-03 16:00:16	43	43.1	0.10	0.01
	2024-04-03 17:00:16	32	32	0.00	0.00
	2024-04-03 18:00:16	30.4	31	0.60	0.36
	2024-04-03 19:00:16	29.4	28.7	-0.70	0.49
	2024-04-03 20:00:16	28.1	28	-0.10	0.01
	2024-04-03 21:00:16	28.2	28	-0.20	0.04
	2024-04-03 22:00:16	28.3	27.5	-0.80	0.64
	2024-04-03 23:00:16	28	27	-1.00	1.00
Day 5	2024-04-04 00:00:16	27.5	27	-0.50	0.25
	2024-04-04 01:00:16	25.5	25.5	0.00	0.00
	2024-04-04 02:00:16	25	25	0.00	0.00
	2024-04-04 03:00:16	25	25	0.00	0.00
	2024-04-04 04:00:16	23	23.5	0.50	0.25
	2024-04-04 05:00:16	23	23	0.00	0.00

	2024-04-04 06:00:16	23	23	0.00	0.00
	2024-04-04 07:00:16	22	22	0.00	0.00
	2024-04-04 08:00:16	23	23	0.00	0.00
	2024-04-04 09:00:16	23.5	24	0.50	0.25
	2024-04-04 10:00:16	25.5	26	0.50	0.25
	2024-04-04 11:00:16	26	26.5	0.50	0.25
	2024-04-04 12:00:16	27	27	0.00	0.00
	2024-04-04 13:00:16	28	28	0.00	0.00
	2024-04-04 14:00:16	28	28	0.00	0.00
	2024-04-04 15:00:16	28	28	0.00	0.00
	2024-04-04 16:00:16	27	27	0.00	0.00
	2024-04-04 17:00:16	27	27	0.00	0.00
	2024-04-04 18:00:16	26	26	0.00	0.00
	2024-04-04 19:00:16	24	24	0.00	0.00
	2024-04-04 20:00:16	24	24	0.00	0.00
	2024-04-04 21:00:16	23	23	0.00	0.00
	2024-04-04 22:00:16	22	22.7	0.70	0.49
	2024-04-04 23:00:16	22	22	0.00	0.00
Mean					**1.89**
RMSC					**1.375**

Following the validation of the outdoor air temperature readings from the house (in-field measurements) against the air temperatures simulated by the program, Table 5.13 presents the RMSC error of 1.375 over a 5-day duration. The RMSC analysis demonstrates the accuracy of DesignBuilder software. Consequently, it can be confidently concluded that the software has undergone rigorous validation and can be deemed reliable for subsequent analyses and applications.

This validation underscores the software's effectiveness in accurately simulating outdoor air temperature dynamics, further enhancing its utility for diverse applications in building performance assessments and environmental analyses.

5.7 SUMMARY

Focusing on a site visit to residential precast concrete buildings in Jubail Industrial City, Saudi Arabia, this chapter offers a comprehensive description and analysis of the selected locations and houses. This sets the stage for a thorough investigation of their thermal efficiency.

Technical data collection from these residences is critical to the assessment of their thermal performance. The research places significant attention on a range of data inputs that affect the buildings' thermal efficiency. Therefore, validation is an important focus of this chapter, conducted through the comparison of in-field temperature measurements (indoor and outdoor) with simulated model outcomes. Despite observing minor temperature variances, attributable to differences in infiltration rates between the actual air temperature and the simulated one, such deviations have important implications for thermal comfort and energy consumption.

The fieldwork visit was undertaken during the challenging conditions of the COVID-19 pandemic, which significantly restricted access to resources. In compliance with safety measures as well as for satisfying research objectives, the researcher collected data from unoccupied homes, thus adhering to one of the research goals of studying vacant properties. Even with the imposed restrictions, the study managed to incorporate three unoccupied houses. Nonetheless, the precision of technical data pertaining to the building envelopes was not fully realised in the acquired technical drawings. To mitigate this, the researcher engaged in a thorough investigation of the thermal characteristics and material properties of precast concrete systems through a review of current research and scholarly publications.

CHAPTER SIX – DISCUSSION OF COMPUTER SIMULATIONS OF CASE STUDY BUILDINGS

6.1 INTRODUCTION

This chapter outlines the analytical phase of evaluating the thermal performance and comfort of the selected precast concrete houses. Employing the thermal modelling software DesignBuilder, it investigates the thermal behaviour of these homes, which is crucial for predicting occupant comfort and assessing potential improvements to enhance indoor thermal conditions and energy efficiency. The analysis was conducted on three houses, each consisting of two zones, resulting in a total of six zones (including two living rooms, three master bedrooms, and one dining room).

Detailed thermal considerations presented in Chapter 5 offered a definitive input data set for integration into the model. Thermal performance for each zone is evaluated monthly, as well as during the hottest and coldest hours of the year, with inter-zone thermal performance comparisons also undertaken. Moreover, the chapter predicts thermal comfort within these zones and examines factors that may influence the indoor thermal environment, such as construction materials and the location of zones within the house. The findings indicate that House 1-J experiences the highest number of total discomfort hours compared to Houses 1-M and 2-M.

6.2 DATA SET, MODELLING INPUT, AND THEIR ARRANGEMENTS

he simulation primarily relied on data related to construction materials. Nevertheless, certain assumptions were required to supplement the dataset with information on precast concrete systems. These assumptions concern the inclusion of materials' thermal properties, contributing to the robustness and accuracy of the simulation inputs.

Additionally, thermal bridges, arising at junctions within precast panels that secure and interconnect the panels, were not distinctly recorded in the gathered data, as these details are typically not specified in project technical drawings. This resulted in a deficiency of detailed technical information regarding the precast concrete panels employed.

It is important to note that modern precast concrete panels do not incorporate steel connectors, as indicated by recent research in this field. Hence, this research assumes the use of conventional concrete connections, aligning with prevalent practices in the precast concrete industry. The literature review examined both historical and current research relevant to this subject, highlighting these factors as crucial for an accurate evaluation of indoor thermal comfort.

This study deliberately narrows its focus to thermal performance via indoor operative temperature, the primary metric of thermal comfort. Other thermal metrics, to be detailed in the following section, are slated for comparison with the refined model at a later research phase. These metrics draw upon established standards such as ASHRAE, and a selection of scholarly publications on thermal comfort and indoor environmental quality (IEQ).

6.3 SOFTWARE DATA CONFIGURATIONS AND SETTINGS

The DesignBuilder software has been verified and extensively utilised in various Saudi energy-related studies, as evidenced by publications from authors such as Al-Tamimi (2022), Taleb and Sharples (2011), Asfour (2020), and others listed. Its applicability and validity concerning the Energy Efficiency Building Codes for Residential Buildings in the GCC have been affirmed by Elnabawi (2021). Subsequently, the ensuing subsections detail pivotal software data configurations.

6.3.1 CLOTHING VALUES

The simulation incorporated clothing insulation values as defined by the EnergyPlus engine for both winter and summer seasons. Specifically, winter clothing insulation (Clo) is set at 1.0, and summer clothing insulation at 0.50, uniformly applied across all occupied zones within the dwellings.

6.3.2 METABOLIC RATE

Metabolic rates are derived from the EnergyPlus database defaults, based on users' gender, with no specific age categorisation applied other than the number of occupants per zone. The standard activity level is set at 1 met, with gender differentiation factors preset (1 for males, 0.85 for females, and 0.75 for children).

6.3.3 OCCUPANCY AND SCHEDULING

Occupancy density and schedules align with the EnergyPlus activity templates, varying according to zone type and associated activities. Circulation zones have an occupancy density of 0.215 people/m². In contrast, bedrooms and living rooms (common areas) are set at 0.0229 and 0.0188 people/m², respectively. Occupancy schedules, spanning weekdays to weekends and holidays, adhere to the ASHRAE 90.1-2007 residential occupancy guidelines, adjusted for each zone's function.

6.3.4 MODEL INFILTRATION RATE

A consistent model infiltration rate (airtightness) is maintained at 0.700 air changes per hour (ac/h), corresponding with the default for most residential buildings in the EnergyPlus configurations. However, it is worth noting that this can vary depending on wind speed. For Dammam, peak summer winds average 11–12 mph, while peak winter winds are slightly lower, averaging 10–11 mph (Windfinder, 2024). These values influence infiltration rates due to varying air pressure gradients during these seasons.

6.3.5 EQUIPMENT POWER DENSITY

Power density for equipment is activated within the simulation as per zone-specific templates, incorporating power density and radiation fraction based on designated schedules. For instance, kitchen power density is set at 30.28 W/m² with a radiant fraction of 0.200, while bedrooms and living rooms are configured at 3.58 and 3.90 W/m², respectively, each with a radiant fraction of 0.200.

6.3.6 APERTURES AND FRESH AIR SCHEDULING

Apertures are standardised at the top opening position, with area open of 25%. Given the full natural ventilation of the houses, ventilation control is assigned to occupants, adhering to the minimum fresh air standard of 10 l/s per person, as recommended by ASHRAE and encoded within EnergyPlus configurations. Additionally, an indoor minimum temperature control is instituted at 24 °C, adjustable by the occupants based on external air temperature conditions.

6.4 PMV AND PPD SOFTWARE ANALYSIS

The DesignBuilder software facilitated the computation of the predicted mean vote (PMV) and predicted percentage of dissatisfied (PPD) for designated areas within the houses. The software calculates metabolic rates, air velocity, and clothing values drawing from the EnergyPlus input data, adhering to the ASHRAE 55-2004 Standard tailored to each zone's occupancy settings. Notwithstanding, users retain the option to specify these variables manually during PMV and PPD evaluations.

Monthly average PPD values have been computed and are presented visually in figures for the zones under investigation. Likewise, PPD values for typical summer and winter days have been determined for these zones. Concurrently, an in-depth analysis of thermal behaviour within the selected zones was conducted by estimating and scrutinising monthly discomfort hours.

6.5 HEAT BALANCE BREAKDOWN

The DesignBuilder software categorizes the load breakdown into three primary segments: (1) Fabric and Ventilation, (2) Airflow, and (3) Internal Gains, as delineated by (EnergyPlus, 2021a).

6.5.1 FABRIC AND VENTILATION SIMULATION

- Glazing: The total heat flow into a zone through glazing, excluding solar radiation, which is accounted for under Solar Gains through Exterior Windows.
- Walls: The cumulative heat gains from the interior surfaces of external walls.
- Roofs: The aggregate heat gains from the interior surfaces of external roofs.
- Ceilings: The total heat gains from the interior surfaces of the ceiling.
- Floors: The overall heat gains from the interior surfaces of internal floors.
- Ground Floors: The sum of heat gains from the inner surfaces of the ground floor.
- Partitions: The cumulative heat gains from the inner surfaces of internal partitions.
- External Infiltration: Heat gain due to air infiltration when employing simple natural ventilation.
- External Air: Heat gain from outside air through external openings when using the calculated natural ventilation option.

Surface conduction data represents heat transfer within the building's surface, inclusive of convection, radiation, and other mechanisms.

6.5.2 AIRFLOW SIMULATION

Air change rate" refers to the rate at which fresh air replaces indoor air. ASHRAE (2016) specifies a minimum of 0.35 air changes per hour, or no less than 15 cubic feet per minute per person. DesignBuilder simulates airflow as a combination of mechanical and natural ventilation, plus infiltration, to maintain acceptable indoor air quality and mitigate health risks.

6.5.3 INTERNAL GAINS SIMULATION

- Heat gains from various sources such as task and general lighting, equipment, and cooking.
- Heat gain from IT equipment.
- Occupant-related gains.
- Solar Gains through Exterior Windows: Short-wave solar radiation transmission through all exterior windows, assuming perfect diffusion by shades.
- Solar Gains through Interior Windows: Not deducted from the external window's reflected solar energy transfer.
- Zone Sensible Cooling: The cooling effect of air introduced into the zone, including 'free cooling' from colder outside air and fan heat effects, represented as negative heat gain.
- Zone Sensible Heating: The heating effect of air supplied into the zone, not synonymous with heat delivered by a heating coil.

The study concentrated on key elements affecting indoor heat balance, such as external/internal walls, solar gains, and total fresh air, acknowledging that roof gains only affect upper-floor zones exposed to external conditions.

6.6 PREDICTED THERMAL COMFORT ZONE BOUNDARIES

Thermal performance across six zones within three selected houses has been evaluated and simulated, analysing variables such as internal temperature and humidity, predicted percentage of dissatisfied (PPD) as estimated by PMV, total discomfort hours, gains breakdown, and airflow within zones. The data pertaining to comfort hours is contingent upon the operative temperature aligning with the comfort zone as delineated in Figures 6.1 and 6.2, which conform to the ASHRAE 55-2004 Standard. Operative temperature is calculated as the mean of the ambient air temperature and the mean radiant temperature. For the purposes of these evaluations, summer conditions assume a clothing level of 0.5 Clo, while winter conditions assume 1.0 Clo. The figures 6.1 and

6.2, stemming from the associated tables, extend the ASHRAE values to a humidity ratio of zero (EnergyPlus, 2021a).

Air Temp(degC)	Humidity Ratio
19.6	0.012
23.9	0.012
26.3	0.000
21.7	0.000

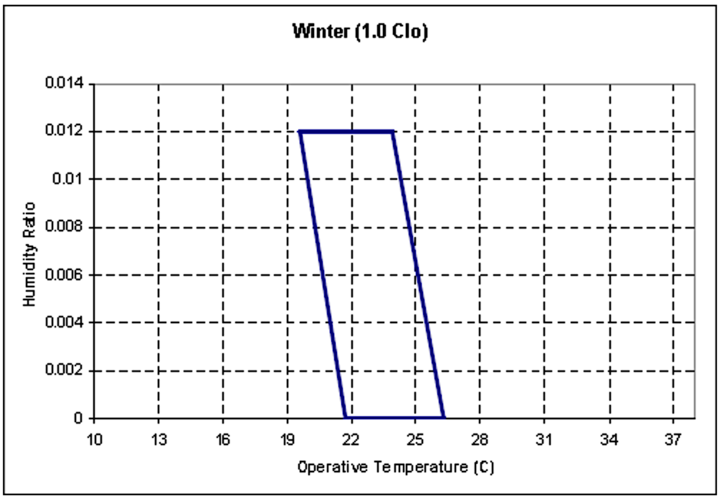

Figure 6.1: Comfort hours zone considering winter clothing. Source: EnergyPlus (2021a).

Air Temp(degC)	Humidity Ratio
23.6	0.012
26.8	0.012
28.3	0.000
25.1	0.000

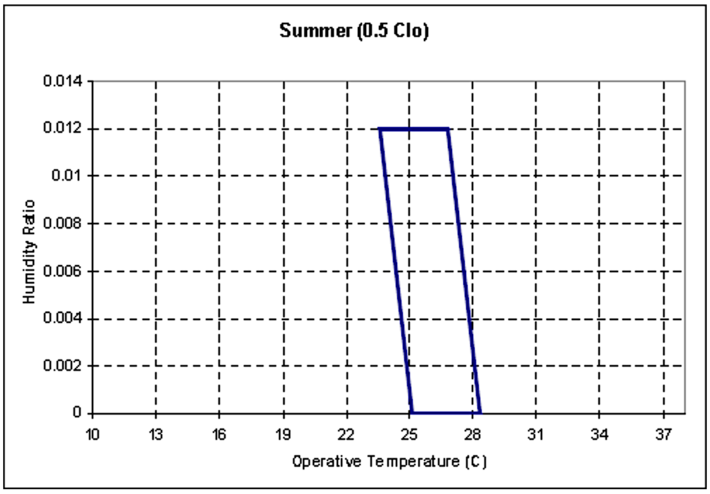

Figure 6.2: Comfort hours zone considering summer clothing. Source: EnergyPlus (2021a).

Operative temperature, a metric recognized by ASHRAE and ISO standards, gauges human thermal comfort by amalgamating air temperature, mean radiant temperature, and air speed into a singular, precise measurement. Therefore, operative temperatures for the living, dining, and bedrooms in each house are forecasted on a monthly basis and for typical days in summer and winter.

Moreover, to provide insight into the interplay between other vital thermal indices, relative humidity (RH) has also been estimated for these zones. Consequently, the analysis of each house is accompanied by a minimum of 16 illustrative figures. The results for the three houses (1-J, 1-M, and 2-M), which encompass two distinct zones each indicative of thermal discomfort hours, are consolidated into a singular figure at this chapter's conclusion.

House 1-J is examined in greater detail, in anticipation of the subsequent chapter's focus on thermal performance enhancements. It is also pertinent to note that the parametric and technical data inputs for all three houses are delineated and discussed.

6.7 HOUSE 1-J THERMAL PERFORMANCE ANALYSIS

6.7.1 TEMPERATURE AND RELATIVE HUMIDITY

Figures 6.3 and 6.4 illustrate the operative temperature and relative humidity, respectively, based on monthly averages for the selected zones. Additionally, Figures 6.5 to 6.8 display these metrics for typical summer and winter days.

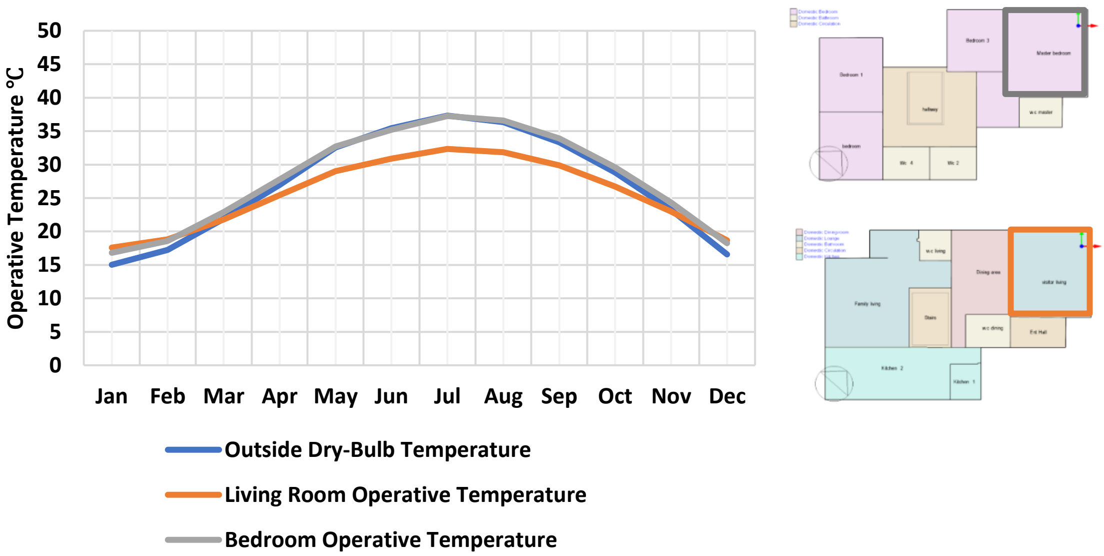

Figure 6.3: Monthly average temperature for the two studied zones as indicated on the plan layouts. Data were obtained from DesignBuilder software and reanalysed using Excel.

As depicted in Figure 6.3, there are significant temperature shifts throughout the year, consistent with the patterns of the external dry-bulb temperature. The summer months (June to August) experience an average peak temperature of 39°C, while the cooler period spans from December to January, with an average low of 14°C. January registers as the coldest month. The indoor operative temperature increases with the external temperature during the summer and decreases with it during the winter.

Notably, the bedroom on the first floor shows a greater temperature range—closely following the external dry-bulb temperature—with a differential of about 6°C higher than the living room temperature, particularly in the summer months. The highest operative temperature for the bedroom is recorded in July, due to inadequate roof thermal insulation, resulting in unmoderated heat gain from the concrete roof's substantial thermal mass, as evidenced in the Heat Balance Breakdown sections of this chapter.

In contrast, the living room, situated on the ground floor, demonstrates a slightly more stable thermal environment (operative temperature) than the bedroom. This stability is attributed to the heat dissipation through the ground floor during the summer, further detailed in the Gains Breakdown section of this chapter.

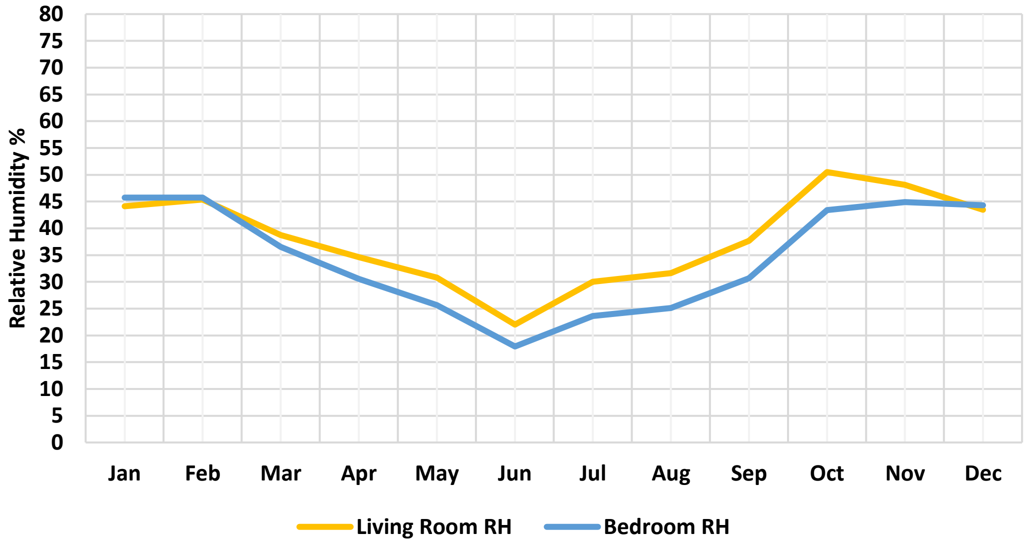

Figure 6.4: Zones' monthly average relative humidity. Data gathered from DesignBuilder software and regenerated using Excel.

Figure 6.4 depicts the zones' monthly average relative humidity. Data from DesignBuilder software have been reprocessed in Excel. The relative humidity for both the living room and bedroom zones decreases to an average of 30% during summer months and increases to around 45% in winter.

The living room, located on the ground floor, consistently records slightly higher relative humidity throughout the year, while the bedroom, situated on the upper floor, shows lower values. This disparity is due to temperature differences between floors, where warmer air on the upper levels holds less moisture, leading to lower humidity.

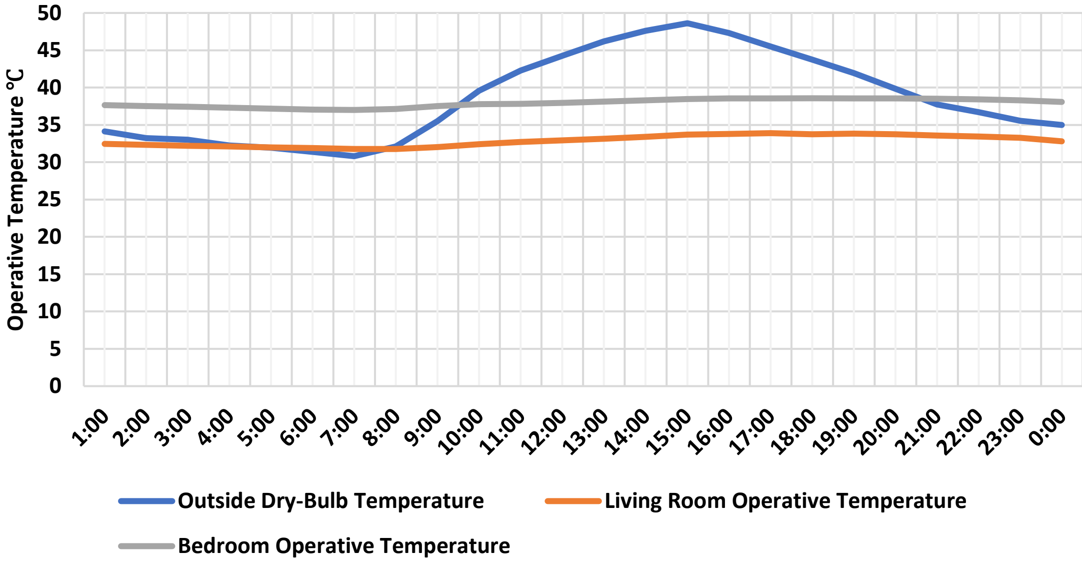

Figure 6.5: Hourly temperature recorded for a typical summer day (24 July). Data gathered from DesignBuilder software and regenerated using Excel.

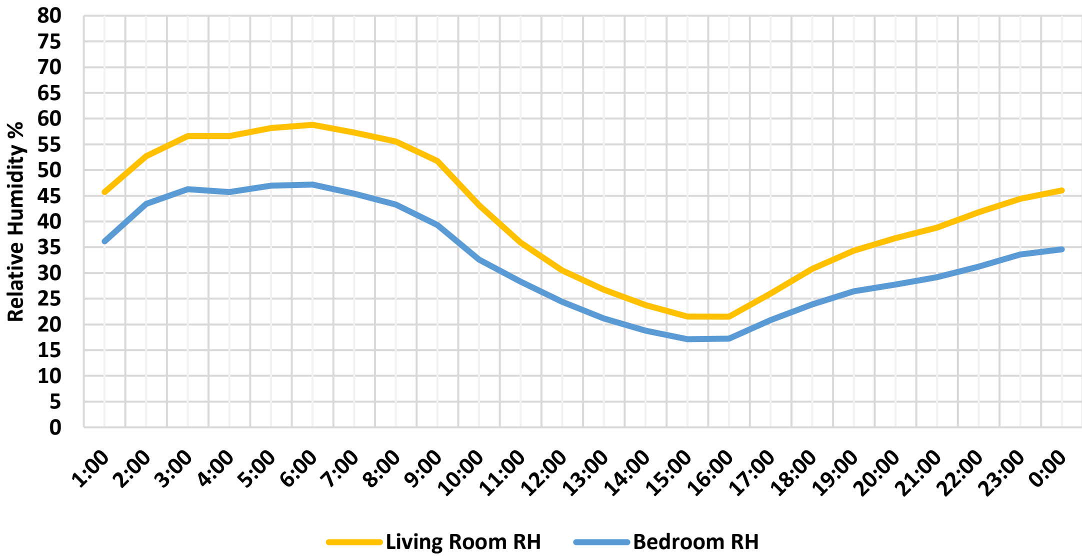

Figure 6.6: Hourly relative humidity recorded for a typical summer day (24 July). Data gathered from DesignBuilder software and regenerated using Excel.

Figures 6.5 and 6.6 illustrate both temperature distribution and relative humidity, respectively throughout the hottest day of the year, which is found to be July 24. Figure 6.5 presents the hourly temperature recorded for a typical summer day (24 July), and Figure 6.6 shows the corresponding hourly relative humidity. The extreme external temperatures of up to 50°C indicate the severity of summer conditions. Hourly indoor operative temperatures demonstrate that the bedroom consistently records higher temperatures than the living room, with a maximum of around 38°C, surpassing the external temperature by about 6°C from late evening to morning. This suggests that the upper-floor zones, particularly those with roof exposure, are subject to more intense heat compared to lower floors.

Relative humidity experiences notable diurnal fluctuations, with the living room ranging from 21% to 59%, and the bedroom from 17% to 47%. The pattern of relative humidity is consistent across both zones, with moderate levels in the early morning and late night, reaching their lowest levels during midday.

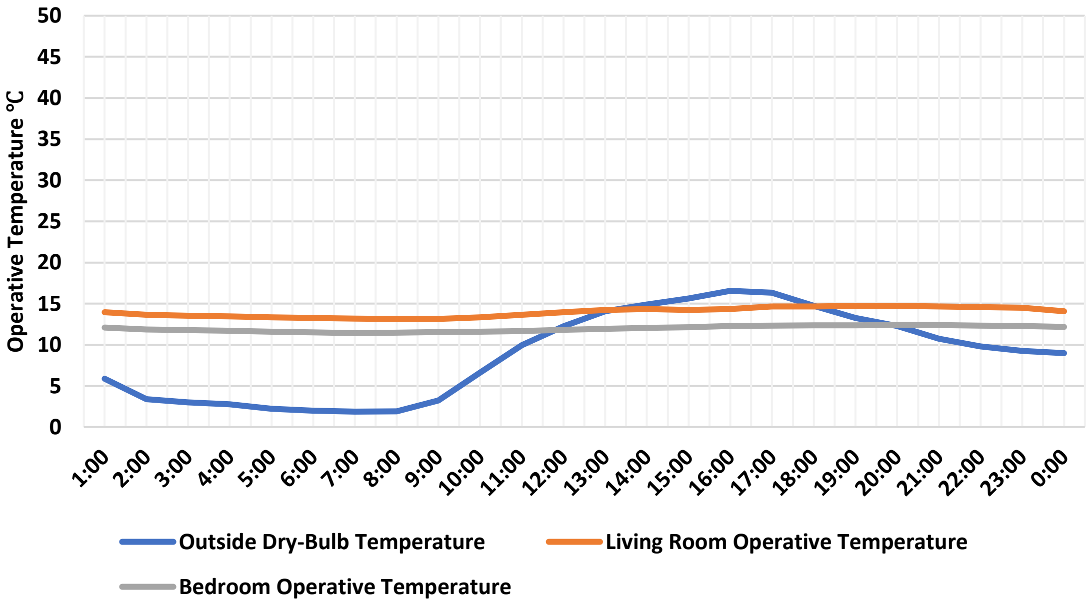

Figure 6.7: Hourly temperature recorded for a typical winter day (23 January). Data gathered from DesignBuilder software and regenerated using Excel.

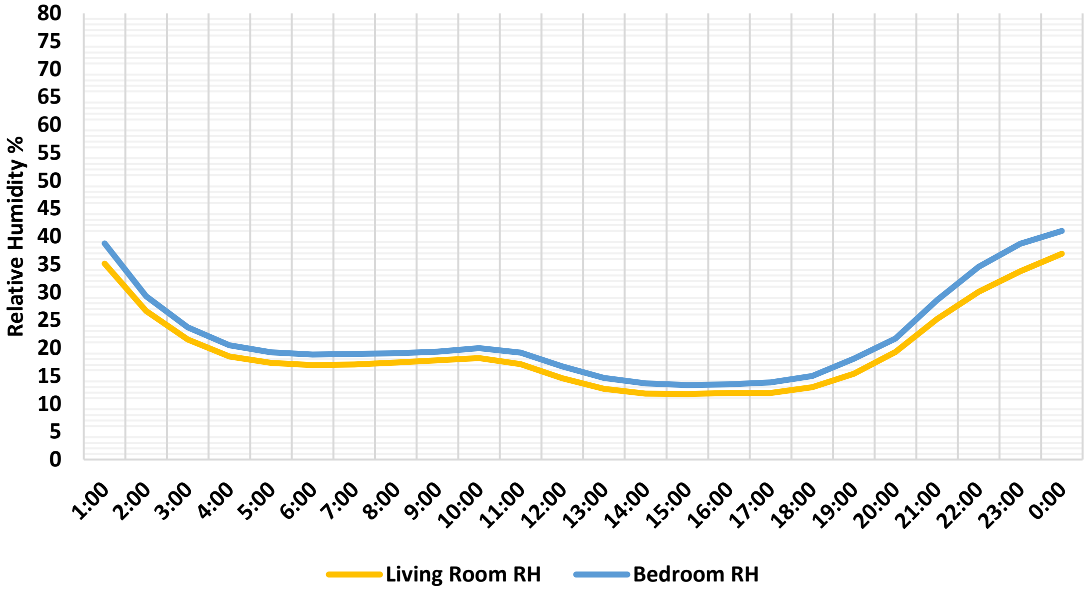

Figure 6.8: Hourly relative humidity recorded for a typical winter day (23 January). Data gathered from DesignBuilder software and regenerated using Excel.

Figures 6.7 and 6.8 capture the hourly temperature and relative humidity for a typical winter day (23 January). The external temperature varies from a low of around 2°C to a high of approximately 17°C. The bedroom experiences the lowest operative temperature, around 11°C, correlating with the early morning external low. Conversely, the living room maintains a higher temperature, approximately 15°C throughout the day.

The living room's operative temperature exceeds that of the bedroom by a maximum of 3°C, a reversal from the summer pattern, implying deficiencies in the house's roof insulation across seasons. Additionally, a pronounced disparity is observed in the early morning, with the living room maintaining a steady temperature between 14°C to 15°C, while the external temperature hovers around 2°C.

The reliance on natural ventilation in the building also means relative humidity significantly influences thermal comfort within the zones. Winter relative humidity values are less variable than in summer, paralleling the more consistent operative temperatures observed in both zones.

6.7.2 PREDICTED PERCENTAGE OF DISSATISFIED (PPD) ANALYSIS

PPD values for both the living room and bedroom have been calculated and analysed, as depicted in Figures 6.9, 6.10, and 6.11. These figures represent monthly averages, a typical summer day, and a typical winter day, respectively. The PPD analysis throughout the year reveals that the living room consistently records lower percentages of dissatisfaction than the bedroom, supporting previous findings that the living room offers better thermal performance.

As demonstrated in Figure 6.9, PPD values for the living room are surprisingly within or below 20% dissatisfaction for several months, notably in March, April, May, October, and November. This lower PPD suggests that the living room remains thermally comfortable for half the year. However, the living room does encounter substantial dissatisfaction levels during other months, peaking at around 71%, 77%, and 75% in January, July, and December, respectively. These peaks signify that the zone is subject to extreme temperature conditions, yet the living room's overall thermal performance exhibits less variance compared to that of the bedroom, indicating a lower dissatisfaction percentage.

Conversely, the bedroom's PPD shows little relief from high dissatisfaction levels throughout the year, as illustrated in Figure 6.9. The PPD values never fall below 28% and often exceed 80%—particularly from June to September—indicating extremely uncomfortable hot conditions during summer. Winter months also see high dissatisfaction levels, suggesting very cold conditions. These stark contrasts in PPD values highlight the poor thermal performance of upper-floor zones that are connected to inadequately insulated roofs.

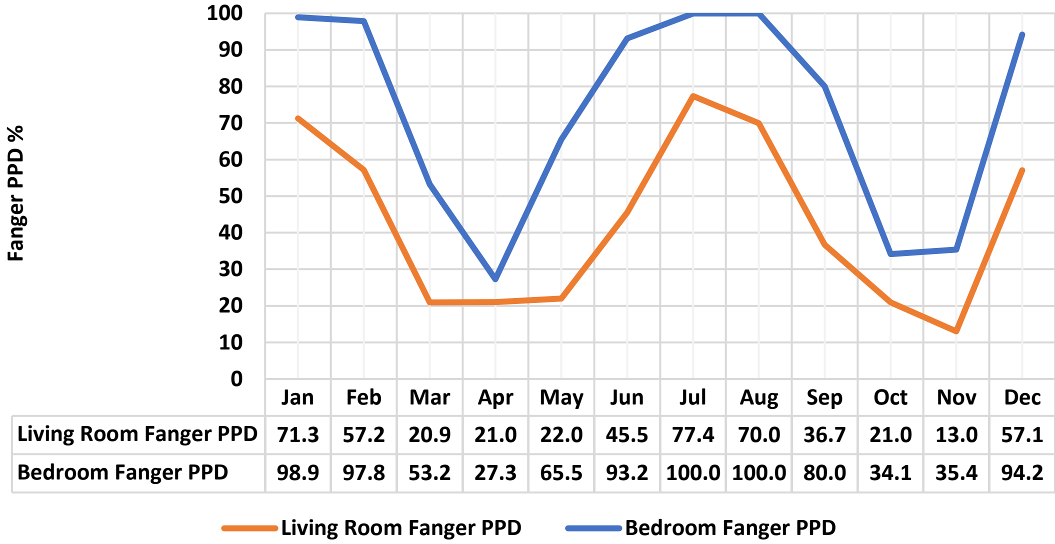

	Jan	Feb	Mar	Apr	May	Jun	Jul	Aug	Sep	Oct	Nov	Dec
Living Room Fanger PPD	71.3	57.2	20.9	21.0	22.0	45.5	77.4	70.0	36.7	21.0	13.0	57.1
Bedroom Fanger PPD	98.9	97.8	53.2	27.3	65.5	93.2	100.0	100.0	80.0	34.1	35.4	94.2

Figure 6.9: Living room and bedroom monthly averaged PPD. Data gathered from DesignBuilder software and regenerated using Excel.

Furthermore, Figure 6.9 shows the living room's PPD peaking in January, July, and December, while reaching its lowest in November at approximately 13%. The bedroom's PPD hits the maximum of 100% during January, February, July, August, and December, with a minimum of 27% in April. The data underscores the necessity for substantial thermal performance improvements in the bedroom to achieve acceptable comfort levels year-round.

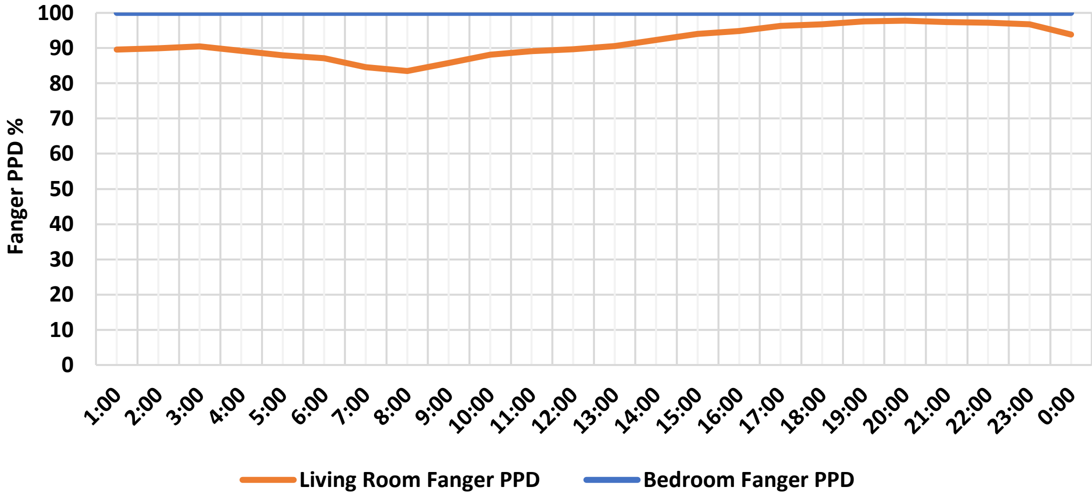

Figure 6.10: Living room and bedroom hourly averaged PPD for a typical summer day (24 July). Data gathered from DesignBuilder software and regenerated using Excel.

On a typical summer day (24 July), Figure 6.10 reveals that the living room's PPD ranges from 83% to 100%, while the bedroom experiences a constant 100% dissatisfaction throughout the day, indicating an overheating issue.

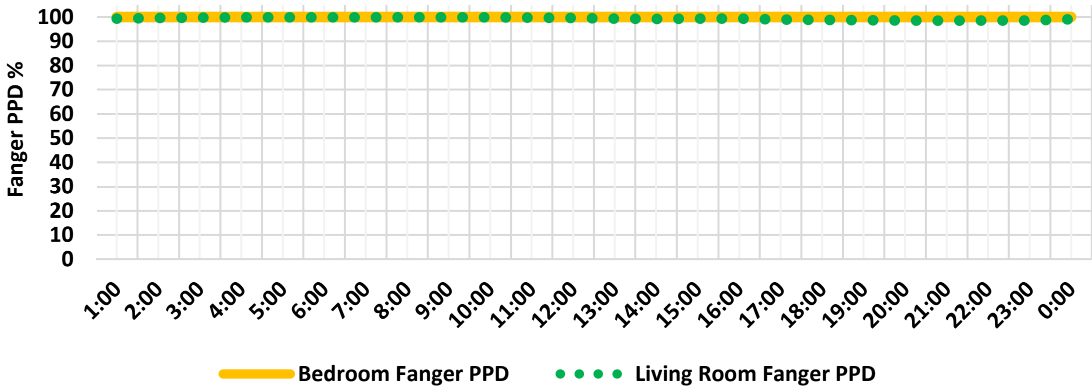

Figure 6.11: Living room and bedroom hourly averaged PPD recorded for a typical winter day (23 January). Data gathered from DesignBuilder software and regenerated using Excel.

During a typical winter day (23 January), shown in Figure 6.11, both the living room and bedroom exhibit a consistent PPD of 100%, indicative of extremely cold conditions and constant dissatisfaction. This uniformity suggests that the house is unable to adequately buffer against external climatic conditions. Therefore, enhancing thermal insulation within the building envelope is imperative for improving thermal comfort.

6.7.3 CALCULATED DISCOMFORT HOURS

To gain a deeper understanding of the thermal comfort in the selected spaces, discomfort hours were analysed monthly throughout the year. These hours were calculated during occupied periods only, given that the total number of hours in a year is 8760, which includes both occupied and unoccupied times, day, and night. For a more realistic assessment of comfort during times when the house is in use, the simulation was confined to occupied hours.

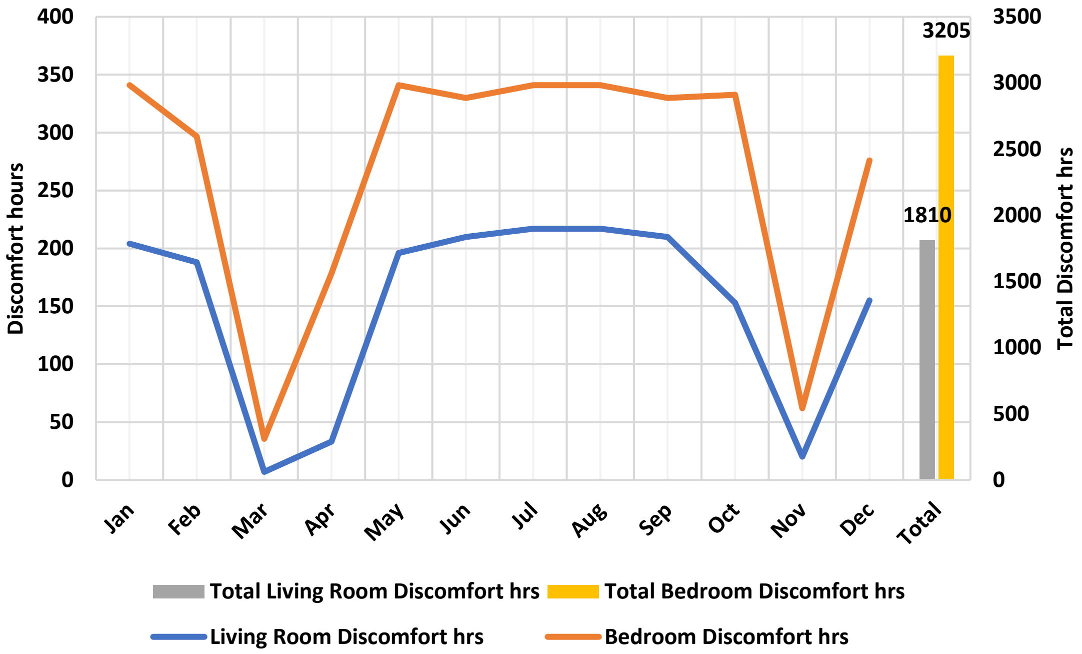

Figure 6.12: House 1-J monthly discomfort hours. Data extracted from DesignBuilder software and reprocessed in Excel.

As depicted in Figure 6.12, the estimation of monthly discomfort hours for both the living room and bedroom shows the lowest discomfort in March and November. The highest levels of discomfort were observed from May to October and from December to February in both zones, indicating that discomfort is especially elevated during the summer and winter months, with the noted exceptions.

Over the course of a year, the bedroom experienced approximately 3205 discomfort hours, while the living room had about 1810 hours. This marks a substantial difference of around 1395 hours between the two zones. The living room, with fewer discomfort hours, demonstrates a comparatively better indoor thermal performance than the bedroom. However, this does not suggest a significant advantage for the living room, as its thermal performance also shows potential for enhancement, especially during months when discomfort hours are at their highest.

6.7.4 SUMMER DAY HEAT BALANCE

The heat balance for both the living room and bedroom during a typical summer day is illustrated in Figures 6.13 and 6.14. These figures highlight significant heat losses in the living room's ground floor and interior floors, with the living room experiencing higher heat losses ranging from approximately 1000 W to 1270 W. This phenomenon is particularly pronounced due to the ground's role as a heat sink during extreme environmental conditions, as noted by Staszczuk and Kuczyński (2018).

In addition, both zones accrue heat through the roof, but the bedroom, being directly exposed to the exterior, registers greater heat gain, peaking at around 430 W. Such a substantial gain is indicative of overheating, attributable to the high thermal mass of the concrete roof, which also releases heat variably from the afternoon to the following midday. The overheating issue during the summer, particularly in the roofing system, is a concern that warrants attention.

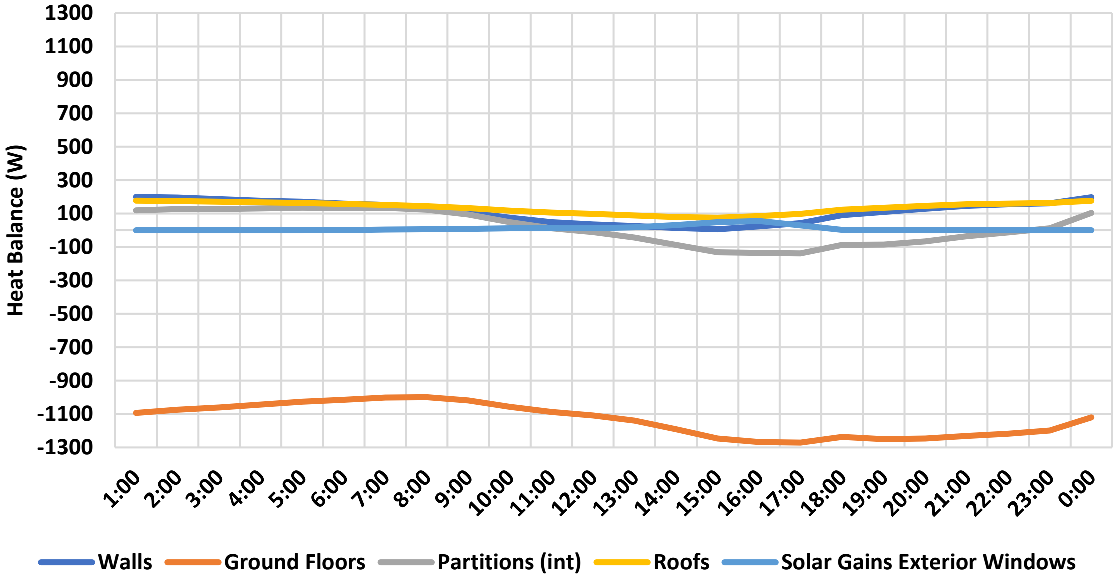

Figure 6.13: Living room summer day heat balance breakdown. Typical summer day (24 July). Data gathered from DesignBuilder software and recalculated using Excel.

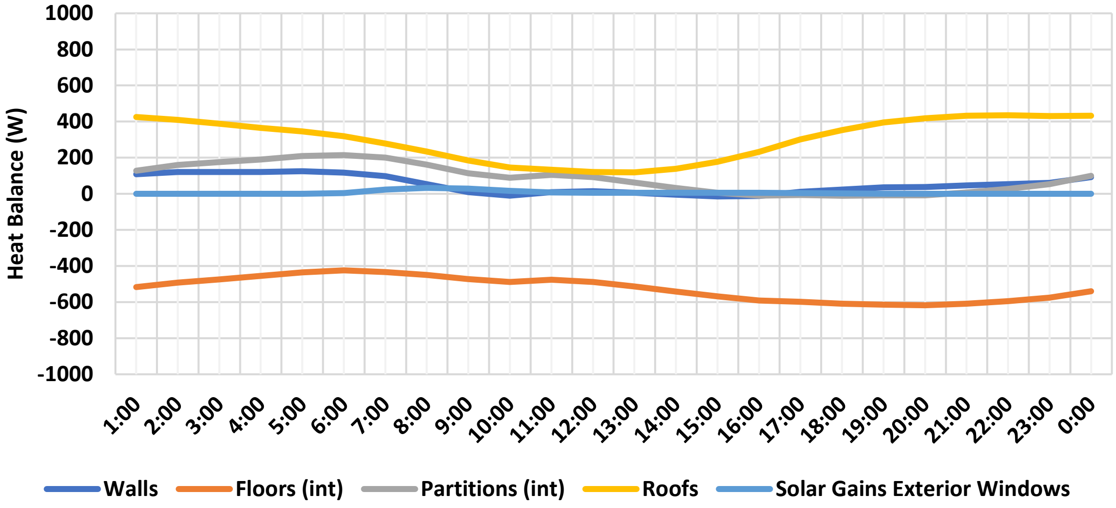

Figure 6.14: Master bedroom summer day heat balance breakdown. Typical summer day (24 July). Data gathered from DesignBuilder software and recalculated using Excel.

The heat gain through external walls is considerable for both zones, with the living room's maximum gain around 200 W and the bedroom's around 100 W, in the mornings. Conversely, from 10 a.m. to 6 p.m., there is a noticeable decrease in wall gains, with the bedroom even recording periods of no external wall gain before it rises again in the late evening. The behaviour of the concrete wall systems, absorbing heat during the day and reradiating it at various times, is evident. Internal partitions reflect similar patterns, with heat gains peaking during the day and dissipating towards the night. Surprisingly, solar gains through the exterior windows are the lowest among the heat gain sources, remaining at a maximum of 50 W throughout the day. This minimal solar gain can be attributed to the effective design and placement of windows, along with a small WWR.

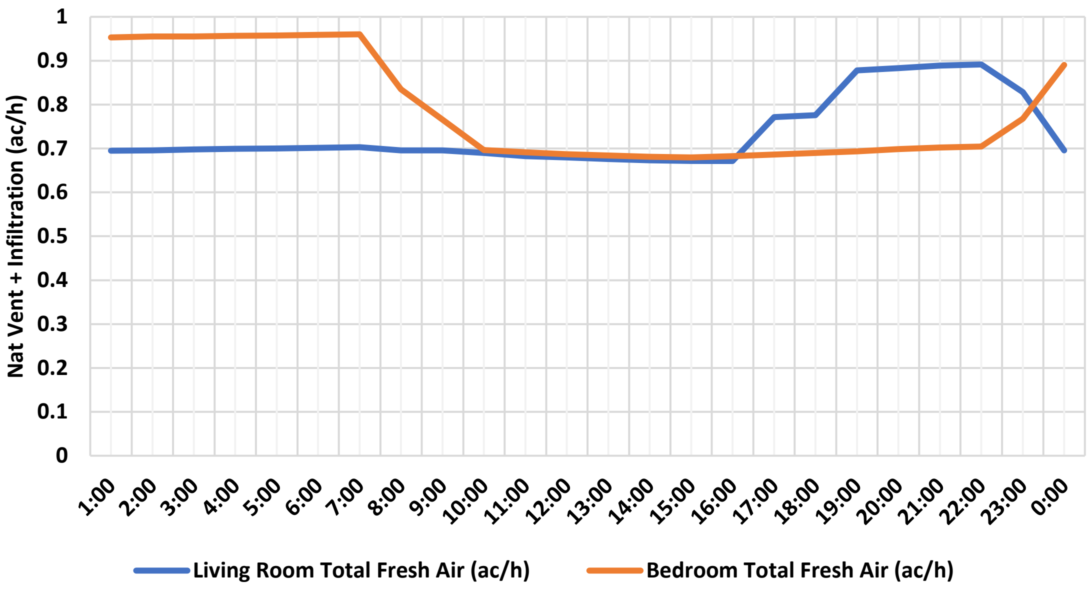

Figure 6.15: Living room and bedroom summer day's total fresh air (24 July). Data gathered from DesignBuilder software and regenerated using Excel.

The total fresh air rates, encompassing natural ventilation and infiltration, are illustrated in Figure 6.15. The bedroom exhibits slight variations, with the highest air change rate at 1 ac/h and the lowest at nearly 0.7 ac/h. The living room maintains a relatively constant air change rate of about 0.7 ac/h throughout the day, with a subtle increase from the late afternoon to late evening.

An increase in the hourly air change rate impacts the indoor heat gain/loss, which correlates with the external environment's conditions. This correlation suggests that the hot air entering from the outside can lead to overheating within the building's zones, especially in summer, as investigated by Ozarisoy and Elsharkawy (2019). This is particularly noticeable in the bedroom from 1 a.m. to 7 a.m., where the air change rate slightly increases, affecting the heat balance of both walls and internal partitions.

6.7.5 WINTER DAY HEAT BALANCE

Figures 6.16 and 6.17 detail the heat balance for the living room and bedroom during a typical winter day. These figures illustrate a noticeable heat gain on the ground floor for the living room and internal floors for the bedroom. Specifically, the living room's ground floor exhibits a slightly higher heat gain, peaking at approximately 460 W around 8:30 a.m., compared to the bedroom, which reaches its highest floor heat gain of about 260 W at around 7 a.m. The additional heat gain in the living room's ground floor likely results from the thermal coupling with the ground, which is known to transfer heat into the space during the winter months.

In contrast to the summer day scenarios depicted in Figures 6.13 and 6.14, the winter day analysis indicates heat loss through the roofs of both the living room and bedroom. The bedroom experiences more significant heat loss (up to -165 W), attributable to the roof's exposure to the cold external environment. The living room's roof, being shielded from direct external exposure, shows a relatively constant heat loss ranging from -50 W to -100 W throughout the day. Notably, the bedroom's roof registers a maximum heat gain of only about 40 W, whereas the living room's roof does not exhibit any heat gain during the day.

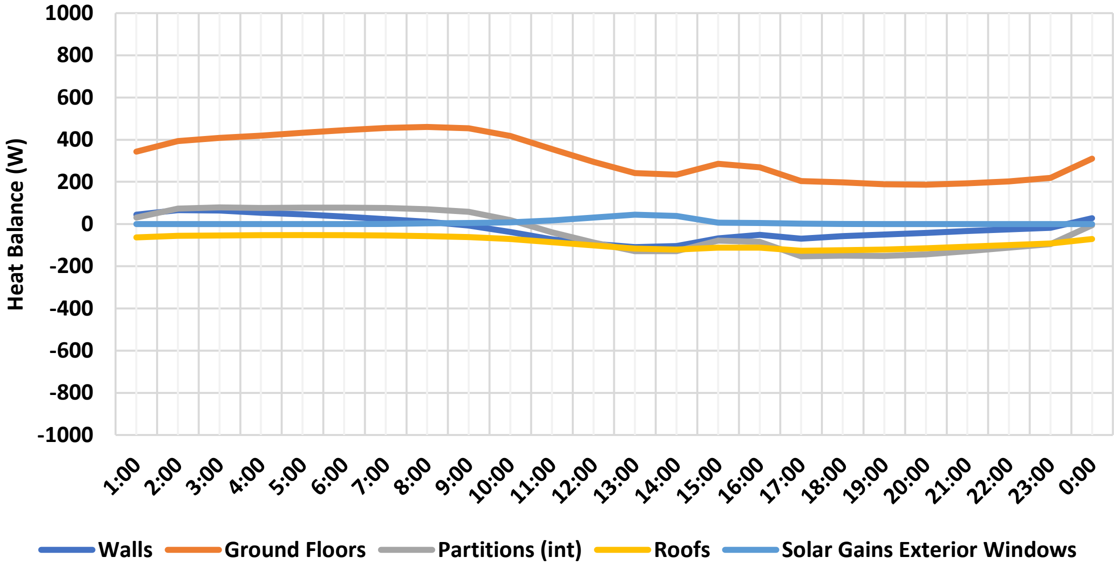

Figure 6.16: Living room winter day heat balance breakdown. Data generated from DesignBuilder software and reanalysed using Excel for a typical winter day (23 January).

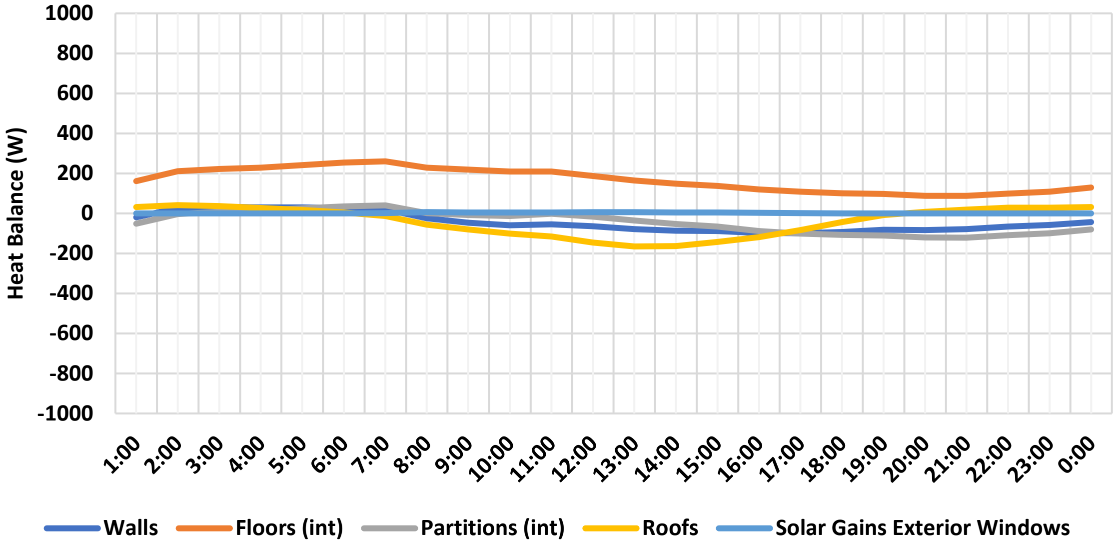

Figure 6.17: Master bedroom winter day heat balance breakdown. Data generated from DesignBuilder software and reanalysed using Excel for a typical winter day (23 January).

Moreover, external wall heat loss for both the living room and bedroom exhibits comparable patterns, with a maximum heat loss of approximately -100 W from 11 a.m. to around 8 p.m. Additionally, a notable heat gain of about 100 W is recorded for the living room from 1 a.m. to 6 a.m. This behaviour is attributed to the thermal mass of dense construction materials, which store heat during the day and reradiate it at night (Zhang et al., 2007).

Internal partitions display similar heat balance trends in both zones, with extra heat loss recorded for the living room, especially during nighttime. The living room also experiences a minor heat gain from 1 a.m. to 9 a.m., while both zones show a heat loss of around -140 W from midday to late evening.

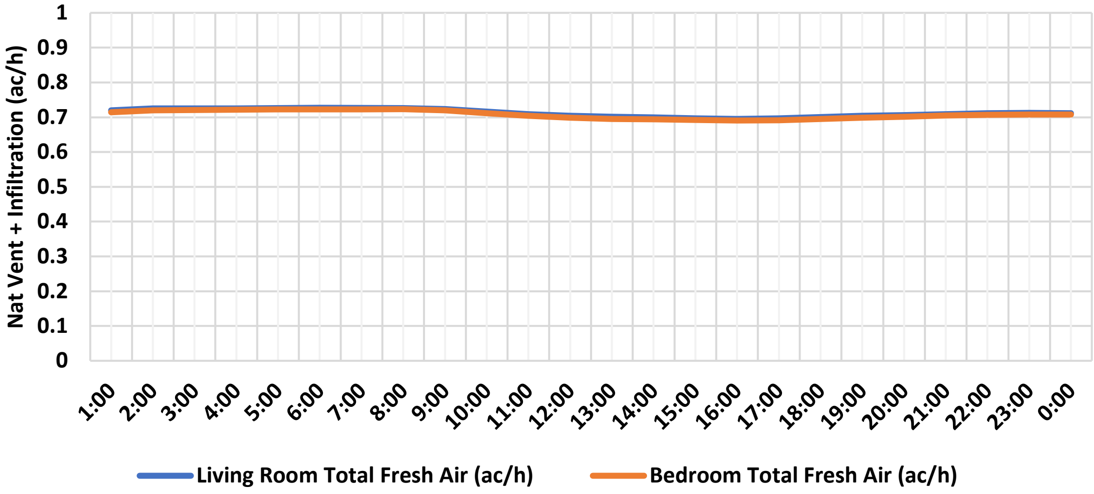

Figure 6.18: Living room and bedroom total fresh air for a typical winter day. Data generated from DesignBuilder software and reproduced using Excel for a typical winter day (23 January).

Consistently throughout the day, the total fresh air rate, including natural ventilation and infiltration, remains at about 0.7 ac/h for both zones. The relationship between convective heat transfer through the building envelope and airflow patterns is crucial (Yan and Li, 2021). This correlation is evidently demonstrated in the heat balance of the building elements, especially under constant airflow conditions, as shown in Figure 6.18.

6.8 HOUSE 1-M THERMAL PERFORMANCE ANALYSIS

6.8.1 TEMPERATURE AND RELATIVE HUMIDITY

Figures 6.19 and 6.20 represent the monthly averages of operative temperature and relative humidity for selected spaces in House 1-M. Additional Figures 6.21 to 6.24 capture the operative temperatures and relative humidity for typical summer and winter days, respectively.

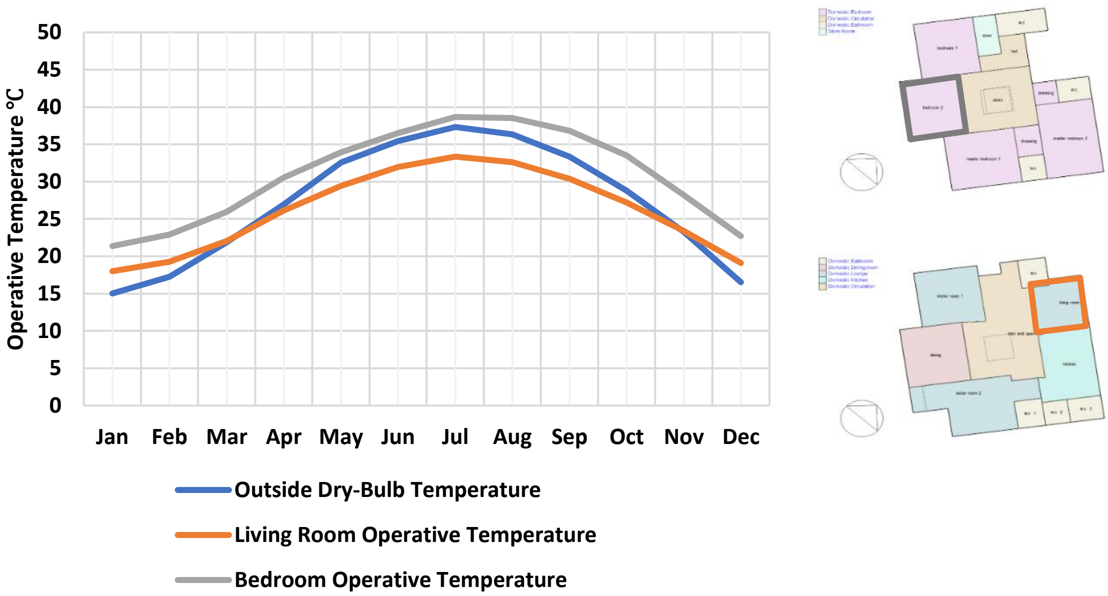

Figure 6.19: Monthly average temperature for the two studied zones, as illustrated on plan layouts. Data gathered from DesignBuilder software and regenerated using Excel.

Figure 6.19 shows the operative temperatures for both the living room and bedroom alongside the outside dry-bulb temperature, which has been previously analysed in this chapter due to their identical location. The temperatures in both zones follow similar patterns throughout the year, with the bedroom's operative temperature consistently registering around 7°C higher than the living room.

During summer months, the bedroom's temperature closely matches the outside dry-bulb temperature, notably from early May to mid-August. It is striking that the bedroom's temperature exceeds the outside temperature for most of the year, a trend that is particularly evident during the winter months, pointing to an overheating issue in the upper-floor zones. The higher bedroom temperatures during the summer months suggest poor thermal performance, particularly in areas directly affected by the roof's thermal properties.

Conversely, in winter, the living room maintains a temperature range within a comfortable thermal comfort zone, likely due to better insulation or ground heat loss effects.

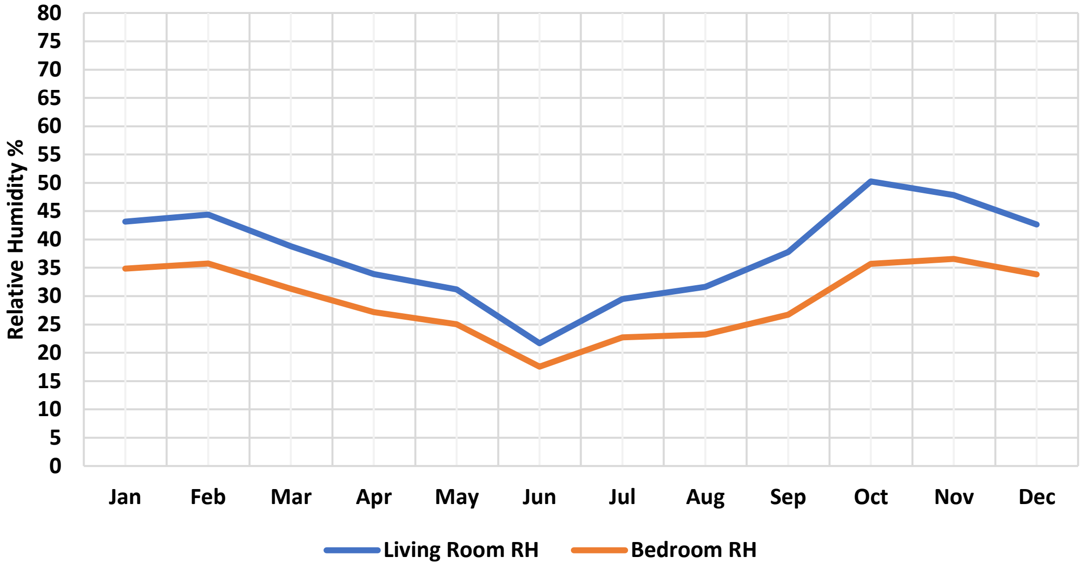

Figure 6.20: Monthly average relative humidity. Data gathered from DesignBuilder software and regenerated using Excel.

The relative humidity, as depicted in Figure 6.20, decreases throughout the summer, and increases during the winter, with both zones displaying similar distribution patterns year-round. However, the living room on the lower floor exhibits higher humidity rates compared to the bedroom on the upper-floor, potentially due to differences in airflow rates between the two floors, as previously investigated in the analysis of House 1-J.

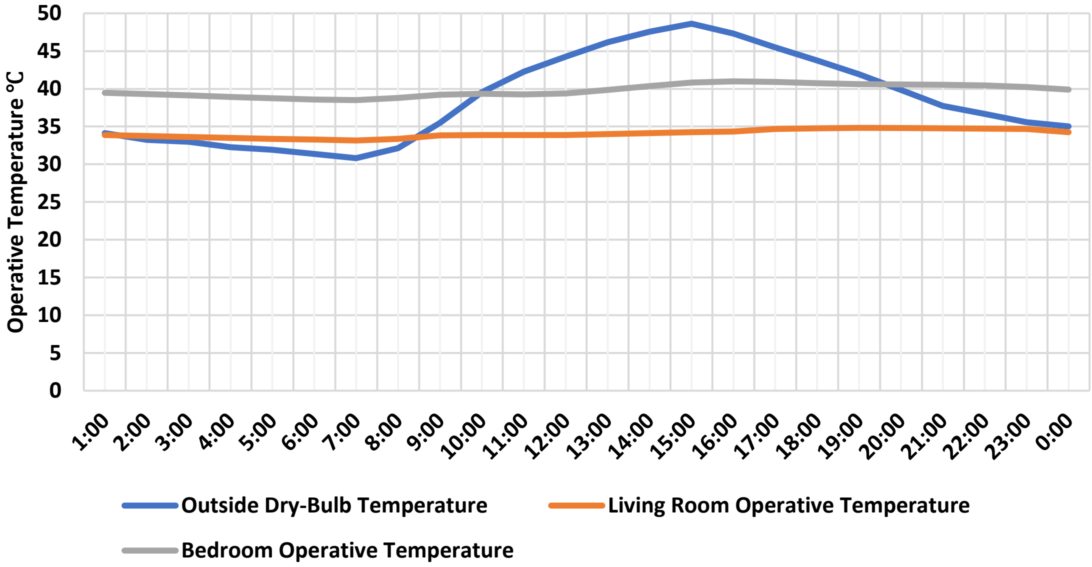

Figure 6.21: Hourly temperature recorded for a typical summer day (24 July). Data gathered from DesignBuilder software and regenerated using Excel.

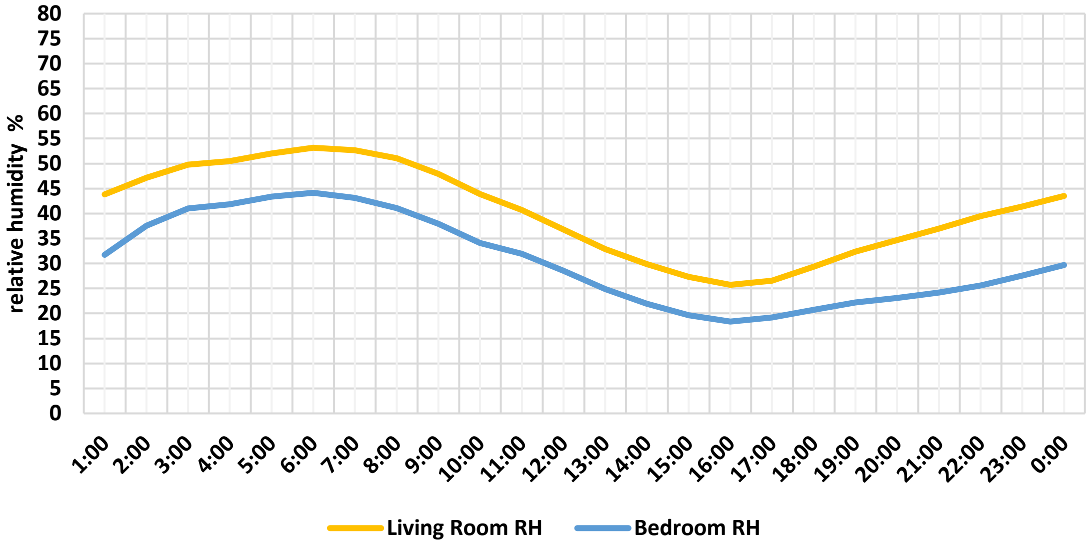

Figure 6.22: Hourly relative humidity recorded for a typical summer day (24 July). Data gathered from DesignBuilder software and regenerated using Excel.

On the hottest day of the year, Figures 6.21 and 6.22 display the distributions of temperature and relative humidity, respectively. With external temperatures soaring to around 50°C, the interior of the house experiences significantly high operative temperatures. In particular, the bedroom's temperature peaks at approximately 40°C.

Notably, the bedroom's temperature surpasses the outdoor dry-bulb temperature from late evening to morning hours, which is indicative of the substantial heat impact on upper-floor zones due to less insulation compared to the ground level. This exacerbates the overheating problem in the bedroom, especially during the night when temperatures typically drop outside but remain high indoors due to the accumulated heat throughout the day.

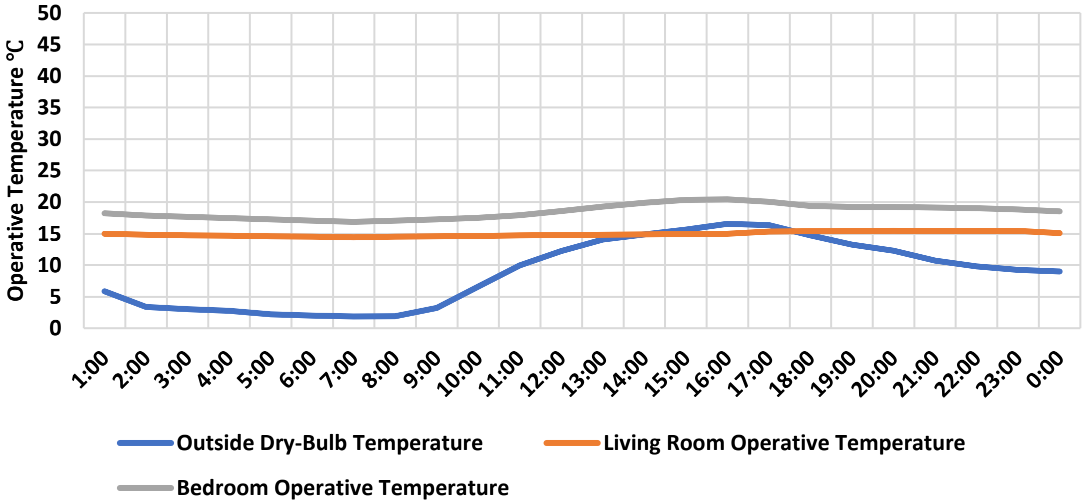

Figure 6.23: Hourly temperature recorded for a typical winter day (23 January). Data gathered from DesignBuilder software and regenerated using Excel.

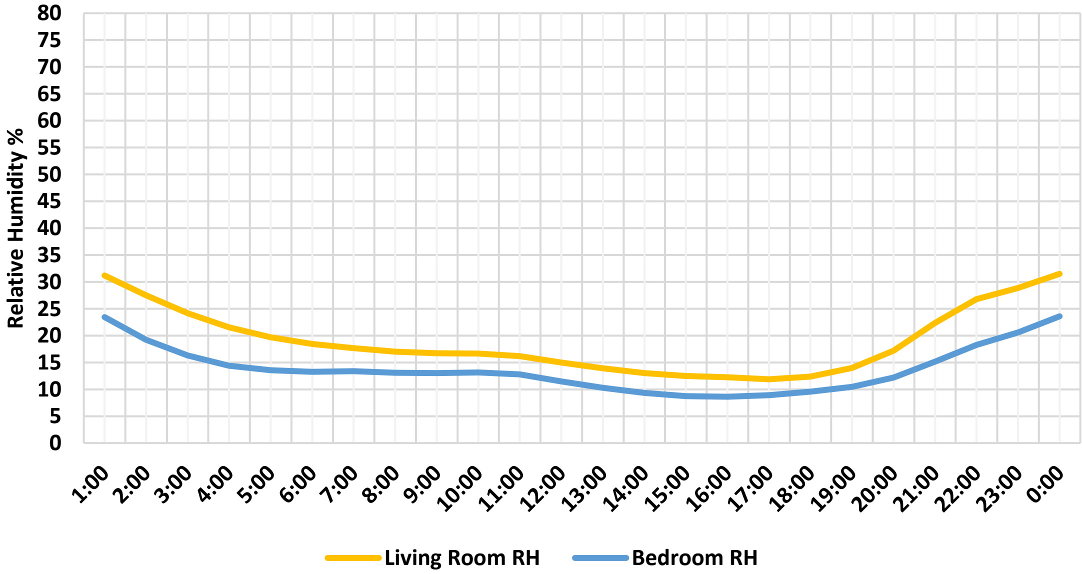

Figure 6.24: Hourly relative humidity recorded for a typical winter day (23 January). Data gathered from DesignBuilder software and regenerated using Excel.

Figures 6.23 and 6.24 offer an in-depth evaluation of temperature and relative humidity distributions during the year's coldest day. External temperatures, observed at a low of around 2 °C in the morning and reaching a high of approximately 17 °C by midday, set the context for analysing the internal thermal conditions of the residence. Both the living room and bedroom maintain consistent operative temperatures, marked at about 15 °C and 20 °C respectively, demonstrating the effectiveness of the building's structure in maintaining a stable interior climate against external temperature fluctuations.

This consistent temperature is particularly noticeable in the bedroom, which sustains a comfortable temperature range, indicating an effective balance of heat retention by its construction materials. Despite the range in external temperatures from the cold of the early morning to the warmth of midday, the internal temperatures of both areas remain relatively steady, confirming the building's ability to uphold a stable and comfortable indoor environment in winter season.

In contrast, the living room, situated on the lower level, tends to have operative temperatures that are consistently about 3 °C cooler compared to the bedroom above throughout the day. This difference reflects the typical heat loss experienced by lower-level floors due to their contact with the ground. The bedroom, on an upper level and receiving direct sunlight, shows higher operative temperatures as a result of the warming effects of solar radiation.

Moreover, the relative humidity levels in the living room and bedroom are quite similar, with the living room showing a slightly higher percentage, exceeding the bedroom by about 5%, as depicted in Figure 6.24. This slight increase in the living room's humidity could be due to its closer proximity to the ground, which is naturally more humid. Therefore, the findings underscore the home's competent thermal management during colder periods, although they also point to opportunities for improving thermal insulation, especially on the lower level, to enhance heat distribution and elevate the comfort within the building.

6.8.2 PREDICTED PERCENTAGE OF DISSATISFIED (PPD) ANALYSIS

The PPD monthly averages, as well as the data for a typical summer day and a typical winter day for both the living room and bedroom, have been estimated and analysed as illustrated in Figures 6.25, 6.26, and 6.27, respectively. The PPD values provide an index reflecting the expected level of occupant dissatisfaction based on thermal environmental conditions.

It is worth mentioning that a mixed-method approach was employed in this research, utilising the adaptive comfort model in conjunction with PPD to evaluate and depict thermal comfort based on the given readings, particularly for naturally ventilated spaces. This approach considers the dynamic environmental factors that influence comfort in such spaces, where temperature and airflow can vary significantly.

As observed from the data, the living room consistently exhibits lower PPD percentages throughout the year when compared to the bedroom, with both zones displaying equivalent PPD values during January, February, and March. This trend suggests a more effective thermal performance in the living room over the bedroom across the analysed periods.

Notably, the living room achieves a PPD below the 20% dissatisfaction threshold during March, April, and November, signifying a thermally comfortable environment for approximately a quarter of the year. However, the remaining months witness significant dissatisfaction levels, peaking at approximately 90% during periods of extreme temperatures.

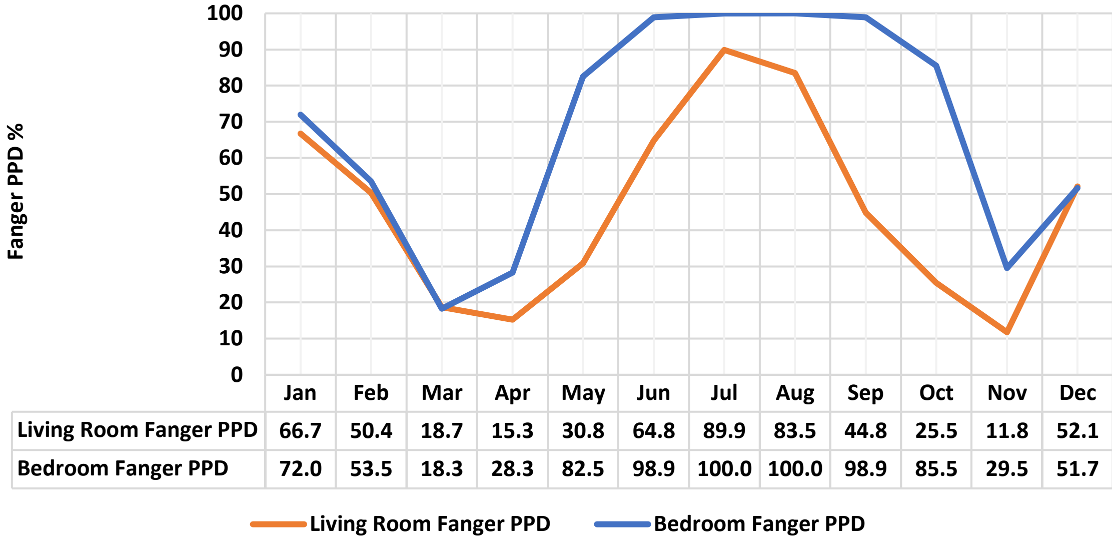

	Jan	Feb	Mar	Apr	May	Jun	Jul	Aug	Sep	Oct	Nov	Dec
Living Room Fanger PPD	66.7	50.4	18.7	15.3	30.8	64.8	89.9	83.5	44.8	25.5	11.8	52.1
Bedroom Fanger PPD	72.0	53.5	18.3	28.3	82.5	98.9	100.0	100.0	98.9	85.5	29.5	51.7

Figure 6.25: Living room and bedroom monthly averaged PPD. Data gathered from DesignBuilder software and regenerated using Excel.

Contrastingly, the bedroom's thermal performance is marked by higher PPD values, especially during the summer months, as depicted in Figure 6.25. March stands out as an exception, with the bedroom's PPD recorded at a mere 18%, aligning with the maximum acceptable dissatisfaction threshold of 20% as delineated by Shaeri and Mahdavinejad (2022).. This finding underscores that the bedroom's environment is within the acceptable dissatisfaction range for only one month of the year.

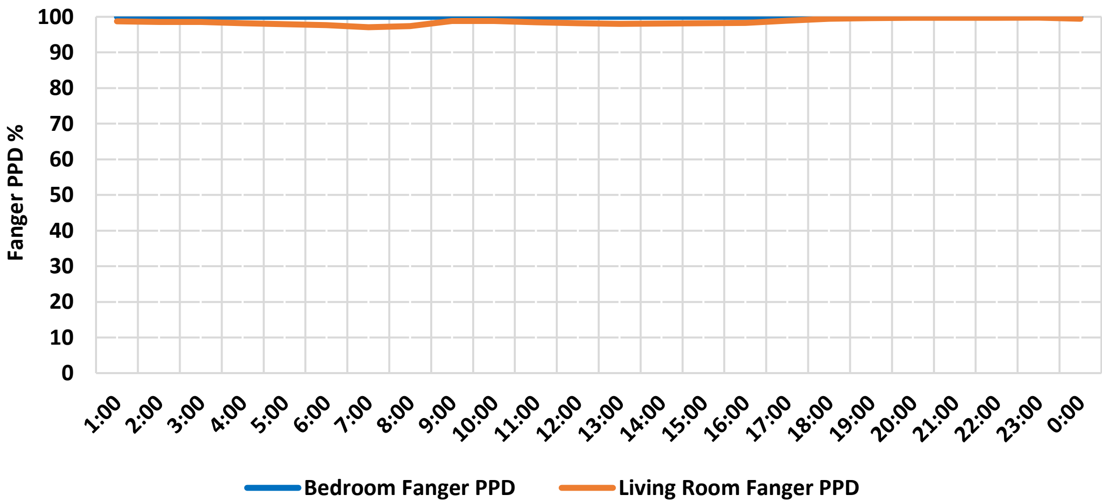

Figure 6.26: Living room and bedroom hourly averaged PPD for a typical summer day (24 July). Data gathered from DesignBuilder software and regenerated using Excel.

Figure 6.26 explains the living room and bedroom hourly averaged PPD for a typical summer day (24 July), revealing a striking 100% PPD throughout the day for both zones. This unity in dissatisfaction underscores a prevalent overheating issue during the peak of summer.

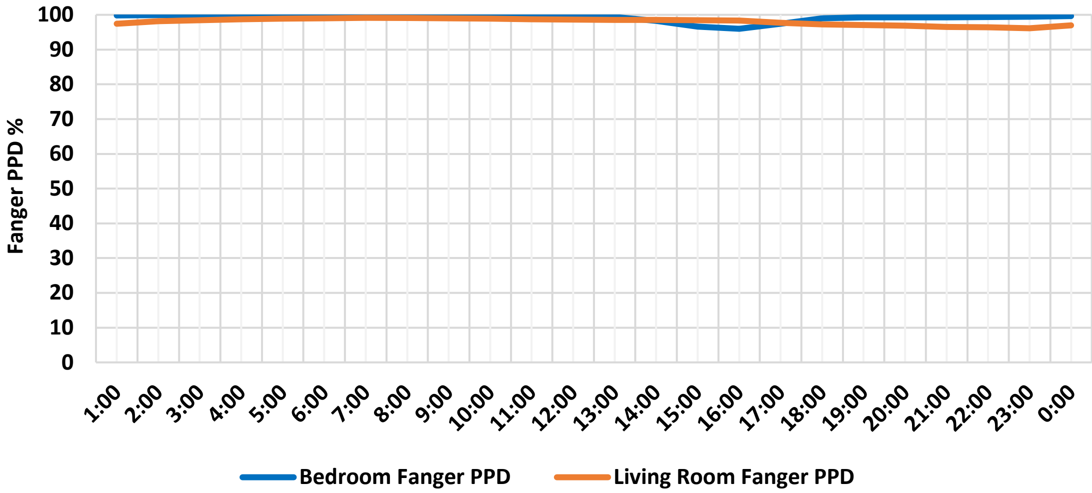

Figure 6.27: Living room and bedroom hourly averaged PPD recorded for a typical winter day (23 January). Data gathered from DesignBuilder software and regenerated using Excel.

Figure 6.27 presents the hourly averaged PPD for a typical winter day (23 January), again registering a 100% dissatisfaction level for both the living room and bedroom throughout the day. Such uniform dissatisfaction from occupants' points to inadequate thermal conditions during the winter's coldest days.

Accordingly, the thermal performance of the analysed zones is deemed unsatisfactory, with occupants likely to experience discomfort during the extremes of summer and winter. Consequently, it is imperative to prioritize enhancements in thermal performance within these spaces to mitigate occupant dissatisfaction.

6.8.3 CALCULATED DISCOMFORT HOURS

Figure 6.28 presents the total discomfort hours for each month throughout the year, considering only the hours when the spaces are occupied. In the living room, the fewest discomfort hours occur in March, April, and November, while the most are recorded from May to October, and from December to January, averaging about 200 hours per month.

In contrast, the bedroom follows a similar pattern but with a consistently higher rate of discomfort hours. From April to October, the bedroom experiences around 350 discomfort hours each month, almost double that of the living room. However, in February and March, the bedroom's discomfort hours drop to 25 and 50 hours, respectively, which is closer to an acceptable range when compared with other months.

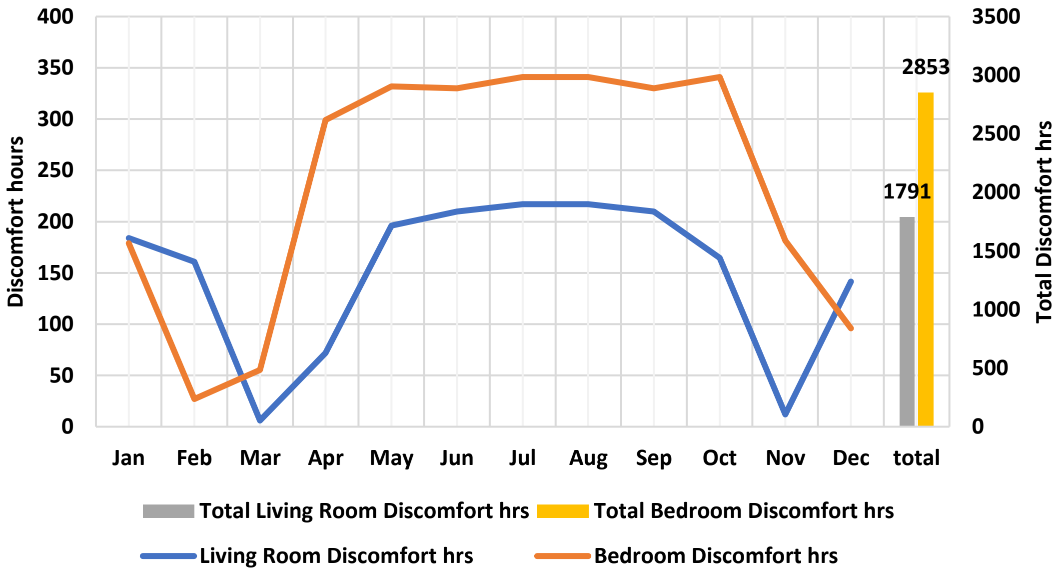

Figure 6.28: Total monthly discomfort hours for House 1-M. Data gathered from DesignBuilder software and reprocessed using Excel.

Cumulatively, the bedroom accumulates about 2853 discomfort hours over the year, while the living room totals about 1791 hours, leading to a difference of 1062 hours between the two areas. Hence, the living room experiences fewer discomfort hours, suggesting a relatively better thermal performance than the bedroom.

Yet, this does not imply that the living room's thermal conditions are satisfactory. There is room for improvement in the living room's thermal management, especially in reducing discomfort hours during the hotter period from May to October, as shown in Figure 6.28.

6.8.4 SUMMER DAY HEAT BALANCE

Figures 6.29 and 6.30 reveal the heat balance for the living room and bedroom, respectively, on a typical summer day. The data indicates a significant heat loss in both the ground floor of the living room and the interior floor of the bedroom.

The living room experiences a relatively steady heat loss ranging from a minimum of about -400 W to a maximum of about -500 W. In contrast, the bedroom exhibits more variable heat loss, ranging from -200 W to a maximum of -650 W, particularly noted between 3 p.m. and 4 p.m. This peak heat loss coincides with a solar heat gain of 700 W through the exterior windows, suggesting a balance between heat gain from the windows and heat absorption by the floor.

Additionally, the heat gain through the roofs is evident for both rooms. However, the bedroom experiences substantial fluctuations, absorbing heat during midday and reradiating it from nighttime into the early morning, indicating a persistent overheating problem throughout the day.

The living room, on the other hand, does not display such pronounced fluctuations, suggesting that its floor's exposure to the external environment is limited. Still, minor heat gains are observed, especially in the early morning and late at night. It is notable that the bedroom's building elements—roof, walls, floors, and internal partitions—tend to lose heat in unison when the airflow reaches its lowest points, as compared to other times of the day (Figure 6.31). This suggests a strong correlation between the heat balance of these elements and the reduction in airflow, particularly between 10 a.m. and 9 p.m. in the bedroom.

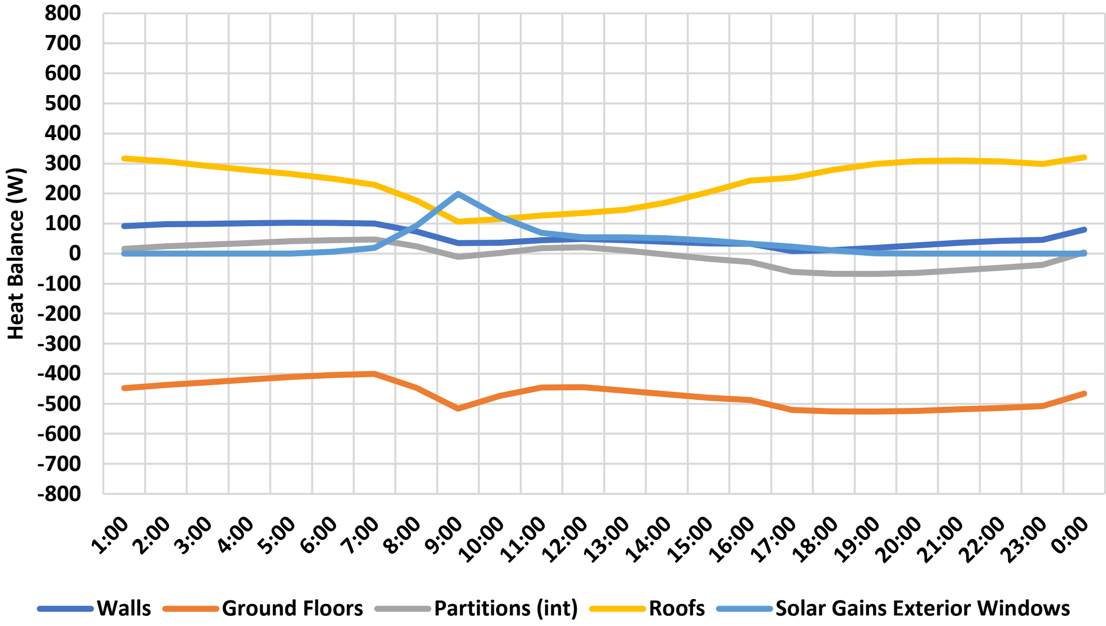

Figure 6.29: Living room summer day heat balance breakdown (24 July). Data gathered from DesignBuilder software and regenerated using Excel.

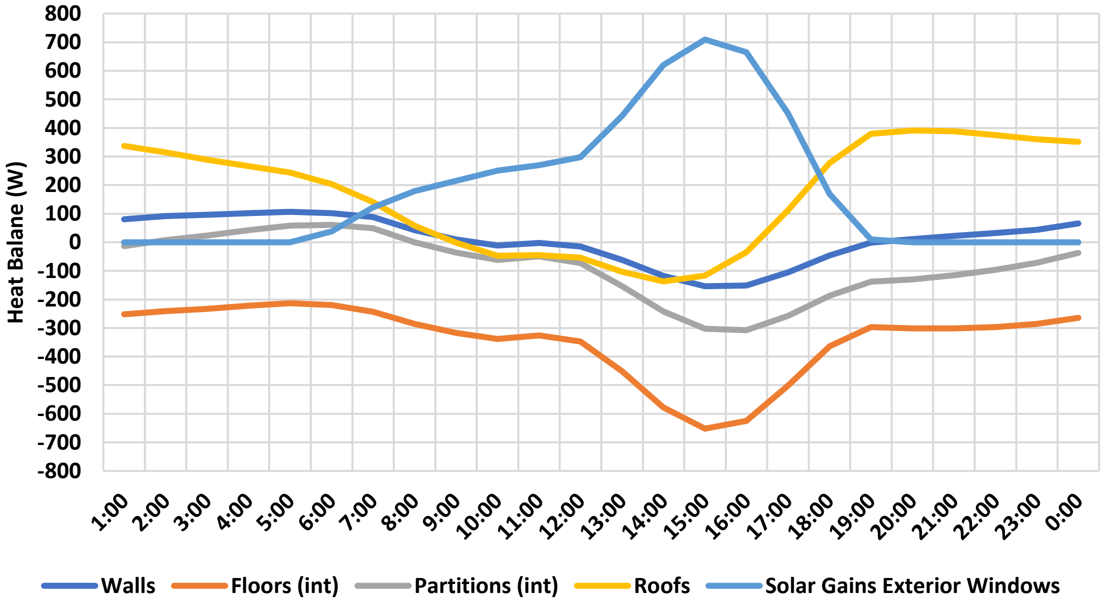

Figure 6.30: Bedroom summer day heat balance breakdown (24 July). Data gathered from DesignBuilder software and regenerated using Excel.

Figures 6.29 and 6.30 demonstrate that, relative to other building components, the external walls of both rooms show less variation in heat balance throughout the day, with a peak heat gain of around 100 W. The exception is a slight heat loss in the bedroom, observed between 12 p.m. and 7 p.m., peaking at approximately 150 W.

The internal partitions within the living room maintain a consistent heat balance, while those in the bedroom display significant fluctuations after 10 a.m., culminating in a maximum heat loss of 300 W at around 4 p.m.

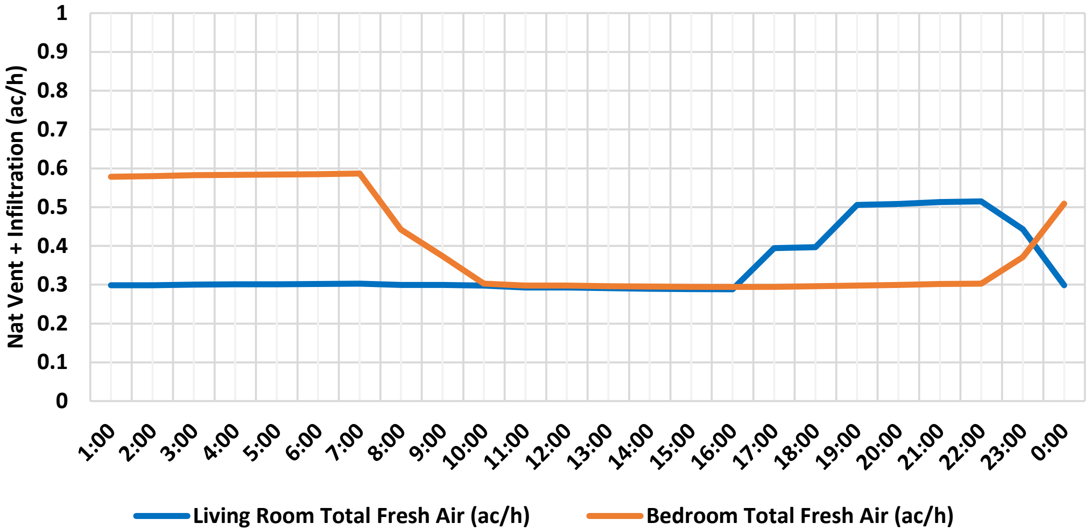

Figure 6.31: Living room and bedroom total fresh air for summer day (24 July). Data gathered from DesignBuilder software and regenerated using Excel.

The airflow patterns on this summer day, as captured in Figure 6.31, exhibit modest variability, particularly in the bedroom. The bedroom's airflow peaks at 0.6 air changes per hour (ac/h) from midnight to 9 a.m., then drops to a minimum of 0.3 ac/h from 10 a.m. to 11 a.m. The living room's airflow remains fairly constant at an average of 0.3 ac/h, with a slight increase to 0.5 ac/h from 6 p.m. to 11 p.m.

The behaviour of the airflow is reflected in the heat balance of the bedroom's elements; a decrease in airflow is mirrored by a decrease in heat gain.

6.8.5 WINTER DAY HEAT BALANCE

Figures 6.32 and 6.33 capture the heat balance within the living room and bedroom, respectively, during a typical winter day. The living room shows modest heat gains in its ground floors and internal partitions, peaking at around 100 W. Solar gains through external windows are observed to be minimal, with a recorded increase of up to 50 W from 10 a.m. to 3 p.m. Conversely, the living room's roof and external walls exhibit significant heat loss, approximately -240 W and -80 W respectively, underscoring the building envelope's inefficiency in retaining heat during the winter season. This thermal behaviour accentuates the need for measures to mitigate heat loss through the building's envelope.

In contrast, Figure 6.33 demonstrates the bedroom's dynamic heat balance, particularly from 9 a.m. to 6 p.m. A pronounced heat gain through the external windows reaches a maximum of 1700 W around 3 p.m., likely due to solar penetration through large window openings from late morning to late afternoon. Simultaneously, the roof registers a peak heat loss of -800 W at 2 p.m., reflecting the absorption of solar heat. The internal floors show significant heat loss as well, with a maximum of -700 W noted at 3 p.m., yet display heat gains at other times, up to 250 W. The external and internal walls maintain a relatively neutral heat balance throughout the day, except for a period of heat loss from 12 p.m. to 5 p.m., peaking at -250 W.

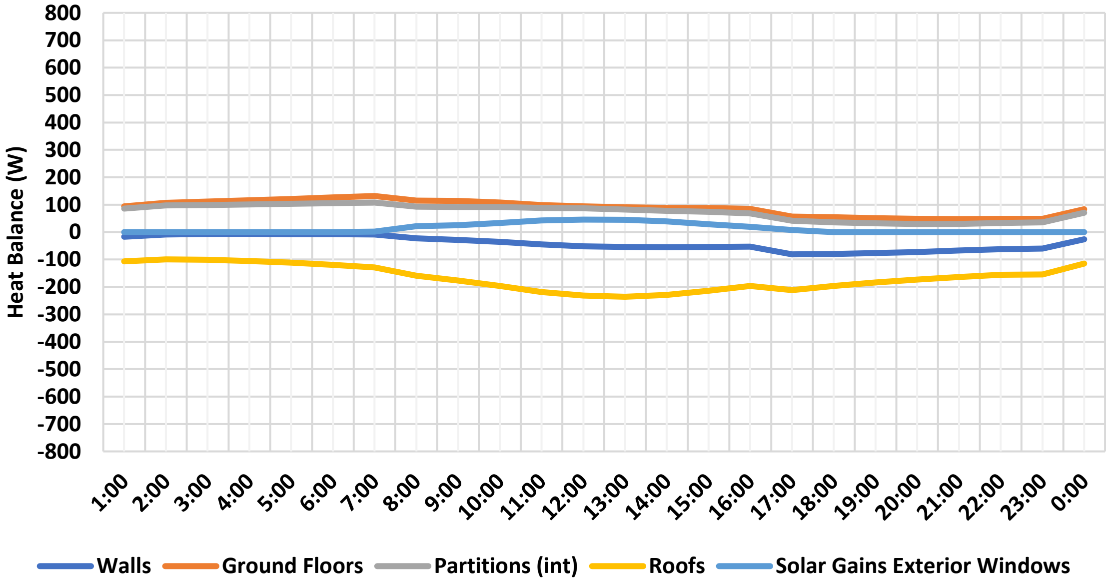

Figure 6.32: Living room winter day heat balance breakdown for a typical winter day (23 January). Data gathered from DesignBuilder software and regenerated using Excel.

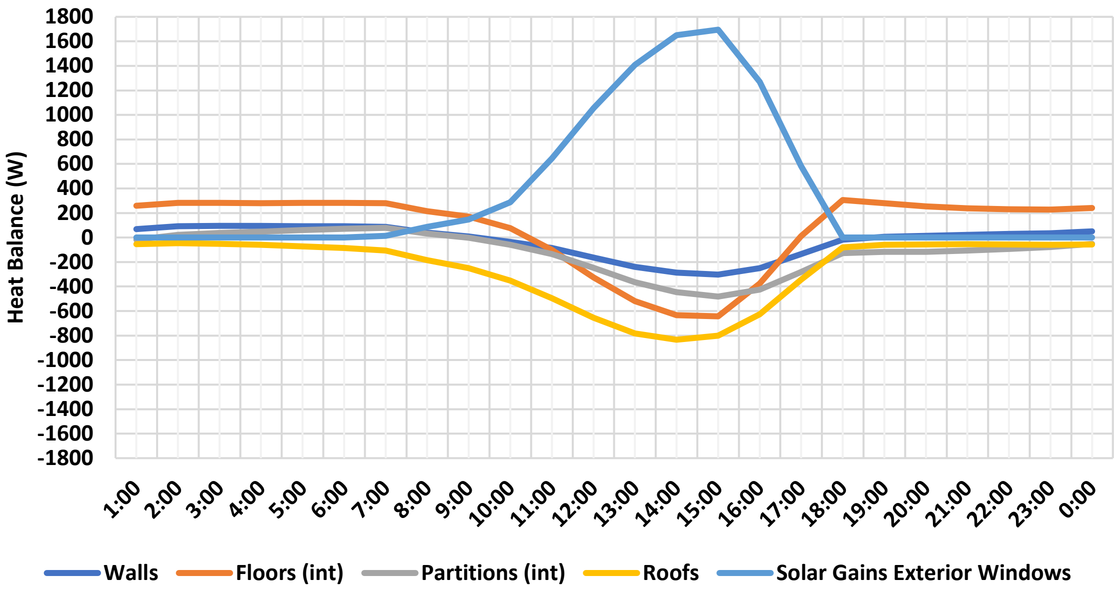

Figure 6.33: Bedroom winter day heat balance breakdown for a typical winter day (23 January). Data gathered from DesignBuilder software and regenerated using Excel.

Airflow dynamics, as illustrated in Figure 6.34, indicate the living room experiences slight fluctuations, varying from a low of 0.3 air changes per hour (ac/h) to a high of 0.5 ac/h. The bedroom, however, maintains a steady airflow of about 0.3 ac/h from morning until late evening and peaks at approximately 0.6 ac/h from the early hours until 7 a.m. These airflow patterns may contribute to the observed heat balance trends within the respective zones.

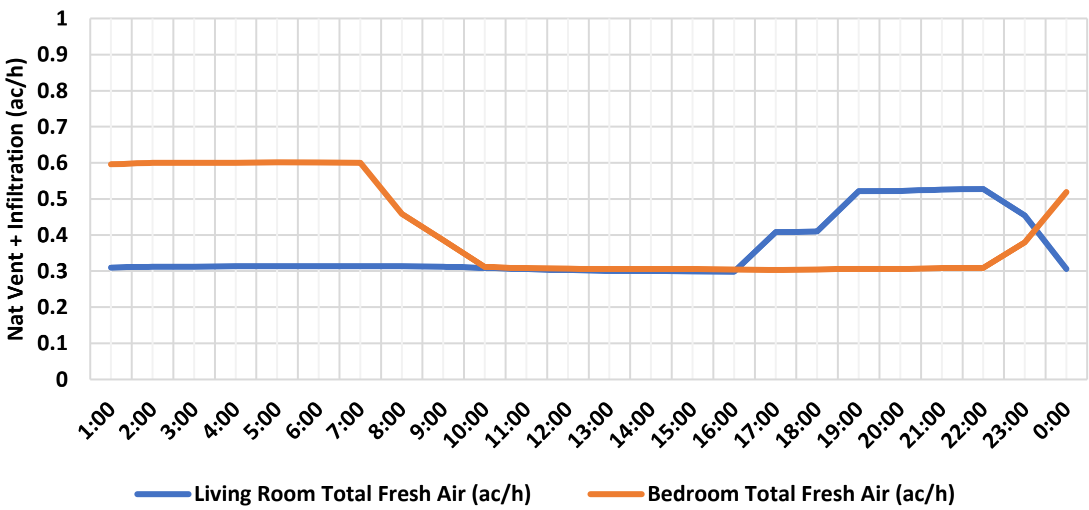

Figure 6.34: Living room and bedroom total fresh air exchange on a typical winter day (23 January). Data gathered from DesignBuilder software and regenerated using Excel.

6.9 HOUSE 2-M THERMAL PERFORMANCE ANALYSIS

6.9.1 TEMPERATURE AND RELATIVE HUMIDITY

Figures 6.35 and 6.36 demonstrate the operative temperature and relative humidity in selected spaces of House 2-M, using monthly averages. In Figure 6.35, the operative temperatures of the dining room and bedroom are closely aligned throughout the year. However, the bedroom experiences an approximately 5°C increase in temperature during the summer months (June, July, and August) compared to the dining room. This notable rise in temperature is indicative of thermal inefficiency, particularly as the bedroom's temperature closely tracks the external dry-bulb temperature, especially from May through August. This pattern is a clear indication of the bedroom's thermal struggle during the summer months due to likely insufficient insulation and high thermal mass, resulting in overheating.

During the winter season, the recorded temperatures in the bedroom show a slight increase, which beneficially impacts the zone by elevating the operative temperature by about 5°C. This suggests that the bedroom's thermal conditions in winter are moderately acceptable and significantly better than during the summer period.

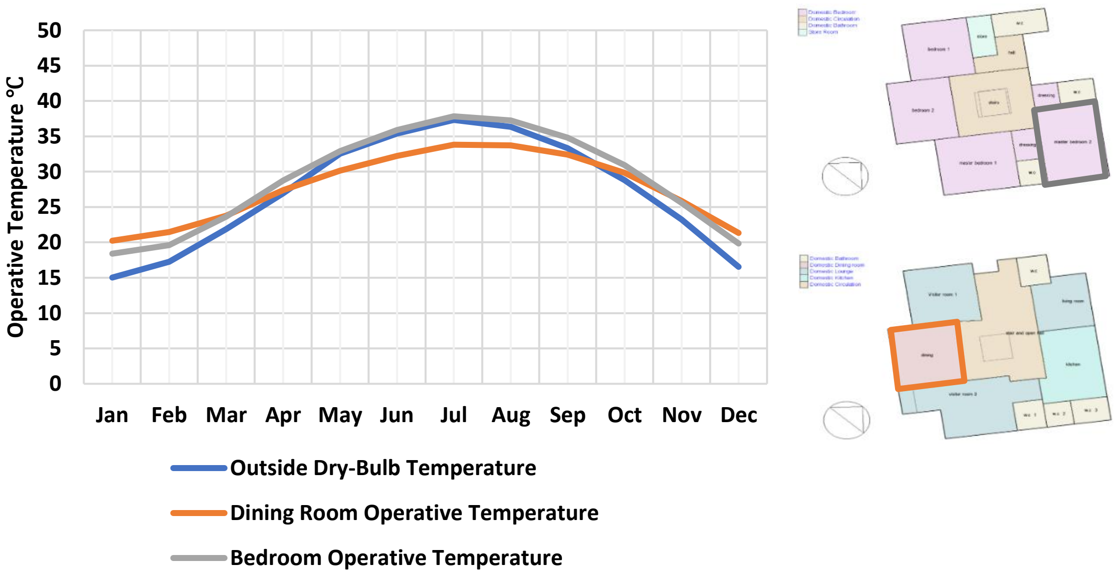

Figure 6.35: Monthly average temperature for the two studied zones as illustrated on plan layouts. Data gathered from DesignBuilder software and regenerated using Excel.

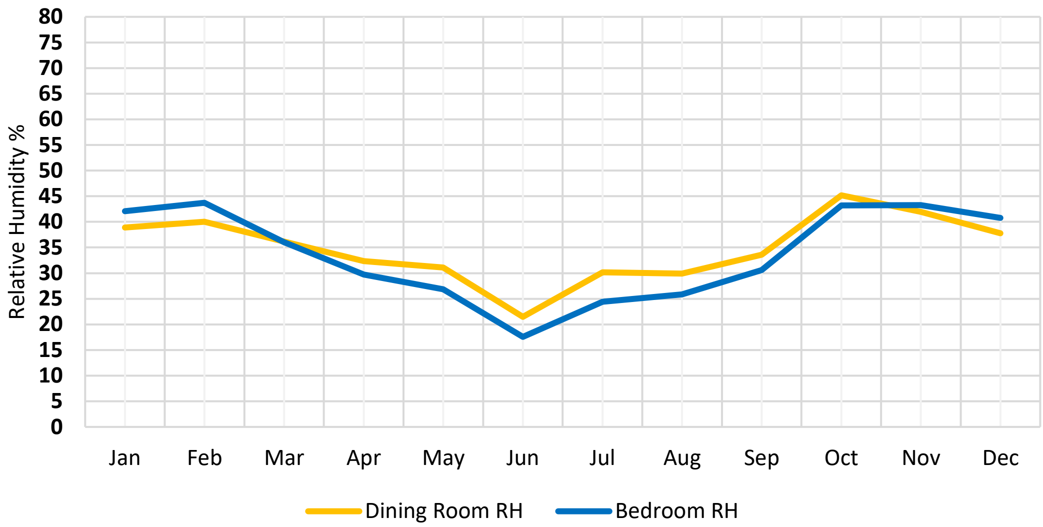

Figure 6.36: Monthly average relative humidity. Data gathered from DesignBuilder software and regenerated using Excel.

Figure 6.36 indicates that both the dining room and bedroom exhibit a decrease in relative humidity during summer and an increase during winter. Specifically, the dining room, located on the ground floor, records marginally higher humidity values during the summer compared to the bedroom. The data ranges from a high of approximately 45% during winter to a low of around 17% during summer months.

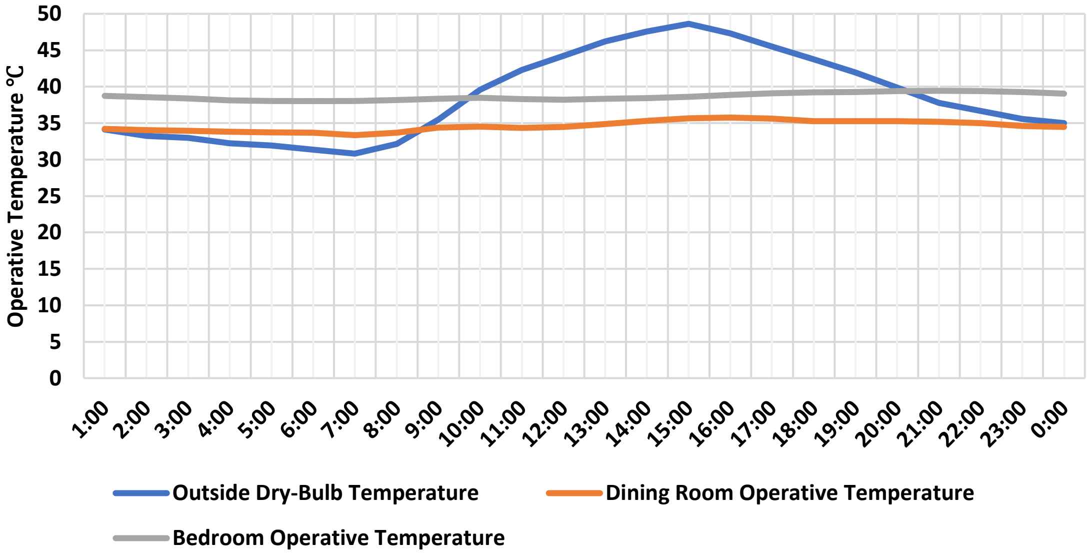

Figure 6.37: Hourly temperature recorded for a typical summer day (24 July). Data gathered from DesignBuilder software and regenerated using Excel.

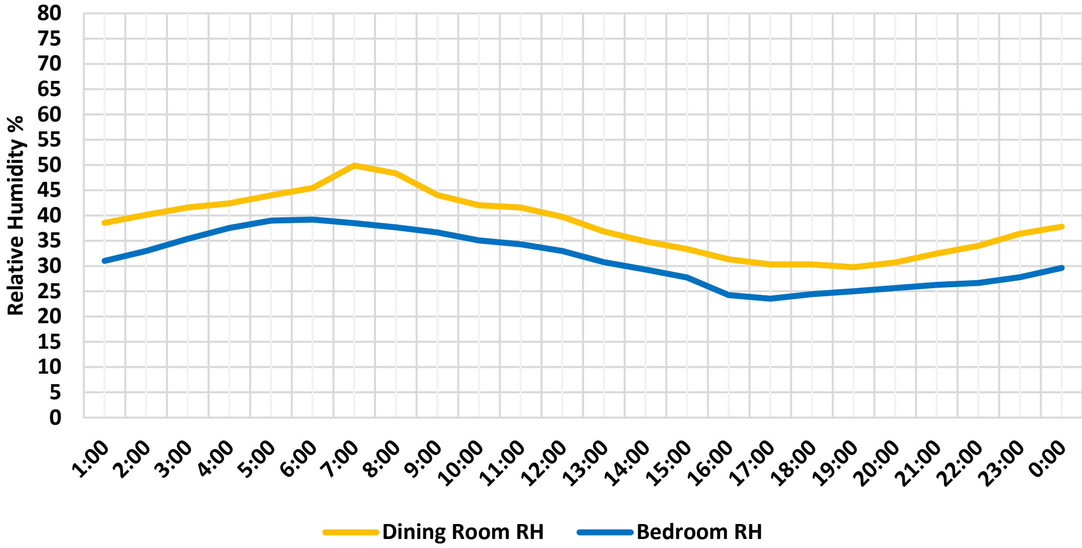

Figure 6.38. Hourly relative humidity recorded for a typical summer day (24 July). Data gathered from DesignBuilder software and regenerated using Excel.

Figures 6.37 and 6.38 highlight the temperature and relative humidity patterns during the peak of summer on 24 July. On this day, the external temperature reaches a high of around 50°C in the afternoon, posing a significant risk of overheating within both the dining room and bedroom.

The bedroom's internal conditions are especially concerning, with operative temperatures reaching around 40°C, which even exceeds the external temperature by about 6°C from late evening to early morning. This is attributed to the bedroom's position on the first floor, where the roof is directly exposed to the extremely hot external climate, in contrast to the ground floor's dining area, which is buffered by its interior position.

Relative humidity on this summer day, as per Figure 6.38, shows that the dining room's humidity is about 6% higher during daytime hours than the bedroom's, with a peak at 50% in the morning and a low at 29% in the evening. The bedroom's humidity reaches its zenith at 39% in the pre-dawn hours and its nadir at 23% in the late afternoon, suggesting slight differences in diurnal humidity patterns between the zones.

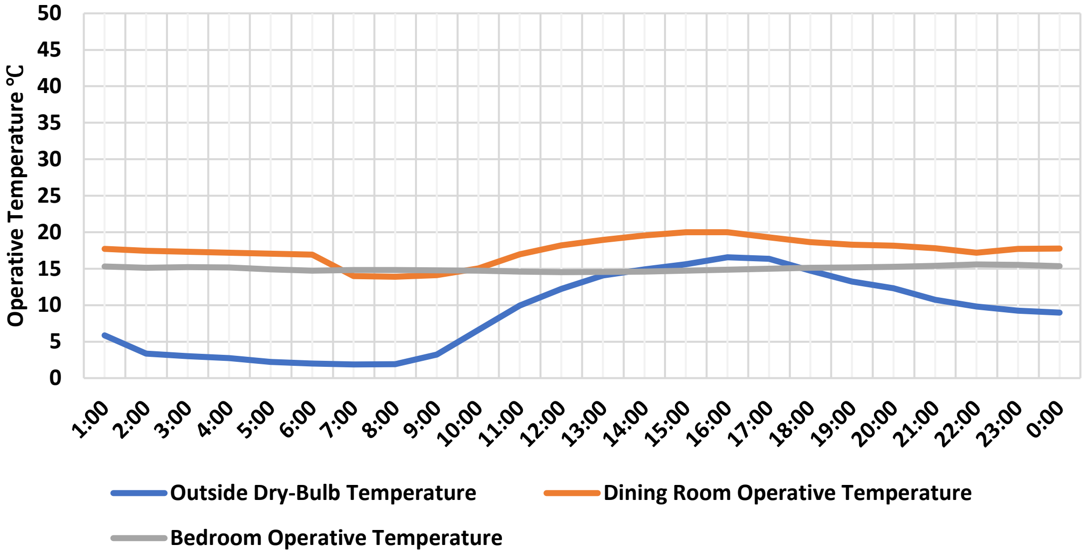

Figure 6.39. Hourly temperature recorded for a typical winter day (23 January). Data gathered from DesignBuilder software and regenerated using Excel.

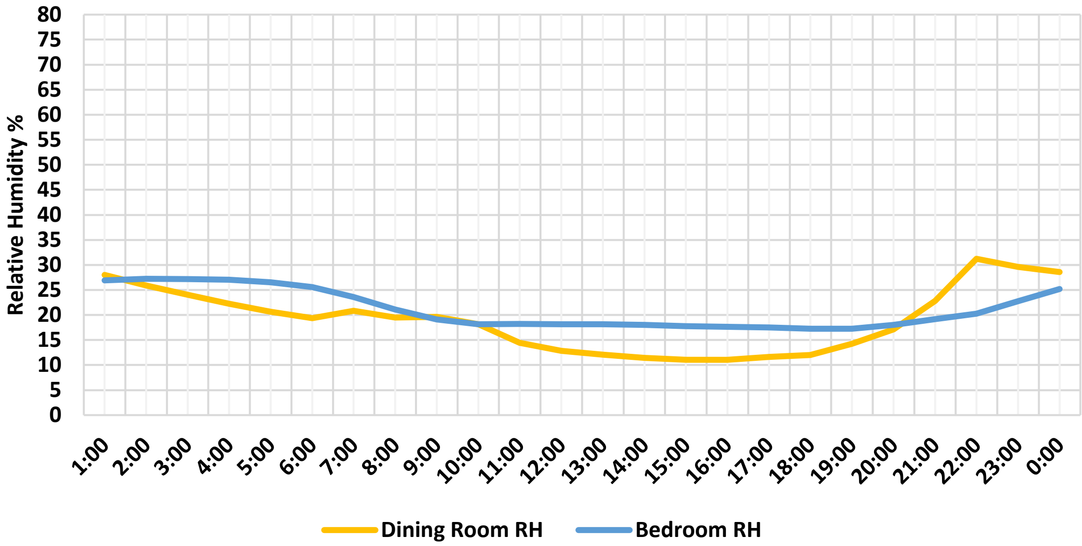

Figure 6.40. Hourly relative humidity recorded for a typical winter day (23 January). Data gathered from DesignBuilder software and regenerated using Excel.

On the coldest day of the year, 23 January, Figures 6.39 and 6.40 depict temperature and humidity distributions, respectively. With the outdoor temperature oscillating between 2°C and 17°C, the dining room and bedroom maintain a relatively stable operative temperature during the day, with a high of 20°C and a low of 15°C.

This temperature consistency in the dining room indicates an adequate thermal response to the coldest day of the year, maintaining comfort levels close to the ideal thermal comfort zone. The bedroom, however, typically records temperatures about 4°C lower than the dining room. Despite external temperature fluctuations, the house appears to be thermally effective in stabilizing indoor temperatures.

Furthermore, the relative humidity values recorded are quite consistent between the two zones during the day, with the bedroom exhibiting a slightly higher humidity, except between 10 p.m. and 12 p.m., when it falls to about 10% lower than that of the dining room, as illustrated in Figure 6.40.

6.9.2 PREDICTED PERCENTAGE OF DISSATISFIED (PPD) ANALYSIS

The PPD for both the dining room and bedroom was analysed and estimated using monthly averages, as well as specific typical summer and winter days. The results are displayed in Figures 6.41, 6.42, and 6.43. The analysis shows that the dining room consistently has lower PPD percentages throughout the year compared to the bedroom, indicating better thermal performance.

Furthermore, the PPD analysis for the dining room indicates that dissatisfaction percentages are surprisingly near or below 20%, particularly during February, March, April, and November. This positions the dining room as a zone of comfort for almost four months of the year. However, considerable dissatisfaction rates are observed during the remaining months, with August reaching a maximum PPD of about 94%, signifying an extremely hot indoor condition.

In contrast, the PPD recorded in the bedroom zone is significantly higher than that of the dining room, suggesting greater occupant dissatisfaction for most of the year, especially during the summer season, as depicted in Figure 6.41. Specifically, from May to September, the PPD values never drop below 70%. Nevertheless, the PPD for the bedroom zone in April and November is recorded at only 21% and 24%, respectively. This results in the bedroom's PPD approaching an 80% satisfaction level for merely two months of the year.

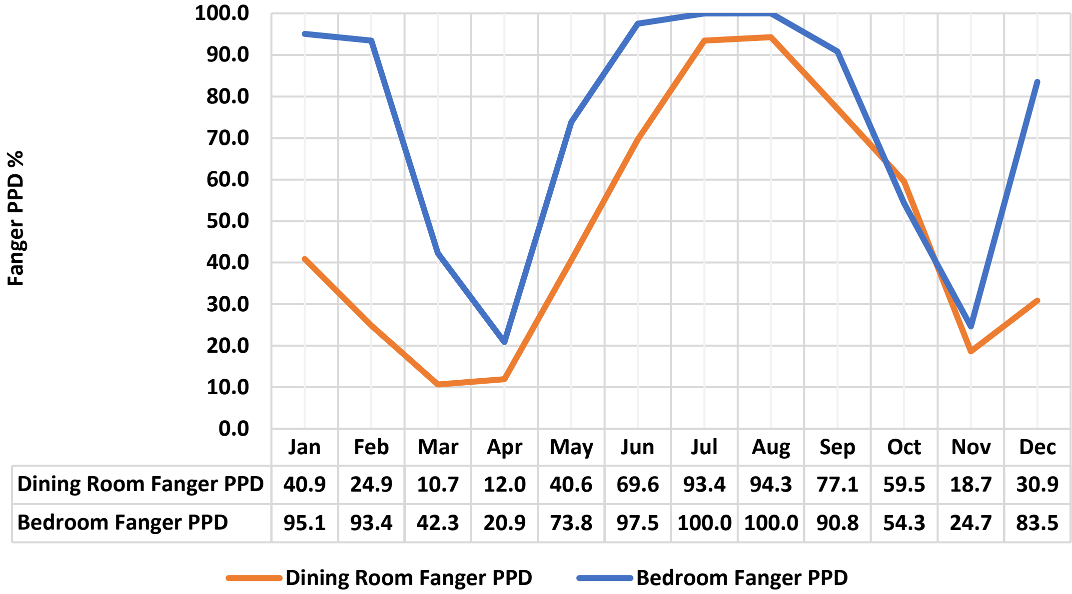

	Jan	Feb	Mar	Apr	May	Jun	Jul	Aug	Sep	Oct	Nov	Dec
Dining Room Fanger PPD	40.9	24.9	10.7	12.0	40.6	69.6	93.4	94.3	77.1	59.5	18.7	30.9
Bedroom Fanger PPD	95.1	93.4	42.3	20.9	73.8	97.5	100.0	100.0	90.8	54.3	24.7	83.5

Figure 6.41: Dining room and bedroom monthly averaged PPD. Data gathered from DesignBuilder software and reprocessed using Excel.

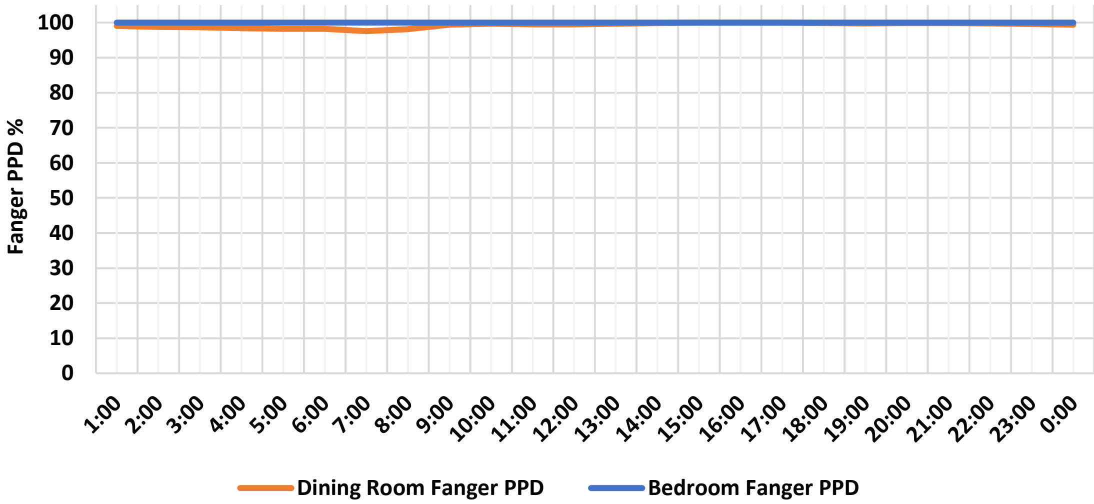

Figure 6.42: Dining room and bedroom hourly averaged PPD for a typical summer day (24 July). Data gathered from DesignBuilder software and regenerated using Excel.

As depicted in Figure 6.42, on a typical summer day, 24 July, both zones recorded an almost constant PPD of 100% throughout the day, indicating a persistent overheating issue during the peak of summer.

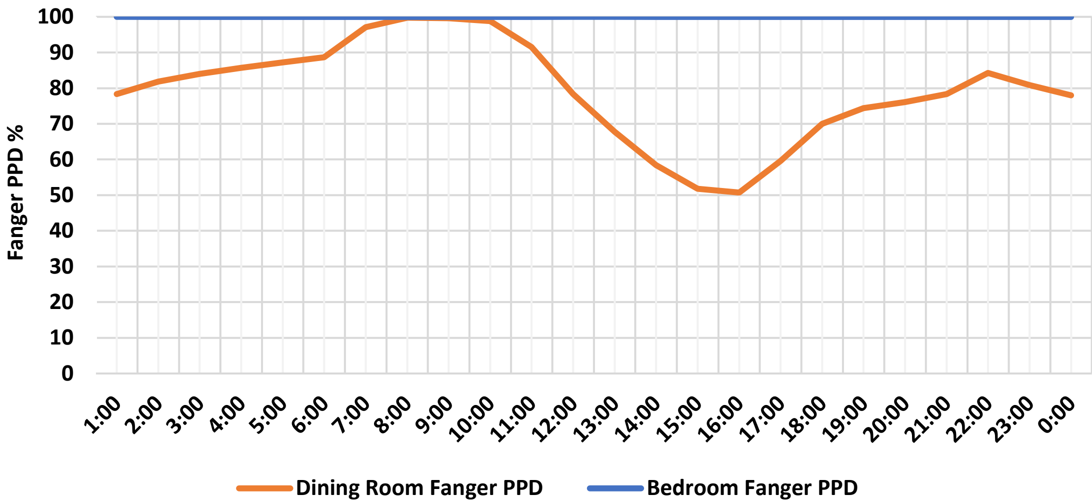

Figure 6.43: Dining room and bedroom hourly averaged PPD recorded for a typical winter day (23 January). Data gathered from DesignBuilder software and regenerated using Excel.

On 23 January, a typical winter day, both the dining room and the bedroom recorded high PPD values, averaging 80% and 100%, respectively. This constant state of discomfort suggests that the thermal performance of these zones is unsatisfactory during the coldest day of the year. However, the dining room exhibited a notable decrease in PPD, around 50%, solely between 3 p.m. and 5 p.m. This reduction in PPD is attributed to substantial solar heat gains through the windows during these hours, as shown in Figure 6.43. Therefore, in this case, increasing the window-to-wall ratio (WWR) could significantly enhance the thermal performance of the zone.

6.9.3 CALCULATED DISCOMFORT HOURS

Figure 6.44 illustrates the total number of discomfort hours per month for the dining room and bedroom throughout the year. As stated earlier, these hours have been calculated based on the periods when the spaces are typically occupied. For both zones, the lowest discomfort hours were recorded in March and November, whereas the highest were observed from May through October. The bedroom exhibits a pattern similar to the dining room but endures an increase of up to 100 discomfort hours during the summer months. For instance, between April and October, the bedroom averages around 350 discomfort hours per month, markedly higher compared to the dining room's 240 hours. This indicates a greater level of thermal discomfort in the bedroom during these warmer months.

The total annual discomfort hours for the bedroom are estimated at approximately 3086 hours, whereas the dining room accrues about 2015 hours, resulting in a notable difference of approximately 1071 hours between the two spaces. Thus, the dining room incurs fewer total discomfort hours, suggesting it has a better thermal comfort level than the bedroom. Despite this, the dining room's thermal environment is not considered completely satisfactory in terms of comfort. There is room for improvement, particularly in reducing the total discomfort hours during the extended summer period from May to October.

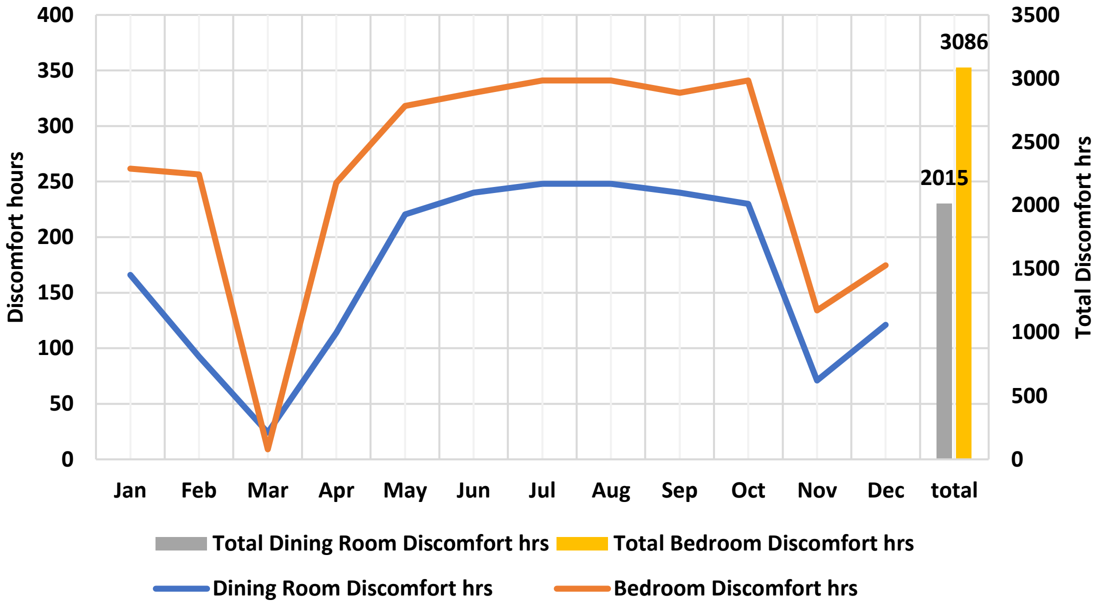

Figure 6.44: Monthly total discomfort hours for the dining room and bedroom. Data gathered from DesignBuilder software and regenerated using Excel.

6.9.4 SUMMER DAY HEAT BALANCE

Figures 6.45 and 6.46 display the heat balance for the dining room and bedroom on a typical summer day. Both zones exhibit notable heat loss, which is significantly higher in the dining room located on the ground floor. The bedroom's floor maintains a steady heat loss ranging between approximately -300 W and -420 W throughout the day. In stark contrast, the dining room's floor experiences substantial fluctuations in heat loss, from a minimum of -575 W to a maximum of -1100 W, with the peak occurring between 3 p.m. and 4 p.m. Coinciding with this peak heat loss, a solar heat gain of 780 W is simultaneously recorded, suggesting that solar heat penetrating through external windows is effectively absorbed by the ground floor, thereby enhancing the thermal performance of the lower floor zones relative to those on the upper floors.

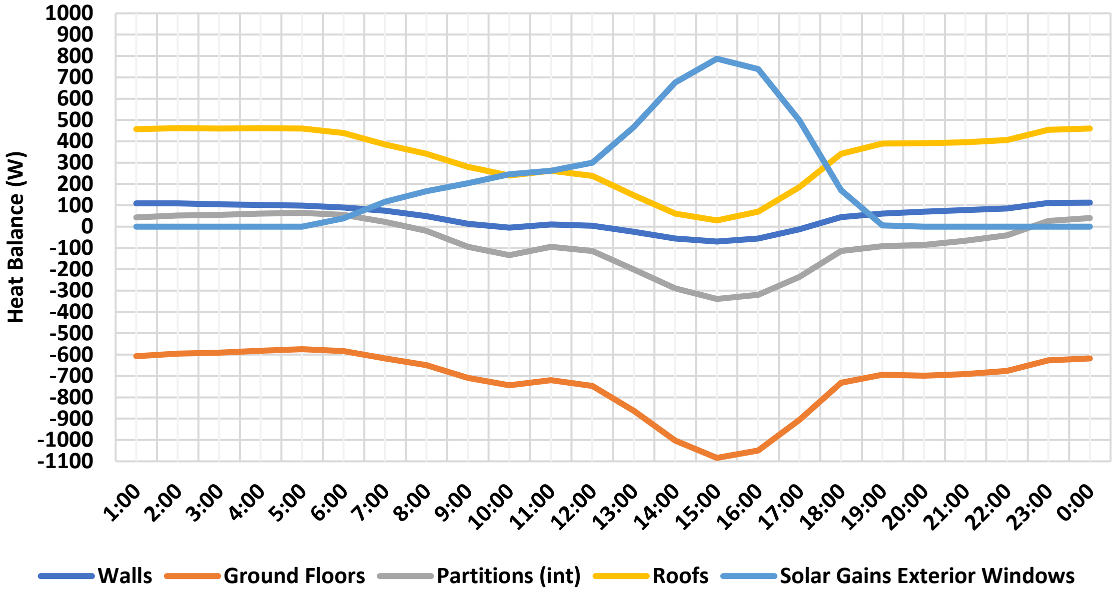

Figure 6.45: Dining room summer day heat balance breakdown (24 July). Data gathered from DesignBuilder software and regenerated using Excel.

Both the dining room and the bedroom also experience heat gains through their roofs. The dining room sees the lowest heat gains, around 29 W, between 1 p.m. and 5 p.m., while the highest gain of approximately 460 W is observed from 9 p.m. to 9 a.m. The bedroom's roof, however, shows a peak heat gain of about 484 W from 6 p.m. to 11 p.m., with the lowest gain, roughly 3 W, noted from 8 a.m. to 11 a.m.

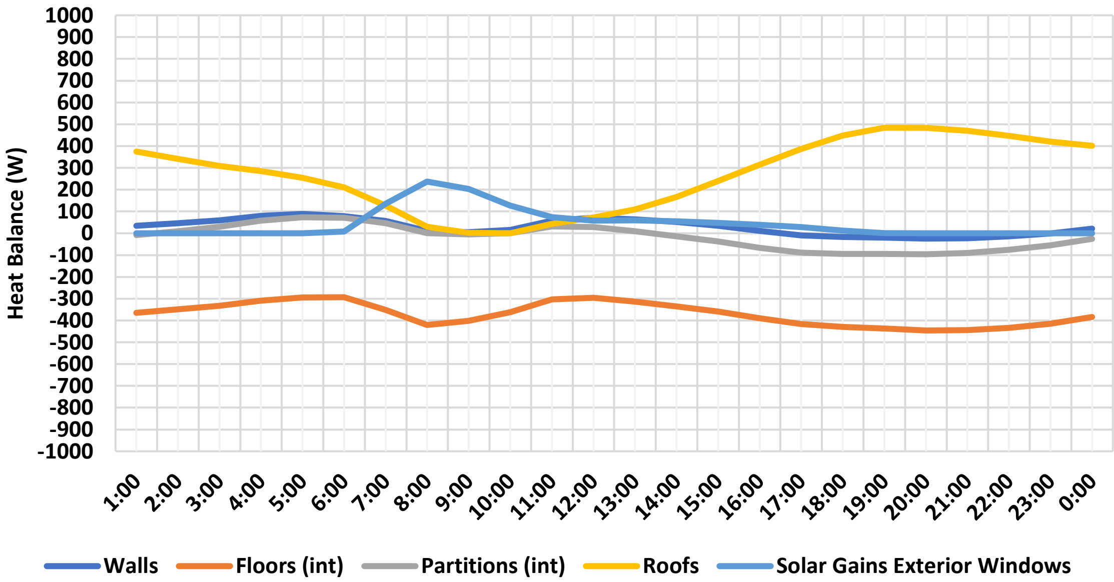

Figure 6.46: Bedroom summer day heat balance breakdown (24 July). Data gathered from DesignBuilder software and regenerated using Excel.

The heat balance of the external walls in both zones presents less variation over the day, with the highest heat gain around 100 W. Nevertheless, both zones do experience some heat loss, with the bedroom and dining room showing a maximum loss of -7 W and -70 W, respectively. The internal partitions in the bedroom exhibit a consistent heat loss of about -50 W throughout the day, whereas the dining room's partitions fluctuate significantly, especially from 9 a.m. to 10 p.m., reaching a maximum loss of -330 W at 3 p.m. Regarding solar gains from external windows, the dining room records substantial solar heat gain in the afternoon, peaking at 780 W at 3 p.m. The bedroom, conversely, maintains a steady heat balance across its external windows, except for a sharp increase of approximately 237 W from 7 a.m. to 10 a.m.

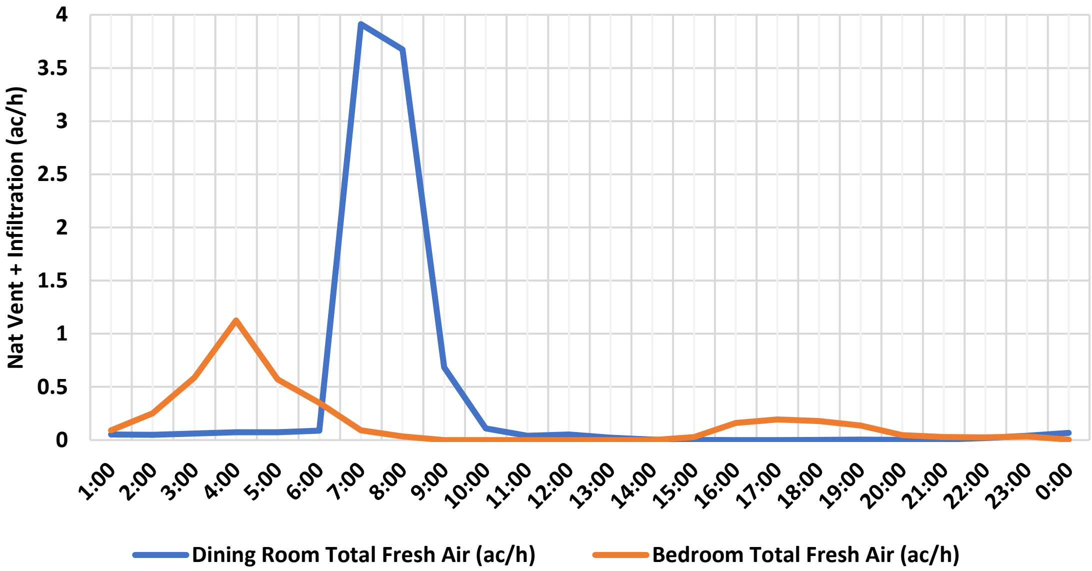

Figure 6.47: Dining room and bedroom summer day total fresh air (24 July). Data gathered from DesignBuilder software and regenerated using Excel.

Figure 6.47 shows the airflow patterns, which are especially turbulent in the dining room, peaking at 4 air changes per hour (ac/h) between 7-8 a.m. However, the dining room's airflow drops to nearly zero ac/h for the remainder of the day. The bedroom's airflow reaches a maximum of about 1 ac/h at 4 am but falls to a minimum for the rest of the day, mirroring the limited ventilation experienced in the dining room.

6.9.5 WINTER DAY HEAT BALANCE

Figures 6.48 and 6.49 present the heat balance breakdown for the dining room and bedroom, respectively, during a typical winter day. The dining room experiences modest heat gains across all components, including the ground floor, roof, partitions, walls, and external windows. These gains range from approximately 10 W to 100 W, predominantly recorded from the early evening at 7 p.m. to the early morning at 6 a.m. Notably, a substantial heat gain is observed through the external windows, peaking at 1961 W around 4 p.m. Concurrently, there is a pronounced heat loss across the ground floor, roof, partitions, and walls, with the ground floor experiencing the most significant loss of up to 936 W and the external walls the least, with a minimum loss of around -280 W.

Conversely, the bedroom maintains a steady heat balance, with minor gains and losses throughout various elements within the space. The roof, in particular, exhibits a turbulent heat balance, suggesting it plays a crucial role in modulating the thermal environment. During daylight hours from 9 a.m. to 2 p.m., the roof incurs a maximum heat loss of about 260 W, effectively reducing discomfort by releasing stored heat. Additionally, an evening heat gain of approximately 63 W is recorded at 8 p.m., which may aid in warming the space during the night through the thermal mass of the concrete.

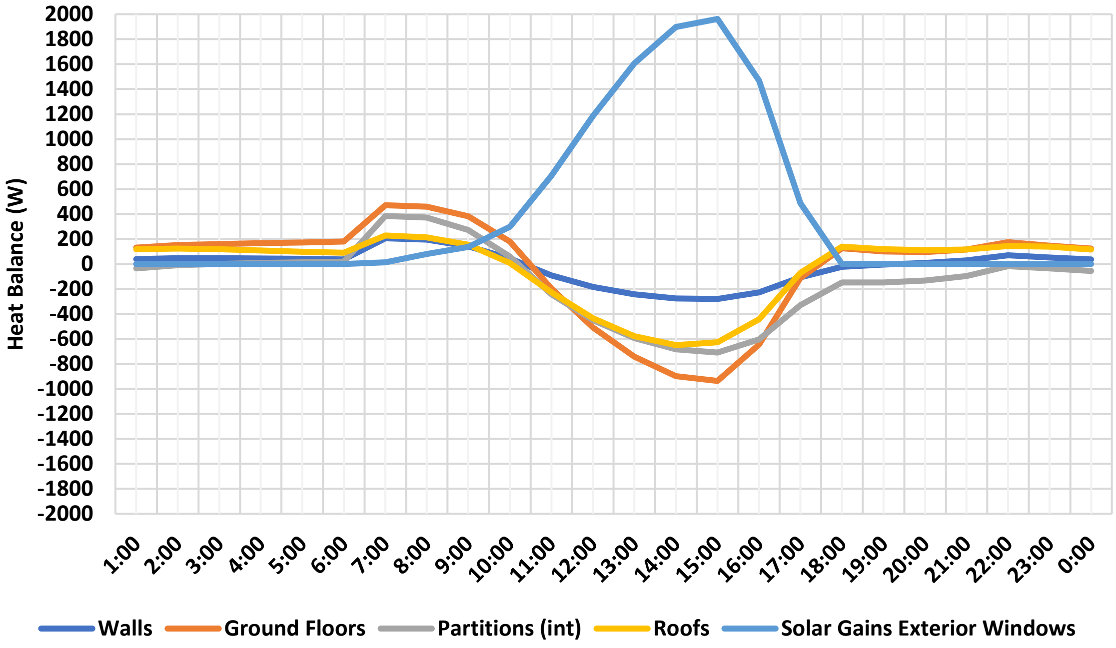

Figure 6.48: Dining room winter day heat balance breakdown (23 January). Data gathered from DesignBuilder software and regenerated using Excel.

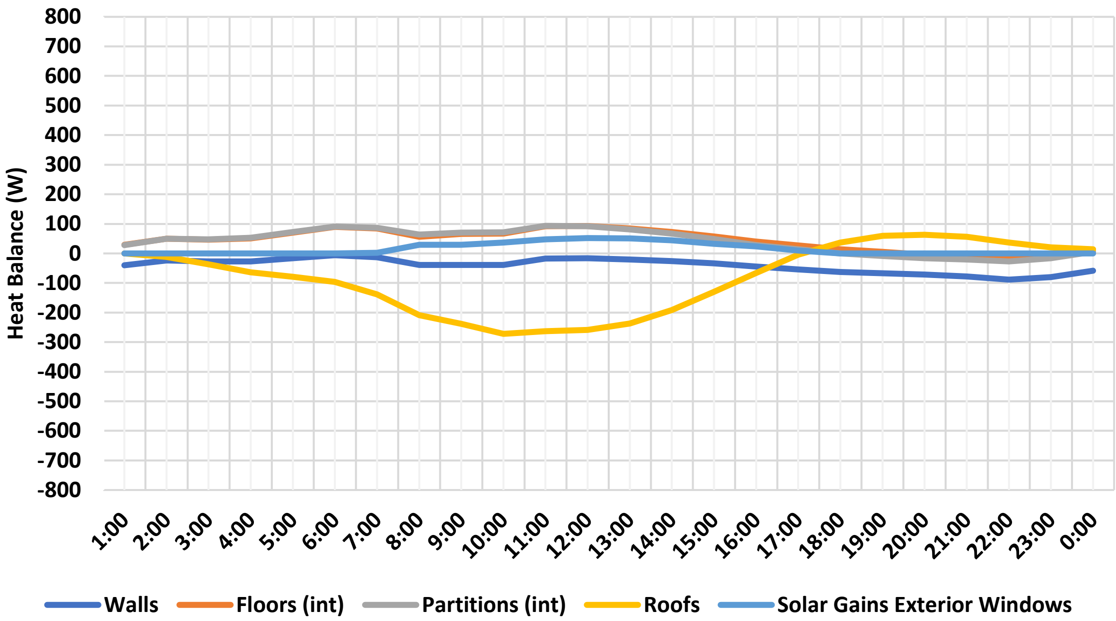

Figure 6.49: Bedroom winter day heat balance breakdown (23 January). Data gathered from DesignBuilder software and regenerated using Excel.

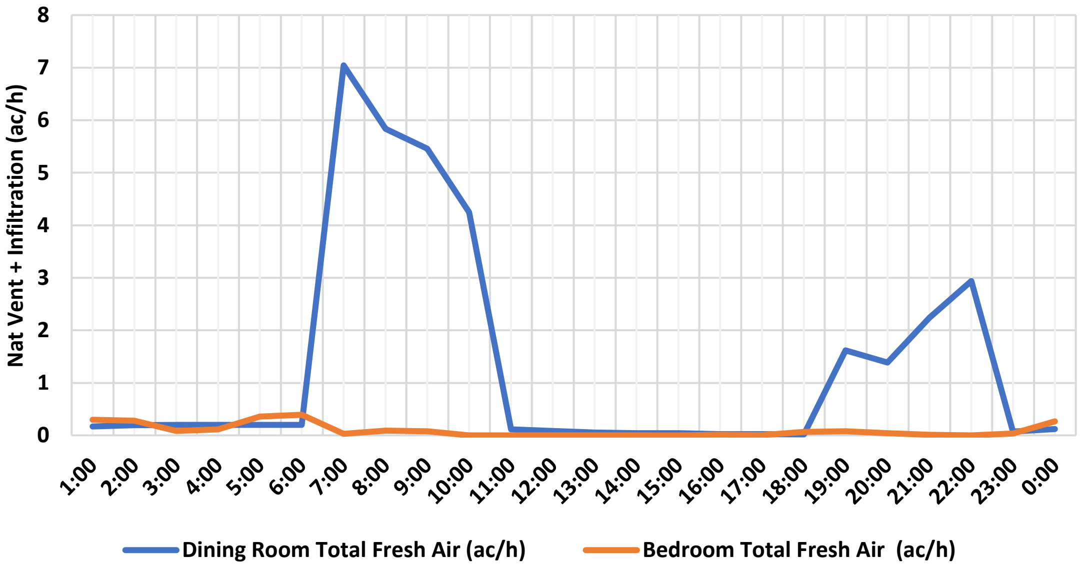

Figure 6.50: Living room and bedroom winter day total fresh air (23 January). Data gathered from DesignBuilder software and regenerated using Excel.

Figure 6.50 presents the airflow readings for the dining room and bedroom. The dining room's airflow exhibits variability, particularly between 6 a.m. to 11 a.m. and from 8 p.m. to 11 p.m., with values ranging from 7 ac/h in the morning to between 1.3 ac/h and 3 ac/h in the evening. The bedroom's airflow, on the other hand, remains consistent at an average of 0.15 ac/h throughout the day, indicating a more stable but limited ventilation compared to the dining room.

6.10 SUMMERY

This study emphasises total thermal discomfort hours as the primary metric for assessing thermal performance. To understand the nuanced thermal behaviours of prefabricated building elements, a range of performance indicators has been analysed. The insights from this analysis will guide the enhancement strategies for the thermal performance of the prefabricated houses under review.

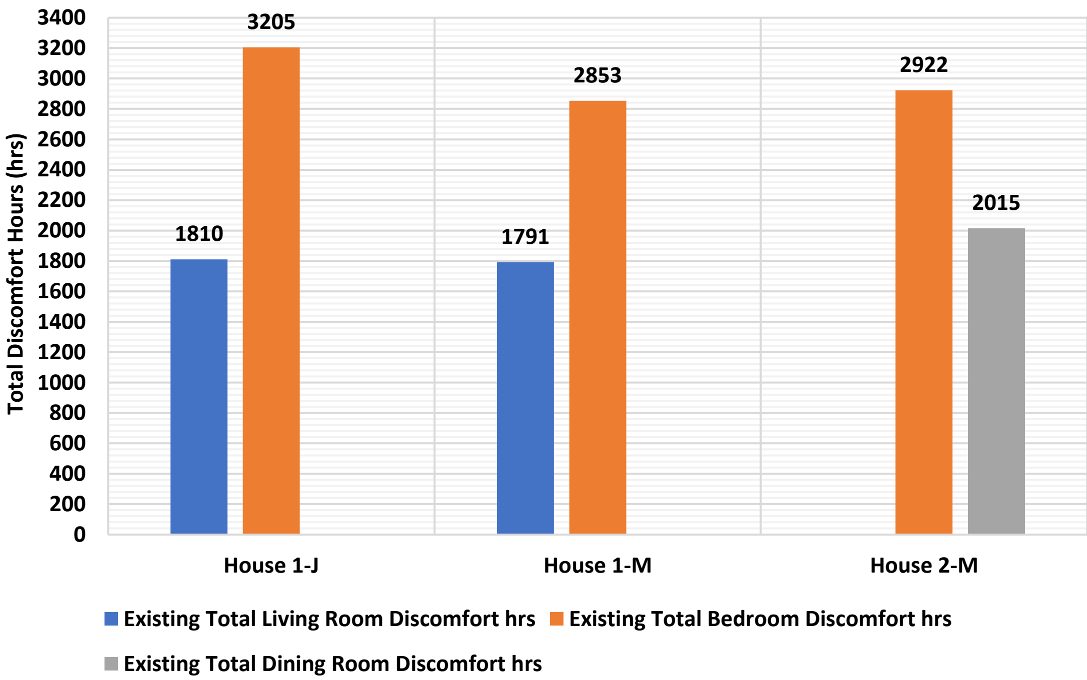

Figure 6.51: Comparative chart of the total annual discomfort hours for the six zones studied across the case study houses. Data was obtained from DesignBuilder software and reproduced using Excel.

Figure 6.51 shows that House 1-J and House 2-M have particularly high indoor temperatures on the upper floors, contributing to annual discomfort hours of 3205 and 2922, respectively. Meanwhile, the lower floors of Houses 1-J, 1-M, and 2-M register fewer annual discomfort hours, with counts of 1810, 1791, and 2015 hours, respectively. This indicates a generally better thermal condition on the lower floors compared to the upper floors.

A slight difference in discomfort hours within the bedroom areas of Houses 1-M and 2-M is observed, likely due to the different locations of these zones within the upper floors and the variation in their specific site locations. Overall, the thermal performance of Houses 1-M and 2-M is marginally better than that of House 1-J, considering they are all subject to the same external climatic influences. The data highlights that the upper floors endure higher discomfort hours year-round, while the lower floors exhibit improved thermal conditions, leading to a reduction in discomfort hours throughout the year.

CHAPTER SEVEN – OPTIMISING PREFABRICATED CONSTRUCTION SYSTEMS FOR BUILDING ENVIRONMENTAL PERFORMANCE AND THERMAL COMFORT

7.1 INTRODUCTION

This chapter is dedicated to enhancing and improving the indoor thermal performance of three selected prefabricated concrete houses. The initial phase involved the use of DesignBuilder software to evaluate the thermal comfort and performance of these residential buildings in Saudi Arabia, a topic thoroughly addressed in the previous chapter. Consequently, the focus here is on optimising the thermal performance of the case study houses, with the understanding that these enhancements could be applicable to similar future building projects, particularly in residential housing developments.

In line with this objective, this chapter focuses on enhancing the indoor thermal performance of three prefabricated concrete houses in Saudi Arabia. Using DesignBuilder software, thermal comfort and performance were assessed in these buildings, as discussed in the previous chapter. The objective here is to optimise thermal performance by addressing key components of the case study houses, with potential applications for future residential housing developments.

Building on this analysis, this chapter investigates improvements aimed at reducing thermal discomfort hours, emphasising the role of building fabric in influencing comfort. Strategies include advanced techniques, such as the incorporation of Phase Change Materials (PCMs), alongside standard construction methods. Simulations conducted for summer and winter conditions highlight the impact of heat transfer through the building envelope on discomfort in specific zones.

However, due to the limitations of modifying precast concrete systems compared to traditional construction methods, the study adopts globally accepted thicknesses and relies on local data. While the houses perform well in their basic configurations, optimisations are explored to demonstrate potential reductions in discomfort hours and energy consumption. The analysis specifically examines walls, floors, and windows, with proposed modifications analysed across two zones per house to highlight improvements during extreme seasons.

Moreover, this chapter aims to provide actionable insights for sustainable construction practices, thereby supporting the development of energy-efficient and thermally comfortable residential buildings in challenging climates.

7.2 PROPOSED CONSTRUCTION SYSTEMS LIMITATIONS

Prior to delving into the detailed evaluation of the proposed systems' thermal performance, it is essential to emphasise the role of scheduled natural ventilation in all simulations. Natural ventilation is a critical factor influencing both heating and cooling dynamics within indoor spaces. The models employed herein represent the volume of air that infiltrates and exits a building over a specific period, which is contingent on occupancy patterns. These patterns are aligned with the EnergyPlus occupancy timing standards and are adjustable within the simulation parameters.

It is crucial to note that these simulations are not based on actual physical openings but rather on predetermined infiltration rates set by the researchers. Therefore, it is vital to establish realistic rates that accurately reflect real-world conditions. Although this approach simplifies the complex dynamics of natural ventilation, it is an effective method that significantly streamlines the simulation process. This simplification facilitates the examination of various scenarios, allowing us to investigate the implications for the building's cooling requirements, how its thermal performance is influenced by construction components, and standard human needs in terms of minimum air changes per hour per occupancy for a naturally ventilated building.

7.2.1 PROPOSED PRECAST WALL DESIGN CONSIDERATIONS

Several design considerations have been addressed when proposing a precast concrete wall panel. The key factors taken into account include total wall thickness, wall thermal mass (construction materials and their varying densities), total estimated thermal conductivity, different insulation materials within the sandwich wall panel, the application of PCM within the precast concrete wall panel, and the position of insulation materials within the precast concrete sandwich wall panel.

It is worth noting that all proposed precast concrete wall panel systems are suitable for real-world applications. However, some of the proposed precast wall panels are intended for architectural applications rather than structural systems. In other words, depending on the concrete panel thickness, some panels have the ability to carry load (load-bearing wall system). Normally, precast concrete panels considered structural walls have a reinforced concrete layer thickness of not less than 7.5 cm, as documented in various previous and up-to-date studies. Furthermore, the proposed wall panels consist of either two or three wythes.

Accordingly, this research evaluated different wall thicknesses and systems to serve as a future reference for diverse design preferences in the prefabricated building construction industry.

Furthermore, several design constraints were considered as follows:

- The proposed precast wall system can be either architectural or structural, depending on the thickness of the provided concrete layer. A reinforced panel with a thickness of 7.5 cm, as recommended by the Precast Concrete Institute (PCI), is considered suitable.
- Different precast wall panel thicknesses have been proposed to provide a variety of options in precast concrete panels, each with different thermal conductivities.
- The proposed precast wall systems are limited to a maximum thickness of 37 cm. This limitation is intended to enhance flexibility and deliverability in off-site construction industries. Additionally, this design allows for flexibility in future architectural recommendations.
- For prefabricated housing construction, the maximum thickness of precast concrete sandwich panels should not exceed 45 cm. However, panels with increased thickness, especially in the insulation layers, may be designed for greater thermal effectiveness.
- All concrete layers in the proposed precast concrete sandwich panel systems incorporate 1% steel reinforcement. This ensures that the panels have sufficient strength to support themselves, though this does not imply they can fully carry the building’s dead and live loads.

7.2.2 PHASE CHANGE MATERIALS CONSIDERATIONS

Phase change materials (PCMs), as previously discussed, are substances that absorb and release substantial amounts of thermal energy during their phase transition processes, such as melting and freezing, depending on the climatic conditions. As highlighted in the literature review chapter, a variety of PCMs are available in the global construction market, with ongoing development of new PCM products. For instance, BioPCM® products represent a proprietary family of PCMs (PCS) with a unique feature differentiating them from traditional PCMs that transition from solid-to-liquid. BioPCM® can change phases between solid-to-gel and solid-to-solid while absorbing and releasing heat. Capable of storing and releasing thermal energy at specific temperatures ranging from -75°C to 175°C, BioPCM® offers optimal energy performance with minimal environmental impact. It also reduces the load on HVAC systems in buildings, data centres, and telecom shelters. However, its application in housing projects is not recommended due to performance limits in residential environments.

Another suitable PCM product for housing applications is Infinite R Phase Change Material. Described by Al-Absi et al. (2021) as a US-patented blend of inorganic hydrated salts, Infinite R functions as a thermal energy sponge, absorbing heat energy and then releasing it gradually. This product, shown in figure 7-1, aids in controlling room temperature and reducing HVAC demands. Safe for various building types, it possesses a Class A fire rating and is non-toxic.

Furthermore, according to WinWerks (2013), it is financially viable, offering a full payback within a maximum of three years post-installation due to significant savings in the short and long term. It also provides immediate thermal comfort improvement upon installation and is highly adaptable in size with an adjustable melting point, making it ideal for home applications within walls, roofs, and ceilings. Given its minimal thickness, Infinite R has been selected for integration in the proposed wall designs incorporating PCMs in this research.

Figure 7.1: Illustration for Infinite R PCMs sheet. Source: WinWerks (2013)

The ideal thickness of PCM varies according to several studies. Al-Yasiri and Szabó (2021) conducted an experiment to estimate the optimal PCM layer thickness for passive application in a composite roof under Iraq's hot climate. They used four test models: one with a standard roof combination and the others incorporating PCM panels with thicknesses of 10, 15, and 20 mm. Their findings indicate that a 20 mm PCM layer can reduce ambient temperature by up to 9°C and provides the best thermal performance in terms of room temperature reduction, decrement factor, and time lag.

There are some limitations to the application of PCMs in the proposed construction systems in this research:

1. The thicknesses of PCMs are limited by their manufacturing design and melting points, which result in varying wall thicknesses when employing different types of PCM.
2. It has been found that PCMs with a melting point of 23°C exhibit optimal thermal behaviour in the studied region under extremely hot conditions.
3. PCMs deliver the best thermal comfort results when placed in the innermost layer of a sandwich wall panel system.

7.2.3 PHASE CHANGE MATERIALS REPAIRS CONSIDERATION

As mentioned earlier in this study, the PCM layer is designed to be positioned within the internal layers of the wall system. This placement aims to stabilise indoor temperature fluctuations by maintaining the desired thermal conditions throughout the hours of occupancy. Additionally, incorporating gypsum board on the innermost side of the wall system facilitates potential future maintenance of the phase change materials.

As a result, in some of the proposed wall systems in this research, gypsum board panels have been integrated on the innermost side of the external wall system. With the PCM attached to the gypsum board, the PCM effectively becomes the second layer from the inside. This design approach enhances the wall system’s maintenance flexibility, allowing easy access to the PCM without compromising the integrity of the entire system.

This technique—particularly the placement of thermal insulation—is a common practice in the construction industry and is often employed in roofing systems that include ceiling panels to integrate various services or equipment. However, despite these maintenance advantages, it was observed that the inclusion of a gypsum board panel marginally diminishes the efficiency of PCM materials in the wall systems analysed in this study.

7.3 SELECTING A SAMPLE HOUSE

Due to the technical limitations of this thesis, it was not feasible to apply the proposed improvements to elements/components across all zones of the examined houses, whose total thermal performance was analysed in the previous chapter. Therefore, for a more in-depth thermal comfort and performance analysis, only two zones in house 1-J were selected.

The enhancements for the remaining two houses (encompassing four zones) will be examined later in a final summary, which will consider the optimal scenario demonstrated in house 1-J. This decision was informed by the findings from the previous chapter, which indicated that house 1-J experienced the highest number of discomfort hours throughout the year, thereby making its zones an ideal candidate for detailed study.

7.4 METHODOLOGICAL APPROACH TO PRECAST WALL SYSTEM ANALYSIS

This section of the research undertakes an extensive evaluation involving a variety of wall types and thicknesses. The aim is to simulate different scenarios to identify the optimal approach for achieving maximum thermal comfort throughout the year. By exploring several proposed precast wall configurations, this study carefully analyses and estimates the total discomfort hours for each system across an entire year. This analysis goes beyond simple comparisons, involving a detailed examination of the impact of these proposed precast walls on operative temperatures during summer and winter, compared to the temperatures in the original house's base case.

In addition to assessing operative temperatures, a significant focus of the analysis is on evaluating the total number of discomfort hours, both monthly and annually. This approach provides a comprehensive understanding of the potential benefits of each proposed precast wall system. The analysis covers a range of factors, including the thermal properties of materials, the placement of insulation within the wall layers, and the architectural integration of these systems within the existing structure.

The subsequent subsections are designed to systematically detail the characteristics of the proposed walls. Each subsection provides a clear overview of the wall designs, followed by a detailed presentation of the simulation results. These findings are intended to illuminate the practical implications of implementing such precast wall systems in real-life settings, highlighting the relationship between theoretical assumptions and real-world data. The aim is to provide insights that are academically robust and practically relevant, contributing to the advancement of sustainable and efficient building design.

7.5 THERMAL PERFORMANCE OPTIMISATION IN PRECAST CONCRETE WALL SYSTEMS FOR CLIMATE ADAPTABILITY

As highlighted in the literature review chapter, several authors have noted the effectiveness of using thermal mass in hot climates. Consequently, the application of thermal mass as a method for minimising diurnal temperature swings is particularly well-suited to hot regions characterised by significant daily temperature fluctuations in the summer and numerous sunny days in winter. It is therefore recommended to apply thermal mass to the walls to evaluate its effectiveness in enhancing thermal comfort.

The use of aerated concrete in the outermost layer of the precast concrete wall panels has been found to promote maximum system performance. Specifically, when lightweight concrete is applied to the exterior surface of a building in extremely hot climates, there is a reduced likelihood of heat transfer compared to the use of higher-density concrete.

Conversely, employing high-density concrete materials on the innermost surface of the wall panel helps maintain stable indoor thermal comfort, closely aligned with the desired air temperature. Additionally, the indoor air temperature tends to remain more consistent throughout the day and between day and night. Thermal analysis, along with the examination of different external walls, reveals that the innermost layer should consistently be made of materials with high thermal mass, while the outermost layer should consist of materials with exceptionally low thermal mass. This design approach in precast panel construction has proven effective, particularly in hot and humid climate regions.

Various insulation materials have been recommended due to their capacity to regulate heat flow through the walls in both directions. However, while insulation may be beneficial in winter, it can be less effective in summer, as heat loss through walls often exceeds heat gain. Consequently, the performance of the proposed walls was evaluated and simulated for each season individually and for the entire year to determine the optimal level of thermal comfort achievable by minimising total discomfort hours.

As described in Chapter 3, a wide range of insulation materials with various insulating properties is available in the global building materials market. However, the options in the Saudi Arabian construction market are more limited. Therefore, this research adheres to the building materials recommended by the Saudi Building Code.

The simulation of the various proposed walls aimed to demonstrate the range of thermal performance (total discomfort hours) achievable by each type of proposed wall. In this study, approximately 120 proposed wall systems were modelled, simulated, and analysed. However, only those systems that demonstrated a significant reduction in total annual discomfort hours and met the criteria for reliable reinforced thicknesses have been included, totalling 16 wall systems. These systems are listed as relevant in various tables.

It is crucial to note that these results are based on specific conditions and assumptions made during testing and may not accurately represent the systems' performance in real-world conditions. Additionally, the results do not consider other factors that could influence wall performance, such as installation quality, environmental conditions, and maintenance requirements.

7.5.1 PROPOSED SANDWICH PANELS' THERMAL ANALYSIS

Tables 7.1 to 7.4 present a comparative analysis of various proposed precast concrete wall panel systems, differentiated by their number of wythes. Each wall system is identified by a unique wall code. The column labelled "Precast Wall Layers" details the composition of each wall system, specifying the materials used, their thickness, and the sequence of layers. The "Cross-Section" column provides an architectural representation of each wall's cross-section, illustrating all layers in their correct order.

The "Panel Thickness (m)" column indicates the total thickness of each wall system in metres. The "U-value (W/m²·K)" column reflects the thermal conductivity of each system; typically, a lower U-value signifies better insulation properties of the wall. Additionally, the "House Total Discomfort Hours (All Clothing) (hrs.) Per Year" column quantifies the total annual discomfort hours for a house equipped with each wall system, considering all Clo values for both summer and winter seasons.

It should be noted that the existing wall (base case) represents the predominant precast wall system type in the region and is widely used in most precast concrete housing constructions. The majority of the proposed walls feature the same exterior and interior finishes as the existing wall, ensuring consistency in comparison and analysis.

Table 7.1: List of wall sections for proposed external precast concrete wall panels featuring a two-wythe configuration. Wall sections were generated using DesignBuilder software and reproduced in PowerPoint for enhanced clarity and presentation.

Wall code	**Precast Wall layers**	**Cross section**	**Panel Thickness (M)**	**U-value (W/m^2-K)**	**House total discomfort hours (All clothing) per year (hrs.)**
W-0 Base case	-Lime sand render -75 mm solid standard concrete -50 mm board Insulation (Glass fibre board) -75 mm solid standard concrete -white paint	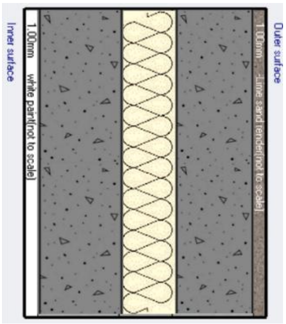	0. 200	0.437	2440
W1	-Lime sand render -75 mm Concrete-aerated -50 mm Expanded polyurethane. -75 mm Concrete-aerated -white paint	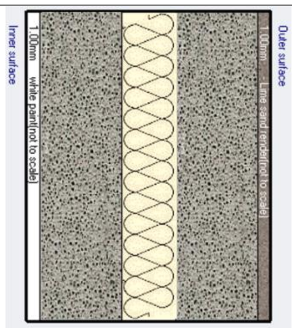	0.200	0.305	2386
W 2	-Lime sand render -75 mm Concrete-aerated -50 mm Expanded polyurethane. -75 mm Concrete-high density -white paint	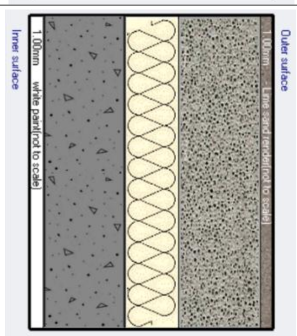	0.200	0.351	2390
W 3	-Lime sand render -75 mm Concrete-aerated -50 mm Phenolic Foam. -75 mm Concrete-high density -white paint	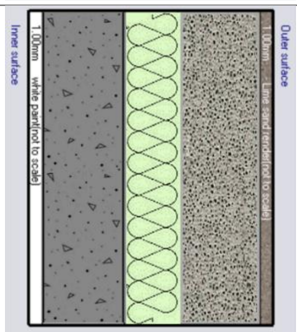	0.200	0.518	2395

W 4	-Lime sand render -80 mm Concrete-aerated - 150 mm Air gap -80 mm Concrete high density -white paint	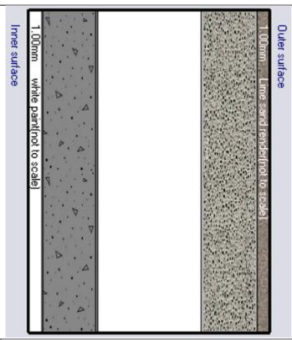	0.310	0.149	2370
W 5	-Lime sand render -75 mm Concrete – aerated. -50 mm Phenolic Foam. -150 mm Air gap -75 mm Concrete – high density -white paint	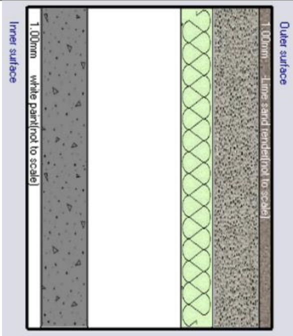	0.350	0.126	2365
W 6	-Lime sand render -75 mm Concrete-aerated -100 mm Phenolic Foam. -100 mm Air gap -75 mm Concrete-high density -white paint	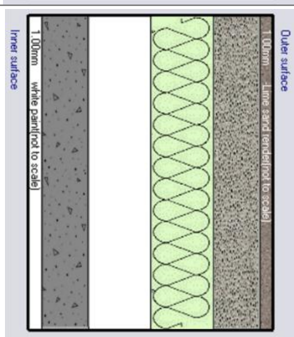	0.350	0.098	2360

From the data provided in Table 7.1, several proposed external precast concrete wall panel systems are highlighted. The table details six distinct wall systems, each characterised by its unique layer composition. Through an analysis of these systems, we can deduce their relative thermal performance, as indicated by their U-values and total discomfort hours. A specific focus is placed on those systems that effectively minimise panel thickness and total discomfort hours.

A common feature across all the proposed systems is their sandwich-like structure, consisting of five layers: lime sand render, a form of concrete, insulation or an air gap, another layer of concrete, and a final coat of white paint. System W-0, serving as the base case, has a panel thickness of 0.2 m, a U-value of 0.437 W/m²·K, and accumulates 2440 discomfort hours per year. The use of standard solid concrete and glass fibre board insulation in this system results in relatively high discomfort hours, highlighting the need for more efficient materials and design to enhance thermal comfort.

Systems W1, W2, and W3, despite sharing the base case's panel thickness, exhibit improved thermal performance. This enhancement is achieved through the integration of aerated and high-density concrete along with different types of insulation. Moreover, systems W4, W5, and W6 introduce a novel approach by incorporating an air gap into their insulation strategy. This design increases their panel thickness (0.31 m for W4 and 0.35 m for W5 and W6) but significantly lowers their U-values and discomfort hours. System W6, in particular, achieves the lowest U-value at 0.098 $W/m^2 \cdot K$ and the fewest discomfort hours at 2360. Despite its larger panel size, this is accomplished by combining a 100 mm phenolic foam layer with an equivalent air gap.

Considering the initial goal of minimising panel thickness and discomfort hours, a trade-off is evident. While system W3 maintains a slender profile, system W6, despite its increased thickness, offers the best overall performance in reducing discomfort hours.

The transition from traditional solid concrete to aerated and high-density versions, along with the integration of advanced insulation materials and air gaps, proves effective in enhancing thermal performance and reducing discomfort hours. Despite the variations in thickness, these design modifications collectively lead to improved thermal comfort and energy efficiency, suggesting a promising direction for the future development of precast concrete wall panel systems.

Table 7.2: List of proposed external precast concrete wall panel systems featuring a two-wythe configuration, including Phase Change Materials. Wall sections were generated using DesignBuilder software and reproduced in PowerPoint for enhanced clarity and presentation.

Wall code	Precast Wall layers	Cross section	Panel Thickness (M)	U-value (W/m^2-K)	House total discomfort hours (All clothing) per year (hrs.)
W 7	-Lime sand render -75 mm Concrete-aerated -75 mm Expanded polyurethane. -75 mm Concrete-aerated -20 mm RPCM - 12.7 mm gypsum board -white paint	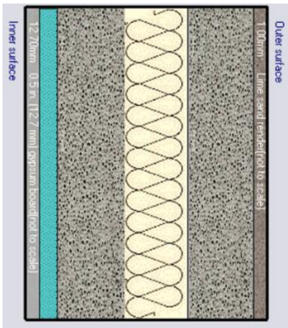	0.2577	0.224	2209
W 8	-Lime sand render -75 mm Concrete-aerated -75 mm Expanded polyurethane. -75 mm Concrete-aerated -30 mm RPCM -12.7 mm gypsum board -white paint	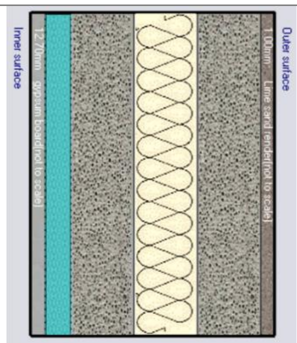	0.2677	0.223	2158
W9	-Lime sand render -75 mm Concrete-aerated -50 mm Vacuum insulation -75 mm Concrete-aerated -30 mm RPCM -12.7 mm gypsum board -white paint	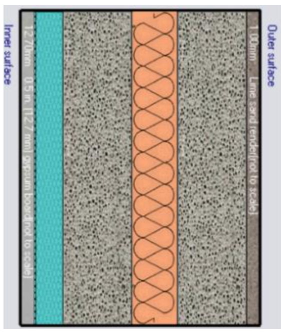	0.2427	0.064	2149

Table 7.2 introduces an innovative approach to precast concrete wall panels by integrating Phase Change Materials (PCMs) into three distinct wall systems, designated as W7, W8, and W9. These PCMs serve as a pivotal element in enhancing thermal regulation, extending beyond the capabilities of traditional insulation. Their unique property of storing and releasing thermal energy during phase transitions, particularly during melting and freezing processes, plays a crucial role in moderating indoor

temperature fluctuations, thereby contributing to a consistently comfortable indoor climate.

The W7 system maintains a similar layering structure to earlier models but introduces a 20 mm layer of BioPCM and a 12.7 mm gypsum board. This combination slightly increases the panel's thickness to 0.257 m but significantly boosts its thermal efficiency, as indicated by a U-value of 0.224 W/m²·K and a reduction in total discomfort hours to 2209 per year. This system demonstrates the effectiveness of BioPCM in optimising thermal performance within a compact wall structure.

Building on the W7 design, the W8 system employs a thicker 30 mm BioPCM layer while keeping the other layers the same. This adjustment results in a slight increase in panel thickness to 0.268 m but further enhances the wall's thermal performance, decreasing the U-value to 0.223 W/m²·K and reducing the annual discomfort hours to 2158. This indicates that increasing the thickness of the BioPCM layer can substantially improve the wall's ability to maintain comfortable indoor temperatures.

W9 marks a significant shift from the previous configurations by replacing standard expanded polyurethane insulation with a 50 mm vacuum insulation panel (VIP). VIPs are renowned for their superior insulation efficiency, and this alteration notably improves the wall's thermal properties, achieving an impressively low U-value of 0.064 W/m²·K. This U-value is the lowest among all the systems analysed, resulting in the fewest discomfort hours at 2149 per year. Additionally, W9 achieves a marginally reduced panel thickness compared to W8, measuring 0.243 m.

With the objectives of minimising panel thickness and discomfort hours in mind, the integration of PCMs and advanced insulation materials like VIPs offers a significant benefit. Among the systems in Table 7.2, W9 stands out as the most effective, achieving the lowest U-value in the two-wythe system and the fewest discomfort hours while maintaining a relatively thinner profile compared to W8.

The strategic inclusion of PCMs introduces a critical enhancement to the thermal performance of these wall systems. By using materials capable of dynamically storing and releasing heat as needed, these systems offer improved comfort and energy efficiency. When combined with advanced insulation technologies such as VIPs, these innovative adaptations represent a significant advancement in the development of precast concrete wall panel systems, particularly in terms of sustainable and comfortable living environments.

Table 7.3: Proposed external precast concrete wall panel systems with three wythes. Wall sections were generated using DesignBuilder software and reproduced in PowerPoint for enhanced clarity and presentation.

Wall code	**Precast Wall layers**	**Cross section**	**Panel Thickness (M)**	**U-value (W/m^2-K)**	**House total discomfort hours (All clothing) per year (hrs.)**
W10	-Lime sand render -50 mm Concrete-aerated 100 mm Expanded polyurethane. -900 mm Concrete-high density -50 mm Air gap -50 mm Concrete-high density -white paint	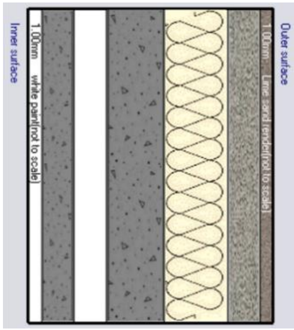	0. 340	0.145	2370
W11	-Lime sand render -50 mm Concrete-aerated -50 mm Expanded polyurethane. -75 mm Concrete-high density -50 mm Expanded polyurethane. -50 mm Concrete-high density -white paint	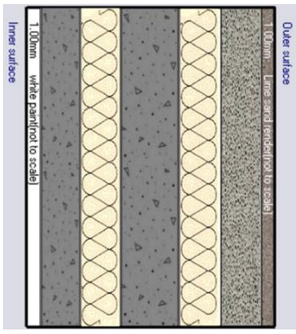	0.275	0.204	2371
W12	-Lime sand render -50 mm Concrete-aerated -50 mm Vacuum insulation -75 mm Concrete-high density -50 mm Vacuum insulation. -50 mm Concrete-high density -white paint	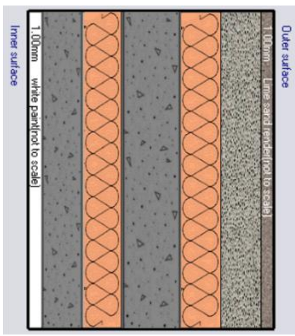	0. 275	0.034	2355

Table 7.3 presents a series of advanced external precast concrete wall panel systems, each characterised by a three-wythe configuration. This design approach, involving an

additional layer of concrete and insulation compared to the two-wythe systems, is aimed at achieving superior thermal performance.

In the W10 wall system, a considerable 90 mm layer of high-density concrete is sandwiched between 100 mm of expanded polyurethane and a 50 mm air gap, complemented by an aerated concrete layer on one end. Despite an increased panel thickness of 0.34 m, this system attains a U-value of 0.145 $W/m^2 \cdot K$ and a total of 2370 discomfort hours per year. The considerable mass of the high-density concrete is likely a key factor in the system's effective thermal performance, serving as a thermal storage medium to stabilise indoor temperature fluctuations.

The W11 system modifies the W10 configuration by substituting the high-density concrete and air gap with an extra layer of expanded polyurethane and a thinner layer of high-density concrete. This alteration leads to a reduced panel thickness of 0.275 m, a slightly higher U-value of 0.204 $W/m^2 \cdot K$, and a marginal increase in total discomfort hours to 2371 per year. The additional insulation layer in W11 indicates a balance between maximising insulation efficiency and leveraging the thermal mass of concrete. This configuration is particularly advantageous when a reduced panel thickness is prioritised.

Significantly, the W12 system stands out for its incorporation of vacuum insulation in place of expanded polyurethane. Maintaining the same panel thickness as W11, W12 remarkably reduces the U-value to an exceptionally low 0.034 $W/m^2 \cdot K$ and brings down the total discomfort hours to 2355 per year. The deployment of vacuum insulation, known for its high-performance insulating properties, is the critical element driving this system's enhanced thermal efficiency.

The analysis of these three systems from Table 7.3 reveals that the integration of an extra wythe, comprising additional insulation and concrete layers, substantially benefits thermal performance and comfort, as demonstrated by the reduced discomfort hours. Notably, the inclusion of vacuum insulation in W12 offers a considerable advantage, achieving the lowest U-value and total discomfort hours among the three systems, despite its moderate thickness. Thus, W12 emerges as the standout performer among the three-wythe systems, striking an impressive balance between panel thickness, thermal efficiency, and overall comfort.

Table 7.4: Proposed external precast concrete wall panel systems with three wythes, including Phase Change Materials. Wall sections were generated using DesignBuilder software and reproduced in PowerPoint for enhanced clarity and presentation.

Wall code	Precast Wall layers	Cross section	Panel Thickness (M)	U-value (W/m^2-K)	House total discomfort hours (All clothing) per year (hrs.)
W13	-Lime sand render -75 mm Concrete-aerated -80 mm Air gap -75 mm Concrete-high density -30 mm RPCM -75 mm Concrete-high density -white paint	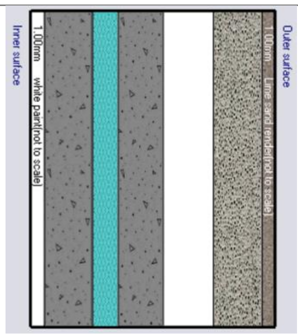	0. 335	0.253	2178
W14	-Lime sand render -75 mm Concrete-aerated -80 mm Air gap -80 mm Exp. polyurethane. -75 mm Concrete-aerated -30 mm RPCM -30 mm Concrete-high density -white paint	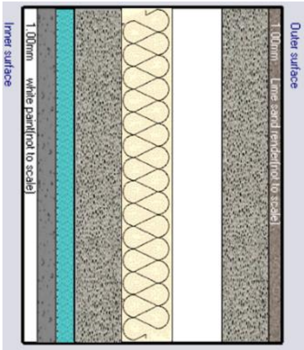	0. 370	0.128	2147
W15	-Lime sand render -75 mm Concrete-aerated -80 mm Phenolic Foam. -75 mm Concrete-aerated - 30 mm RPCM -75 mm Concrete-high density -white paint	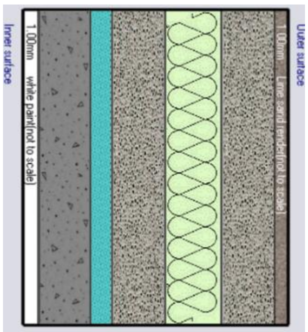	0. 335	0.178	2163
W16	-Lime sand render -75 mm Concrete-aerated -80 mm Phenolic Foam. -75 mm Concrete-aerated - 30 mm RPCM -50 mm Concrete-high density -white paint	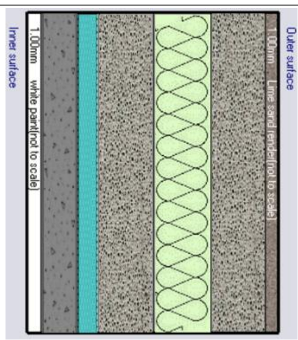	0.310	0.178	2156

W17	-Lime sand render -75 mm Concrete-aerated -80 mm Expanded polyurethane. -75 mm Concrete-aerated -15 mm RPCM -75 mm Concrete-high density -white paint	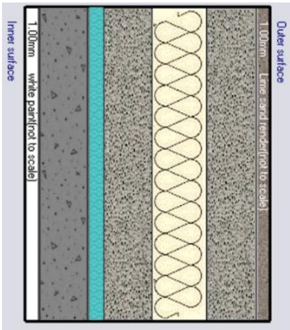	0. 320	0.215	2262
W18	-Lime sand render -50 mm Concrete-aerated -50 mm Expanded polyurethane. -75 mm Concrete-high density -30 mm RPCM -50 mm Concrete-high density -white paint	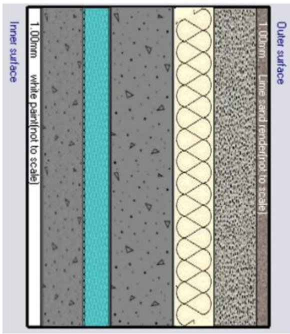	0.255	0.363	2151
W19	-Lime sand render -75 mm Concrete-aerated -30 mm Vacuum insulation -75 mm Concrete-aerated -30 mm RPCM -50 mm Concrete-high density -white paint	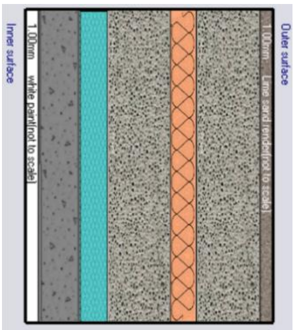	0. 260	0.103	2139

Table 7.4 lists the development in the design of external precast concrete wall panel systems, now incorporating PCMs into a three-wythe configuration. This innovative approach is designed to optimise thermal performance and comfort by combining additional insulation layers with the thermal storage capabilities of BioPCMs.

The table lists a range of systems, W13 through W19, each uniquely combining materials, thicknesses, and BioPCMs to achieve specific thermal outcomes, as indicated by their U-values and total annual discomfort hours. Notably, systems W14 and W19 stand out for their exceptional thermal performance.

W14, with the largest panel thickness in this series at 0.370 m, attains a remarkably low U-value of 0.128 W/m²·K and a total of 2147 discomfort hours per year. This efficiency is attributable to its composition, which includes an air gap, expanded polyurethane, and BioPCM. The integration of these materials provides a balanced approach to thermal insulation and storage, resulting in enhanced comfort.

Conversely, W19, with a more modest panel thickness of 0.260 m, leverages the highly efficient vacuum insulation alongside BioPCM. This combination yields an impressive U-value of 0.103 W/m²·K and the lowest total discomfort hours of 2139 per year. The use of vacuum insulation, known for its superior insulating properties, coupled with the adaptive thermal properties of BioPCM, marks W19 as a particularly effective system in terms of thermal management.

The analysis of these systems from Table 7.4 highlights the significant impact that the right combination of materials and technology can have on the thermal performance of wall systems. By strategically incorporating PCMs and varying insulating materials, these wall systems demonstrate the potential for enhanced comfort and energy efficiency in building design. Systems like W14 and W19, in particular, represent the forefront of this innovation, successfully balancing panel thickness with outstanding thermal performance and comfort.

Note: The placement of PCMs between two concrete panels may present practical risks, such as expansion due to the nature of PCMs. However, these systems serve as guidelines for engineers and can be adapted to mitigate any risks in the future as required.

7.5.2 IDENTIFICATION OF OPTIMAL HIGH-PERFORMANCE PRECAST WALL SYSTEMS

In summarising the thermal performance of various wall systems presented across the four tables, it becomes evident that significant improvements have been achieved through the incorporation of innovative materials and design changes. The pinnacle of this progression is observed in the systems that integrated high-performance insulation materials like vacuum insulation and PCMs, particularly in the form of prefabricated wall systems. Among all evaluated systems, W19 stands out, offering the best thermal performance. It achieves the lowest number of total discomfort hours (2139 hours per year) and an impressively low U-value, while maintaining a reasonable panel thickness. This optimal balance of comfort, thermal efficiency, and structural feasibility positions W19 as an exemplary choice for an external precast concrete wall panel system.

These findings indicate that the future development of wall panel systems should focus on the utilisation of high-performance insulation materials, potentially in combination with PCMs. This approach, coupled with careful design and layering strategies, could further boost thermal performance, augment occupant comfort, and enhance overall energy efficiency in the field of prefabricated buildings.

The subsequent sections in this chapter will delve deeper into the thermal performance and comfort offered by the selected precast concrete wall panel system. By analysing the system's effectiveness in maintaining a comfortable indoor environment and reducing energy consumption, this study aims to guide the decision-making process in selecting the most suitable wall system for future development. The overarching goal of this research is to provide a comprehensive understanding of the thermal dynamics of precast concrete wall panel systems, thereby advocating for the adoption of building practices that are both thermally comfortable and energy efficient.

7.6 THERMAL PERFORMANCE OPTIMISATION IN PREFABRICATED ROOF SYSTEMS

The case study houses under investigation typically feature precast hollow-core concrete roofing systems with a thickness of 200 mm. To understand the effectiveness of the original roof system design in terms of total thermal discomfort hours, construction layers such as insulation and tiles were analysed according to the original specifications in the base case simulation. The base case, representing the original building configuration, recorded a total of 2440 discomfort hours per year.

In response to this research challenge, several alternative roofing systems have been developed and investigated with the goal of enhancing indoor thermal conditions. These proposed systems aim to reduce total discomfort hours throughout the year, thereby decreasing annual energy consumption. This reduction is particularly significant as it is often driven by the need for active air conditioning systems to maintain desirable indoor temperatures within a comfortable range.

It is essential to highlight that improvements in the thermal performance of the roof system have a direct and positive impact on the overall thermal comfort of the house, especially in the upper floor zones. This underscores the importance of considering roof system design as a critical component in the overall strategy to enhance energy efficiency and comfort in residential buildings. Through these investigations, the study seeks to identify roofing system designs that not only reduce discomfort hours but also contribute to a more sustainable approach to managing indoor climates.

In response to the research challenge, several alternative roofing systems have been developed and investigated with the goal of enhancing indoor thermal conditions. These proposed systems aim to reduce total discomfort hours throughout the year, thereby decreasing annual energy consumption. This reduction is particularly significant, as it is often driven by the need for active air conditioning systems to maintain desirable indoor temperatures within a comfortable range.

It is essential to highlight that improvements in the thermal performance of the roof system have a direct and positive impact on the overall thermal comfort of the house, especially in the upper floor zones. This underscores the importance of considering roof system design as a critical component in the overall strategy to enhance energy efficiency and comfort in residential buildings. Through these investigations, the study seeks to identify roofing system designs that not only reduce discomfort hours but also contribute to a more sustainable approach to managing indoor climates.

7.6.1 MODELLING DESCRIPTION OF PROPOSED ROOF SYSTEMS

The proposed roof systems have been meticulously designed, focusing on varying construction layers and adjusting their thicknesses to achieve the most significant reduction in total discomfort hours. It is crucial to note that these designs maintain the structural integrity of the roof by utilising the standard hollow-core system, a prevalent feature across the majority of prefabricated housing projects examined in Saudi Arabia.

Additionally, the construction layers in the proposed systems adhere to standard worldwide thicknesses for concrete buildings, from the top tiles to the inner insulation layers. This compliance ensures that the systems meet globally recognised building standards while striving to optimise thermal comfort.

A key feature of these proposed roof systems is the strategic integration of PCMs. These materials are incorporated within the innermost layer of the roof systems, following standard recommendations for roofing systems that include PCMs. The placement of PCM on the inner side of the envelope system is known for its high flexibility and enhanced performance. Furthermore, for a comprehensive understanding, several roof systems embodying these design elements and materials are detailed in tables within the next subsections. These tables display a range of roofing solutions capable of significantly reducing discomfort hours, thereby contributing to more efficient energy use and improving occupant comfort throughout the year.

Additionally, the construction layers in the proposed systems adhere to standard worldwide thicknesses for concrete buildings, from the top tiles to the inner insulation layers. This compliance ensures that the systems meet globally recognised building standards while striving to optimise thermal comfort.

A key feature of these proposed roof systems is the strategic integration of PCMs. These materials are incorporated within the innermost layer of the roof systems, following standard recommendations for roofing systems that include PCMs. The placement of PCMs on the inner side of the envelope system is known for its flexibility and enhanced performance. Furthermore, for a comprehensive understanding, several roof systems embodying these design elements and materials are detailed in the tables within the next subsections. These tables display a range of roofing solutions capable of significantly reducing discomfort hours, thereby contributing to more efficient energy use and improving occupant comfort throughout the year.

7.6.2 THERMAL ANALYSIS OF PROPOSED ROOF SYSTEMS

This section conducts a thorough thermal evaluation of the buildings, focusing on the impact of seasonal variations on roofing systems. During the peak summer months, the analysis reveals considerable heat gains through the roofs, which exceed the rate of heat loss. Conversely, in the winter season, this dynamic shift, with heat loss through the roofs surpassing heat gains. To address these seasonal challenges, the study proposes several roofing systems designed with lower thermal conductivity than the existing system. The objective is to mitigate heat loss in winter and reduce heat gain in summer, thereby enhancing overall thermal efficiency.

Table 7.5 provides a comparative analysis of four proposed roofing systems, primarily based on hollow-core concrete slabs and standard insulation materials. Each system is uniquely defined by its layer configuration and respective thicknesses. The U-values for each system, a critical indicator of heat transfer rate, are included for comparative purposes. Moreover, the table details the total house discomfort hours per year, offering a comprehensive perspective on the impact these roofing systems have on maintaining thermal comfort throughout the year.

Furthermore, this section introduces the innovative application of PCMs within these roofing systems, with the goal of significantly enhancing their thermal regulation properties. Table 7.6 delves into the specifics of these advanced roofing solutions, detailing their compositions, layer thicknesses, thermal conductivities, and the extent to which they reduce annual discomfort hours. The use of PCMs, an advanced material in thermal performance optimisation, is anticipated to substantially improve the energy efficiency and comfort levels of these buildings. This exploration of integrating traditional insulation methods with PCMs aims to establish a new benchmark in prefabricated concrete roofing system design, emphasising optimal thermal comfort and energy efficiency.

Table 7.5: Proposed roofing systems with common insulation materials. Roof sections were generated using DesignBuilder software and reproduced in PowerPoint for enhanced clarity and presentation.

Roof code	**Roofing system**	**Cross section**	**Panel Thickness (M)**	**U-value (W/m^2-K)**	**House total discomfort hours (All clothing) per year (hrs.)**
R-0 Base case	-50mm Roof Tile -1.50mm UPVC -30mm slop Concrete -50mm Structural Concrete topping -200mm Hollow-core Concrete.	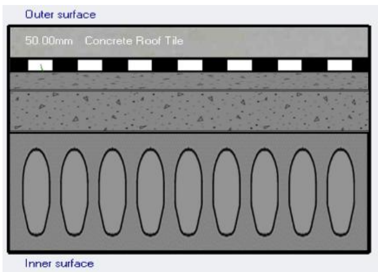	0.3315	1.9	2440
R-1	-50mm Roof tile -1.50mm UPVC -30mm slop Concrete -50mm structural Concrete topping -100 mm exp polyurethane -200mm Hollow core Concrete	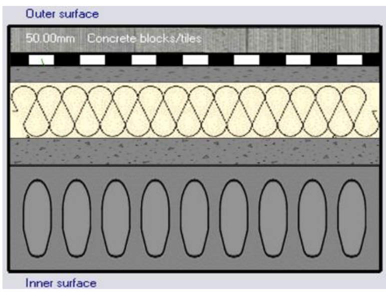	0.4315	0.206	2367

R-2	-50mm - gravel -50mm roof tiles aerated -1.50mm UPVC -30mm slop Concrete -100 mm exp polyurethane -200mm Hollow core Concrete	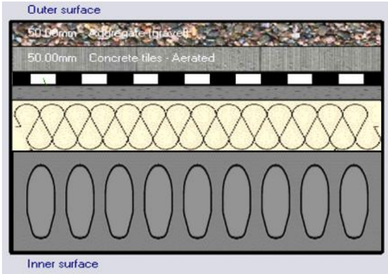	0.4315	0.199	2352
R-3	-80mm gravel -1.50mm UPVC -30mm slop Concrete -100mm exp polyurethane -200mm Hollow core Concrete	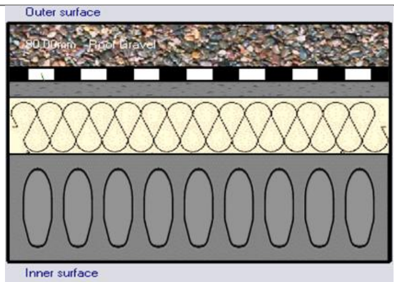	0.4115	0.208	2350
R-4	-50mm gravel -50mm concrete tiles-aerated -1.50mm UPVC -30mm slop concrete -150mm exp polyurethane -50mm structural Concrete topping -200mm aerated concrete slab	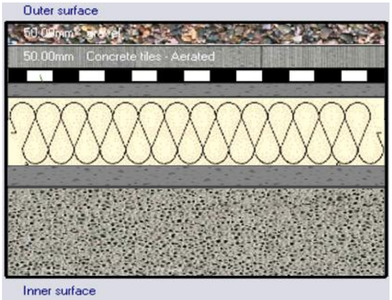	0.5315	0.119	2340

Table 7.5 provides a detailed overview of five distinct proposed roofing systems, including the base case (R-0) and four innovative alternatives (R-1 to R-4), each uniquely assembled with a combination of common insulation materials and structural elements. These systems collectively demonstrate a range of approaches to enhancing thermal efficiency in roofing designs.

The base case, R-0, sets the standard for comparison with a U-value of 1.9 W/m²·K and the highest number of discomfort hours annually at 2440. This system's lack of advanced insulative materials, such as expanded polyurethane, underscores its relatively inferior thermal performance when compared to the proposed alternatives.

The alternative systems, R-1 through R-4, highlight significant improvements in U-values and discomfort hours, primarily due to the integration of expanded polyurethane. This material, known for its exceptional thermal resistance, plays a pivotal role in elevating the thermal efficiency of these roofing configurations. R-1 and R-2, both characterised by a panel thickness of 0.4315 m, deliver comparably low U-values. However, R-2 achieves a marginally lower number of discomfort hours, benefiting from the addition of both aerated roof tiles and gravel, which enhance its thermal efficiency.

Moreover, R-3, distinctively utilising an 80 mm gravel layer instead of roof tiles, slightly reduces the panel thickness to 0.4115 m. This system maintains a thermal performance comparable to R-2, with a mere two-hour annual difference in discomfort hours, indicating its effectiveness.

Notably, R-4, despite having the greatest panel thickness of 0.5315 m, stands out with the lowest U-value of 0.119 $W/m^2 \cdot K$ and the fewest annual discomfort hours at 2340. The combination of a 150 mm layer of expanded polyurethane and an aerated concrete slab contributes significantly to this system's enhanced thermal performance.

In evaluating these systems, R-3 emerges as an attractive option, balancing thermal performance with structural efficiency. However, if the primary focus is on maximising thermal efficiency, R-4, despite its larger thickness, offers the most effective solution, achieving the lowest U-value and the minimum number of discomfort hours.

Table 7.6: Proposed roofing systems with Phase Change Materials. Roof sections were generated using DesignBuilder software and reproduced in PowerPoint for enhanced clarity.

Roof code	Roofing system	Cross section	Panel Thickness (M)	U-value (W/m^2-K)	House total discomfort hours (All clothing) per year (hrs.)
R-5	-50mm gravel -50mm concrete tiles - aerated -1.50mm UPVC -30mm slop concrete -150mm Exp polyurethane -50mm structural concrete topping -200mm Hollow core Concrete -15 mm RPCM -12.7 mm gypsum board.	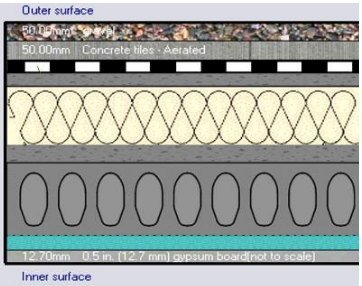	0.5742	0.136	2228
R-6	-50mm gravel -50mm concrete tiles - aerated -1.50mm UPVC -30mm slop Concrete -50mm V. Insul -50mm Structural Concrete topping -200mm Hollow core Concrete -15 mm RPCM -12.7 mm gypsum board.	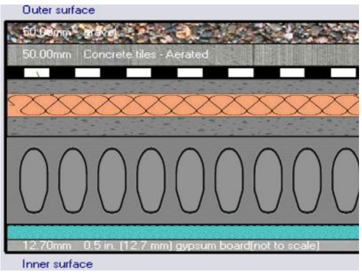	0.4742	0.066	2176
R-7	-50mm gravel -50mm concrete tiles - aerated -1.50mm UPVC -30mm slop conc. -80mm V. Insul. -50mm Structural Concrete topping -200mm Hollow core Concrete -30 mm RPCM -12.7 mm gypsum board.	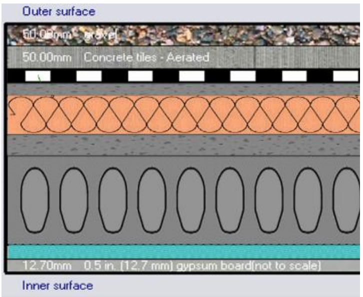	0.5042	0.042	2172

Table 7.6 highlights three advanced proposed roofing systems (R-5 to R-7), each integrating PCMs, specifically BioPCM, and, in some configurations, Vacuum Insulation (V. Insul). These advanced systems share certain structural elements such as gravel, aerated concrete tiles, UPVC, sloped concrete, a structural concrete topping, a hollow-core concrete slab, BioPCM, and a gypsum board layer. The distinction between these innovative systems primarily resides in their choice and thickness of insulation materials.

System R-5 utilises 150 mm of expanded polyurethane for insulation, achieving a panel thickness of 0.5742 m and a U-value of 0.136 W/m²·K. This system results in 2228 total discomfort hours per year, representing a significant 8.7% reduction compared to the base case R-0.

Further, System R-6 represents a further advancement in thermal insulation by replacing expanded polyurethane with 50 mm of vacuum insulation, renowned for its excellent insulative properties. This alteration reduces the panel thickness to 0.4742 m and lowers the U-value to 0.066 W/m²·K, leading to a total of 2176 discomfort hours per year — a substantial 10.8% improvement over R-0.

The most sophisticated of these systems, R-7, amplifies the insulation effect seen in R-6 by incorporating 80 mm of vacuum insulation and enhancing the BioPCM layer to 30 mm. Despite a slight increase in panel thickness to 0.5042 m, R-7 achieves an extremely low U-value of 0.042 W/m²·K and further reduces discomfort hours to 2172 per year, culminating in an 11% decrease in discomfort hours relative to the base case R-0.

Thus, among these advanced roofing systems, R-6 emerges as the optimal choice for balancing thermal performance with structural efficiency, particularly in terms of minimising discomfort hours and panel thickness. However, for ultimate thermal efficiency, R-7, despite a slight increase in thickness, offers the most effective solution with the lowest U-value and the fewest annual discomfort hours, positioning it as the preferred system for maximising thermal comfort in this study.

7.7 WINDOWS OPTIMISATIONS CONSIDERATIONS

In this section, an extensive thermal evaluation of buildings is provided, with a special emphasis on the significant impact of windows on overall thermal performance, as explored in the literature review chapter. Windows are particularly crucial due to the substantial heat gains through glazing caused by solar exposure. Such solar heat gains can contribute to up to 50% of total discomfort hours throughout a year (Calama-González et al., 2019). The heat gain through windows is influenced by several factors, including the window-to-wall ratio (WWR), the orientation of windows in relation to the building's overall direction, and the effectiveness of internal and external shading devices. Notably, the choice of glazing materials has been shown to be pivotal in reducing unwanted solar heat gains through windows.

Across the globe, various glazing systems have been developed, ranging from single-pane to triple-pane systems. These systems, acknowledged for their thermal performance in the glazing industry, often include different types of gases such as air, xenon, and argon to enhance their insulation properties. The efficiency of these gases in glazing systems has been extensively studied by scholars.

Accordingly, Table 7.7 presents several proposed glazing systems, considering the original WWR and their impact on total house discomfort hours. This analysis uses data compiled using DesignBuilder software for accuracy and comprehensiveness.

Table 7.7: Proposed glazing systems, their specifications, and thermal performance. Data were gathered using DesignBuilder software.

Systems' code	Glazing type	Total solar transmission (SHGC)	U-value (W/m^2-K)	Discomfort Hours (All Clothing) (hr)
WD-0 (Base case)	Dbl Blue 6mm/6mm Air	0.212	2.89	2440
WD-1	Dbl Ref-A-H Tint 6mm/13mm Arg	0.197	2.185	2424
WT-1	Trp LoE (e5=.1) Clr 3mm/13mm Air	0.579	1.256	2420
WT-2	Trp LoE (e5=.1) Clr 3mm/13mm Arg	0.579	1.058	2418
WT-3	Trp LoE Film (55) Clr 6mm/13m Air	0.310	1.202	2430
WT-4	Trp LoE Film (55) Bronze 6mm/13mm Air	0.222	1.202	2432

This table lists a range of proposed glazing systems, along with their specifications and the resulting thermal performance. The base case system, WD-0, consists of double-pane blue glazing, each pane being 6 mm thick, with an air gap in between. It is characterised by a total solar transmission (SHGC) of 0.212, a U-value of 2.89 W/m²·K, and results in 2440 discomfort hours annually. The other proposed systems exhibit varied specifications, leading to different thermal performances. Generally, systems with lower SHGC and U-value are more effective in thermal insulation, transmitting less solar radiation.

Among these systems, WT-2, featuring triple-pane low-E clear glazing with 3 mm and 13 mm thicknesses and argon gas filling, achieves the lowest U-value at 1.058 W/m²·K. Additionally, systems WT-3 and WT-4, incorporating Triple Low-E Film glazing, have lower SHGC values of 0.310 and 0.222, respectively. However, in terms of total discomfort hours, which indicate the likely comfort level of occupants under different glazing systems, there is minimal variation across all proposed systems, with values ranging from 2418 to 2440 hours.

Controlled air exchange between indoor and outdoor environments (infiltration) is also a crucial factor in maintaining indoor thermal comfort. Minimised infiltration rates are associated with improved indoor thermal performance and energy efficiency, especially when mechanical heating or cooling systems are in full operation (Tian et al., 2019). Thus, the proposed glazing systems in this study were simulated with the effect of minimum infiltration rates considered, aligning with the study's aim to enhance indoor thermal comfort while reducing total energy consumption. It is important to note that these simulations were based on the base case WWR of only 4% for the case study house, indicating a need for further exploration to optimise the reduction of total discomfort hours. This aspect will be addressed in the subsequent section.

7.7.1 PROPOSED ADVANCED VARIABLES FOR ENHANCING OVERALL WINDOWS THERMAL PERFORMANCE

Considering the data presented in Table 7.8, it becomes clear that the case study houses possess a relatively small WWR. Consequently, any attempt to enhance the building's thermal performance is unlikely to yield substantial improvements solely through modifications to the window system. Nevertheless, this research sought to explore the maximum potential for improving overall thermal performance by experimenting with variations in the WWR. Additionally, the study analysed the impact of other crucial elements like window shading devices and various indoor blind systems. These factors play a significant role in dictating the thermal efficiency of glazing, as evidenced by their influence on reducing total discomfort hours throughout the year.

This thorough analysis was performed using over 100 detailed simulations in DesignBuilder software, enabling the pinpointing of the most advantageous correlation points among the proposed variables to achieve optimal indoor thermal conditions. This method offered a comprehensive understanding of the complex interplay among these factors, leading to valuable insights into the most effective strategies for enhancing the thermal performance of window systems, especially in extremely hot climates.

The application of this advanced optimisation analysis provided profound insights into the complex relationship between the proposed variables, deepening the understanding of their collective impact on overall thermal performance. This methodical approach facilitated the identification of the most optimal combinations of these variables. This knowledge is invaluable for future decision-making processes, offering a pathway for more efficient strategies to optimise thermal performance in various construction projects. Accordingly, Table 7.8 lists the simulated variables and their correlations, highlighting their impact on indoor thermal performance, specifically in terms of total discomfort hours.

Table 7.8. Simulated variables within proposed window systems and their thermal performance. Data were gathered using DesignBuilder software.

System code	Glazing type	WWR%	Outer local shading type	Inner Window blind type	Discomfort (All Clothing) (hr)
WV-1	Dbl LoE (e2=.1) Clr 6mm/13mm Arg	11	1.5 m projection Louvre	Blind with medium reflectivity slats	2322
WV-2	Dbl LoE (e2=.1) Clr 6mm/13mm Arg	21	1.5 m projection Louvre	Blind with medium reflectivity slats	2317
WV-3	Dbl Clr 3mm/13mm Arg	11	No shading	Micro Louvre	2323
WV-4	Dbl Clr 3mm/13mm Arg	11	No shading	Blind with high reflectivity slats	2315
WV-5	Trp LoE (e2=e5=.1) Clr 3mm/13mm Arg	19	0.5m Overhang	Micro Louvre	2290
WV-6	Dbl LoE (e3=.1) Clr 3mm/13mm Arg	25	1.5 m projection Louvre	Blind with low reflectivity slats	2295
WV-7	Trp LoE (e2=e5=.1) Clr 3mm/13mm Arg	29	No shading	Micro Louvre	2260

Table 7.8 meticulously details the thermal performance of various window systems, each uniquely defined by a combination of several critical variables: glazing type, WWR, the type of outer local shading, and the choice of inner window blinds. This comprehensive analysis aims to pinpoint the most efficacious systems in terms of minimising total discomfort hours. As previously underscored in the research, total discomfort hours serve as a pivotal measure of thermal comfort. They are defined as the aggregate number of hours during which occupants are likely to endure discomfort owing to suboptimal thermal conditions. Therefore, systems with lower discomfort hours are indicative of superior thermal comfort performance.

Spanning different window system configurations, the table presents a rich tapestry of potential solutions. Each system is characterised by its own unique blend of features: the type of glazing employed, which determines insulating properties; the WWR, influencing solar radiation penetration; the type of shading used externally, such as overhangs or louvres; and the style of window blinds used internally, such as blinds or micro-louvres.

A key aspect of this analysis is identifying the system that yields the minimum discomfort hours. The standout system, WV7, achieves a remarkable reduction in discomfort hours to 2260. This system is exemplary in its thermal performance, optimising indoor conditions by reducing discomfort hours annually. Furthermore, several other systems also demonstrate reasonable reductions in discomfort hours, thereby offering viable alternatives:

- System WV-5: Incorporates triple low emissivity (e2=e5=.1) clear 3mm/13mm argon glass, complemented by a 0.5m overhang and Micro Louvre inner window blind, culminating in 2290 discomfort hours.
- System WV-6**:** Consists of double low emissivity (e3=.1) clear 3mm/13mm argon glass, accompanied by a 1.5m projection louvre and a blind with low reflectivity slats, achieving 2295 discomfort hours.

The compilation of data in this table underscores the critical role of selecting the appropriate combination of glazing type, WWR, external shading techniques, and internal blind types in achieving enhanced thermal performance and occupant comfort. These findings offer valuable guidance to architects and building designers, aiding them in making informed decisions for the design of building envelopes and window systems.

Considering this study, the WV7 window combination is selected for its optimal thermal performance, marking its integration into the proposed system combination in the subsequent section of this research. This expanded analysis not only heightens our understanding of the intricate interplay between these variables but also solidifies the importance of meticulous design considerations in optimising building thermal performance.

7.8 COMBINATION OF ENHANCED BUILDING ELEMENTS

This section converges the individual elements of walls, roofs, and windows, each meticulously selected for their superior thermal performance, into a cohesive system. The previous sections have laid the groundwork by isolating and examining the thermal efficiency of various proposed systems. Now, the focus shifts to integrating these optimal components into a unified scenario, aiming to significantly enhance the overall thermal performance of the houses while simultaneously reducing reliance on energy-intensive air conditioning systems.

The central aim of this research is twofold: firstly, to elevate the thermal comfort within the dwellings, and secondly, to minimise the total energy consumption, predominantly used for air conditioning, thereby reducing total discomfort hours across the year. This approach implies a decreased dependency on mechanical climate control systems during specific periods, contributing to energy savings and enhanced indoor comfort.

The culmination of this research is the formulation of a final optimised scenario, combining the best-performing systems from the prior analyses. This scenario represents a synthesis of elements that not only achieve minimal total discomfort hours but also embody the peak of thermal efficiency within the constraints of this study. Due to time limitations, multiple system combinations were explored, but only the most effective one, in terms of both thermal performance and discomfort hour reduction, has been extensively analysed and presented in this chapter.

A key metric in this final evaluation is the comparison of total energy consumption before and after implementing the optimised combination of building elements. The reduction in discomfort hours serves as an indirect assessment of decreased HVAC usage, thus implying a lower energy requirement for maintaining indoor thermal comfort. This analysis will shed light on the tangible benefits of integrating these optimised building elements, not only in terms of enhancing living conditions but also in contributing to more sustainable and energy-efficient building practices.

In essence, this section is not merely about combining various building elements; it represents the culmination of a comprehensive and methodical approach to developing an integrated solution that addresses both thermal comfort and energy efficiency in residential buildings. The results from this integrated approach are anticipated to offer valuable insights and guidelines for future construction projects, particularly those aimed at achieving high thermal performance in challenging climatic conditions.

By integrating optimal proposed systems that accomplish minimal total discomfort hours into one combined scenario, the goal of this research can be achieved: to improve the thermal performance (comfort) of the house as well as reduce total energy consumption across the three studied houses.

7.9 SELECTION OF OPTIMAL DESIGN

In the quest to enhance the thermal performance of residential buildings, a meticulous selection process was undertaken to identify the most effective combination of building elements. This process, detailed in Table 7.9, involved a comprehensive analysis of various proposed systems for walls, roofs, and windows. The primary criteria for selection were the systems' capabilities to significantly reduce the total annual discomfort hours and their efficacy in improving thermal comfort during both the summer and winter seasons.

Table 7.9: Conclusion for optimal systems selection.

Building Element	System Code	Description and Impact	Calculated Reduction in Discomfort Hours
Wall System	W-19	Exhibits the least annual total discomfort hours with a significant 12.4% reduction, offering enhanced thermal comfort.	12.4%
Roof System	R-7	Optimal thermal performance among roof systems, contributing to an 11% reduction in discomfort hours and optimising heat balance.	11%
Glazing System	WV-7	Achieves a 6.2% reduction in annual discomfort hours, with cost-effective design and enhanced daylight and ventilation features.	6.2%

7.9.1 JUSTIFICATIONS FOR SYSTEMS SELECTIONS

- Wall System (W-19): This system was meticulously chosen due to its unparalleled efficiency in reducing total discomfort hours throughout the year by 12.4%. Its integration into the building significantly elevates the thermal conditions within the primary living areas, ensuring enhanced comfort levels during both the hot summer months and the cold winter periods. The choice of this system confirms the early literature claiming that aerated concrete is a technique used for optimising the thermal performance and especially used for external walls. Also, as early mentioned within the literature review, the use of vacuum insulation panels exhibit a thermal conductivity that is 5 to 8 times lower than that of traditional thermal insulation materials (Ciobanu and Iacob, 2013). Hence, considering its low thermal conductivity, its contribution in improving the thermal performance is significant.

- Roof System (R-7): R-7 emerged as the leading candidate among the roofing options, demonstrating exceptional thermal performance. By facilitating an 11% reduction in total discomfort hours annually (a reduction of 268 hours per year), this system plays a pivotal role in harmonizing heat gains during summer with heat losses in winter. Such optimisation is instrumental in achieving a balanced and energy-efficient heat exchange for the residence.
- Glazing System (WV-7): The selection of WV7 was driven by multiple factors. Primarily, it stands out for minimising annual discomfort hours, indicating a 6.2% reduction. Additionally, the system's design, which includes an inner Micro Louvre and the absence of external shading devices, not only reduces construction costs but also enhances the building's aesthetic appeal. The increased WWR of 29% further enhances the entry of natural light and facilitates better ventilation, aligning with sustainable design principles. This confirms the importance of such high performance windows systems in hot climates as earlier discussed by Alshenaif (2015) in the literature section of this research.

The combination of these selected elements – W19 for walls, R-7 for roofs, and WV7 for glazing – represents an integrated approach to achieving the goals of this research: improving the thermal performance and comfort of residential structures while simultaneously reducing the reliance on energy-intensive HVAC systems. The implementation of this strategically optimised combination marks a significant advancement in the design of energy-efficient and comfortable living spaces.

7.10 HOUSE 1-J OPTIMISED THERMAL PERFORMANCE ANALYSIS

The subsequent section presents a comprehensive thermal performance analysis, synthesising a combination of the optimal scenarios previously examined. This integrated approach offers a holistic view of the potential improvements and overall efficacy of the proposed solutions in enhancing the thermal performance of prefabricated houses.

7.10.1 TEMPERATURE AND RELATIVE HUMIDITY

The dataset under examination provides a comprehensive and rigorous exploration of the comparative thermal performance between existing and optimised building elements. The optimisation process, which represents a significant evolution in residential thermal performance, has been facilitated by the incorporation of superior, high-performance components. These include specifically enhanced walls, roofing, and windows, each contributing to a marked enhancement in thermal efficiency.

The analytical focus of this research is the year-long thermal performance within two key zones of a standard prefabricated (precast) house: the living room and the bedroom. These zones were selected due to their centrality in daily residential activities and their consequential exposure to varying thermal demands. By investigating these areas over an annual cycle, the study aims to offer a nuanced understanding of how optimised building elements influence thermal comfort, thereby elucidating the long-term implications of these modifications on the overall comfort and energy efficiency within prefabricated housing.

As illustrated in Figure 7.2, the operative temperatures in these zones have a close linkage to the outdoor conditions. The thermal profiles for both the existing and optimised building elements exhibit a pattern that mirrors the existing pattern of the external dry-bulb temperature over a calendar year. While this link is a predictable attribute of building design, its impact on interior temperatures can be moderated through detailed building elements and the adoption of state-of-the-art materials, as demonstrated in the optimised scenario. Comparing the operative temperatures in the optimised scenario with the existing elements, it is observed that the existing scenario maintains a consistently higher level throughout the year in both the living room and the bedroom. This indicates a more effective thermal performance, expected due to the enhanced insulation properties of the optimised building elements.

The benefits of this optimisation are most prominent during the colder months (January, February, and December), when the temperatures achieved with the optimised building elements considerably surpass those of the existing elements. This advancement, considering naturally ventilated building, could potentially result in a significant reduction in reliance on mechanical or electrical heating systems, thereby promoting energy conservation and financial savings.

Furthermore, it is notable that the temperatures achieved with the optimised building elements in both the living room and the bedroom demonstrate a smaller range of fluctuation compared to those with the existing elements. This diminished variability suggests a more stable and evenly distributed thermal performance throughout the building subsequent to the integration of optimised elements. Such uniform temperature distribution could be deemed advantageous for overall occupant comfort.

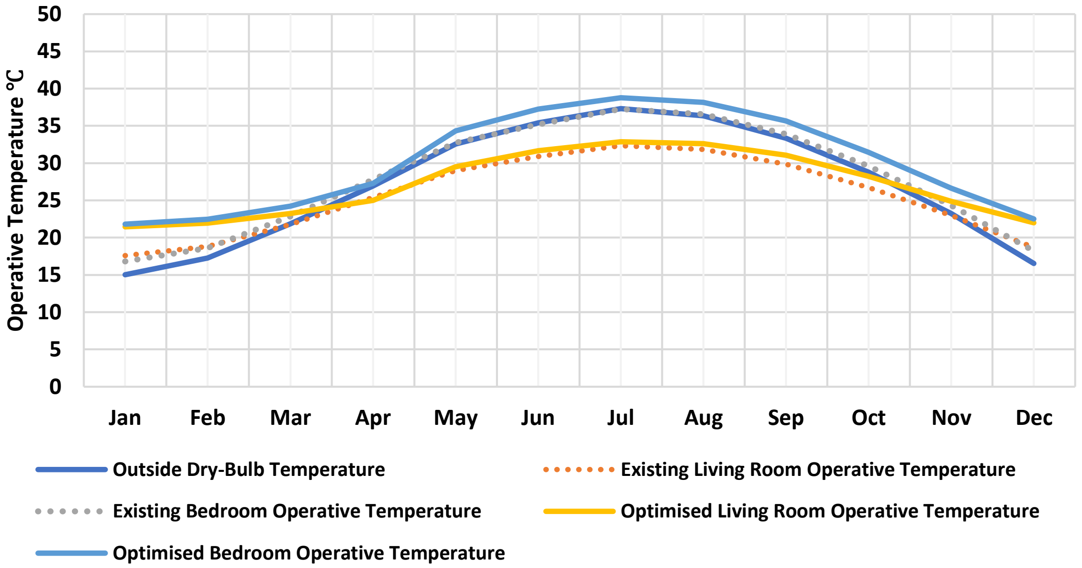

Figure 7.2:Optimised monthly average temperature. Data were gathered using DesignBuilder software.

Nevertheless, it is crucial to approach these findings with circumspection. While the enhanced insulation could diminish heating requirements during colder months, it might conversely result in elevated temperatures during the summer months, as proved by Al-Sanea et al. (2012). Evidently, the zones with optimised building elements exhibit a slight rise in temperatures during these periods, which could culminate in thermal discomfort. This underscores the norm, which is the need for active cooling requirements to ensure a balanced building design in extremely hot conditions, striving for improved thermal performance without compromising occupant comfort during the summer peak.

Accordingly, this primary analysis emphasises the potential benefits of integrating the proposed building elements, as evidenced by the optimised thermal performance. Concurrently, it underscores the potential challenges associated with ensuring year-round comfort in such harsh environments. The essence of effective building design lies in striking an optimal balance between thermal performance and comfort, considering the specific local climatic conditions (both extreme hot and cold climates). Hence, this data-driven analysis is an indispensable step towards achieving this balance.

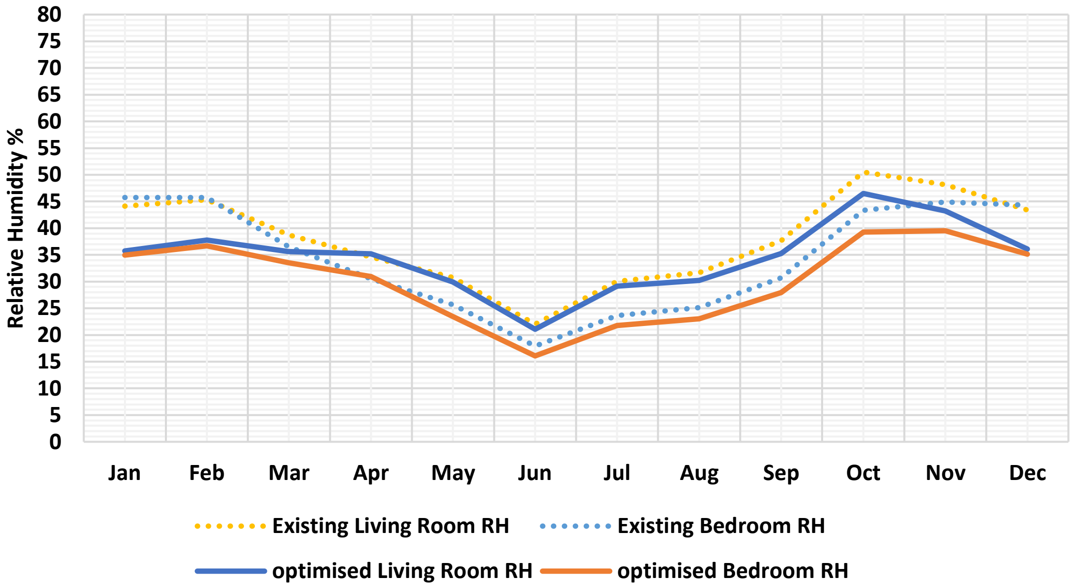

Figure 7.3: Optimised monthly average relative humidity. Data were gathered using DesignBuilder software.

Figure 7,3 illustrates a comparison of the relative humidity (RH) between the existing and optimised building elements in a living room and a bedroom throughout the year. It is observable that the RH in these zones is likely influenced by outdoor conditions, similar to the operative temperatures discussed previously. The RH profiles of both the existing and optimised scenarios demonstrate seasonal trends, which indicates an interaction between the building design and climatic conditions. Moreover, across both zones, the optimised scenario consistently demonstrates lower RH than the existing scenario throughout the year. This suggests a more efficient control over the moisture levels within these areas, feasibly attributable to the superior humidity regulation properties of the optimised building elements as claimed by Martínez-Molina et al. (2016).

The impact of this optimisation is particularly notable during the months of high humidity (September, October, and November), where the RH in the optimised scenario is noticeably lower than in the existing base case scenario. This outcome could potentially contribute to a more comfortable indoor environment by mitigating the potential for mould growth and other humidity-related issues as also claimed by Baughman and Arens (1996).

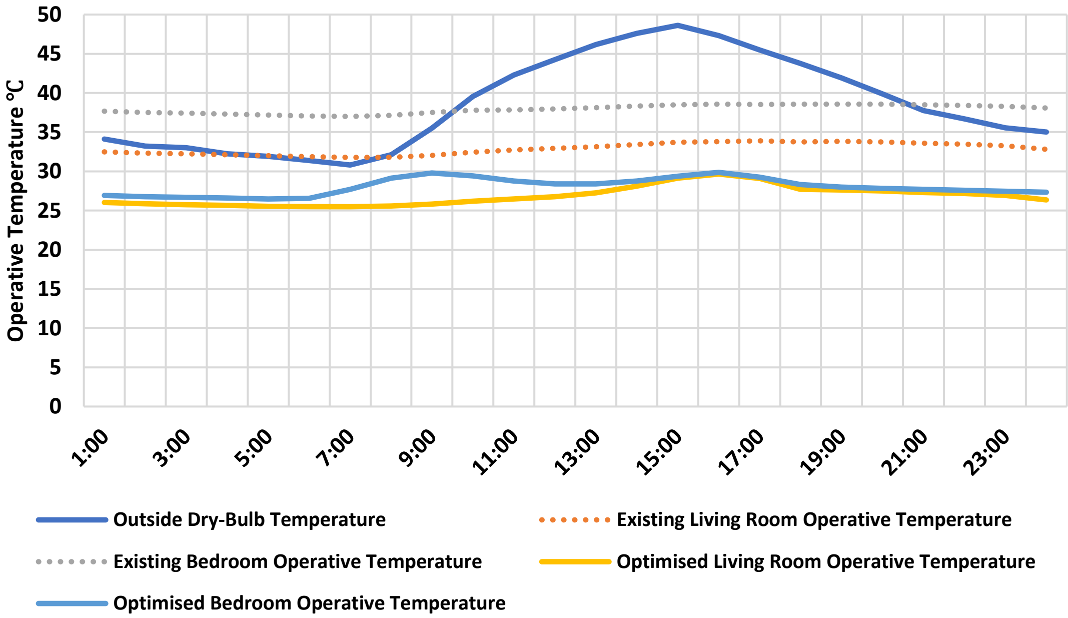

Figure 7.4: Optimised Hourly Temperature Recorded for a Typical Summer Day (24 July). Data were gathered using DesignBuilder software.

Figure 7.4 displays the hourly distribution of operative temperatures on a typical summer day, 24 July, comparing both existing and optimised building elements for a living room and a bedroom. As previously mentioned, the optimisation of these elements has been achieved using advanced building components, such as enhanced walls, roofing, and windows. In the existing scenario, the operative temperature in the bedroom is alarmingly high during the day, particularly reaching 38.6°C between 3 p.m. and 9 p.m. Such elevated temperatures are likely to cause severe discomfort and may demand extensive cooling, leading to increased energy consumption.

On the other hand, the operative temperatures in the optimised scenario remain notably lower throughout the day in both the living room and bedroom. The peak temperature in the optimised living room is recorded at 29.7°C at 4 p.m., while in the optimised bedroom, it reaches 29.9°C at the same time. This reflects a substantial improvement in thermal performance over the existing building elements, indicative of the enhanced insulation and heat dissipation capabilities of the optimised components.

Additionally, it is important to note the noticeable temperature fluctuation in the optimised bedroom during the morning hours. The temperature here rises from 26.6°C at 6:00 a.m. to a peak of 29.8°C at 9:00 a.m., then decreases to 28.4°C at 12:00 p.m. before ascending again in the afternoon. This fluctuation, although within an acceptable comfort range, may be due to significant solar heat gain through the roof during these hours. Thus, the detailed analysis indicates that the use of advanced building components in the optimised scenario substantially enhances thermal performance during a peak summer day, maintaining lower operative temperatures compared to the existing building elements. This underscores the potential benefits of material optimisation in contributing to energy efficiency and improved comfort.

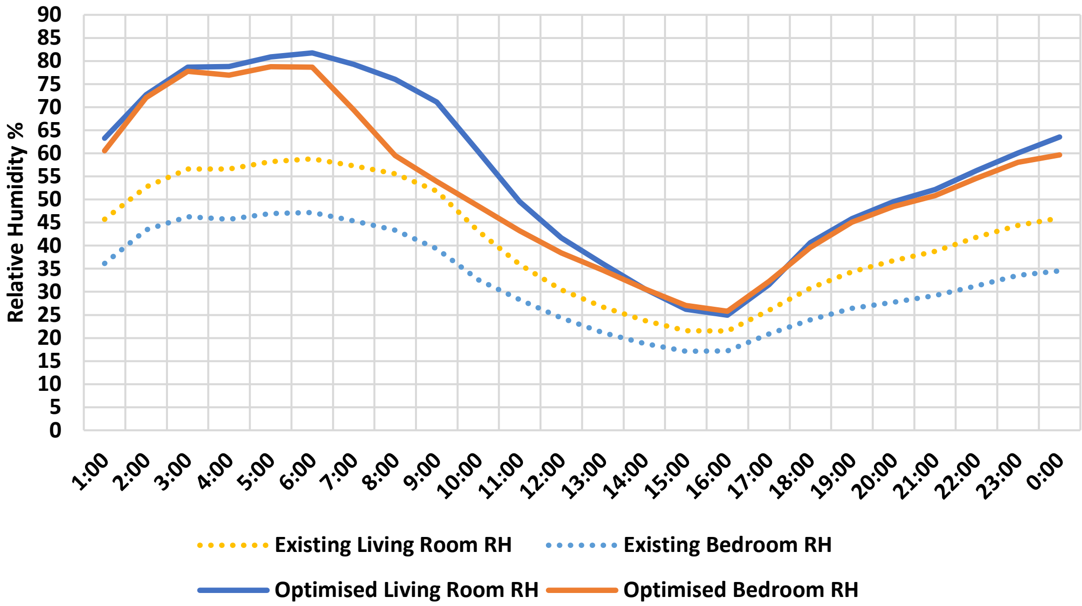

Figure 7.5: Optimised hourly relative humidity recorded for a typical Summer Day (24 July). Data were gathered using DesignBuilder software.

Figure 7.5 presents the relative humidity (RH) for a living room and bedroom in both existing and optimised building scenarios on a typical summer day, 24 July. It is generally observed that the relative humidity exhibits an inverse relationship to the outside dry-bulb temperature; that is, relative humidity increases as temperature decreases, and vice versa.

In the existing living room scenario, the highest relative humidity is recorded at 58.8% at 6:00 a.m., coinciding with the early morning when temperatures are at their lowest. Similarly, the peak relative humidity in the existing bedroom scenario is 47.2% at 6:00 am. It is notable that both of these values fall within the generally accepted comfort zone of 30-60% relative humidity, which is conducive to human comfort. In contrast, the optimised scenario shows higher overall relative humidity levels throughout the day, which could be attributed to better insulation and air tightness of the optimised building components. The peak relative humidity in the optimised living room and bedroom are 81.8% at 6:00 a.m. and 78.7% at 6:00 a.m., respectively.

Additionally, the optimised bedroom demonstrates a considerable decrease in relative humidity from 78.7% at 6:00 am to 59.5% at 8:00 a.m., possibly due to increased ventilation within the upper floor level. Nevertheless, the relative humidity remains within a comfortable range for most of the day.

The hourly analysis indicates that while optimised building elements can achieve lower operative temperatures, they may also result in higher relative humidity levels. This underscores that although advanced building components can significantly enhance thermal comfort, a comprehensive approach is necessary to maintain a balance of both temperature and humidity. Attention must be directed to the potential risk of increased relative humidity, which might necessitate mitigation measures such as adequate ventilation or dehumidification strategies as indicated by Sudhakar et al. (2019).

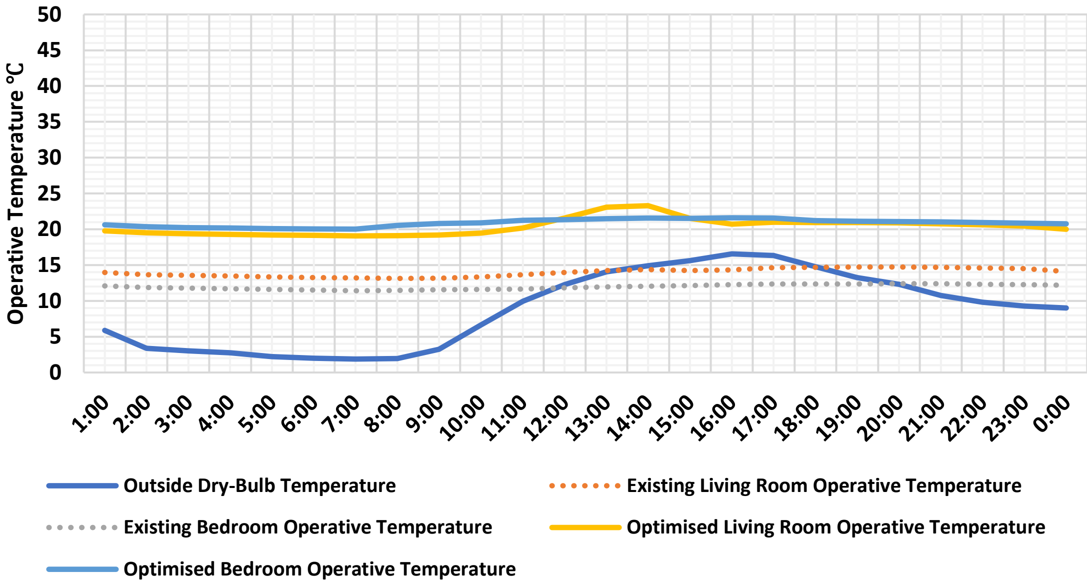

Figure 7.6: Optimised hourly temperature recorded for a typical winter Day (23 January). Data were gathered using DesignBuilder software.

Figure 7.6 illustrates hourly temperature readings for a typical winter day, 23 January, for both existing and optimised zones. Beginning with the existing building elements scenario, the operative temperature in the living room varies from 13.1°C at 8:00 a.m. to 14.7°C at 9:00 p.m. and 10:00 p.m., and from 7:00 p.m. to 8:00 p.m. The bedroom temperatures display a narrower range, with the lowest being 11.4°C at 7:00 a.m. and the highest 12.4°C at 6:00 p.m., 8:00 p.m., and 9:00 p.m. These temperatures are reasonably higher than the outside dry-bulb temperature, which ranges from 1.9°C at 7:00 a.m. and 8:00 a.m. to 16.6°C at 4:00 p.m. However, this can be attributed to the existing insulation in the building elements and poor ventilation, which do not maintain a comfortable indoor operative temperature compared to the outdoor levels.

In contrast, the optimised building elements scenario presents a more favourable setting during winter. The operative temperature in the optimised living room varies from 19.1°C at 6:00 a.m., 7:00 a.m., and 8:00 a.m. to 23.3°C at 2:00 p.m. Meanwhile, the operative temperature in the optimised bedroom ranges from 20.0°C at 6:00 a.m. to 21.6°C at 2:00 p.m., 3:00 p.m., and 4:00 p.m. Despite the coldest day of the year, the optimised building elements noticeably maintain a relatively warm and comfortable environment, well adjacent to the typical comfort threshold.

Interestingly, both the optimised living room and bedroom show a remarkable increase in operative temperatures during the day. Also, during the time when the outdoor temperature begins to rise, both zones remain constant in value, which clearly demonstrates the optimised building elements' thermal performance. Therefore, this analysis affirms the effectiveness of the optimised building elements in enhancing thermal performance during winter.

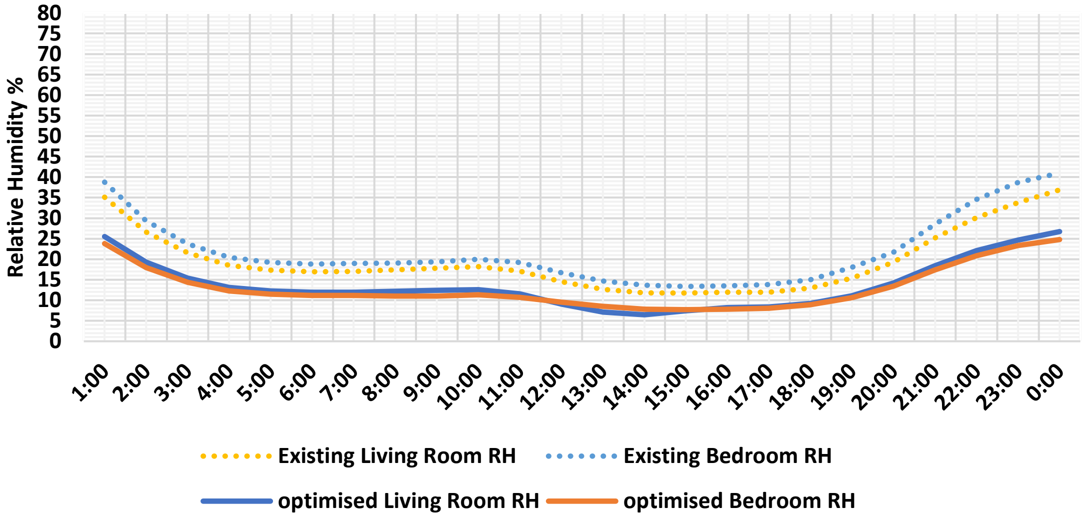

Figure 7.7: Optimised hourly relative humidity recorded for a typical winter day (23 January). Data were gathered using DesignBuilder software.

Figure 7.7 shows the optimised hourly relative humidity (RH) analysis recorded for a typical winter day, the 23 January, which provides important insights into the impact of optimised building elements on indoor humidity levels. Interestingly, the optimisation appears to have led to a reduction in RH compared to the existing scenario, despite the relatively low RH levels.

In the existing scenario, the RH in the living room ranges from a minimum of 11.8% at 2:00 p.m. to a maximum of 36.9% at 12:00 a.m. Bedroom RH fluctuates between 13.4% at 3:00 p.m. to a maximum of 41.0% at 12:00 a.m. Although these levels span a wide range, they fall within the generally accepted comfort range for most individuals. After the implementation of optimised building elements, there is a noticeable decrease in RH. The optimised living room RH varies between 6.5% at 2:00 p.m. and 26.7% at 12:00 a.m., while the optimised bedroom RH ranges from 7.7% at 3:00 p.m. to 24.8% at 12:00 a.m. This indicates that the optimised elements contribute to a further reduction in RH, even from the already low levels observed in the existing scenario.

This significant reduction in RH under the optimised scenario is notable, particularly given the initial RH was not excessively high. Typically, one would expect that optimisation of building elements would be more focused on decreasing high RH levels in indoor environments. However, the data indicates that other factors, possibly the increased airtightness of the optimised building elements, have contributed to this further reduction in RH.

7.10.2 PREDICTED PERCENTAGE OF DISSATISFIED (PPD) ANALYSIS

The data presented in Figure 7.8 outlines the Predicted Percentage Dissatisfied (PPD) for both existing and optimised scenarios in two distinct zones—the living room and bedroom—throughout the year. As previously mentioned, the PPD index, developed by Povl Ole Fanger, is a widely accepted thermal comfort metric used to estimate the percentage of people likely to be dissatisfied with a given thermal environment. In this analysis, a higher PPD value indicates a higher percentage of occupants who are likely to be dissatisfied within the indoor thermal comfort conditions.

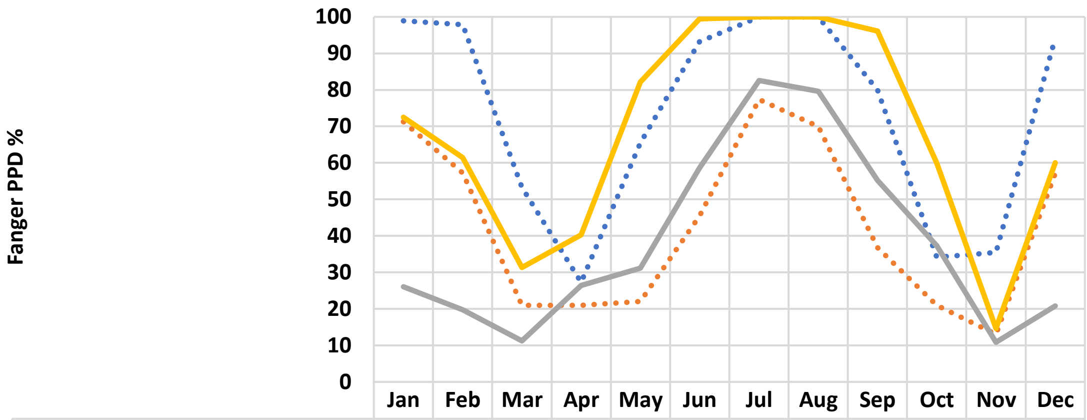

	Jan	Feb	Mar	Apr	May	Jun	Jul	Aug	Sep	Oct	Nov	Dec
Existing Living Room Fanger PPD	71.3	57.2	20.9	21.0	22.0	45.5	77.4	70.0	36.7	21.0	13.0	57.1
Existing Bedroom Fanger PPD	98.9	97.8	53.2	27.3	65.5	93.2	100.0	100.0	80.0	34.1	35.4	94.2
Optimised Living Room Fanger PPD	26.1	19.8	11.2	26.4	31.1	58.6	82.6	79.6	55.2	37.3	10.9	20.8
Optimised Bedroom Fanger PPD	72.5	61.5	31.3	40.3	82.1	99.5	100.0	100.0	96.1	60.0	14.6	60.1

Figure 7.8: Optimised living room and bedroom monthly averaged PPD. Data were gathered using DesignBuilder software.

For the existing base case scenario, PPD levels in both the living room and bedroom peak during the summer months, with July highlighting significant thermal discomfort. In the living room, the PPD reaches a high of 77.4%, while in the bedroom, dissatisfaction is absolute, with a PPD of 100%. This indicates that under existing conditions, thermal comfort during the summer months is notably challenging.

The optimised scenario presents a markedly different picture, with a dramatic decrease in PPD during the winter months. In the optimised living room, the PPD for January is reduced to 26.1%, indicating a reduction in dissatisfaction of more than 45%. Similarly, in the bedroom, the PPD decreases to 72.5% in January—a significant decrease of over 26% from the existing condition. Although there is a slight increase in PPD during the summer in the optimised scenario, particularly in the living room, the values do not diverge drastically from those in the existing configuration. This marginal increase in summer PPD could be considered a trade-off for the substantial improvements in thermal comfort experienced during the winter. Notably, the optimised living room's summer PPD peaks at 82.6% in July, which is only 5.2 percentage points higher than the existing scenario.

Accordingly, the optimised building scenario offers considerable benefits, particularly during the winter months, contributing to improved occupant comfort and potential energy savings. While the average summer PPD levels are slightly elevated, they remain within a range comparable to existing conditions, suggesting that the advantages of winter improvements likely outweigh the summer trade-offs.

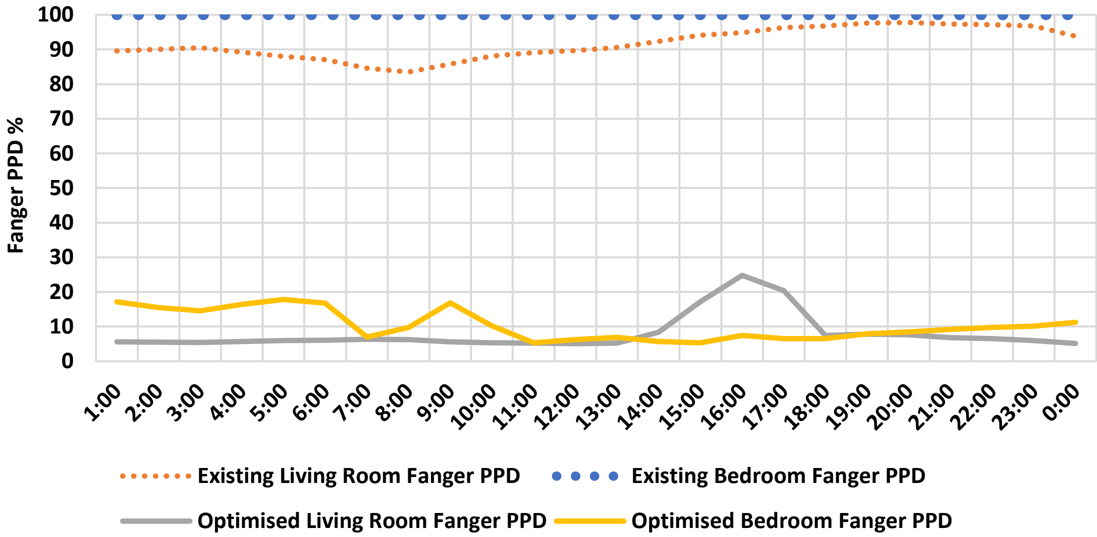

Figure 7.9: Optimised living room and bedroom hourly averaged PPD for typical summer day (24 July). Data were gathered using DesignBuilder software.

Moreover, when comparing the Predicted Percentage Dissatisfied (PPD) values between the existing and optimised scenarios over a typical summer day, 24 July, as shown in Figure 7.9, there is a significant shift towards increased comfort in the optimised scenario. The benefits of such improvements extend beyond merely enhancing occupant comfort to potential energy savings, as the need for cooling might be reduced under optimised conditions.

In the existing scenario, the living room records consistently high levels of dissatisfaction throughout the day, with PPD values hovering around 90% for most hours and reaching a peak of 97.8% at 8:00 p.m. The bedroom exhibits an even more severe level of discomfort, with a sustained PPD of 100% throughout the day, suggesting that occupants would likely feel extremely uncomfortable, potentially leading to a heavy reliance on cooling appliances.

In contrast, the optimised scenario demonstrates a significant reduction in PPD values, indicating substantially improved thermal comfort conditions. The PPD in the optimised living room starts as low as 5.38% at 3:00 a.m. and remains within a comfortable range for the entirety of the day, peaking at only 24.8% at 4:00 p.m. This is a marked decrease in discomfort when compared to the existing scenario. Additionally, the bedroom's PPD in the optimised scenario follows a similar pattern, with the lowest value being 5.3% at 11:00 a.m., and while there is an increase towards the later hours, it only peaks at 17.2% at 1:00 a.m., representing a drastic improvement from the existing conditions where extreme discomfort would have been likely throughout the day.

The data indicates that the optimised building elements significantly enhance occupant comfort on a typical summer day, potentially reducing the dependence on active cooling strategies. Lower levels of thermal dissatisfaction imply that occupants are less likely to rely on energy-intensive cooling methods, promoting potential energy savings and aligning with sustainable building practices.

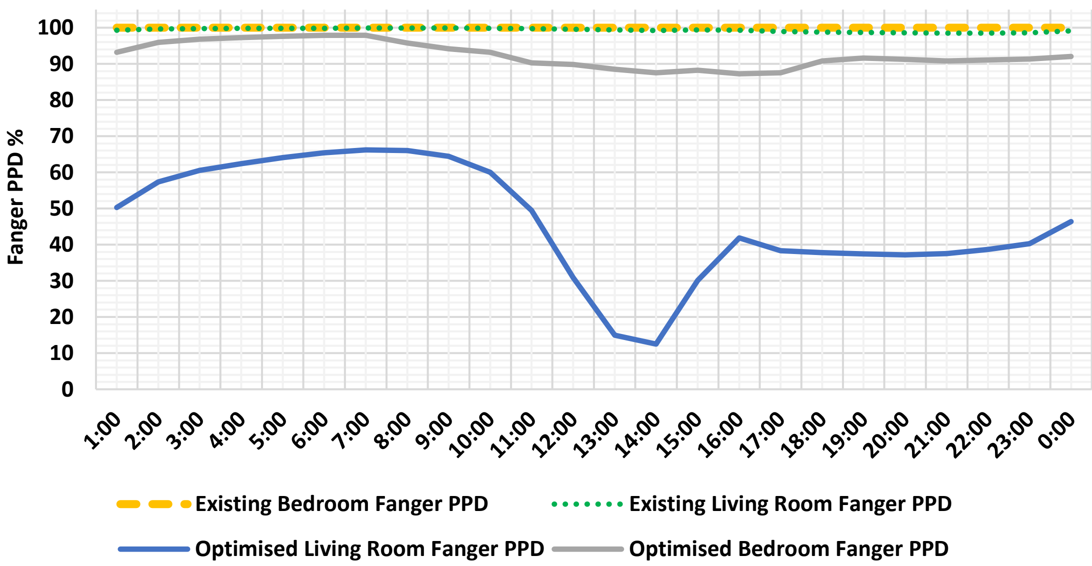

Figure 7.10: Optimised living room and bedroom hourly averaged PPD recorded for typical winter day (23 January). Data were gathered using DesignBuilder software.

Figure 7.10 provides a comparative analysis of the PPD values for both the existing and optimised scenarios over a typical winter day, 23 January. Although the optimised scenario does not eliminate discomfort, it does introduce significant reductions, indicating potential benefits for both energy consumption and occupant thermal comfort. Hence, in the existing scenario, the living room and bedroom both demonstrate severe discomfort throughout the day. The living room's PPD peaks at 100% for most of the day.

Similarly, the bedroom maintains a PPD of 100% across all hours. This extremely high level of dissatisfaction implies that occupants would likely be dependent on heating appliances throughout the day, leading to increased energy consumption and costs. Conversely, the optimised scenario shows a marked improvement in occupant comfort. The living room's PPD starts at 50.3% at 1:00 a.m. and reaches a peak of 66.2% at 7:00 a.m. By midday, the PPD significantly decreases, dropping to as low as 12.5% at 2:00 p.m. Despite a slight increase in the later hours, the PPD remains substantially lower than that of the existing scenario.

The optimised bedroom's PPD indicates a less pronounced but still noticeable improvement over the existing conditions. PPD values in the optimised bedroom stay in the mid-90s for most of the day, with the lowest recorded at 87.2% at 5:00 p.m. Although these values are still high, they suggest a reduced load on heating appliances compared to the existing scenario. Overall, while the optimised scenario does not completely resolve thermal discomfort on a typical winter day, it mitigates the extremes of discomfort found in the existing scenario. These improvements are significant for the occupants' thermal comfort and could potentially reduce the need for energy-intensive heating solutions.

7.10.3 CALCULATED DISCOMFORT HOURS

The monthly discomfort hours for existing and optimised zones reveal substantial improvements in thermal comfort due to the optimisation of building elements, as shown in Figure 7.11. For the existing living room zone, the total discomfort hours for the year amount to 1,810. In contrast, the optimised living room shows a significant reduction to a total of 1,348 hours, demonstrating a decrease of about 25%. This reduction suggests that the optimised scenario leads to an increased level of thermal comfort, which is a considerable benefit, especially in a naturally ventilated environment where maintaining comfort can be challenging due to fluctuating outdoor conditions. Similarly, for the bedroom zone, the total annual discomfort hours in the existing scenario are alarmingly high at 3,205 hours. However, with optimised building elements, this total is reduced to 2,406 hours, representing an impressive 25% decrease in discomfort. These results reiterate the effectiveness of optimisation in reducing discomfort hours and thus enhancing the living conditions within the house.

Upon closer examination of the monthly discomfort hours, it is evident that optimisation has the most significant impact during the winter months, such as January. In the existing living room, discomfort hours are high at 204 hours for January, whereas in the optimised scenario, this figure is drastically reduced to just 32 hours. This vast reduction during the colder months implies that optimisation effectively improves the building's thermal performance and, consequently, the occupants' comfort.

Moreover, optimisation proves highly beneficial during transitional months like April and October, when heating or cooling demands are typically lower, but discomfort can still occur due to fluctuating conditions. The discomfort hours during these months are considerably reduced in the optimised zones, further demonstrating the advantages of optimised building elements. However, even in the optimised scenario, substantial discomfort hours persist during the summer months, indicating that the need for active or passive cooling systems remains essential in extremely hot environmental conditions.

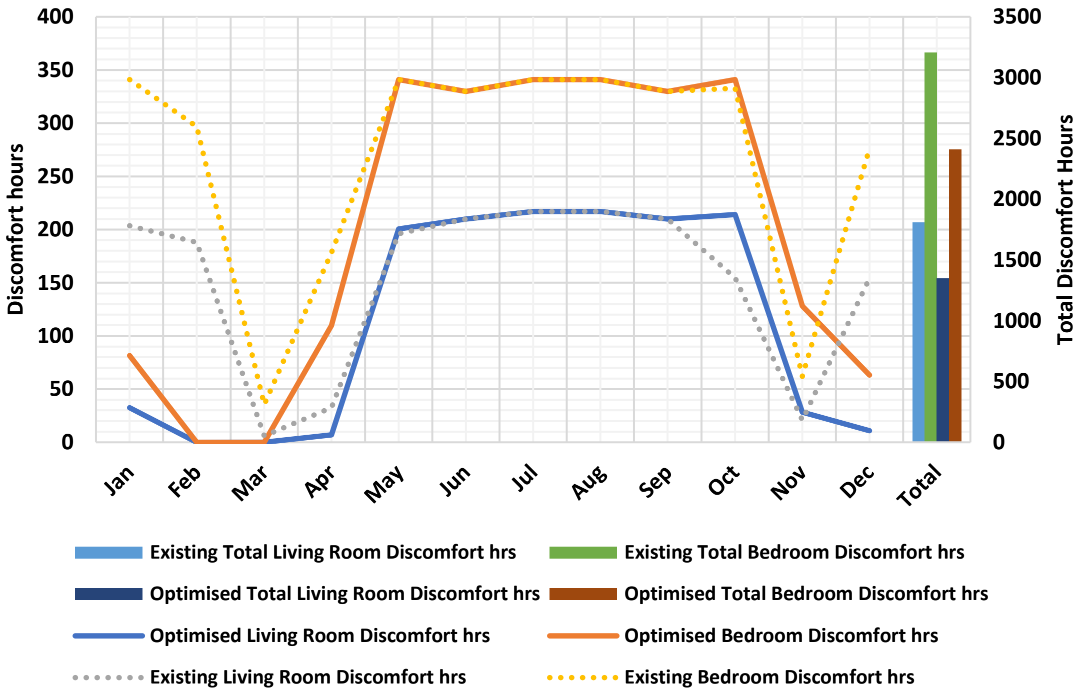

Figure 7.11: House 1-J existing and optimised zones monthly discomfort hours. Data were gathered using DesignBuilder software.

The detailed evaluation of discomfort hours provides insightful revelations into the efficacy of building optimisation. Specifically, the optimisation yields a marked decrease in the number of hours occupants experience thermal discomfort, as evidenced by a 25% reduction in both living and bedroom areas over the course of the year. This improvement is particularly pronounced during the colder months, with January displaying a dramatic decline in discomfort hours from 204 to 32 in the living room, exemplifying the enhanced insulation and thermal performance of the optimised elements. However, the data also brings to light the limitations of optimisation alone in addressing summer discomfort, emphasising the essential role of cooling systems to maintain comfort in peak heat conditions. These insights are crucial for informing strategies to achieve a year-round thermally comfortable and energy-efficient living environment.

7.10.4 SUMMER DAY HEAT BALANCE

The comparison of summer day heat balances in both existing and optimised living room scenarios on a typical summer day (24 July) exemplifies the impact of building element optimisation on the variation of heat gains and losses. Indicated in Figure 7.12, the optimised scenario highlights a marked improvement in heat gain/loss balance over the existing conditions, primarily attributed to the integration of phase change materials (PCMs).

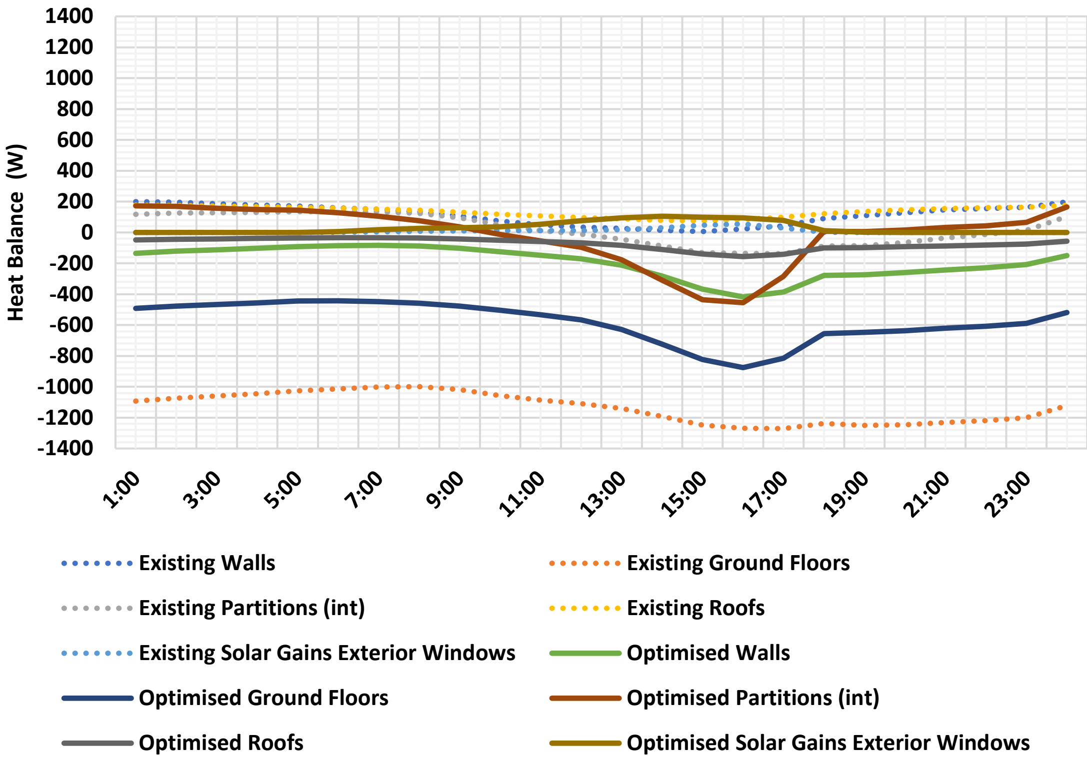

Figure 7.12: Existing and optimised living room's summer day heat balance breakdown on a typical summer day (24 July). Data were gathered using DesignBuilder software.

PCMs are adept at absorbing and releasing thermal energy as they oscillate between solid and liquid states, functioning as latent heat storage (LHS) systems. During the heat absorption phase, a PCM transitions from a solid to a liquid state, sequestering energy which is then released back into the living space as it solidifies, coinciding with a drop in ambient temperatures.

In the existing scenario, the walls start with a considerable heat gain of 200 W at 1:00 a.m., which then decreases to 6 W by 3:00 p.m., before rising back to 160 W at 11:00 p.m. Ground floors show a significant heat loss early in the morning at -1094 W, peaking at -1271 W at 5:00 p.m., highlighting a substantial energy loss. Internal partitions exhibit a shift from gaining heat to losing it from 11:00 a.m. onwards, while solar gains through exterior windows consistently influence the space from the early hours until the late afternoon (6:00 a.m. to 4:00 p.m.).

The optimised scenario presents a different dynamic, reflecting better control over both heat gain and loss. Moreover, the heat loss from the optimised elements is primarily associated with the performance of PCMs. Accordingly, the optimised walls show a steady heat loss from -135 W (1:00 a.m.) to -417 W (4:00 p.m.) before decreasing to -209 W (11:00 p.m.). Despite this apparent disadvantage, it has the positive effect of absorbing excessive heat, potentially preventing overheating within the living area. The ground floors within the optimised scenario undergo heat loss throughout the day, peaking at -875 W (4:00 p.m.), again aiding in the absorption of excess heat.

For internal partitions, the optimised design achieves a heat gain that persists until 9:00 a.m., after which it reverses to a loss, contributing to the thermal balance. Enhanced solar gains through exterior windows, starting at 5.5 W at 6:00 a.m. and peaking at 105 W at 2:00 p.m., underscore an effective use of passive solar heat gain, a feature particularly beneficial during the colder seasons.

Through a critical lens, it is apparent that the optimised scenario offers superior control over both heat gains and losses. While increased heat loss may initially appear detrimental, in this context, it aids in controlling the accumulation of excess heat within the living room during the hottest summer day. Also, by absorbing excessive stored heat, it contributes towards maintaining thermal comfort and increasing the building's overall thermal performance. Moreover, the heat loss might seem disadvantageous, the utilisation of PCMs transforms this phenomenon into a beneficial aspect. By absorbing excess heat, they prevent potential heat flow in the living room during peak temperature hours. This latent heat storage strategy allows the living room to maintain a more consistent and comfortable temperature range throughout the day, enhancing its thermal comfort and energy efficiency.

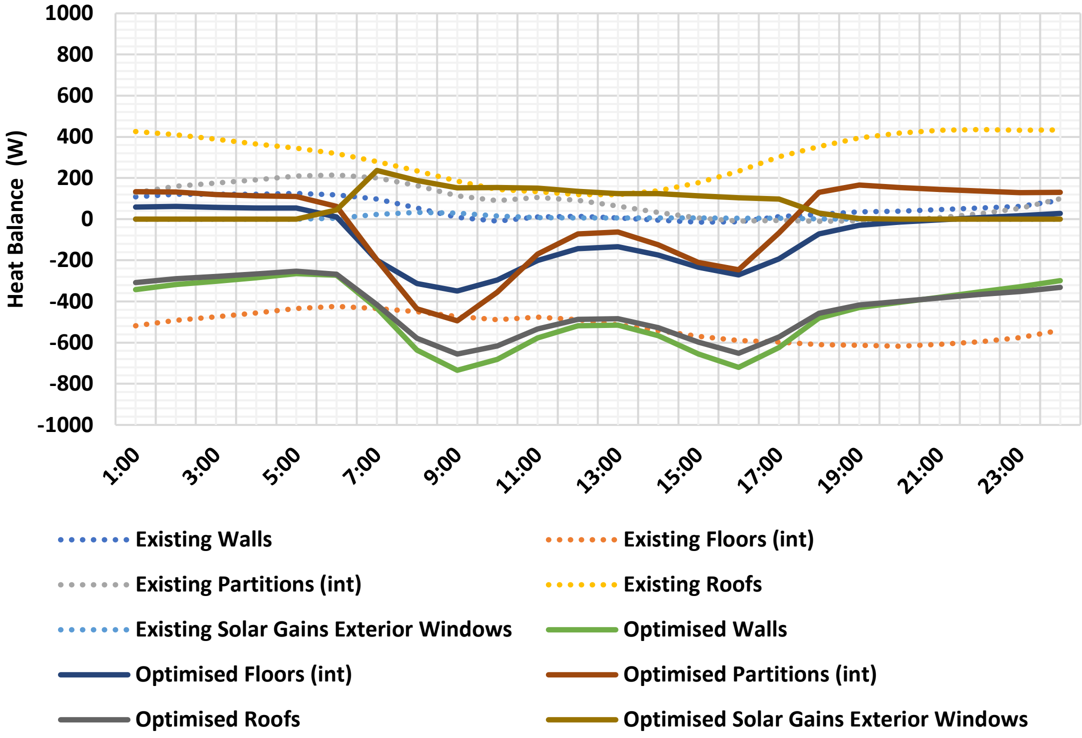

Figure 7.13: Existing and optimised master bedroom summer day heat balance breakdown. Typical summer day (24 July). Data were gathered using DesignBuilder software.

Figure 7.13 illustrates the heat balance for the existing and optimised Master Bedroom on a typical summer day, the 24th of July, providing an analytical understanding into the influence of phase change materials (PCMs) and optimised building elements on heat gain and loss.

In the existing scenario, heat gain is predominantly sourced from the walls, internal floors, internal partitions, and roofs, with the roofs peaking at a heat gain of 435 W at 10:00 p.m. Additionally, moderate solar gains through exterior windows are noted during daylight hours. Conversely, the internal floors exhibit a pronounced heat loss, with a maximum of -617 W at 8:00 p.m., revealing significant energy loss from the bedroom.

In contrast, the optimised scenario illustrates the effective placement of PCMs within the master bedroom. Optimised walls, floors, partitions, and roofs predominantly display heat loss throughout the day, signifying efficient heat absorption by PCMs. The most substantial heat loss occurs at the walls, reaching -720 W at 4:00 p.m., and at the optimised roofs, with a peak of -651 W, also at 4:00 p.m. These heat losses are advantageous as they represent the thermal energy being stored within the PCMs during peak heat, mitigating the risk of overheating.

Furthermore, the optimised floors show less noticeable heat loss, peaking at -200 W at 7:00 a.m., as they absorb the morning's warmth. The internal partitions also contribute to thermal regulation, with a notable heat loss of -246 W at 4:00 p.m., demonstrating the comprehensive approach to improving the room's thermal performance. Notably, solar gains through the optimised exterior windows increase, with a peak gain of 236 W at 7:00 a.m., a benefit attributed to the enhanced WWR, which promises added advantages during the winter season.

The strategic incorporation of PCMs in the optimised Master Bedroom significantly refines the heat balance, with pronounced heat losses during daylight reflecting the PCMs' heat absorption. This heat is later released as temperatures decline, preventing overheating and maintaining a comfortable thermal environment. This sensible balance of heat absorption and release, along with solar gains, underscores the potential of advanced construction materials and design strategies to boost thermal comfort and energy efficiency within modern prefabricated buildings.

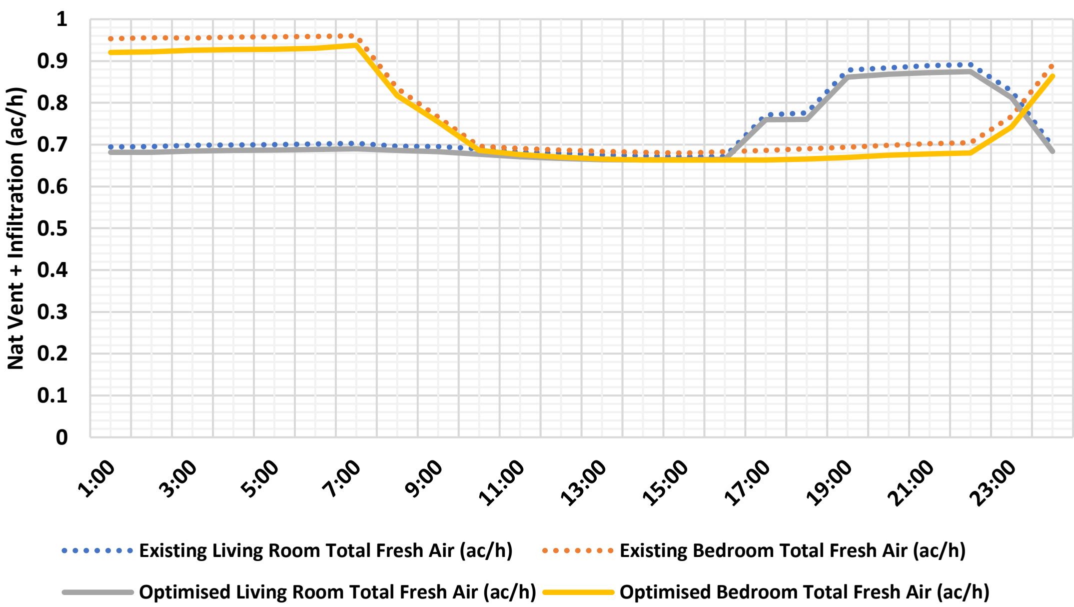

Figure 7.14: Existing and optimised living room and bedroom total fresh air for summer day (24 July). Data were gathered using DesignBuilder software.

Figure 7.14 presents a comparison of the total fresh air rates in both the living room and bedroom under existing and optimised conditions during a typical summer day, 24 July. The data suggests nominal differences between the two scenarios, indicating that the design optimisations implemented, which may include alterations to the WWR, have not markedly impacted natural ventilation rates.

In the existing scenario, the living room experiences airflow variations from 0.67 to 0.89 air changes per hour (ac/h), and the bedroom from 0.68 to 0.96 ac/h. These figures fall within a range considered comfortable for residential spaces, ensuring adequate air exchange throughout the day. In contrast, the optimised scenario demonstrates a comparable airflow pattern, with the living room's airflow ranging from 0.66 to 0.87 ac/h, and the bedrooms from 0.66 to 0.93 ac/h. Despite slight variations, these adjustments in airflow rates are minor and maintain the original pattern of air circulation.

Thus, this consistency in airflow rates, despite optimisations, suggests that the building's natural ventilation mechanisms remain effectively preserved post-optimisation. It underscores the possibility of enhancing other aspects of building performance without compromising on ventilation—a critical component of indoor air quality and occupant comfort. The data from this day in summer reflects a balance between the need for fresh air and the requirements of maintaining a thermally comfortable environment, affirming the design's alignment with sustainable and comfortable indoor living conditions.

7.10.5 WINTER DAY HEAT BALANCE.

Figure 7.15 illustrates the heat balance in the living room of both existing and optimised scenarios on a typical winter day, 23 January, highlighting the enhancements achieved through optimisation. The integration of phase change materials (PCMs) plays a pivotal role in these improvements.

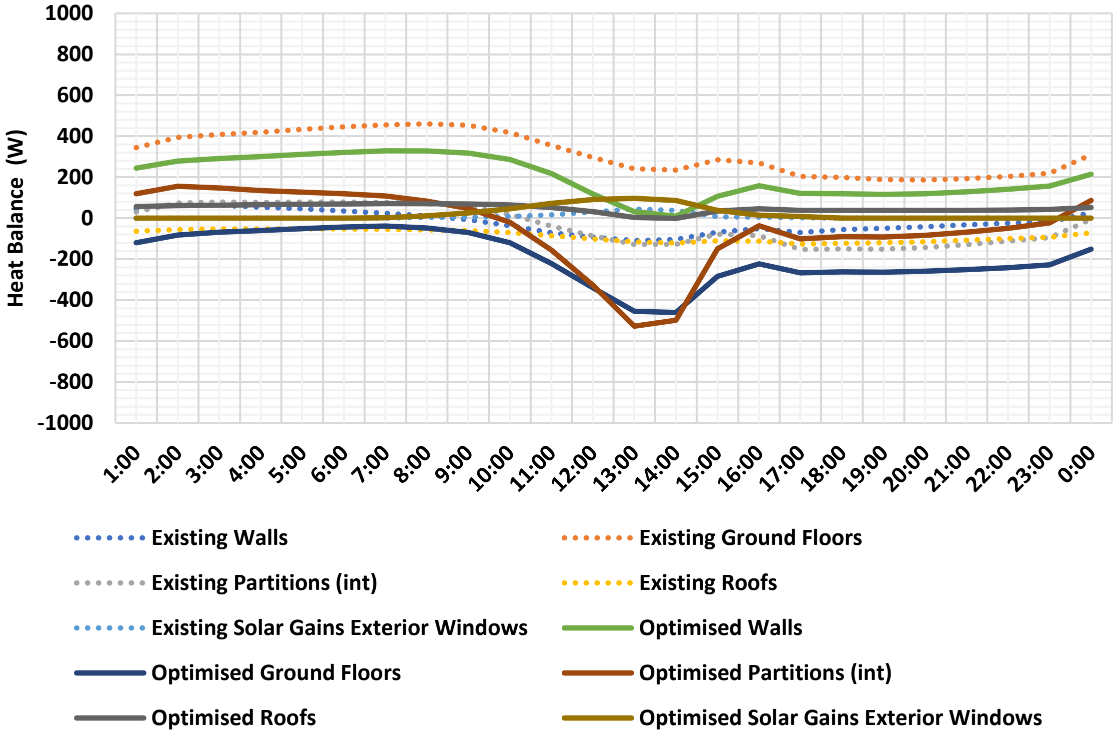

Figure 7.15: Both existing and optimised living room winter day heat balance breakdown on a typical winter day (23 January). Data were gathered using DesignBuilder software.

In the existing design, the walls start with a heat balance of 44 W at 1:00 a.m., narrowing to 27 W by midnight. After optimisation, the walls experience a notable increase in heat balance, indicating superior heat retention. This enhancement is attributed to the PCMs which absorb and store heat, thus slowing down the heat transfer through the walls and contributing to a warmer indoor environment.

The ground floors in the optimised scenario undergo a significant shift, suggesting a 'heat sink' effect where the PCMs incorporated within them absorb excess heat during the day and release it steadily, promoting a balanced indoor temperature over time. Furthermore, the partitions' heat balance in the optimised scenario demonstrates a notable improvement, maintaining more balanced values during the day that indicate a more effective thermal performance compared to the existing scenario state, where the partitions failed to regulate indoor temperatures efficiently.

Roof performance in the optimised scenario exhibits a marked improvement, shifting from consistently negative to predominantly positive values. This shift implies enhanced thermal performance, crucial during the winter months. Additionally, optimised solar gains through exterior windows are exploited more effectively, with positive values recorded from early morning to late afternoon (7:00 a.m. until 6:00 p.m.), indicating efficient use of solar energy. This captured energy is preserved within the building and gradually released, aiding in sustaining a comfortable interior temperature even after sunset, in stark contrast to the negligible solar gains in the existing scenario.

Overall, the optimised scenario reveals an advanced heat balance profile throughout the day, primarily due to the PCMs' ability to moderate interior temperatures by storing and then gradually releasing excess heat. This dynamic contributes to a more comfortable living environment and reduces the need for external heating sources, thereby enhancing energy efficiency and sustainability in residential environments.

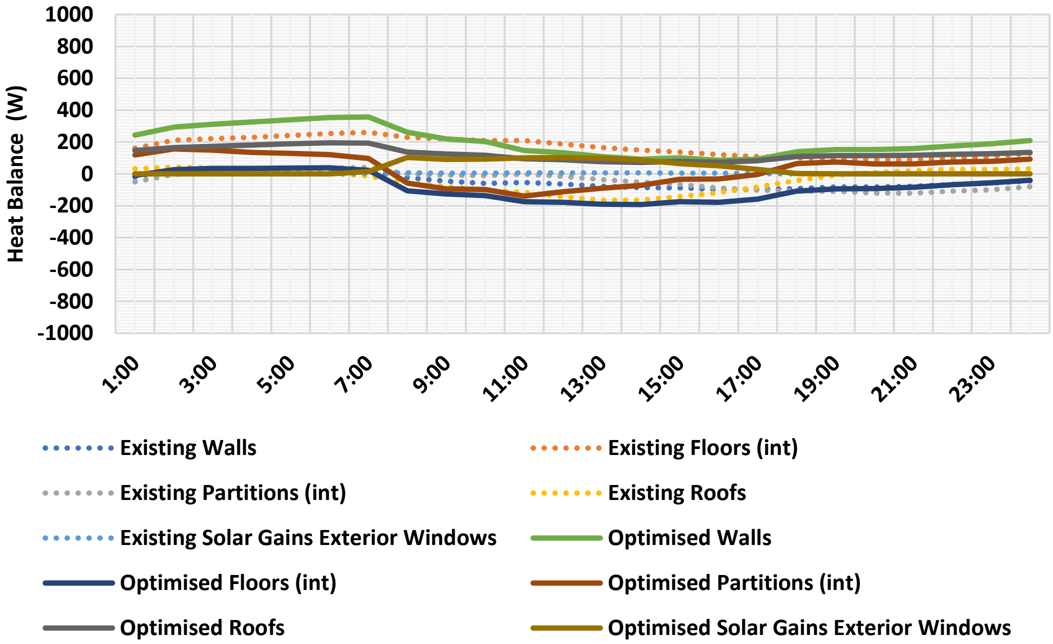

Figure 7.16: Both existing and optimised master bedroom winter day heat balance breakdown on a typical winter day (23 January). Data were gathered using DesignBuilder software.

Figure 7.16 demonstrates the heat balance for the master bedroom’s existing and optimised components on a typical winter day, 23 of January. The graph reveals a marked improvement in thermal preservation and regulation due to the integration of PCMs within the building fabric.

In the existing scenario, the walls start with a heat loss, indicating an initial heat balance of -20 W at 1:00 a.m., which signifies a loss of heat from the zone. In contrast, the optimised walls begin at an advantageous 243 W at the same hour, maintaining a positive heat balance throughout the day. This significant difference highlights the PCMs' effectiveness in enhancing wall insulation, thereby reducing heat loss, and contributing to a warmer indoor climate.

Additionally, moving to the interior floors, an interesting shift is noted from positive heat balance values in the existing scenario to negative values in the optimised model. This indicates that the optimised floors are functioning as a heat storage, absorbing excess heat during peak hours and releasing it slowly, contributing to a balanced indoor temperature and enhancing occupant comfort.

In the case of partitions, the optimised scenario shows a positive heat balance maintained throughout the day, denoting an enhanced, steady thermal environment. This outcome, coupled with brief periods of heat loss during the early morning, implies that the partitions suggest efficient heat absorption and release dynamics, facilitating a steady temperature within the room. It is enhanced with the optimised other components in the zone, absorb heat efficiently when it is abundant and subsequently release it slowly, regulating room temperature effectively.

Furthermore, the roofs in the optimised scenario exhibit a consistently improved heat balance compared to the existing scenario, reflecting improved insulation properties and the strategic use of PCMs to retain heat, which is particularly advantageous during the colder months.

Solar gains through exterior windows are significantly higher in the optimised scenario, with noticeable heating contributions from early morning, from 7:00 a.m. until the evening. This solar heat is effectively captured and stored, then slowly released, enhancing thermal comfort and reducing the need for additional heating, thereby optimising energy use. Conversely, the existing scenario shows minimal solar gains, underlining the optimised design's superior thermal performance.

Overall, the optimised master bedroom exhibits a superior thermal performance across various components, with notable thermal behaviour enhancements in the walls, partitions, roofs, and solar gains. Such advancements lead to a more thermally regulated environment, promoting occupant comfort and contributing to energy conservation during the winter months, highlighting the substantial benefits of utilising PCMs in building design.

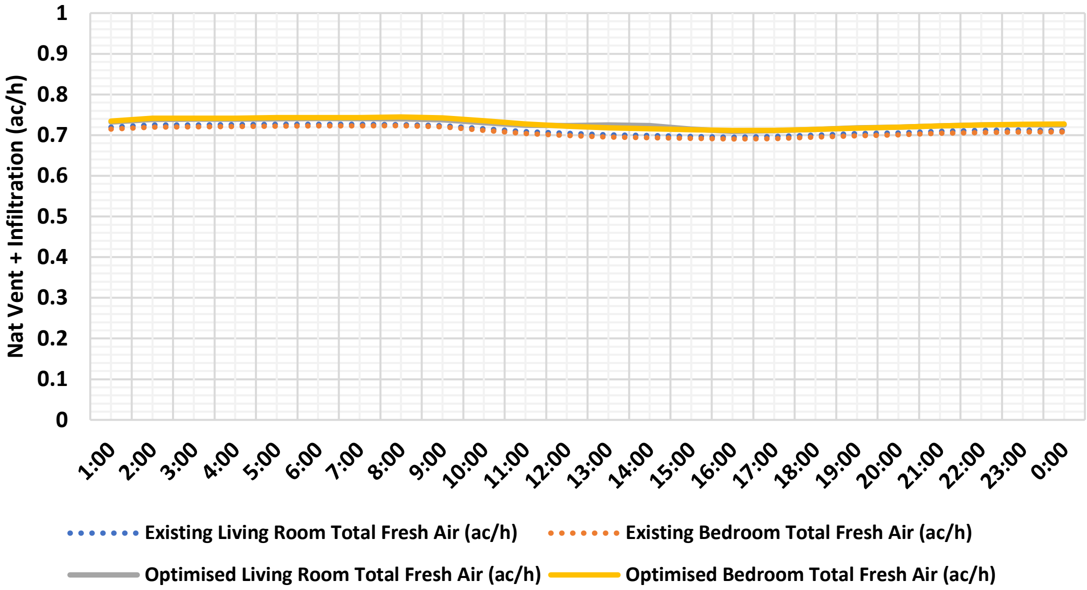

Figure 7.17: Both existing and optimised living room and bedroom total fresh air for a typical winter day (23 January). Data were gathered using DesignBuilder software.

The analysis of the airflow rates for the living room and bedroom on a typical winter day, 23 January, reveals a comparable airflow trend between the existing and optimised scenarios. Figure 7.17 illustrates that the optimisation process preserves the airflow distribution patterns, with minimal variances in the rates observed. These findings suggest that the optimisation efforts, which may encompass modifications to the building envelope and ventilation strategies, have not adversely affected the natural ventilation performance. Instead, they have sustained, or slightly improved, the fresh air supply rates.

The preservation of similar airflow characteristics in both scenarios indicates a successful balance in the design approach. The optimisation has been achieved without compromising the essential aspect of air exchange, which is crucial for ensuring a healthy and comfortable indoor environment during the winter months. Maintaining such airflow rates is essential for occupant health, particularly when buildings are sealed to conserve heat, as it helps to mitigate issues related to indoor air quality and moisture accumulation.

7.11 OPTIMISATION ANALYSIS SUMMERY

Based on the comprehensive data provided in Figure 7.18, a complete evaluation of total discomfort hours is conducted across three residential buildings—House 1-J, House 1-M, and House 2-M. This analysis observes the one-year effects of optimisation on the living room, bedroom, and dining room.

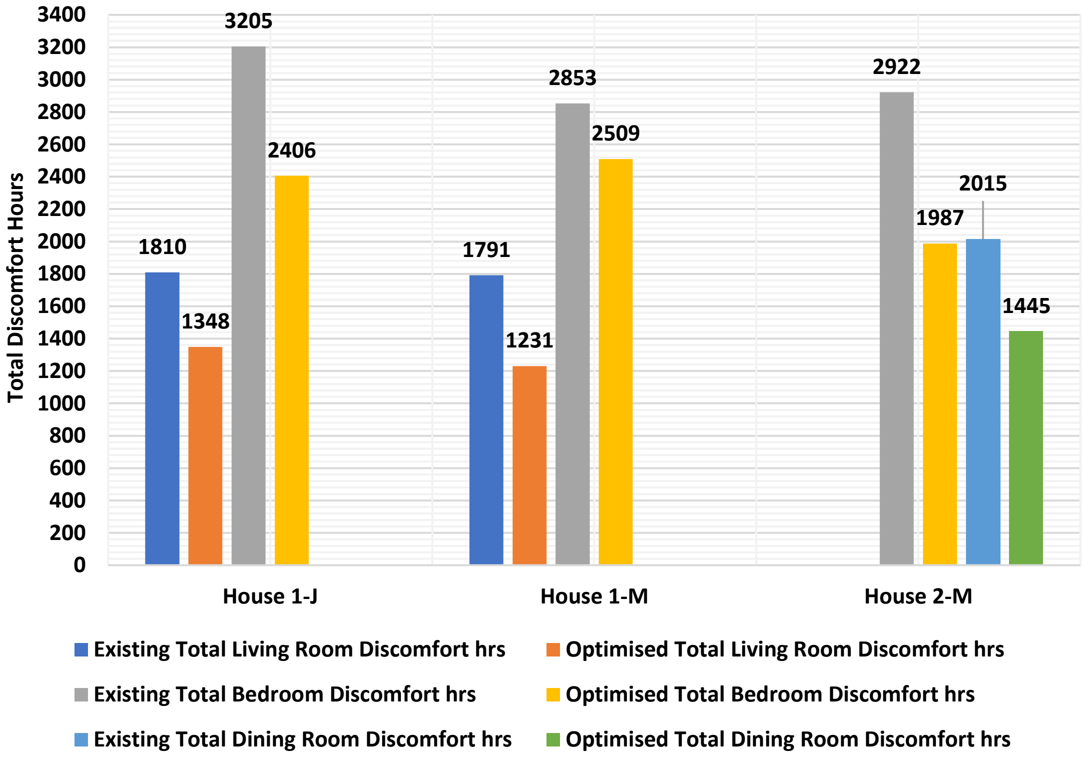

Figure 7.18: A summary illustrating total discomfort hours before and after optimisation throughout a year for the studied 6 zones within the 3 investigated houses. Data were gathered using DesignBuilder software.

For the living rooms of House 1-J and House 1-M, the optimisation process yielded a substantial reduction in total discomfort hours. House 1-J recorded a 25.5% decrease, from 1810 to 1348 hours, while House 1-M achieved an even greater reduction of 31.3%, decreasing from 1791 to 1231 hours. These figures highlight the optimisation's effectiveness in significantly enhancing comfort levels in these selected zones.

In the bedrooms of the three houses, the improvements are consistently positive. House 1-J observed a 24.9% decrease in total discomfort hours, from 3205 to 2406 hours, and House 2-M showed an impressive 32% reduction, from 2922 to 1987 hours. The bedroom of House 1-M also noted a reduction, although more reasonable at 12.1%, from 2853 to 2509 hours. These results collectively demonstrate the substantial impact of the optimisation process on bedroom comfort levels. Furthermore, the dining room of House 2-M exhibited a notable 28.3% decrease in total discomfort hours following optimisation, from 2015 to 1445 hours. This reduction clearly indicates the successful application of optimisation techniques in enhancing the comfort of dining zones.

In summary, the findings from Figure 7.18 confirm that the optimisation process has been markedly successful across all studied zones within the three houses. The significant reduction in total discomfort hours across the living rooms, bedrooms, and dining rooms not only improves overall comfort levels but also highlights the profound potential of optimisation to enhance thermal performance in residential environments. These outcomes underline the importance of such processes in advancing the quality of living and sustainability of modern prefabricated housing.

7.12 ADVANCED PREDICTION OF MAJOR SAUDI ARABIAN CITIES USING OPTIMAL VARIABLES

The examination of various major cities and areas within the Kingdom of Saudi Arabia has involved thorough consideration of diverse hourly weather and climate data. Consequently, six distinct climate zones have been subjected to detailed analysis and testing, employing comprehensively optimised variables.

Table 7.10 presents the selected major cities and regions, highlighting the significant variables aimed at minimising total discomfort hours over the span of a year. It is important to emphasise that House 1-J has been designated as the prototype for simulation across all six cities, serving as an essential reference point for understanding the impact of different optimised scenarios and combined variables on thermal performance within the house across each climate zone. This approach not only facilitates a deeper understanding of the interactions between various design variables and climatic conditions but also contributes to the advancement of architectural practices tailored to the distinctive environmental context of Saudi Arabia.

The table analyses thermal performance using total discomfort hours as the primary performance indicator for the proposed systems and design variables. The table includes major regions and cities in Saudi Arabia, each with its optimal design to minimise total discomfort hours throughout the year. It is significant that the optimised scenarios are tailored to achieve fully naturally ventilated houses. This implies that no HVAC systems or any air conditioning systems have been utilised.

To understand the performed analysis of the thermal performance, it is essential to consider the regional climatic variations and their impact on natural ventilation efficiency. As earlier mentioned in this research, Saudi Arabia's diverse climatic conditions, ranging from arid deserts to humid coastal areas, necessitate tailored design approaches to optimise thermal comfort. In this case, the table likely reflects these variations, highlighting the necessity of region-specific strategies in natural ventilation design approach.

Moreover, the reliance on natural ventilation underscores the importance of architectural design and material selection. The optimisation process presumably involves a detailed analysis of building orientation, window opening level, WWR, window glazing system, wall system, roof system, shading devices, and infiltration rate. These factors collectively influence the indoor thermal environment and the overall comfort of the occupants. These variables, therefore, influence various climatic parameters, such as temperature, humidity, and airflow, to quantify the deviation from thermal comfort standards over time. By minimising total discomfort hours, the proposed scenarios aim to enhance occupant thermal comfort and reduce reliance on artificial cooling, thus contributing to energy efficiency and sustainability. The focus on minimising total discomfort hours highlights the critical role of climate-responsive design in achieving thermal comfort without mechanical systems. This approach not only supports sustainable building practices but also aligns with the broader goals of environmental stewardship and resource conservation.

Table 7.10: Advancing optimal design and variables strategies for predicting lowest possible discomfort hours for residential buildings in different KSA regions. A developed comprehensive study using House 1-J as a prototype for optimal design strategy comparison in different climate zones in Saudi Arabia.

Variables	**Dammam**	**Riyadh**	**Jeddah**	**Dhahran**	**Tabuk**	**Qassim**
Wall System	W-16 or W19	W19	W9	W-16 or W19	W19	W19
Roof System	R-7	R-7	R4	R-7	R-7	R-7
Glazing	Quadruple LoE Films (88) 3mm/8mm Krypton	Dbl Ref-C-Clr 6mm/13mm Air	Quadruple LoE Films (88) 3mm/8mm Krypton	Quadruple LoE Films (88) 3mm/8mm Krypton	Trip Clr 3mm/13mm Air	Dbl Ref-A-M Clr 6mm/13mm Arg
WWR	13%	7%	23%	13%	7%	7%
Shading	0.5 m Overhang	1.5m Overhang	1 m Overhang	1 m Overhang	Louvre, 0.5m overhangs and sidefins	0.5 Overhang
External Window open	43%	55%	29%	43%	14%	16%
Orientation	North	North	290° (NW)	North	North	North
Infiltration	0.2 ac/h	0.2 ac/h	0.2 ac/h	0.2 ac/h	0.2 ac/h	0.2 ac/h
Total Discomfort Hours	1292 hrs	850 hrs	2713 hrs	1905 hrs	618 hrs	918 hrs

As shown in table 7.10, Riyadh achieved the minimum total discomfort hours with around 850 hrs. during the year. Conversely, both Jeddah and Dhahran recorded the highest total discomfort hours, which is undoubtedly associated with the climatic conditions of these areas. As deeply investigated in analysis chapter, high temperature and high relative humidity are particularly believed to be highly correlated with the increased discomfort hours in these cases.

Furthermore, this exploration of ideal scenarios provides valuable insights into the potential limits of thermal optimisation under extreme conditions. Riyadh's achievement of minimal discomfort hours underscores the effectiveness of the proposed optimisations in a relatively dry climate. The city's climatic conditions likely facilitate better natural ventilation performance, contributing to the reduced discomfort hours.

In contrast, the higher discomfort hours recorded in Jeddah and Dhahran highlight the challenges posed by humid climates. The high relative humidity in these regions significantly impacts indoor thermal comfort. This correlation between high humidity and discomfort hours suggests that additional measures beyond natural ventilation, such as dehumidification or hybrid ventilation systems, may be necessary to improve comfort in these areas.

Furthermore, the examination of these scenarios emphasises the need for region-specific solutions. The difference in performance across different cities illustrates that a one-size-fits-all approach is inadequate for optimising thermal comfort in diverse climates. Tailored strategies that consider local climatic conditions, construction practices, and economic constraints are essential for developing feasible and effective solutions.

Moreover, as shown in Table 7.10, it is evident that a reduced infiltration rate results in better thermal performance across all studied climate zones. Additionally, the use of advanced glazing systems, WWR, and window opening percentages are optimised to fit the best possible scenario for each studied zone. These findings can serve as a valuable reference point for future improvements and optimisation using prefabricated construction systems in different climatic conditions. This analysis is considered one of the main outcomes of this study. However, it is important to note that implementing these advanced solutions may be associated with high construction and material costs in the real world.

The reduced infiltration rate, as explained, plays a crucial role in enhancing thermal performance by minimising unwanted air exchange, thus maintaining indoor thermal conditions more effectively. This is particularly beneficial in extreme climates where maintaining a stable indoor environment is challenging. The optimised window systems and their respective parameters ensure maximum efficiency in natural ventilation and thermal control, tailored to the specific requirements of each climate zone.

Using prefabricated construction systems, which offer precision and consistency, can further enhance the implementation of these optimised parameters. Prefabrication can reduce construction time and waste while ensuring that the high-performance standards required for low infiltration rates and advanced glazing systems are met. This approach not only supports the practical application of the research findings but also promotes sustainability through efficient resource use and reduced environmental impact.

Thus, the insights gained from Table 7.10 underscore the importance of reduced infiltration rates and optimised window systems in achieving superior thermal performance. These findings provide a solid foundation for future research and practical applications, particularly through prefabricated construction systems. However, addressing the associated high costs will be essential for making these advanced solutions viable and accessible in real-world settings.

7.12.1 LIMITATIONS OF ADVANCED PREDICTIONS

It is important to mention that the proposed variables do not meet the minimum requirements set by international standards such as ASHRAE. Instead, the optimised variables in this section focus on achieving the minimum discomfort hours. This approach may anticipate high construction and materials costs. For instance, the cost of installing quadruple-pane windows incorporating Specialised gas between the panes would require custom orders with high specifications. Additionally, achieving an exceptionally low infiltration rate, such as 0.2 ac/h, ideally involves precise construction work using high-standard construction techniques. Consequently, this approach necessitates higher construction costs compared to the previously proposed scenario for house 1-J in this chapter, which this research has already considered for more feasible and practical scenario.

Moreover, the reliance on Specialised materials and construction techniques highlights the importance of balancing theoretical optimisation with practical feasibility. While the theoretical models may demonstrate significant improvements in thermal comfort, the real-world application must account for budget constraints, availability of materials, and local construction capabilities. It is essential to develop solutions that are not only effective but also economically viable and implementable within the existing construction industry framework. Therefore, future research should aim to strike a balance between achieving optimal thermal performance and ensuring practical feasibility. This includes exploring cost-effective materials and construction methods that align with international standards while remaining accessible and affordable for real-world applications.

7.13 SUMMARY

The optimisation process has been decisively validated to enhance indoor thermal comfort levels in various zones of all three examined houses. The notable decrease in total discomfort hours offers a robust testament to the potential of such optimisation in elevating residential thermal comfort.

The analysis emphasises the effectiveness of integrating high thermal mass materials on the inner surfaces of external precast walls. These materials leverage their thermal attributes to moderate indoor temperature fluctuations, sustaining ambient temperatures within a desirable comfort range for extended periods, especially with proper indoor ventilation. The strategic inclusion of Phase Change Materials (PCM) within the building's elements markedly amplifies this thermal regulation. By absorbing or releasing heat during phase changes, PCMs function as thermal energy reservoirs, thereby stabilizing indoor temperature variations and bolstering comfort levels.

Conversely, the external surface of the precast wall is susceptible to outdoor climatic influences, such as intense solar radiation and elevated temperatures. The use of low thermal mass materials, like lightweight concrete, has been shown to significantly limit heat absorption by the materials and the overall thermal conductivity across the wall system. This leads to a pronounced reduction in heat transfer from the exterior to the interior of the wall, enhancing thermal performance.

When considering the placement of PCMs for improving thermal performance, it is essential to address the precise location and composition of the PCM within the wall system. In this context, the PCM has been accurately placed next to the inner concrete layer, with a melting point regulated to 23°C. Such a methodical placement ensures a synergistic interaction between high thermal mass materials internally and low thermal mass materials externally, optimising the wall's thermal attributes and thus, its overall efficacy.

In hot climates, this method shows promise in not just enhancing indoor thermal comfort but also in diminishing reliance on air conditioning, courtesy of the PCMs' capacity to balance internal temperatures, absorbing excess heat by day and releasing it at night. This integrated approach indicates a sustainable approach to achieving exceptional thermal performance in building design, contributing to more energy-efficient and comfortable indoor environments.

Additionally, in regions with extreme heat, the application of PCMs is particularly advantageous in lessening the dependency on air conditioning systems during the cooler seasons and effectively reducing cooling loads in the warmer months that proved by reducing discomfort hours. Nevertheless, the summer heat presents a challenge that persists despite the use of optimised components. However, a marked reduction in cooling loads has been recorded, with all three houses, due to the optimised scenarios, achieving the most significant reduction. This unique combination minimises overheating in buildings and optimises natural airflow within the house.

The developed comprehensive study used House 1-J as a prototype in different climate zones in Saudi Arabia. Thus, it is worth mentioning that the provided advanced predictions scenarios represent the best possible and most advanced outcome within the limitations of this research, considering the designated optimisation parameters only. Accordingly, future studies can build upon this research by incorporating additional variables, such as other sustainable design options, and parameters, and systems better suited to the studied zones.

These advanced predictions scenarios highlight the potential of optimising thermal performance through natural ventilation and other passive design strategies. To achieve greater applicability and effectiveness, future research should explore a broader range of sustainable design elements. For example, integrating renewable energy sources, advanced insulation materials, and adaptive building technologies could further enhance thermal comfort and energy efficiency of buildings in various climatic conditions.

CHAPTER EIGHT –DISCUSSION AND COMPARISON OF ENERGY ANALYSIS FOR EXISTING AND OPTIMISED CASE STUDY BUILDINGS

8.1 INTRODUCTION

This chapter undertakes a comprehensive analysis of energy consumption within the selected case study houses, drawing comparisons between existing and optimised scenarios. Additionally, it explores in detail the impact of optimisation on energy savings throughout the year. The primary focus of the initial part is on energy savings attributed to the utilisation of HVAC systems, clarifying the significant role these systems play in influencing energy consumption in Saudi Arabian homes.

The subsequent part of this chapter shifts attention to the broader range of overall energy consumption. This encompasses a holistic examination of various equipment and appliances, including lighting and hot water supply. Notably, an emphasis is placed on the influential role of increasing the window-to-wall ratio (WWR) in diminishing the reliance on artificial lighting, subsequently reducing the lighting load. Thus, the findings reveal that optimisation not only yields energy savings specifically related to HVAC systems but also extends to an overall reduction in building energy consumption. This insight serves to underscore the motivation for embracing optimised scenarios in future prefabricated concrete buildings.

8.2 ENERGY SAVINGS ANALYSIS

As emphasised in earlier sections of this research, the enhancement of a building's thermal comfort can lead to substantial reductions in the overall annual energy consumption, particularly that which is attributed to air conditioning systems. This research posits that by improving the thermal performance of prefabricated building components throughout the year, there has been a consequential and significant reduction in the energy consumed by air conditioning systems. To quantify the overall energy savings in the case study houses that have undergone these improvements, a comparison has been drawn between the original scenarios and the optimised scenarios in terms of their annual energy consumption.

It is crucial to highlight that any improvement in thermal performance within specific zones is symbolic of an upgrade in the thermal efficiency of the houses. This general enhancement in indoor thermal performance implies that the improvements are not isolated but rather prevalent throughout the entire dwelling. Accordingly, the energy savings analysis presented in this section encompasses a full assessment of each house in its total, considering all zones collectively. This approach to analysing total house energy consumption provides an extensive view of the total energy savings realised due to the reduced reliance on air conditioning systems.

8.2.1 ENERGY ANALYSIS LIMITATIONS

Several key considerations have been meticulously accounted for during the energy analysis phase. Firstly, to ensure a precise understanding and estimation of the energy consumed solely by air conditioning systems, energy usage from other household utilities has been deliberately excluded from first stage of the analysis. Such utilities encompass indoor lighting, outdoor lighting, kitchen appliances, office equipment, domestic hot water (DHW), and various miscellaneous items. Consequently, the focus of the energy consumption estimation has been narrowed down exclusively to the air conditioning systems across both the original case scenarios and the optimised scenario. Moreover, the second stage of the energy analysis incorporates all building equipment and appliances to produce a complete overview of energy analysis in the real world.

In addition to this, it is significant to mention that both heating and cooling set points, along with other design and thermal parameters considered, have been previously defined in Chapter 6. This inclusion ensures that all parameters align with the established criteria for thermal performance and energy consumption, providing a comprehensive foundation for the subsequent analysis.

8.2.2 TEMPERATURE SET POINTS FOR ENERGY ANALYSIS

According to a study from the collaborative King Abdullah Petroleum Studies and Research Centre (KAPSARC) and UNESCWA project, *Energy Productivity in the GCC* by Dubey et al. (2016), the efficacy of optimal design and operational strategies for electricity usage, potential energy savings, and peak demand reduction in residential buildings across five KSA sites is captured in Table 8.1. The study also posits that implementing energy efficiency programs in buildings could result in up to a 27% decrease in electricity usage and a 30% reduction in peak electricity demand across Saudi Arabia.

The research evaluated various cooling set points, specifically at 22°C, 24°C, and 26°C, to optimise energy use. However, the cooling and heating temperature settings for residential buildings, as delineated in the Saudi Building Code (SBC), are set at 25.5°C for cooling and 20°C for heating. Nonetheless, a cooling set point of 26°C was identified as optimal in achieving a balance between thermal comfort and energy conservation in residential settings, particularly in Dhahran city, which shares similar climatic conditions with the Jubail industrial city.

Considering the above, this study, particularly during the simulation phase, adopted 26°C and 20°C as the cooling and heating set points, respectively, for the HVAC system in the baseline scenarios of the three identified houses (1-J, 1-M, and 2-M).

Table 8.1: Compilation of optimal design and operational strategies, anticipated energy usage, and peak demand savings for residential buildings in five KSA regions. Source: KAPSARC, cited by Dubey et al. (2016).

EEM	Riyadh	Jeddah	Dhahran	Tabuk	Abha
Wall insulation	RSI-2.0	RSI-2.0	RSI-3.0	RSI-1.0	No insulation
Roof insulation	RSI-3.0	RSI-3.0	RSI-3.0	RSI-3.0	RSI-3.0
Glazing	Double Bronze	Double Bronze	Double Bronze	Single Clear	Single Clear
Shading	Projection 0.2 m	Projection 0.5 m	Projection 0.2 m	Projection 0.2 m	Projection 0.2 m
Azimuth	0	0	0	0	0
WWR	10%	10%	10%	10%	10%
Lighting	2.2 W/m²	2.2 W/m²	2.2 W/m²	2.2 W/m²	2.2 W/m²
Infiltration	0.21 ACH	0.21 ACH	0.21 ACH	0.21 ACH	0.84 ACH
Cooling Set Point	26°C	26°C	26°C	26°C	26°C
Refrigerator	Typical (800 kWh/year)	Class 1 (280 kWh/year)	Class 2 (440 kWh/year)	Class 3 (560 kWh/year)	Typical (800 kWh/year)
HVAC COP	4.0	4.0	4.0	3.5	3.0
Total Energy Savings	71.1%	70.5%	71.2%	63.1%	54.2%
Life Cycle Cost	$111,640	$115,070	$113,860	$104,660	$92,116
Peak Demand (W)	9,461	8,573	9,409	10,954	10,101
Peak Savings	76.3%	74.2%	76.2%	69.6%	58.9%
Peak Time	07/28 6 p.m.	08/19 6 p.m.	07/29 6 p.m.	07/29 6 p.m.	06/12 6 p.m.

Additionally, given the hot climate of Saudi Arabia, the study explores appropriate temperature set points for cooling and heating in residential buildings. The SBC prescribes specific temperature settings of 25.5°C for cooling and 20°C for heating.

Furthermore, the study corroborates that 26°C serves as an effective cooling set point that not only ensures thermal comfort but also promotes energy efficiency in residential buildings within Dhahran, Saudi Arabia.

8.2.3 ESTIMATED COOLING LOADS

Figures 8.1 and 8.2 demonstrate the estimated monthly and total annual cooling loads for three residential prefabricated houses, comparing both original and optimised scenarios. The analysis of the data reveals significant reductions in cooling loads, achieved through optimisation strategies, thereby affirming the efficiency of optimised prefabricated components in enhancing energy conservation in residential buildings.

In the original scenarios, all houses exhibit pronounced cooling load peaks during the summer months—June, July, and August. Specifically, House 1-J reaches its highest load in July, registering at 6438 kWh. Similarly, House 1-M and House 2-M also peak in July, with 6650 kWh and 6649 kWh, respectively, indicating a significant demand for cooling during these months.

Following optimisation, all three houses experience notable reductions in their summer cooling loads. House 1-J records a decrease from 6438 kWh to 3808 kWh in July, representing a reduction of over 40%. For House 1-M, the cooling load in July drops from 6650 kWh to 3139 kWh, equating to a reduction of nearly 53%. Likewise, House 2-M's cooling load in July decreases by approximately 52%, falling from 6649 kWh to 3191 kWh.

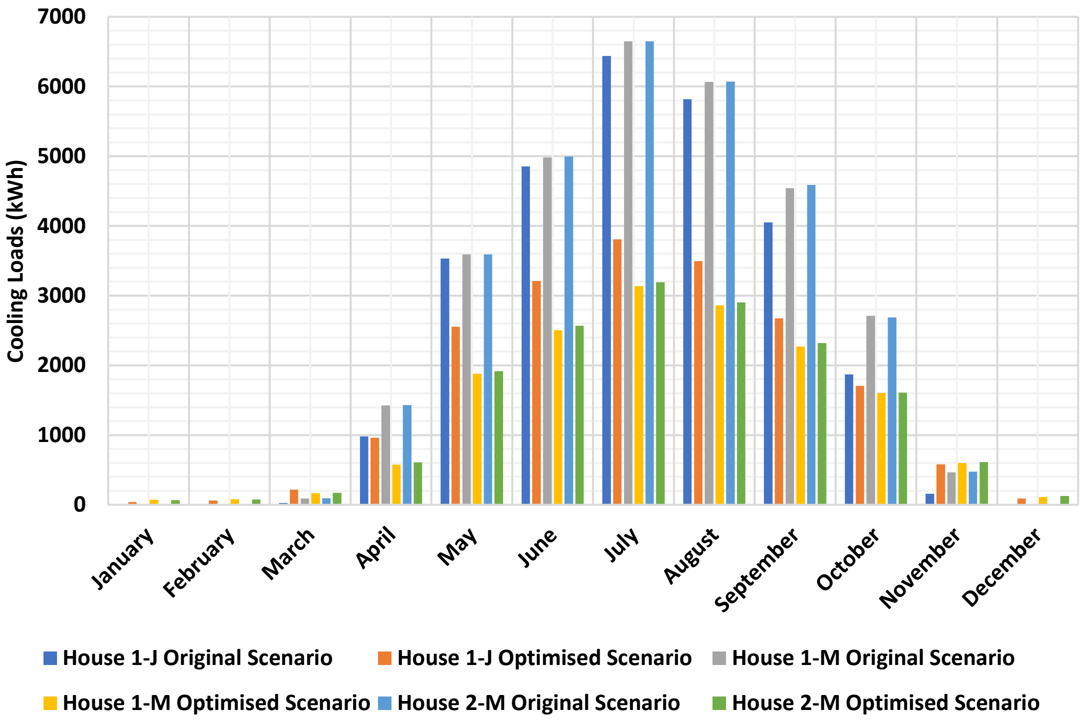

Figure 8.1: Estimated monthly cooling loads among the three houses before and after optimisation. Data gathered from DesignBuilder software and reproduced using Excel.

Conversely, the optimised scenario reveals a slight but reasonable rise in cooling loads during the cooler months, such as January and February, likely due to improved insulation. For instance, House 1-J's cooling load increases from 0 kWh to 60 kWh in February. Similarly, House 1-M and House 2-M see their February cooling loads climb from 0 kWh to approximately 78 kWh and 74 kWh, respectively. These trends suggest that the optimised prefabricated components are highly effective in reducing the cooling load during the intense summer heat, while also slightly increasing the load during the colder months. This balance indicates a strategic enhancement of energy efficiency, reducing excessive summer loads and distributing energy usage more evenly throughout the year.

The observed trends in the data clearly demonstrate the efficacy of optimised prefabricated components in reducing the cooling load during periods of intense summer heat, while simultaneously facilitating a moderate increase in the load during colder winter months. This balance represents a strategic improvement in energy efficiency. By diminishing the excessive cooling loads required during the summer and sensibly distributing energy consumption more uniformly across the year, these optimisation strategies underscore a promising approach to achieving sustainable and energy-efficient prefabricated systems for residential buildings.

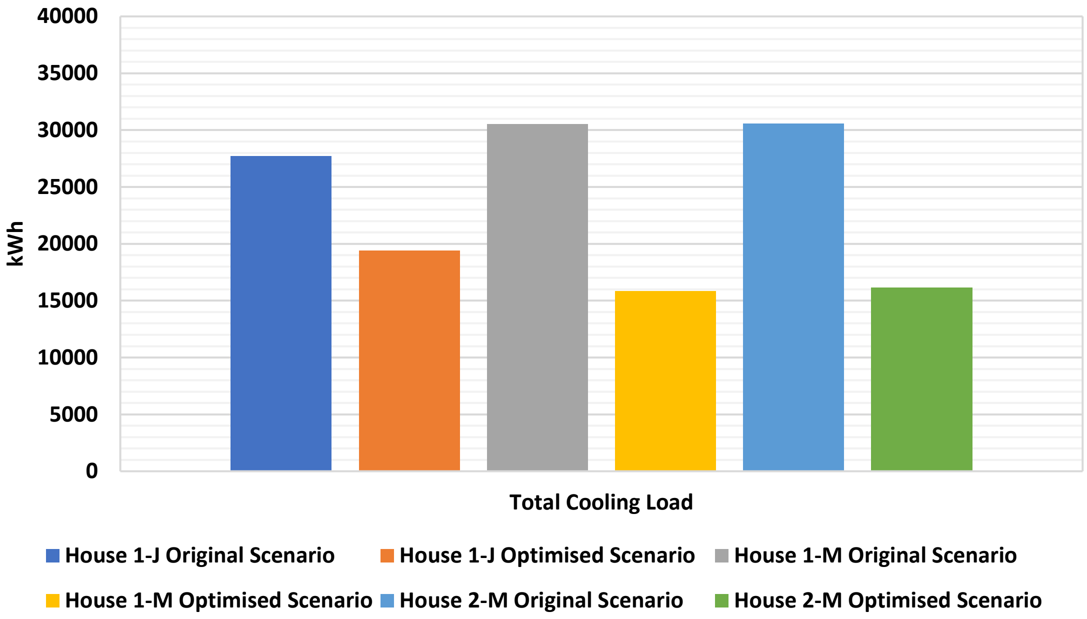

Figure 8.2: Estimated total annual cooling loads among the three houses before and after optimisation. Data gathered from DesignBuilder software and reproduced using Excel.

Delving into the total annual cooling load as represented in Figure 8-2, the optimisation process yields significant energy savings across the scale of housing scenarios. Taking House 1-J as a primary example, we witness a reduction in the total cooling load from 27,722 kWh in the original scenario to 19,396 kWh in the optimised scenario, indicating a substantial decrease achieving 30%. This pronounced reduction in energy consumption is strong evidence to the effectiveness of the optimisation strategies employed, underlining their fundamental role in enhancing energy efficiency.

House 1-M similarly presents a remarkable decrease in its total cooling load, reducing from the initial figure of 30,528 kWh to a mere 15,858 kWh post-optimisation, signifying a near 48% reduction. This outcome is indicative of the exceptional efficiency achieved through the optimised design, effectively dividing the cooling load by almost half in stark contrast to the original condition. In a comparable trend, House 2-M illustrates the impact of optimisation, achieving a remarkable reduction in its annual cooling load, which falls from 30,581 kWh to 16,169 kWh, corresponding to a considerable reduction of approximately 47%.

It is imperative to acknowledge that these overall reductions have been represented despite a slight increase in cooling loads during the winter months within the optimised scenario, further illustrating how efficacious these optimisation strategies are at balancing energy usage throughout the differing seasons. By alleviating the peak loads during the hot summer and modestly enhancing loads during the winter, the optimised scenario ultimately results in a significantly reduced and more evenly distributed total annual cooling load. These observing insights solidify the argument for the prevalent application of optimised prefabricated components in residential buildings, which stand to substantially elevate energy efficiency and limit total cooling loads requirements.

8.2.4 ESTIMATED HEATING LOADS

Figure 8.3 delineates the estimated monthly heating loads for three residential houses—House 1-J, House 1-M, and House 2-M—across both original and optimised scenarios. This figure reveals a distinct pattern opposite to that of the cooling load analysis, with the winter months—January, February, and December—predominantly bearing the effect of the heating load in the original scenario. The optimised scenario, however, shows a substantial reduction in heating demands, with figures narrowed to near-zero heating loads.

Within the original scenario, House 1-J recorded the most substantial heating load in the middle of winter—January and December—registering 2030 kWh and 1461 kWh, respectively. Meanwhile, House 1-M and House 2-M, though recording lesser loads than House 1-J, reached their peak heating loads during these same months. Notably, House 1-M recorded 1115 kWh in January and 779 kWh in December, while House 2-M recorded 1119 kWh and 800 kWh for the same months.

In the optimised scenarios, the data shows a significant shift in heating load numbers. For House 1-J, the January heating demand significantly falls from 2030 kWh to a mere 4 kWh, and the December demand similarly reduces from 1461 kWh down to just 1 kWh. These dramatic decreases are not just marginal improvements but rather indicate an almost total removal of the need for heating.

Similarly, House 1-M and House 2-M exhibit notable reductions. House 1-M's heating requirement in January drops sharply from 1115 kWh to only 2 kWh, and the December load reduces to 1 kWh from 779 kWh. House 2-M follows similar trends with January's heating load falling sharply from 1119 kWh to a minimal 0.6 kWh, and December's heating load dropping from 800 kWh to practically negligible at 0.1 kWh.

These figures provide clear evidence of the success of the optimisation strategies applied. The strategies have not just reduced the cooling load substantially but have also all but eliminated the heating load. This indicates a significant potential for increasing energy efficiency across the board. The significance of these reductions suggests a clear trend towards sustainability and supports the potential for adopting optimised prefabricated components more broadly in the construction of residential buildings. Adopting such strategies demonstrates a clear commitment to drastically reducing energy use, directing prefabricated building industries towards the development of more energy-efficient prefabricated homes.

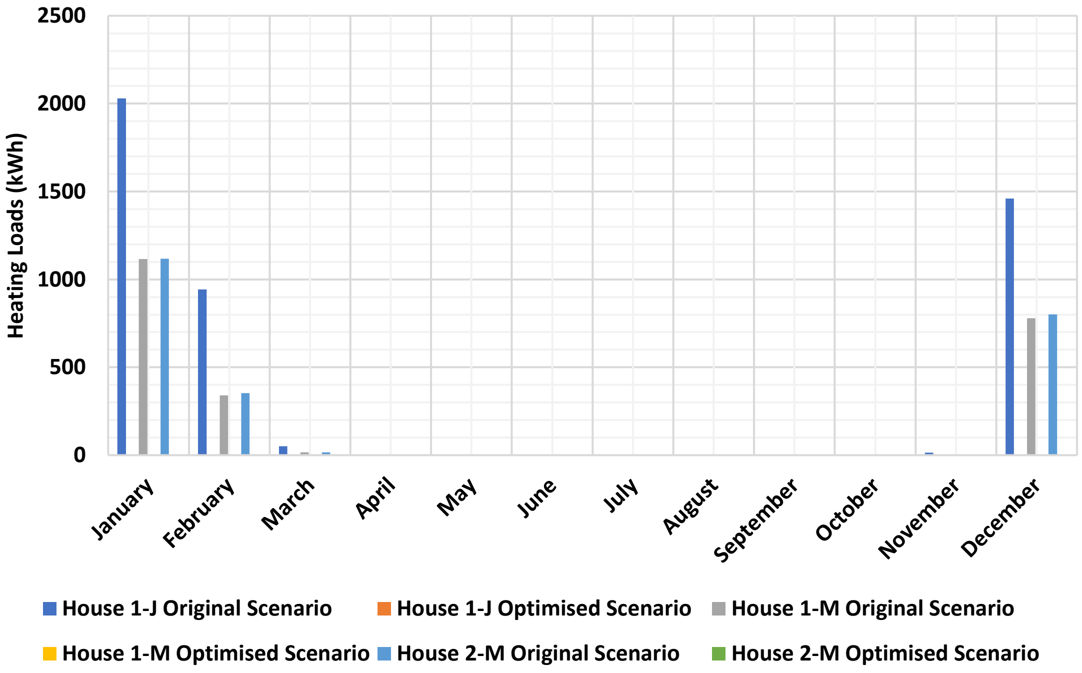

Figure 8.3: Estimated monthly heating loads among the three houses before and after optimisation. Data gathered from DesignBuilder software and reproduced using Excel.

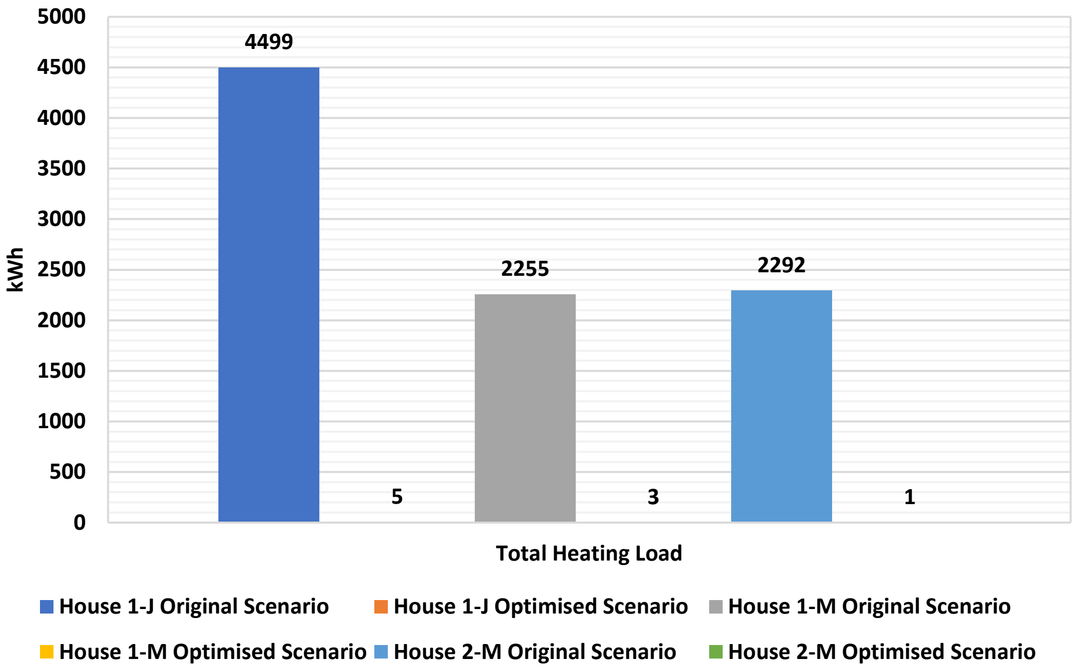

Figure 8.4: Estimated total heating loads among the three houses before and after optimisation. Data gathered from DesignBuilder software and reproduced using Excel.

Furthermore, Figure 8.4 demonstrates the total annual heating loads for the three houses—House 1-J, House 1-M, and House 2-M—comparing their original and optimised scenarios. The figure effectively captures the substantial decrease in heating loads that result from the integration of optimised prefabricated components, which stands as evidence to the efficacy of such enhancements.

In the original scenario, House 1-J's heating load was the most significant, corresponding at 4499 kWh. This figure establishes a high decline to a nominal 5 kWh in the optimised scenario, indicating an incredible 99.9% reduction. This remarkable decrease not only signifies the extreme reduction of energy required for heating but also serves as a clear indicator of the profound influence optimisation strategies have on the conservation of energy.

Similarly, the heating load for House 1-M, originally recorded at 2255 kWh, undergoes a dramatic reduction, settling at a minor 3 kWh post-optimisation, which also mirrors a reduction of approximately 99.9%. House 2-M's scenario mirrors this pattern, with its initial heating load of 2292 kWh reducing to around 1 kWh in the optimised scenario, again illustrating a reduction of nearly 99.9%.

These pronounced decreases in heating loads, brought about through accurate optimisation efforts, strongly advocate for the broader application of such strategies within the residential sector. Beyond the marked reduction in cooling loads, these strategies are shown to nearly eliminate heating demands, substantially sustaining the energy efficiency of these prefabricated houses.

The implications of such extensive energy savings are significant, indicating a shift toward more sustainable practices in prefabricated housing development and potentially offering considerable contributions to the reduction of the overall carbon footprint associated with residential structures.

8.2.5 ESTIMATED TOTAL HVAC SYSTEM ENERGY SAVING

Table 8.2 presents the estimated yearly savings in cooling loads for the three houses, with the optimised scenarios resulting in notable reductions when compared to the original scenarios. Specifically, House 1-J achieved a 30% energy saving, House 1-M showed an impressive 48% reduction, and House 2-M experienced a 47% decrease.

Table 8.2: Estimated yearly cooling load savings. Data sourced from DesignBuilder software and reproduced using Excel.

House	Original Scenario (kWh)	Optimised Scenario (kWh)	Savings (%)
House 1-J	27722	19396	30.09
House 1-M	30528	15858	48.03
House 2-M	30581	16169	47.16

Table 8.3: Estimated total heating loads savings throughout the year. Data gathered from DesignBuilder software and reproduced using Excel.

House	**Original Scenario (kWh)**	**Optimised Scenario (kWh)**	**Savings (%)**
House 1-J	4499	5	99.88
House 1-M	2255	3	99.86
House 2-M	2292	1	99.95

In contrast, Table 8.3 shows the estimated yearly heating load savings. The optimised houses scenarios display significant reductions in heating needs compared to the original scenarios. Houses 1-J, 1-M, and 2-M all achieved remarkable savings of 99.88%, 99.86%, and 99.95%, respectively, indicating a significant decrease in heating requirements. These percentages emphasise how effective the optimised scenarios are in reducing heating loads during cold months.

Table 8.4: Total annual air conditioning load (cooling and heating loads) and their estimated savings. Data gathered from DesignBuilder software and reproduced using Excel.

House	**Original Scenario (kWh)**	**Optimised Scenario (kWh)**	**Savings (%)**
1-J	32221	19400	39.80
1-M	32782	15860	51.60
2-M	32872	16172	50.87

Table 8.4 represents a complete picture of the estimated total annual energy savings for the three houses, considering both cooling and heating loads, in the original and optimised scenarios. The optimised scenarios have led to significant cuts in the total annual energy usage when compared to the original scenarios. Specifically, House 1-J has seen a notable decrease in its total energy use by 39.80%, showing that the energy-

saving steps taken are effective for both cooling and heating. House 1-M stands out with a remarkable 51.60% reduction in its overall energy use, which points to major improvements in energy efficiency for this home. Similarly, House 2-M has also shown a considerable saving, with a 50.87% reduction in its total energy use for the year. These results emphasise just how effective the optimised scenarios are in driving down energy use and achieving significant energy savings over the course of the year.

8.3 INTERNAL LOADS SIMULATION CONSIDERATIONS

HVAC systems play a pivotal role in maintaining thermal comfort within buildings, and their efficiency is significantly influenced by internal heat gains originating from various sources. Internal heat gains encompass the heat generated by lighting systems, appliances, and equipment within a building. As these elements produce thermal energy, they contribute to the overall heat load within the interior space. Consequently, the HVAC system must contend with additional cooling demands to offset the rise in temperature induced by these internal heat sources.

In simulations and analyses of HVAC performance, it is imperative to consider and quantify these internal heat gains comprehensively. Such considerations are essential for accurate modelling of the thermal dynamics within a building, enabling engineers and designers to optimise HVAC systems for energy efficiency and occupant comfort. The variables involved in these simulations may include the wattage of lighting systems, the heat output from electronic appliances, and other pertinent factors that collectively contribute to the internal heat gain profile within a given space. Table 8.5 includes a list of included load sources within the simulation.

Table 8.5: A list of included load source within the total energy simulation and available values for calculated energy consumption: Data used in DesignBuilder software.

Load Source	Load Values
General Lighting	Led 2.5 W/m^2 per100 lux
Miscellaneous Equipment	0 W/M2
DHW (Instant)	1.8 (Coefficient of Performance)
Air Con (American Society of Heating and Air-Conditioning Engineers)	1.8 (Coefficient of Performance)
Air Con (Cooling)	1.8 (Coefficient of Performance)

Furthermore, it is noteworthy that "surface heat gain" refers to heat transfer from the inside surface of building elements to the zone. Due to scope of study, the study focuses on key elements and variables influencing indoor heat balance, encompassing external walls, solar gains from exterior windows, roofs, and total fresh air (the sum of natural ventilation and infiltration rate). It is essential to highlight that roof gains exclusively occur within upper-floor zones exposed to external environmental conditions and solar beams. In contrast, lower-floor zones situated on the ground floor experience no roof gains (as discussed in detail in chapters 6 and 7).

8.4 ESTIMATED TOTAL BUILDING ENERGY SAVING

The subsequent subsection provides an in-depth analysis and discussion concerning energy consumption within the studied three prefabricated houses, exploring both existing and optimised scenarios. This thorough examination extends beyond HVAC systems to encompass a broader spectrum of energy usage, including considerations for lighting and hot water supply. The overarching objective is to elucidate the effectiveness of optimisation strategies in mitigating overall energy consumption within residential contexts in Saudi Arabia.

By thoroughly examining these aspects, this study aims to underscore the potential benefits derived from implementing optimisation strategies. Specifically, the impact of increasing the WWR)is explored, revealing its role in reducing the reliance on artificial lighting and thereby facilitating significant energy savings. This analysis provides valuable insights into the interaction between design interventions and energy efficiency outcomes, informing future strategies for sustainable residential development in the region.

8.4.1 HOUSE 1-J TOTAL ENERGY SAVING ANALYSIS

Based on the provided analysis in Figure 8.5 for House 1-J's total energy consumption under the original existing scenario, several critical insights can be derived. The figure illustrates the distribution of electricity load across different end uses, quantified in kilowatt-hours (kWh).

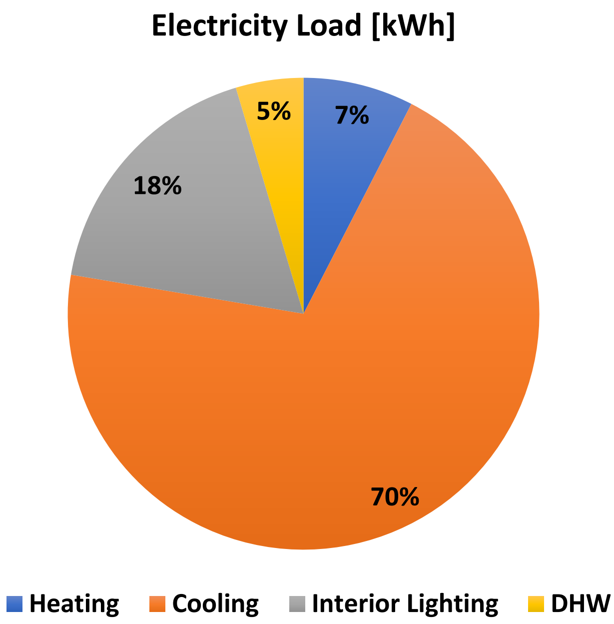

Figure 8.5: Estimated total electricity loads among house 1-J before optimisation. Data gathered from DesignBuilder software and reproduced using Excel.

Firstly, cooling constitutes the most significant portion of the electricity load, accounting for approximately 70% of the total energy consumption. This observation underscores the substantial energy demand associated with maintaining indoor thermal comfort, particularly in climates like Saudi Arabia, which are characterised by high temperatures.

Following cooling, interior lighting represents a notable portion of the energy consumption, comprising approximately 18% of the total electricity load. This finding emphasises the importance of efficient lighting within the house considering its small WWR. Moreover, heating, and domestic hot water (DHW) collectively contribute to the remaining portion of the electricity load, with each representing relatively smaller shares compared to cooling and interior lighting.

In summary, the critical energy analysis of House 1-J's original existing scenario reveals a significant reliance on cooling, followed by interior lighting, heating, and DHW in descending order of energy consumption. Addressing these areas through targeted optimisation strategies presents opportunities for substantial energy savings and enhanced sustainability in residential buildings.

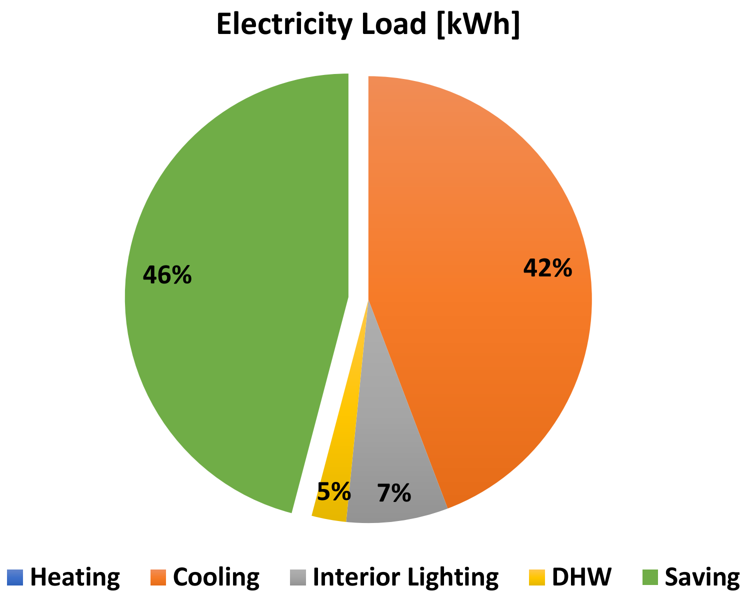

Figure 8.6: Estimated total electricity loads among house 1-J after optimisation. Data gathered from DesignBuilder software and reproduced using Excel.

As depicted in Figure 8.6, the optimised scenario reflects significant reductions in energy consumption across various end uses compared to the original existing scenario. Notably, heating has been eliminated in the optimised scenario, indicating a successful implementation of energy-efficient strategy. This achievement represents a substantial reduction in energy demand and underscores the effectiveness of optimisation strategies in minimising energy consumption associated with heating.

Furthermore, cooling remains a significant contributor to electricity load, although with a notable reduction compared to the original existing scenario. This reduction indicates the implementation of improved building envelope design (Refer to optimisation chapter) to mitigate heat transfer and enhance indoor thermal comfort while reducing energy consumption.

Interior lighting also demonstrates a noticeable decrease in energy usage in the optimised scenario. This reduction is likely due to the adoption of an increased WWR as part of the best optimisation strategy, which reduces the reliance on artificial lighting by maximising natural daylight. However, this finding aligns with the study by Asfour (2020), which cautions that increasing the WWR beyond 50% can elevate cooling demands and the risk of thermal discomfort, underscoring the need for a balanced approach to energy optimisation.

Overall, the optimised scenario demonstrates substantial energy savings across all end uses, resulting in a total electricity load of 23,917 kWh, compared to 44,217 kWh in the original existing scenario. This significant reduction in energy consumption, amounting to 20,299 kWh, underscores the effectiveness of optimisation strategies in enhancing energy efficiency and reducing environmental impact in residential buildings.

8.4.2 HOUSE 1-M TOTAL ENERGY SAVING ANALYSIS

The critical analysis of House 1-M's energy consumption distribution, based on the provided data, offers valuable insights into the factors influencing energy usage within residential buildings. Notably, the comparison between House 1-M and House 1-J reveals distinct differences in energy consumption patterns, attributable to various architectural and environmental factors.

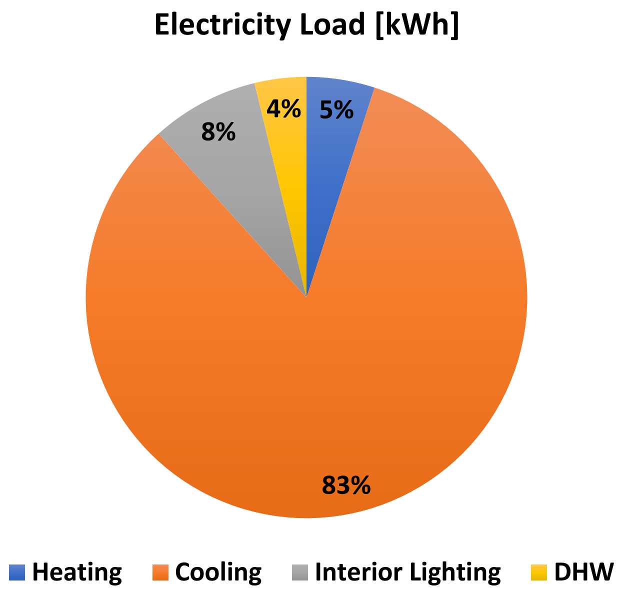

Figure 8.7: Estimated total electricity loads among house 1-M before optimisation. Data gathered from DesignBuilder software and reproduced using Excel.

The analysis of House 1-M's total electricity loads before optimisation underscores several critical insights regarding energy consumption distribution. Notable among these is the substantial proportion of energy allocated to cooling, which comprises approximately 83% of the total electricity load. This dominance of cooling-related energy expenditure underscores the significance of effective cooling strategies in maintaining indoor thermal comfort, particularly pertinent in regions characterised by high temperatures such as Saudi Arabia (Figure 8.7).

In addition to cooling, as shown in Figure 8.7, interior lighting represents a small contributor to energy consumption, constituting around 8% of the total electricity load. This underscores the importance of implementing efficient lighting technologies and design practices to minimise energy usage associated with illumination. Moreover, optimising lighting systems not only reduces energy consumption but also contributes to improved indoor environmental quality and occupant comfort, thereby enhancing the overall sustainability of residential buildings.

Furthermore, while heating accounts for a relatively smaller share of the electricity load compared to cooling and interior lighting, comprising approximately 5% of the total energy consumption, its optimisation remains crucial for comprehensive energy conservation efforts. Although heating demand may be lower in climates like Saudi Arabia, efficient heating systems and strategies can still contribute significantly to reducing energy consumption and enhancing overall building performance.

Lastly, domestic hot water (DHW) usage, although representing a reasonable portion of the energy consumption at approximately 4% of the total electricity load, warrants attention for optimisation. Implementing energy-efficient hot water systems and adopting strategies to reduce hot water consumption are essential steps toward achieving comprehensive energy savings and sustainability goals in residential buildings.

In summary, the existing analysis of House 1-M's energy consumption distribution highlights the dominant role of cooling, followed by interior lighting, heating, and DHW. Addressing these areas through targeted optimisation strategies presents opportunities for substantial energy savings, improved building performance, and enhanced environmental sustainability in residential construction.

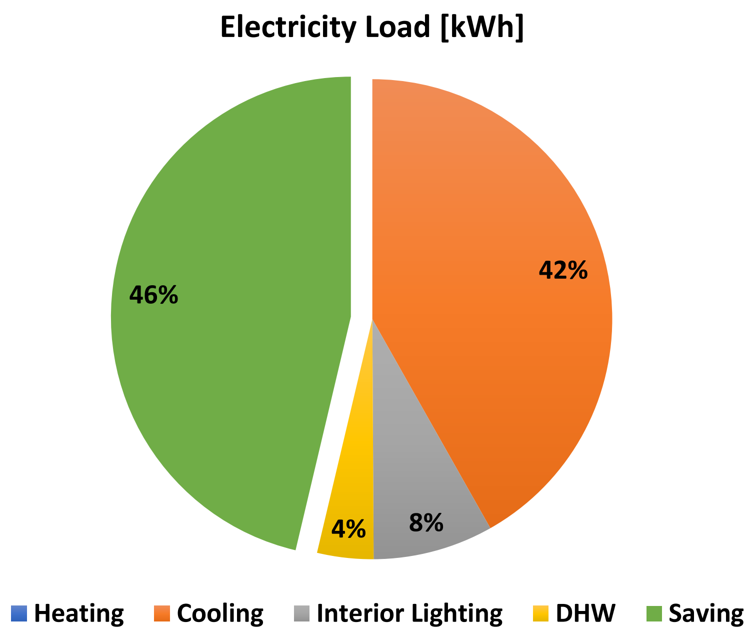

Figure 8.8: Estimated total electricity loads among house 1-M after optimisation. Data gathered from DesignBuilder software and reproduced using Excel.

The analysis of House 1-M's optimised scenario, incorporating savings percentages, provides critical insights into energy consumption distribution and the effectiveness of optimisation strategies, as shown in Figure 9.8.

Cooling, accounting for approximately 42% of the total electricity load in the optimised scenario, remains a substantial component of energy consumption. Despite experiencing a notable reduction compared to the original existing scenario, this underscores the ongoing importance of implementing efficient cooling systems and passive cooling techniques to ensure indoor thermal comfort while minimising energy usage in precast concrete buildings.

Interior lighting constitutes around 8% of the total electricity load in the optimised scenario, indicating a decrease compared to the original existing scenario by around 1700 kwh. This underscores the continued relevance of optimising lighting systems and adopting energy-efficient lighting technologies to reduce energy consumption.

A notable achievement in the optimised scenario is the complete elimination of heating, resulting in substantial energy savings. This signifies successful implementation of energy-efficient design to the insulation materials and PCSP system, contributing to a reduction in energy demand and highlighting the effectiveness of optimisation strategies used in chapter 8.

Incorporating the savings percentages, the total energy savings amount to approximately 46% in the optimised scenario. This underscores the significant reduction in overall energy consumption achieved through optimisation attempts, highlighting the potential for ongoing optimisation endeavours to further advance sustainability in residential prefabricated buildings.

8.4.3 HOUSE 2-M TOTAL ENERGY SAVING ANALYSIS

As shown in Figure 8.9, The analysis of House 2-M's existing energy consumption distribution mirrors patterns observed in the previously examined House 1-M existing scenario. Hence, cooling dominates energy consumption, accounting for approximately 83% of the total electricity load.

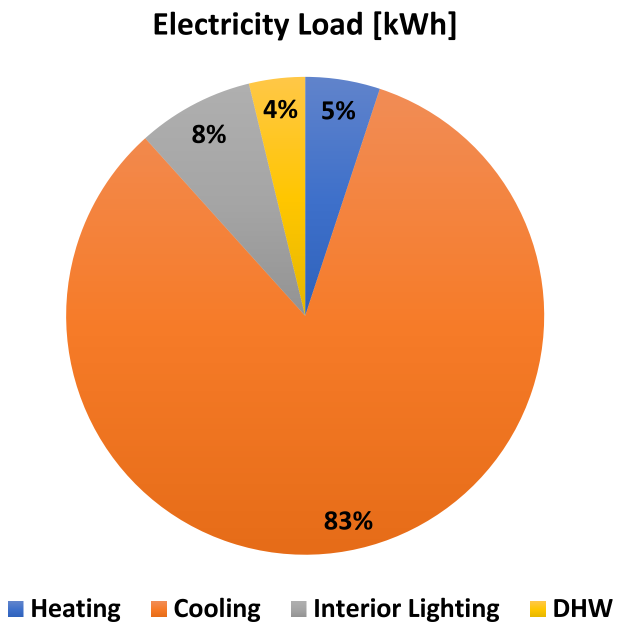

Figure 8.9: Estimated total electricity loads among house 2-M before optimisation. Data gathered from DesignBuilder software and reproduced using Excel.

Also, interior lighting represents around 8% of the total electricity load, while total heating and domestic hot water usage contribute relatively small portions of the electricity load, similar to the House 1-M existing scenario. Thus, the energy consumption distribution in House 2-M's existing scenario aligns closely with patterns observed in the previously analysed House 1-M scenario, regardless of their surrounding buildings. Both underscore the importance of optimising strategies to achieve significant energy savings in residential buildings.

It is worth noting that in a controlled environment with HVAC systems, the energy consumption differences between House 1-M and House 2-M for both existing and optimised models are minimal. However, in uncontrolled indoor settings, such as free-run buildings without air conditioning systems, disparities in occupant thermal comfort satisfaction become apparent (refer to thermal comfort analysis in Chapter 6 and 7).

This discrepancy is particularly notable due to the potential influence of adjacent buildings, which may create possible wind corridors. In the case of House 1-M, superior ventilation facilitated by adjacent structures could enhance air circulation and ventilation, resulting in a more comfortable indoor environment. It is important to acknowledge that this study does not encompass an assessment of the impact of adjacent houses on wind corridors. Therefore, future research endeavours may explore the effects of possible wind corridors created by adjacent buildings on indoor occupant thermal comfort in such prefabricated houses, providing valuable insights for optimising building designs to maximise natural ventilation.

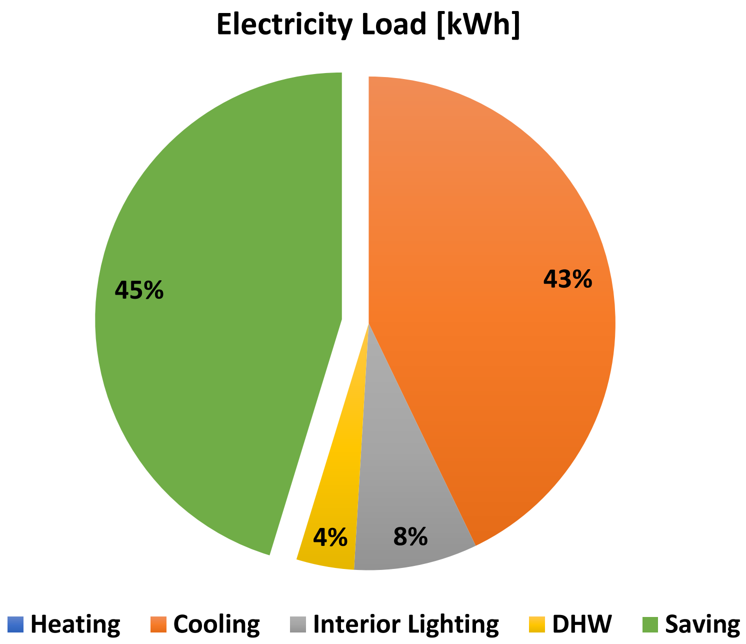

Figure 8.10: Estimated total electricity loads among house 2-M after optimisation. Data gathered from DesignBuilder software and reproduced using Excel.

In House 2-M's optimised scenario as shown in figure 9-10, the cooling load represents 43%, representing a significant reduction from the original existing scenario. However, when compared to House 1-M's optimised scenario, the cooling load is slightly higher by 1%. This difference may indicate variations in building surroundings as explained in previous subsection. Similarly, interior lighting and DHW loads in House 2-M's optimised scenario show comparable values to House 1-M's optimised scenario. Remarkably, the total energy saving in House 2-M's optimised scenario amounts to 45%. Besides, while both House 1-M and House 2-M exhibit energy savings in their respective optimised scenarios, A 1% difference in total energy savings indicates minor difference in optimisation results.

8.5 SUMMARY

To conclude, the comprehensive analysis of heating and cooling loads affirms the significant advantages of employing optimisation strategies in the precast construction of residential buildings. The data reveals dramatic cuts in energy consumption for both cooling and heating, with optimisation leading to a cooling load reduction of up to 48% and an almost complete elimination of the heating load by approximately 99.9%. This substantial drop in energy usage accentuates the transformative impact of optimised prefabricated components on residential buildings. Such advancements are fundamental in boosting energy efficiency, lowering homeowners' energy expenses, and substantially contributing to the mitigation of climate change through reduced carbon emissions.

In a controlled environment with HVAC systems, the disparity in energy consumption between House 1-M and House 1-J is marginal for both existing and optimised models. However, the significance of this difference becomes pronounced in uncontrolled indoor conditions, particularly in free-run buildings devoid of air conditioning systems. In such settings, House 1-M exhibits a clear advantage in occupant thermal comfort satisfaction (illustrated in Chapter 7), attributed to superior ventilation facilitated by a number of factors such as adjacent buildings and larger WWR. This enhanced air circulation and ventilation in free-run conditions contribute to a more comfortable indoor environment in House 1-M compared to House 1-J.

Nevertheless, it is crucial to acknowledge that this study does not encompass an assessment of wind corridors concerning adjacent buildings. Therefore, future research endeavours may consider exploring the impact of external wind corridors on indoor occupant thermal comfort in buildings. Such investigations could provide valuable insights into optimising building designs to leverage natural ventilation and improve occupant comfort while minimising energy consumption.

Additionally, the architectural differences between House 1-M and House 1-J, such as the number of floors, necessitate consideration when evaluating overall energy consumption percentages. House 1-M's two-floor structure may influence energy consumption patterns differently compared to House 1-J's three-floor configuration.

Thus, any comparative analysis should account for these architectural variations to provide accurate assessments of energy efficiency and consumption profiles.

The critical analysis of House 1-M's energy consumption, contextualised within the broader architectural and environmental considerations, highlights the importance of natural ventilation and building design in influencing energy usage and occupant comfort. Future research endeavours should explore these factors comprehensively to inform optimised building designs that prioritize energy efficiency and occupant thermal comfort.

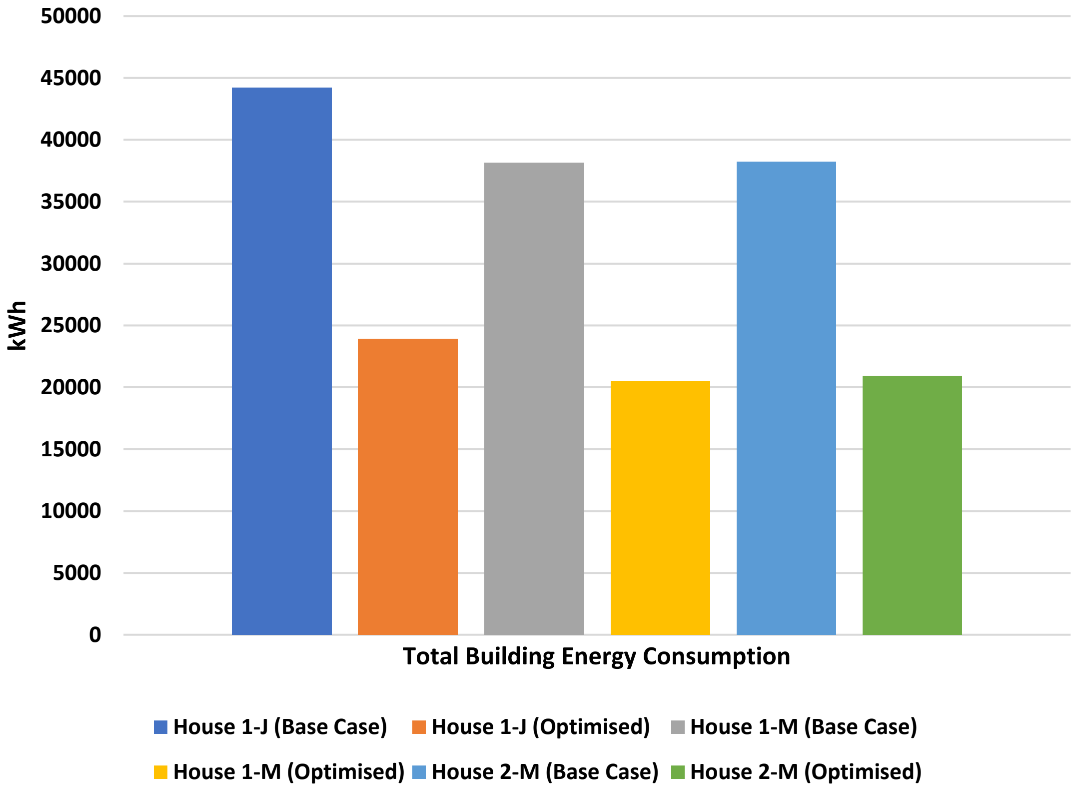

Figure 8.11: Estimated total electricity loads, in kWh among the three studied houses before and after optimisation. Data gathered from DesignBuilder software and reproduced using Excel.

In Figure 8.11, the total energy consumption in kWh is presented for each house before and after optimisation. The comparison reveals significant reductions in energy consumption following optimisation across all three houses. House 1-J, for instance, experienced a notable decrease from 44217.24 kWh in the base case to 23917.53 kWh after optimisation. Similarly, House 1-M and House 2-M also demonstrated substantial reductions in energy consumption post-optimisation. These findings underscore the efficacy of optimisation strategies in achieving energy savings and improving overall energy efficiency in residential buildings.

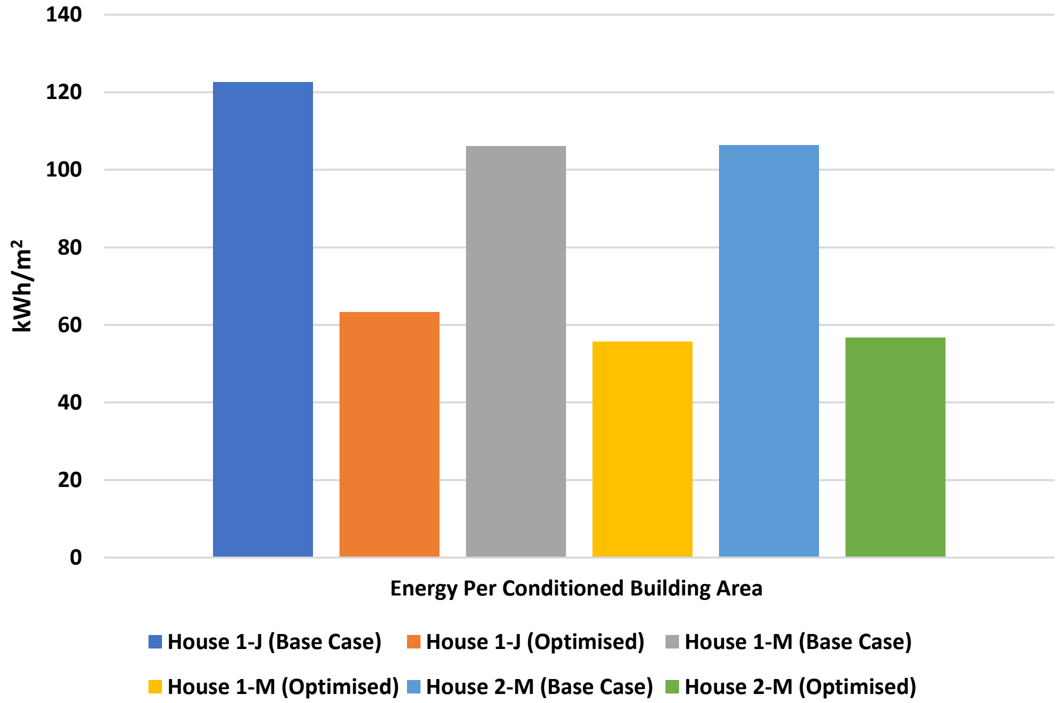

Figure 8.12: Estimated total electricity loads, in kWh/m^2 among the three studied houses before and after optimisation. Data gathered from DesignBuilder software and reproduced using Excel.

Furthermore, Figure 8.12 provides insights into energy consumption per conditioned building area, measured in kWh/m^2, before and after optimisation. This metric allows for a standardised comparison of energy efficiency across the studied buildings. The data indicate that, on average, energy consumption per conditioned building area decreased significantly after optimisation for all three houses. Notably, House 1-J exhibited the most substantial reduction in energy consumption per m^2, decreasing from 122.54 kWh/m^2 in the base case to 63.34 kWh/m^2 after optimisation. Similarly, House 1-M and House 2-M also demonstrated notable decreases in energy consumption per m^2 following optimisation. These findings highlight the effectiveness of optimisation strategies in improving energy efficiency in a conditioned area.

Overall, the figures underscore the importance of optimisation strategies in reducing energy consumption and enhancing energy efficiency in prefabricated residential buildings in the region. The significant reductions observed in energy consumption post-optimisation reflect the potential for implementing sustainable building practices to mitigate environmental impact and promote energy conservation in the built environment.

CHAPTER NINE – CONCLUSIONS AND RECOMMENDATIONS FOR FUTURE RESEARCH

9.1 INTRODUCTION

This chapter interprets and concludes the research findings in connection with the research goals. Additionally, previous studies and literature referenced throughout this research are linked and critically examined in this chapter. Furthermore, the analyses and results presented in earlier chapters (5–8) are critically reflected upon in this chapter, illustrating the significant outcomes of the study. Specifically, the outcomes of the investigations described in previous chapters are discussed and related to the research objectives and questions outlined in Chapter One of this dissertation:

1. *What are the indoor thermal conditions of prefabricated buildings in the extremely hot climate of Saudi Arabia?*
2. *To what extent do prefabricated houses maintain conditions conducive to thermal comfort throughout the year?*
3. *How effectively can the optimisation of prefabricated building components in Saudi Arabia deliver optimal thermal performance over the course of a year?*

Climate change, driven by rising temperatures and natural disasters, presents a significant global challenge. The building sector accounts for a substantial portion of energy use, with residential buildings contributing 22%. Meeting the goal of limiting global warming to 2°C by 2050 requires a 77% reduction in carbon emissions from this sector. In Saudi Arabia, high energy consumption in residential buildings, coupled with a lack of specific standards for insulation and thermal performance in prefabricated construction, hinders the efficient adoption of these methods, despite their growing popularity in the harsh climate.

This research aimed to meet the demand for affordable and energy-efficient housing in Saudi Arabia by comparing the thermal performance of existing prefabricated houses with more advanced and enhanced prefabricated structures. The study analysed case study data using DesignBuilder software to assess the thermal performance and energy efficiency of typical Saudi prefabricated houses. The focus was on identifying energy savings and improving indoor thermal comfort, thereby offering insights into the potential advantages of advanced prefabricated construction in environments with high energy demands.

The current state of prefabricated housing in Saudi Arabia requires thorough evaluation, particularly regarding energy and thermal efficiency. While active ventilation systems are often employed to manage indoor heat, the challenge of reducing dependence on HVAC systems and ensuring thermal comfort in severe climates persists. As awareness of sustainable development grows in Saudi Arabia, it is imperative for architects and engineers to integrate sustainable practices from the inception of the design process. Although guidelines and standards exist to aid in material selection, a clear categorisation and classification of prefabricated envelope systems are essential. This would provide a comprehensive reference for construction professionals specializing in various types of prefabricated construction, ensuring informed decisions and optimised outcomes.

9.2 THERMAL PERFORMANCE EVALUATION AGAINST ASHRAE

The thermal performance evaluation was conducted using DesignBuilder software (version 6.1.8.021). This involved assessing total discomfort hours across two distinct zones in each house. Specifically, the living room and bedroom were chosen for evaluation in Houses 1-J and 1-M, while the dining room and bedroom were selected for House 2-M. Consequently, six zones in total underwent thorough thermal analysis.

Several metrics were employed to gauge the thermal performance of these houses, including zone operative temperature and relative humidity, PPD based on estimated PMV, total discomfort hours, heat balance breakdown, and zone airflow (estimated total fresh air). For each zone, monthly averages, conditions on the hottest day of summer, and the coldest day of winter were meticulously calculated and critically analysed. This approach facilitated a comprehensive understanding of the thermal behaviour of each zone across different seasons.

Adhering to ASHRAE 55 thermal comfort parameters, the simulated models were set to reflect naturally ventilated houses. Scheduling for occupancy hours and window opening times was determined based on the standard used by the Energy Plus software engine, which defaults to the ASHRAE adaptive model. Personal parameters, such as clothing insulation values and metabolic rate, were automatically adjusted for summer and winter conditions. Furthermore, to ensure accuracy and clarity, the thermal output results from the three houses were transposed and visualised using Microsoft Excel. Each thermal metric was individually depicted in figures for enhanced precision in the results.

9.3 RESEARCH KEY FINDINGS

In this section, the research questions are addressed, clearly demonstrating their relationship to the main findings of the study. Each subsection will precisely analyse and clarify the significant outcomes, linking them directly to the research questions posed at the beginning. This approach is designed to offer a systematic understanding of the essential findings derived from the research.

9.3.1 KEY FINDINGS AMONG BASE CASE SCENARIOS ANALYSIS

The analysis of the base case scenarios has unveiled several key findings about the indoor thermal conditions of prefabricated buildings in Saudi Arabia's extremely hot climate, particularly focusing on naturally ventilated buildings. The following points address the first research question of this thesis.

It is important to recall that the acceptable indoor operative temperature, considering various personal and environmental factors, has been defined in Chapter 3. The analysis encompassed a total of 8760 hours, accounting for both occupied and unoccupied periods throughout the year (365 days) and including both daytime and nighttime.

Generally, the analysis revealed that the least discomfort hours were recorded in March and November, while the most discomfort hours occurred from May to October and from December to February, indicating high discomfort levels during summer and winter, except for March and November.

Among the studied zones within the three houses, it was consistently observed that upper floors experienced higher operative temperatures compared to lower floors, often reaching the external dry bulb temperature. This was particularly evident in bedrooms located on the upper floors, highlighting a significant need for thermal performance improvements to achieve acceptable indoor conditions year-round. This issue was largely attributed to inadequate roof thermal insulation, which led to excessive heat gains due to the roof's high thermal mass from heavy concrete materials.

In contrast, living rooms on the ground floor demonstrated slightly better thermal conditions, benefiting from heat loss through the ground floor slab in summer. For instance, the living room in House 1-J experienced a high percentage of Predicted Percentage Dissatisfaction (PPD), ranging between 83% and 100% during the hottest day of the year, while the bedroom on the top floor consistently recorded 100% PPD, indicating a high level of occupant dissatisfaction and an inability to cope with external climatic conditions.

Furthermore, the analysis indicated that during the summer season, the inflow of hot air through windows led to significant overheating in the buildings. This issue was particularly noticeable in the studied zones, especially in the heat balance of walls and internal partitions, where an increase in air changes per hour during the summer aggravated the overheating condition. This led to the identification of a fundamental correlation between convective heat transfer through the building envelope and airflow patterns, playing a key role in regulating the heat balance within the building's materials and components.

Moreover, it was observed that a smaller WWR resulted in reduced natural ventilation, thereby increasing the chance of overheating in the summer while maintaining warmer indoor conditions in the winter. The study also found that the presence and orientation of surrounding buildings significantly affected the rate of natural ventilation, greatly impacting the overall thermal condition of the houses. These neighbouring structures impede the flow of natural air into the buildings and contribute to heat retention due to their high thermal mass concrete materials.

In summary, the key findings derived from the analysis of the base case scenarios clearly indicate that prefabricated buildings in the extremely hot climate of Saudi Arabia, particularly those relying on natural ventilation, encounter significant challenges in maintaining indoor thermal comfort. To effectively address these challenges, the study underscores the importance of focusing on enhanced thermal insulation, optimising ventilation strategies, and considering the thermal impacts exerted by surrounding buildings. These insights make a valuable contribution to answering the first research question of this thesis, laying a solid foundation for future research endeavours and potential solutions aimed at improving the thermal performance of prefabricated buildings in such demanding climates.

9.3.2 KEY FINDINGS AMONG OPTIMISED SCENARIOS ANALYSIS

The simulation results highlight that the heat balance (gain or loss) within the building envelope is a pivotal factor influencing discomfort levels within the building, regardless of the season. The analysis revealed that the thickness and density of materials in the outer layer of precast concrete wall panels are crucial in reducing the total discomfort hours experienced within the building. Additionally, the study discovered that enhancing the thermal performance of external walls has a beneficial effect on the thermal performance of internal walls. This improvement aids in regulating indoor thermal conditions more effectively relative to external ambient temperatures. This relationship is consistent in both hot and cold climates, with the significant thermal mass of internal walls playing an integral role in this synergistic thermal effect.

Moreover, partitions within the optimised zones demonstrated improved heat balance and notable enhancement in the overall indoor thermal condition, attributed to their high thermal mass materials. Additionally, it was observed that augmenting the thickness, material density, and arrangement of layers in precast sandwich wall panels is instrumental in minimising total discomfort hours.

Additionally, the thermal analysis revealed that when evaluating different external walls, it is imperative to construct the innermost layer using materials with high thermal mass. In contrast, the outermost layer of the system should consist of materials with exceptionally low thermal mass. This specific design approach in the precast sandwich panel system has proven to be particularly effective, especially in regions with hot and humid climates. This strategic layering sequence not only optimises thermal comfort but also enhances the overall energy efficiency of the building, aligning with the principle of sustainable construction.

Throughout the analysis, it became evident that internal walls, or partitions, are significantly influenced by the thermal performance of the external building envelope. For instance, when the external walls are thermally optimised, the internal walls exhibit improved thermal performance. This indicates that the thermal behaviour of indoor building components is largely dictated by ambient thermal conditions, particularly when the internal walls are constructed with high thermal mass materials, as was the case in this study. This phenomenon has been observed in both hot and cold conditions, where internal walls play a critical role in regulating indoor thermal conditions. These conditions are affected by the thermal performance of the building envelope, which directly influences the ambient environment within the building.

The study also delved into the effects of using different insulation materials within the Precast Concrete Sandwich Panels (PCSP). It was observed that incorporating air cavities within the system yielded thermal performance results comparable to those achieved with polyurethane foam. This similarity was particularly noticeable in terms of indoor thermal discomfort hours experienced throughout the year. Furthermore, the strategic selection and sequencing of proper thermal insulation materials within the PCSP were found to significantly enhance the building's overall thermal performance. This finding underscores the importance of careful material choice and layer arrangement in optimising the thermal performance of prefabricated building systems.

Overall, the analysis addressed the role of building openings, specifically the WWR. It was discovered that increasing the WWR to 29% and implementing shading devices, such as Micro Louvre on the interior and overhangs and side fins on the exterior, can markedly enhance indoor thermal performance. These modifications play a significant role in mitigating the risk of overheating, demonstrating the importance of thoughtful architectural design in managing indoor climate conditions effectively.

9.3.3 THE ROLE OF PCM IN ENHANCING PCSP PERFORMANCE

In the context of Saudi Arabia, achieving indoor thermal comfort without air conditioning systems is nearly impossible, particularly in densely populated residential areas. The integration of Phase Change Materials (PCMs) with a moderate melting point of 23°C within Precast Concrete Sandwich Panels (PCSP) has been demonstrated to effectively regulate indoor temperatures, maintaining them within the desired range throughout the day and night. This results in considerable energy savings, particularly during periods of high cooling demand.

Although the direct, day-to-day effects of PCMs may not be immediately evident, the results indicate significant long-term energy savings. Therefore, it is recommended to combine high thermal mass concrete with PCM materials on the inner side of the wall system. At the same time, the use of low thermal mass materials on the outermost side of the wall system is critical to preventing unwanted heat storage during extreme weather conditions. This dual-layered strategy proves particularly beneficial in regions with year-round reliance on active air conditioning systems.

Furthermore, PCMs with a 23°C melting point have demonstrated optimal thermal behaviour. When strategically placed on the inner side of the sandwich wall panel system, they contribute significantly to enhanced thermal comfort during periods of natural ventilation. Additionally, their inclusion has shown to support energy savings when air conditioning systems are in operation, offering a practical solution for improving energy efficiency in residential buildings in hot climates.

In certain proposed PCSP systems, Gypsum board panels are attached to PCM materials on the innermost side of the external wall. This placement aims to preserve the PCM and facilitate ease of access and maintenance over time. However, it has been observed that the effectiveness of PCM materials is somewhat diminished due to the low thermal conductivity of the Gypsum board. Further analysis revealed that a PCM with a 30 mm thickness and a 23 °C melting point, integrated within the building envelope systems, can reduce the operative temperature by approximately 10 °C on a typical hot summer day. Conversely, it can increase the indoor operative temperature by about the same margin on a typical winter day. It was also discovered that the correct sequencing of material layers in a PCSP integrating PCM significantly enhances the system's thermal performance. However, simply increasing the thickness of PCM within a component system does not inherently lead to better thermal performance but may result in additional costs.

Furthermore, the role of natural ventilation in regulating indoor thermal conditions is pivotal. Controlling natural ventilation is essential for optimising the behaviour of PCM materials in buildings that rely on natural airflow. The study found that PCM materials effectively maintain warm indoor conditions during winter and store cooler temperatures generated by air conditioning systems in summer. This dual functionality leads to reduced energy consumption during periods of extreme heat and decreased reliance on heating systems in colder seasons.

However, the design of shading devices is critical; if not configured properly, they can hinder airflow and negatively impact natural ventilation, reducing the building's overall thermal performance. Additionally, during periods of extreme heat, closing windows can enhance the PCM's ability to regulate indoor conditions in conjunction with air conditioning systems. This combined effect between air conditioning and PCM materials optimises energy efficiency by storing the desired ambient temperature within the system and releasing it later when the air conditioning is not in use.

Evidently, controlling natural ventilation is essential to optimising the efficiency of Phase Change Materials (PCMs), highlighting the critical role of infiltration and ventilation rates in buildings utilising PCM technology. Furthermore, the incorporation of PCM materials within a Precast Concrete Sandwich Panel (PCSP) system under Saudi Arabia's climatic conditions demonstrates significant potential for reducing energy demands. Specifically, it can decrease total cooling loads by up to 48%, reduce heating loads by as much as 99.95%, and cut total energy consumption by air conditioning systems by up to 51.60%. These findings underscore the effectiveness of PCM integration in enhancing energy efficiency and significantly lowering the energy footprint of residential buildings.

9.4 PREFABRICATED BUILDING SYSTEMS OPPORTUNITIES

In Saudi Arabia, characterised by its hot climate, prefabricated building systems present significant opportunities to address the region's unique environmental challenges. These building solutions offer numerous benefits, including faster construction times, reduced waste, enhanced energy efficiency, and improved thermal comfort. Prefabricated systems enable quicker construction compared to traditional methods, which is particularly advantageous in a rapidly developing country like Saudi Arabia, where infrastructure growth must keep pace with the increasing demand for housing, commercial spaces, and public facilities.

The hot climate of Saudi Arabia underscores the necessity for energy-efficient building designs to mitigate cooling costs. Prefabricated systems can be tailored with superior insulation, reflective surfaces, and strategic ventilation to reduce heat gain and optimise energy use. Additionally, prefabricated buildings facilitate better quality control, as components are produced in controlled factory environments. This approach also proves cost-effective, owing to reduced labour costs, shorter construction periods, and more efficient material usage. Consequently, prefabricated building systems are becoming an increasingly attractive option for developers and investors in the Saudi Arabian housing construction sector.

9.5 PREFABRICATED BUILDING MATERIALS OPPORTUNITIES

The increasing demand for affordable and sustainable housing in Saudi Arabia presents significant opportunities for the implementation of prefabricated building systems. A key innovation in this realm is the incorporation of Phase Change Materials (PCMs) into Precast Concrete Sandwich Panels, which enhances the energy efficiency of buildings and contributes to sustainability objectives. An interesting source of PCMs in Saudi Arabia could be the waste petroleum waxy by-products, which are abundant in paraffins. Paraffins are particularly effective due to their latent heat storage capabilities, making them ideal candidates for PCMs. These materials serve as energy reservoirs, absorbing excess heat during the daytime and releasing it at night or during cooler periods. This process aids in stabilising indoor temperatures, reducing the reliance on active cooling systems. As a result, this leads to a reduction in energy consumption and peak energy demands, aligning with the goals of energy efficiency and sustainability in the building sector.

The use of waste petroleum waxy by-products contributes to waste reduction and promotes sustainability. Additionally, these materials are chemically stable, making them safe and easily prepared for use in construction applications. Consequently, there are opportunities for further research on PCMs to optimise their integration into precast systems, develop new PCM formulations, and explore their compatibility with local climatic conditions. Finally, the potential correlation between the availability of raw materials, such as waste petroleum waxy by-products, and the improvement of prefabricated buildings lies in the utilisation of these materials as phase change materials. This contributes to enhanced energy efficiency, reduced reliance on air conditioning, and lower carbon emissions. Rigorous scientific investigation and research are necessary to fully explore and exploit this potential correlation.

Furthermore, the incorporation of aerated concrete in precast sandwich panels offers multiple advantages. Its inherent thermal insulation properties reduce the need for supplementary insulation materials, while its lightweight characteristics simplify transportation and installation procedures. Additionally, aerated concrete contributes to sound insulation, enhancing the overall acoustic performance of buildings. As it is locally available in Saudi Arabia, aerated concrete presents a cost-effective option that can be utilised to foster the growth of domestic manufacturing and innovation.

Moreover, VIPs, with their ultra-high thermal performance, represent another valuable addition to precast concrete sandwich panels. Their remarkably low thermal conductivity ensures superior insulation capabilities, thereby enhancing energy efficiency in hot climate conditions. Despite being thinner than conventional insulation materials, VIPs maintain their insulation efficacy, resulting in potential space savings and reduced transportation expenses. Nonetheless, attention must be given to their fragility, as VIPs require careful handling during transport and installation. The long-term energy savings offered by VIPs can, however, offset the initial investment costs.

Eventually, the integration of such high thermal performance materials in prefabricated construction systems, particularly in precast concrete sandwich panels, holds significant potential for enhancing building performance in hot climates like Saudi Arabia. These materials offer enhanced thermal efficiency, lightweight characteristics, and other beneficial properties, making them promising candidates for sustainable and energy-efficient construction practices. Consequently, further research and development in this area can lead to innovative solutions that address the challenges posed by hot climates and contribute to the advancement of prefabricated building practices in the region.

9.6 RESEARCH ASSUMPTIONS AND LIMITATIONS

This section outlines several key assumptions and limitations that have been considered in this research:

9.6.1 RESEARCH NATURE LIMITATIONS

The focus of this study is primarily on Saudi Arabia and regions with extremely hot climatic conditions. It investigates indoor thermal comfort by examining operative temperature and total discomfort hours, using various thermal comfort metrics and indicators as detailed in the analysis chapter. These thermal metrics are aligned with established standards, such as those of ASHRAE, and draw upon a number of published papers in the field of thermal comfort and Indoor Environment Quality (IEQ) studies. Consequently, the research is primarily geared towards improving the prefabricated envelope system, including external walls, roofs, and openings. It is important to note, however, that the thermal performance of other building components is inherently enhanced due to the positive impact of the optimised systems on ambient indoor temperature.

9.6.2 RESEARCH STANDARDS LIMITATIONS

In the thermal optimisation chapter, due to the depth of analysis required and the constraints of the research's scope and content, the study focused primarily on one house (House 1-J). While the other two houses were also optimised and analysed, with their results included in the chapter, the detailed investigation of proposed component improvements was limited to House 1-J. Consequently, the analysis of total discomfort hours was specifically conducted for House 1-J, focusing on two zones, as this house demonstrated the poorest original thermal performance among the three. This limitation in the scope of practical testing provides a focused but representative insight into the efficacy of the proposed improvements within the context of extremely hot climates.

9.6.3 SITE VISIT AND CASE STUDY HOUSES LIMITATIONS

The research entailed reviewing several local projects in the Kingdom of Saudi Arabia that utilised various prefabricated building systems, with a particular focus on projects employing prefabricated concrete systems. These projects were investigated theoretically (Appendix A), without direct communication with any involved parties. It is important to acknowledge that there may be other new prefabricated housing projects not identified due to the limitations of this study and the methods used for data collection.

Information about these projects was primarily sourced from online resources and official government websites. While steel construction was utilised in some of these projects, it was not a focus of this research. Consequently, the study centred specifically on prefabricated concrete systems, without an in-depth examination of steel construction applications in prefabricated housing.

Regarding the selection criteria for the case study houses, these were comprehensively discussed in the methodology chapter of this research. In line with the study's nature, the chosen case study houses are unoccupied properties. This decision was made from the outset to minimise potential complications that could arise from evaluating occupied homes. Additionally, due to the limited availability of technical data concerning the investigated houses, the research necessitated several assumptions. These assumptions were based on existing literature and standard knowledge within the field. This approach was adopted to ensure a comprehensive analysis, despite the constraints posed by the lack of specific technical information on the case study houses.

The simulation data input primarily utilised the collected data regarding the thermal and physical properties of construction materials. However, given the specific nature of Precast Concrete Sandwich Panel (PCSP) systems, some assumptions were required to supplement the available data. These assumptions, particularly concerning certain materials' thermal properties, were made to ensure more accurate and reliable data input for the model simulation. Furthermore, thermal bridging—a phenomenon typically occurring at the connection regions within precast panels that support and attach the panels to each other—was considered.

While these connections have been extensively studied in the literature, they were not explicitly detailed in the technical working drawings of the selected projects. This omission led to a gap in technical information for the chosen precast concrete houses. To address this, assumptions were drawn from data obtained in the literature. For instance, modern precast concrete panels, as identified in recent research, do not typically use steel connectors. Consequently, in this study, the thermal bridging materials were assumed to be normal concrete connections, like those commonly used in most precast concrete industries globally.

9.6.4 PRECAST CONCRETE SANDWICH PANEL DESIGN ASSUMPTIONS

Several design constraints for PCSPs were considered in this research, as outlined below:

- The proposed precast wall system was design to function either as an architectural or structural system, depending on the thickness of the provided concrete layer. A reinforced panel with a thickness of 7.5 cm, as recommended by the Precast Concrete Institute (PCI), was adopted for this study.
- A range of precast wall panel thicknesses was explored to evaluate various precast concrete panel options with differing thermal conductivities.

- The maximum thickness of the proposed panels was limited at 37 cm. This limitation was set to enhance the flexibility and deliverability of the product within offsite construction industries.
- For the purposes of this study, all concrete wythes within the proposed PCSP systems included 1% steel reinforcement. This inclusion ensures that the panel possesses the necessary strength for self-support and allows for a realistic estimation of the panel’s thermal performance.
- The dimensions of PCSPs can vary depending on project specifications, form size, handling equipment capabilities, transportation constraints, worksite limitations, and design requirements. In this study, the primary focus regarding dimensions was directed towards the total panel thickness to investigate its impact on thermal performance.

9.6.5 OPTIMISATION APPROACHES AND CONSTRAINTS IN PREFABRICATED HOUSING

The study proposed several optimised materials for thermal enhancement, ranging from various concrete material densities to different insulation materials, considering variable thicknesses. Additionally, diverse glazing materials were proposed, alongside a range of shading systems and techniques. Other strategies, such as optimising the WWR and the house orientation, were also considered. While the literature review highlighted several sustainable design techniques and strategies, these were excluded from the current study's optimisation due to time constraints and word limitations, but they offer valuable directions for future research.

In terms of natural ventilation, it was actively incorporated, with a window opening percentage set at 20% for the three studied houses. In the simulation, this was triggered only when the air change per hour rate fell below the standard average, leading to significant increases in fresh air rates at certain times of the day. Addressing this issue in future studies could involve implementing a smart fresh air management system, reducing the need for manual intervention. Notably, Houses 1-M and 2-M exhibited varying energy savings throughout the year, indicating that total energy savings could be further enhanced by effectively controlling natural ventilation. Moreover, the study's application of Phase Change Materials (PCMs) within the proposed construction systems faced several limitations:

- The thickness of PCMs was restricted to manufacturing design specifications, considering a variety of PCM types and their respective melting points.
- The literature review, particularly focusing on the use of PCMs in extremely hot climates, highlighted challenges in selecting melting points. For hot regions, the evaluated PCM melting points ranged from 20°C to 50°C, with 23°C identified as optimal for indoor applications.
- The phase change materials studied and simulated were limited to those available within the DesignBuilder library template.

9.6.6 ENERGY SAVINGS ANALYSIS LIMITATIONS

This study, while aiming to optimise indoor thermal conditions, also focuses on reducing total energy consumption attributed to active air conditioning systems. To clearly understand and estimate the energy consumed solely by air conditioning, utilities such as indoor and outdoor lighting, kitchen equipment, office equipment, domestic hot water (DHW), and miscellaneous loads have been excluded from the analysis. Therefore, the energy consumption estimated in this research is specific to air conditioning systems across both the original and optimised scenarios. The specific heating and cooling set points, along with other relevant design and thermal parameters, are detailed in Chapter 4.

In the energy analysis, the air conditioning system used for all three houses is modelled as a basic FCU system. Notably, in the optimised scenarios, substantial energy savings are achieved through the control of natural ventilation, which depends on occupant behaviours. The simulation sets limits on the preferred external natural ventilation temperatures, with minimum and maximum thresholds set at 20°C and 24°C, respectively.

The reliability of the results related to PCM performance presented in the thesis depended on the validity of the software. The software needs verification and validation for PCM modelling in particular for building comfort applications under extremely hot or cold climatic conditions where phase change would not be expected to occur (no benefit from the PCM) and other climatic conditions where the phase change processes in a daily cycle would not be complete (partial benefit), to ensure that the output from the software in terms of building energy savings using the PCM reflects the environment-dependent performance rather than the full potential at all times.

9.7 SUMMARY

This research has comprehensively addressed three critical questions concerning the thermal performance of prefabricated buildings in Saudi Arabia's extreme hot climate, with a particular emphasis on naturally ventilated structures. Accordingly, the first question investigated the indoor thermal conditions of these buildings. Findings from the base case scenarios indicated significant challenges in maintaining thermal comfort. In response, the study recommends optimising thermal insulation, improving ventilation strategies, and considering the impact of surrounding structures on thermal comfort.

Addressing the second question, the study examined the thermal comfort range provided by precast houses throughout the year. The analysis of optimised scenarios brought forth several important findings. Notably, the heat balance within the building envelope was identified as a crucial determinant of comfort levels, irrespective of the season. Factors such as the thickness and material density of the outer layer of the precast concrete wall panel, coupled with the sequence of these layers, play a pivotal role in reducing discomfort hours. The research suggests that design improvements in precast sandwich wall panels, specifically employing high thermal mass materials for the inner layers and lightweight materials for the outer layers, can significantly enhance thermal comfort.

The third research question delved into the capacity of Saudi Arabia's prefabricated building industry to deliver optimally insulated building components and systems. A key discovery was the comparable thermal performance of air cavities and polyurethane foam within PCSP. Moreover, the strategic choice and arrangement of thermal insulation materials were found to substantially enhance building thermal performance. The study also highlighted that increasing WWR and incorporating shading devices can markedly improve indoor thermal performance and minimise overheating risks.

Furthermore, the role of PCMs in enhancing PCSP thermal performance was scrutinised. The study revealed that PCMs, particularly those with a melting point of 23 °C positioned on the inner side of the PCSP, effectively regulate indoor temperature and lead to notable energy savings. This optimal performance is achieved by combining high thermal mass concrete with PCM materials internally and applying low thermal mass materials on the exterior. The employment of this approach was shown to significantly reduce total cooling loads by up to approximately 48%, heating loads by up to 99.95%, and overall energy consumption by air conditioning systems by up to 51.60%.

In conclusion, the findings from this research offer valuable insights into improving the thermal performance and energy efficiency of prefabricated buildings in extremely hot climates, such as those found in Saudi Arabia. The study underscores the importance of specific design interventions and material choices that can greatly enhance thermal comfort in prefabricated construction. Also, it is evident that this research primarily focused on reducing total discomfort hours by enhancing and optimising various prefabricated systems and materials. Consequently, by treating the building as a naturally ventilated structure and optimising its thermal performance, substantial energy savings were realised.

REFERENCES

ABERGEL, T., DEAN, B. & DULAC, J. 2017. Towards a zero-emission, efficient, and resilient buildings and construction sector. *Global Status Report 2017*, 1-48.

ADEYEMI, A. B., OHAKAWA, T. C., OKWANDU, A. C., IWUANYANWU, O. & IFECHUKWU, G.-O. 2024. Energy-Efficient Building Envelopes for Affordable Housing: Design Strategies and Material Choices. *Energy,* 13**,** 248-254.

ADILKHODJAEV, A., HASANOV, B., SHAUMAROV, S. & KONDRASHCHENKO, V. Aerated concrete with predetermined pore parameters for the exterior walls of energy efficient buildings. IOP Conference Series: Materials Science and Engineering, 2021. IOP Publishing, 012006.

AGUILAR-SANTANA, J. L., JARIMI, H., VELASCO-CARRASCO, M. & RIFFAT, S. 2019. Review on window-glazing technologies and future prospects. *International Journal of Low-Carbon Technologies,* 15**,** 112-120.

AHMAD, A., MASLEHUDDIN, M. & AL-HADHRAMI, L. M. 2014. In situ measurement of thermal transmittance and thermal resistance of hollow reinforced precast concrete walls. *Energy and Buildings,* 84**,** 132-141.

AHMED, W., ASIF, M. & ALRASHED, F. 2019. Application of Building Performance Simulation to Design Energy-Efficient Homes: Case Study from Saudi Arabia. *Sustainability,* 11.

AL-ABSI, Z., MOHD ISA, M., ISMAIL, M. & GHAZALI, A. 2021. Towards Sustainable Development: Building's Retrofitting with PCMs to Enhance the Indoor Thermal Comfort in Tropical Climate, Malaysia. *Sustainability,* 13**,** 3614.

AL-GHAMDI, S. G. & AL-FERIDAH, A. K. Potential energy saving and peak shaving of electric in single family houses in Saudi Arabia. Proceedings of Conference: People and Buildings held at the offices of Arup UK, 23rd September 2011. London, 2011. 1-6.

AL-MOFEEZ, I. A. 1991. *Insulation in the opaque envelope: effects on thermal performance of residential buildings in hot-arid climates.* Texas A&M University.

AL-SAGGAF, A., NASIR, H. & TAHA, M. 2020. Quantitative approach for evaluating the building design features impact on cooling energy consumption in hot climates. *Energy and Buildings,* 211**,** 109802.

AL-SANEA, S. A. & ZEDAN, M. 2011. Improving thermal performance of building walls by optimizing insulation layer distribution and thickness for same thermal mass. *Applied Energy,* 88**,** 3113-3124.

AL-SANEA, S. A., ZEDAN, M. F. & AL-HUSSAIN, S. N. 2012. Effect of thermal mass on performance of insulated building walls and the concept of energy savings potential. *Applied Energy,* 89**,** 430-442.

AL-SHAYEB 2021. Typical Precast Concrete Sandwich Panel Details in Saudi Prefabricated Housing Construction Industries. AL-SHAYEB CONSULTANT ENGINEERING.

AL-TAMIMI, N. 2022. Building Envelope Retrofitting Strategies for Energy-Efficient Office Buildings in Saudi Arabia. *Buildings,* 12**,** 1900.

AL-TAMIMI, N. A. 2015. Toward sustainable building design: Improving thermal performance by applying natural ventilation in hot–humid climate. *Indian Journal of Science and Technology,* 8**,** 1-8.

AL-YASIRI, Q. & SZABÓ, M. 2021. Case study on the optimal thickness of phase change material incorporated composite roof under hot climate conditions. *Case Studies in Construction Materials,* 14**,** e00522.
AL SURF, M. S. & MOSTAFA, L. A. 2017. Will the Saudi's 2030 Vision Raise the Public Awareness of Sustainable Practices? *Procedia Environmental Sciences,* 37**,** 514-527.
ALAIDROOS, A. & KRARTI, M. Impact of Passive Cooling Strategies on Energy Consumption Reduction of Residential Buildings in the Kingdom of Saudi Arabia. ASME 2015 9th International Conference on Energy Sustainability collocated with the ASME 2015 Power Conference, the ASME 2015 13th International Conference on Fuel Cell Science, Engineering and Technology, and the ASME 2015 Nuclear Forum, 2015a. V002T17A002.
ALAIDROOS, A. & KRARTI, M. 2015b. Optimal design of residential building envelope systems in the Kingdom of Saudi Arabia. *Energy and Buildings,* 86**,** 104-117.
ALAIDROOS, A. & KRARTI, M. 2016. Evaluation of passive cooling systems for residential buildings in the Kingdom of Saudi Arabia. *Journal of Solar Energy Engineering,* 138.
ALASSAF, Y. 2024. Comprehensive Review of the Advancements, Benefits, Challenges, and Design Integration of Energy-Efficient Materials for Sustainable Buildings. *Buildings,* 14**,** 2994.
ALAYED, E., O'HEGARTY, R. & KINNANE, O. 2021. Thermal envelope analysis for new code compliance of Saudi Arabian dwellings. *Energy and Buildings,* 243**,** 110997.
ALBOGAMI, S. & BOUKHANOUF, R. 2019. Residential building energy performance evaluation for different climate zones. *IOP Conference Series: Earth and Environmental Science,* 329**,** 012026.
ALDABESH, A., SOUFI, J., OMER, S. & HAREDY, A. 2021. Unlocking the Residential Retrofitting Potential in a Three-Degree World: A Holistic Approach to Passive Design in Hot Climates. *Buildings,* 11**,** 228.
ALMUJAHID, A. & KANEESAMKANDI, Z. 2013. Construction of a test room for evaluating thermal performance of building wall systems under real conditions. *measurement,* 2.
ALRASHDAN, A., GHALEB, A. M., AHMAD, K. H. & DAOUD, A. N. 2024. Integration of Phase Change Materials in Service Areas of Building Envelopes for Improved Thermal Performance: An Experimental Study in Saudi Arabia. *Buildings,* 14**,** 904.
ALRASHED, F. & ASIF, M. Challenges facing the application of zero-energy homes in Saudi Arabia: Construction industry and user perspective. Proceedings of the ZEMCH 2012 International Conference, Glasgow, UK, 2012. 20-22.
ALRASHED, F. & ASIF, M. 2014. Trends in residential energy consumption in Saudi Arabia with particular reference to the Eastern Province. *Journal of Sustainable Development of Energy, Water and Environment Systems,* 2**,** 376-387.
ALRASHED, F. A. 2015. *Design and application of zero-energy homes in Saudi Arabia.* Glasgow Caledonian University.
ALSAADANI, S. & DE SOUZA, C. The social component of building performance simulation: Understanding architects. Proceedings of the 2012 Building Simulation and Optimization Conference, Loughborough University, Loughborough, UK, September, 2012. 10-11.

ALSHENAIF, M. 2015. *High performance homes in Saudi Arabia Revised Passivhaus principles for hot and arid climates.* M. Sc. Thesis, Philadelphia University.

ALSHUHAIL, K. & TALEB, H. 2020. Thermal performance and experimental assessment of building orientations in the United Arab Emirates (UAE). *Science and Technology for the Built Environment,* 26**,** 1461-1489.

ALWETAISHI, M., BALABEL, A., ABDELHAFIZ, A., ISSA, U., SHARAKY, I., SHAMSELDIN, A., AL-SURF, M., AL-HARTHI, M. & GADI, M. 2020. User Thermal Comfort in Historic Buildings: Evaluation of the Potential of Thermal Mass, Orientation, Evaporative Cooling and Ventilation. *Sustainability,* 12**,** 9672.

ALYAMI, M. 2024. The Impact of the Composition and Location of Thermal Insulation in the Building Envelope on Energy Consumption in Low-Rise Residential Buildings in Hot Climate Regions. *Arabian Journal for Science and Engineering,* 49**,** 5305-5351.

AMERICAN SOCIETY OF HEATING, R. & AIR-CONDITIONING ENGINEERS, I. 2021 ASHRAE® Handbook - Fundamentals (SI Edition). American Society of Heating, Refrigerating and Air-Conditioning Engineers, Inc. (ASHRAE).

ANG SOON ERN, P., MEI LING, L., KASIM, N., ABD HAMID, Z. & BIN MASROM, M. A. N. 2017. Thermal Performance of Precast Concrete Sandwich Panel (PCSP) Design for Sustainable Built Environment. *IOP Conference Series: Materials Science and Engineering,* 245**,** 032073.

ASADI, I. 2018. Thermal conductivity of concrete – A review.

ASB. 2020. *Annual Statistical Bulletin* [Online]. Available: https://www.opec.org/opec_web/en/publications/202.htm [Accessed at 10 March 2020].

ASCIONE, F., BIANCO, N., DE MASI, R. F., DE' ROSSI, F. & VANOLI, G. P. 2014. Energy refurbishment of existing buildings through the use of phase change materials: Energy savings and indoor comfort in the cooling season. *Applied Energy,* 113**,** 990-1007.

ASDRUBALI, F., D'ALESSANDRO, F. & SCHIAVONI, S. 2015. A review of unconventional sustainable building insulation materials. *Sustainable Materials and Technologies,* 4**,** 1-17.

ASFOUR, O. S. 2020. A comparison between the daylighting and energy performance of courtyard and atrium buildings considering the hot climate of Saudi Arabia. *Journal of Building Engineering,* 30**,** 101299.

ASHRAE. 2016. *How much ventilation do I need in my home to improve indoor air quality?* [Online]. EPA: United States Environmental Protection Agency. Available: https://www.epa.gov/indoor-air-quality-iaq/how-much-ventilation-do-i-need-my-home-improve-indoor-air-quality [Accessed on 2 of March 2023].

ASHRAE. 2023. *ANSI/ASHRAE Standard 55 Thermal Environmental Conditions for Human Occupancy* [Online]. Available: https://www.ashrae.org/technical-resources/bookstore/standard-55-thermal-environmental-conditions-for-human-occupancy?utm_source=chatgpt.com [Accessed on 12 of December 2024].

ASHRAE, A. 2010. Standard 55-2010: Thermal environmental conditions for human occupancy. 2010. *American Society of heating, Refridgerating and Airconditioning Engineers: Atlanta*.

ASHRAE, A. 2013. Standard 55-2013: Thermal environmental conditions for human occupancy. *American Society of Heating, Refrigerating, and Air-Conditioning Engineers, Inc. Atlanta*.

ASIF, M., DEHWAH, A. H. A., ASHRAF, F., KHAN, H. S., SHAUKAT, M. M. & HASSAN, M. T. 2017. Life cycle assessment of a three-bedroom house in Saudi Arabia. *Environments,* 4**,** 52.

ATTIA, S., BELTRÁN, L., DE HERDE, A. & HENSEN, J. "Architect friendly": A comparison of ten different building performance simulation tools. Proceedings of 11th International Building Performance Simulation Association Conference and Exhibition, 2009. International Building Performance Simulation Association (IBPSA).

ATTIA, S., GRATIA, E., DE HERDE, A. & HENSEN, J. L. 2012. Simulation-based decision support tool for early stages of zero-energy building design. *Energy and buildings,* 49**,** 2-15.

AULICIEMS, A. & DEAR, R. D. 1998. Thermal adaptation and variable indoor climate control. *Human Bioclimatology***,** 61-86.

BAGARIĆ, M., BANJAD PEČUR, I. & MILOVANOVIĆ, B. 2020. Hygrothermal performance of ventilated prefabricated sandwich wall panel from recycled construction and demolition waste – A case study. *Energy and Buildings,* 206**,** 109573.

BALABEL, A., EL-ASKARY, W., ALAHMADI, A. & ALZAED, A. 2024. Development of a passive strategy for buildings' sustainability using green roofs techniques in Taif City, Saudi Arabia. *Journal of Umm Al-Qura University for Engineering and Architecture,* 15**,** 31-45.

BANHAM, R. 1980. *Theory and design in the first machine age*, MIT press.

BAUGHMAN, A. & ARENS, E. A. 1996. Indoor humidity and human health--Part I: Literature review of health effects of humidity-influenced indoor pollutants.

BENA, A., GILLOTT, M. & BOUKHANOUF, R. 2019. Review of Strategy for Assessing the Thermal Performance of Institutional Building Form in Hot Dry Climate of Nigeria.

BOLTZMANN, S. 2021. *Emissivity Coefficients common Products* [Online]. The Engineering ToolBox. Available: https://www.engineeringtoolbox.com/emissivity-coefficients-d_447.html [Accessed 26 of December 2021].

BOUCHLAGHEM, N. 2000. Optimising the design of building envelopes for thermal performance. *Automation in construction,* 10**,** 101-112.

BULLETIN, A. S. 2024. *Saudi Arabia facts and figures* [Online]. OPEC. Available: https://www.opec.org/opec_web/en/about_us/169.htm?utm_source=chatgpt.com [Accessed on 12 of December 2024].

BUTCHER, K. J. 2006. *Environmental design : CIBSE guide A / editor, Ken J. Butcher*, London : CIBSE.

CALAMA-GONZÁLEZ, C. M., SUÁREZ, R., LEÓN-RODRÍGUEZ, Á. L. & FERRARI, S. 2019. Assessment of Indoor Environmental Quality for Retrofitting Classrooms with An Egg-Crate Shading Device in A Hot Climate. *Sustainability,* 11**,** 1078.

CANDIDO, C. & DEAR, R. D. 2012. From thermal boredom to thermal pleasure: a brief literature review. *Ambiente Construído,* 12**,** 81-90.

CAO, X., LI, X., ZHU, Y. & ZHANG, Z. 2015. A comparative study of environmental performance between prefabricated and traditional residential buildings in China. *Journal of cleaner production,* 109**,** 131-143.

CEMENT, S. 2023. About the Company's Business for The Extra-Ordinary General Assembly Meeting. *Annual Report 2023.* Saudi Cement.

CHEN, Y., TONG, Z. & MALKAWI, A. 2017. Investigating natural ventilation potentials across the globe: Regional and climatic variations. *Building and Environment,* 122**,** 386-396.

CIOBANU, A.-A. & IACOB, A. 2013. A PARAMETRIC STUDY OF THERMAL PERFORMANCE OF AN EXTERIOR WALL INSULATED WITH VACUUM INSULATION PANELS. *Buletinul Institutului Politehnic din lasi. Sectia Constructii, Arhitectura,* 59**,** 37-45.

CLARKE, J., YANESKE, P. & PINNEY, A. 1991. *The harmonisation of thermal properties of building materials,* Building Research Esablishment.

CORRADO, V., SERRA, V. & VOSILLA, A. Performance analysis of external shading devices. Proceedings of PLEA, 2004.

CORREIA, J. R., FERREIRA, J. & BRANCO, F. A. 2006. A rehabilitation study of sandwich GRC facade panels. *Construction and Building Materials,* 20**,** 554-561.

CRAWLEY, D. B., HAND, J. W., KUMMERT, M. & GRIFFITH, B. T. 2008. Contrasting the capabilities of building energy performance simulation programs. *Building and environment,* 43**,** 661-673.

DE DEAR, R. 1985a. Validation of the predicted mean vote model of thermal comfort in six Australian field studies. *ASHRAE Transactions, B,* 91**,** 452-468.

DE DEAR, R. Recent enhancements to the adaptive comfort standard in ASHRAE 55-2010. Proceedings of the 45th annual conference of the Architectural Science Association, Sydney, Australia, 2011a. Citeseer, 16-19.

DE DEAR, R. 2011b. Revisiting an old hypothesis of human thermal perception: alliesthesia. *Building Research & Information,* 39**,** 108-117.

DE DEAR, R. & BRAGER, G. S. 1998. Developing an adaptive model of thermal comfort and preference.

DE DEAR, R. & SCHILLER BRAGER, G. 2001. The adaptive model of thermal comfort and energy conservation in the built environment. *International journal of biometeorology,* 45**,** 100-108.

DE DEAR, R. J. 1985b. *Perceptual and adaptational basis for the management of indoor climate: A study in warm Australian environments.* University of Queensland.

DE DEAR, R. J. & BRAGER, G. S. 2002. Thermal comfort in naturally ventilated buildings: revisions to ASHRAE Standard 55. *Energy and buildings,* 34**,** 549-561.

DENG, J., YAO, R., YU, W., ZHANG, Q. & LI, B. 2019. Effectiveness of the thermal mass of external walls on residential buildings for part-time part-space heating and cooling using the state-space method. *Energy and Buildings,* 190**,** 155-171.

DESIGNBUILDER. 2022. *Simulation Hourly Weather Data* [Online]. Available: https://designbuilder.co.uk/helpv2/Content/Hourly_Weather_Data.htm [Accessed 20 Feb 2022].

DUBEY, K., HOWARTH, N. & KRARTI, M. 2016. Evaluating building energy efficiency investment options for Saudi Arabia. *Riyadh, Kapsarc*.

EFEOMA, M. O. & UDUKU, O. 2014. Assessing thermal comfort and energy efficiency in tropical African offices using the adaptive approach. *Structural Survey*.

EL-ABIDI, K. M. A. & GHAZALI, F. E. M. 2015. Motivations and Limitations of Prefabricated Building: An Overview. *Applied Mechanics and Materials,* 802**,** 668-675.
EL BAKKUSH, A., LASKER, W. & HARRIS, D. J. 2015. On-site measurements of thermal performance of a residential building in a hot-arid region. *International Journal for Housing Science and its Applications,* 39**,** 135-145.
ELNABAWI, M. H. 2021. Evaluating the Impact of Energy Efficiency Building Codes for Residential Buildings in the GCC. *Energies,* 14**,** 8088.
ENERGYPLUS. 2021a. *Comfort Analysis* [Online]. energyPlus. Available: https://designbuilder.co.uk/helpv2/Content/Comfort_Analysis.htm [Accessed 6 April 2022].
ENERGYPLUS, D. W. 2021b. *ASHRAE 140-2017 Validation Report, Building Thermal Envelope and Fabric Load Tests* [Online]. Available: https://designbuilder.co.uk/download/documents [Accessed 29 Sep 2021].
ERBAS, I. & VAN DIJK, S. 2012. A survey for the improvement of decision support tools for effective sustainable architectural design. *International Journal of Sustainable Building Technology and Urban Development,* 3**,** 294-305.
EVANS, M. 1980. *Housing, climate, and comfort / Martin Evans,* London : New York, London : Architectural Press

New York : John Wiley & Sons.
FAGEHI, H. & HADIDI, H. M. 2022. Toward buildings with lower power demand in the smart city of NEOM-incorporating phase change material into building envelopes. *Sustainable Energy Technologies and Assessments,* 53**,** 102494.
FAHMY, M., ATTIA, W., AL SAYED, A. A.-K. A. & IBRAHIM, H. 2024. Shear performance of X and Z configuration wythe ties for insulated precast concrete sandwich panels using different FRP materials. *Journal of Building Engineering,* 85**,** 108701.
FANGER, P. O. 1970. Thermal comfort. Analysis and applications in environmental engineering. *Thermal comfort. Analysis and applications in environmental engineering.*
FLANSBJER, M., WILLIAMS PORTAL, N., VENNETTI, D. & MUELLER, U. 2018. Composite behaviour of textile reinforced reactive powder concrete sandwich façade elements. *International Journal of Concrete Structures and Materials,* 12**,** 1-17.
FRANKL, B., LUCIER, G., RIZKALLA, S., BLASZAK, G. & HARMON, T. Structural behavior of insulated prestressed concrete sandwich panels reinforced with FRP grid. Proceedings of the Fourth International Conference on FRP Composites in Civil Engineering (CICE2008), Zurich, Switzerland, 2008.
FRANKL, B. A., LUCIER, G. W., HASSAN, T. K. & RIZKALLA, S. H. 2011. Behavior of precast, prestressed concrete sandwich wall panels reinforced with CFRP shear grid. *PCI journal,* 56**,** 42-54.
GEETA, B., BHADAURIA, S. & SALEEM, A. 2013. A Review: Recent Innovations in Self Compacting Concrete. *International Journal of Scientific & Engineering Research,* 4.
GENERAL AUTHORITY FOR STATISTICS. 2024. *Population estimates* [Online]. Available: https://www.stats.gov.sa/en/node [Accessed at 9 of December 2024].
GLEICH, H. 2007. New carbon fiber reinforcement advances sandwich wall panels. *Structure.*

GREGORY, K., MOGHTADERI, B., SUGO, H. & PAGE, A. 2008. Effect of thermal mass on the thermal performance of various Australian residential constructions systems. *Energy and buildings,* 40**,** 459-465.

HAASE, M. & AMATO, A. 2009. An investigation of the potential for natural ventilation and building orientation to achieve thermal comfort in warm and humid climates. *Solar Energy,* 83**,** 389-399.

HAMMARBERG, E. & ROOS, A. 2003. Antireflection treatment of low-emitting glazings for energy efficient windows with high visible transmittance. *Thin Solid Films,* 442**,** 222-226.

HARRISON, H., BIRKS, M., FRANKLIN, R. & MILLS, J. Case study research: Foundations and methodological orientations. Forum qualitative Sozialforschung/Forum: qualitative social research, 2017. 1-17.

HASHIM, N. H. 1991. *Evaluation of alternative thermal strategies for the precast concrete system houses in Jeddah, Saudi Arabia.* University College, Cardiff.

HASSAN, T. K. & RIZKALLA, S. H. 2010. Analysis and design guidelines of precast, prestressed concrete, composite load-bearing sandwich wall panels reinforced with CFRP grid. *PCI journal,* 55**,** 147.

HAUSLADEN, G., DE SALDANHA, M. & LIEDL, P. 2006. ClimaSkin. Concepts for better thermal insulation and lower energy consumption; ClimaSkin. Konzepte fuer Gebaeudehuellen, die mit weniger Energie mehr leisten.

HEGGER, J., WILL, N. & HORSTMANN, M. 2009. Summary of Results for the Project INSUSHELL-of the Institute of Structural Concrete (IMB). *RWTH Aachen University*.

HIEN, W. N. & ISTIADJI, A. D. Effects of external shading devices on daylighting and natural ventilation. Proceedings of the 8th International IBPSA Conference, Eindhoven, The Netherlands, 2003. 475-482.

HORSTMANN, M. & HEGGER, J. 2011. Sandwich façades made of Textile Reinforced Concrete-Experimental investigations. *Bautechnik,* 88**,** 281-291.

HOU, H., JI, K., WANG, W., QU, B., FANG, M. & QIU, C. 2019. Flexural behavior of precast insulated sandwich wall panels: Full-scale tests and design implications. *Engineering Structures,* 180**,** 750-761.

HOUGHTON, C., CASEY, D., SHAW, D. & MURPHY, K. 2013. Rigour in qualitative case-study research. *Nurse researcher,* 20.

HUANG, J.-Q., XU, Y.-Y., HUANG, H. & DAI, J.-G. 2022. Structural behavior of FRP connector enabled precast geopolymer concrete sandwich panels subjected to one-side fire exposure. *Fire Safety Journal***,** 103524.

HÜLSMEIER, F. vakutex-Vacuum-Insulated Textile Concrete Facade Elements. 2nd Annu. Int. Conf. Archit. Civ. Eng. ACE, 2014. 235-241.

ISO, E. 2007. 6946: Building components and building elements–Thermal resistance and thermal transmittance–Calculation method (ISO 6946: 2007). *German version EN ISO,* 6946.

JAGDEEP VERMA, H. C. 2023. *Cement in Saudi Arabia* [Online]. Available: https://www.globalcement.com/magazine/articles/1335-cement-in-saudi-arabia?utm_source=chatgpt.com [Accessed on 12 of December 2024].

JAWDHARI, A., FAM, A. & KADHIM, M. M. A. 2022. Thermal bowing of reinforced concrete sandwich panels using time-domain coupled-field finite element analysis. *Engineering Structures,* 252**,** 113592.

JING, S., LI, B., TAN, M. & LIU, H. 2013. Impact of relative humidity on thermal comfort in a warm environment. *Indoor and Built Environment,* 22**,** 598-607.

JITHIN, P. U. & JOSEPH, A. Thermal and Structural Behavior of Precast Concrete Sandwich Panels. *In:* MARANO, G. C., RAHUL, A. V., ANTONY, J., UNNI KARTHA, G., KAVITHA, P. E. & PREETHI, M., eds. Proceedings of SECON'22, 2023// 2023 Cham. Springer International Publishing, 511-522.

JOHANSSON, P. 2012. Vacuum insulation panels in buildings: Literature review.

JOHANSSON, R. 2007. On case study methodology. *Open house international*.

JOSEPH, J. D. R., PRABAKAR, J. & ALAGUSUNDARAMOORTHY, P. 2018. Flexural behavior of precast concrete sandwich panels under different loading conditions such as punching and bending. *Alexandria engineering journal,* 57**,** 309-320.

KAPSARC. 2020. *Electricity Consumption by Sectors,* [Online]. Available: https://datasource.kapsarc.org/explore/dataset/electricity-consumption-by-sectors/information/?disjunctive.region&disjunctive.type_of_consumption [Accessed on 10 November 2020].

KAYELLO, A., GE, H., ATHIENITIS, A. & RAO, J. 2017. Experimental study of thermal and airtightness performance of structural insulated panel joints in cold climates. *Building and Environment,* 115**,** 345-357.

KEENEHAN, J., CONCANNON, K., HAJIALIZADEH, D. & MCNALLY, C. Numerical Asessment of The Thermal Performance of Structural Precast Panels. Proceedings of the 1st International Conference on Numerical Modeling Strategies for Sustainable Concrete Structures, 2012.

KHAN, N., SU, Y. & RIFFAT, S. B. 2008. A review on wind driven ventilation techniques. *Energy and buildings,* 40**,** 1586-1604.

KHAYYAMINEJAD, A. & FARTAJ, A. 2024. Unveiling the synergy of passive cooling, efficient ventilation, and indoor air quality through optimal PCM location in building envelopes. *Journal of Energy Storage,* 89**,** 111633.

KIM, Y. J. & ALLARD, A. 2014. Thermal response of precast concrete sandwich walls with various steel connectors for architectural buildings in cold regions. *Energy and Buildings,* 80**,** 137-148.

KNAACK, U. 2012. *Prefabricated systems : principles of construction / Ulrich Knaack, Sharon Chung-Klatte, Reinhard Hasselbach,* Basel, Basel : Birkhauser.

KNAACK, U., CHUNG-KLATTE, S. & HASSELBACH, R. 2012. *Prefabricated systems: Principles of construction*, Walter de Gruyter.

KRARTI, M., ALDUBYAN, M. & WILLIAMS, E. 2020. Residential building stock model for evaluating energy retrofit programs in Saudi Arabia. *Energy,* 195**,** 116980.

KUMAR, S., SINGH, M. K., MATHUR, A., MATHUR, S. & MATHUR, J. 2018. Thermal performance and comfort potential estimation in low-rise high thermal mass naturally ventilated office buildings in India: An experimental study. *Journal of Building Engineering,* 20**,** 569-584.

KUMAR, S., TEWARI, P., MATHUR, S. & MATHUR, J. 2017. Development of mathematical correlations for indoor temperature from field observations of the performance of high thermal mass buildings in India. *Building and Environment,* 122**,** 324-342.

LAMEIRAS, R., BARROS, J. A. O., VALENTE, I. B., POLETTI, E., AZEVEDO, M. & AZENHA, M. 2021. Seismic behaviour of precast sandwich wall panels of steel fibre reinforced concrete layers and fibre reinforced polymer connectors. *Engineering Structures,* 237**,** 112149.

LASKER, W. J. A. 2016. *The impact of construction and building materials on energy consumption on Saudi residential buildings.* Heriot-Watt University.

LEE, B.-J. & PESSIKI, S. 2004. Analytical investigation of thermal performance of precast concrete three-wythe sandwich wall panels. *PCI journal,* 49**,** 88-101.

LEE, B.-J. & PESSIKI, S. 2006. Thermal performance evaluation of precast concrete three-wythe sandwich wall panels. *Energy and Buildings,* 38**,** 1006-1014.

LEE, B.-J. & PESSIKI, S. 2008a. Experimental evaluation of precast, prestressed concrete, three-wythe sandwich wall panels. *PCI journal,* 53.

LEE, B.-J. & PESSIKI, S. 2008b. Revised zone method R-value calculation for precast concrete sandwich panels containing metal wythe connectors. *PCI journal,* 53.

LEE, B. D., SUN, Y., AUGENBROE, G. & PAREDIS, C. J. Towards better prediction of building performance: a workbench to analyze uncertainty in building simulation. 13th International Building Performance Simulation Association Conference, Chambéry, France, 2013.

LEE, H. 2016. *Sustainability of precast sandwich panel: Possible development towards Korean market.* Civil Engineering, Helsinki Metropolia University of Applied Sciences.

LEE, J.-H., KANG, S.-H., HA, Y.-J. & HONG, S.-G. 2018. Structural behavior of durable composite sandwich panels with high performance expanded polystyrene concrete. *International Journal of Concrete Structures and Materials,* 12**,** 1-13.

LI, Y. & YAM, J. C. W. 2004. Designing thermal mass in naturally ventilated buildings. *International Journal of Ventilation,* 2**,** 313-324.

LIND, J., MÖLLERSTRÖM, E., AVERFALK, H. & OTTERMO, F. 2023. Energy flexibility using the thermal mass of residential buildings. *Energy and Buildings,* 301**,** 113698.

LIPING, W. & HIEN, W. N. 2007. The impacts of ventilation strategies and facade on indoor thermal environment for naturally ventilated residential buildings in Singapore. *Building and Environment,* 42**,** 4006-4015.

LIU, P., WU, W., DU, B., HUA TIAN, G. & GONG, Y. F. 2022. Study on the heat and moisture transfer characteristics of aerogel-enhanced foam concrete precast wall panels and the influence of building energy consumption. *Energy and Buildings,* 256**,** 111707.

LOLLI, N. & ANDRESEN, I. 2016. Aerogel vs. argon insulation in windows: A greenhouse gas emissions analysis. *Building and Environment,* 101**,** 64-76.

LOMAS, K. J. & GIRIDHARAN, R. 2012. Thermal comfort standards, measured internal temperatures and thermal resilience to climate change of free-running buildings: A case-study of hospital wards. *Building and Environment,* 55**,** 57-72.

LOSCH, E. D., HYNES, P. W., ANDREWS JR, R., BROWNING, R., CARDONE, P., DEVALAPURA, R., DONAHEY, R., FREEDMAN, S., GLEICH, H. A. & GOETTSCHE, G. 2011. State of the art of precast/prestressed concrete sandwich wall panels. *PCI journal,* 56**,** 131-176.

LUO, M., WANG, Z., KE, K., CAO, B., ZHAI, Y. & ZHOU, X. 2018. Human metabolic rate and thermal comfort in buildings: The problem and challenge. *Building and Environment,* 131**,** 44-52.

MAGZOUB, M., ALHAJI MOHAMMED, M., BUDAIWI, I. M. & AL-HOMOUD, M. S. 2024. Assessment of thermal performance of energy-active window systems in hot climates. *Energy and Buildings,* 318**,** 114473.

MAHMOUD, R., KAMARA, J. & BURFORD, N. 2020. Opportunities and Limitations of Building Energy Performance Simulation Tools in the Early Stages of Building Design in the UK. *Sustainability,* 12.

MARANI, A. & MADHKHAN, M. 2021. Thermal performance of concrete sandwich panels incorporating phase change materials: An experimental study. *Journal of Materials Research and Technology,* 12**,** 760-775.

MARTÍNEZ-MOLINA, A., TORT-AUSINA, I., CHO, S. & VIVANCOS, J.-L. 2016. Energy efficiency and thermal comfort in historic buildings: A review. *Renewable and Sustainable Energy Reviews,* 61**,** 70-85.

MCCARTNEY, K. & HUMPHREYS, M. 2002. Thermal comfort and productivity. *Proceedings of Indoor Air,* 2002**,** 822-827.

MEZAIEN, A. A. & BALTAZAR, J.-C. 2024. Potential Regenerative Impact of Implementation of Cultural Vernacular Elements (Rowshan) in Jeddah, Saudi Arabia. *Energies,* 17**,** 1995.

MOSTAFAEIPOUR, A., GOUDARZI, H., SEDAGHAT, A., JAHANGIRI, M., HADIAN, H., REZAEI, M., GOLMOHAMMADI, A.-M. & KARIMI, P. 2019. Energy efficiency for cooling buildings in hot and dry regions using sol-air temperature and ground temperature effects. *Journal of Engineering, Design and Technology*.

MOTOYAMA TATAMI SHOP. 2016. *The Japanese flooring* [Online]. Available: https://en.wikipedia.org/wiki/Tatami#inauspicious [Accessed on 30 March 2020].

MOUSA, W. A. Y., LANG, W. & YOUSEF, W. A. 2017. Simulations and quantitative data analytic interpretations of indoor-outdoor temperatures in a high thermal mass structure. *Journal of Building Engineering,* 12**,** 68-76.

MUJEEBU, M. A. & ALSHAMRANI, O. S. 2016. Prospects of energy conservation and management in buildings–The Saudi Arabian scenario versus global trends. *Renewable and Sustainable Energy Reviews,* 58**,** 1647-1663.

MUNIZ, P. A. 1985. *The geometry of external shading devices as related to natural ventilation, daylighting and thermal comfort, with particular reference to tropical hot-humid climates,* Virginia Polytechnic Institute and State University.

NATIONAL CENTER FOR METEOROLOGY. 2020. *Climate of the Kingdom of Saudi Arabia* [Online]. Available: https://ncm.gov.sa/ar/Pages/default.aspx [Accessed at 8 March 2020].

NATIONAL GEOGRAPHIC. 2017. *Mongolian Yurt ; A yurt is a portable, circular dwelling made of a lattice of flexible wood and covered in felt.* [Online]. Available: https://www.nationalgeographic.org/encyclopedia/yurt/ [Accessed on 29 March 2021].

NEJAT, P., JOMEHZADEH, F., TAHERI, M. M., GOHARI, M. & MAJID, M. Z. A. 2015. A global review of energy consumption, CO2 emissions and policy in the residential sector (with an overview of the top ten CO2 emitting countries). *Renewable and sustainable energy reviews,* 43**,** 843-862.

NEWS, A. 2024. *New report focuses on cultural sector sustainability in Saudi Arabia* [Online]. ARAB NEWS. Available: https://www.arabnews.com/node/2569966/saudi-arabia [Accessed on 9 of December 2024].

NIALL, D. & WEST, R. 2024. Development of Concrete Façade Sandwich Panels Incorporating Phase Change Materials. *Energies,* 17**,** 2924.

NICOL, J. F. & HUMPHREYS, M. A. 1973. Thermal comfort as part of a self-regulating system.

NIELSEN, H. 2019. *Literacy in Saudi Arabia: Striving for Excellence* [Online]. Available: https://www.fawco.org/global-issues/education/education-articles/4158-literacy-in-saudi-arabia-striving-for-excellence [Accessed at 9 of March 2020].

O'HEGARTY, R. & KINNANE, O. 2020. Review of precast concrete sandwich panels and their innovations. *Construction and Building Materials,* 233**,** 117145.

O'HEGARTY, R., KINNANE, O., GRIMES, M., NEWELL, J., CLIFFORD, M. & WEST, R. 2021. Development of thin precast concrete sandwich panels: Challenges and outcomes. *Construction and Building Materials,* 267**,** 120981.

O'HEGARTY, R., REILLY, A., WEST, R. & KINNANE, O. 2020. Thermal investigation of thin precast concrete sandwich panels. *Journal of Building Engineering,* 27**,** 100937.

OLIVIERI, L., TENORIO, J. A., REVUELTA, D., NAVARRO, L. & CABEZA, L. F. 2018. Developing a PCM-enhanced mortar for thermally active precast walls. *Construction and Building Materials,* 181**,** 638-649.

OPEC. 2019. *Saudi Arabia facts and figures* [Online]. Organization of The Pertoleum Exporting Countries. Available: https://www.opec.org/opec_web/en/about_us/169.htm [Accessed 10 of March 2020].

OZARISOY, B. & ELSHARKAWY, H. 2019. Assessing overheating risk and thermal comfort in state-of-the-art prototype houses that combat exacerbated climate change in UK. *Energy and Buildings,* 187**,** 201-217.

PATHIRANA, S., RODRIGO, A. & HALWATURA, R. 2019. Effect of building shape, orientation, window to wall ratios and zones on energy efficiency and thermal comfort of naturally ventilated houses in tropical climate. *International Journal of Energy and Environmental Engineering,* 10**,** 107-120.

PEREIRA, P. F. D. C. & BRODAY, E. E. 2021. Determination of Thermal Comfort Zones through Comparative Analysis between Different Characterization Methods of Thermally Dissatisfied People. *Buildings,* 11**,** 320.

PORTAL, N. W. 2013. *Sustainability and flexural behaviour of textile reinforced concrete*, Chalmers Tekniska Hogskola (Sweden).

PORTAL, N. W., FLANSBJER, M., ZANDI, K., WLASAK, L. & MALAGA, K. 2017. Bending behaviour of novel Textile Reinforced Concrete-foamed concrete (TRC-FC) sandwich elements. *Composite Structures,* 177**,** 104-118.

PUNGERCAR, V., ZHAN, Q., XIAO, Y., MUSSO, F., DINKEL, A. & PFLUG, T. 2021. A new retrofitting strategy for the improvement of indoor environment quality and energy efficiency in residential buildings in temperate climate using prefabricated elements. *Energy and Buildings,* 241**,** 110951.

RABABA, W. & ASFOUR, O. S. 2024. Façade Retrofit Strategies for Energy Efficiency Improvement Considering the Hot Climatic Conditions of Saudi Arabia. *Applied Sciences,* 14**,** 10003.

REILLY, A. & KINNANE, O. 2017. The impact of thermal mass on building energy consumption. *Applied Energy,* 198**,** 108-121.

RIBEIRO, K. B. 2024. Experimental analysis of precast sandwich panels with EPS core and mortar wythes under axial load.

RICHARD, O., WEST, R., REILLY, A. & KINNANE, O. 2019. Composite behaviour of fibre-reinforced concrete sandwich panels with FRP shear connectors. *Engineering Structures,* 198**,** 109475.

ROAF, S., FUENTES, M. & THOMAS-REES, S. 2014. *Ecohouse*, Routledge.
RODRIGUES, E., FERNANDES, M. S., GASPAR, A. R., GOMES, Á. & COSTA, J. J. 2019. Thermal transmittance effect on energy consumption of Mediterranean buildings with different thermal mass. *Applied Energy,* 252**,** 113437.
ROHLES, F. 1974. The effects of air movement and temperature on the thermal sensations of sedentary man. *ASHRAE transactions,* 80**,** 101-119.
ROYAL COMMISSION FOR JUBAIL AND YANBU INDUSTRIAL CITY 2011. Housing Technologies in Royal Commission Projects.
SAH, T. P., LACEY, A. W., HAO, H. & CHEN, W. 2024. Prefabricated Concrete Sandwich and Other Lightweight Wall Panels for Sustainable Building Construction: State-of-the-Art Review. *Journal of Building Engineering***,** 109391.
SAKANI. 2019. *Achievements of the Ministry of Housing* ‹[Online]. sakani housing. Available: https://www.housing.gov.sa/en/node [Accessed 16 November 2020].
SARı, A., BICER, A., KARAIPEKLI, A. & AL-SULAIMAN, F. A. 2018. Preparation, characterization and thermal regulation performance of cement based-composite phase change material. *Solar Energy Materials and Solar Cells,* 174**,** 523-529.
SAUDI ARABIAN CULTURAL MISSION. 2020. *Culture, Traditions and Art of Saudi Arabia* [Online]. Available: https://sacm.org.au/culture-traditions-and-art/ [Accessed at 9 March 2020].
SAUDI BUILDING CODE NATIONAL COMMITTEE. 2019. *Saudi Building Code Application Law,* [Online]. Available: https://www.sbc.gov.sa/Ar/BuildingCode/Pages/system.aspx [Accessed on 24 Nov 2020].
SAVVIDES, A. Urban Design as a Tool for Preservation and Adaptive Reuse of Public Space in Historic Districts. 2013. International Conference on Architecture and Urban Design.
SBC. 2021. *THERMAL INSULATION IN BUILDINGS; The Guide for Thermal Insulation in Buildings* [Online]. Saudi Electricity Company. Available: https://www.se.com.sa/en-us/Pages/ThermalInsulationinBuildings.aspx [Accessed 4 July 2021].
SCHIAVONI, S., BIANCHI, F. & ASDRUBALI, F. 2016. Insulation materials for the building sector: A review and comparative analysis. *Renewable and Sustainable Energy Reviews,* 62**,** 988-1011.
SEC. 2019. *saudi electricity company, Annual electricity consumption by sector* [Online]. Available: http://www.se.com.sa [Accessed 2019].
SENGUL, O., AZIZI, S., KARAOSMANOGLU, F. & TASDEMIR, M. A. 2011. Effect of expanded perlite on the mechanical properties and thermal conductivity of lightweight concrete. *Energy and Buildings,* 43**,** 671-676.
SHAERI, J. & MAHDAVINEJAD, M. 2022. Prediction Indoor Thermal Comfort in Traditional Houses of Shiraz with PMV/PPD model. *International Journal of Ambient Energy,* 43**,** 8316-8334.
SHAMS, A., HORSTMANN, M. & HEGGER, J. 2014. Experimental investigations on Textile-Reinforced Concrete (TRC) sandwich sections. *Composite Structures,* 118**,** 643-653.
SHAMS, A., STARK, A., HOOGEN, F., HEGGER, J. & SCHNEIDER, H. 2015. Innovative sandwich structures made of high performance concrete and foamed polyurethane. *Composite Structures,* 121**,** 271-279.

SHAREEF, S., MUSHTAHA, E. S., ABU DABOUS, S. & ALSYOUF, I. 2024. Holistic analysis for the efficiency of the thermal mass performance of precast concrete panels in hot climate zones. *Engineering, Construction and Architectural Management,* 31**,** 4184-4206.

SOARES, N., COSTA, J. J., GASPAR, A. R. & SANTOS, P. 2013. Review of passive PCM latent heat thermal energy storage systems towards buildings' energy efficiency. *Energy and Buildings,* 59**,** 82-103.

STASZCZUK, A. & KUCZYŃSKI, T. Using the ground as a heat sink in residential buildings during heat waves. IOP Conference Series: Earth and Environmental Science, 2018. IOP Publishing, 012034.

STRAUBE, J. & ENG, P. 2008. Insight: Can Highly Glazed Building Façades Be Green? *Building Science Insights,* 6.

SU, X. & ZHANG, X. 2010. Environmental performance optimization of window–wall ratio for different window type in hot summer and cold winter zone in China based on life cycle assessment. *Energy and buildings,* 42**,** 198-202.

SUDHAKAR, K., WINDERL, M. & PRIYA, S. S. 2019. Net-zero building designs in hot and humid climates: A state-of-art. *Case Studies in Thermal Engineering,* 13**,** 100400.

SZOKOLAY, S. 2014. *Introduction to Architectural Science: The Basis of Sustainable Design,* London, London: Routledge.

TAKAGI, J., SHIMONISHIKIDA, S., KITAYAMA, K. & MINAMI, S. 2012. Development of static analysis models of existing wall-type precast reinforced concrete residential buildings. *Journal of Structural and Construction Engineering,* 77**,** 113-120.

TALEB, H. M. & SHARPLES, S. 2011. Developing sustainable residential buildings in Saudi Arabia: A case study. *Applied Energy,* 88**,** 383-391.

TANTASAVASDI, C., SREBRIC, J. & CHEN, Q. 2001. Natural ventilation design for houses in Thailand. *Energy and buildings,* 33**,** 815-824.

TECHCON, G. 2020. *What is Cellular Concrete?* [Online]. Available: https://qgreentech.com/cellular-concrete/ [Accessed 05/10 2023].

THOMPSON, A. 2014. *Major Greenhouse Gas Reductions Needed by 2050: IPCC,* [Online]. Available: https://www.climatecentral.org/news/major-greenhouse-gas-reductions-needed-to-curtail-climate-change-ipcc-17300 [Accessed on 9 November 2020].

TIAN, Z., YANG, J., LEI, Y. P. & YANG, L. 2019. Sensitivity Analysis of Infiltration Rates Impact on Office Building Energy Performance. *IOP Conference Series: Earth and Environmental Science,* 238**,** 012019.

TOFTUM, J. 2004. Air movement--good or bad? *Indoor air,* 14**,** 40-45.

TOMLINSON, D. G. 2015. Behaviour of partially composite precast concrete sandwich panels under flexural and axial loads. *Queen's University, Kingston, Ontario, Canada. A. Ahmad and N. Mohamad (2012). Structural Behaviour of Precast Lightweight Foamed Concrete Sandwich Panel under Axial Load: An Overview*.

TROUP, L., PHILLIPS, R., ECKELMAN, M. J. & FANNON, D. 2019. Effect of window-to-wall ratio on measured energy consumption in US office buildings. *Energy and Buildings,* 203**,** 109434.

TRUBIANO, F. 2013. Energy Free Architectural Design: The Case of Passivhaus and Double Skin Facades. *Design and Construction of High Performance Homes***,** 37-54.

TSOKA, S., THEODOSIOU, T., PAPADOPOULOU, K. & TSIKALOUDAKI, K. 2020. Assessing the Energy Performance of Prefabricated Buildings Considering Different Wall Configurations and the Use of PCMs in Greece. *Energies,* 13.

TSSC. 2024. *Know why developers prefer TSSC for custom-made sandwich panels in Saudi Arabia* [Online]. Harwal Group. Available: https://tsscgroup.com/saudi-arabia/sandwich-panels/?utm_source=chatgpt.com [Accessed on 7th of December 2024].

TURNER, S. C. 2011. What's New in ASHRAE's Standard on Comfort. *ASHRAE Journal,* 53**,** 42.

UNIFIED NATIONAL PLATFORM. 2019. *Emerging economy for Saudi Arabia* [Online]. Available: https://www.my.gov.sa/wps/portal/snp/content/1economic/!ut/p/z1/jY_RCoIwGIWfxSfY-Zczb5cWIeQcU7PdyK5kUBYRPX-yiyAo89z98H0_5zDLOmZH9_SDe_jr6M7TfbJJX1RpTBKkIDMBbeqk5CrlBmDHAJS0xZ7iCYj5DjrPZSlqKqhNmF3ivwG1Ehvo7LBW0rQEiGU-fkTiv28DMrfg88eXigGY6WDcnd0uTdPBV4OMohdeVQ3-/dz/d5/L0lHSkovd0RNQUZrQUVnQSEhLzROVkUvZW4!/ [Accessed at 9 of March 2020].

VOELLINGER, T., BASSI, A. & HEITEL, M. 2014. Facilitating the incorporation of VIP into precast concrete sandwich panels. *Energy and buildings,* 85**,** 666-671.

WILDE, J. 2023. *Indoor Thermal Standards: What's The Difference Between ASHRAE 55 AND ISO 7730?* [Online]. SIMSCALE. Available: https://www.simscale.com/blog/ashrae-55-and-iso-7730/?utm_source=chatgpt.com [Accessed on 10 of December 2024].

WILLIAMS PORTAL, N., FLANSBJER, M., ZANDI, K., WLASAK, L. & MALAGA, K. 2017. Bending behaviour of novel Textile Reinforced Concrete-foamed concrete (TRC-FC) sandwich elements. *Composite Structures,* 177**,** 104-118.

WILLIAMSON, T. J. 2010. Predicting building performance: the ethics of computer simulation. *Building Research & Information,* 38**,** 401-410.

WINDFINDER. 2024. *Wind & weather statistics for Dammam* [Online]. Windfinder. Available: https://www.windfinder.com/windstatistics/dammam_eastern_province_saudi arabia [Accessed at 1st of Dec 2024].

WINWERKS. 2013. *Infinite R Phase Change Material Facts* [Online]. Available: https://www.winwerksipd.com/infinite-r-facts [Accessed on 21 November 2023].

WOLISZ, H., KULL, T. M., MÜLLER, D. & KURNITSKI, J. 2020. Self-learning model predictive control for dynamic activation of structural thermal mass in residential buildings. *Energy and Buildings,* 207**,** 109542.

WOLTMAN, G., NOEL, M. & FAM, A. 2017. Experimental and numerical investigations of thermal properties of insulated concrete sandwich panels with fiberglass shear connectors. *Energy and Buildings,* 145**,** 22-31.

YAN, S. & LI, X. Comparison of space cooling/heating load under non-uniform indoor environment with convective heat gain/loss from envelope. Building Simulation, 2021. Springer, 565-578.

YAO, R., LI, B. & LIU, J. 2009. A theoretical adaptive model of thermal comfort – Adaptive Predicted Mean Vote (aPMV). *Building and Environment,* 44**,** 2089-2096.

YOON, H.-S., LIM, T.-K., JEONG, S.-M. & YANG, K.-H. 2020. Thermal transfer and moisture resistances of nano-aerogel-embedded foam concrete. *Construction and Building Materials,* 236**,** 117575.

ZHAI, X., WANG, Y. & WANG, X. 2018. Thermal performance of precast concrete sandwich walls with a novel hybrid connector. *Energy and Buildings,* 166**,** 109-121.

ZHANG, Y., ZHOU, G., LIN, K., ZHANG, Q. & DI, H. 2007. Application of latent heat thermal energy storage in buildings: State-of-the-art and outlook. *Building and Environment,* 42**,** 2197-2209.

ZHAO, J., ABDUL AZIZ, F., DENG, Y., UJANG, N. & XIAO, Y. 2024. A Review of Comprehensive Post-Occupancy Evaluation Feedback on Occupant-Centric Thermal Comfort and Building Energy Efficiency. *Buildings,* 14**,** 2892.

APPENDICES

APPENDIX A

The following table (Table A-1) displays a total of 22 local projects in the Kingdom of Saudi Arabia where various prefabricated building systems were developed.

These projects employ more than one technology under the broad category of prefabricated construction systems. Therefore, some projects have utilised steel, while others have used concrete systems. As previously mentioned, this study focuses primarily on precast concrete projects. However, it also includes some projects that use non-concrete systems, as long as they fall within the scope of prefabricated systems. Accordingly, during this phase of the study, the projects were categorized based on their locations, project year, project type, project size, construction system used, executing agency, contractor, and the feasibility of visiting the project.

Table A 1: List of prefabricated housing projects in Saudi Arabia. Source: sakani (2019).

Project	Location	Project year	Project type	Project size m²/cap	Prefabricated construction system	Executing / contractor	Availability
Al-Wajiha housing complex	Dammam, Eastern Province	2021	Residential house	185,734 (574 house)	Precast concrete system	Alhakmiah	Not completed project.
Mutrafiah housing project	Jubail industrial city.	2013	housing	769,888 (3,600 villas)	Precast concrete system	Azmeel contracting & construction company. Precaster: Al-Rashid abetong co. Ltd.	Empty building available
Sabic mega housing projects - Jalmudah	Jubail industrial city.	2012	Housing and facilities	1280 villa	Precast concrete system	Precaster: bceg, Qanbar Dywidag	Empty building unavailable
Sabic housing project	Al-Meshaireef, Yanbu Industrial city	2013	Housing and facilities	444,857 (384 villas)	Precast concrete system	Azmeel contracting. Precaster: bceg, Qanbar Dywidag	Remote location
MOI housing project	Najran region, South border	2016	Housing and apartments	1,000 villas and more than 600 apartments.	Precast concrete system	Al-seif construction company	Remote location
Murcia housing developments	Riyadh	2020	Housing	491,639 (936 villas)	Precast concrete system	Dar and Emaar	Not completed project.
Saraya narges	Riyadh	Late 2019	Housing	750,324 (1,984 villas)	Precast concrete system	Dar and Emaar	Not completed project.

Ishraq living	Riyadh	2018	Housing	554,879 (2,229 units)	Precast concrete system	Alliance	Remote location
Shams Al-Diyar	Al-Gwan suburb. Riyadh	2018	Housing	343,478 (503 units)	Precast concrete system	Aldiyar Al-Arabiya (shhum)	Remote location
Al-Jawhara buildings	Al-Gwan suburb. Riyadh	2018	Housing	15,473 (112 units)	Precast concrete system	Abdulrahman bin saad Al-Rashed and his sons	Remote location
Riyadh housing 1	Al-Gwan suburb. Riyadh	2018	Housing	13,983 (168 units)	Precast concrete system	Salman Abdullah bin Saedan	Remote location
Asdaf Al-Khobar	Al-Khobar, eastern province	2020	Housing	38,530 (115 units)	Autoclaved aerated concrete panels	Saudi acico co. Ltd.	Empty building unavailable
Residence heights	Riyadh	2020	Housing	120,704 (476 units)	Precast concrete system	Maskan Arabia company	Remote location
Abha housing - Abha hills	Southern region of Asir	2018	Housing	1,023,100 (1,243 villas)	Precast concrete system	Ali shar real estate	Remote location
Dahiyat Al wahaka - sunset hills (Townhouse)	Dammam, eastern province	2019	Housing	134,346 (442 units)	Precast concrete system	Sany Al-amria company	Empty building unavailable
Al bairaq villas (Mubarraz)	Al-Ahsa ،eastern province	2018	Housing	180,000 (192 units)	Autoclaved aerated concrete panels	Innovative investments real estate development	Empty building unavailable
Dammam housing, al bairaq.	Dammam, Eastern province, Saudi Arabia	2019	Housing	519,627 (959 units)	Autoclaved aerated concrete panels	Innovative Investments Real Estate Development	Empty building unavailable
Diyar Rabigh housing	Rabigh	2018	Housing	260,707 (350 units)	Precast concrete system	Ali shar real estate	Not completed project.
Al Qatif housing project	Qatif, eastern province	2018	Housing	221,383 (942 units)	Precast concrete system	Al Tamimi company	Not completed project.
Ras Tanura residential community	Ras Tanura, Eastern Province	2015	Site, housing, and facilities.	80 units villas	Precast concrete system	Saudi Aramco (client), khonaini international company (contractor)	Empty building unavailable
Jalmudah housing project (Sabic)	Jalmudah, Jubail ind. City	2015	Site, housing, and facilities.	234 Units	Precast concrete system	Saudi Arabian basic industries corporation (client) khonaini international company (contractor)	Empty building available
Housing project (Saudi KAYAN)	Jalmudah, Jubail Ind. City, Saudi Arabia	2015	Site, housing, and facilities.	248 Units	Precast concrete System	Saudi Kayan Petrochemical Company (Client), and khonaini international company (contractor)	Empty building available

APPENDIX B

Houses 1-J Simulated Model using DesignBuilder:

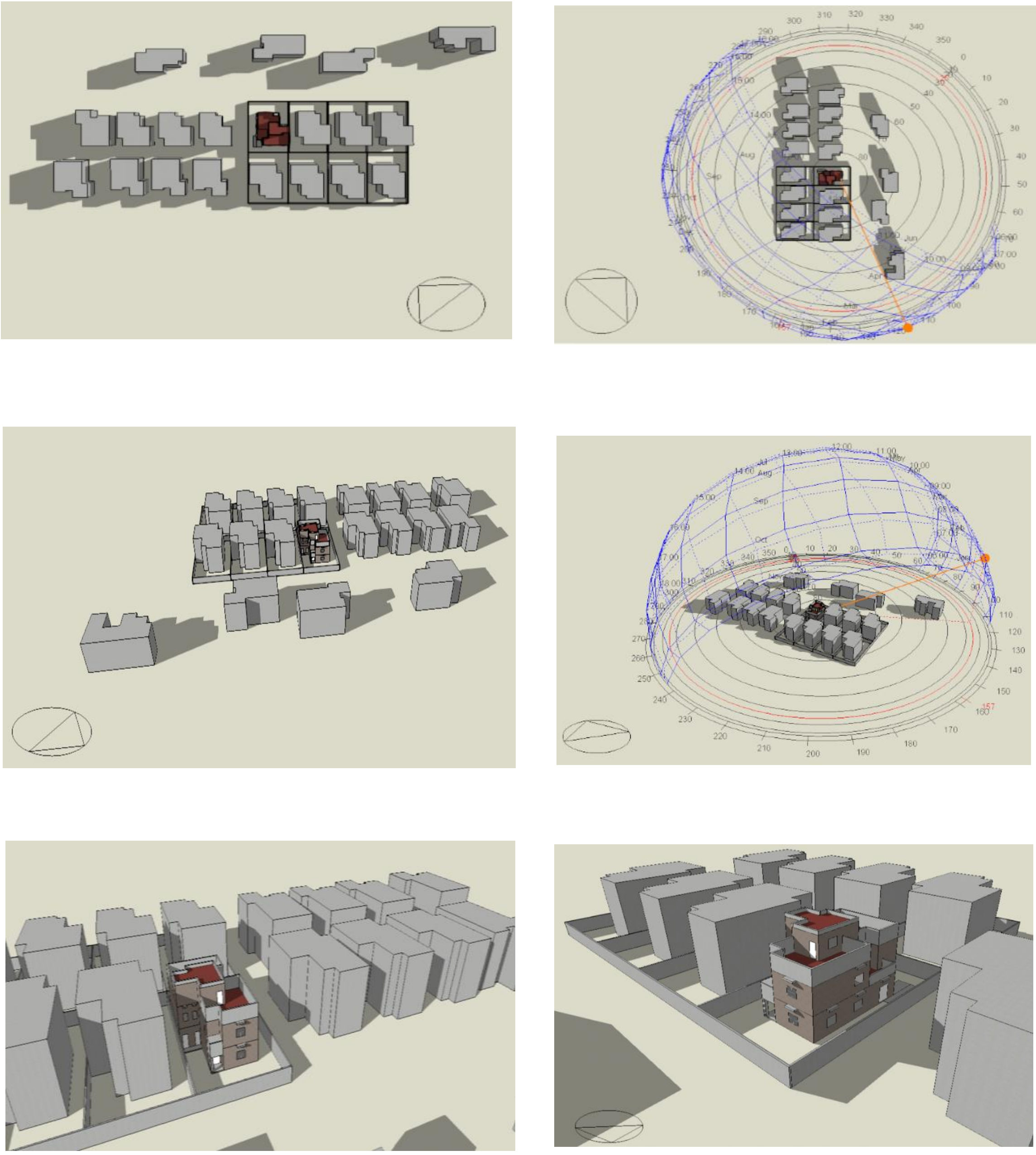

Figure B-1: Images showing house 1-J simulated in DesignBuilder.

Houses 1-J Simulated Zones using DesignBuilder:

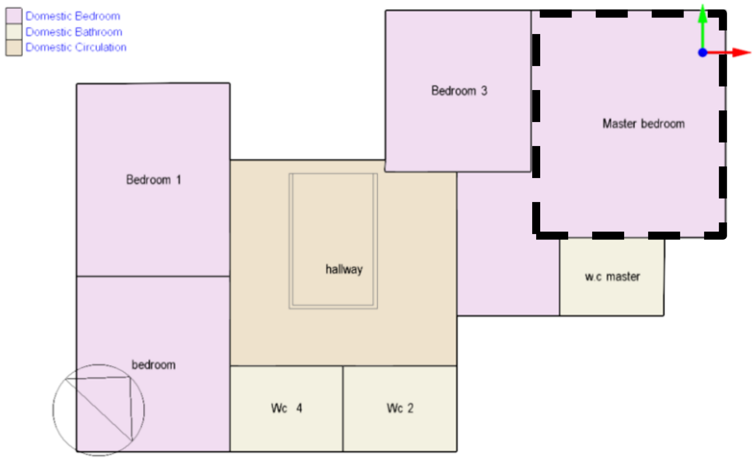

Figure B-2: Simulated image illustrates house 1-J ground floor zones.

Figure B-3: Simulated image illustrates house 1-J first floor zones.

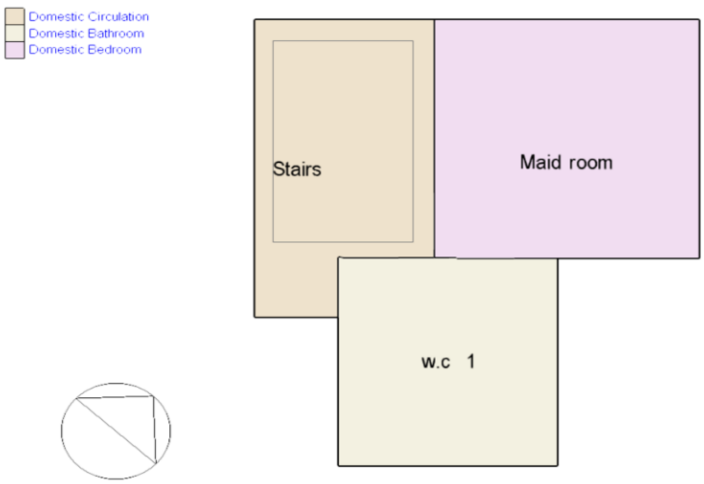

Figure B-4: Simulated image illustrates house 1-J top floor zones.

Houses 1-M Simulated Model using DesignBuilder:

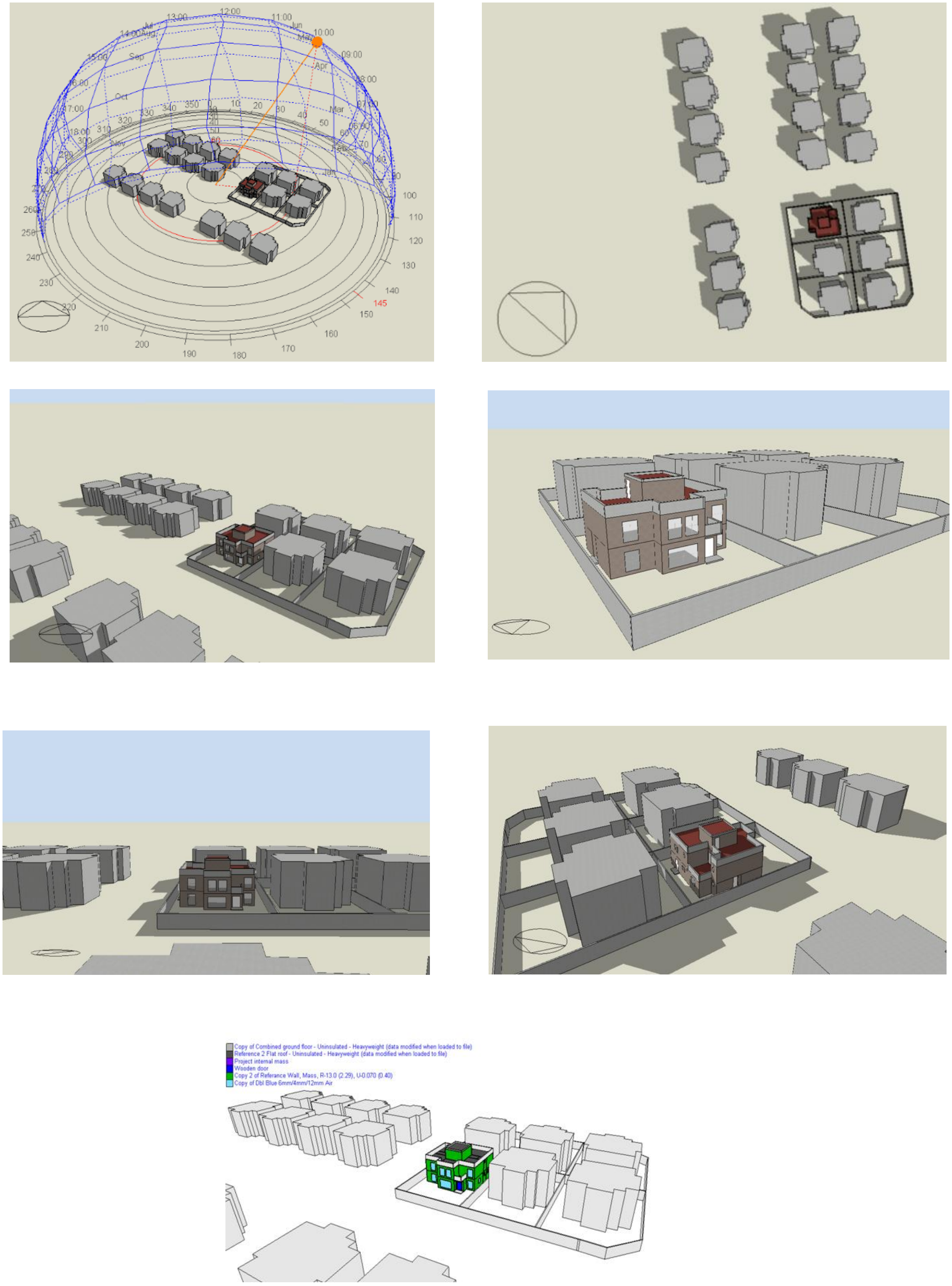

Figure B-5: Images illustrate house 1-M simulated model in different angles.

Houses 2-M Simulated model using DesignBuilder:

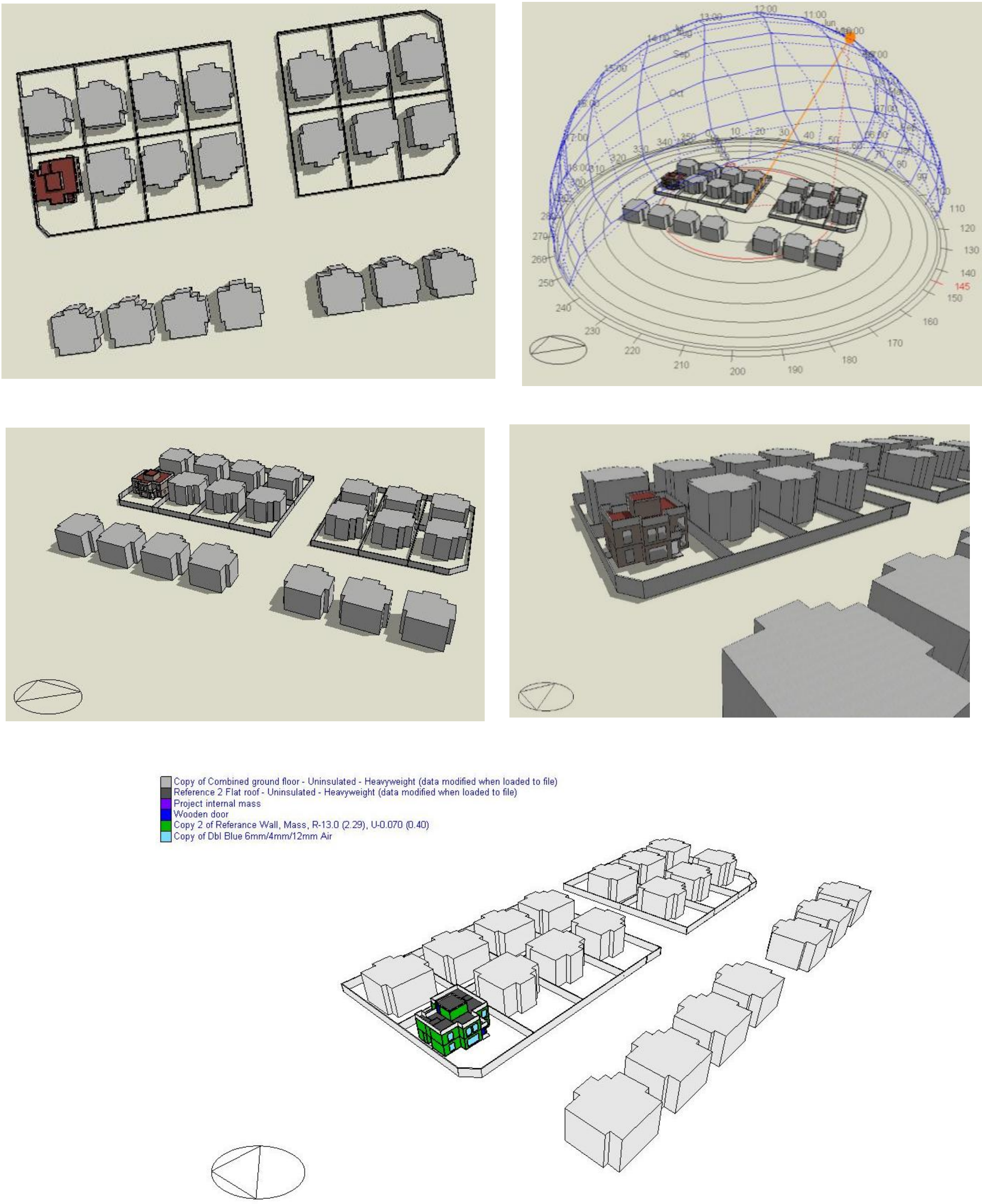

Figure B-6: Images illustrate house 2-M simulated model in different angles using DesignBuilder software.

Houses 1-M & 2-M Simulated zones using DesignBuilder:

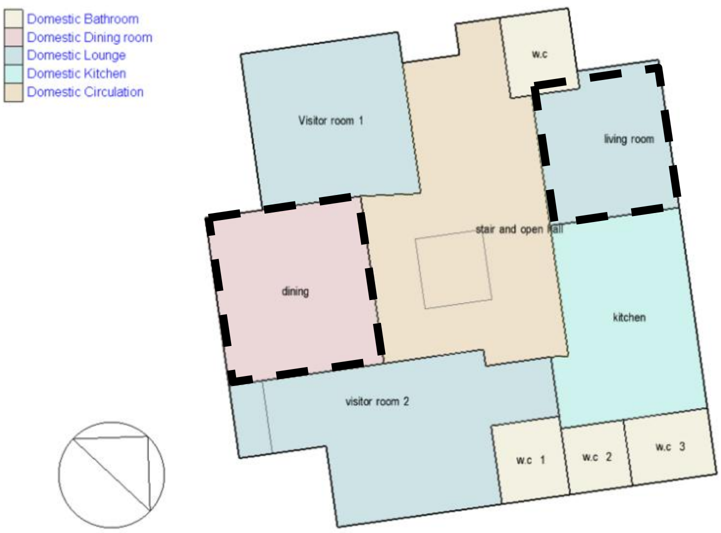

Figure B-7: Simulated image illustrates house 1-M & 2-M ground floor plan.

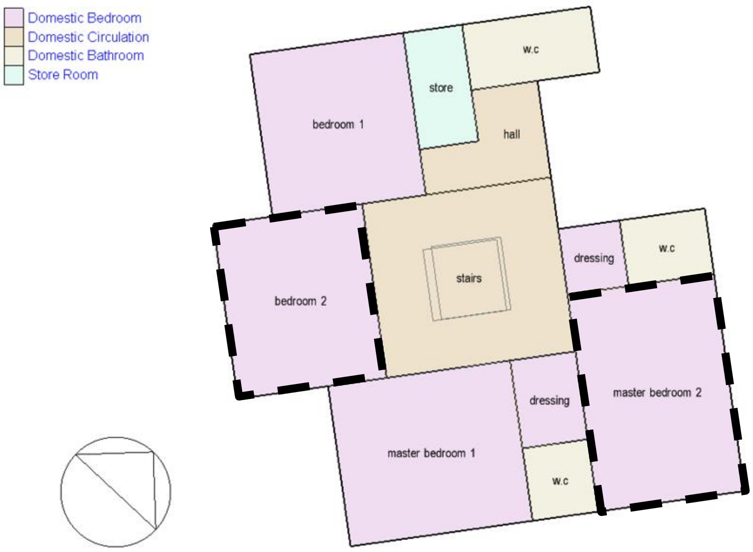

Figure B-8: Simulated image illustrates house 1-M & 2-M first floor plan.

APPENDIX C

Estimated energy savings using DesignBuilder:

House 1-J Base case scenarios

Table C-1: House 1-J total existing energy usage . Date exported from DesignBuilder software.

Site and Source Energy

	Total Energy [kWh]	Energy Per Total Building Area [kWh/m2]	Energy Per Conditioned Building Area [kWh/m2]
Total Site Energy	35973.15	99.69	99.69
Net Site Energy	35973.15	99.69	99.69
Total Source Energy	50712.77	140.54	140.54
Net Source Energy	50712.77	140.54	140.54

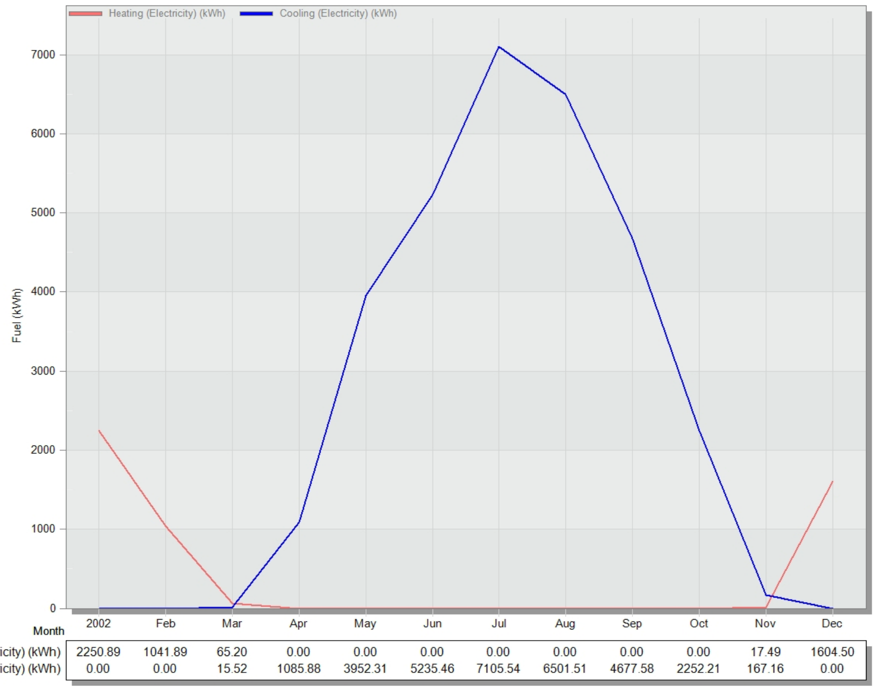

Figure C-1: Images illustrate house 1-J estimated energy usage. Data exported from DesignBuilder software.

House 1-J Optimised scenario

Table C 2: House 1-J total optimised energy usage. Data exported from DesignBuilder software.

Site and Source Energy

	Total Energy [kWh]	Energy Per Total Building Area [kWh/m2]	Energy Per Conditioned Building Area [kWh/m2]
Total Site Energy	26644.16	70.56	70.56
Net Site Energy	26644.16	70.56	70.56
Total Source Energy	28891.78	76.51	76.51
Net Source Energy	28891.78	76.51	76.51

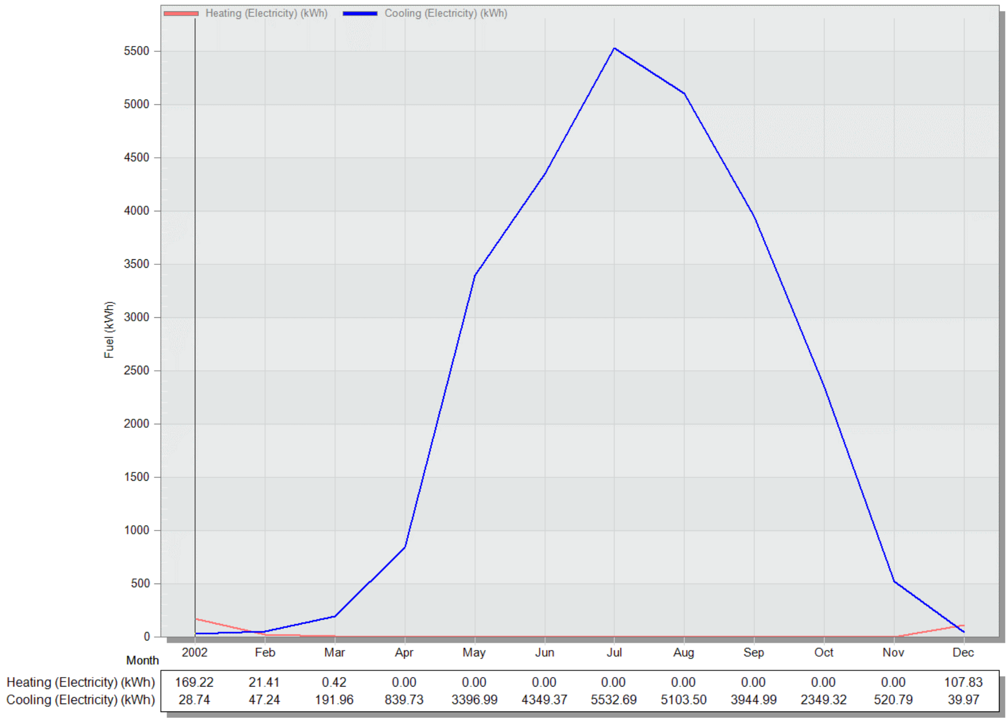

Figure C-2: Images illustrate house 1-J optimised energy. Data exported from DesignBuilder software.

House 1-M base case scenarios

Table C 3: House 1-M total existing energy usage. Data exported from DesignBuilder software.

Site and Source Energy

	Total Energy [kWh]	Energy Per Total Building Area [kWh/m2]	Energy Per Conditioned Building Area [kWh/m2]
Total Site Energy	28422.49	79.04	79.04
Net Site Energy	28422.49	79.04	79.04
Total Source Energy	34695.57	96.49	96.49
Net Source Energy	34695.57	96.49	96.49

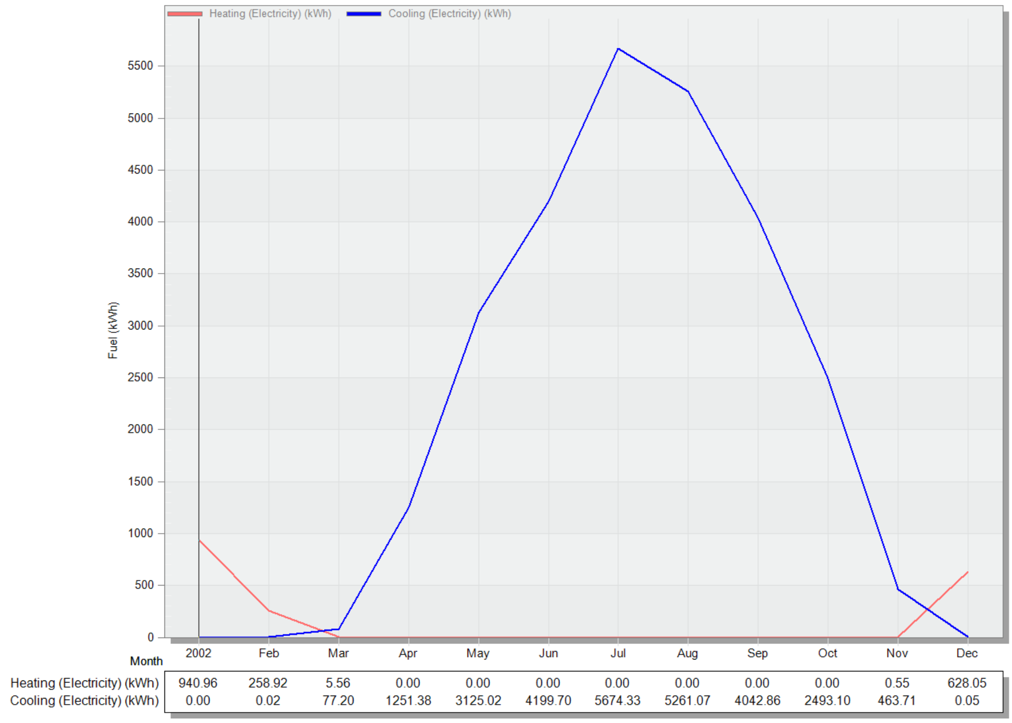

Figure C-3: Images illustrate house 1-M existing energy usage. Data exported from DesignBuilder software.

House 1-M optimised scenarios

Table C 4: House 1-M total optimised energy usage. Data exported from DesignBuilder software.

Site and Source Energy

	Total Energy [kWh]	Energy Per Total Building Area [kWh/m2]	Energy Per Conditioned Building Area [kWh/m2]
Total Site Energy	17600.82	47.80	47.80
Net Site Energy	17600.82	47.80	47.80
Total Source Energy	18643.07	50.63	50.63
Net Source Energy	18643.07	50.63	50.63

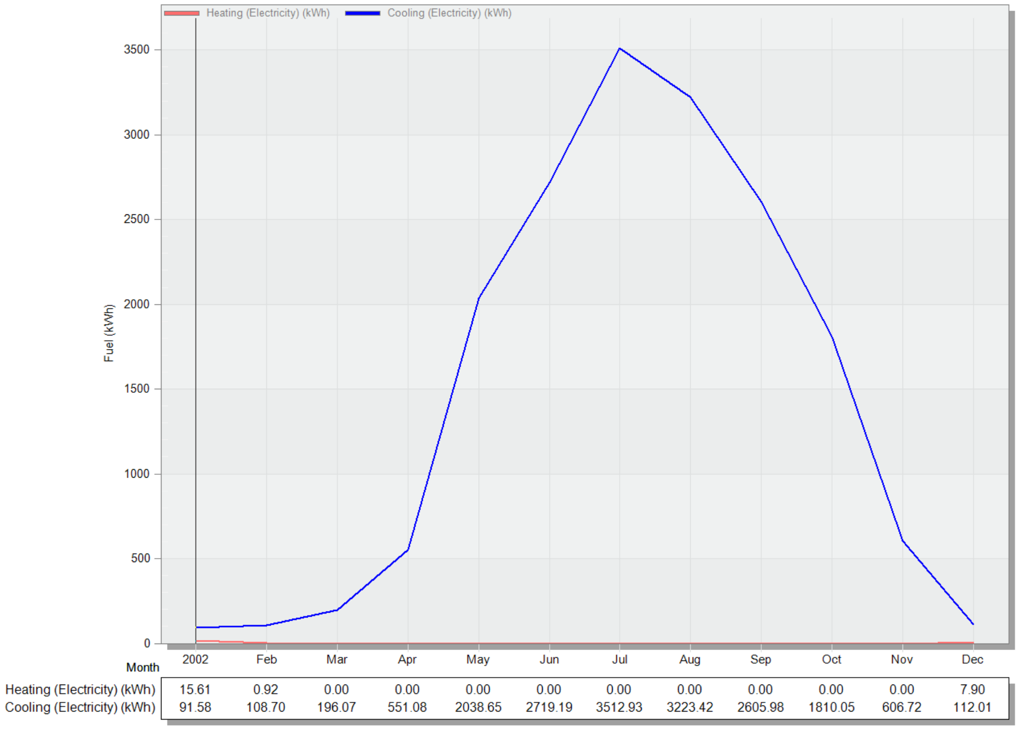

Figure C-4: Images illustrate house 1-M optimised energy usage. Data exported from DesignBuilder software.

House 2-M base case scenarios

Table C 5: House 2-M total existing energy usage. Data exported from DesignBuilder software.

Site and Source Energy

	Total Energy [kWh]	Energy Per Total Building Area [kWh/m2]	Energy Per Conditioned Building Area [kWh/m2]
Total Site Energy	32872.94	91.42	91.42
Net Site Energy	32872.94	91.42	91.42
Total Source Energy	40564.20	112.81	112.81
Net Source Energy	40564.20	112.81	112.81

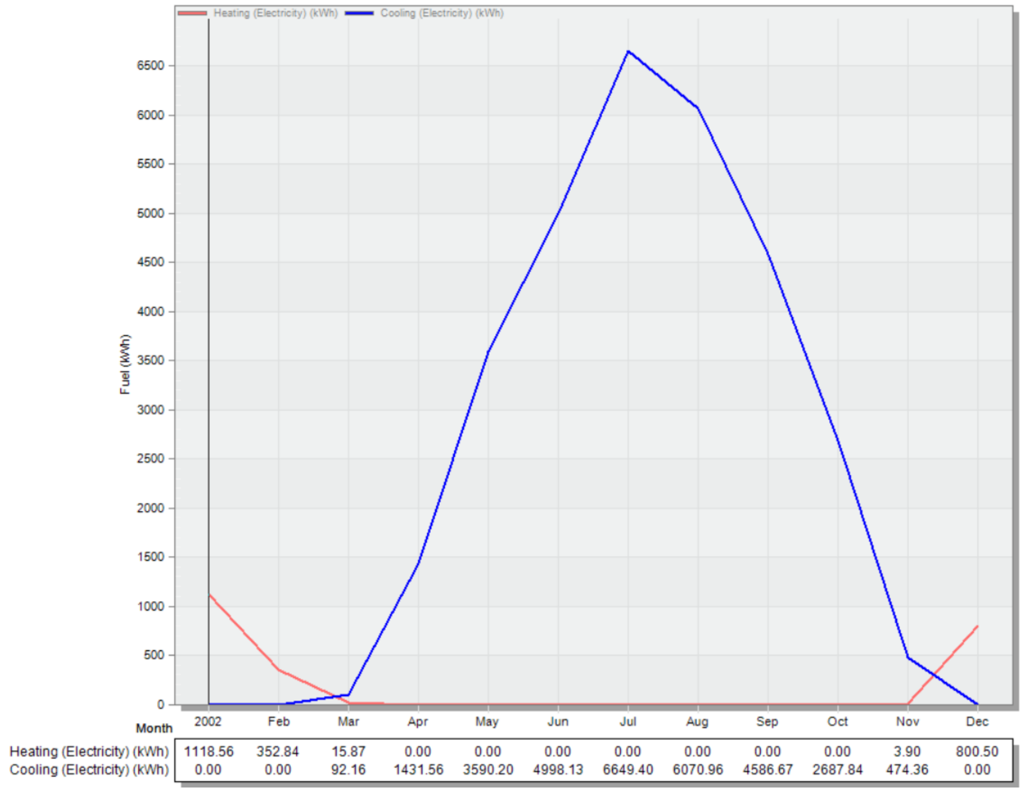

Figure C-5: Images illustrate house 2-M existing energy usage. Data exported from DesignBuilder software.

House 2-M optimised scenarios

Table C 6: House 2-M total optimised energy usage. Data exported from DesignBuilder software.

Site and Source Energy

	Total Energy [kWh]	Energy Per Total Building Area [kWh/m2]	Energy Per Conditioned Building Area [kWh/m2]
Total Site Energy	23447.12	63.67	63.67
Net Site Energy	23447.12	63.67	63.67
Total Source Energy	24797.96	67.34	67.34
Net Source Energy	24797.96	67.34	67.34

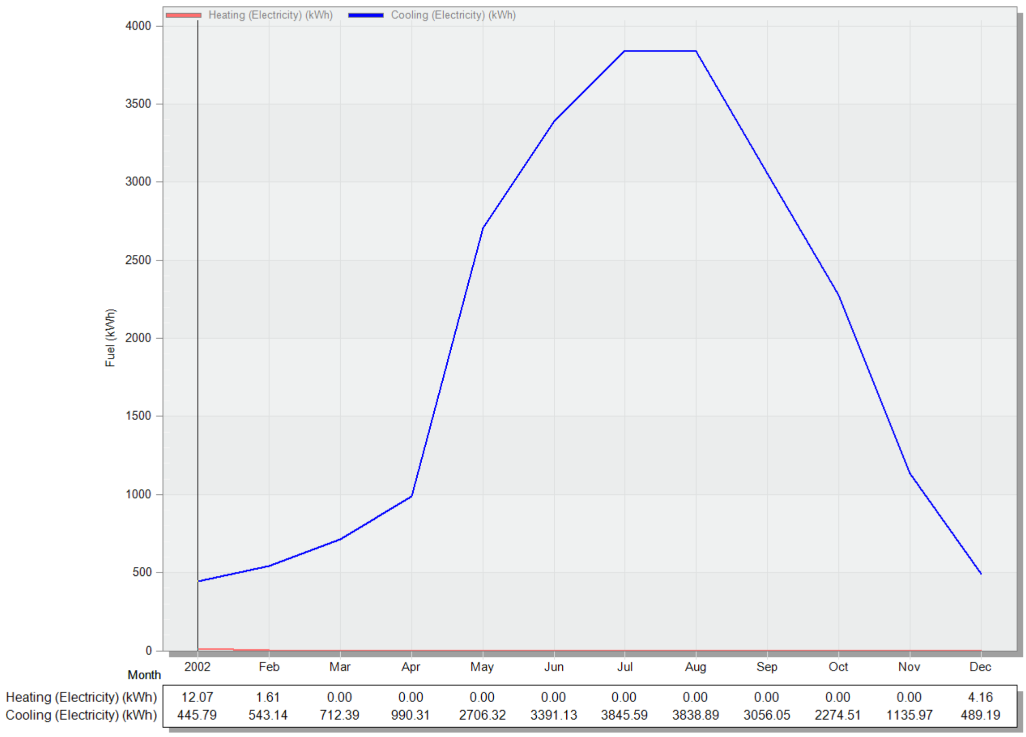

Figure C-6: Images illustrate house 2-M optimised energy usage. Data exported from DesignBuilder software.

APPENDIX D

Certificate of Calibration 1

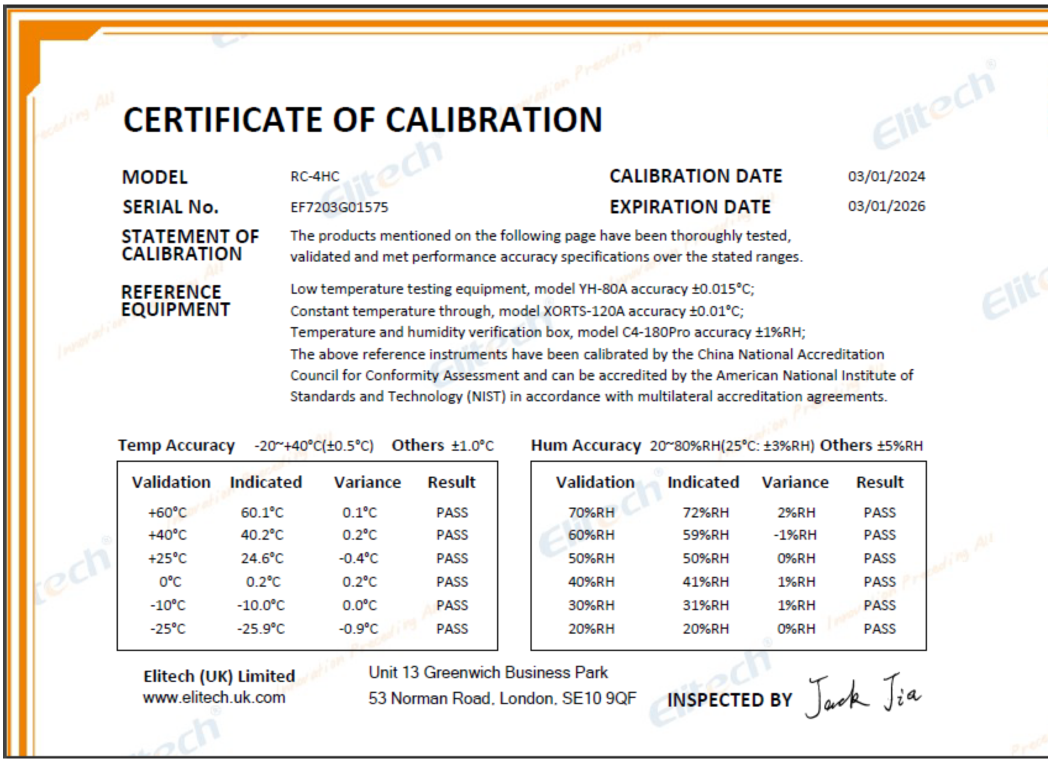

CERTIFICATE OF CALIBRATION

MODEL	RC-4HC	CALIBRATION DATE	03/01/2024
SERIAL No.	EF7203G01575	EXPIRATION DATE	03/01/2026

STATEMENT OF CALIBRATION The products mentioned on the following page have been thoroughly tested, validated and met performance accuracy specifications over the stated ranges.

REFERENCE EQUIPMENT Low temperature testing equipment, model YH-80A accuracy ±0.015°C;
Constant temperature through, model XORTS-120A accuracy ±0.01°C;
Temperature and humidity verification box, model C4-180Pro accuracy ±1%RH;
The above reference instruments have been calibrated by the China National Accreditation Council for Conformity Assessment and can be accredited by the American National Institute of Standards and Technology (NIST) in accordance with multilateral accreditation agreements.

Temp Accuracy -20~+40°C(±0.5°C) **Others** ±1.0°C

Validation	Indicated	Variance	Result
+60°C	60.1°C	0.1°C	PASS
+40°C	40.2°C	0.2°C	PASS
+25°C	24.6°C	-0.4°C	PASS
0°C	0.2°C	0.2°C	PASS
-10°C	-10.0°C	0.0°C	PASS
-25°C	-25.9°C	-0.9°C	PASS

Hum Accuracy 20~80%RH(25°C: ±3%RH) **Others** ±5%RH

Validation	Indicated	Variance	Result
70%RH	72%RH	2%RH	PASS
60%RH	59%RH	-1%RH	PASS
50%RH	50%RH	0%RH	PASS
40%RH	41%RH	1%RH	PASS
30%RH	31%RH	1%RH	PASS
20%RH	20%RH	0%RH	PASS

Elitech (UK) Limited
www.elitech.uk.com

Unit 13 Greenwich Business Park
53 Norman Road, London, SE10 9QF

INSPECTED BY Jack Jia

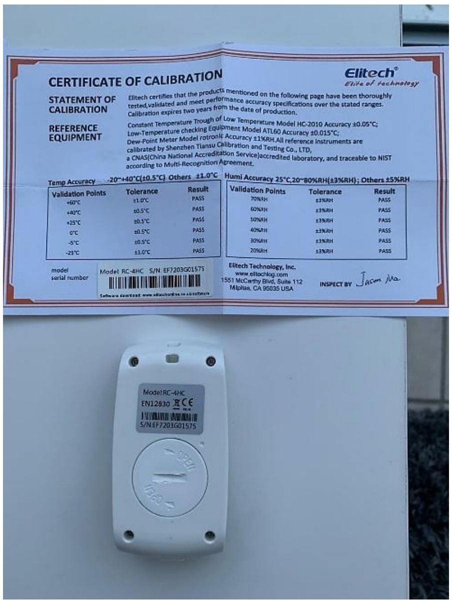

Figure D-1: Images illustrate original certificate of calibration with related matching device’s serial number.

Certificate of Calibration 2

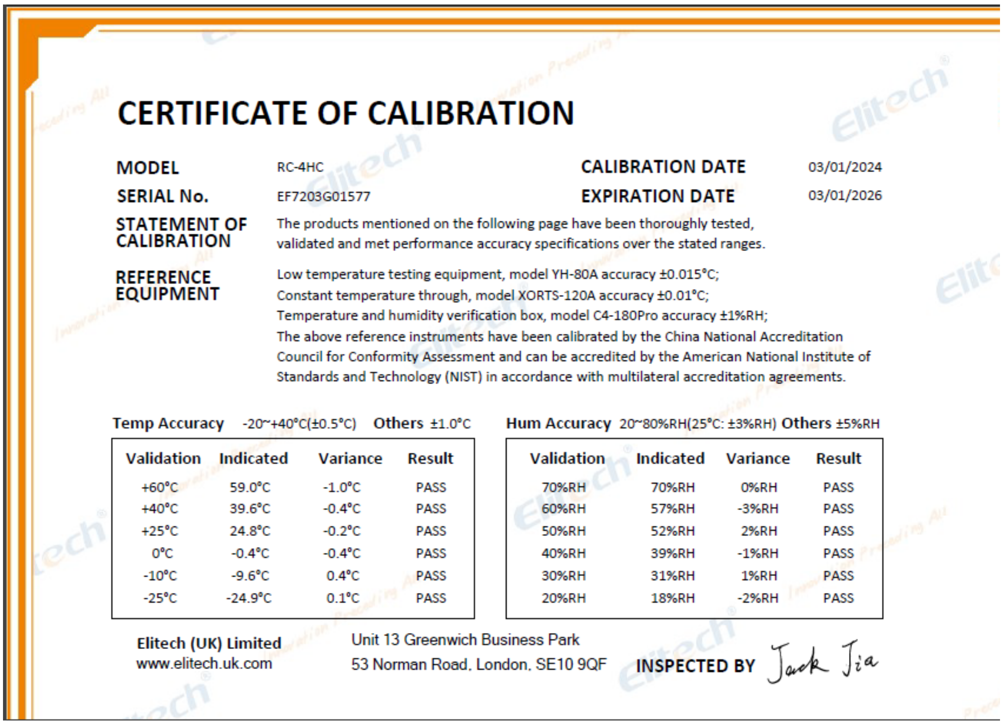

CERTIFICATE OF CALIBRATION

MODEL	RC-4HC	**CALIBRATION DATE**	03/01/2024
SERIAL No.	EF7203G01577	**EXPIRATION DATE**	03/01/2026

STATEMENT OF CALIBRATION The products mentioned on the following page have been thoroughly tested, validated and met performance accuracy specifications over the stated ranges.

REFERENCE EQUIPMENT Low temperature testing equipment, model YH-80A accuracy ±0.015°C;
Constant temperature through, model XORTS-120A accuracy ±0.01°C;
Temperature and humidity verification box, model C4-180Pro accuracy ±1%RH;
The above reference instruments have been calibrated by the China National Accreditation Council for Conformity Assessment and can be accredited by the American National Institute of Standards and Technology (NIST) in accordance with multilateral accreditation agreements.

Temp Accuracy -20~+40°C(±0.5°C) **Others** ±1.0°C

Validation	Indicated	Variance	Result
+60°C	59.0°C	-1.0°C	PASS
+40°C	39.6°C	-0.4°C	PASS
+25°C	24.8°C	-0.2°C	PASS
0°C	-0.4°C	-0.4°C	PASS
-10°C	-9.6°C	0.4°C	PASS
-25°C	-24.9°C	0.1°C	PASS

Hum Accuracy 20~80%RH(25°C: ±3%RH) **Others** ±5%RH

Validation	Indicated	Variance	Result
70%RH	70%RH	0%RH	PASS
60%RH	57%RH	-3%RH	PASS
50%RH	52%RH	2%RH	PASS
40%RH	39%RH	-1%RH	PASS
30%RH	31%RH	1%RH	PASS
20%RH	18%RH	-2%RH	PASS

Elitech (UK) Limited
www.elitech.uk.com

Unit 13 Greenwich Business Park
53 Norman Road, London, SE10 9QF

INSPECTED BY Jack Jia

Figure D-2: Images illustrate original certificate of calibration with related matching device’s serial number.

Certificate of Calibration 3

CERTIFICATE OF CALIBRATION

MODEL	RC-4HC	**CALIBRATION DATE**	03/01/2024
SERIAL No.	EF7203G01576	**EXPIRATION DATE**	03/01/2026

STATEMENT OF CALIBRATION The products mentioned on the following page have been thoroughly tested, validated and met performance accuracy specifications over the stated ranges.

REFERENCE EQUIPMENT Low temperature testing equipment, model YH-80A accuracy ±0.015°C;
Constant temperature through, model XORTS-120A accuracy ±0.01°C;
Temperature and humidity verification box, model C4-180Pro accuracy ±1%RH;
The above reference instruments have been calibrated by the China National Accreditation Council for Conformity Assessment and can be accredited by the American National Institute of Standards and Technology (NIST) in accordance with multilateral accreditation agreements.

Temp Accuracy -20~+40°C(±0.5°C) **Others** ±1.0°C

Validation	Indicated	Variance	Result
+60°C	59.4°C	-0.6°C	PASS
+40°C	40.3°C	0.3°C	PASS
+25°C	24.6°C	-0.4°C	PASS
0°C	-0.5°C	-0.5°C	PASS
-10°C	-10.4°C	-0.4°C	PASS
-25°C	-24.1°C	0.9°C	PASS

Hum Accuracy 20~80%RH(25°C: ±3%RH) **Others** ±5%RH

Validation	Indicated	Variance	Result
70%RH	69%RH	-1%RH	PASS
60%RH	61%RH	1%RH	PASS
50%RH	50%RH	0%RH	PASS
40%RH	39%RH	-1%RH	PASS
30%RH	27%RH	-3%RH	PASS
20%RH	20%RH	0%RH	PASS

Elitech (UK) Limited
www.elitech.uk.com

Unit 13 Greenwich Business Park
53 Norman Road, London, SE10 9QF

INSPECTED BY Jack Jia

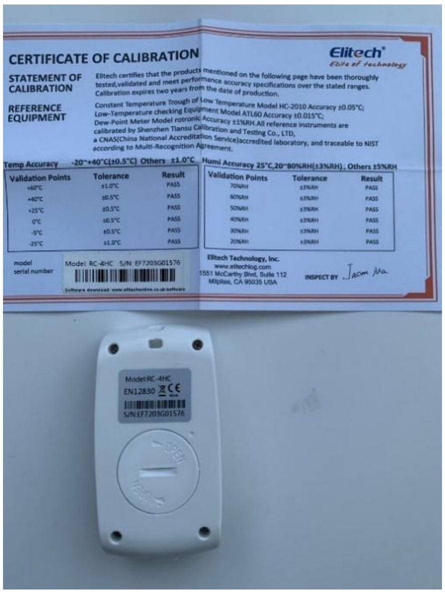

Figure D-3: Images illustrate original certificate of calibration with related matching device’s serial number.

APPENDIX E

Previous Research into the Use of BEPS Tools

Over the past five decades, the building energy industry has witnessed the evolution and extensive application of numerous building energy simulation tools. Alrashed (2015) reviewed a study by Crawley et al. (2008) that meticulously compared the technical capabilities of various BEPS tools, as detailed in Tables E-1 to E-5. This research furnished comprehensive tables, offering an unbiased comparison of the tools based on features detailed by their developers. The categories evaluated included general programme features, zone loads, building envelope, daylighting and solar aspects, renewable energy systems, electrical systems, HVAC systems, environmental emissions, and economic assessments. This comprehensive comparison stands out in the literature, making it a dependable source for tool selection within the purview of the current study.

However, the implications of prior research exploring the efficacy of BEPS tools cannot be understated for this study's orientation. Challenges abound in predicting input parameters, understanding occupancy dynamics, and deciphering operation strategies, as these elements exhibit considerable variability across buildings (Lee et al., 2013). Additionally, meteorological factors can be erratic. Thus, energy modelling through BEPS tools offers approximations rife with uncertainties. Given the significance of modelling outcomes for optimal design and informed decision-making, it is imperative to recognise and navigate these uncertainties (Williamson, 2010, cited in Alrashed, 2015). Furthermore, Attia et al. (2009) evaluated the user-friendliness of ten simulation tools. Their assessment highlighted the Integrated Environmental Solutions Virtual Environment (IES-VE) as the most intuitive tool for architects during that period.

Note: In the subsequent tables, X indicates a commonly used feature or capability; P indicates a partially implemented feature; O signifies an optional feature; R denotes a feature used for research; E implies a feature requiring domain expertise; I represents a feature with challenging-to-source inputs.

Table E-1: Comparison illustrating zone loads evaluation capabilities for each BEPS tool. Source: Crawley et al. (2008).

	BLAST	BSim	DeST	DOE-2.1E	ECOTECT	Ener-Win	Energy Express	Energy-10	EnergyPlus	eQUEST	ESP-r	IDA ICE	IES 〈VE〉	HAP	HEED	PowerDomus	SUNREL	Tas	TRACE	TRNSYS
Interior surface convection																				
• Dependent on temperature	X	X					P		X		X	X	X		X	X	X	X		X
• Dependent on air flow	X						X		P		X		X		X			X		E
• Dependent on surface heat coefficient from CFD									E		E		X							
• User-defined coefficients (constants, equations or correlations)		X	X	X	X				X		E	R	X		X	X	X	X		X
Internal thermal mass	X	X	X	X	X	X	X	X	X	X	X	X	X		X	X	X	X	X	X
Automatic design day calculations for sizing																				
• Dry bulb temperature	X	X	X	X	X	X	X	X	X	X		X	X	X	X	P		X	X	
• Dew point temperature or relative humidity			X	X		X	X		X	X		X	X	X				X	X	
• User-specified minimum and maximum			X	X		X	X		X	X		X	X	X	X			X	X	
• User-specified steady-state, steady-periodic or fully dynamic design conditions			X									X	X	X				X	X	X

Table E-2: Comparison illustrating Building envelop, daylighting and solar evaluation capabilities for each BEPS tool. Source: Crawley et al. (2008).

	BLAST	BSim	DeST	DOE-2.1E	ECOTECT	Ener-Win	Energy Express	Energy-10	EnergyPlus	eQUEST	ESP-r	IDA ICE	IES 〈VE〉	HAP	HEED	PowerDomus	SUNREL	Tas	TRACE	TRNSYS
Outside surface convection algorithm																				
• BLAST/TARP	X								X										X	
• DOE-2				X					X	X									X	
• MoWiTT									X		X								X	
• ASHRAE simple	X					X		X	X				X		X			X	X	
• Ito, Kimura, and Oka correlation											X	X								
• User-selectable			X						X		X	X	X			X		X	X	X
Inside radiation view factors		X	X						X		X	X	X				P	X		
Radiation-to-air component separate from detailed convection (exterior)		X	X						X	X	X	X	X				X	X	P	X
Solar gain and daylighting calculations account for inter-reflections from external building components and other buildings		P			X				X		X		X			P				X

Table E-3: Comparison illustrating infiltration, ventilation, room air and multizone airflow evaluation capabilities for each BEPS tool. Source: Crawley et al. (2008).

	BLAST	BSim	DeST	DOE-2.1E	ECOTECT	Ener-Win	Energy Express	Energy-10	EnergyPlus	eQUEST	ESP-r	IDA ICE	IES 〈VE〉	HAP	HEED	PowerDomus	SUNREL	Tas	TRACE	TRNSYS
Single zone infiltration	X	X	X	X	X	X	X	X	X	X	X	X	X	X	X	X	X	X	X	X
Automatic calculation of wind pressure coefficients		X	P						P				X				X	X		
Natural ventilation (pressure, buoyancy driven)		X	P						X	P	X	X	X			X	X	X		O
Multizone airflow (via pressure network model)		X	P						X		X	X	X				X	X		O
Hybrid natural and mechanical ventilation		X	P			X					I	X	X			X		X		O
Control window opening based on zone or external conditions			X			X			X		X		X			P	X			O
Displacement ventilation									X		X	X	X					X		O
Mix of flow networks and CFD domains			X								E									
Contaminants, mycotoxins (mold growth)		P									R					P				

Table E-4: Comparison illustrating HVAC system/components and renewable energy system evaluation capabilities for each BEPS tool. Source: Crawley et al. (2008).

	BLAST	BSim	DeST	DOE-2.1E	ECOTECT	Ener-Win	Energy Express	Energy-10	EnergyPlus	eQUEST	ESP-r	IDA ICE	IES 〈VE〉	HAP	HEED	PowerDomus	SUNREL	Tas	TRACE	TRNSYS
Renewable Energy Systems (12 identified, X+O)	1	2	2	1	4	0	0	2	4	2	7	1	3	0	0	1	2	2	0	12
Idealized HVAC systems	X		X		X	X			X		X	X	X				X			X
User-configurable HVAC systems		X	X				P		X		X	X	X	X	X	X	R	X	X	X
Pre-configured systems (among 34 identified, X+O)	14	14	20	16	0	16	5	7	28	24	23	32	28	28	10	8	1	23	26	20
Discrete HVAC components (98 identified, X+O)	51	24	34	39	0	24	8	15	66	61	40	52	38	43	7	15	3	26	63	82

Table E-5: Comparison illustrating economic evaluation capabilities for each BEPS tool. Source: Crawley et al. (2008).

	BLAST	BSim	DeST	DOE-2.1E	ECOTECT	Ener-Win	Energy Express	Energy-10	EnergyPlus	eQUEST	ESP-r	IDA ICE	IES 〈VE〉	HAP	HEED	PowerDomus	SUNREL	Tas	TRACE	TRNSYS
Simple energy and demand charges		X	X	X	X	X	X	X	X	X	X	X	X	X	X	X		X	X	X
Complex energy tariffs including fixed charges, block charges, demand charges, ratchets		X	X	X			X		X	X			X	X	X	P			X	E
Scheduled variation in all rate components		X	X	X					X	X		X	X	X	X	P		X	X	X
User selectable billing dates				X					X	X					X	P			X	E

Few studies have delved into the real-world application of BEPS by examining architectural practices. In a survey conducted in the Netherlands by Erbas and van Dijk (2012), cited by Mahmoud et al. (2020), 149 individuals, mainly architects, were surveyed. They highlighted the need for tools that offer flexibility across various design stages. Prior work showed architects' interest in integrating Design Authoring Software

(DAS) with third-party extensions, such as Revit and SketchUp (Mahmoud et al., 2020).

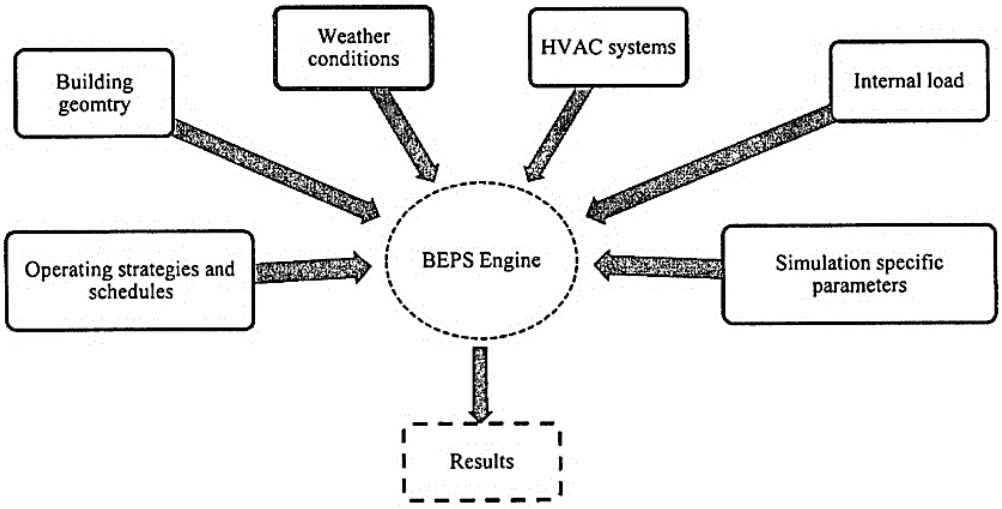

Figure E-1: General data flow of BEPS tool. Source: Alrashed (2015).

Historically, BEPS tools catered to engineers focused on HVAC systems. Recently, there has been a push towards adapting these tools for broader users, like architects. This is seen in the evolution of software like IES-VE and the development of new tools such as Sefaira. However, BEPS tools always require specific input data, including building elements, loads, and user behaviour. The accuracy of these tools depends on the input precision. Maile et al. (2007), referenced by Alrashed (2015), divided input variables into six categories, illustrated in Figure E-1.